CR 85010

INTERIM SCIENTIFIC REPORT

PHASE DIFFERENCE NAVIGATION SATELLITE STUDY

JUNE 1967

Prepared for:

ELECTRONICS RESEARCH CENTER
NATIONAL AERONAUTICS AND SPACE ADMINISTRATION
CAMBRIDGE, MASSACHUSETTS

Contract NAS-12-509

RADIO CORPORATION OF AMERICA ■ DEFENSE ELECTRONIC PRODUCTS
SYSTEMS ENGINEERING, EVALUATION AND RESEARCH, MOORESTOWN, N. J.

Mr. Leo Keane
Technical Monitor
NAS 12-509
Electronics Research Center
575 Technology Square
Cambridge, Massachusetts 02139

INTERIM SCIENTIFIC REPORT

PHASE DIFFERENCE NAVIGATION SATELLITE STUDY

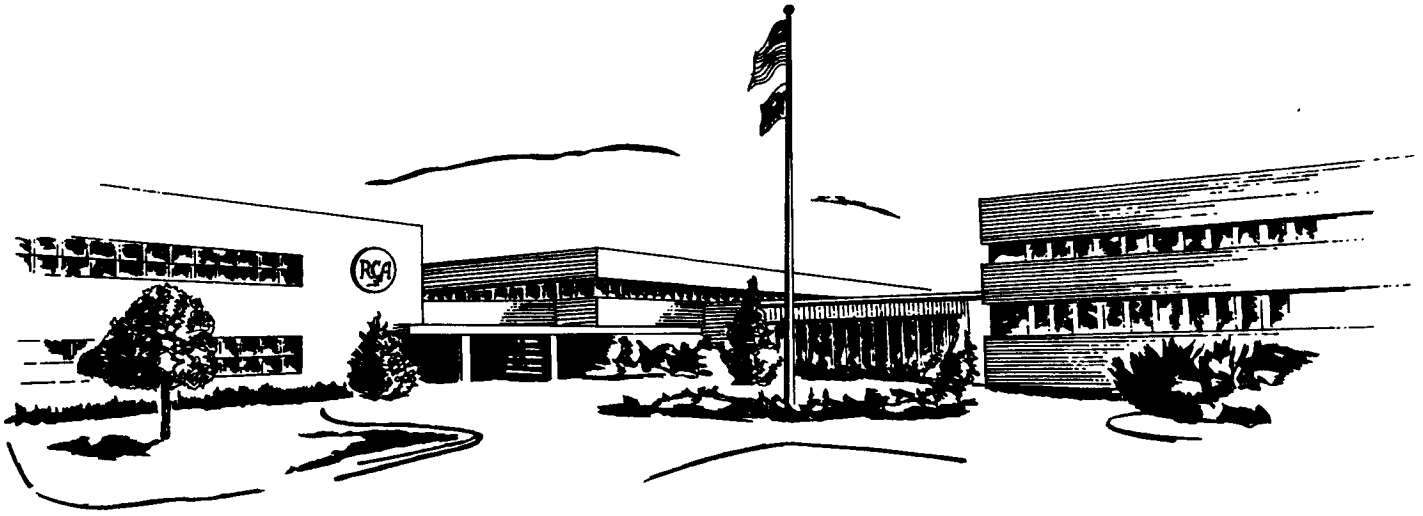

JUNE 1967

Prepared for:

ELECTRONICS RESEARCH CENTER
NATIONAL AERONAUTICS AND SPACE ADMINISTRATION
CAMBRIDGE, MASSACHUSETTS

Contract NAS-12-509

RADIO CORPORATION OF AMERICA ■ DEFENSE ELECTRONIC PRODUCTS
SYSTEMS ENGINEERING, EVALUATION AND RESEARCH, MOORESTOWN, N. J.

CONTENTS

ILLUSTRATIONS

TABLES

Section 1

INTRODUCTION AND SUMMARY

The contents of this Interim Scientific Report represents a comprehensive record of the analyses and investigations performed by RCA under contract NAS 12-509, during the period 15 November 1966 through 15 May 1967. The objective of the Phase Difference Navigation Satellite Study is to investigate the feasibility of selected alternative implementations of the SPOT (Speed, Position, and Track) navigational satellite technique which employs phase difference measurements for navigation and traffic control.

The scope of the study program is defined in five task statements as follows:

1. Define the requirements for navigation and traffic control for the variety of potential marine and aircraft users of the satellite navigational system. Requirements will be stated in terms of anticipated numbers and types of users, rates of fix, and accuracy required. The requirements model will be based on previously conducted NASA studies, other agency and industry studies, and contacts to be made early in the program with pertinent agencies and users. The model will be derived with the North Atlantic environment, projected to 1975 as a basis.

2. Study both the tri-spherical and hyperbolic passive ranging schemes in sufficient detail to define ground station, satellite and user equipment and equipment stabilities required to perform such measurements. The user equipment will include antenna, receiver, and position computer. Investigate requirements and recommend techniques for the distribution of satellite position data. Study the possible use of charts, tables, and hand computations in place of a totally automated navigation measurement.

3. Examine the possibility of making relative position measurements using phase difference techniques of a higher order accuracy by transponding both directly to a computation center and through a marker or buoy. Perform a detailed error analysis to estimate relative positioning accuracy due to the major geometric, atmospheric, instrumentation and other anticipated error.

4. Recommend a unified approach which, in consonance with the model developed under I, will provide the capabilities outlined under 2 and 3 as well as the required traffic control capability. Study the integration time requirements for data relay and examine and detail the format of the information relayed through the satellite for traffic control and a navigation fix. Perform a comprehensive error analysis estimating the various fix accuracies including all major anticipated error sources during simultaneous use by (1) in a traffic control loop, (2) passive navigators, and operators who are making relative navigation measurements. Estimate the maximum number of users which could enter the traffic control system. The carrier frequency to be considered is the 1540-1660 MHz radio navigation band.

5. Identify critical aspects of the selected approach and recommend laboratory, aircraft, or satellite tests which should be initiated to confirm feasibility.

Toward the end of study period, six critical areas were jointly selected by NASA and RCA for additional investigation. An extension to the subject contract was awarded to RCA covering the period from 15 May 1967 through 15 September 1967. A final report will be submitted on 15 October summarizing results and conclusions as a consequence of the entire 10-month effort. The final report will also include identification of a unified system which will provide simultaneous passive user navigation and traffic control; instrumentation characteristics including detailed specifications and block diagrams of user and satellite equipment; identification of all critical aspects of the unified system; and recommendations for additional study, laboratory test and development, and a field test and feasibility demonstration program. It is anticipated that the results of the extension period will alter, to some degree, the statements presented in this interim report concerning system configuration, instrumentation, and performance.

1.1 REPORT CONTENT

1.1.1 GENERAL CONTENT

A description of navigation and traffic control systems concepts, including traffic control surveillance, passive or self-navigation by user vehicles and relative navigation appears in Section 2. The ground, satellite and user equipment requirements are defined for both circular and hyperbolic ranging techniques.

At the beginning of the study, a requirements model for navigation and traffic control of aircraft and marine users projected to 1975 was postulated using data from the Ad Hoc Joint Navigation Satellite Committee of May 1966 and several traffic traffic survey and study reports sponsored by NASA, the FAA, the Department of Commerce and other cognizant agencies. Descriptions of the potential user vehicles and operations, and estimates of their numbers, position fix accuracy requirements and traffic densities relative to a traffic control system for the North Atlantic environment appears in Section 3.

A detailed analysis of the process of position determination is presented in Section 4. The geometries involved in circular and hyperbolic ranging are depicted in graphical form, and mathematical solutions are provided for manual computations (with the aid of charts and tables) as well as fully automated processes for determining position fixes with the use of computers. Techniques are recommended for the distribution of satellite position data, including periodically up-dated almanacs, for manual navigation. A glossary of terms covering Section 4 appears in Appendix 4A. Appendix 4B provides an analysis of the generalized fix problem, and the associated uncertainty ellipses.

Section 5 provides results of a comprehensive simulation of error transformation of ranging from measurement errors into position fix errors. A description of the GDOP (Geometric Dilution Of Precision) computer program is included. Among the

parameters studied are: altitude of user; minimum elevation angle; orbital inclination, height and nodes; number of satellites in orbit; relative orbital geometry; and user position, in latitude and longitude.

A detailed analysis of the system performance parameters associated with RF propagation from the earth to satellites and vice-versa and signal processing at the ATC facility, satellite and user vehicle are developed in Section 6. Link analyses are shown for the traffic control mode the passive navigation mode. Identified are environmental factors, such as tropospheric and ionospheric refraction and background noise, are identified as are equipment instabilities and sensitivities which contribute to errors in range or range difference measurements. Modulation techniques for optimization of phase measurements are investigated, and error magnitudes are determined for several combinations of signal processing and anticipated RFI environments. A matrix identifying these combinations follows:

RFI Environment	Signal Processing Technique		
	Homodyne	Band Pass Filter	Phase Lock Loop
White Noise	X	X	X
White Noise + Specular Multi-Path	X	X	X
White Noise + Diffuse Multi-Path	X	X	X

A summary of the error budget for carrier and tone frequencies recommended for the Phase-Difference Satellite Navigation System appears at the end of Section 6.

The integration time requirements for data relay and address of the various users through the satellite for traffic control and a navigation fix is analyzed in Section 6.3.11 and 6.3.12 for a time division multiplexing format. Also, the maximum number of users and number of position fixes per hour per channel reserved for traffic control purposes are estimated.

1.1.2 CONCEPTUAL HARDWARE DESIGNS

The conceptual hardware designs and justification at this state in the development of the system for the Phase Difference Satellite Navigation System are given in several sections of this report. For the purpose of unification and ease we now describe this location and content.

Receiver - User and Control Center receiver are described in Sections 6.2 and 6.2.4. Phase detector configurations and analyses are shown in Section 6.5. Details of the Phase-Lock-Loop carrier demodulation are given in Section 6.4.2.

User Antenna - The user antenna configuration is shown in Section 6.3.4.

Transmitters - The satellite transmitters are shown in Sections 6.3.7 and 6.3.10. The user transponder is essentially the same as the satellite transponder. The control center power amplifier is the same as the satellite power amplifier for the distribution of the field signal.

Equipment time-delay errors are shown in Section 6.3.7.

Further details of the conceptual hardware design are also given in the Link Analysis, Section 6.3.9, Data Link Requirements, Section 6.3.11 and Channel Capacity - Traffic Control Mode, Section 6.3.12

1.2 CONTRIBUTORS TO THE STUDY

The RCA participants in the Phase Difference Satellite Navigation Study are: Jerome Barnla, Program Manager; Jack Breckman, Technical Director, System Concepts, Position Determination and Error Transformations; Gilbert Lieberman and Edward Spaans, Signal Processing Analysis and Error Determinations; Leroy Tangradi, Link Analysis and Communications; Sheppard Wenglin, Tropospheric and Ionospheric Refraction; Dr. R.S. Johnson, Computational Analyses; Dr. Jacobo Farber, Multipath. Propagation and Antenna; and M. W. Mitchell, Requirements Model. Mr. Leo Keane contributed many suggestions and critiques as study Technical Monitor for NASA.

1.3 INTERIM CONCLUSIONS

A brief review of the Phase D fference Satellite Navigation System study results lead to the following conclusions:

- The system can perform world-wide Navigation/Traffic Control functions on a 24 hr/day basis to satisfy aircraft and marine user requirements projected to 1975 and beyond. At the radio navigation band of 1540-1660 MHz, no interruptions are anticipated from variations in weather conditions, tropospheric and inonospheric effects, or other environmental influences.

- The short sampling interval (about 1.0 second) which gives an accurate fix, coupled with the frequent interrogation of the vehicle allows the generation of a virtually continuous track at the Air Traffic Control Center, thus providing a capability for collision warning.

- The traffic control system can meet the maximum traffic densities (North Atlantic region) projected to 1975, and possibly to 1980, utilizing only one data channel. It is assumed that navigation tones will be propagated continuously on an adjacent channel serving both traffic control and passive (self-navigation) users.

- The system provides navigational tones at two or more frequencies to offer non-ambiguous position fixes to the widest categories of aviation and marine users.

- The system can provide position fix accuracies which will meet a wide spectrum of user requirements (. 01 to 2 nmi) from survey vehicles to commercial air traffic, and is contingent upon the refinement and cost of the user equipment.

- User equipment costs for the passive navigation mode can be made attractive to many users by employing simple receivers and antennas in conjunction with manual computations. Updated almanacs would be distributed periodically (on about a 60-day cycle) to assist in the computations.

- The satellites used for navigation are compatible, from the viewpoint of location and equipment characteristics, for use as communication relays.

- The ground station, satellite and user equipment requirements are within the present state-of-the-art. Similar equipments have already been developed and successfully demonstrated. A possible exception is an L-band antenna for aircraft. However, this does not pose any unusual problems, and should be a straightforward development.

Section 2

SYSTEM CONCEPTS

This report and the final report to follow contain the details of performance analysis and implementation for a system of navigation whose concepts were presented in the initial proposal for this contract.[2-1]* Work reported here has confirmed the broad conception, and the modes and configurations envisioned at the time are the bases on which further work will build.

In order to provide continuity for readers to whom the earlier descriptions are not at hand, the conceptual material is reproduced here, with minor modifications in the illustrative numbers and diagrams.

2.1 FIELD AND BURST SIGNALS

The principle involved in phase navigation is illustrated in Figure 2-1. In this figure the center transmits an RF carrier modulated by a continuous "tone" of lower frequency. To picture the situation more easily, the tone may be considered an envelope on the carrier (although an operational system may use phase modulation). The center signal is beamed at a near-synchronous satellite, where it is frequency translated and repeated toward the earth into the field of users. Hence this signal, originating at the center and repeated toward the earth, is called the field signal.

When the signal arrives back on the earth, points of the same slant range from the satellite will experience the same phase of the tone at every moment, since there are as many wavelengths from the satellite to one of these points as there are from the satellite to another of these points. Sets of such points may be connected into lines of equal phase, each of these being a circular line on the earth. If now a particular user were to transpond the field signal back to the center via the satellite, the phase difference of the envelope, measured at the center between its signal generator and the returned signal, will be an indication of the particular circular line of position (LOP) occupied by the user. This transponded signal is called the burst signal, because it will generally be returned in a burst, gated at the user.

2.2 COARSE AND FINE TONES

If the tone envelope were 10-kHz, for example, then LOP's differing in slant range by a half wavelength, or 15 km in this case, would return the same phase to the center. The strips between adjacent LOP's of the same phase are called bands. Hence a 10-kHz tone would be satisfactory in determining the LOP of a user without ambiguity where the initial uncertainty in his LOP did not exceed the horizontal equivalent of 15 km in slant range. The 10-kHz tone may be thought of as a coarse, or resolving tone whose primary function is to identify the lane of the user without ambiguity.

*References are listed in Section 7.

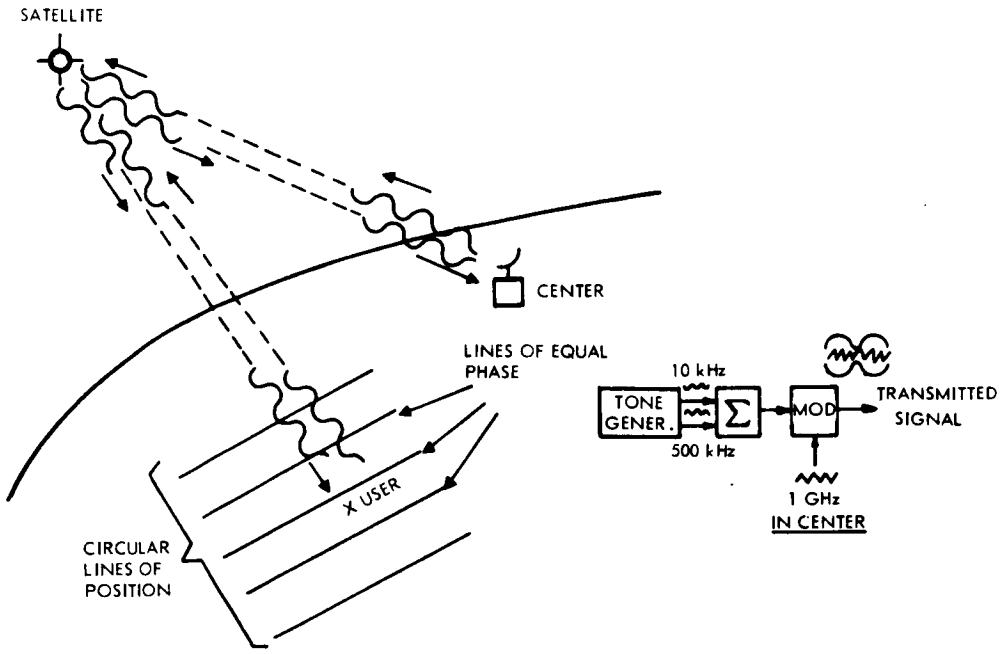

Figure 2-1. Basic Principle of Phase Navigation

In addition to the resolving tone, the signal also carries a tone at higher frequency, 300-kHz for example, whose half wavelength is about 500 meters. (The generation of this composite signal is indicated schematically in the figure.) This is the fine or tracking tone, and subdivides each 10-kHz lane into 30 lanes. A 3% measurement (1 part in 30) on the 10-kHz tone is sufficient to identify which lane is involved in a particular cycle of the fine tone. If in turn the fine tone phase is measured to 10%, the LOP of the user is selected to within the horizontal equivalent of 50 meters.

2.3 TWO-SATELLITE NAVIGATION

Figure 2-2 shows the phase principle applied via two satellites simultaneously. It has been shown that one of these satellites, say A, results in the determination of a user LOP at the center. The addition of another satellite B now gives a second LOP, whose intersection with the first establishes a fix of user position.

This figure shows the basic configuration of a traffic control system. Field signals are generated at the center for repeat back to the earth via satellites A and B into a large field of users. These signals are uninterrupted and continuously available to every user simultaneously. From time to time, at intervals determined by data processing equipment at the center, a particular user is selected from the field to return a burst of field signal currently impinging on him.

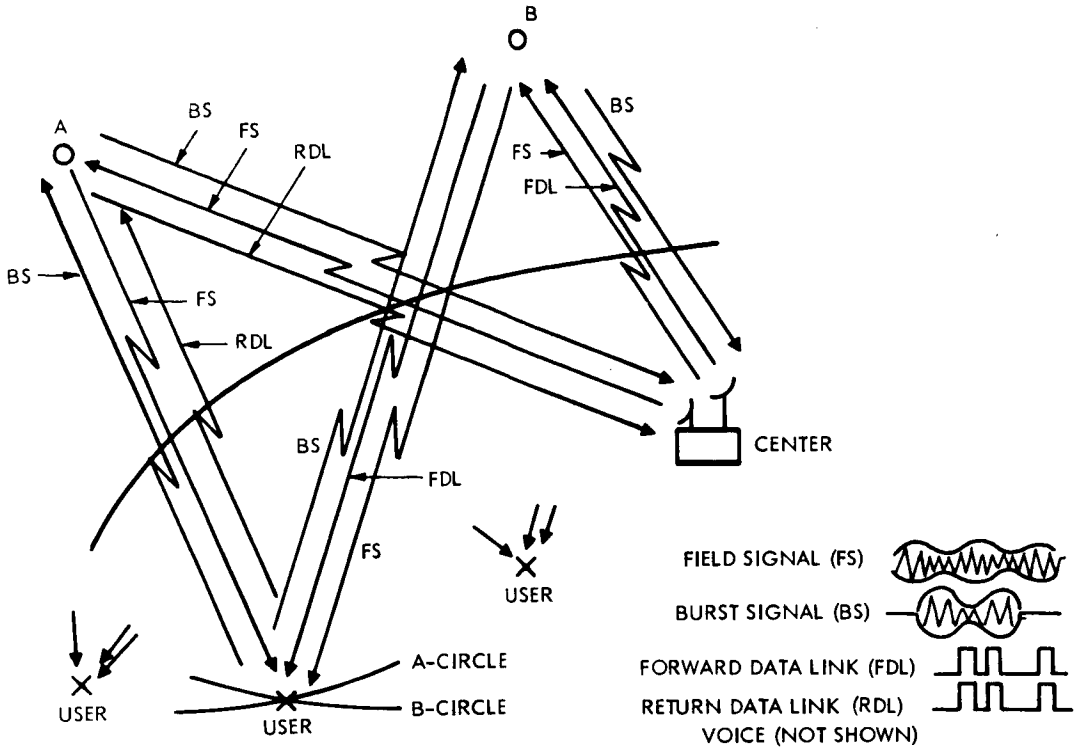

Figure 2-2. Traffic Control

While the antennas at the center are highly directional, the user in general will have an isotropic antenna. His burst of the A field signal will return via A, and the burst of the B field signal will return via B. The center now has the phase information to establish the user at the intersection of two circular LOP's.

2.4 INTERROGATION AND REPLY

The selection of a particular user from the field is accomplished by the transmission of a distinctive digital address which is recognized by that user and no other. Accompanying this address may be any of several digital control signals, to call for a particular receiver configuration at the user, or to display some selected information to him. At present, however, the chief concern is only with the control signal, which means in effect "return a burst m milliseconds long," where m might be 50, 100, 1000, etc., and may change from user to user or even from interrogation to interrogation of the same user.

The user's burst is accompanied by his digital address which identifies the source of the burst, thus providing the center with an authentication signal, confirming that the burst it is receiving at any time originated at the user intended. In addition to the identification, the user may send digital status and measurement data representing the configuration and status of his equipment, or some measurement on his ambient environment made enroute.

In an operational system the whole process of interrogation via address and control, and reply via burst, identification, and status, will be automatic. The center data processor will decide the interrogation interval, which will vary from user to user and even for a particular user, depending on the present state of knowledge of his track at the center or on changing requirements during a flight for fineness of detail; on similar grounds the data processor will decide on the length of burst for any particular interrogation.

At initial operation the number of users will probably be relatively small, so that after a particular interrogation is sent out the center may wait for the reply before issuing the next interrogation. However, the elapsed time between initiating the interrogation and receiving the reply will be between one-half and one second — a significant period of time to dwell on each user. As the user population increases, it may be necessary to generate the interrogations under the control of the center processor so that replies are stacked in space on a non-interfering basis. This procedure may improve the duty cycle four-fold at the expense of an additional computer burden. However, in a late operational era even this improvement may not be sufficient, and more channel capacity may be required aboard the satellites.

2.5 VOICE/TELETYPE

In addition to the automatic channels, the center may desire to exchange information with the user field via voice or teletype. This kind of exchange may involve weather, flight status, airport closures, safety advisories, and other categories requiring ad hoc formatting and content. It is anticipated that such conventional communications channels will be available in the navigation satellite, at least to the extent of a single simple teletype channel, for order wire and urgent bulletins. Of course voice and teletype messages may be sent via purely communications satellites but this would complicate rather than simplify the navigation system. First it would require the concurrent mutual visibility of both communications and navigation satellites to the user and the center (or it will require multi-hop capability to the center); second, it would require that the center processor keep track of the visibility of the communication satellites for each of its users; third, in time-sharing communication systems it would require coordination with another agency for access via a coordination procedure not perfectly compatible with immediate control by the center in emergency situations; and fourth, more antennas would be required at the center and perhaps at the user.

2.6 SATELLITE ORBIT DETERMINATION

Figure 2-3 illustrates the principle of satellite tracking, so that the satellite positions may be known continuously to a precision compatible with user fix requirements. The center itself and two other fixed locations constitute a sub-class of "user" (this is the minimum ground support system for satellite location; the operational system may involve four or five stations). The location of each of these stations is known to first-order precision in a geodetic frame, established either via conventional means or via geodetic satellite surveys. From time to time the center interrogates each of these stations, requiring a burst of returned signal. The usual equations of position determination are now inverted at the center processor, the inputs being ground station

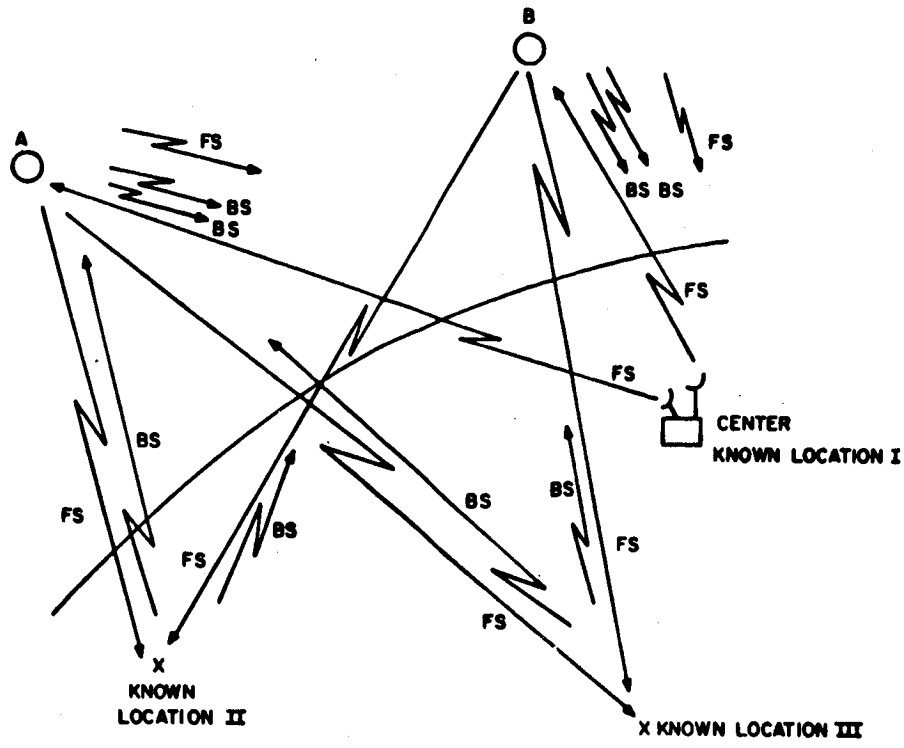

Figure 2-3. Ground Support for Satellite Tracking

locations and the outputs being satellite location. Hence the satellite-finding procedure is perfectly coherent from a signal and computation viewpoint, with the user-finding procedure, and errors in user position due to satellite uncertainty are directly controllable by the tightness of the geodetic base.

2.7 THE LOCAL CENTER

Figure 2-4a shows the extension of the basic system to include control of a cluster of the field via a local center. This configuration may arise in control of incoming traffic at some terminal point, perhaps by one of the thousands of airports around the world not already equipped with an instrument landing system (ILS); it may arise in weather-balloon tracking and control from some local station; or it may arise in passing enroute control to a local center in congested regions, because of the increased precision available in proximate control for reasons discussed below.

In these configurations the signal center serves primarily as the source of field signal only; the actual interrogation, computation and tracking are done at the local center. Where the users are within line of sight of the local center, the return bursts may be via the line-of-sight path instead of the satellite. In this case, the LOP's defining the user are ellipses, with the satellite at one focus and the local center at the other. If the bursts are returned via the satellites, the LOP's are circles as before.

In any case, when the local center and its cluster of users are relatively close, errors due to satellite uncertainty tend to vanish, as well as errors due to refractive variations.

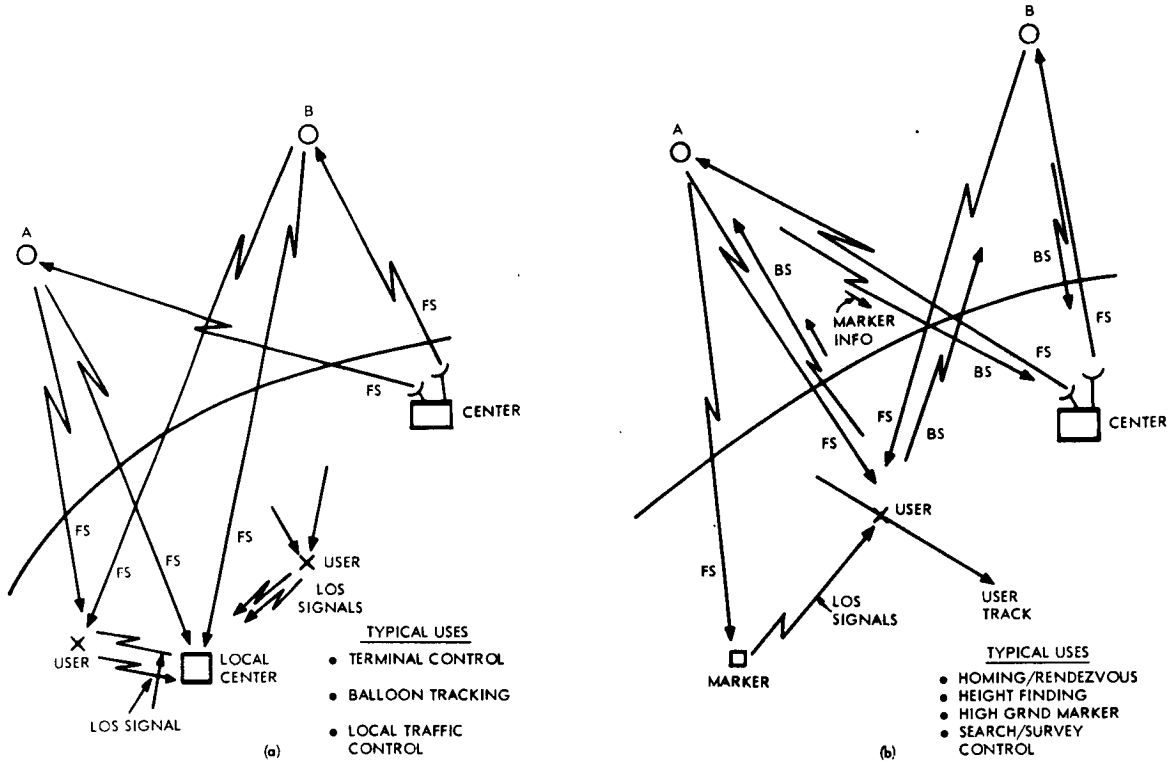

Figure 2-4. Relative Navigation

Hence relative position finding under such circumstances may improve to the order of tens of meters, if satellite and refraction uncertainties are the limiting factors in absolute position-finding. In other words, the system described has an inherent precision-tightening characteristic in situations where measurement and maintenance of relative spacing are of primary concern.

2.8 EARTH REPEATERS: MARKERS AND BUOYS

Figure 2-4b illustrates another use of proximate transponders. In this figure the marker represents a ground station (perhaps unattended) which continuously repeats the field signal from a satellite into the region of its line-of-sight vicinity. In effect this provides a third "satellite" for users in the vicinity, allowing height determination within the system instead of relying on external instrumentation to give height information. The user burst includes a sample of marker field signal as well as samples of the A and B field signals. If the marker burst is returned via satellite A, the third surface of position is an ellipsoid whose foci are the marker and satellite A.

Such markers may be used along segments of routes where system-coherent height information is important, and may also be used to mark high ground in particularly hazardous regions. In some applications the marker itself may represent a home or rendezvous point, and the user moves to null the phase.

In another application such as precision sea search or survey control, a set of one or more such markers or buoys placed on an ad-hoc basis makes possible relative

navigation in the vicinity of such markers; position relative to the markers may have a precision in the order of tens of feet because of primary error cancellations.

2.9 ATTITUDE REFERENCE

Figure 2-5 illustrates the use of the system to develop a heading reference for a ship, or a complete attitude-reference/control on an airplane. Consider three spacially separate antennas on the vehicle, perhaps on 10-foot centers. (On an airplane, for example, these may be 6- to 12-inch slots flush with the aerodynamic surface.) Phase differences among the signals entering these antennas, measured aboard the craft, establish an interferometer effect and determine the three Euler angles characterizing the displacement of two planes: the plane formed by the three antennas, and the plane formed by the satellite pair and the vehicle. Each of these planes has associated with it an arbitrary principal direction; for example, the principal direction of the antenna plane may be the longitudinal axis of the vehicle; the principal direction of the space plane may be the line of sight to one of the satellites or the line joining the satellites. In any case the configuration should provide a statement of ship's heading or aircraft attitude to within a few minutes of arc when used in conjunction with a suitably chosen attitude tone.

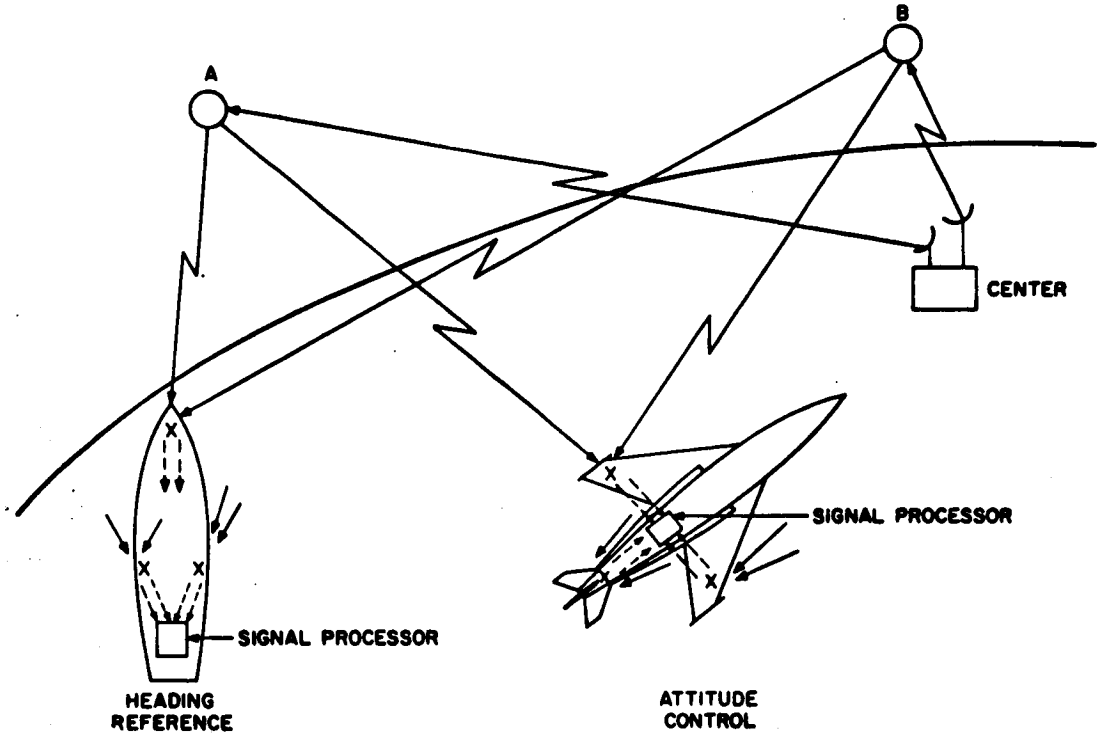

Figure 2-5. Angle References

2.10 RANGE-RANGE NAVIGATION

Figure 2-6 illustrates one of two general modes of operation wherein the user may operate passively to determine his own position. The position may be found onboard automatically by a computer, or manually with the aid of charts, tables, and hand calculations. It is expected that large groups of users will operate with the system in this way, perhaps because they are not part of the control pattern, or because their mission requires passive navigation.

In the configuration shown the user is assumed to know the location of his starting point with respect to the general grid he is about to traverse. He carries a local oscillator which generates tones for him of the same frequency as those on the field signal. In one channel he adjusts the phase of this local tone to match that of the incoming A-tone; in another channel he matches the incoming B-tone. He now begins his trip.

As he moves off his initial A-LOP he will begin to accumulate a phase difference in his A-channel, designated ΔP_A. Similarly he accumulates a ΔP_B in the B-channel. The number pair (ΔP_A, ΔP_B) is a continuous statement in LOP coordinates of his position relative to the LOP grid he is traveling. Notice that his phase accumulations must keep account of the number of tone cycles traversed, as well as fractions thereof. The reader will recognize this mode as a form of range-range navigation.

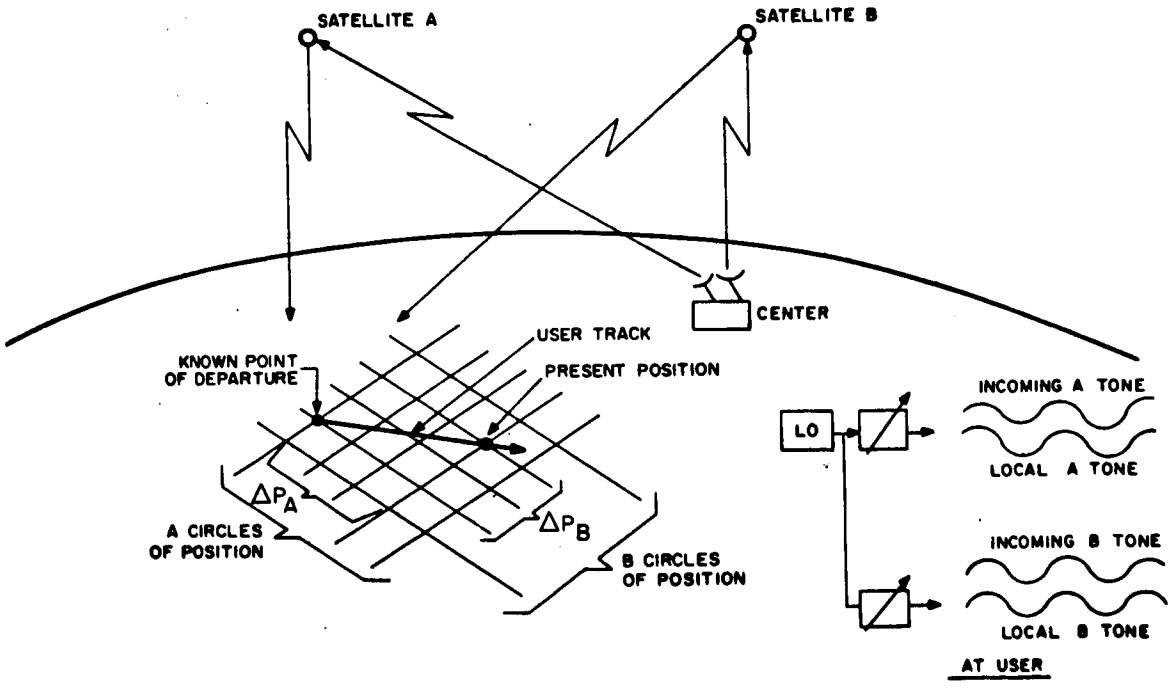

Figure 2-6. Self-Navigation With Local Oscillator

2.11 HYPERBOLIC NAVIGATION

In the self-navigation mode just described, the user was able to operate with two satellites, but he needed a local oscillator of either substantial long-term stability or a well-calibrated drift rate. Either one or the other is available to him in present-day oven-controlled crystal oscillators (his drift rate being recalibrated when he touches another known point in his itinerary). However, there is a mode of self navigation which makes use of a third satellite when one is available, and dispenses with the precision oscillator aboard the vehicle. This mode is illustrated in Figure 2-7.

Here the A and B phases are compared in one channel while the A and C phases are compared in another channel. The AB phase difference available from the first channel defines a particular hyperbolic LOP; the AC difference from the second channel defines a second hyperbolic LOP whose intersection with the first establishes the user fix.

An alternative way of operating assumes the user starts his trip from a known point in the grid about to be traversed. At the start, each channel is brought to zero phase difference by an adjustable delay in the A-tone, one in each channel. Now the trip begins and the accumulated phase difference in each channel is a coordinate in the LOP grid system, giving a continuous indication of the track traversed. In effect, the local oscillator of the previous mode has been exchanged for Satellite A of the present mode.

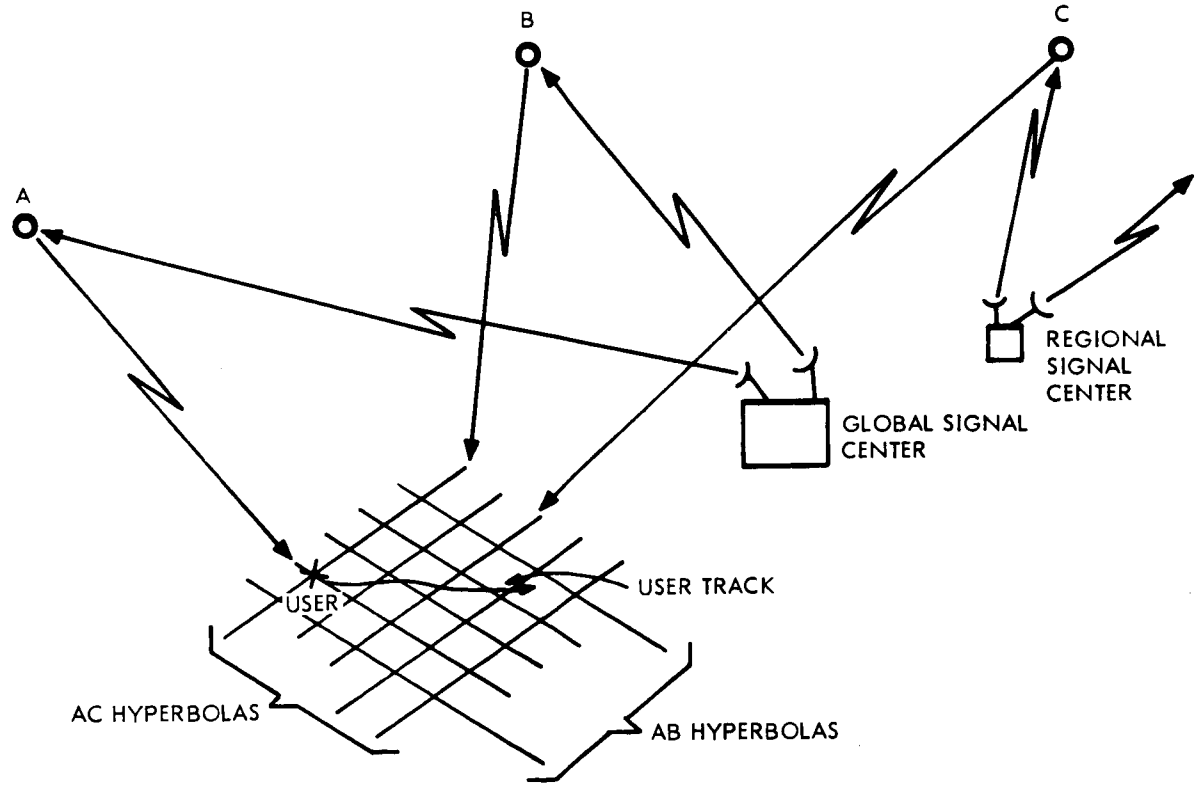

Figure 2-7. Self-Navigation Without Local Oscillator

2.12 EPHEMERIDES DISTRIBUTION

To perform self-navigation the user must know the positions of the various satellites at the time of his fix. There are several ways of distributing this information to the field. One is to broadcast the position of each satellite periodically over an automatic data link and/or the voice teletype link. This form may be supplemented or replaced by a broadcast of orbital coefficients, again at appropriate intervals. For synchronous satellites a broadcast of elements every several days or even weeks may be sufficient. Also, satellite element bulletins can be issued to the field on a weekly or monthly basis in the form of hard copy for those users who do not have facilities for receiving the broadcast data.

2.13 INTERFERENCE AND JAMMING

An important system feature highlighted by the possibility of self-navigation is the use of this mode as a fail-soft characteristic. It is not difficult to imagine that any universal navigation system on whose efficient and reliable operation an important segment of the economic, civil, and commercial communities depend will become a possible military target, legitimate or not, in the event of a hot war, or even a warmer cold war. Furthermore such a system, depending as it does on access to the satellites (at least for the retransmission of the field signal) is a sitting duck for jammers of moderate power whose only mission is to saturate the satellite or even only distort the signal at the satellite input. This form of sabotage is so cheap and easy for a hostile power and its impact on the totality of civil commerce so catastrophic that it would be imprudent to ignore this possibility. The validity of the entire argument becomes even stronger if our own military finds the system useful for some of its activity and begins to use it either openly or subrosa.

The Fail-Soft Backup - One way to implement the system to cope with deliberate interference is to equip each satellite with a self-contained oscillator, perhaps a ruggedized atomic clock. The self-contained package would be designed to go into operation whenever some activating code fails to appear on schedule. The circuitry carried aloft would be capable of generating tones identical to the field signal, and in addition would signal the entire field to revert to the self-navigation mode. Of course, all vital vehicles will be equipped to do this, even if in some cases it means manual calculation. (In anticipation of such an emergency, all such vehicles will also carry the latest hard copy bulletin describing the satellite orbital motions.)

The No-Transient Changeover - If it is decided to implement the system for continuity of operation under interference conditions, such continuity may be enhanced by exciting each satellite (during normal operation) in such a way that should normal operation be denied, the self-contained backup goes into operation without changing the tone phase emanating from each satellite. In other words, the transition from normal to backup should proceed without changing the phase as received at any user. Now since each of the individual oscillators in the various backup packages aboard the several satellites has its own phase, unrelated to any other phase in the system, one way to accomplish this is to arrange that during normal operation the field signal arrives at each satellite in phase with the oscillator within that satellite.

Individual Phase Synchronization - Figure 2-8 shows how each satellite can be excited in phase with its own oscillator. The signal from a signal source is passed through a variable delay and thence transmitted as the field signal; the satellite receives this signal and transponds it back to the center. From time to time the local oscillator aboard the satellite is interrogated and sends a burst down to the center via the burst channel. Both the returned field signal and the burst are phase compared and the output is used to drive the signal delay toward a comparator null. When this happens, the center generated signal arrives at the satellite in phase with the internal satellite oscillator. Hyperbolic self-navigators need to know the relative phases of the field signals as they leave the satellites. These relative phases will change slowly for a well-stabilized atomic oscillator, and the relative phase information may be included in the broadcasts and bulletins precisely as if they were ephemeris data.

During the backup mode of operation when access is denied, the relative phases are continuously monitored and the hard copy bulletins are updated from time to time (about every two weeks for stabilities currently available from ruggedized rubidium oscillators).

Note that it is not desirable to keep the backup equipment on all the time (and so permanently replace the ground excitation), because the life of the atomic oscillator aloft depends on the load placed on it. To extend this life, the local oscillator is sampled from time to time on an extremely low duty cycle.

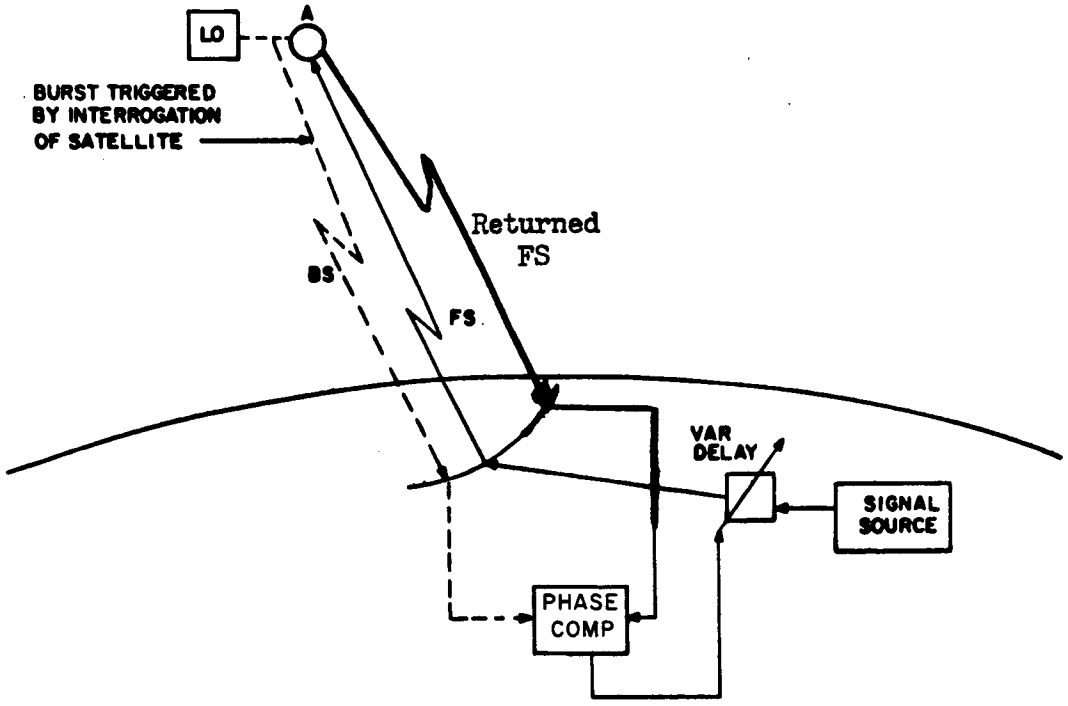

Figure 2-8. Signal Center Exciting a Satellite in Phase With the Satellite's Local Oscillator

2.14 SATELLITE CHANNELS

Figure 2-9a shows a possible division of channels on the early operational satellites. Each satellite will carry a 4-channel amplifier. The field channel is for coarse and fine tones; the service channel is for time distribution and satellite position; the burst channel is for the user-returned tones; and the data channel carries a pulse-modulated carrier for the address, identification, control and status signals. The upcoming frequencies of these four channels are designated as f_1, f_2, f_3, f_4; the downgoing frequencies are each shifted an amount Δf. The bandwidths, power, noise figures, and other pertinent characteristics to be expected of these channels are discussed in Section 6.3. Note that there will probably be no atomic oscillator or control circuitry aboard the early satellites.

Figure 2-9b shows a possible configuration of a later operational satellite with seven channels. As in Figure 2-9a, it carries a field signal channel and a service signal channel. Two burst signal channels are included: one for the exclusive use of an air traffic control center; and the other to be shared by any or all other centers which may join the system as it grows, including meteorological centers, oceanographic centers, military control centers, home office centers, terminal control centers, and the system signal centers. The data link channel is similarly duplicated, one for the air traffic control center and the other for the general centers. A voice/teletype channel is also available for the exchange of ad-hoc verbal information (as the system develops, more voice/teletype channels may become necessary). The satellite also carries logic and control circuitry to perform various switching functions on command, and a self-contained navigation package based on an oscillator of good long-term stability.

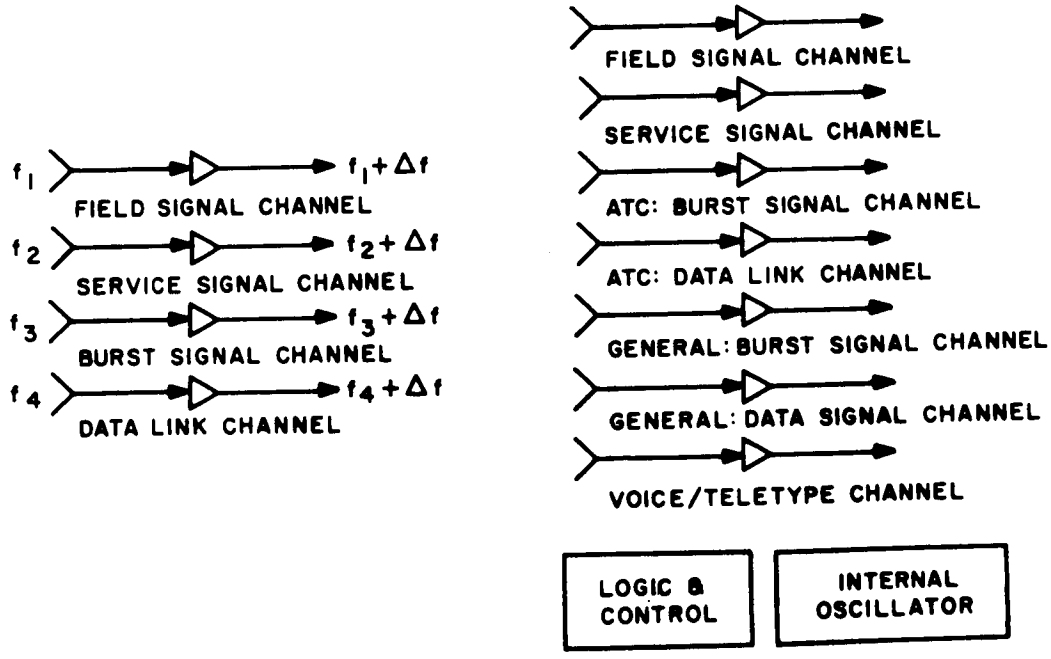

a. Early Operational Satellite b. Later Operational Satellite

Figure 2-9. Operational Satellites

2.15 SIGNAL GENERATION AND SYSTEM CONTROL

The Global Signal Center (GSC) and Regional Signal Centers (RSC), shown in Figure 2-10 generate the field signals consisting of the carriers, the tones, the time distribution, and satellite ephemeris and phase data. These centers control the time sharing of the general data link and burst signal channels by assigning certain time slots to the various centers (except the Air Traffic Control Center, which has a data link channel and burst signal channel in each satellite for its exclusive use). They also allocate the access and use of the voice/teletype channels to the various centers and their user clusters.

Among the general centers using the general channels are the GSC and RSC's themselves, for the interrogation of the orbit-finding stations (to keep track of the satellites), and for the interrogation of the satellite local oscillators (to excite each satellite in phase with its own oscillator). The GSC and RSC's distribute the satellite position and initial phase information automatically over the field signal channel: by teletype over the teletype channel, and by hard copy bulletins to the field. They "survey" into the system new centers and fixed ground stations as they join the system.

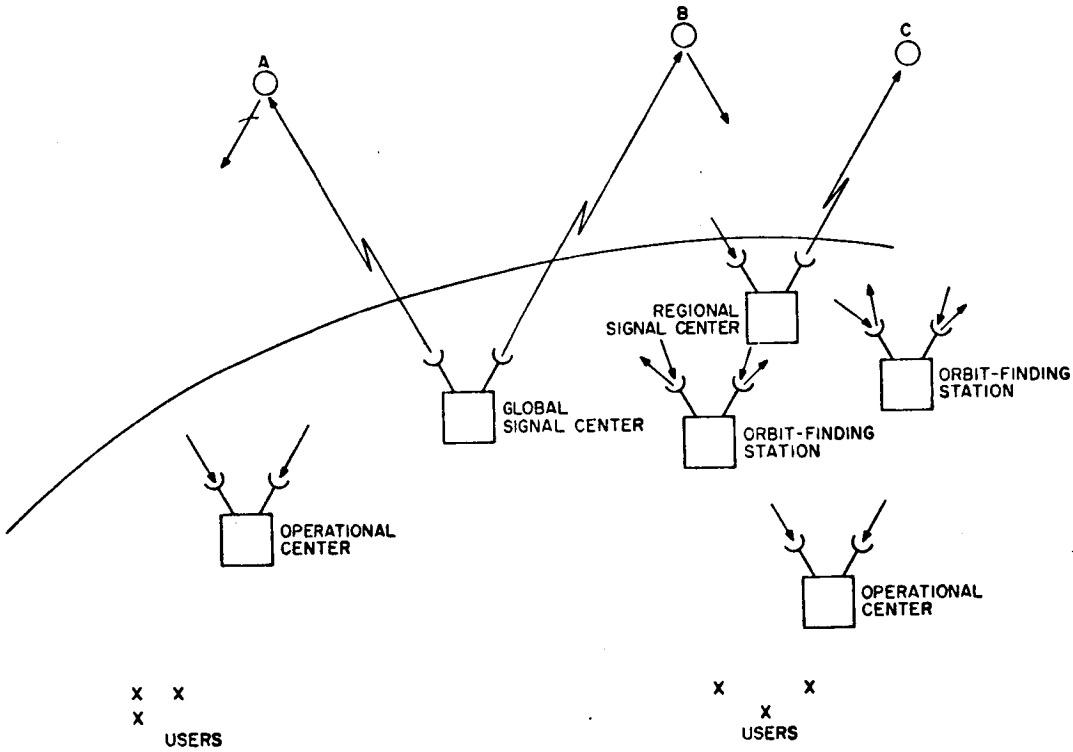

Figure 2-10. Global Signal Center and Its Environment

2.16 ENROUTE CONTROL

The Air Traffic Control Center originates interrogations to its cluster of users, keeping for each a sample track of appropriate precision. Table 2-1 shows some of the control and status signals which may be exchanged between center and user. Earth repeaters may act as "local satellites," providing a third dimension in the positional fix, especially along route segments where a system-compatible height measurement from each craft is important. Other earth repeaters may act essentially as high-ground markers in hazardous terrain, or as accurate delineators of route corridors.

2.17 EMERGENCY AND ENROUTE REPORTS

When any of the users in the Air Traffic Control cluster encounters an emergency, he may press a button which sends a digital signal up the data link, repeated every 200 msec for a two-second interval. Simultaneous with the digital identifying information, position-locating bursts are sent up on the burst return channels for a period of two seconds. On receipt of such signals the ATC goes into an emergency mode for that user.

In the course of flight an airplane pilot may encounter several situations he should report to the ATC, such as weather conditions, unexpected air turbulence, wind velocities, temperature and pressure gradients, etc. In general these data are not of an emergency nature, and can wait till an appropriate interrogation time for that user. In such cases the information is recorded (most conveniently on a magnetic tape recorder) along with the flight log record of his track (which is made by continuously recording the incoming phase information) and a time marker. When the user is interrogated by the ATC the relevant segments on the tape record are consulted and sent forward, giving the ATC a timely account of unusual flight conditions, where they were encountered, and when.

The phase navigation system is compatible with a continuous flight record of the vehicle track, and is available for a moment-by-moment replay of that track from departure to arrival in a post-flight analysis.

2.18 ATC LOCATION

The ATC may be co-located with the Global Signal Center. However, it is anticipated that the growth of the system will ultimately involve several traffic control centers, and perhaps several Regional Signal Centers (to continue satellite excitation around the world). In the course of this development, the growing numbers of these stations and their separate specializations may make it inconvenient to house the two kinds of operations at the same geographic locations; hence the present discussion assumes the more general situation of independent facilities. Also, in the paragraphs to follow, several other kinds of operational control centers are mentioned. Here again any combination of these may be co-located or separately housed as the situation warrants.

TABLE 2-1. PARTIAL ROSTER OF DATA LINK SIGNALS

From ATC	From User
ADDRESS PLUS SOME COMBINATION OF THE FOLLOWING	IDENTIFICATION PLUS SOME COMBINATION OF THE FOLLOWING:
• Return a burst, m milliseconds long • Return data via satellite X • Return burst via satellites X and Y • Report in by voice • Your position is: (in appropriate form) • Your velocity is: (in appropriate form) • Send other data (e.g., height, speed, wind, temperature, heading) • Read & record all satellite marker phases for later interrogation by center • Send recorded segment	• Emergency • Responding to your (burst / other) request • I want a voice contact • Read my flight record, it has hazard information • Give me my position (and/or velocity)

2.19 WEATHER BUREAU

The Meteorological Center may control specially equipped airplanes, ships, and balloons. In addition, many ordinary airplanes and ships may be able to make and report observations on one aspect or another of their weather environment. The center will ripple through this composite cluster of users by interrogations independent of the (perhaps fully loaded) ATC, via the general burst signal channel, which it shares with all other low-load control centers. The automatic response to this interrogation will carry the position of the craft (via the burst signal), and some preformatted information responses (via the general data link). In addition, ad hoc information may be passed along via the time-shared voice/teletype channel. The Meteorological Center, like the ATC, is fully prepared to make the necessary position calculations because it too receives the field signal and is continually informed on the satellite locations via the service channel.

2.20 OCEAN CONDITION AND SURVEYS; SEA TRAFFIC

The Oceanographic Center operates like the Meteorological Center, and indeed may be co-located with it. Also, certain of the oceanographic ships may require precision relative tracking during some critical aspect of their survey. This situation is represented in Figure 2-4b, where an ad-hoc, taut wire marker buoy is used to provide fine relative tracks. The marker buoy may be located on an absolute basis with improved precision by reading its locations back to the Oceanographic Control Center with extended bursts (perhaps a minute or more; by providing it with high-gain, directional antennas and by equipping its receiver with a very-low-noise front end).

Many aerial surveys have similar requirements for precision relative oceanographic tracks, especially when surveying trackless regions (i.e., magnetometer surveys over ocean or search and rescue operations). Here again, ad-hoc ground markers or sea buoys provide the local reference and may themselves be located with precision on the absolute grid.

The Ship Traffic Control Center operates like the ATC, and at least in the early operational era may be co-located with it. Of course its interrogation rates per vessel will be somewhat lower, but the number of its subscribers active at any given moment will be considerably higher, reaching possibly into the tens of thousands.

2.21 TERMINAL CONTROL

Airport control (stylized in Figure 2-4a) may be implemented at many of the thousands of airports throughout the world, large and small, which are without adequate conventional ILS facilities. There are hundreds of such general-aviation airports in the U.S. where an economical, universal system would extend their operability into marginal weather and visibility conditions which now cause total shutdown. Also many dozens of foreign airports, presently using substandard ILS facilities or none at all, will become accessible to U.S. traffic under circumstances now prohibitive. Harbor control is another use of the system, potentially applicable to many of the thousands of ports over the world with inadequate approach facilities in dense fog, darkness, or closed-in weather.

2.22 MILITARY NAVIGATION

The Military Air and Ship Centers are examples of the possible extension of the system into the military domains. Such centers have obvious reasons for separating their activities from the civilian traffic control centers, but may use the same navigational satellites either via the general burst signal and data link channels, or by added military burst signal and data link channels. For many military missions during peacetime, active cooperation with a center by military craft is entirely acceptable. However, there will be a class of missions and craft which must operate covertly. For these situations some combination of the following precautions may be taken:

(1) The user navigates in the passive mode.

(2) When a center must know the user's position, the craft may be outfitted with a small, highly-directional dish or phased-array antenna, appropriately located with respect to the aerodynamic surfaces. This will minimize detectability but will not entirely eliminate it.

(3) The vehicle's transponding equipment uses a pre-arranged psuedo-random delay on the returned burst signals, removable only at the center which has an identical code stream. These artificial delays can range up to tens of milliseconds, giving apparent positions many thousands of miles away from the true position.

(4) When access is denied to a particular satellite by hostile interference or jamming, the satellite backup self-contained mode is automatically brought into operation, and all users navigate passively.

2.23 BUSINESS AND COMMERCE

The Home Office Center concept illustrates the possible use of the public system by the owners and operators of fleets of ships or aircraft, including commercial air carriers, passenger and freight ships, fishing fleets, and oil tankers. The home office interest in the current operations of these craft will extend to their present whereabouts, environment, and condition. Other uses include issuing advisories on minimum-time maximum-safety weather-routing, airport and harbor facilities, and administrative information and instructions.

2.24 SPACE NAVIGATION

It is expected that the field signal from near-synchronous satellites will be present in the space surrounding the earth, perhaps to a height of 500 nmi. In an era of full global coverage, this signal makes phase navigation available to several categories of space operation, including insertion, correction, and rendezvous. This last is typified in Figure 3-4b, where the dock carries a field signal repeater and the approaching space vehicle is homing in by flying toward zero phase.

2.25 GUIDANCE AND CONTROL

The continuous presence of the navigation signal throughout the entire field of users makes possible not only a complete flight log of every track detail, but also the use of the signal for vehicle guidance and control, either in an autopilot or via a flight director displaying control indication to the pilot. For example, a particular desired track at some point may involve a ratio of LOP-coordinate differential phase changes $\Delta P_A / \Delta P_B$. This desired ratio is set in via appropriate controls (either manually or by a computer) and the craft constrained to move to fulfill this ratio, until replaced by another along the track.

Table 2-2 summarizes the several applications touched on in the preceding paragraphs. This list emphasizes the more important and immediate areas of civilian and commercial application. In addition there are several areas in military, space, and land-vehicle navigation that are not mentioned here. A full catalog of uses of phase navigation is being collected and documented and will be available in the course of subsequent system studies and development.

2.26 USER EQUIPMENT

It is intended that user configurations will be built up by modular components, so that no user need buy and install more facility than he requires for his operation. The general craft will use a hemispheric isotropic stub or slot antenna, with a modest gain of 3 or 4 dB; the front end may have a noise figure somewhere between 5 and 10 dB. Special users with a need for improved precision may use 2-foot or even larger directional antennas, with gains ranging to 18 dB and upward. Certainly signal centers, control centers, orbit-finding stations, earth repeaters, and many markers and buoys should be so equipped.

TABLE 2-2. APPLICATIONS SUMMARY

• Absolute & relative position finding	• Height, velocity, heading, attitude
• Enroute traffic control of planes & ships	• Guidance & control signals
• Terminal control	• Flight recording-air, sea, ground
• Pin-pointing CAT & other hazards	• Time distribution
• Aerial surveys - land & sea	• Search & rescue
• Markers: runway & harbor buoys	• Markers: high ground & sea hazards
• Satellite tracking by inverse system	• Space rendezvous & docking

Every user will need two field signal receivers, each of which extends from the IF strip through the phase detector. The self-navigator's equipment may end here, with the only additional requirement either a local oscillator or a third field signal receiver. It is the current expectation that the user cost of minimum self-navigation equipment will not exceed $1000.

From this point on, user configurations can develop in many different directions. Some self-navigators may want to subscribe to the service channel of one or more satellites and will need a receiver for each channel alongwith the decoders to read their digital information.

2.27 PARTICIPATING TRANSMITTERS AND RECEIVERS

Users cooperating with one or more control centers will need one (or two) data link receivers and two transmitters (for the two burst signal channels). However, such users will not need a separate data link transmitter, because one of the burst transmitters can send the digital information after the burst. Also there is no need for an additional pair of burst transmitters to report to a second center; a single pair will suffice by reporting first to the ATC, for example, and then to the second interrogation. Some users will subscribe to the voice/teletype channels, and such users will carry at least a receiver (for broadcasts) and at their option, a transmitter.

2.28 PROCESSING

Many users will self-navigate manually; others will use an on-board computer for this function. The bulk of center subscribers will probably do neither, but will get their position from the center. In any case a variety of input-output devices, displays, and computers will be available to match the requirements of each vehicle.

Figures 2-11 and 2-12 show some possible configurations of phase-measuring devices. Figure 2-11a uses a closed-loop resolver circuit and may give its indication either on a dial or digitally via an optical shaft encoder (not shown). Figure 2-11b shows a similar circuit for use when the tone frequency is beyond the range of direct resolver implementation. In such cases, a local reference frequency is used to excite the resolver.

Figure 2-12 shows a circuit which delivers the phase in digital Gray code, to avoid reading errors larger than one quantum cell of the code. Such a phasemeter uses no moving parts.

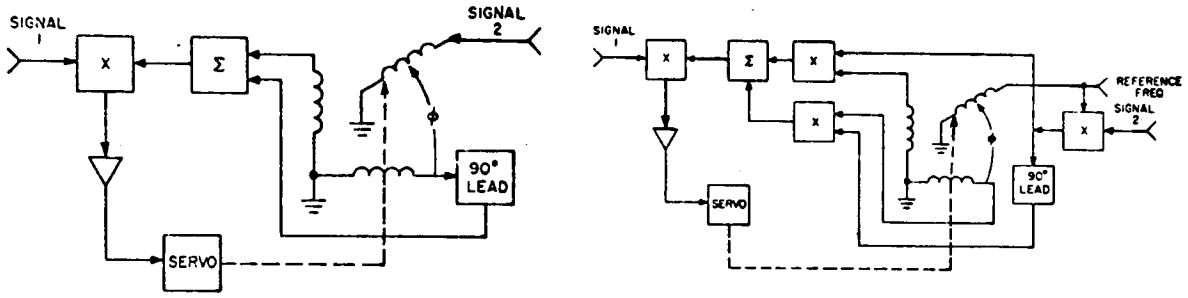

Figure 2-11. Phase Measurement Using a Resolver

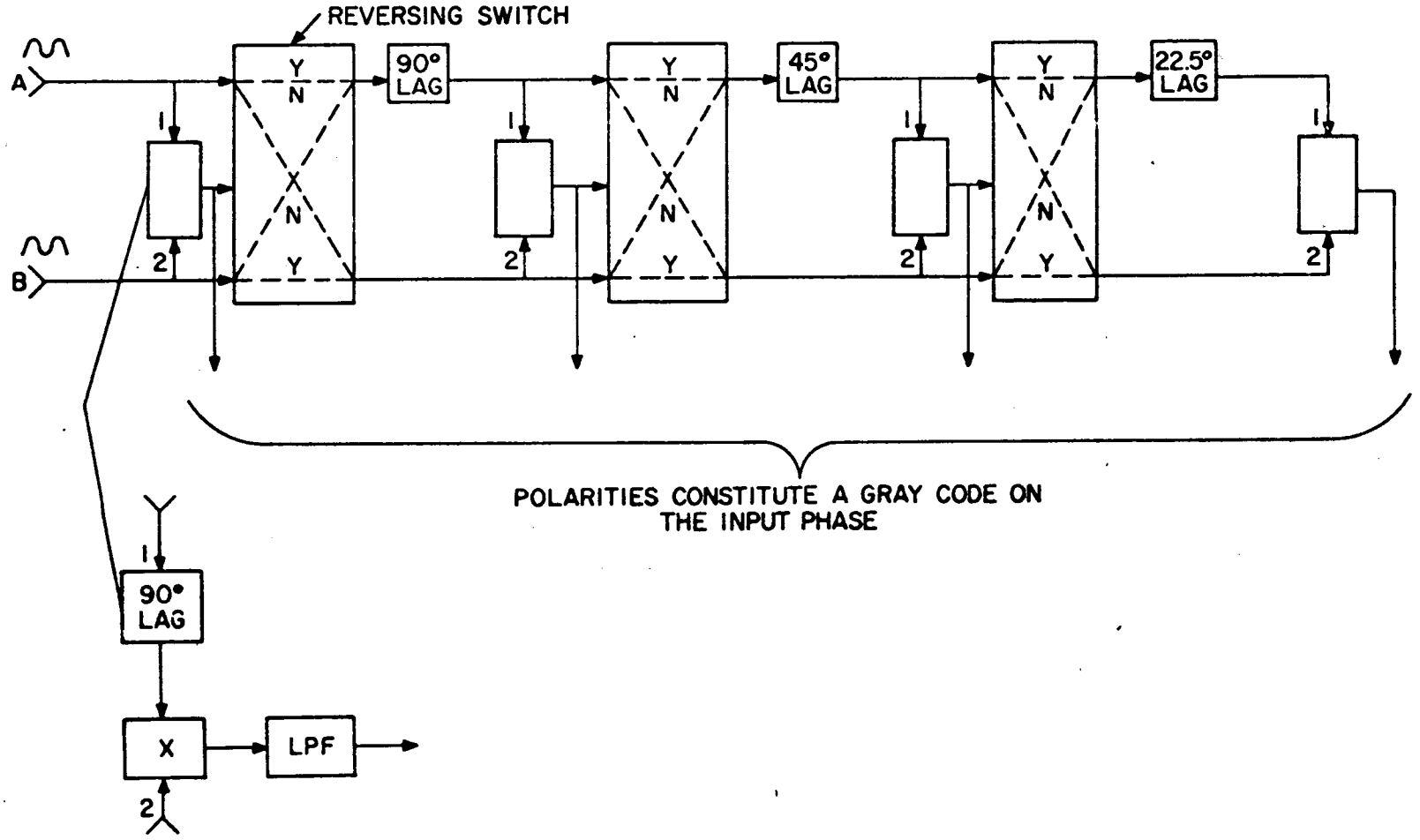

Figure 2-12. A Phase-to-Gray Code Converter for Phase Measurement

Section 3

REQUIREMENTS MODEL

3.1 INTRODUCTION

Navigation and traffic control requirements for non-military aircraft and marine vessels traveling over or on international waters has been the subject of several surveys and studies by the National Aeronautics and Space Administration, Federal Aviation Agency, Department of Commerce, and other U.S. government agencies. The particular concern of these investigations was to determine whether existing systems or those in an advanced state of development and implementation were capable of meeting future traffic coordination and safety requirements, specifically within the next decade. The Final Report of the Ad Hoc Joint Navigation Satellite Committee (JNSC), dated May 1966, offers a distillation of the survey data which was accumulated and draws some pertinent conclusions on this subject. These can be summarized as follows:

(a) A need exists for a more efficient air traffic control or coordination system over the North Atlantic within a few years. A desirable feature would be a surveillance capability by air traffic control centers where aircraft positions can be determined independently of cockpit derived navigation fixes.

(b) Future air and marine navigation and communications requirements probably will not be met with existing systems.

(c) Economic benefits would accrue from an improved world-wide navigation and communication system.

(d) Satellite systems show sufficient promise to warrant further technical and economic investigations of their feasibility to fulfill future world-wide navigation and communication requirements.

In addition to offering recommendations on the course of future investigations which would be of benefit to the U.S., the JNSC report [3-1]* provides data for configuring a technical requirements model for navigation and traffic control surveillance of aircraft and marine vehicles for the next decade. The requirements model for this study, which is developed in this section, draws primarily on this data. To insure proper interpretation and, in a few instances, extrapolation of the data, several additional survey reports were used as references (3-2, -3, -4, and -5). The criteria for the requirements model were based upon the following operational parameters for each type of vehicle in a network.

(1) Position fix accuracies: longitude, latitude, and altitude where applicable.

(2) Frequency of position fixes for traffic surveillance and navigation.

(3) Number of users during peak traffic conditions.

*References are listed in Section 7.

Other data which will be identified are those vehicle dynamic characteristics which may affect the navigation function, such as aircraft velocities. The environmental conditions of operation are presumed to include the full spectrum of meteorological variations on the surface and in the atmosphere of the earth, and the full variation of ionospheric densities and temperatures attendant with seasonal changes and solar activity cycles. Nominal geographical coverage requirements will be world-wide and up to 100,000 feet in altitude.

Based on previous studies, the North Atlantic region headed the list of transoceanic areas with high traffic densities including marine as well as air traffic by a substantial margin. It is assumed that a traffic control surveillance system capable of meeting the demands of the North Atlantic region could be expanded, without major perturbations, to a world-wide network. Also, in terms of a timetable of implementation, the logical first choice would be the North Atlantic since saturation of the air traffic control system, based on current standards of vehicle separation, appears imminent within a few years.[3-1] Therefore, the North Atlantic environment projected to 1975 was selected to represent the model for estimating maximum traffic densities.

3.2 AIRCRAFT

3.2.1 USER CATEGORIES

Civil aircraft of the next decade which would be utilizing an advanced transoceanic navigation and traffic control system are described below:

Subsonic Transports - Commercial passenger and cargo craft will constitute the largest user category from the viewpoint of the number of airplanes and the number of flights. Most of these vehicles will be turbo-jet powered, subsonic, fixed wing aircraft of the type in current use. By 1970, the large "aerobus" (500 to 600 passengers) versions are expected to become operational. Approximately 90 Boeing 747's are currently on order by U.S. and European Airlines.[3-6] Initial use will probably take place over the Continental U.S., with a subsequent expansion to North Atlantic service. Since each aerobus has three to four times the handling capacity of present models, increases in the number of commercial aircraft will probably level off compared to recent rates of growth. Some turbo-prop and piston engine aircraft will also be flying across the North Atlantic, but these are expected to decline steadily in number.

Supersonic Transports (SST) - Early estimates of the production of SST's by England-France (Concorde) and the United States (Boeing and Lockheed) indicated that approximately 150 to 200 SST's will be in commercial service by 1975. These estimates are undergoing revisions due to development schedule stretch-outs. U.S. models may barely be coming off the production lines by 1975. At best, only a few aircraft will be in commercial service.[3-6] The Anglo-French model is scheduled for operation by 1971 or 1972. The planned production rate of Concordes is three per month with possibly one-third to one-half of them being used for North Atlantic service. In broad terms, this means approximately 40 aircraft assigned to the North Atlantic routes. Each Concorde is capable of two round trips per day between Europe and the U.S. From the viewpoint of numbers and commercial impact, the SST's will not be

significant contributors to the air lanes by 1975, and their high altitudes of operation over subsonic aircraft will not add to the congestion of air traffic in the North Atlantic. However, the SST with its relatively high speed and high altitude flight characteristics must be considered as an important factor in the synthesis of a Requirements Model.

Search and Rescue (SAR) Aircraft - The principal agency which conducts and coordinates SAR activities in waters adjacent to the United States is the U.S. Coast Guard. This agency maintains a ship and aircraft surveillance function through its Atlantic Merchant Vessel Report (AMVR) system. When an emergency situation occurs and a search is initiated for a ship or aircraft in distress, the Coast Guard alerts its squadrons and those of the U.S. military with SAR responsibilities and conducts whatever operations the emergency dictates. Civil aircraft may be diverted from their planned flight to participate in a search, but this is usually a minor activity compared to the effort of the U.S. Coast Guard and military. European coast countries have comparable rescue facilities and international agreements have been concluded to coordinate SAR activities over international waters. Past experiences by the U.S. Coast Guard and military, as reflected in their reports on SAR missions, will provide some insight in defining future navigation and traffic handling requirements for this type of user. Also, a precise navigation and surveillance system should reduce the number of vehicles and flights required in a typical SAR operation. The type of aircraft employed vary from helicopters to long range jets (C-130's).

Oceanographic and Ice Patrol Aircraft - The U.S. Coast Guard patrols sea lanes and alerts marine traffic to the existence of hazards. The sea areas for which individual countries are responsible are determined by international agreements. It is obvious that coverage of the entire North Atlantic is desirable if a navigation system is to serve this function in addition to the others.

Survey Aircraft - Geodetic agencies, it is generally acknowledged, require better navigation and position fix accuracies than are available at the present time when they are conducting surveys in regions extending beyond the line of sight (i.e., beyond the range capabilities) of coastal radar or radio navigation stations. These specialized, highly instrumented survey aircraft are very limited in number.

General Aviation - Most of the "private" aircraft which are capable of transoceanic flights will likely be owned by business concerns. Their contributions to North Atlantic traffic is expected to be relatively small.

3.2.2 GENERAL REQUIREMENTS AND CONSTRAINTS

The JNSC panel, in its summarization, indicated that the present civil aviation environment in the North Atlantic would impose the following rules and constraints in

configuring an improved navigation and traffic control surveillance system which could be implemented within a few years:

(1) Air traffic control will be conducted from ground installations. (For the North Atlantic, this constraint implies locations on the Eastern Seaboard of the United States - in the vicinity of New York and New Jersey - and at existing terminals in Europe.)

(2) Air separation standards and decision functions will be the responsibility of the control agency: the FAA for civilian air traffic and the addition of the Coast Guard in SAR operations.

(3) Aircraft position determination by the Air Traffic Control (ATC) center should be independent of the primary system used by the aircraft navigator.

(4) Direct voice communication between pilots and ATC personnel is required.

(5) Ground control centers will have direct voice and digital data communication links with each other.

(6) Navigation is solely the pilot's responsibility.

(7) The communication of timely meteorological data and forecasts between aircraft and ground stations would be desirable.

(8) The above functions should be operational for all weather conditions.

3.2.3 POSITION FIX REQUIREMENTS

The JNSC panel's estimate of position fix accuracy requirements for each category of aircraft for the 1975 period is shown in Table 3-1. The fix accuracies range from ±0.5 to ±3.0 nmi based on an "absolute" geographic reference. The term "absolute" here refers to any vehicle position on or near the surface of the Earth which is referenced to any arbitrarily selected geodetic point on the Earth. Greenwich, England, for example, contains the origin from which longitude is measured. For this study, a traffic control center located in New York may constitute a more appropriate reference point from which all vehicle positions are measured. For convenience, the geometric point of origin should be well within view of any satellite or satellite system. On the other hand, errors associated with handover of a vehicle traveling from one satellite coverage zone to another can be minimized by locating permanent geodetic stations, whose positions are accurately predetermined, at the coverage zone interfaces.

Commercial aircraft have the more relaxed requirement of ±3.0 nmi; a factor which reflects in their favor since weight, size, and power requirements of airborne equipment is more restrictive on transports than on specialized vehicles such as SAR, patrol and survey aircraft.

"Relative" position determinations encompass small zones or areas in which vehicle fixes are referenced to local geodetic markers, buoys or other predetermined points. Oceanographic and coastal surveys by aircraft require relative position accuracies of

TABLE 3-1. POSITION FIX REQUIREMENTS OF NON-MILITARY AIRCRAFT FOR NORTH ATLANTIC AIR TRAFFIC CONTROL & SURVEILLANCE TO 1975 PERIOD

Aircraft Category	Position Fix Requirements*		Position Fix Intervals#
	Absolute** (nmi)	Relative## (ft.)	(Minutes)
Subsonic Transports	±3.0		10
Supersonic Transports	±3.0		5
Search and Rescue	±1.0	1000	10
Oceanographic & Ice Patrol	±0.5		10
Survey	±0.5	300	10
General Aviation	±3.0		15
Altitude Determination	250 ft	250 ft	

*From Reference 3-1.
#From References 3-1 and 3-2.
**"Absolute" pertains to coordinate references of large geodetic areas (transoceanic and larger).
##"Relative" pertains to coordinate references of small geodetic areas (about 300 miles in radius) or between successive position fixes.

300 feet according to the JNSC report. Also, SAR aircraft, while scanning an area for downed aircraft or distressed shipping, need assurances that they are neither missing nor excessively overlapping the area to be surveilled. Accuracies between successive position fixes of 1000 feet are required for this "relative" navigation mode. By these definitions, a local area may encompass two or three hundred nmi. Navigation to this degree of precision is intended primarily for the user's benefit and, as such, is a self-navigation function which is not reflected in the traffic control requirements model. Thus, the user may prefer to lock onto the RF navigation tone and navigate continuously without interrupting the traffic control system.

Figure 3-1 shows the evolutionary requirements for position accuracies to the end of this century.(3-1)

The estimated interval for obtaining position fixes of aircraft in an air traffic control surveillance mode is also shown in Table 3-1. The intervals for the specialized aircraft were obtained from the JNSC report. The intervals for the transports were based on a projection of tightened standards of separation and safety for the 1975 period. Current separation requirements for aircraft in the North Atlantic is 120 nmi laterally, 15 minutes along the flight path, and 2000 feet vertically. The current position reporting procedures for pilots in transoceanic flight of 5° of longitude for

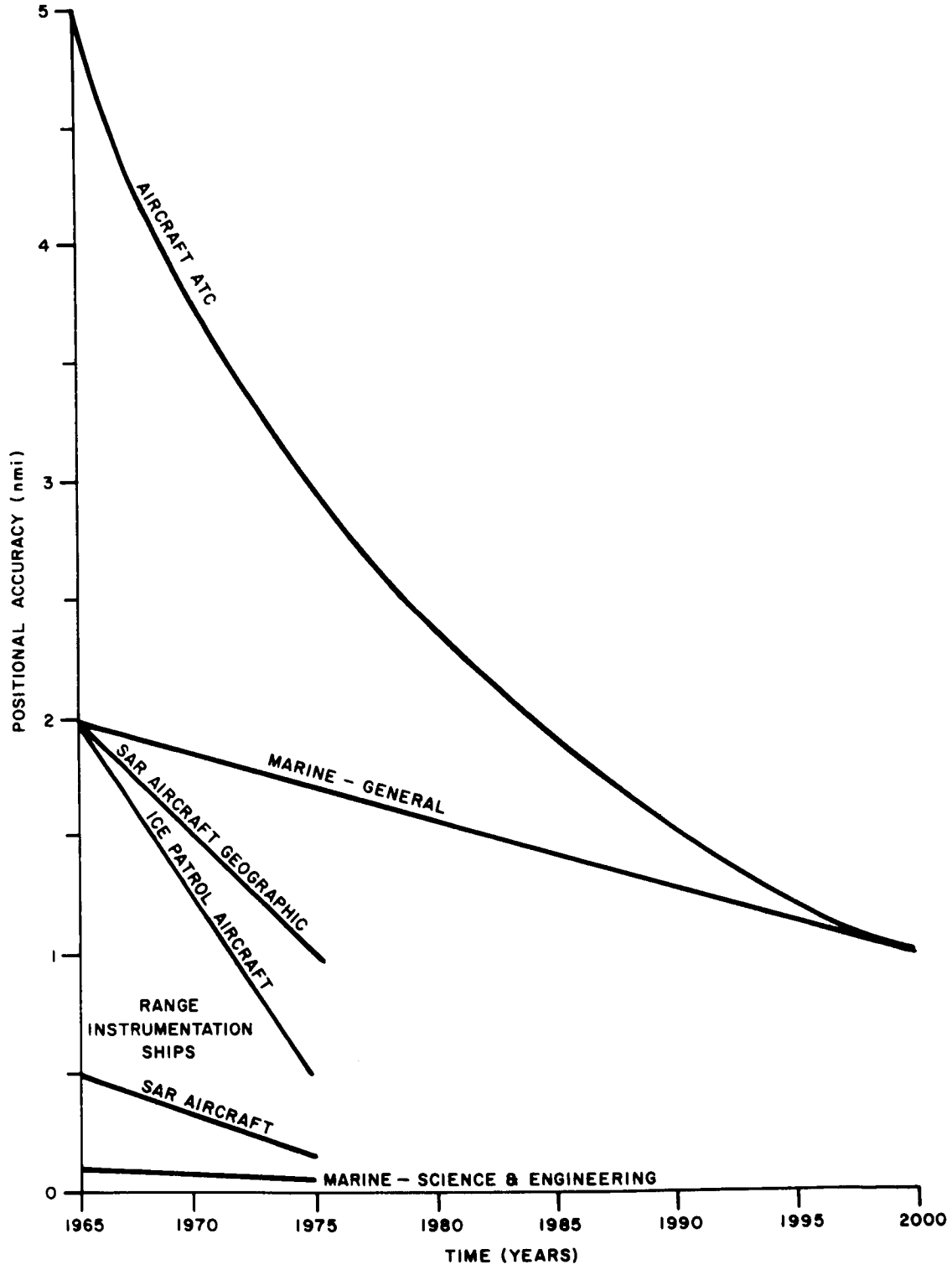

Figure 3-1. Positional Accuracy Requirements
(Data from Reference 3-1)

propeller aircraft and 10° for jet aircraft (about every one-half hour over the North Atlantic air lanes) appear to be too infrequent for an advanced traffic control mode. For this study model, a position fix interval of 10 minutes for subsonic jet transports, and 5 minutes for SST's was selected. This means the maximum flight distance between traffic control interrogation intervals for any aircraft would be 150 nmi.

3.2.4 TRAFFIC DENSITY AND POSITION FIX RATE

In order to estimate the number of potential users and traffic densities of a world-wide navigation and traffic surveillance system, several attempts have been made to predict the growth of Civil Aviation in the next one and two decades. The consensus of a number of reports is that passenger miles and cargo tonnage will increase exponentially. The International Civil Aviation Organization (ICAO) estimated the North Atlantic traffic growth rate to be about 13% per year.[3-3] New commercial aircraft, however, are continually increasing in size and payload capability and their numerical growth may be relatively modest. For example, current jet subsonic aircraft can carry about 120 passengers and cross the Atlantic Ocean in an average period of 6 hours. The future jet aerobus, traveling at the same velocity, is expected to have a 500 to 600 passenger capacity, an increase in passenger miles of approximately four to one. Concordes are designed for about 120 passengers, and are expected to take an average of 3 hours for a transatlantic trip. The SST's being developed by the U.S. are designed to carry up to 300 passengers and cross the Atlantic in about 2.5 hours with a corresponding increase in passenger miles over current aircraft of about six to one. Any valid prediction of the number of civil aircraft plying the North Atlantic by 1975 would have to take into cognizance the rate of introduction of advanced models.

Table 3-2 shows the results of surveys conducted during 1963-64 which reported the number of air transports and civil aircraft in the world inventory as of that time.[3-1] The inventory for the North American continent and Europe is shown in Table 3-3 and reveals the domination of aircraft ownership by the two continents bordering the North Atlantic. The aircraft in transoceanic service are mainly transports over 20,000 lbs.

More to the point for the establishing of a technical traffic model for this study is the instantaneous count of aircraft over the North Atlantic projected to 1975. This would indicate the number of airplanes which would have to be handled by an air traffic control surveillance system at the same time.

Table 3-4 shows a projection of civil aircraft in simultaneous flight over the North Atlantic to 1972. The rate of growth column apparently reflects the introduction of new aircraft with larger and larger passenger and cargo handling capacities. By following the trend of Table 3-4, the absolute peak count for 1975 would be about 240 aircraft. The addition of approximately 20 aircraft for the contingency of SAR or ice survey activities would make the total instantaneous count about 260.

Using the position fix intervals in Table 3-1 as a guide, the maximum traffic density model evolves as shown in Table 3-5.

TABLE 3-2. WORLD INVENTORY OF NON-MILITARY AIRCRAFT* (TRANSPORTS AND CIVIL AIRCRAFT)**

Aircraft		July '64 Transport A/C			Dec. '63 Civil A/C
Type	Weight	ICAO#	Non-ICAO##	Total	ICAO
Jet	Over 20,000 lbs.	953	185	1,138	838
	Under 20,000 lbs.				42
Turboprop	Over 20,000 lbs.	897	307	1,204	986
	Under 20,000 lbs.				23
Piston	Over 20,000 lbs.	3,739	1,741	5,480	4,381
	Under 20,000 lbs.				104,508

*From Reference (3-1): a) ICAO Digest of Stat. No. 111, Civil A/C on Register as of December 31, 1963; and b) "Boeing Air Transport Fleets of the World," July 1964.

**Transports refer to aircraft which were registered as commercial carriers, and civil aircraft include private and corporation aircraft as well as transports.

#International Civil Aviation Organization (ICAO): 73 Countries (includes all major countries with the exception of below)

##Non-ICAO: Russia, Bulgaria, Hungary, Czechoslovakia, Rumania, China Mongolia.

TABLE 3-3. CIVIL AND TRANSPORT AIRCRAFT INVENTORY FOR NORTH AMERICA AND EUROPE (ICAO COUNTRIES)*

Aircraft		Transport Aircraft		Civil Aircraft	
Type	Weight	N.A.	Europe	N.A.	Europe
Jet	Over 20,000 lbs.	533	284	491	262
	Under 20,000 lbs.			20	20
Turboprop	Over 20,000 lbs.	344	251	533	246
	Under 20,000 lbs.			5	18
Piston	Over 20,000 lbs.	1,438	830	2,439	754
	Under 20,000 lbs.			87,055	10,652

*Please refer to notes at bottom of Table 3-2 for explanation of data.

TABLE 3-4. INSTANTANEOUS AIRBORNE COUNTS (IAC) - NORTH ATLANTIC (0500 ZEBRA)

(Number of Aircraft)*

Fiscal Year	Absolute Peak	Average Peak	Rate of Growth**
1962	94#	64##	
1963	103	70	10
1964	113	77	10
1965	124	85	10
1966	136	93	10
1967	150	102	10
1968	165	112	10
1969	180	122	9
1970	194	132	8
1971	208	141	7
1972	220	149	6

*Prepared by FAA Office of Policy Development, PO-30, January 8, 1965.

**IAC growth rates were derived from peak day traffic forecasts developed in support of the FAA SPANAT program.

#Source: SRDS Report No. 150-2s: North Atlantic Region Air Traffic Survey, FY 1962.

##The average of twelve observations covering the peak IAC in each month during FY 1962.

TABLE 3-5. PEAK TRAFFIC DENSITIES FOR AIRCRAFT IN NORTH ATLANTIC FOR 1975

Aircraft Type	Number in Simult. Flight	Position Fix Interval (Minutes)	Density of Position Fixes No./Hr.
Supersonic Transports (Concordes)	20	5	240
Subsonic Transports	220	10	1440
Others (Non-Military)	20	10	120
		TOTAL	1800

The rationale for the number of SST's above is based on 40 aircraft in North Atlantic service making two round trips per day per aircraft for an average of 6.7 crossings per hour. Since the trip takes about three hours, about 20 aircraft would be in the air at one time. The subsonic transports include conventional jets and the future aerobus models. This projection is derived primarily from the JNSC estimates which took into consideration the increased capacities of future transports to meet the anticipated 13% per annum increases in passenger and cargo traffic.

The "Others" category of 20 flights is intended to cover the contingency of air rescue and/or search and navigation aid flights. Thus, the maximum number of position fix rates during peak traffic conditions in the North Atlantic for 1975 is estimated to be 1800 per hour.

Military flights, although excluded from the above model, could have a perturbing effect on a traffic control system. In 1961, it was estimated[3-2] that on peak days as many as 200 military aircraft overflew the Atlantic. Statistics are not readily available on how many aircraft were in the air simultaneously. However, it is assumed that they avoided civil air lanes and were not subject to the same peak schedule restraints as the commercial airlines. For this study, no cognizance will be made of military air traffic other than that separate RF channels may be required in a satellite traffic control system to monitor military aircraft flying near to or across civil air lanes.

3.2.5 AIRCRAFT CHARACTERISTICS

The flight characteristics of commercial transports and their normal operational altitudes over the North Atlantic are shown in Table 3-6. The envelope of velocity and altitude capabilities extend to 1600 knots and 80,000 feet, respectively.

TABLE 3-6. CIVIL AIRCRAFT FLIGHT CHARACTERISTICS*

Aircraft	No. of Passengers	Velocity (knots)		Altitude (kilofeet)#	
		Maximum	Normal	Maximum	Normal
Subsonic Transport	200 - 700	600	440 - 490	43	35 ± 6
SST (Concorde)	126	Mach 2.2	Mach 2.2	80	60 - 80
SST (U.S.)	200 - 300	Mach 2.7	Mach 2.7	80	60 - 80
Turbo Prop	80	420	250 - 420	37	29 ± 6
Piston (Pressure)	90	350	190 - 250	25	18 ± 6
(Non-Pressure)	90	220	140 - 220	15	9 ± 4

*From Reference 3-1.

#Climb Rate 300 to 5000 feet per minute

3.3 MARINE CRAFT

3.3.1 USER CATEGORIES

The following categories of ocean vessels are potential users of a world-wide navigation system.

Merchant Marine - The U.S. Department of Commerce's statistical records of merchant shipping in the world divides ships which gross 1000 tons or over into four major types: combination passenger and cargo ships, freighters, bulk carriers, and tankers. As of December 31, 1964, the total world fleet of ships over 1000 tons was reported[3-4] as 18,115 ships of which the predominant number, 11,686, were freighters. The U.S. Registry numbered 2598 ships, of which only 1014 were operational.[3-1] Considerable inaccuracies can result in deriving an estimate of potential maritime users from these gross statistics. Using the U.S. experience as an example, it would be reasonable to assume that only half of the world fleet is operational. The case for smaller vessels is even more sketchy.

As of December 31, 1964, the world merchant fleet contained 21,000 vessels grossing between 100 and 1000 tons and 120,000 vessels between 5 and 100 tons.[3-2] Most of these ships operate on rivers, inland lakes, and coastal regions and would not be good prospects for a world-wide navigation system. Based on discussions with personnel from the Maritime Administration of the U.S. Department of Commerce,[3-2, 3-7] it was estimated that less than 5% of the 100 to 1000 ton vessels would benefit from an advanced navigation system by 1970, if it were available, and the price was modest. A generous estimate may be 10% by 1975. The potential for the smaller vessels is considerably less and will not be included in the traffic model for this study.

For the larger ocean going vessels, precise navigation capabilities would result in economic benefits by reducing the time it takes to travel over broad ocean expanses. The dead weight tonnage of ocean-going merchant vessels has been increasing during the 1960's at the rate of approximately 5% per year, but due to the construction of larger vessels (in particular, bulk carriers and tankers) the number of vessels has increased a modest 1% per year. This trend is expected to continue.

Commercial Fishing - The Bureau of Commercial Fisheries of the U.S. Department of Interior reported 11,747 motorized fishing vessels of five gross tons or larger licensed by the U.S. in 1964.[3-5] About 60% of these vessels are under 50 feet in length and operate close to shore. Of the remainder about 3000 to 4000 are likely to venture on the high seas.[3-1, 3-8]

Countries which exceeded the U.S. in fishery catches during the 1960's were Peru, Russia, China, and Japan. Of an average world annual catch during this period of about 100 billion pounds, the U.S. contributed about 5 billion pounds or 5% of the world total. (1964 was a bad year for the U.S. and showed a downward trend. To counter it, the U.S. government is subsidizing the fishing industry in the construction of larger and more efficient fishing vessels.) Using U.S. statistics as a means of

determining the ratio of ships to fishery catches, the operational world fishing fleet would then approximate 75,000 ocean going vessels. It has been roughly estimated that 40% of these ships would operate in the Atlantic Ocean, and be on the high seas 50% of the time.[3-2] With respect to growth projection to 1975, personnel in the Bureau of Commercial fisheries[3-8] estimated that the number of vessels would remain static because of the introduction of larger and more efficient vessels to replace those which become obsolete.

Navigation requirements for fishing vessels are greatly influenced by the type of fishing operations. Travel to and from fishing sites and rendezvous with storage or factory ships require accuracies of one or two nautical miles, consistent with these functional requirements. Locating specific fishing grounds for bottom fishing, or following schools of fish require relative accuracies of 0.05 to 0.10 nmi and is currently being accomplished by underwater sounding devices.

Research and Survey (R&S) Vessels - Oceanographic research vessels, commercial resources exploration vessels, cable laying, range instrumentation (NASA) and the like have navigation requirements which exceed the accuracy of the general marine user. The location or relocation of sites for oceanographic observations, cable repairs, oil and mineral explorations can be improved with navigation precisions of ±0.1 nmi or better. A desirable goal of ±0.05 nmi by 1975 was expressed by the JNSC panel.

At present the U.S. has approximately 150 research and survey vessels. The World inventory of R&S vessels probably number about 1000 if the ratio of U.S. to World merchant shipping also prevails here. A growth rate of 3% per annum appears reasonable.

Oceanographic and meteorological data is also obtained from some commercial ships in a voluntary program identified as "Ships of Opportunity." These ships, in the normal course of their travels, make periodic reports to a central office. Improvements in the accuracy of reported positions relative to observations would enhance the value of this data. About 1800 ships are presently participating in this program with predictions indicating a doubling in this number by 1975.[3-1] Most of these ships, however, are included under the category of Merchant Marine.

Deep Sea Yachting - Navigation aids for this type of user will be highly dependent upon the nominal cost of equipment and its operation, and does not appear to constitute a significant category of user by the 1975 period.

Coast Guard Vessels - The U.S. Coast Guard maintains approximately 120 ships for such functions as search and rescue, aids to navigation, ice breaking, and oceanographic and ice patrol. These ships are highly instrumented from the point of view of navigation. The Coast Guard also operates a voluntary ship reporting system (AMVER) for use in emergencies. A rough estimate of the World high seas Coast Guard fleet or its equivalent is 1000 ships.

3.3.2 GENERAL REQUIREMENTS AND CONSTRAINTS

There is no compulsory traffic control system for maritime vessels traveling in international waters as there is for aircraft. There are voluntary procedures arrived at by international agreement, and services furnished by various countries to aid navigation, search and rescue operations, weather advisories, medical advisories, etc. A summary of features which would appear desirable for a North Atlantic navigation and surveillance system, and some constraints are listed below.

(1) Navigation capability should be available in all weather to all users on a 24-hour per day basis.

(2) Navigation is the sole responsibility of the ship's captain.

(3) Shipboard navigation equipment should be simple to operate, reliable and low in cost.

(4) Position determination should be free of ambiguity.

(5) Communication capability between ships and Coast Guard stations and other advisory agencies should be available in all weather to all users on a 24-hour per day basis.

(6) Communication of timely oceanographic, meteorological and hazards data to all users is highly desirable.

(7) Automation of ship navigation by 1975 is a goal. Automatic track and heading error indication would constitute a requirement to meet this goal.

3.3.3 POSITION FIX REQUIREMENTS

The navigation requirements for shipping by 1975 appear to be primarily concerned with the ability of the ship's navigator to reliably obtain position fixes whenever, wherever, and to the accuracy the situation demands. The concept implies a self-navigation mode in which use is made of a world-wide or transoceanic navigation system. The implementation of a reliable ship-to-shore and ship-to-ship communication system would satisfy the flow of information which is required for safe and efficient operation of shipping on the high seas.

A traffic control and surveillance function in which vessel locations are determined independent of the ship's navigator does not appear to be in the offing for non-military ships in the next two or three decades. A notable exception, however, may be ships that are designed for automatic navigation. To meet this capability, a traffic control center would require a surveillance system. One could elaborate on the requirements for such a system and the interfaces with other ocean craft and obstacles that would need to be identified, but it is sufficient to state for this study that the navigation system for ocean vessels to the 1975 era should be capable of growth for the accommodation of a traffic surveillance mode.

Estimates of position fix accuracies for each category of vessel by 1975 are listed in Table 3-7, along with required time intervals between fixes. Position accuracies based on a world-wide or transoceanic geodetic reference range from about 2.0 nmi

TABLE 3-7. POSITION FIX GOALS FOR MARINE VESSELS ON HIGH SEAS PROJECTED TO 1975 BASED ON NAVIGATION REQUIREMENTS

Type of Vessel	Position Fix Accuracy		Position Fix Interval (Minutes, Except as Noted)
	Absolute (±nmi)	Relative (± ft)	
Merchant Marine	2		2 Hrs.
Fishing Vessels	1	300	10
Research & Survey Vessels	1	300	10
Coast Guard:			
SAR	1.0	1,000	10
Ocean Stations	1.0		1 Hr.
Ice Patrol	0.5		10
Ice Break	2.0		1 Hr.
Range Instrumentation	0.5		10
Pleasure Boats	2.0		2 Hrs.

NOTE

1. Absolute refers to world-wide or transoceanic geodetic reference.
2. Relative refers to local geodetic reference or relative to successive position fixes.
3. Position Fix Intervals refers to navigation by absolute references. Relative navigation may require continuous position determinations.
4. Data based on JNSC report, Ref. 3-1.

for general shipping to 0.5 nmi for the special functions of some Coast Guard activities and range instrumentation ships used in support of the NASA Apollo Program. Survey ships and some fishing vessels may require position accuracies of 0.05 nmi with reference to local geodetic markers within a radius of 200 or 300 nmi or relative to successive position fixes. The frequency with which position fixes are required reflect the importance of maintaining precise tracks and are predicated upon the functions being performed by each type of vessel. Survey and rescue operations obviously require higher standards than general marine travel. The position fix intervals shown in Table 3-7 are based on requirements for the ship's navigator when he is performing at his most precise capabilities. For instance, fishing or survey vessels enroute to a distant destination would not require position fixes every ten minutes, but may determine their position every few hours. The same applies to any traffic control mode, also. A reporting interval of every few hours on the high seas would appear to be reasonable for the 1975 environment.

3.3.4 TRAFFIC DENSITY

Commercial and specialized vessels plying the oceans are potential users of a satellite navigation system. However, the likelihood of widespread use of any navigation system is dependent upon many factors, the most important being whether the cost of shipboard implementation is reasonable, and financial advantages accrue by its implementation. For this study, the ship's traffic model will be derived from data on existing inventories and growth rates with a projection to 1975 which will result in a liberal estimate of the number of users. This may be a moot point in those cases where the user will be employing a self-navigation mode in which position is derived from a broadcasted RF tone. The number of simultaneous users can be infinite without affecting the basic design of the navigation system. In other instances, however, such as automatic or remote controlled navigation operations and traffic surveillance, the number of users will be important to the system designer. Table 3-8 lists the number of non-military marine vessels which constitute the world ocean fleet, and their projection to 1975. The sources for this data and the estimates relative to percent of the total fleets which are on the high seas at any one time are referenced at the bottom of the Table. The growth rate in number of vessels for each category was discussed in Section 3.3.1. The total number of ships plying the Atlantic Ocean for this traffic model amounted to approximately 20,000 by 1975 of which 22% are merchant marine, 75% fishing vessels, and about 3% navigation aid and research vessels.

The questions which still remain are: (1) what portion of these ships would take part in a voluntary traffic surveillance system and (2) what portion would prefer to use only the self-navigation mode of a satellite navigation system? The preference, according to present trends and predictions, leans heavily towards self-navigation concepts. However, to obtain some perspective of the traffic densities which may be imposed on a surveillance system, plots of number of fixes per hour versus percent participation of each type of user is shown in Figure 3-2. It was assumed that on the average, fishing boats would report positions every 12 hours, merchant marine and survey vessels every 2 hours, and Coast Guard ships every 1/4 hour. On this basis, the maximum participation by all categories in the Atlantic Ocean would result in a requirement for about 5000 position fixes per hour by 1975.

3.3.5 OCEAN VESSEL CHARACTERISTICS

The size and speed of ocean vessels will not have a discernible effect on the navigation system performance requirements. The ships in this model range in size from 50 feet to several hundred feet in length, and from 100 tons to over 100,000 tons in weight. Some of the larger modern vessels reported in Reference 3-4 were capable of speeds of 30 to 35 knots. It is likely that 40-knot velocities will be attainable by 1975. The majority showed average velocities between 15 and 20 knots.

TABLE 3-8. HIGH SEAS MARINE TRAFFIC ESTIMATE

Category	1964 Estimate		1975 Projection	
	World Inventory (No.)	Atlantic Ocean Traffic (No. of Simul. Vessels)	World Inventory (No.)	Atlantic Ocean Traffic (No. of Simul. Vessels)
1. Merchant Marine				
a) 1000 tons and over	18,000	3,200	20,000	3,600
b) 100 to 1000 tons	21,000	600	24,000	700
2. High Seas Fishing Vessels	75,000	15,000	75,000	15,000
3. Ocean Research and Survey	1,000	200	1,400	300
4. Ocean Coast Guard or equivalent	1,000	200	1,400	300
TOTAL	116,000	19,200	121,800	19,900

Data Sources: (Note discussion in Section 3.3.1 for World Inventory Numbers.)

1. (a) Of Inventory: 50% are operational (Ref. 3-1); approximately 60% on high seas at one time (Ref. 3-1); approximately 60% in Atlantic (Ref. 3-2).
   (b) Of Inventory: 50% are Operational (Ref. 3-1); 10% on High Seas at one time; approximately 60% in Atlantic (Ref. 3-2).
2. Of Inventory: Numbers reflect Operational vessels; 50% on High Seas at one time (Refs. 3-1, 2); 40% in Atlantic Ocean (Ref. 3-2).

3 &

4. Of Inventory: Assume 50% on high seas at one time (Ref. 3-1), assume 40% in Atlantic Ocean.

3.4 SUMMARY

The elements of the requirements model which directly influence the design and performance characteristics of the navigation system are:

(1) Position accuracy requirements of each user,

(2) Frequency with which position fixes need to be made,

(3) Number of simultaneous potential users or number position fixes per unit time,

(4) Range of velocities of the user vehicles.

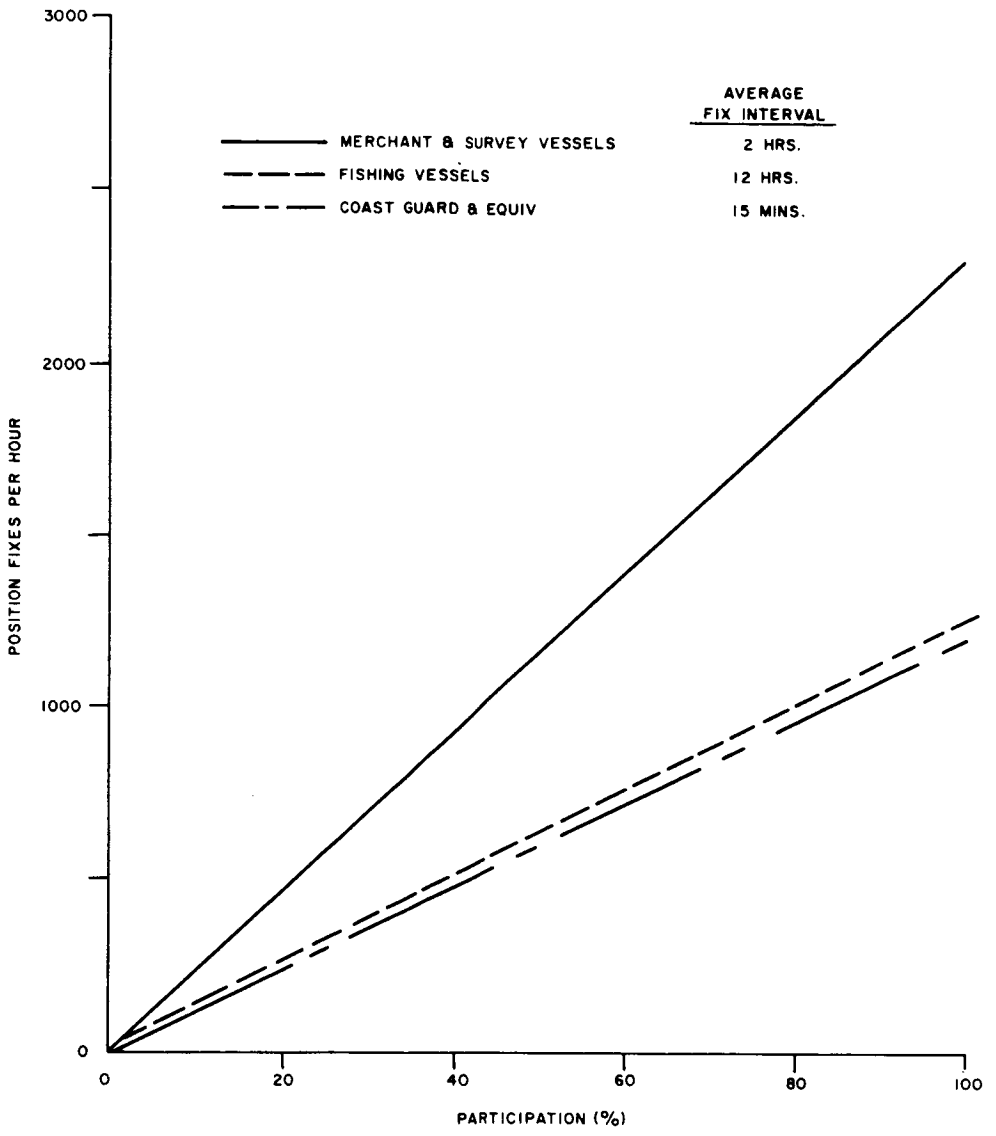

Figure 3-2. Ship Traffic Surveillance Requirements for Atlantic Ocean by 1975

A summary of this data appears in Tables 3-9 through 3-12. The data and the rational used for the traffic projections to 1975 are based upon the same sources as those utilized in the Final Report of the Ad Hoc Joint Navigation Satellite Committee (Ref. 3-1).

An initial assumption which influenced the results was that population and traffic growth would proceed on the same pattern as in the past 10 years. In addition, international and national agencies responsible for the conduct of international travel and safety are expected to encourage the formation and use of a world-wide navigation and traffic control system by the 1970's.

The model presented herein is probably optimistic in its forecasts. Thus, a navigation and traffic control system capable of meeting these requirements would likely reflect some growth potential into the late 1970's.

TABLE 3-9. TRAFFIC CONTROL AND NAVIGATION MODEL FOR 1975 ENVIRONMENT

User	Position Fix	
	Accuracy (nmi)	Rate (Fixes/Hr)
Aircraft:		
Subsonic Transports	± 3.0	6
Supersonic Transports	± 3.0	12
Search and Rescue Aircraft	± 1.0	6
Navigation Aid Aircraft	± 0.5	6
Scientific Survey Aircraft	± 0.5	6
General Aviation	± 3.0	4
Marine Vessels:		
Merchant Marine	± 2.0	1/2
Fishing	± 1.0	6
SAR & Nav. Aid (Max. Req'ts.)	± 0.5	6
Range Instrum. (Space Program)	± 0.5	6
General	± 2.0	1/2

TABLE 3-10. PRECISION NAVIGATION REQUIREMENTS FOR 1975 ENVIRONMENT

User	Position Fix	
	Accuracy (ft)	Rate (Fixes/Hr)
Aircraft:		
Search and Rescue	± 1000	Continuous
Survey	± 300	Continuous
Marine Vessels:		
Fishing	± 300	6 to Continuous
Oceanic Survey	± 300	6 to Continuous
Search and Rescue	± 1000	6 to Continuous

TABLE 3-11. PEAK TRAFFIC DENSITY MODEL FOR NORTH ATLANTIC PROJECTED TO 1975

User	No. of Simul. Users	Position Fix Rate (Fixes/Hr)	
		Individual	Total
Aircraft:			
Supersonic Transports	20	12	240
Subsonic Transports	220	6	1,320
Others	20	6	120
		TOTAL	1,680
Marine Vessels (High Seas):			
Merchant (100 tons & over)	4,300	1/2	2,150
Fishing	15,000	1/12	1,250
Oceanic Survey	300	1/2	150
SAR & Nav. Aid	300	4	1,200
		TOTAL	4,700

TABLE 3-12. VEHICLE PERFORMANCE CHARACTERISTICS

User	Maximum Velocity (knots)	Maximum Altitude (ft)
Aircraft:		
Supersonic	1,700	80,000
Subsonic	600	41,000
Marine Vessels:	40	----

Section 4

POSITION DETERMINATION

4.1 INTRODUCTION

In this section we identify the elements which enter into a determination of position in each of the major navigational modes, and outline the more important computational methods for locating the vehicle in some appropriate coordinate system. Preliminary versions of formulas are presented to show the scope of the operations and to call attention to the tractability of on-line user computation. Because a special vocabulary is needed for the concise and explicit representation of the ideas, a glossary is provided in Appendix 4A for immediate reference.

In the course of the discussions we include numerous diagrams which are to be read not as a supplement to the text material, but as an integral part of it. The drawings have been designed to clarify concepts, define terms, display formulas, and in some cases provide textual detail and annotation. Therefore, all figures should be perused with some care in the descriptive sequence.

Finally it is not always convenient to define every word or phase at its first occurrence in the material; while it may be logically desirable to do so, it sometimes breaks the continuity of the reading. When the reader encounters a new term as yet undefined or an old word in a new setting, he is advised to consult the glossary in Appendix 4A.

4.2 NAVIGATION MODES

The principal modes with which we deal in these discussions are circular and hyperbolic navigation. In circular navigation we measure the equivalent of range from the user to the satellite: lines of equal range are circles on a plane or spherical surface. In hyperbolic navigation we measure the equivalent of difference in the ranges between the user and two satellites: lines of equal range-difference are hyperbolas on a plane or near-plane.

4.3 NAVIGATION TONES

The navigation signal apprehended by the user consists in the present concept, of two cw tones suitably modulated on the RF carrier. The frequencies of these tones are in some simple ratio; in our discussions we take them at 10 kHz for the coarse tone and 300 kHz for the fine tone, with respective wavelengths of about 30 km and 1 km. The navigation satellites are excited from the ground so that the tones appear to originate within the satellites, synchronously in phase and in frequency.

4.4 LOP: LINE OF POSITION

The fundamental quantity indicated to the navigator or delivered to the computer is the LOP, the line of position. This concept is classical in celestial navigation, and is familiar to the modern navigator in LORAN, VOR and several other electronic aids to navigation. Its use here is entirely continuous with the usual

notion of line of position. However, because it does arise in a somewhat different geometric context and several of its properites are isolated as basic parameters, we shall define LOP again from our present point of view, along with its related vocabulary.

Figure 4-1 shows the development of LOP in a circular system; however the definitions in a hyperbolic system are analogous and need little elaboration. We picture the satellite as the center of a system of concentric spherical shells, extending into and beyond the regions of the earth. Each shell constitutes an SOP (surface of position) in that all points on such a surface are at the same range from the satellite. We identify as cardinal SOP's those shells whose radii are integral coarse-tone wavelengths: the interval between two consecutive cardinal shells we call a band, which is seen to be a coarse-tone repetition interval. We now consider every such interval as being further partitioned by shells spaced apart by a fine-tone wavelength. This smaller interval is called a lane; a lane is a fine-tone repetition interval. Finally, we arbitrarily sub-divide every lane into 1000 parts, and call each of these parts a line. The choice of 1000 in the definition of a line is suggested by the practicalities of distinguishing sub-divisions of a fine cycle from each other. The operational limits of phase discrimination, like virtually all analog measurements in the field, is in the order of one part in a thousand.

In hyperbolic navigation, the SOP's are loci of equal range difference from two satellites. In this case the surface designated as 0000:00.000 is the plane everywhere equidistant from the satellities, that is, the perpendicular bisector of the line joining them. The idea of band as a coarse-tone repetition interval is carried over into the hyperbolic mode. In this mode a band is not equal to a coarse-tone wavelength, or any simple multiple or function of it. In fact, the distance between consecutive band surfaces is not constant, even for the same pair of surfaces. What is invariant in the idea of a band in any navigation mode, is that it is the interval over which the phase differences in the coarse-tone channel begin to repeat. Similarly a lane is a fine-tone repetition interval with again 30 lanes to a band, and 1000 lines to a lane.

The idea of band, lane, and line may be particularized from partitions in space to partitions on a surface, especially a horizontal plane through the user. In this case the planar band, lane, and line are the intersections between the plane and the spatial band, lane, line. In fact, this latter usage is so frequent that we assume these words refer to surface partitions unless the context indicates otherwise. Furthermore the phrase LOP will always refer to such an intersection, and ever though the navigation meters actually read the instantaneous SOP's occupied by the vehicle, they are considered to indicate the LOP intersections between those SOP's and the user plane.

4.5 THE LOP-METER

Figure 4-2 is a conceptual view of the navigation meter, intended to fix ideas as well as to represent a possible operational version of the meter for low-cost, manual navigation.

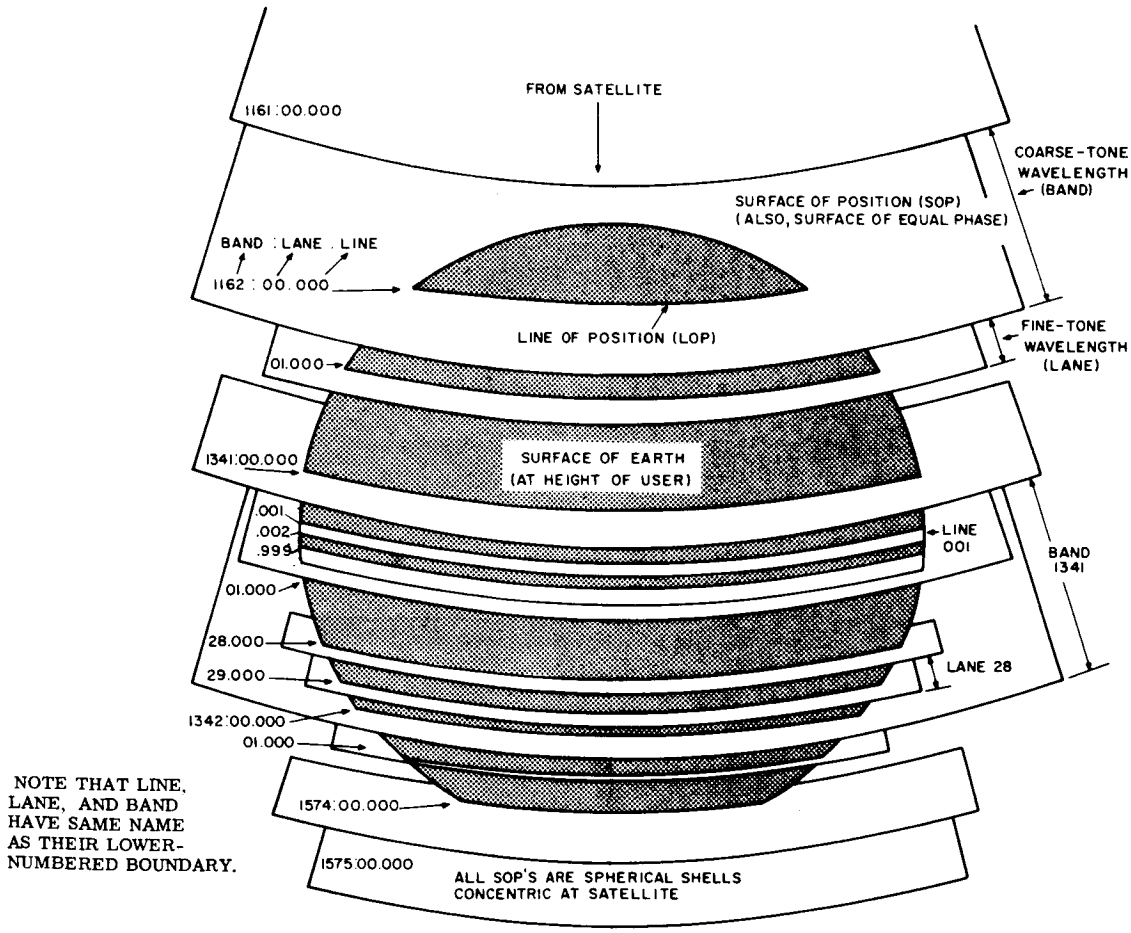

NOTE: .GURE SHOWS RANGE SURFACES OF POSITION FROM SYNCHRONOUS-HEIGHT SATELLITE, INTERSECTING THE EARTH. COARSE TONE 10 KC, FINE TONE 300 KC; THAT IS, BANDS ARE ABOUT 30 KM LONG, AND LANES ABOUT 1 KM LONG, ALONG A LINE-OF-SIGHT. THERE ARE 30 LANES TO A BAND, AND, FOR A NOMINAL READING RESOLUTION OF A THOUSANDTH OF A FINE CYCLE, 1000 LINES TO A LANE.

Figure 4-1. Definition of Band, Lane, and Line

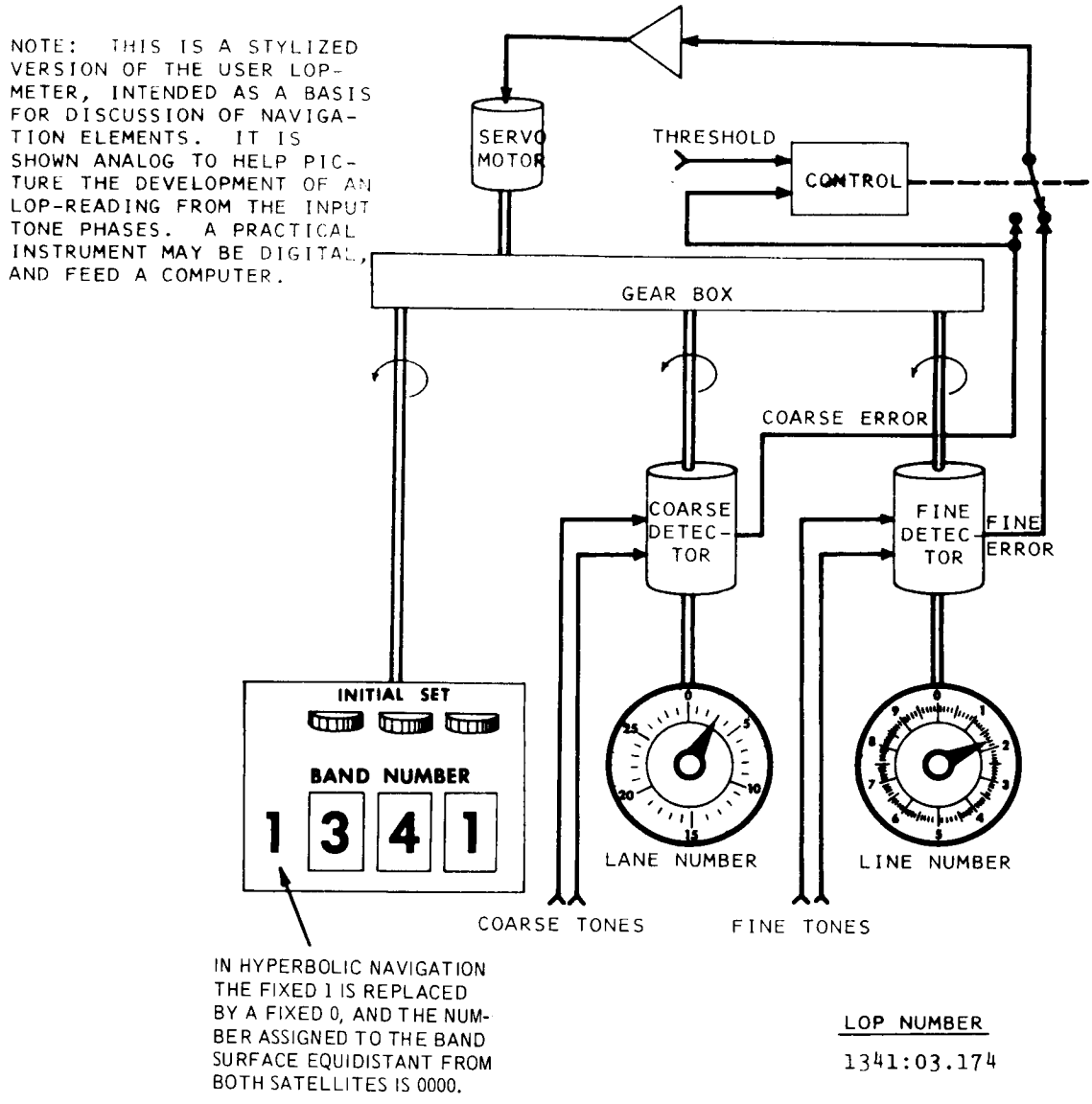

Figure 4-2. LOP-Meter

The two demodulated tones of the coarse channel (either from two satellites, or from one satellite and a tone-local oscillator) drive a coarse detector until the error in the loop is less than that attributable to half a fine-shaft cycle. At this point the fine-channel error signal takes control, driving the fine error to zero. Under either control, the servo motor drives the fine shaft, which drives the coarse shaft. The coarse shaft, in turn, drives the rightmost band-digit decade, and the rotation continues to propagate to the left.

The INITIAL-SET controls allow the user to insert his appropriate band number either at the start of a flight, or enroute, for reset or change of satellite. In an automatic system, this function is driven by the computer. For a coarse wavelength of 30 km, the fourth band digit in the vicinity of the earth is uniformly 1 in the circular mode, and 0 in the hyperbolic mode. Hence, only three band windows are needed in any case. Furthermore, negative LOP numbers cannot occur in the circular mode, and are indicated in the hyperbolic mode by the presence of a digit greater than 5 in the third (i.e., the coarsest) band window.

4.6 LOP-PARAMETERS

Figure 4-3 introduces the fundamental parameters in the description of an LOP-family in the vicinity of the user. The family of lines is pictured as being in the user plane, or in some contexts the base plane, both of which are horizontal and near the earth. The family is characterized by the distance-value p of the line passing through the user or basepoint, the gradient G of the lines, and the direction φ of the gradient. p is the range, double-range, or range-difference in one-way circular, two-way circular, or hyperbolic navigation respectively. G is seen to be the ratio of a small change in LOP-distance to the shortest horizontal distance experiencing that change; φ is the direction of most rapid change, measured clockwise from true north.

The LOP-distance p which has linear dimensions is related to the LOP-value P, whose units are LOP-cycles and which is dimensionless, by

$$p = P\lambda_f$$

where λ_f is the fine-tone wavelength. It is convenient in the sequel to use P rather than p, because P is the observed quantity, and we want to bring our discussions to operational formulations as directly as possible.

4.7 PARAMETER FORMULA

Figure 4-3 displays the formula for the LOP-parameters, in terms of the topocentric coordinates of the LOP-satellites, R, θ, E: range, azimuth and elevation angle at the user or basepoint. In the formula for P the symbol $\underline{\circ}$ is used to indicate the equivalence rather than the equality of the LOP-value and the LOP-distance.

φ gives the direction of increasing P, that is, positive G. In circular navigation where the expressions for G is always positive, φ is always directed away from the LOP-satellite. In hyperbolic navigation, G may be given as positive or negative depending on the arbitrary assignment of A and B to the satellites. No difficulty results however,

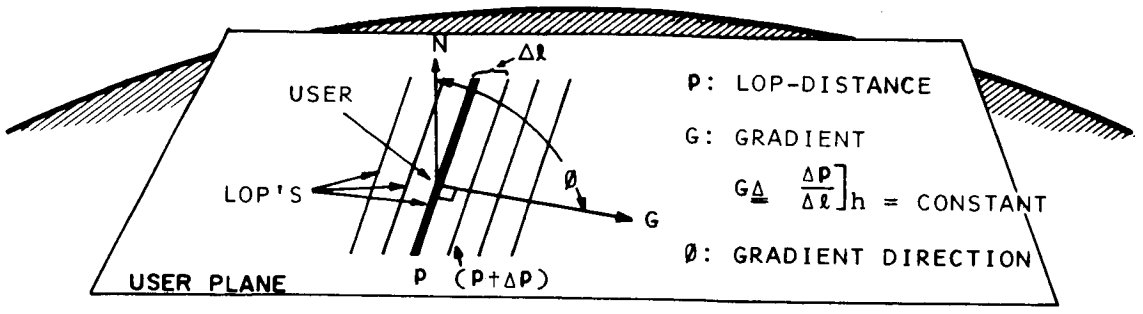

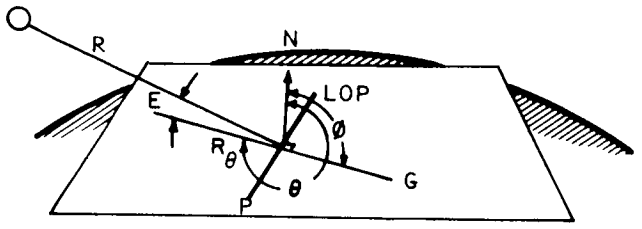

ONE-WAY CIRCULAR

$P \triangleq R$

$\emptyset = \theta - 180°$

$G = \cos E$

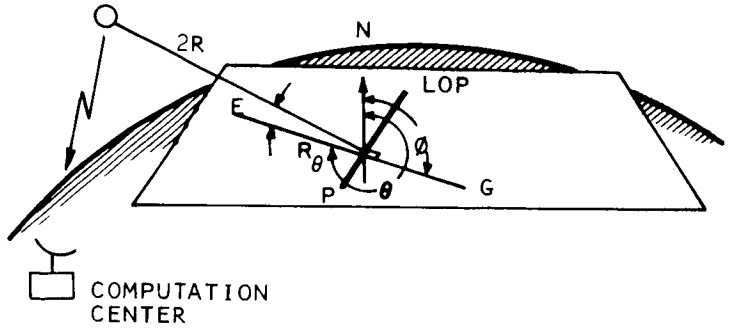

TWO-WAY CIRCULAR

$P \triangleq 2R$

$\emptyset = \theta - 180°$

$G = 2 \cos E$

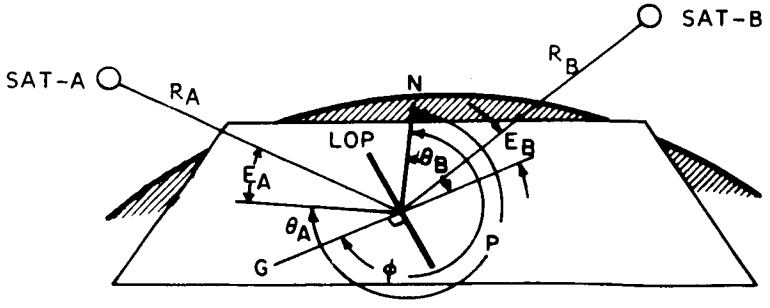

HYPERBOLIC

$P \triangleq \delta R = R_B - R_A$

$$\phi = \theta - \tan^{-1} \frac{\cos E_B \sin(\theta_B - \theta_A)}{\cos E_A - \cos E_B \cos(\theta_B - \theta_A)}$$

$$G = \cos E_A \cos(\theta_A - \phi) - \cos E_B \cos(\theta_B - \phi)$$

Figure 4-3. LOP Parameters for Circular and Hyperbolic Navigation Modes

because the same assignment applies to the computation of φ; hence, when G is negative the sense of positive G is given by the reverse of φ. In other words, the pair (G,φ) is a valid gradient-vector in any mode, and for any arbitrary assignment of A and B in the hyperbolic mode.

The magnitude of G is at most 1 in the one-way circular mode, and 2 for two-way circular navigation. In fact, the gradient for two-way circular is always twice that for the same geometry in one-way circular; however no significant error-transformation advantage is expected from this property, because the measurement error in P is seen to be virtually twice as great also. In hyperbolic navigation the G-magnitude may be as high as 2, but again the apparent error-transformation advantage over one-way circular is compromised somewhat by the observation that the error in the hyperbolic P may be estimated as 40% higher ($\underline{\circ}\ \sqrt{2}$) than the error in the circular P involving as it does the difference of two ranges.

4.8 HEIGHT-SENSITIVITY (Figure 4-4)

The height-sensitivity H is another of the describing parameters of an LOP-family. It is the ratio of height increment to the least horizontal displacement needed to remain on the same SOP. It's direction is φ, the gradient direction. Like the gradient also, it is positive in circular navigation, but may be negative in the hyperbolic mode; in any case (H, φ) is a valid vector.

Of course both the gradient and height-sensitivity are partial derivatives, the gradient at constant altitude and the height-sensitivity at constant LOP-value. An analytic treatment would generate the same results, which in the limit are given by the geometric ratios. The geometric derivation however is pictorial, goes immediately to the formulation most suitable for user computation, and points the way to convenient experimental determination of the parameters, given an LOP-meter and a tapemeasure.

4.9 LANE-WIDTH

The lane-width L along a horizontal surface is a combination of gradient and fine-tone wavelength. As shown in Figure 4-5 it is given by

$$L = \lambda_f / G$$

It is not precisely equal to the fine-tone repetition interval which includes the user, because G is not constant over this interval. However for practical navigation using a tone at 1 km, the difference is in the order of a foot and quite negligible therefore. In any case L is an intuitive figure of merit easily visualized, combining the system geometry and the system signal.

A related characterizing parameter is line density D given by

$$D = 1000/L$$

That is, D is the density of lines per length in the horizontal plane, and is given by such expressions as 828 lines/mile or 604 lines/km.

A related number is the granularity g of the LOP-family:

$$g = 1/D$$

g is given in feet or meters, and indicates the (approximate) minimum horizontal displacement which may show up on the user's instruments. Hence to say that the granularity of a given LOP-family is 5 feet means that the user's motion will be detected when he moves about 5 feet (along the gradient).

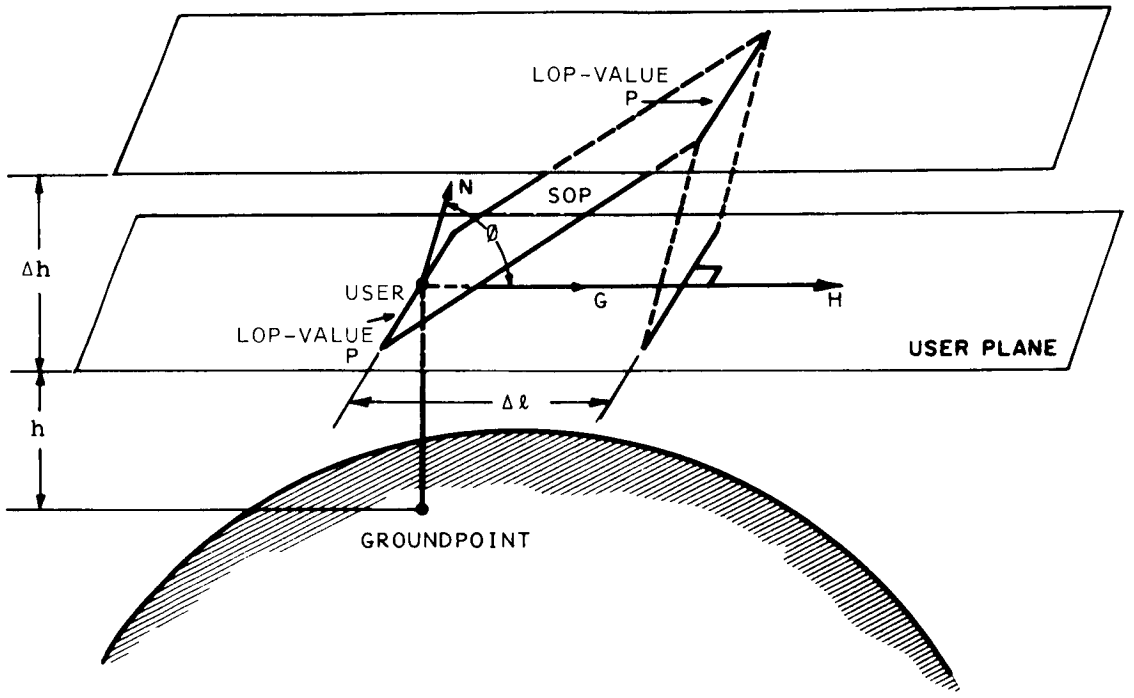

$$H \triangleq \left[\frac{\Delta h}{\Delta \ell}\right]_{P\,=\,\text{CONSTANT}}$$

ONE-WAY CIRCULAR: $H = \cot E$

TWO-WAY CIRCULAR: $H = 2 \cot E$

HYPERBOLIC: $H = \dfrac{\cos E_A \cos(\theta_A - \phi) - \cos E_B \cos(\theta_B - \phi)}{\sin E_B - \sin E_A}$

Figure 4-4. The Height Sensitivity H, of an LOP Family

4.10 PARAMETER BEHAVIOR

Figures 4-6 and 4-7 provide further insight into the nature of the various LOP-parameters and their relation to satellite displacements as viewed from the user.

In the circular mode, a line-of-sight displacement in the satellite or, equivalently, an error in slant range due to an imperfect ephemeris results only in a translation of the LOP-family; the gradient and height-sensitivity vectors are unaffected. An azimuthal displacement or error causes only a rotation in the family; the LOP-value and vector magnitudes are unchanged. An elevation displacement or error causes a stretching or tightening as of a rubber sheet; the LOP-value and LOP-direction remain the same.

In hyperbolic navigation, line-of-sight error again means only LOP-value discrepancy; the sensitivity vectors are invariant. However, azimuth and elevation are so interwoven that a change in either will both rotate the family and stretch (or tighten it), but leave the LOP-value as it was. Hence, in general, both vectors are disturbed in magnitude and direction, with an angular displacement in either satellite.

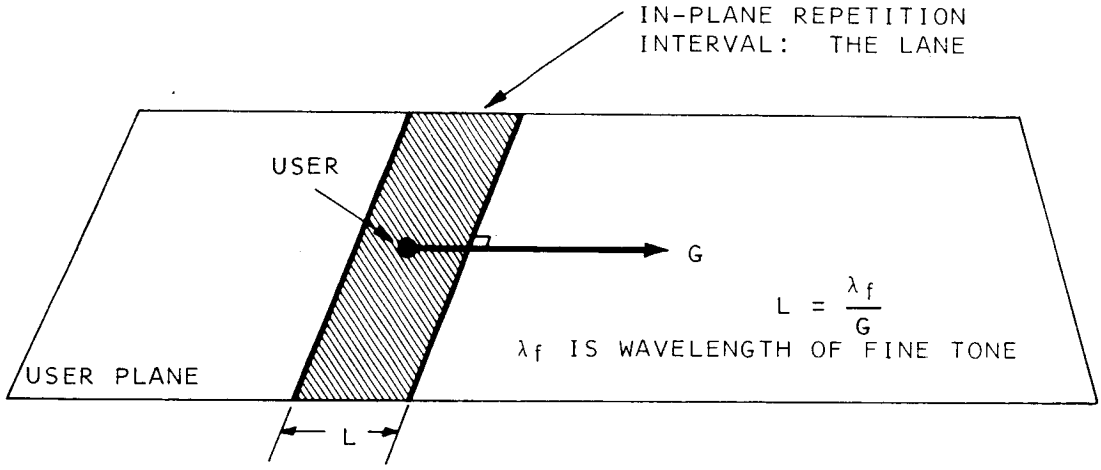

Figure 4-5. The Lane-Width Parameter

4.11 THE FIX: ABSOLUTE NAVIGATION

Figures 4-8 and 4-9 introduce the elements of absolute navigation, defining the terms, giving the computation formula, and outlining a representative algorithm. The situation is described here in terms of one-way circular navigation, but the formula and methods are directly applicable to the two-way circular and the hyperbolic modes. We shall proceed through the flow chart, which is keyed by circled lower case letters to appropriate elements in the diagram of Figure 4-8. All computations are presumed to be performed automatically.

The process starts with the determination of satellite position (a) by use of the global ephemeris coefficients for the selected satellites, and the time of

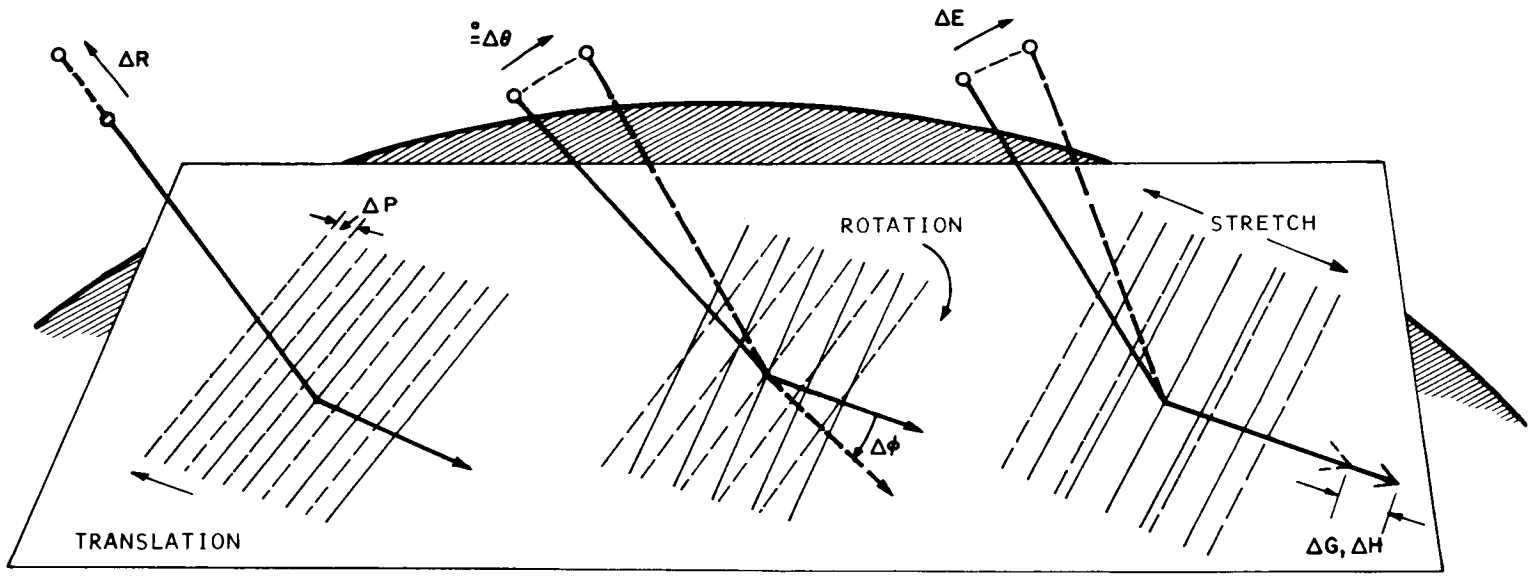

LINE-OF-SIGHT DISPLACEMENT		AZIMUTHAL DISPLACEMENT		ELEVATION DISPLACEMENT	
LOP - FAMILY TRANSLATES (ONLY LOP-VALUE CHANGES)		LOP-FAMILY ROTATES (ONLY GRADIENT-DIRECTION CHANGES)		LOP-FAMILY CONTRACTS OR EXPANDS (ONLY GRADIENT & HEIGHT SENSITIVITY CHANGE)	
ONE-WAY	TWO-WAY	ONE-WAY	TWO-WAY	ONE-WAY	TWO-WAY
$\Delta P \doteq \Delta R$	$\Delta P \doteq 2\Delta R$	$\Delta\phi = \Delta\theta$	$\Delta\phi = \Delta\theta$	$\Delta G = -\Delta E \sin E$ $\Delta H = -\Delta E \csc^2 E$	$\Delta G = -2\Delta E \sin E$ $\Delta H = -2\Delta E \csc^2 E$

Figure 4-6. Effect of Satellite Displacement on LOP-Family, Circular Navigation

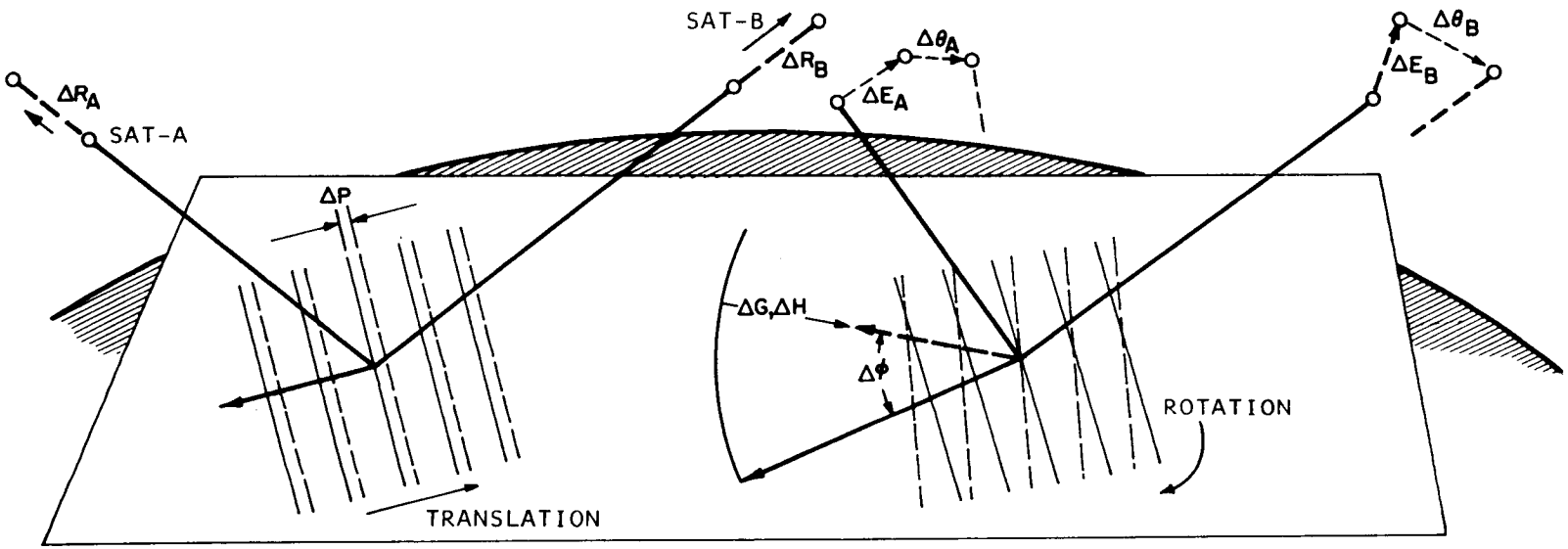

LINE-OF-SIGHT DISPLACEMENT

LOP - FAMILY TRANSLATES
(ONLY LOP-VALUE CHANGES)

$$\Delta P \stackrel{\circ}{=} \Delta R_B - \Delta R_A$$

AZIMUTHAL AND/OR ELEVATION DISPLACEMENT

LOP-FAMILY ROTATES AND CONTRACTS OR EXPANDS
(DIRECTION, GRADIENT AND HEIGHT SENSITIVITY CHANGES;
LOP-VALUE REMAINS UNCHANGED)

$$\Delta Q = \frac{2Q}{2\theta_A}\Delta\theta_A + \frac{2Q}{2\theta_B}\Delta\theta_B + \frac{2Q}{2E_A}\Delta E_A + \frac{2Q}{2E_B}\Delta E_B$$

WHERE Q REPRESENTS: Ø; G; H

Figure 4-7. Effect of Satellite Displacement on LOP-Family, Hyperbolic Navigation

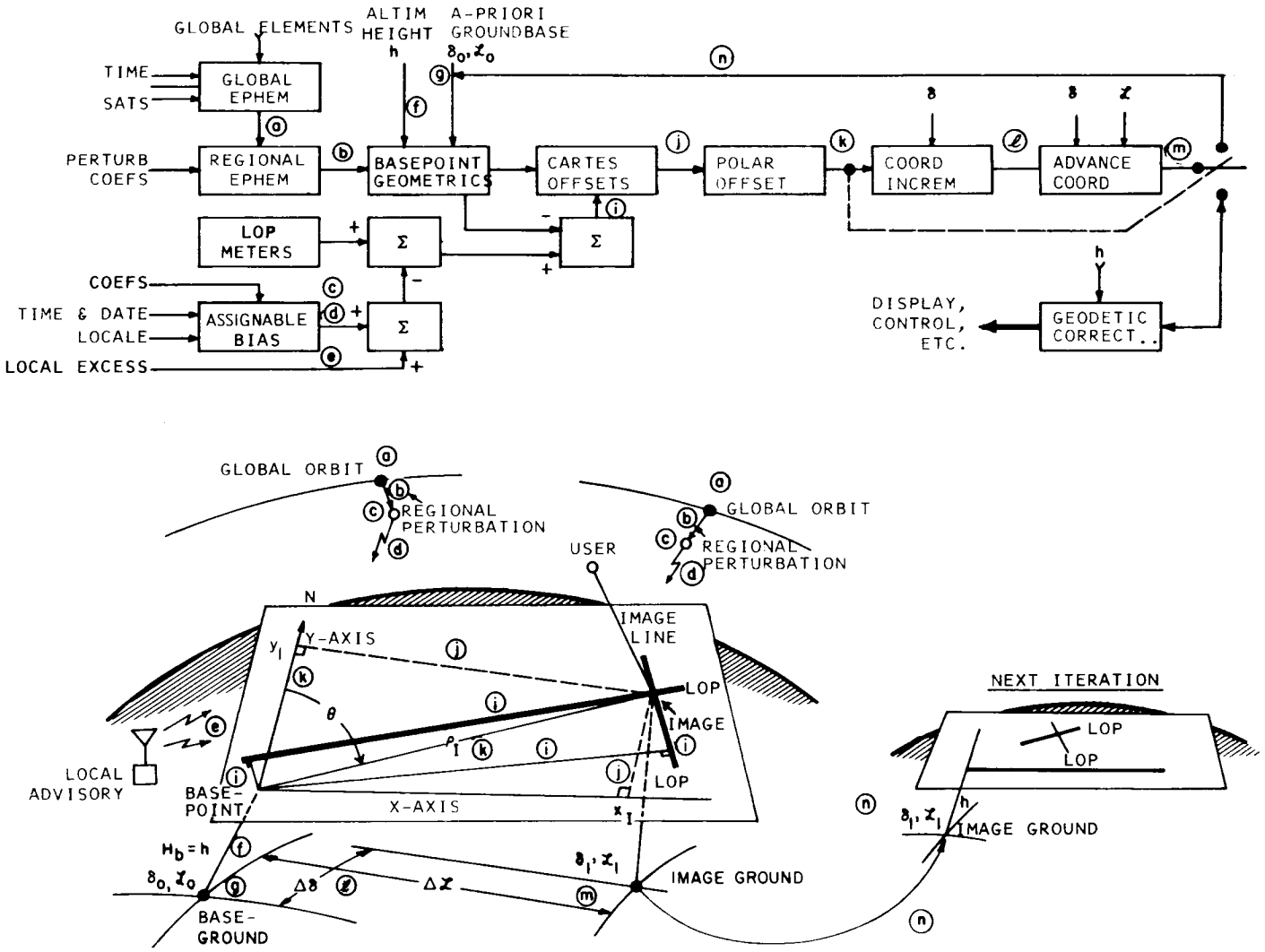

Figure 4-8. Flow of Computation in Absolute Navigation

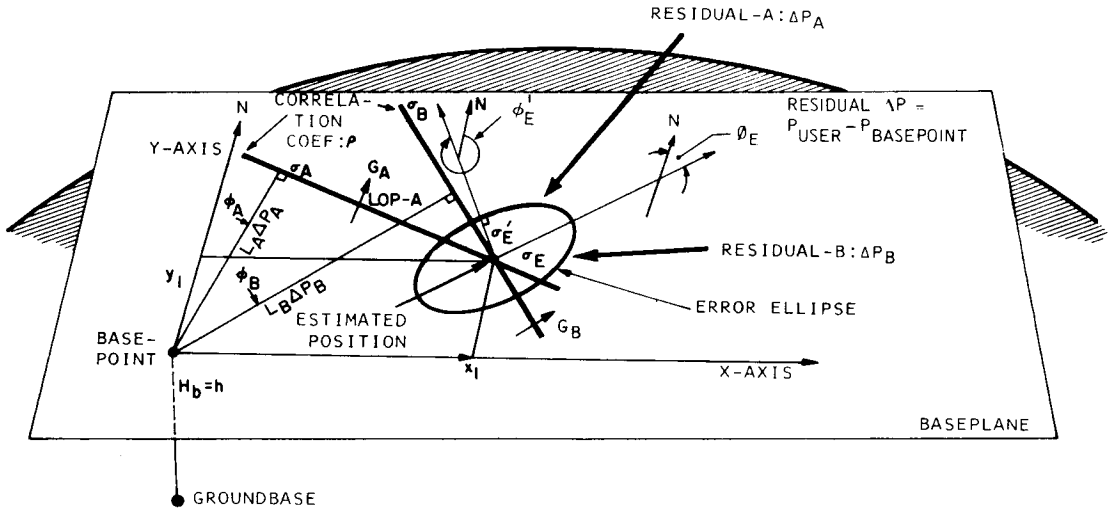

ESTIMATED POSITION

$$x_I \sin \phi_A + y_I \cos \phi_A = L_A \Delta P_A$$

$$x_I \sin \phi_B + y_I \cos \phi_B = L_B \Delta P_B$$

WHENCE:

$$x_I = -\frac{L_A \cos \phi_B}{\sin (\phi_B - \phi_A)} \Delta P_A + \frac{L_B \cos \phi_A}{\sin (\phi_B - \phi_A)} \Delta P_B$$

$$y_I = \frac{L_A \sin \phi_B}{\sin (\phi_B - \phi_A)} \Delta P_A - \frac{L_B \sin \phi_A}{\sin (\phi_B - \phi_A)} \Delta P_B$$

ERROR ELLIPSE

$$\phi_E = \frac{1}{2} \tan^{-1} \frac{\sigma_B^2 \sin 2\phi_A + \sigma_A^2 \sin 2\phi_B - 2\rho\sigma_A\sigma_B \sin (\phi_A + \phi_B)}{\sigma_B^2 \cos 2\phi_A + \sigma_A^2 \cos 2\phi_B - 2\rho\sigma_A\sigma_B \cos (\phi_A + \phi_B)}$$

$$\phi'_E = \phi_E - 90°$$

$$\sigma_E = \sqrt{(1-\rho^2)} \left[\frac{\sin^2 (\phi_A - \phi_E)}{\sigma_A^2} + \frac{\sin^2 (\phi_B - \phi_E)}{\sigma_B^2} - 2\rho \frac{\sin (\phi_A - \phi_E) \sin (\phi_B - \phi_E)}{\sigma_A \sigma_B} \right]^{-1/2}$$

$$\sigma'_E = \sqrt{1-\rho^2} \left[\frac{\cos^2 (\phi_A - \phi_E)}{\sigma_A^2} + \frac{\cos^2 (\phi_B - \phi_E)}{\sigma_B^2} - 2\rho \frac{\cos (\phi_A - \phi_E) \cos (\phi_B - \phi_E)}{\sigma_A \sigma_B} \right]^{-1/2}$$

Figure 4-9. Two LOP's - The Determined Case, Absolute Navigation

observation.* The regional ephemeris coefficients are now applied to get the corrected satellite position (b), where more accuracy is needed.

The assignable biases currently experienced at the LOP-meters is computed by means of operational coefficients which give the nominal phase drift (c) (in back-up oscillator operation), and the nominal refraction (d), when the time of fix, date, and (approximate) user location is entered. Also, where local excess (e) is available, it is added to the biases at this point; the net bias is then subtracted from the LOP-values delivered to the computer by the LOP-meters.

The altimeter height (h) is entered at (f) as the height of the baseplane, and the first assumed location of the basepoint is entered at (g) in terms of its latitude δ_o and longitude $\mathcal{L}_o$. These quantities allow a computation of the basepoint geometries, which are then subtracted from the respective bias-corrected LOP-value to give the residuals ΔP_A and ΔP_B, at (i). The residuals are used in the formula for x_I, y_I which are in the form

$$x_1 = A_1 \ \Delta P_A + A_2 \ \Delta P_B$$

$$y_1 = B_1 \ \Delta P_A + B_2 \ \Delta P_B$$

where x_1, y_1 are the cartesian coordinates of the image-point.** These are converted to a polar coordinate statement (k) of the horizontal displacement of the user from the basepoint. This in turn is used to compute the increments in latitude and longitude (ℓ), and the new absolute coordinate pair $(\delta, \mathcal{L})$ at (m).

When the polar offset (k) is less than a pre-set threshold, the current estimate of δ and $\mathcal{L}$ are corrected for the local geodesy where necessary for accuracy, and the results delivered to user display and/or controls. When the offset is not within the threshold, the cycle is repeated at (n), using the up-dated user position as the new basepoint.

Where the user requires an estimate of the position error, the dimensions and directions of the principal axes of the error ellipse are computed from the formula given in Figure 4-9, where σ_E, $\sigma_E{}'$ are the semi-axes and φ_E, $\varphi_E{}'$ are their respective directions.

---

* A minor nicety of computation may be mentioned here in passing. The satellite position ultimately required in high accuracy computations is the position at the time the now-received signal was impinging on the satellite. More particularly, we require the time-average position over the interval corresponding to the current sample. Such details appear to be necessary only for non-equatorial satellites, and then only when fine accuracy is required. In any case there is no difficulty in including them, and the final report will elaborate on this point. It will include as well the formula and procedures for satellite position determination, and precise geodetic correction.

** Several new phrases and symbols are introduced into this discussion. The reader is referred to Appendix 4A, and to Figures 4-8, 4-9 and 4-10 for explicit definitions of these terms.

The solution described in Figures 4-8 and 4-9 refer to the determined case of two LOP's. The general solution for the over-determined case is presented in Appendix 4B.

Ephemeris Coefficients - The global elements and the regional perturbations used in the computation of satellite position are made available to the field of users in several ways. The global coefficients are generated at a regional service center as of some convenient epoch, perhaps the beginning of the month, in terms of the Keplerian elements (and their rates including some second derivatives) to a total of about 15 numbers. It is expected that most navigators need only the six zero-order elements, and perhaps two or three first-order rates. In any case, the coefficients pertaining to a particular satellite are promulgated periodically (once an hour) via that satellite over both its digital data channel, and one of its voice/teletype channels; such broadcasts include also late updating information. Assuming as many as eight decimal digits per coefficient, this form and frequency of distribution is seen to put a negligible load on the communication facility (about 500 bits per hour).

The global elements are also issued in hard copy bulletins, emanating from the regional centers, to the community of users who subscribe to this service including especially those who do not have the benefit of the communications channels. The logistics of this form is estimated at about a single printed page per month, mailed to the user.

The regional perturbations are corrections on the global position. They also originate in the regional service center, prepared from the data provided by the regional tracking network. They give the vector displacement of the actual (regional) satellite from the apparent (global) satellite in a cartesian coordinate system, whose principal plane is the global orbit, and whose vertical axis is the radius to the global satellite. It is estimated that a quadratic Taylor series in each dimension is sufficient for the more demanding users; hence nine perturbation coefficients are contemplated, again on the order of monthly epochs. These coefficients also are broadcast and printed, and do not noticeably change the load on data logistics.

4.12 THE FIX: RELATIVE NAVIGATION

Figures 4-10 and 4-11 present the concepts and formula necessary for the computation of relative navigation. While some of the terms used here were anticipated in the previous discussion, they are perhaps more clearly discerned in the present context.

In Figure 4-10 the user is shown somewhere above the baseplane, which is generally tangent to the earth at the basepoint. This point is the origin of cartesian axes X and Y, positive to the east and north respectively. The imageline is the locus of points which produce the same pair of LOP-readings as observed at the user. Its intersection with the baseplane is the image point, and constitutes an important intermediary in the process. The intersection of the user's vertical with the baseplane is the piercepoint, and with the earth is the ground-point; the projection of the user on the baseplane is the foot.

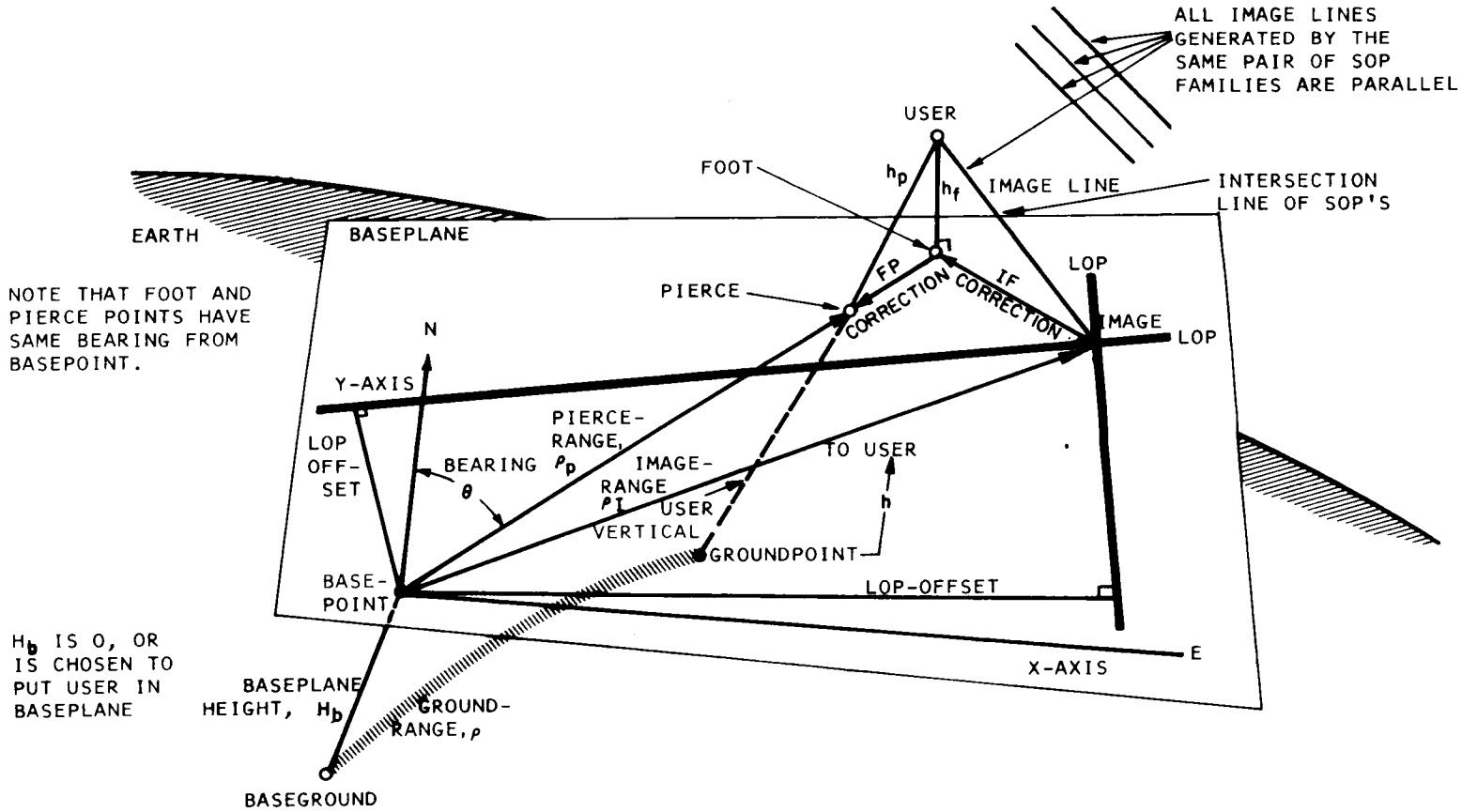

Figure 4-10. Illustrating Geometric Terms Used in Relative Navigation

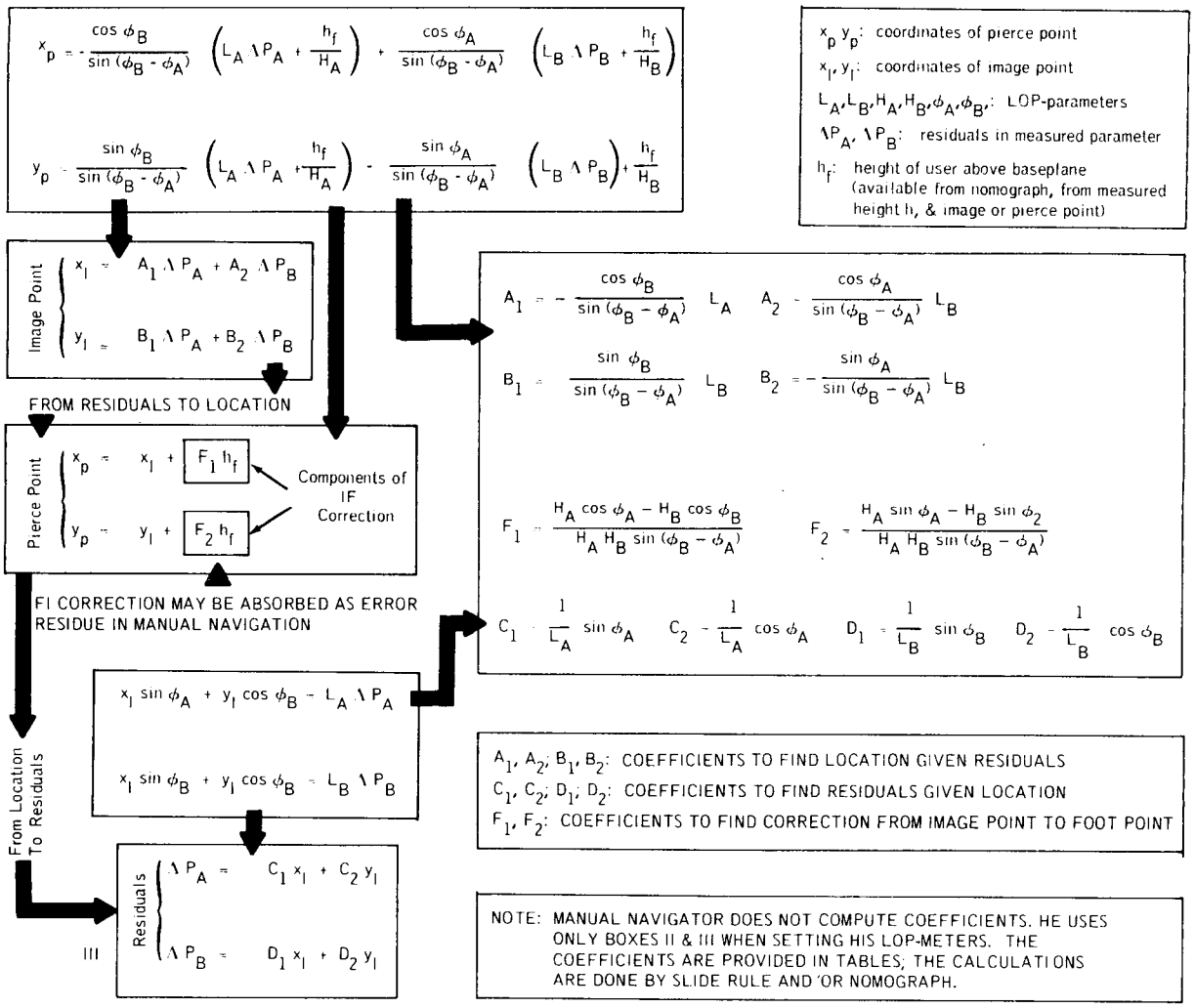

Figure 4-11. Computation Formula for Relative Navigation

Figure 4-11 shows the formula relating the observations to the relative offsets, via the geometric coefficients and LOP-family parameters. The image-coordinates are just linear mixtures of the residuals, and the pierce-coordinates are given by linear corrections to the image-values.

4.13 THE LOP ALMANAC

Figure 4.12 shows the flow of computation for manual navigation, and a representative page from the LOP-almanac carried by the user.

The almanac is a chronological tabulation of coefficients needed by the navigator for his calculations, which he performs with one or more aids such as sliderule, nomograph, or chart. Each almanac is prepared for a specific base domain. Postulating basepoints on about 200-nmi centers, the United States for example, is covered by something less than 100 base domains. The almanacs are issued perhaps on a bi-monthly basis to an individual distribution center serving the subject domain, as well as to regional centers serving domain groups. Each page in the almanac lists the coefficients for a civil day for a selected pair of LOP's. Hence a manual user contemplating a flight through one or more base domains requests the appropriate pages from the distribution centers, either in advance of the flight or at intermediate points while the flight is in progress. In this regard it is expected that all airports will subscribe to the almanac of their local base demain as well as to contiguous domains, and issue current sheets on request, using one of the several on-the-spot reproduction processes now available.

The master almanacs are prepared at a regional or national computation and distribution center. On the assumption that all the computation and printing is done at a single location, we estimate the average computation burden per day as follows:

(a) number of base domains: 100

(b) number of navigation modes in each domain: 2

(c) number of LOP-pairs per basepoint (i.e., pages per almanac) : 3

(d) number of rows per page: 49

(e) number of coefficients per row: 12

(f) number of milliseconds needed for the computation of each coefficient (slow machine): 10

(g) total computation time per day, for all almanacs: 60 minutes

(h) total printing time per day, at 600 lines per minute: 50 minutes

(i) time required per day to prepare master almanacs for the entire United States, using a single computer and a single printer but recognizing that one batch may be printed while the next batch is being computed: about one hour, or 4% timeload

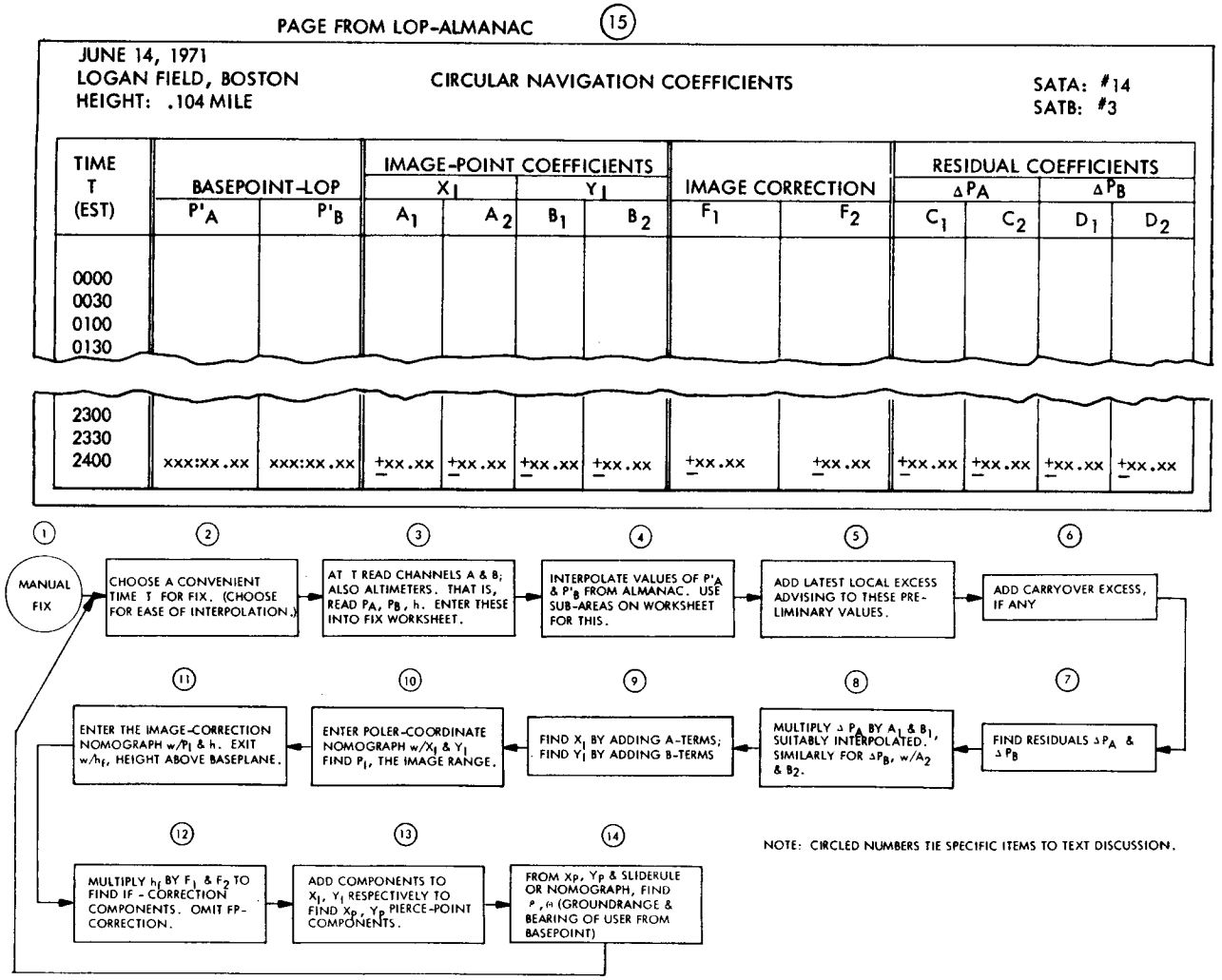

Figure 4-12. Flow Chart for Manual Fix and Page From LOP-Almanac

4.14 MANUAL RELATIVE NAVIGATION

The computation at the user is indicated in the flow chart of Figure 4-12. Block 3 refers to a Fix Worksheet,* which is a prepared form designed to take the user step-by-step thru the computation, and to provide suitably arranged blank spaces to receive the numerical entries. It is estimated that 4 by 7 inch card-formats will provide sufficient working space, even including the interpolation work space needed in blocks 4, 8 and 12.

The Polar-Coordinate Nomograph* referenced in block 10 is a single card the user may elect to carry among his working aids, which graphically converts cartesian coordinates to polar (or vice versa). The Image-Correction Nomograph* of block 11 is again a single card, which is entered with baseplane range and vehicle height, and exited with height of user above the baseplane.

4.15 CHART NAVIGATION

Figures 4-13 and 4-14 illustrate an alternative method of manual navigation, using a base chart and a LOP-almanac designed to give the appropriate coefficients for this option. When the preparation of this almanac is added to the computation load and account made for its 8 columns rather than 12, about 40 minutes of computation time are added, and about 35 minutes of print time. The limiting load-time (i.e., computation) is then about 100 minutes, or 7% capacity.

In the chart procedure the graphical construction which recovers the user position is made either directly on the geographic background or on conventional aeronautic flight charts. This allows the user to correlate immediately his position determination with visible landmarks or LOP-indications from other sources. Figure 4-15 is an improvised example of chart navigation, using an aeronautical chart around Boston's Logan Airport as a base.

4.16 BASEPLANE CORRECTIONS

Figure 4-16 shows some additional detail for relative navigation when the computation is automatic. In this case the foot-pierce correction need not be ignored as a nuisance as it is in manual computation, but is included in the correction loop.

The note in Figure 4-16 refers to still another possibility. The relative navigation intended in Figures 4-12 thru 4-16 assumes a baseplane tangent at the basepoint. The note refers to a computational procedure where the height of the baseplane above (or below) the basepoint is adjusted until the plane contains the user.

4.17 NAVIGATION IN REVERSE

Figure 4-17 shows the flow of manual computation when the inverse navigation problem faces the user: given a knowledge of position, what should the instruments read?

The first of these situations, block 1, occurs at the onset of a trip or having touched down at, or passed close to, a well-known intermediate point. It is initialization of the

---

* These devices will be detailed in the final report.

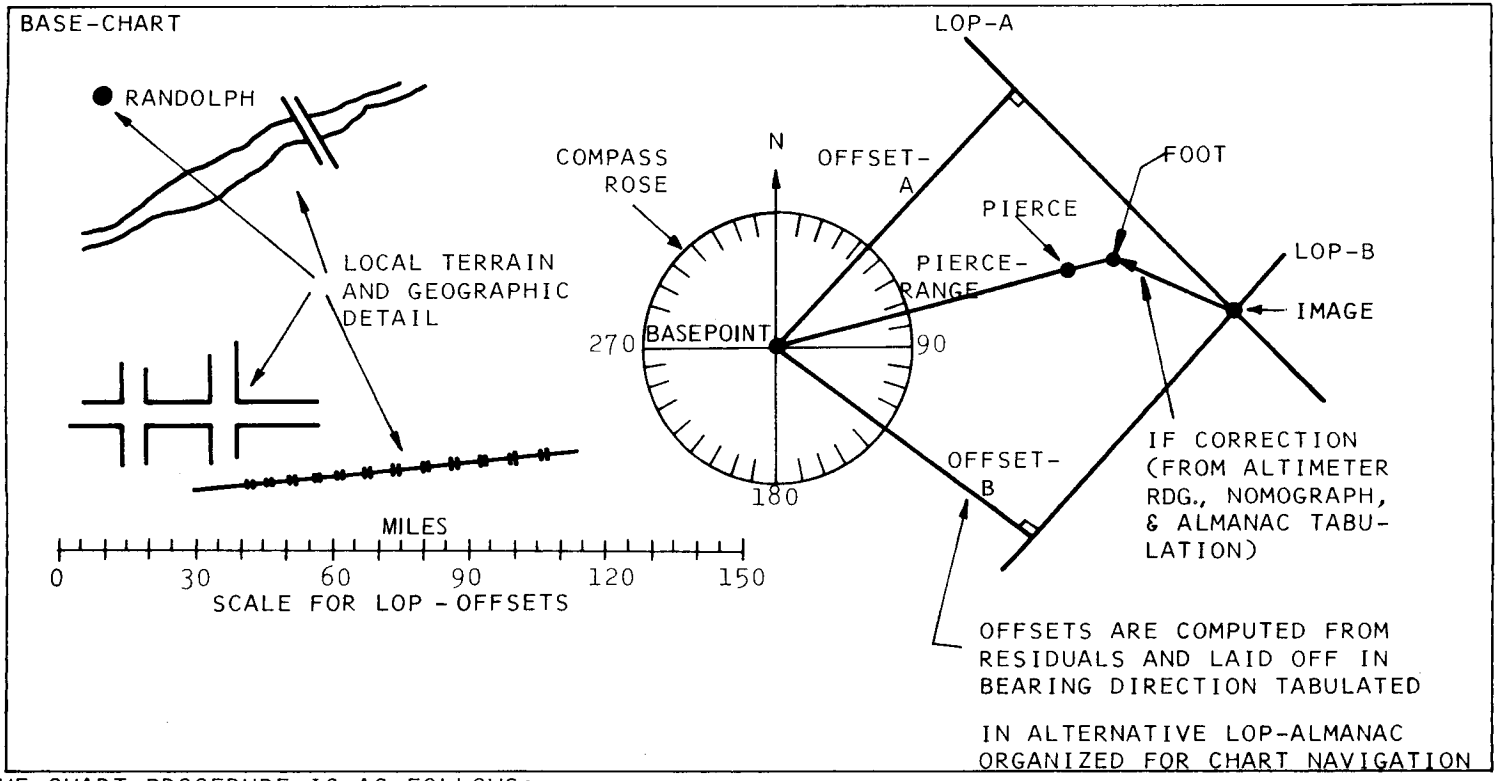

NOTE: THE CHART PROCEDURE IS AS FOLLOWS:

(1) FIND THE RESIDUALS BETWEEN THE LOP-METER READINGS, AND THE TABULATED BASEPOINT LOP'S.
(2) LAY OFFSETS ALONG GRADIENT DIRECTIONS, WITH LENGTHS GIVEN BY GRADIENT MULTIPLICATION OF RESIDUALS
(3) ERECT PERPENDICULARS, AND FIND INTERSECTION AT IMAGE-POINT
(4) APPLY IF-CORRECTION, USING MULTIPLIER AND DIRECTION TABULATED IN ALMANAC
(5) THE GEOGRAPHIC LOCATION IS READ OFF THE CHART BACKGROUND. GROUND-RANGE IS AVAILABLE FROM BACKGROUND CIRCLES. NOTICE THAT OFFSET LENGTHS ARE IN BASEPLANE LENGTHS, NOT GROUND LENGTHS. THE BASEPLANE SCALE IS LINEAR; THE GROUND-RANGE SCALE IS NOT. HOWEVER, THE DIFFERENCES MAY BE NEGLECTED FOR CHART NAVIGATION.

Figure 4-13. Alternative Manual Fix: Chart Navigation

JUNE 14, 1971
LOGAN FIELD, BOSTON
HEIGHT: .104 MILE

SAT A: #14
SAT B: #3

CIRCULAR NAVIGATION PARAMETERS

TIME T (EST)	BASEPOINT-LOP		LANE-WIDTH				IMAGE-FOOT CORRECTION	
			LOP-A OFFSET		LOP-B OFFSET			
	P'_A	P'_B	L_A	ϕ_A	L_B	ϕ_B	F	ϕ_F
0000								
0030								
0100	xxx:xx.xx	xxx:xx.xx	±x.xxx	xxx.x	±x.xxx	xxx.x	xx.xx	xxx.x

NOTE: NO SPECIAL COLUMNS NEED APPEAR FOR RECOVERY OF THE RESIDUALS, GIVEN THE LOCATION. FOR THIS PROBLEM THE RESIDUALS ARE FOUND BY REVERSING THE FIX PROCEDURE, THAT IS,

(1) TO THE BASEPLANE POSITION (PIERCE-POINT), APPLY THE FI-CORRECTION
(2) ERECT THE LOP'S PERPENDICULAR TO THE TABULATED DIRECTIONS
(3) DRAW OFFSET THRU THE BASEPOINT
(4) DIVIDE THE OFFSET LENGTHS BY THE TABULATED LANE WIDTHS

Figure 4-14. Alternative Almanac Format for Chart Navigation

LOP-meters. The P_A and P_B referred to in block 9 are the final LOP-values to be inserted. The band number components of each LOP is inserted via the INITIAL SET controls of Figure 4-2. For circular one-way navigation the lane number and line number of LOP-A are inserted via the A-channel variable delay, shown in Figure 4-18. The lane and line components of LOP-B are inserted via the B-channel delay. These delays are adjusted until the contents of the respective LOP-meter are as required for time T, and then the instrument is released; that is, the variable delays retain their last setting and the meters are free to follow the phase excursions of the incoming signal. For hyperbolic navigation there is of course no tone-LO and no variable delays to set; the lane and line numbers find their natural values on comparing the incoming phases.

Block 11 introduces the procedure applicable to cross-over; that is, the transition from one base domain to another. It is similar to initialization, and requires some

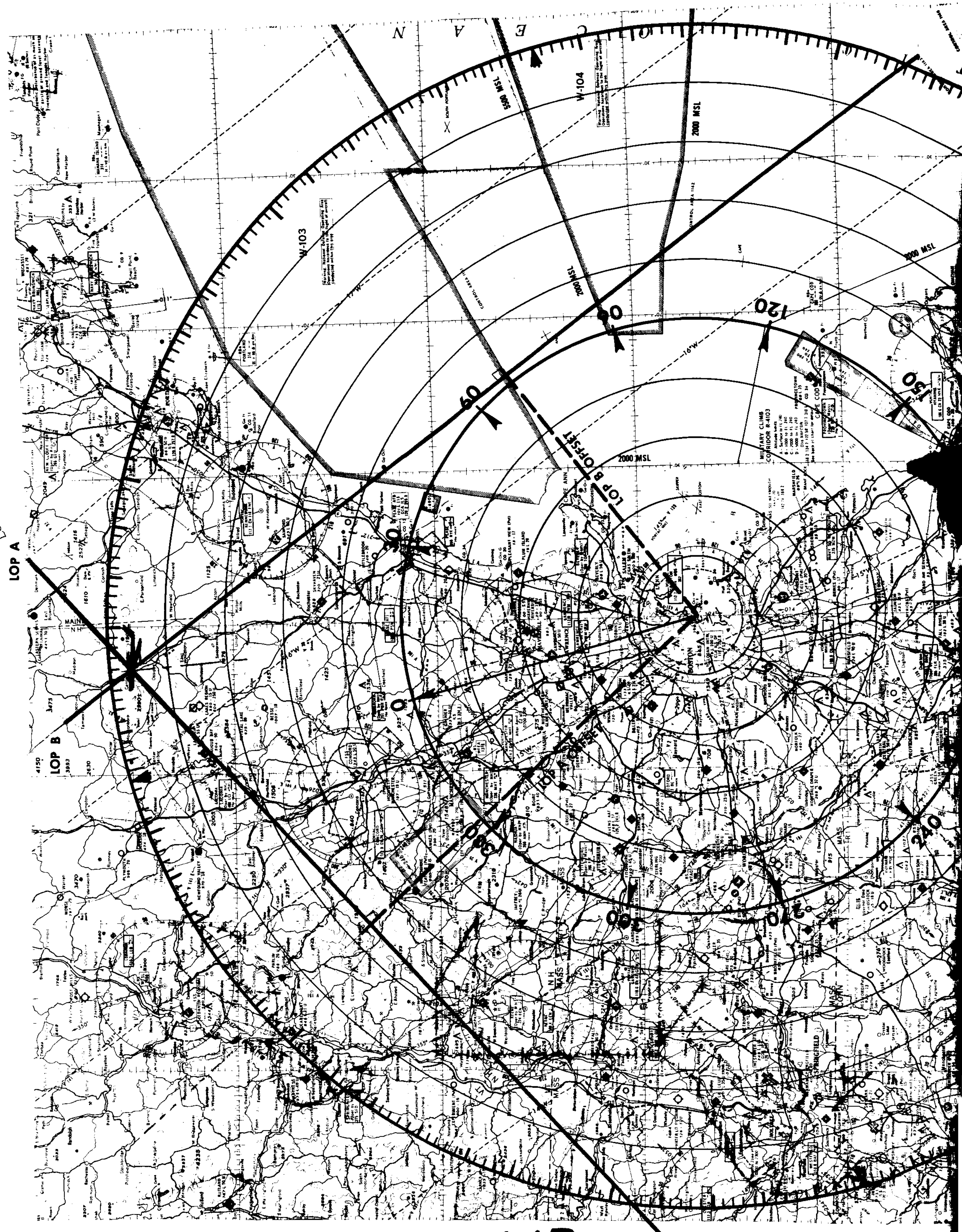
LOP A
LOP B
LOP B OFFSET
W-103
W-104
5500 MSL
2000 MSL
MILITARY CLIMB CORRIDOR R-4103
BOSTON
CAPE ANN
MAINE
N H
MASS
CONN
SPRINGFIELD
60
90
120
150
240
O C E A N

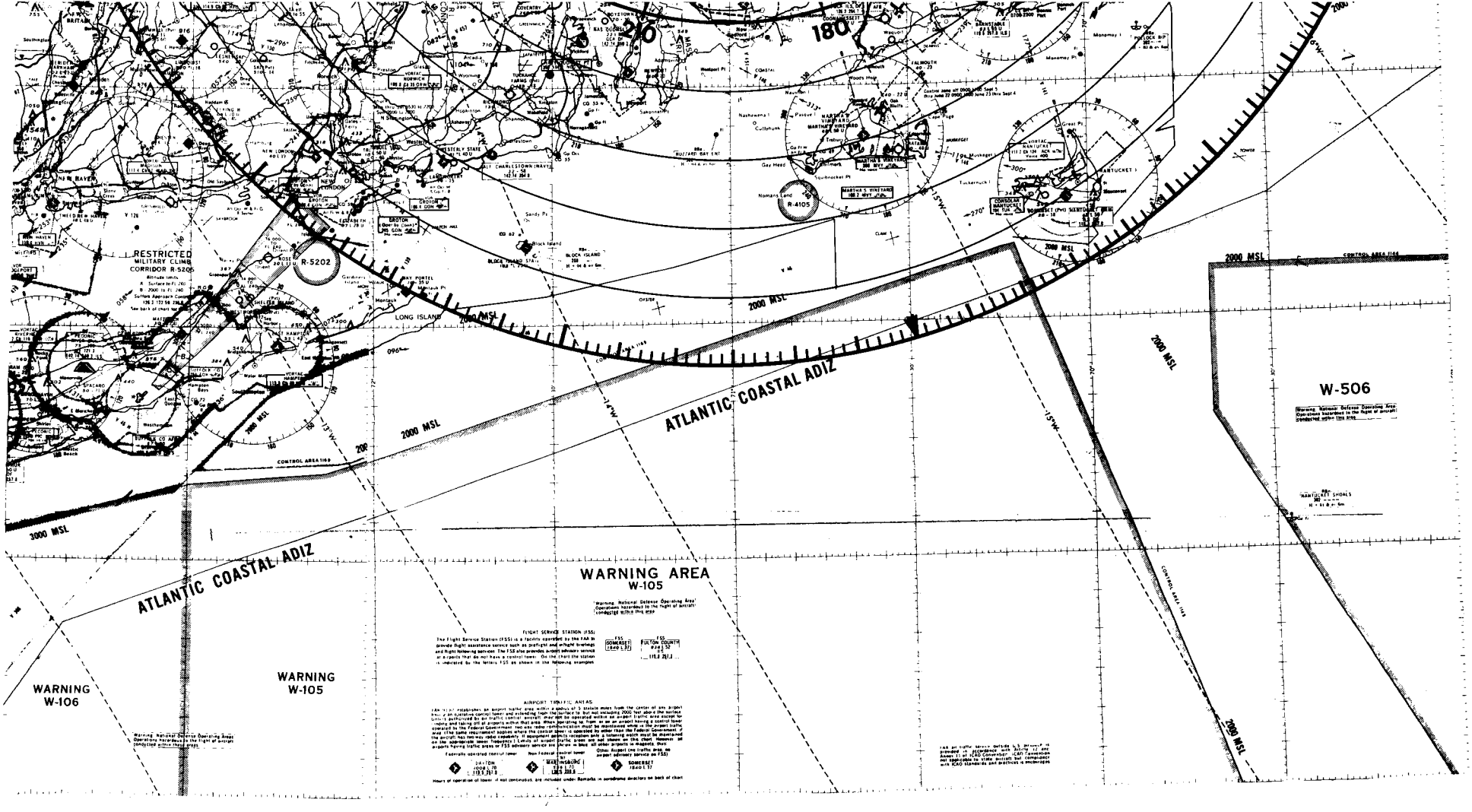

Figure 4-15. Boston Region Satellite Navigation Chart

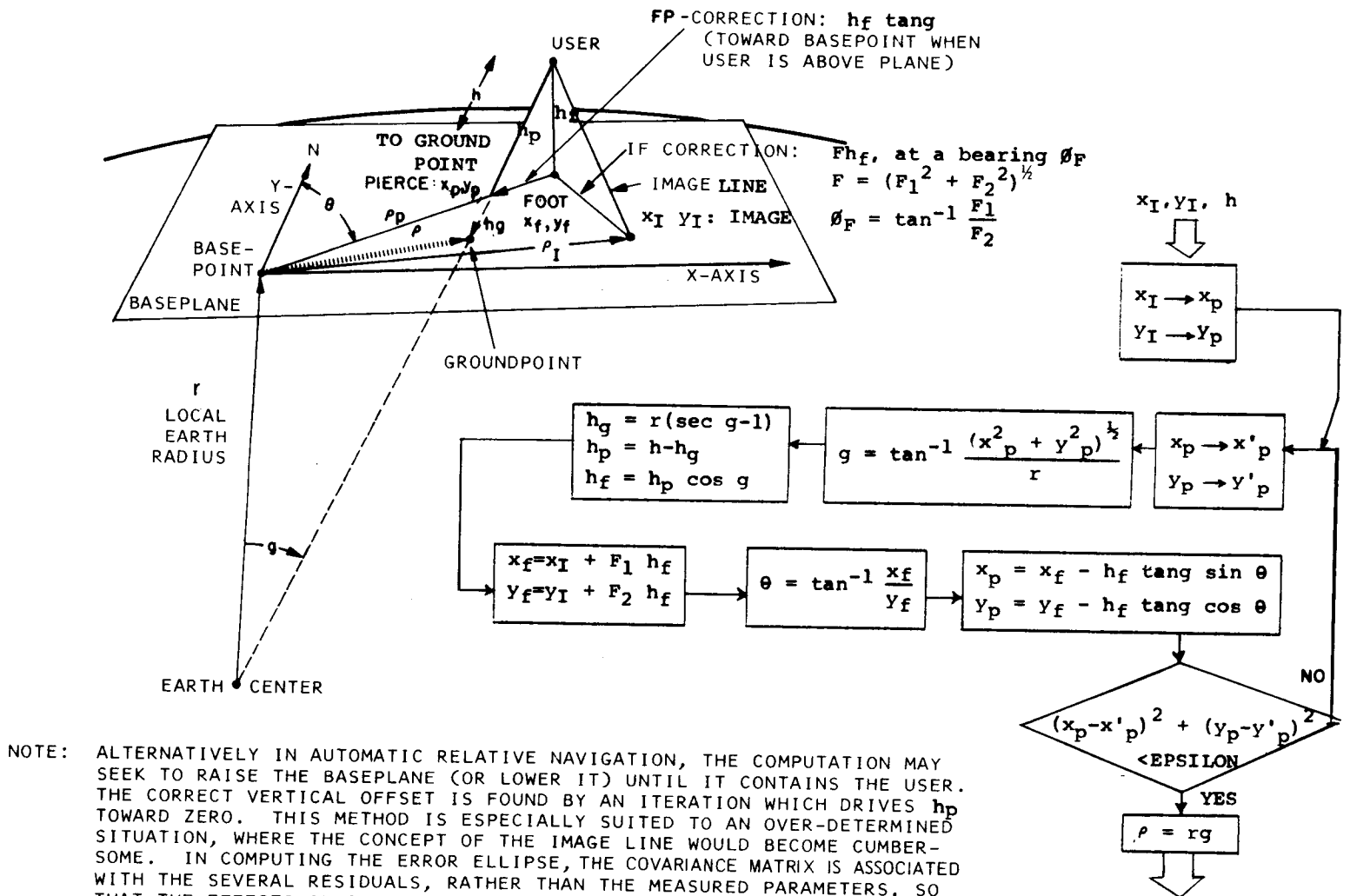

NOTE: ALTERNATIVELY IN AUTOMATIC RELATIVE NAVIGATION, THE COMPUTATION MAY SEEK TO RAISE THE BASEPLANE (OR LOWER IT) UNTIL IT CONTAINS THE USER. THE CORRECT VERTICAL OFFSET IS FOUND BY AN ITERATION WHICH DRIVES h_p TOWARD ZERO. THIS METHOD IS ESPECIALLY SUITED TO AN OVER-DETERMINED SITUATION, WHERE THE CONCEPT OF THE IMAGE LINE WOULD BECOME CUMBERSOME. IN COMPUTING THE ERROR ELLIPSE, THE COVARIANCE MATRIX IS ASSOCIATED WITH THE SEVERAL RESIDUALS, RATHER THAN THE MEASURED PARAMETERS, SO THAT THE EFFECTS OF COMMON ERRORS ARE PROPERLY DISCOUNTED.

Figure 4-16. Baseplane Correction Loop in Automatic Relative Navigation

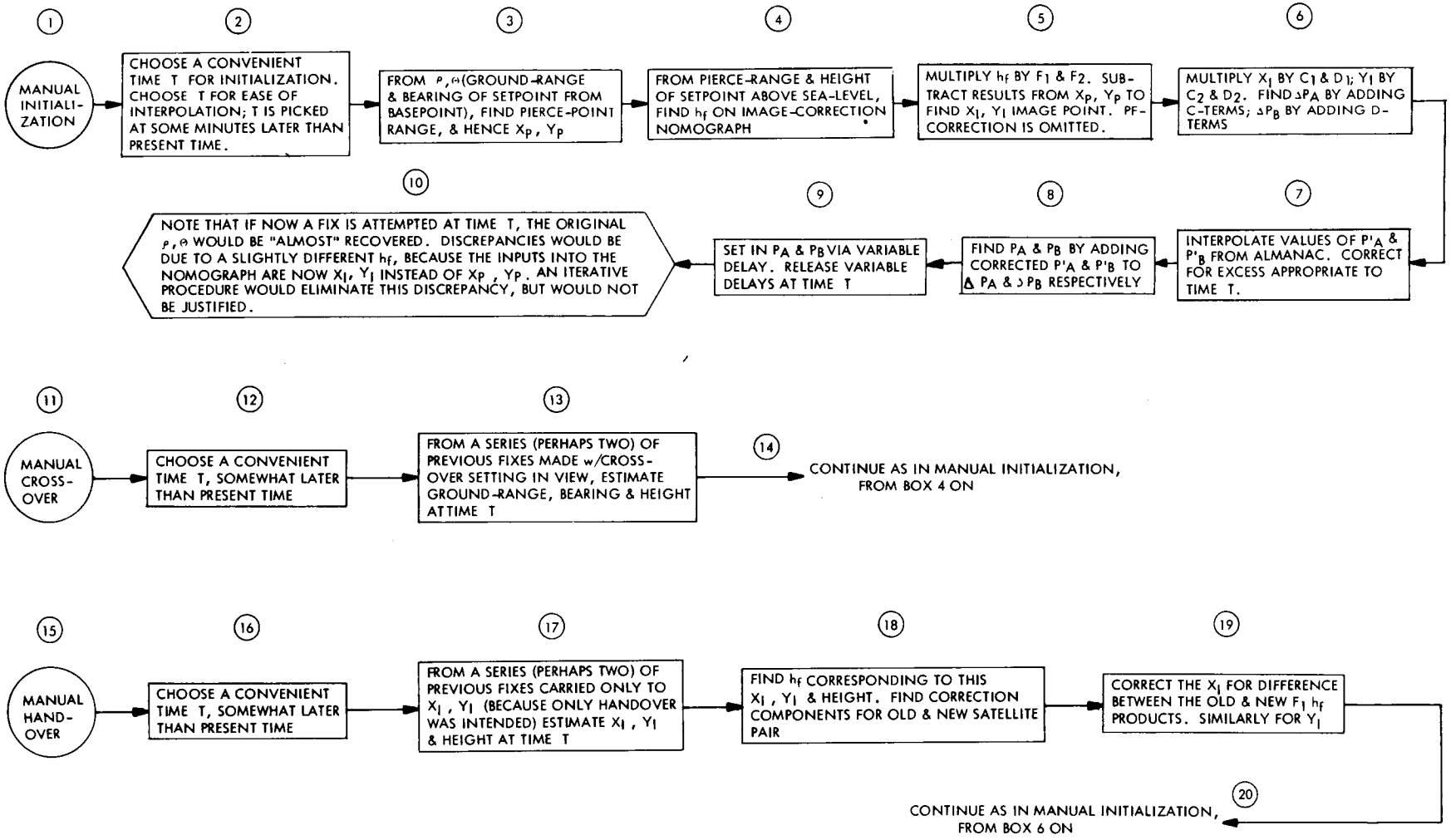

Figure 4-17. Flow Charts for Manual Intialization, Carry-Over, and Handover

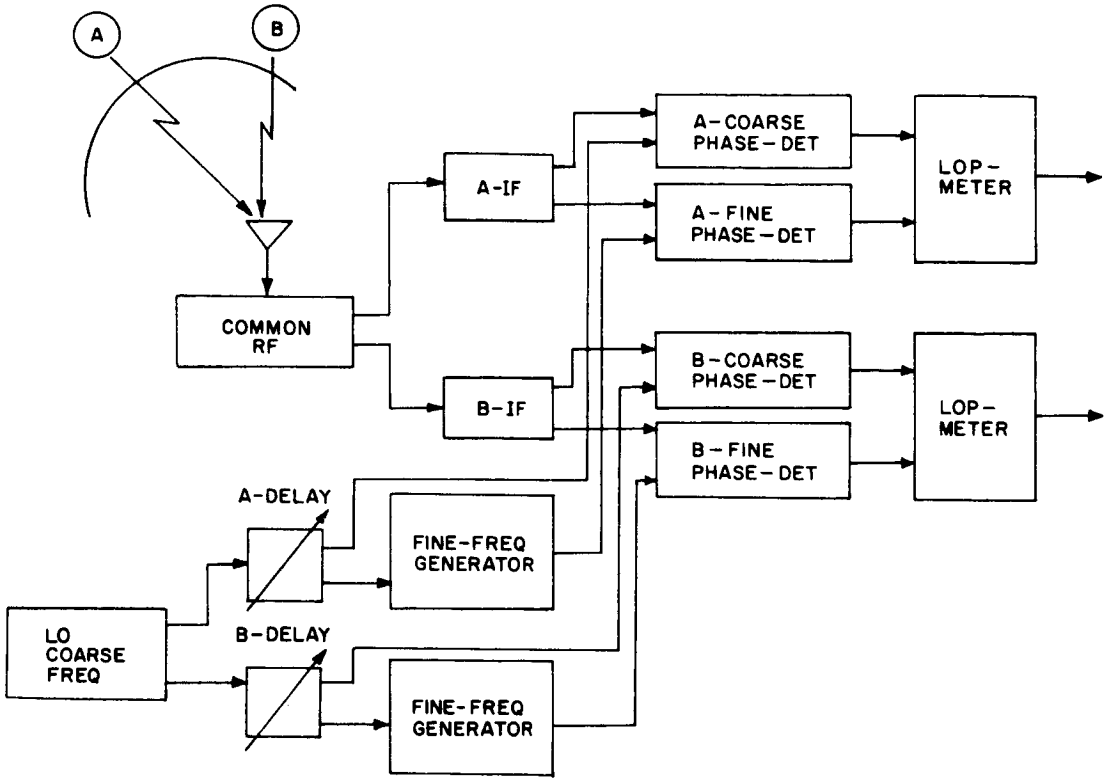

Figure 4-18. Variable Delay Control of LOP-Meter: Circular, One-Way Navigation

in-flight preparation as specified in block 13. Block 15 refers to the dropping of one LOP (perhaps because of setting of one of its associated satellites below the communications horizon), and its replacement by another LOP. This is in-flight handover. Again special preparations are needed, as specified in block 17.

4.18 TWO-WAY NAVIGATION

The navigation procedures discussed up to this point refer to one-way navigation. For active (i.e., two-way) navigation such as required in air traffic control, the situation is not changed in essentials. Of course, we do not contemplate manual computation in such a case; furthermore, the hyperbolic mode is not relevant, and explicit relative navigation is not necessary. Hence two-way navigation devolves to absolute circular navigation, automatically computed.

Hyperbolic navigation is not used in ATC because where three satellites are available to position a user, information is discarded in merely settling for two range-differences; instead, three ranges are observed, which over-determine the user's position, resulting in an uncertainty ellipse somewhat tighter than the ellipse associated with the two-LOP fix, even allowing for the apparent gradient advantage of the hyperbolic mode.

Explicit relative navigation is not necessary in ATC because a set of nominal absolute fixes for a cluster of users in some locality, although each has moderate error, generally results in a derived set of relative positions of considerably improved accuracy because of common error cancellation. However Figure 4-19 illustrates an explicit relative procedure which could be used for ATC computation. It is analogous to the one-way relative navigation algorithm already discussed, and is given here to round out the catalog of options available to the center.

4.19 ABSOLUTE VS. RELATIVE NAVIGATION

Figure 4-20 contrasts the absolute and relative navigation procedures. In addition to the notes included in that figure, we add the following distinguishing characteristics:

(a) absolute navigation

  (1) compensation in some measure for refraction bias, by computation.
  (2) operating in large time and space resulting in tone-LO drifts non-compensating refraction errors, and non-compensating ephemeris errors.
  (3) successive basepoints are stated in absolute coordinates to allow calculation of basepoint parameters from computed satellite position.

(b) relative navigation

  (1) as a result of the setting process (initialization, crossover, or handover) cancellation in large measure of tone-LO ephemeris bias and refraction bias.
  (2) operates in restricted time and space, so that these cancellations remain effective.
  (3) manual navigator need not know the absolute coordinates of his basepoint.

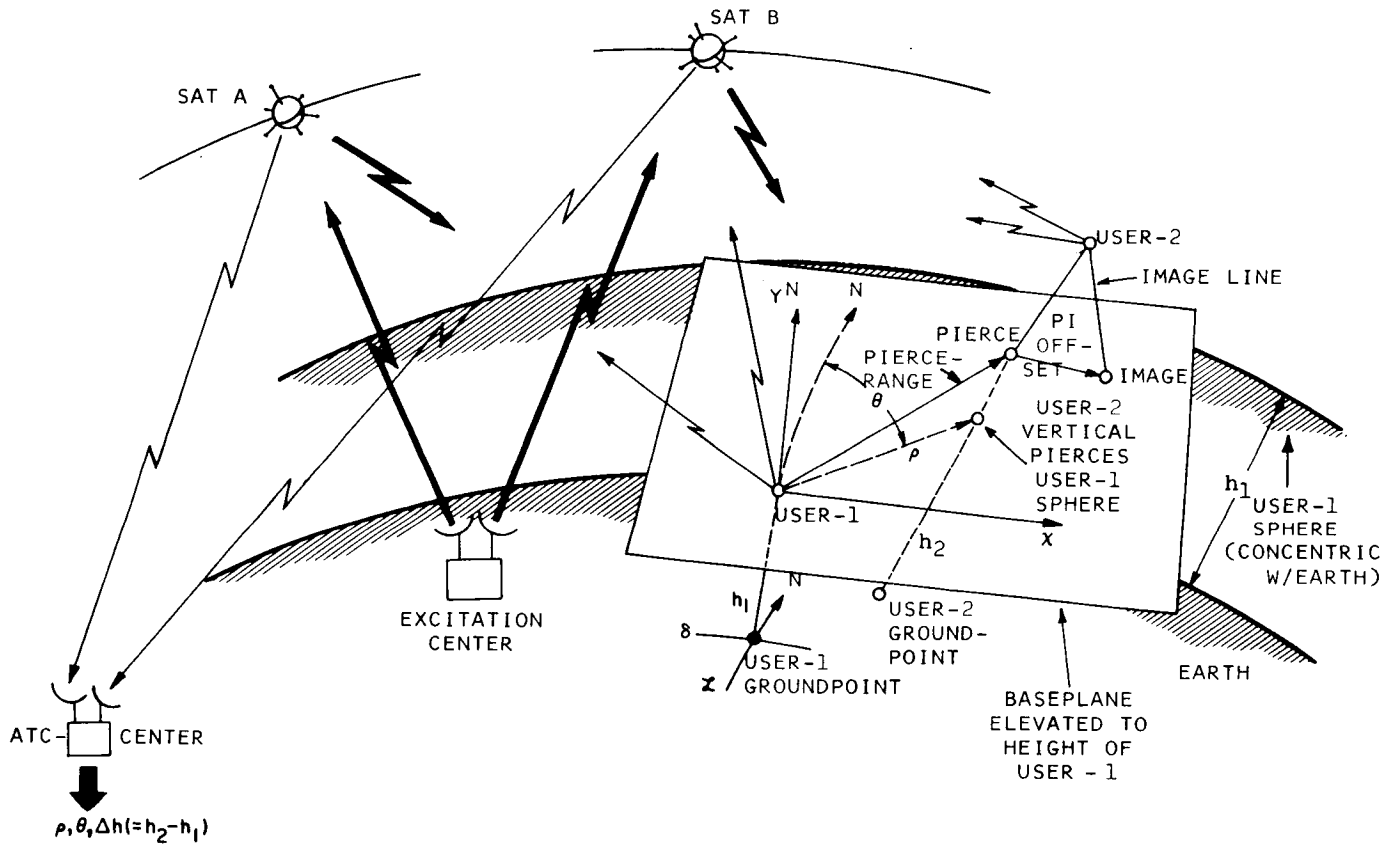

NOTE: IN THIS NAVIGATION MODE, THE ATC ASSUMES A BASEPOINT AT USER-1, AND FINDS HIS ABSOLUTE POSITION WITH MODEST PRECISION. THE ABSOLUTE POSITION (δ, χ) IS USED TO FIND THE EXPANSION COEFFICIENTS IN THE EXPRESSIONS GIVING THE PIERCE-RANGE. THE RESIDUALS APPEARING AS ARGUMENTS IN THESE EXPRESSIONS ARE GIVEN DIRECTLY BY THE PHASE DIFFERENCES AVAILABLE AT THE ATC-CENTER. THESE DIFFERENCES ARE ALREADY FULLY BIAS-COMPENSATED.

Figure 4-19. Alternative Two-Way Relative Navigation

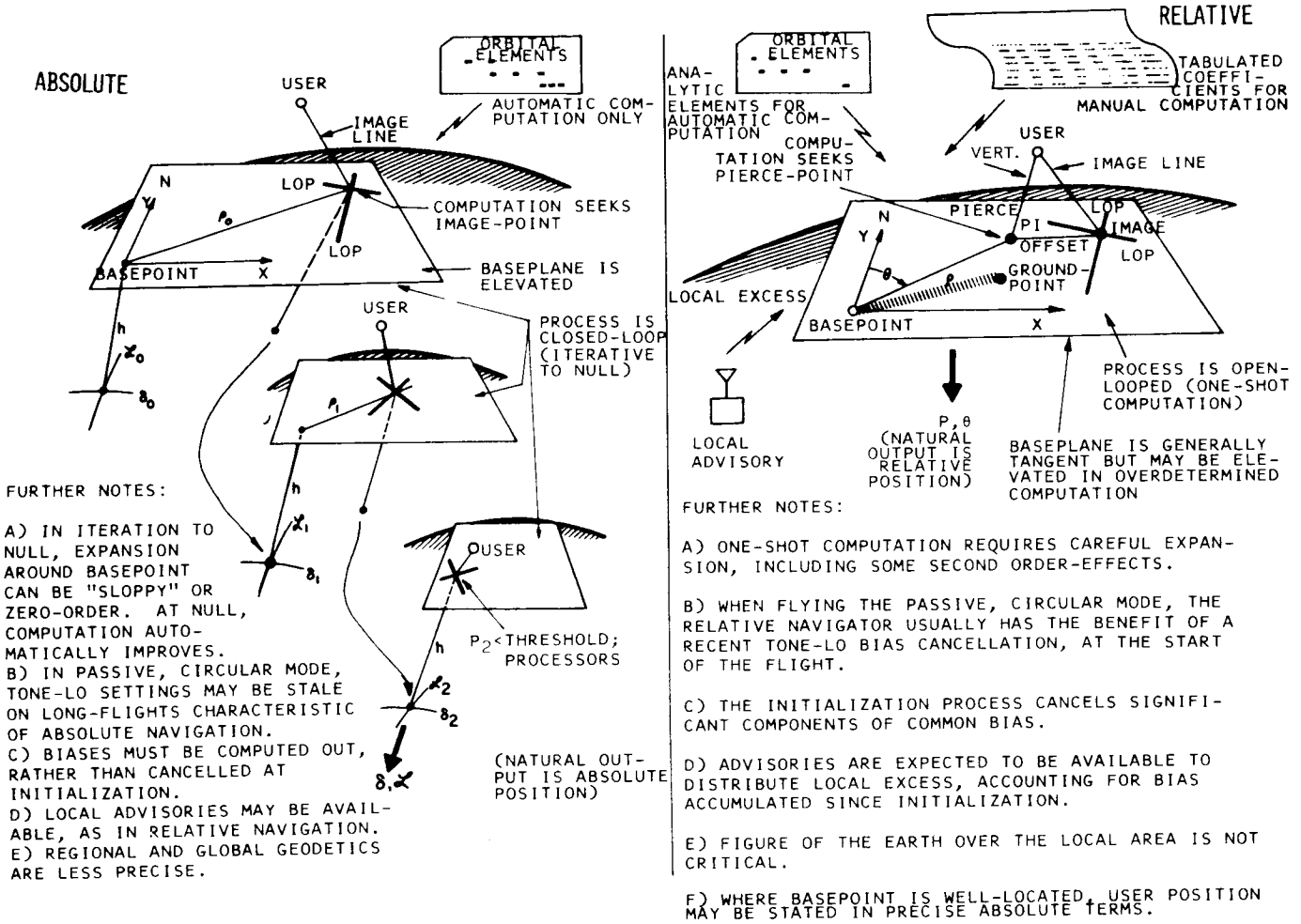

Figure 4-20. Contrasts Between Absolute and Relative Navigation; Both Processes Involve Only Straight-Line Geometry

Section 5

ERROR TRANSFORMATION BEHAVIOR

5.1 GEOMETRIC DILUTION OF PRECISION (GDOP)

GDOP is a computer program that generates details and statistics on the transformation of errors between observed parameters and plan position in the horizontal plane. The present program considers the geometric aspects insofar as they amplify or attenuate the input errors; a later development will game the input errors as well, and generate outputs in terms of operational error, rather than error ratios.

5.2 INPUT DATA

The program accepts an orbiting population consisting of two or three circular orbits, each of arbitrary inclination, ascending node, height, and number of satellites, uniformly disposed around the orbit. The user is described in terms of his position, his height above the earth, and the minimum elevation angle capability of his antenna. The computational modes include a specification of hyperbolic or circular navigation, or both.

5.3 PROGRAM PROCESS

The program proceeds by moving the user from one latitude to another through an arbitrary number of (uniformly spaced) latitude steps. At each latitude, the user is moved in longitude through 360° in equally spaced discrete steps of arbitrary increment. Each longitudinal position of the user constitutes a frame, at which a variety of details, averages, and dispersions are calculated.

5.4 COMPUTATION AND OUTPUTS

Each frame constitutes a specific relative geometry between the user and the orbiting system; however, the inter-orbital phase relations among the satellites in their separate planes is a degree of freedom which must be made specific in order to proceed with the computation. Because the respective periods in the orbital planes can never be quite commensurate one with another (nor does there seem to be any point in operating the system to make them commensurate) a long-term average situation was generated by computing the error ellipses at discrete phase steps, running thru the spectrum of all possible phase relations.

In the hyperbolic mode for example, the computation of a frame begins with a determination of the three LOP-gradients, for the central situation in each orbit. The central configuration is the one wherein the two satellites (in a given orbit) involved in the hyperbolic LOP are symmetrically disposed with respect to the user, that is, they are at equal elevation angles. The program output lists these elevation angles, the accompanying gradients, and their associated azimuthal directions.

The program now takes the three gradients in pairs, and for each gradient pair computes the maximum, minimum, and mean dimensions of the confidence ellipse, listing

these dimensions in an output tabulation. From a consideration of these confidence ellipses, the program decides which of the orbital pairs it will couple in a computation of the hyperbolic details for the user-orbit geometry implicit in this particular frame. The details consist in the dimensions of all confidence ellipses generated by stepping the inter-orbital satellite phases through their full spectrum. An output tabulation lists the weighted averages of these dimensions and their standard deviations over all the detailed ellipses.

Of course, where only two orbital planes are inputted rather than three, there is no competition to resolve at each frame among contending orbital pairs, and the program launches immediately into a computation of details. Also, for circular navigation the computation proceeds essentially as described above, except that the central configuration is the one which gives a maximum elevation angle at the user.

5.5 OUTPUT SUMMARY

In addition to the tabulations of frame details and statistics the program also generates an overall average confidence ellipse, giving the respective average of the maximum, minimum, and geometric mean dimensions of all the detailed confidence ellipses on that latitude, and the standard deviations for these overall distributions. Finally, the output summary also lists the percentage of frames on that latitude for which a LOP-choice exists, as opposed to those situations where only one pair of LOP's offer; these percentages constitute a summary of the geometric coverage provided by the postulated orbital system.

5.6 SUMMARY PLOTS (Illustrations presented at end of Section)

Figures 5-1, 5-2, and 5-3 are presentations of the overall latitudinal average fix confidence for several representative system configurations. In the Figure 5-3 set of plots (consisting of 11 illustrations, Figures 5-3a through 5-3k), the control plot is shown in Figure 5-3a for a set of standard conditions, against which variation runs were made, to show the sensitivity of the confidence ellipse to each important geometric parameter.

In particular, what is plotted in these figures is the average of the (geometric) mean dimension of all detail confidence ellipses at a particular latitude, as a function of user latitude. The result is a single number, the average fix confidence characterizing the GDOP encountered at this latitude. The fix confidence may be interpreted as a number which divides the error in the measured parameter (range in circular navigation, range-difference in hyperbolic navigation) to produce the error in plan-position. Hence confidence coefficients less than one represent error amplification; coefficients greater than one represent error attenuation. In the plots the standard condition results are shown as solid lines; the variation results are shown dotted.

Also, the variation conditions are shown in a table by means of an entry only at the variation parameter. Parameters not varied in a particular run are indicated in the variation table by a short dash. The figures show results for both hyperbolic and circular modes, in each case for one-way (passive) navigation.

5.7 THE STANDARD PLOTS

As a preliminary to the variational plots, Figure 5-1 shows the summary results for the standard situation, consisting of three mutually orthogonal orbital planes (one equatorial, two polar) of synchronous height, each deploying six satellites with uniform spacing. The user is 6 nmi above sea level, with an antenna elevation cut-off at 5°. The plots show the maximum, minimum, and (geometric) mean dimensions for both the hyperbolic mode (solid lines), and circular mode (dashed lines).

With respect to the behavior of the mean, notice that the confidence coefficients for hyperbolic navigation are uniformly greater than one (i.e., error attenuation), with a relatively small variation over the latitude band, ranging from about 1.02 near 40° latitude to about 1.06 at the equator and the poles.

On the other hand, the mean coefficients for circular navigation are seen to amplify measurement errors through all latitudes, with minimum amplification (highest divider) occurring in the middle latitudes, with a worsening toward the equator and especially toward the poles. It must be remarked, however, that the error which the circular one-way mode amplifies significantly (doubling it through the important latitude band) is perhaps 70% of the error encountered in a range-difference (hyperbolic) system, where two ranges enter the determination of a single LOP. The GDOP advantage of the hyperbolic system for the standard conditions is therefore better estimated as 1.4 to 1, rather than 2 to 1.

Figure 5-2 shows the standard deviations which accompany these averages. Notice that the hyperbolic mode distributions are much better behaved in terms of variation; in particular the deviation on the geometric mean dimension is uniformly less than half that for the circular mode, and that the worst hyperbolic behavior is better in this regard than the circular mean. In any case, the dispersion of confidence ellipse dimensions over the latitudinal band shows a relatively consistent error transformation for either mode throughout the navigation domain.

5.8 USER HEIGHT VARIATION

Figure 5-3a shows the effect of user height on the confidence coefficient. The sensitivity is so slight that moving the user from 6 nmi (the standard height) to sea level (the variational height) results in no discernible difference on the plot: the variational dotted lines fall on the standard solid lines, for both circular and hyperbolic navigation.

5.9 MINIMUM ELEVATION VARIATION

Figure 5-36 shows the effect of minimum elevation angle of the user antenna: the hyperbolic coefficients do not change perceptibly at any latitude while the circular coefficients are unchanged through the main latitude band. The plots reflect the fact that for standard conditions the number of optimum hyperbolic opportunities are not affected by the elevation change, while for circular navigation they are affected only at the latitude extremes, and then moderately.

These results have some interesting implications. If geometric optimality is not very sensitive with respect to antenna elevation cut-off, the antenna taper design becomes more tractable, antennas become smaller and lighter, and installations more economical. Furthermore, analysis shows that the extent of multipath interference is quite sensitive to elevation cut-off, so that a favorable trade-off situation exists, where modest geometric compromises are made in exchange for significant multipath suppression.

In Section 5.14, we will discuss another geometric aspect of an early elevation cut-off, that of coverage opportunities, (that is, the opportunities available to the user to make a fix in a given mode). It will be seen that his primary opportunities are not degraded at all, but some back-up capability is reduced.

5.10 PLANE VARIATION

Figures 5-3c, d, and e show the effect of considerable variation in orbital plane parameters. In Figure 5-3c the nominal equatorial orbit is operated at 10° inclination rather than 0°; in Figure 5-3d one of the nominally polar orbits is operated at 80° inclination; and in Figure 5-3e, the angle between the polar orbits is 80° rather than 90°. In all the cases, the geometric effect on hyperbolic navigation seems negligible while circular navigation is only moderately affected, and virtually not at all in the central latitudinal band. Again, the implications of these results are valuable, in that precision launches and insertion are not indicated, at least with respect to orbital plane, nor are plane-keeping controls and fuels required once aloft.

5.11 ORBITAL HEIGHT VARIATION

Figures 5-3f and 5-3g show the effect of variation in orbital height. In Figure 5-3f the height of one of the polar orbits was increased 1000 nmi beyond synchronous height; in Figure 5-3g all three orbital heights were increased 1000 nmi. The effect of this change on either hyperbolic or circular navigation is seen to be negligible, so that orbital height and, by implication, eccentricity need not be carefully controlled, either at insertion or in operation.

5.12 SATELLITE VARIATION

Figures 5-3h, i, and j show the effect of changing the numbers of satellites in the orbits. In Figure 5-3h, the equatorial satellites are decreased from 6 to 5; in Figure 5-3i one of the polar orbits is operated at 5; and in Figure 5-3j, all orbits are operated at 5. In all cases, the decrease in the number of satellites is seen to improve the confidence coefficients uniformly: the hyperbolic coefficients rather significantly, and the circular coefficients mildly.

This seeming paradox (of improved coefficients) is explained by the improvement in LOP-gradient with decreasing elevation angle. With 5 equally spaced satellites in orbit, the average elevation angle involved in a fix is somewhat reduced, with respect to a 6-equally-spaced-satellite case. Also it will be seen in Figure 5-4 that the LOP availability is virtually unaffected, for either primary or secondary opportunities.

The full implications of these results cannot be weighed until more specific information is available on the economics of launch and multiple-seeding, the frequency of replenishment, and the statistics of refraction degradation with approach to the horizon. It is possible that these results will have more influence on the strategy of navigation given an operational system, than they will on the system configuration itself.

5.13 ORBITAL SYSTEM VARIATION

Figure 5-3k shows the effect of a major change in the orbital system. While the standard configuration is three orthogonal planes, one equatorial and two polar, the variation system is three planes concurrent in the nodes, one equatorial and two at 60°.

The hyperbolic coefficients are seen to degrade uniformly from error attenuation to error amplification, with the degradation becoming rather marked in the polar regions. For circular navigation the effect is an improvement over the upper half of the latitude band, and a degradation over most of the lower half. These results indicate that a system designed primarily around the circular mode may benefit from configurations such as the one explored here, but unless subsequent detailed simulation shows more promise, the range of improvement does not justify the near-deterioration of the hyperbolic mode.

5.14 COVERAGE CHART

Figure 5-4 shows the changes in LOP-availability with selected variations from the standard conditions. The upper presentations show the situation for the hyperbolic mode; the lower chart for the circular mode. The singly-hatched areas show the availability of exactly two LOP's; the crossed-hatched area shows the availability of three LOP's, giving a choice or a back-up.

Notice that all variations shown, at all latitudes and in both modes, have at least primary coverage; that is, all areas are hatched. Also for any variation as well as for the standard, there is little to distinguish the hyperbolic coverage from the circular coverage.

The change in antenna at cut-off from 5° to 15° causes the most noticeable change in coverage, at low and high latitudes. However, a primary opportunity always remains; it is only the back-up availability which is affected at these latitudes. On the other hand the decrease in satellite numbers from 6 to 5 has only a mild affect on LOP availability. Finally, the change in orbital system to the nodal-concurrent configuration improves the back-up availability at the equator and the poles, and degrades it slightly in the middle latitudes.

5.15 LATITUDE PLOTS

Figures 5-5 through 5-8 show the mean confidence coefficients as a function of user longitude, on selected latitudes, for the standard configuration (Figures 5-5 and 5-6) and the nodal-concurrent configuration (Figures 5-7 and 5-8); in all plots, latitudes 0°, 15°, and 30° are shown with solid lines; and latitudes 45°, 60°, 75° and 90° with dashed lines, in an attempt to separate the plots where they fall on each other, and make them more readable.

Figure 5-5 presents the longitudinal behavior for the standard, hyperbolic mode. Notice that the plots cluster over all latitudes, and within any latitude, especially as compared to the behavior in the succeeding figures. Figure 5-6 gives the standard, circular behavior, in which sizeable swings occur within some latitudes (e.g., 0°) and among the latitudes. Similarly, Figures 5-7 and 5-8 show the variational hyperbolic and circular modes respectively, again showing considerable dispersion both within and between the user latitudes.

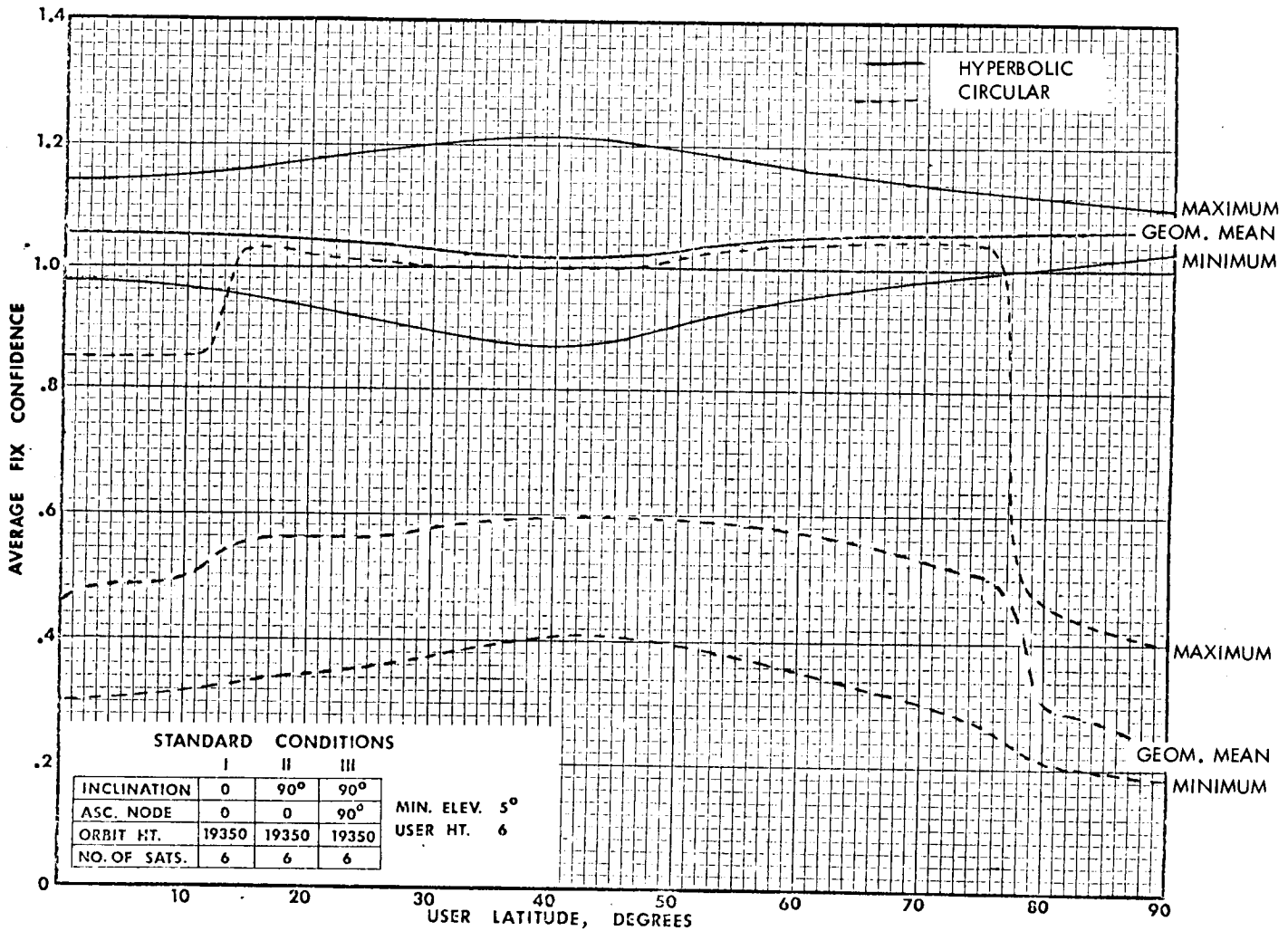

Figure 5-1. Average Fix Confidence vs User Latitude; Standard Conditions

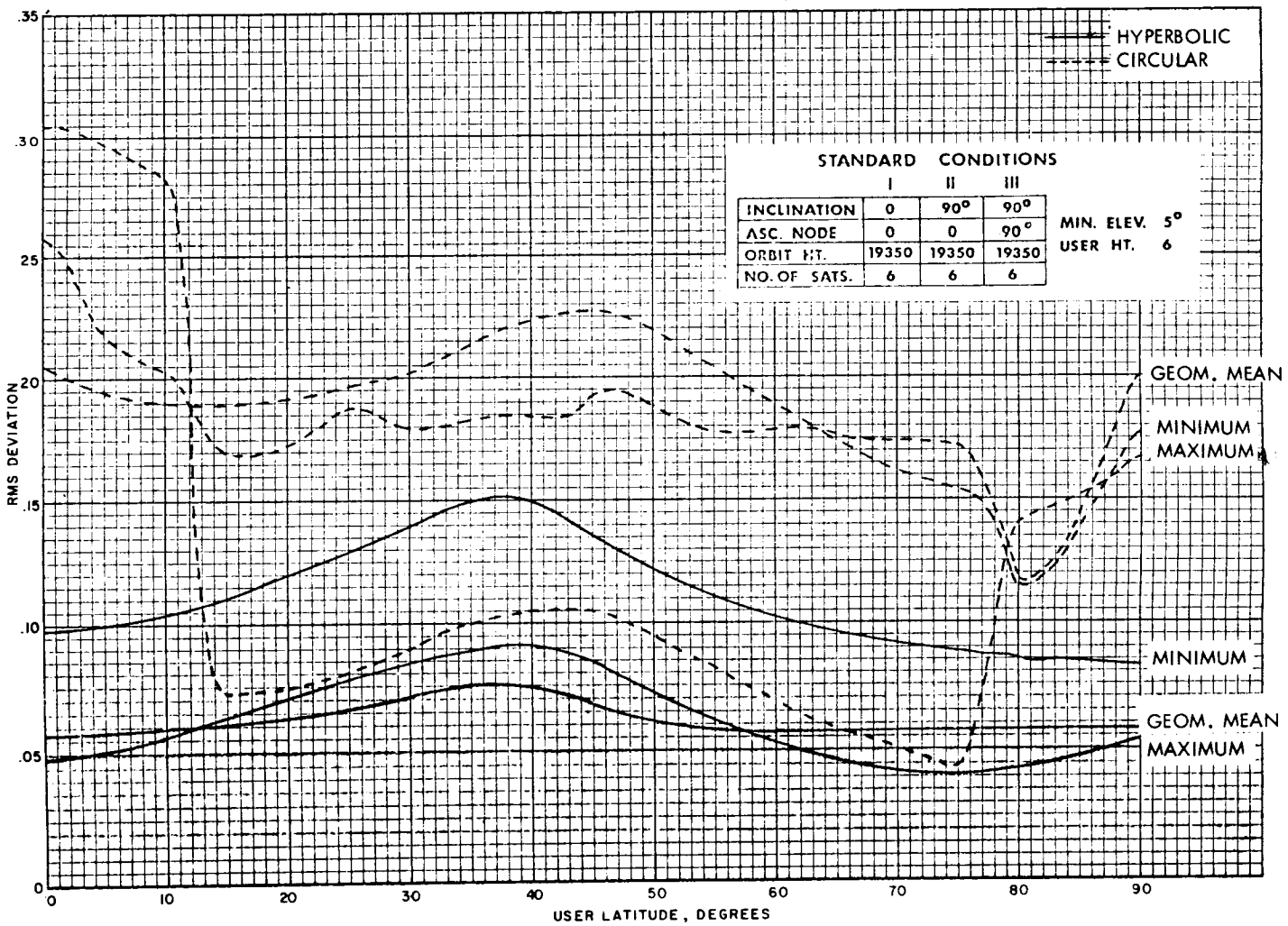

Figure 5-2. RMS Deviation in Fix Confidence vs User Latitude, Standard Conditions

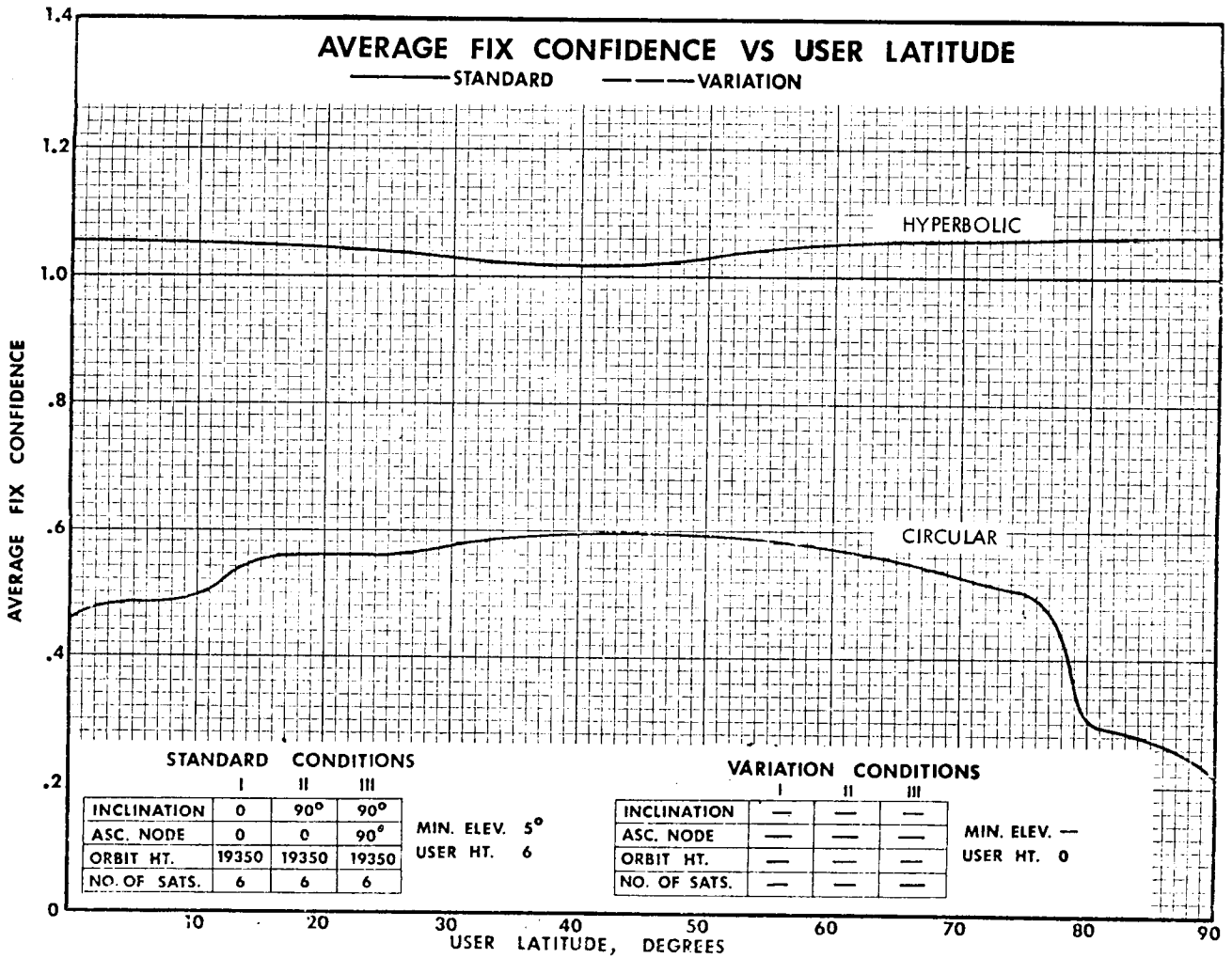

Figure 5-3a. Average Fix Confidence vs User Latitude

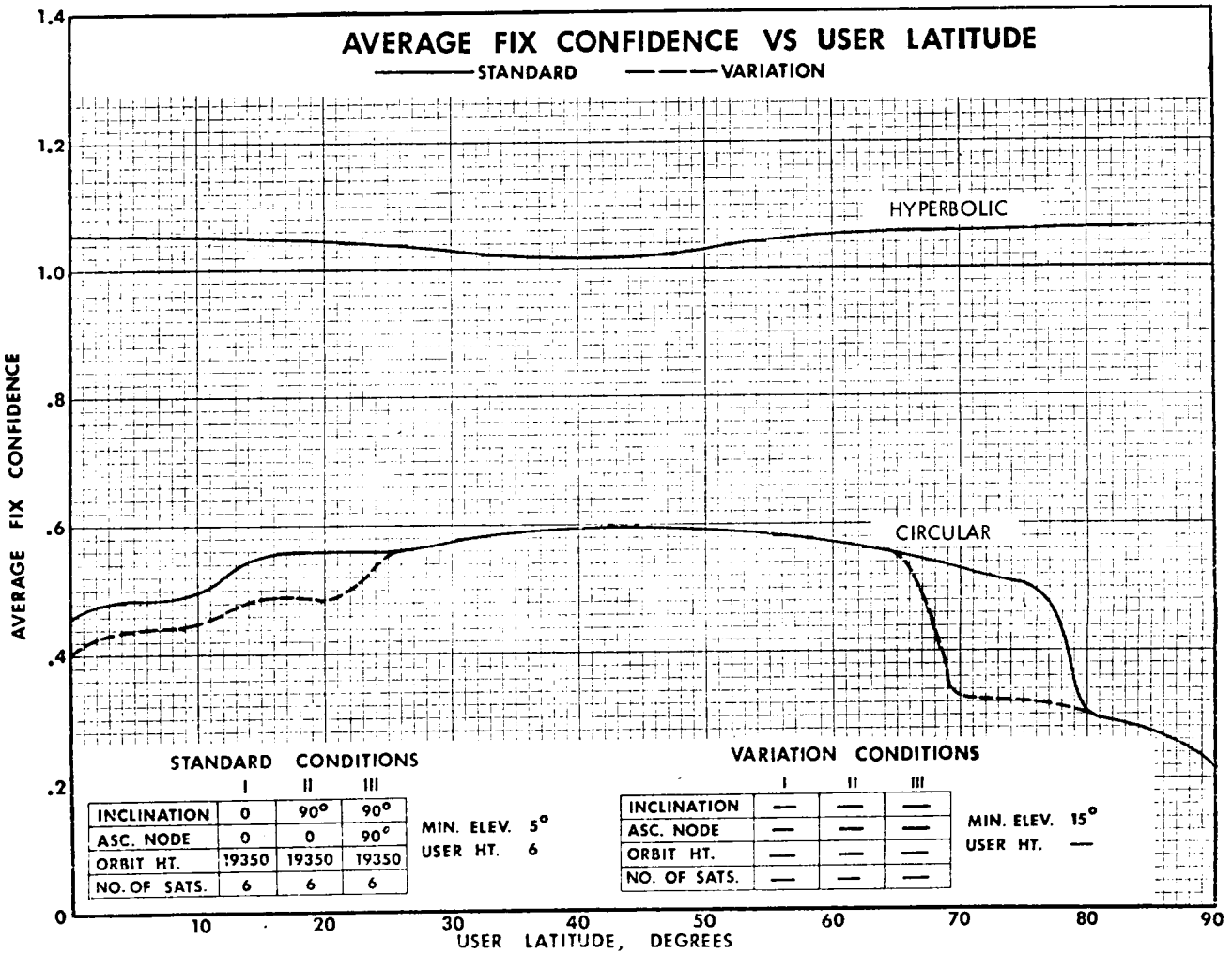

Figure 5-3b. Average Fix Confidence vs User Latitude

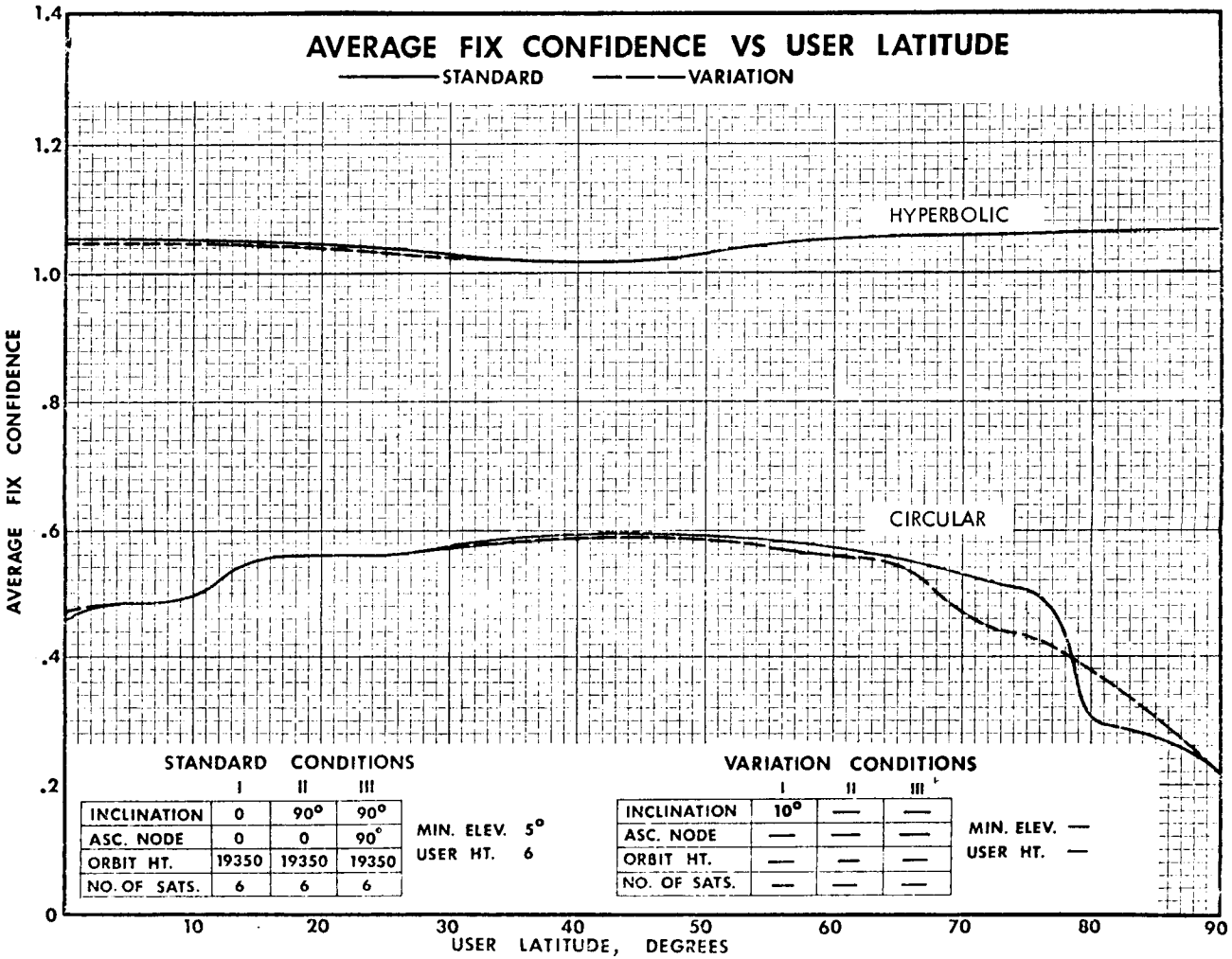

Figure 5-3c. Average Fix Confidence vs User Latitude

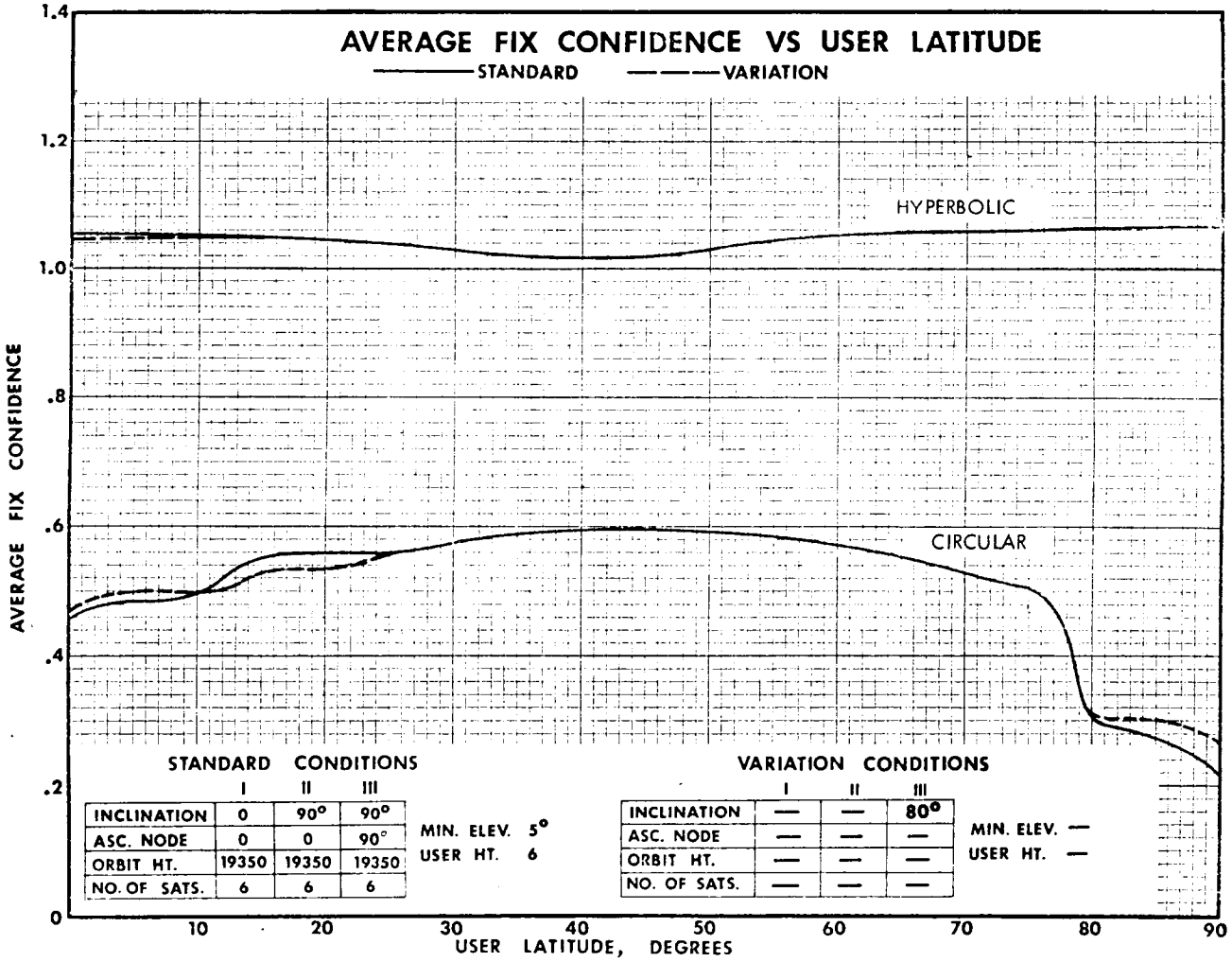

Figure 5-3d. Average Fix Confidence vs User Latitude

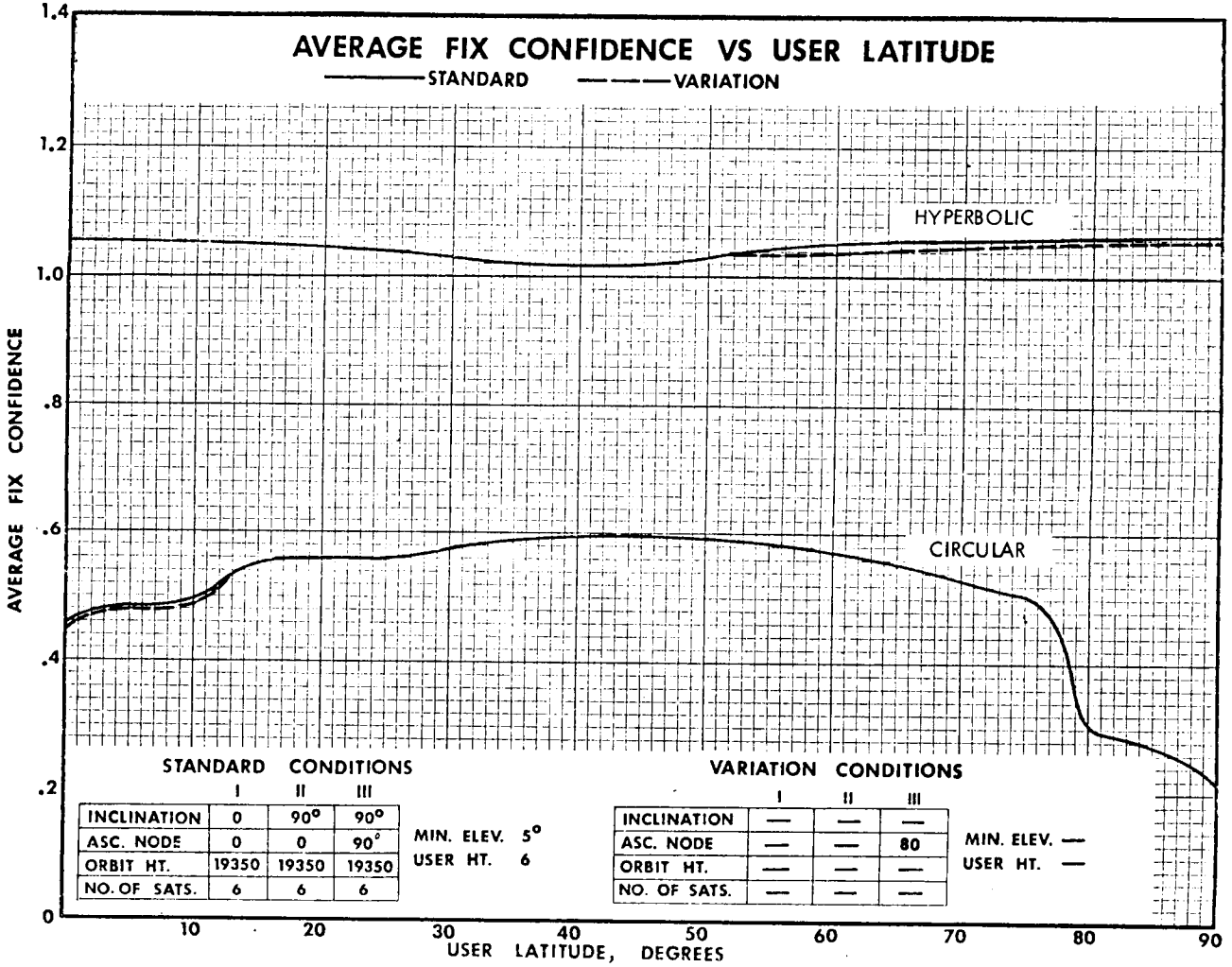

Figure 5-3e. Average Fix Confidence vs User Latitude

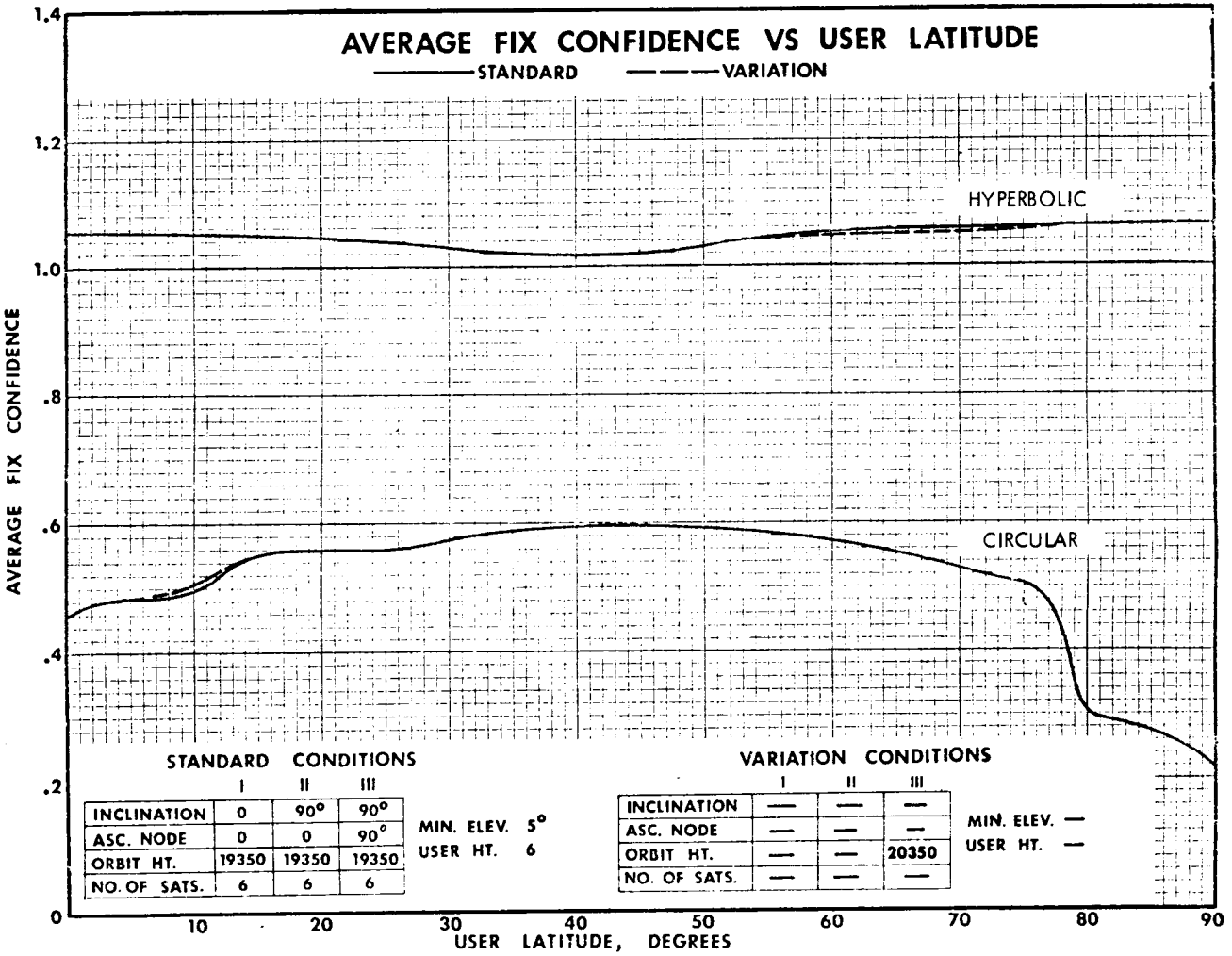

Figure 5-3f. Average Fix Confidence vs User Latitude

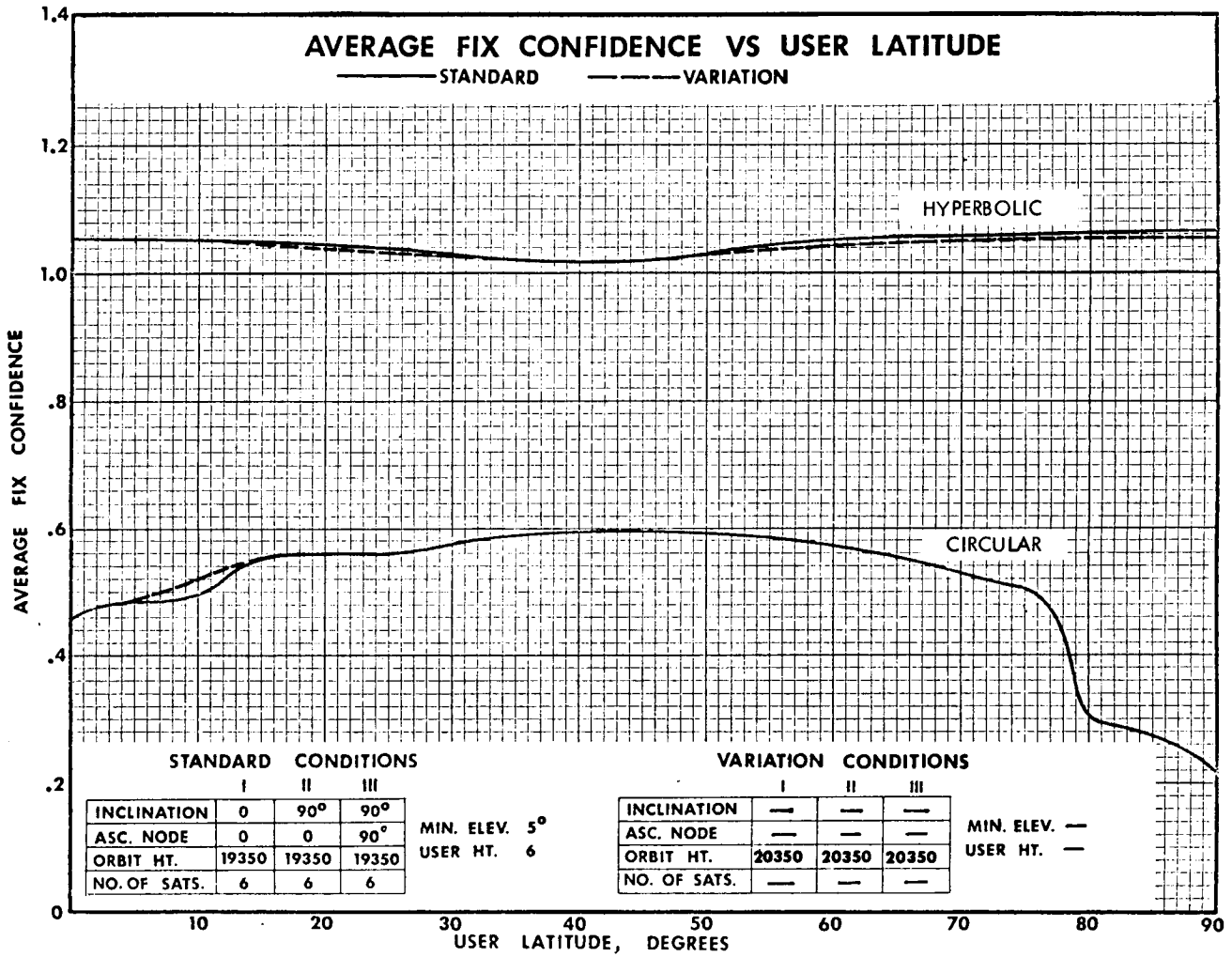

Figure 5-3g. Average Fix Confidence vs User Latitude

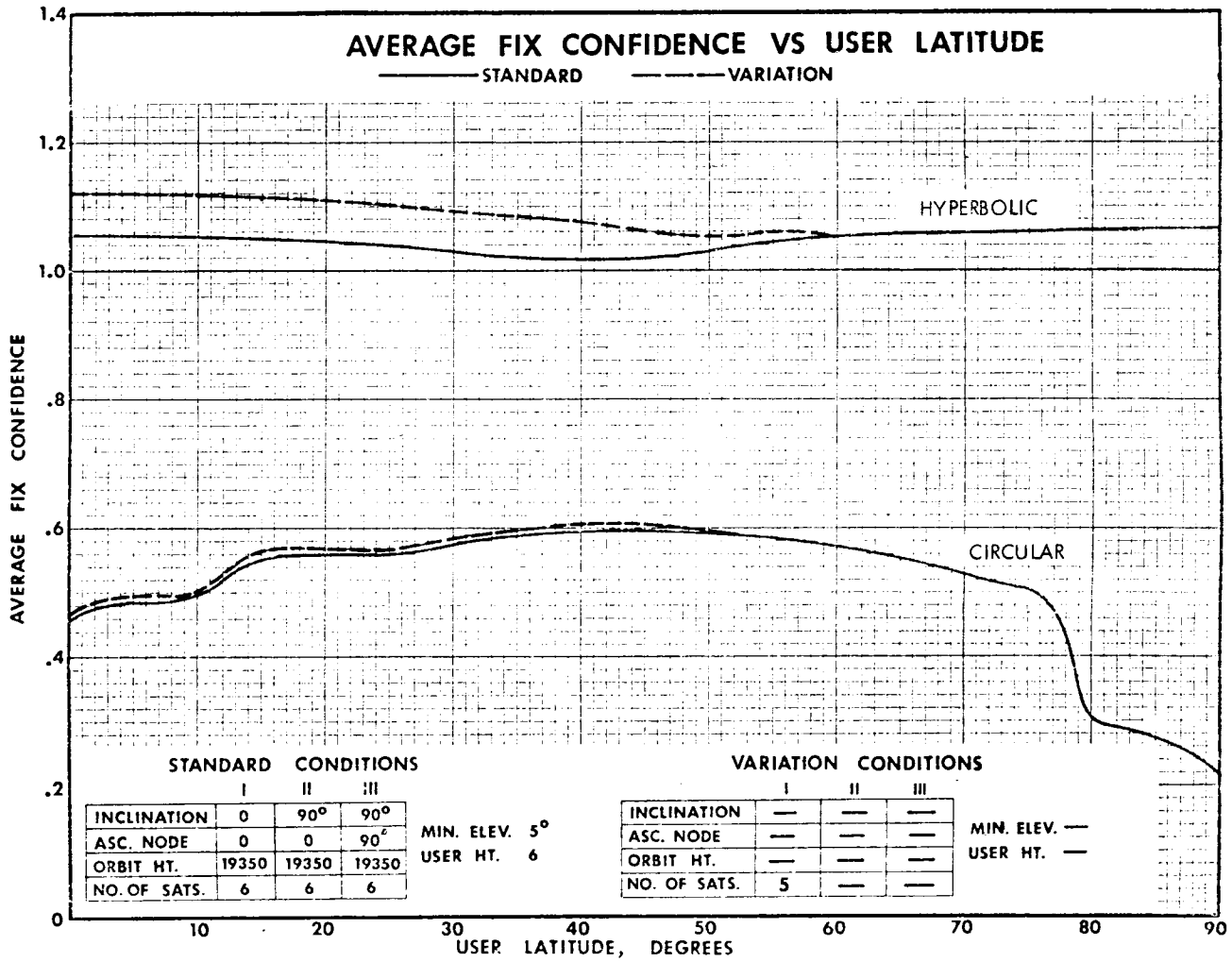

Figure 5-3h. Average Fix Confidence vs User Latitude

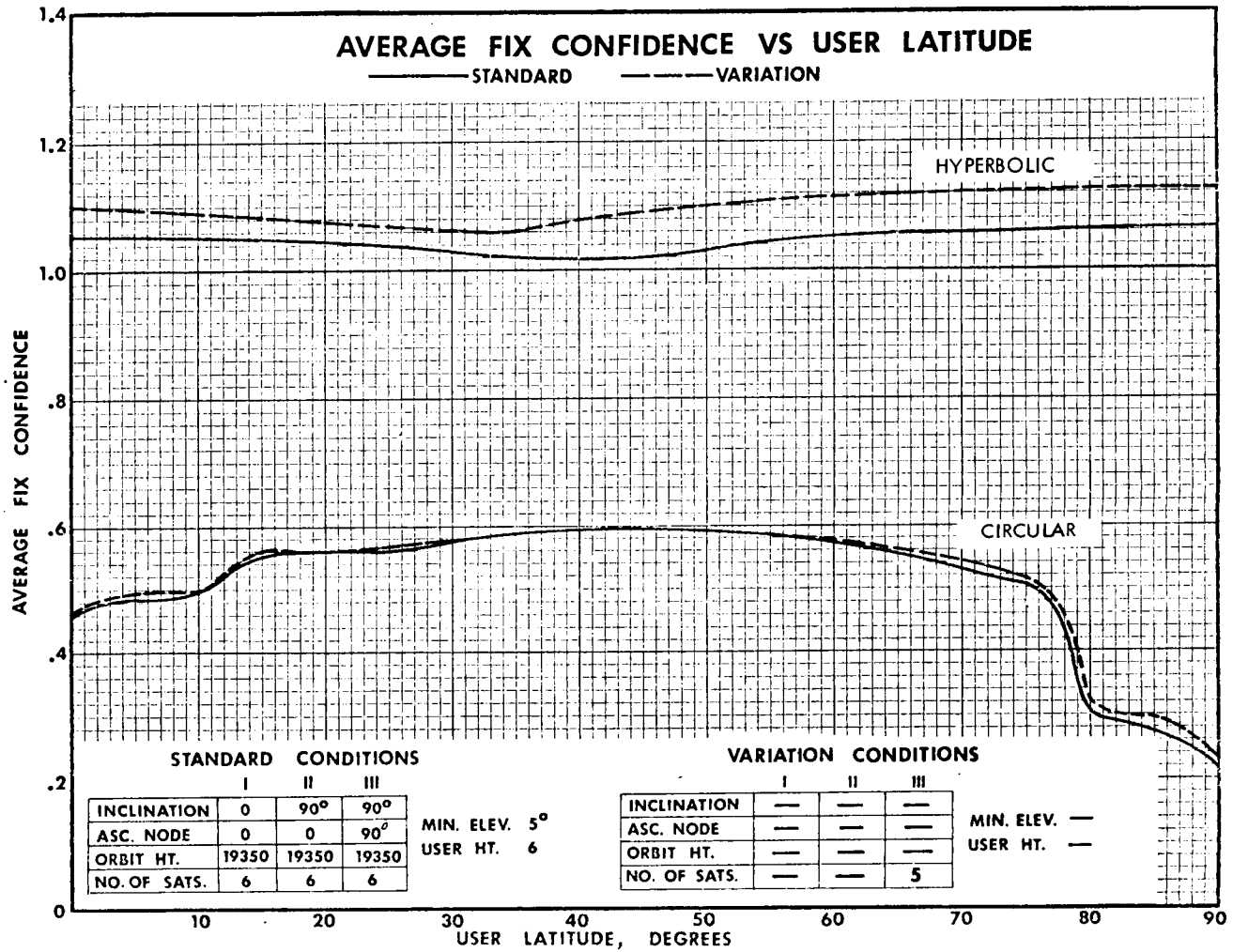

Figure 5-3i. Average Fix Confidence vs User Latitude

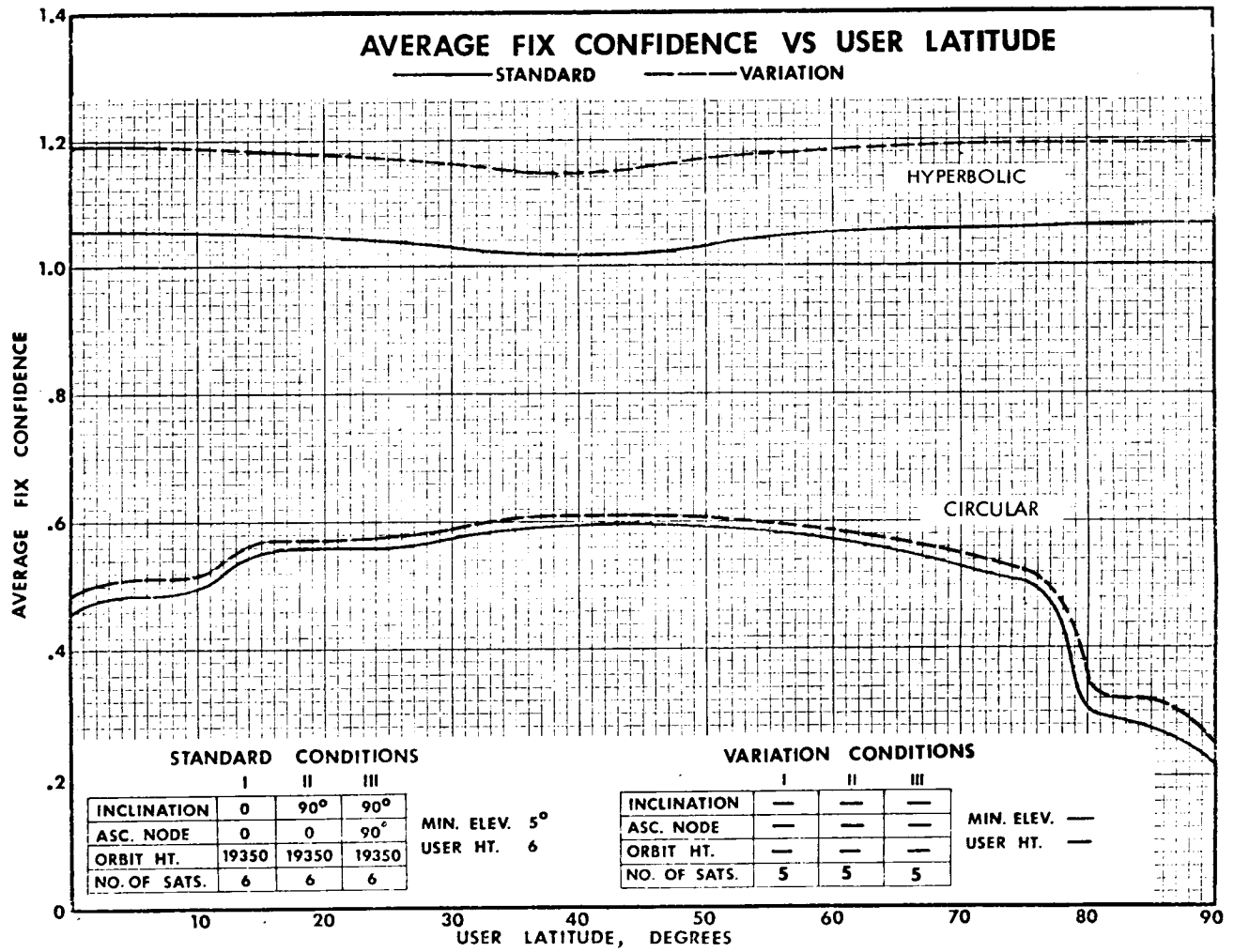

Figure 5-3j. Average Fix Confidence vs User Latitude

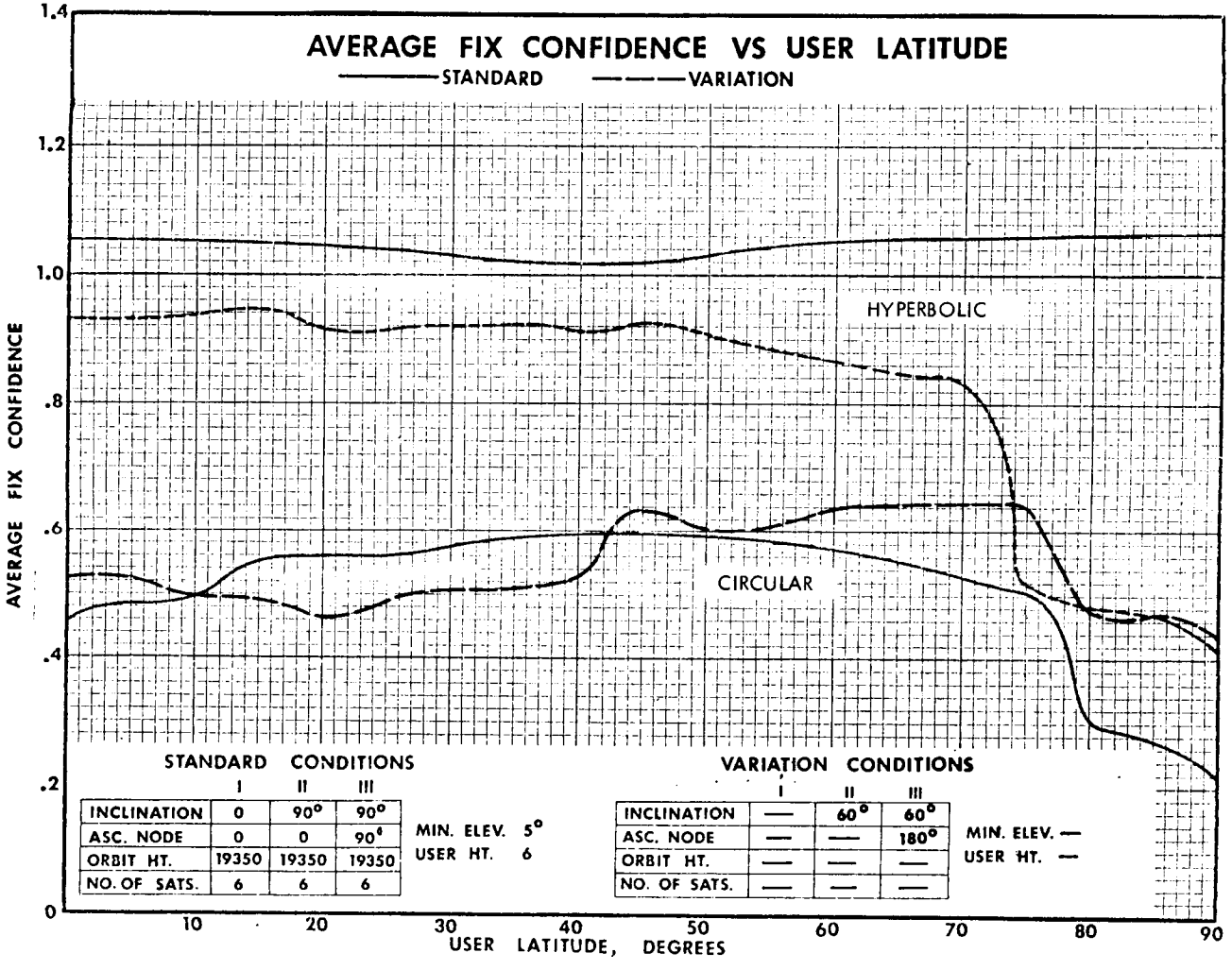

Figure 5-3k. Average Fix Confidence vs User Latitude

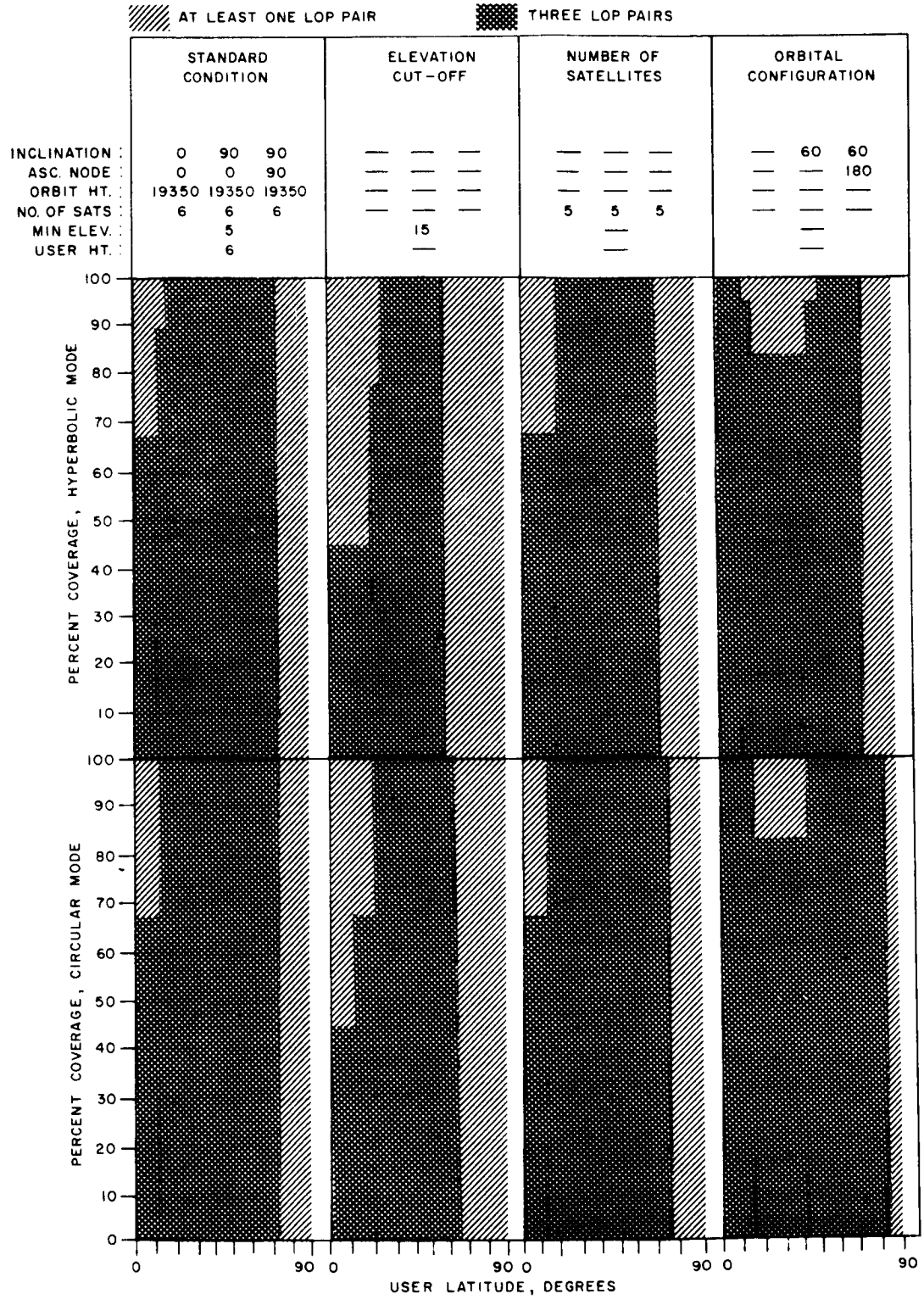

Figure 5-4. Availability of LOP Pairs vs User Latitude

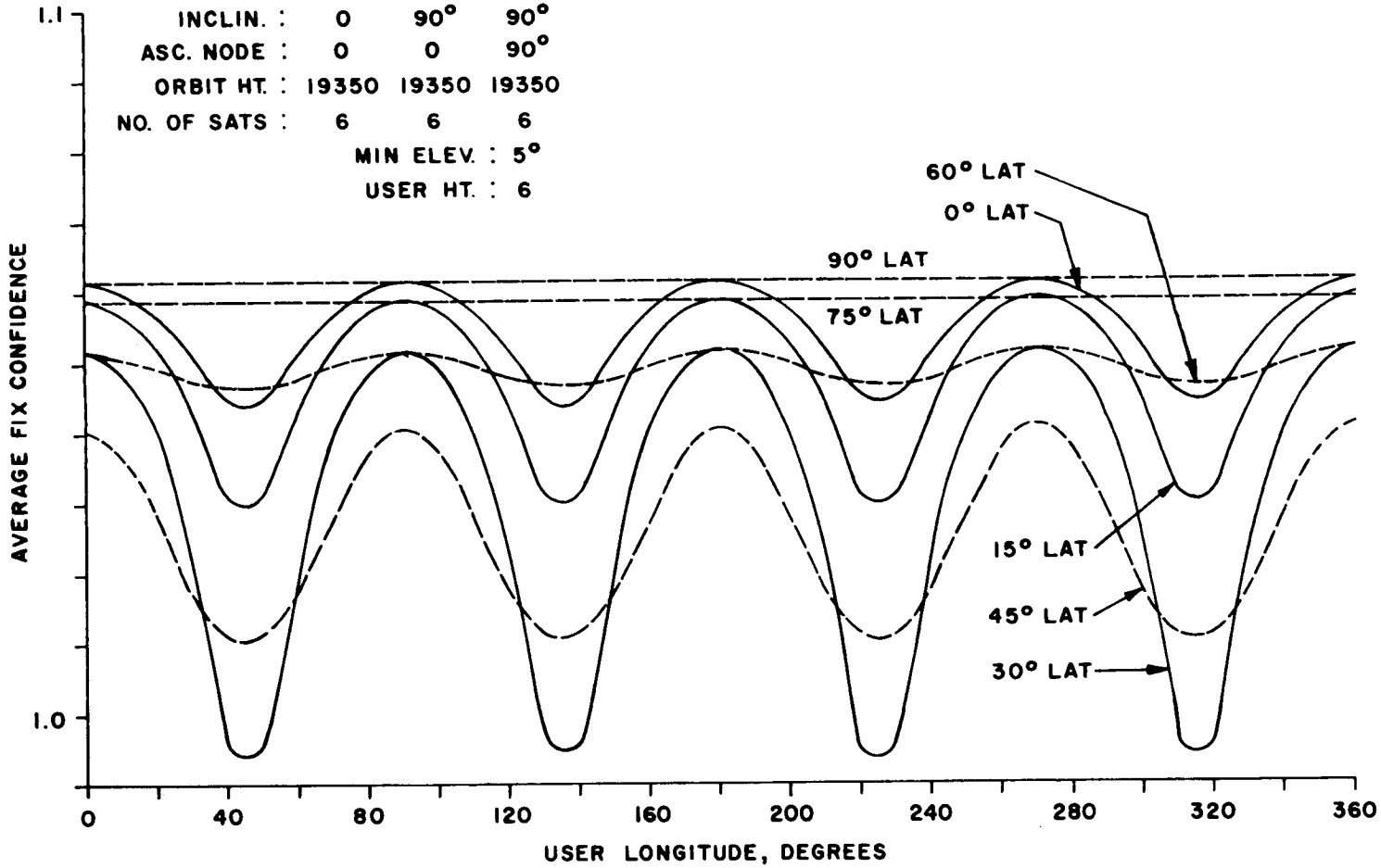

Figure 5-5. Average Fix Confidence vs User Longitude at Several Latitudes, Hyperbolic Mode - Standard Configuration

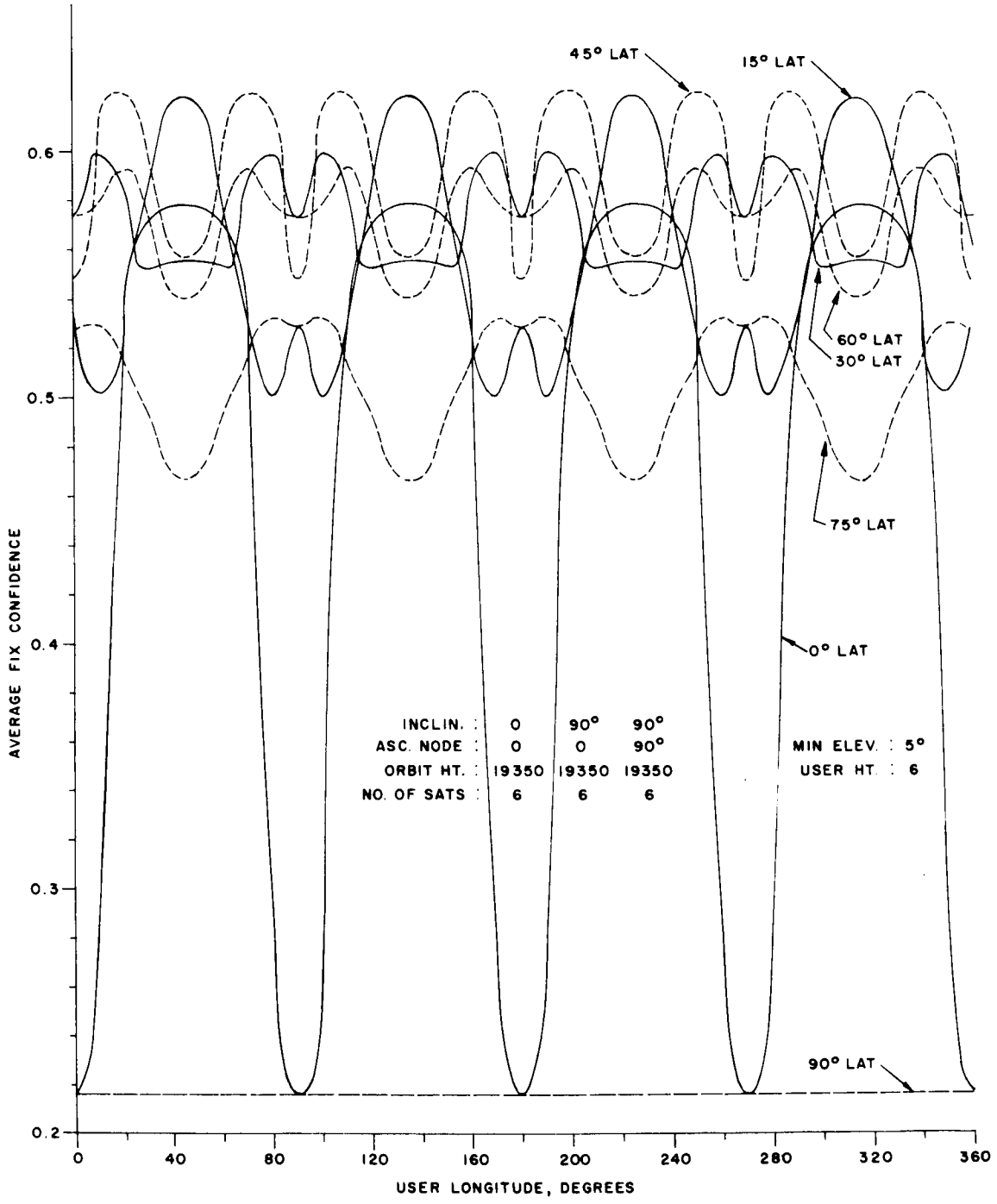

Figure 5-6. Average Fix Confidence vs User Longitude at Several Latitudes, Circular Mode - Standard Configuration

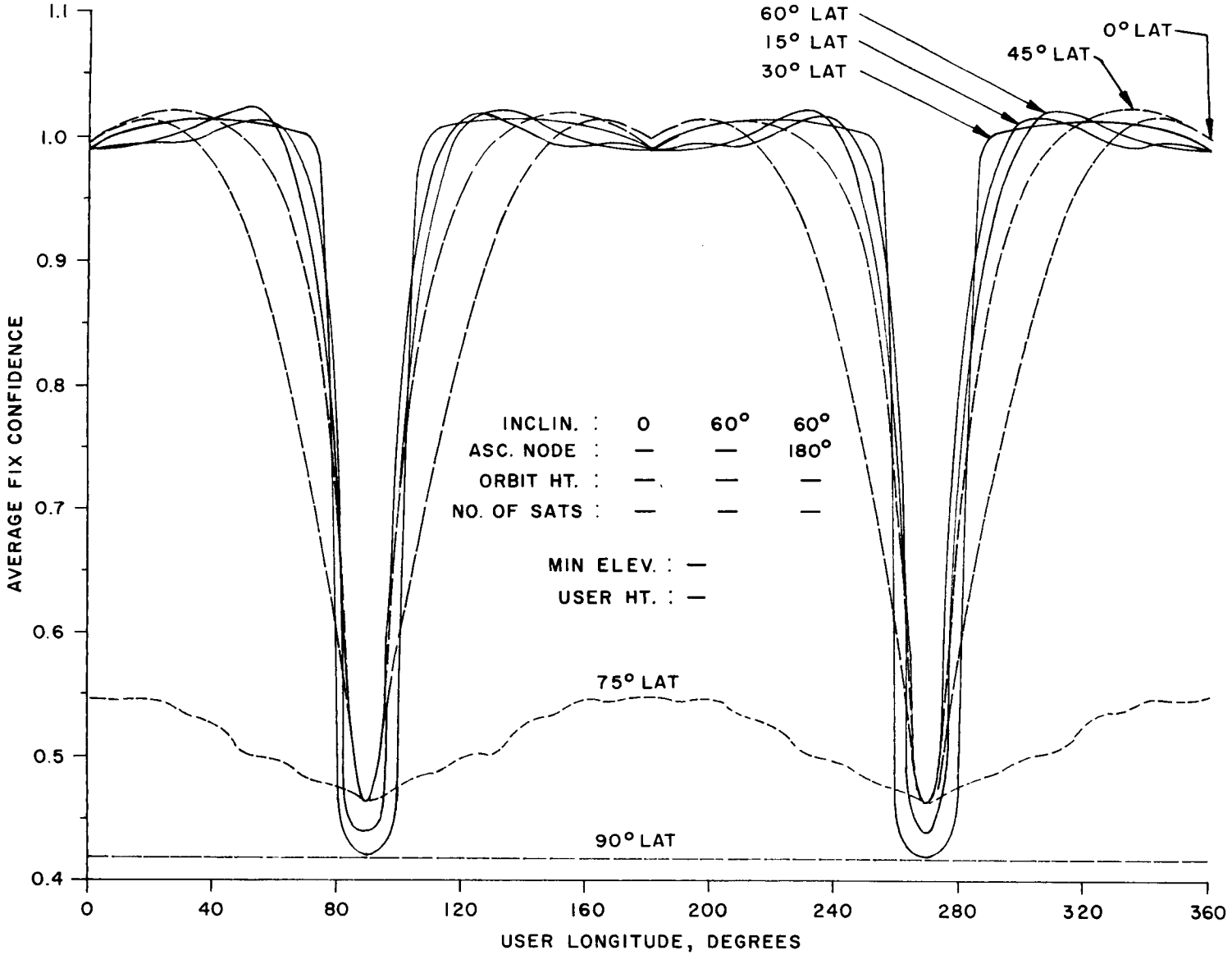

Figure 5-7. Average Fix Confidence vs User Longitude at Several Latitudes, Hyperbolic Mode - Variational Configuration

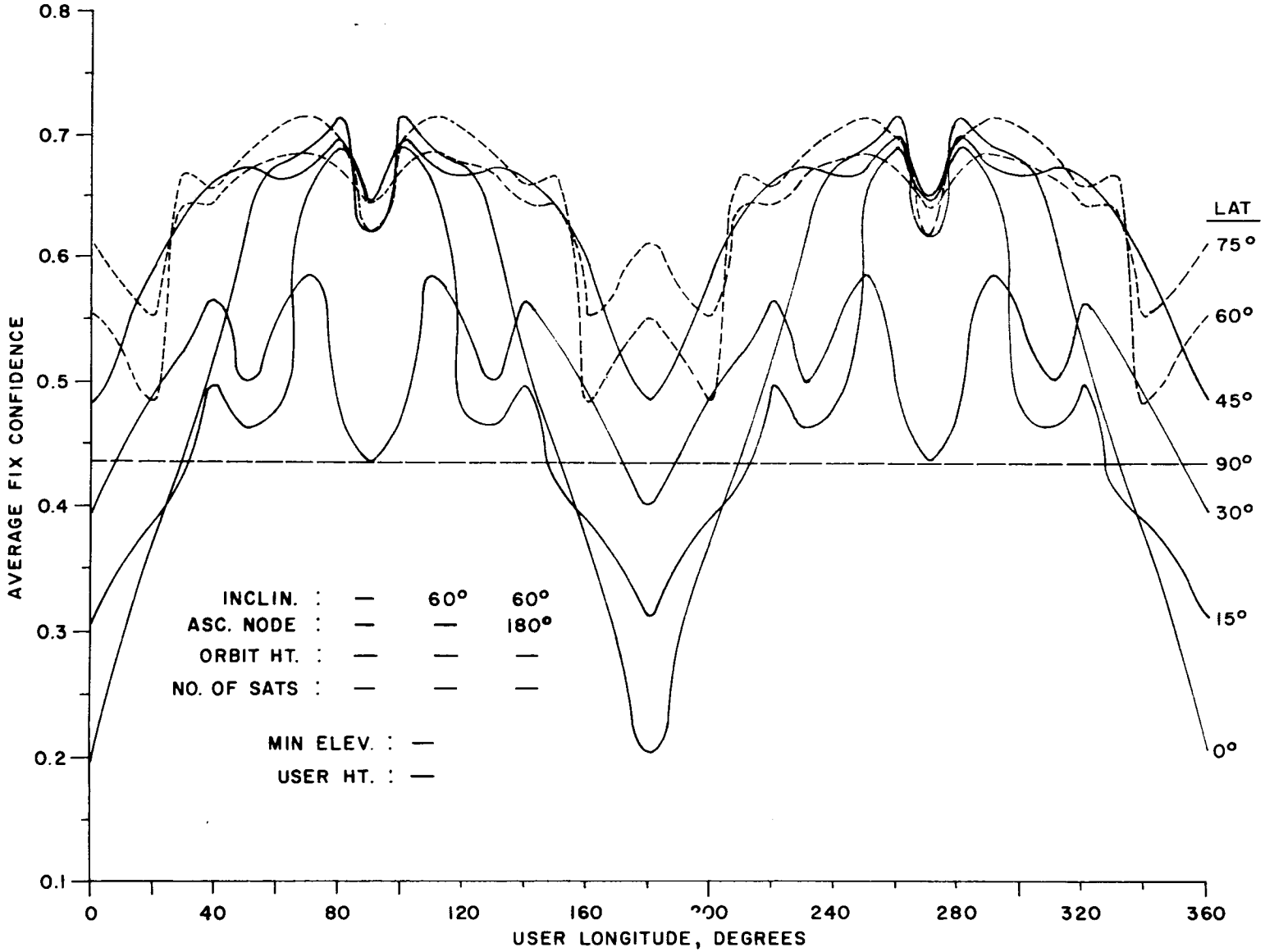

Figure 5-8. Average Fix Confidence vs User Longitude at Several Latitudes, Circular Mode - Variational Configuration

Section 6

SYSTEM ANALYSIS

6.1 INTRODUCTION

In order to calculate meaningful error budgets, it is necessary to quantitatively describe the complete position measurement process in detail, starting from the ground-based center transmitter through the satellite repeater, to the receiver tone demodulators, phase difference measurement, and the ultimate coarse and fine position calculations. This analysis is divided here into the following categories:

(1) Channel characterization

  (a) Mathematical models
  (b) Physical models and data

(2) Description of receiver signal-processing

(3) Analysis of receiver tone demodulator

(4) Phase measurement analysis

(5) Analysis of range measurement errors

The channel characterization process will take into account the following error sources:

(1) Additive noise due to cosmic noise, receiver noise, and man-made interference at the satellite, and the ground receiver.

(2) Uplink and downlink atmospheric refraction.

(3) Downlink multipath.

(4) Oscillator frequency instability and noise.

(5) Variations in path length due to satellite and receiver motion.

(6) Satellite and downlink receiving equipment time delays.

The mathematical modeling describes these error sources in a general way, specifying required channel parameters. The physical models and data provide typical experimental and/or theoretical values for these channel parameters.

Given a mathematical channel model, one can analyze the effects of the above-mentioned error sources on the processes of carrier and tone demodulation, phase difference measurement and position determination. The physical channel data can then be applied to calculate actual error magnitudes.

As a standard of comparison, it is possible to calculate a lower bound on the standard deviation of a typical range measurement in the presence of noise for any given

modulation method. For band-limited white Gaussian noise and double-sided AM modulation, Goblick [6-1]* has shown that this lower bound is:

$$\sigma_{min} = \frac{C}{\pi W \left(\frac{2 E_s}{N_o}\right)^{1/2}} \tag{1}$$

where,

C = Speed of light

W = Transmitted signal bandwidth

E_s = Received signal energy

N_o = White noise spectral density

This assumes that the AM side bands are located at $f_c \pm W/2$, where f_c is the carrier frequency. The quantity E_s includes the time-delay measurement integration time, since it equals the product of the received signal power P_r and the integration time T. Equation (1) is applicable when the tone phase-modulates the carrier, provided the modulation index is small. In this case AM and PM are approximately equivalent.

Equation (1) is a special case of the more general formula: [6-1, 6-2]

$$\sigma_{min} = \frac{C}{2\pi B \left(\frac{2 E_s}{N_o}\right)^{1/2}} \tag{2}$$

where,

$$B^2 = \frac{\int_{-\infty}^{\infty} f^2 \left|S(f)\right|^2 df}{\int_{-\infty}^{\infty} \left|S(f)\right|^2 df} \tag{3}$$

and $\left|S(f)\right|^2$ is the double-sided transmitted signal power spectrum. Equation (2) gives a lower bound on the standard deviation of a range measurement based on the Cramer-Rao inequality of statistical estimation theory.

In the case of a sinusoidal transmitted signal of frequency f_o,

$$\left|S(f)\right|^2 = \frac{P}{2}\left[\delta(f - f_o) + \delta(f + f_o)\right] \tag{4}$$

*References are listed in Section 7.

Applying (4) to (3), $B = f_o$, in which case

$$\sigma_{min} = \frac{C}{2\pi f_o \left(\frac{2E_s}{N_o}\right)^{1/2}} \tag{5}$$

In the case of double side-band AM discussed above, the actual signal used for range measurement is a tone of frequency $f_o = W/2$. Therefore (1) follows from (5).

Comparison of (1) and (5) shows that when the tone used for fine ranging modulates the carrier, the measurement precision is limited by the available RF bandwidth W, whereas in actuality one could use an RF frequency for fine ranging. Therefore, the "ultimate" limitation in ranging precision is not the RF bandwidth, but the RF frequency.

This "ultimate" limitation should not be confused with the actual limitations imposed by the real-life error sources enumerated above. For example, there is no point in trying to range on a 150 MHz tone, which has a 2 meter wave length, when the total range errors due to refraction, geodetic errors, and equipment errors are of the order of 2000 meters. In other words, additive noise is only one of several key error sources. In the above example, the noise does not provide the ultimate limitation. Therefore, a signal design based on white noise may not be optimum for such situations.

6.2 DESCRIPTION OF USER RECEIVER SIGNAL PROCESSING

The receiver signal processor must extract the coarse and fine tone modulation from each IF output. Each IF output corresponds to a different satellite transmission. Once the tones are extracted, in the 3-satellite position measurement scheme, coarse and fine tone phase differences are measured for each pair of IF outputs. Figure 6-1 shows the signal processing for two IF channels with phase-locked-loop IF carrier demodulation. If only two satellites are available, but the user transmitter and receiver have accurate frequency standards, position measurements can be based on phase comparisons between coarse and fine tone filter output signals, and corresponding reference tone frequencies.

In Figure 6-1, the carrier narrow-band filter output consists of the IF carrier frequency plus noise since the purpose of this filter is to reject all the sidebands of the original phase-modulated carrier. The width of this filter is determined by the maximum IF frequency uncertainty due to long-term oscillator drift, and Doppler shift. This filter output is then processed in a phase-locked loop (PLL) in order to extract the IF carrier frequency. The narrower the loop filter bandwidth, the longer the lock-up time, but the smaller the phase jitter on the voltage controlled oscillator (VCO) output after lock-up. As shown in Figure 6-1, the IF frequency is extracted by multiplying the VCO output and the IF output. The resulting product is then processed in the coarse and fine tone filters.

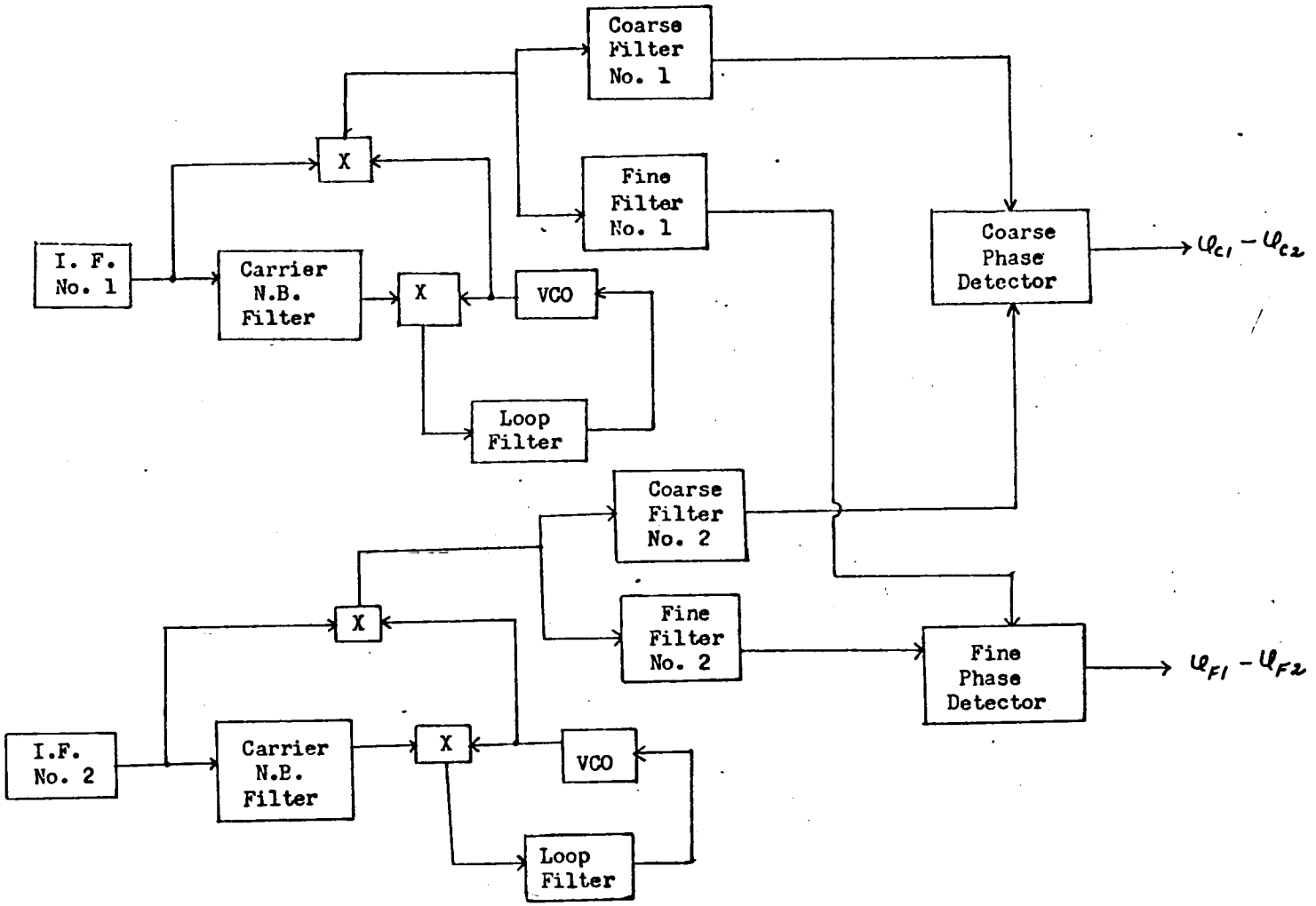

Figure 6-1. User Receiver Signal Processing With Phase-Locked Loop IF Carrier Demodulator

If the IF carrier frequency is known, the phase-lock demodulator can be replaced by a local oscillator (LO) at the known IF frequency, as shown in Figure 6-2a. If the IF carrier frequency is not known, but the IF carrier frequency uncertainty is relatively small, the carrier extraction can be accomplished by a narrow-bandwidth filter as shown in Figure 6-2b. The demodulator in Figure 6-2a is of interest because an analysis of the receiver performance with known IF carrier frequency determines the most optimistic signal-processing system performance. Furthermore, this analysis is the simplest.

Demodulator 6-2b is of interest because of its simplicity, and because its performance can be analyzed in a straightforward manner in the presence of multipath-fading signals. The performance of the phase-locked loop demodulator for multipath fading input signals is not completely understood. The occurrence of multipath can result in loss of lock, causing the VCO output frequency to deviate from the desired IF carrier frequency by more than the tone filter bandwidths. When this occurs, the tone signal information will be lost. A possible approach to combat this situation is to broaden the tone filters and to employ phase-locked loops at the outputs of each filter. These phase-locked loops are used in this manner as narrow bandwidth frequency and phase-tracking filters.

The final portion of the receiver signal-processing shown in Figure 6-1 is the phase comparison process. Figure 6-3 shows block diagrams of two phase detectors; (1) a zero crossing phase detector, and (2) an analog quadrature phase detector.

For phase-detector input signal-to-noise ratios greater than 10 dB, the performance of these phase detectors in stationary white noise is approximately the same, with zero mean phase error and phase error variance equal to that of a maximum likelihood phase-detector. This variance equals one-half the sum of the reciprocals of the signal-to-noise power ratios at the output of each tone filter. When the comparison is made with a noiseless reference, the reference tone channel signal-to-noise ratio is infinite, in which case the variance equals the reciprocal of twice the tone-filter output signal-to-noise ratio.

6.2.1 MODULATION REQUIREMENTS

6.2.1.1 SINGLE-TONE ANALYSIS

The tone modulated carrier can be denoted by

$$X(t) = \cos(\omega_c t) + m \sin(\omega_1 t) \qquad (1)$$

where $m = \Delta f / f_1$, Δf is the frequency deviation of the carrier caused by the modulation frequency f_1, and m represents the maximum phase shift of the carrier. Expanding in terms of Bessel functions:

$$X(t) = J_o(m) \cos \omega_c t - J_1(m) \left[\cos(\omega_c - \omega_1)t - \cos(\omega_c + \omega_1)t\right]$$

$$+ J_2(m) \left[\cos(\omega_c - 2\omega_1)t + \cos(\omega_c + 2\omega_1)t\right]$$

(Equation Continued)

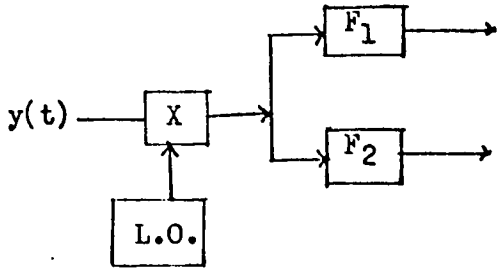

(a) KNOWN CARRIER FREQUENCY; IDEAL HOMODYNE DETECTOR

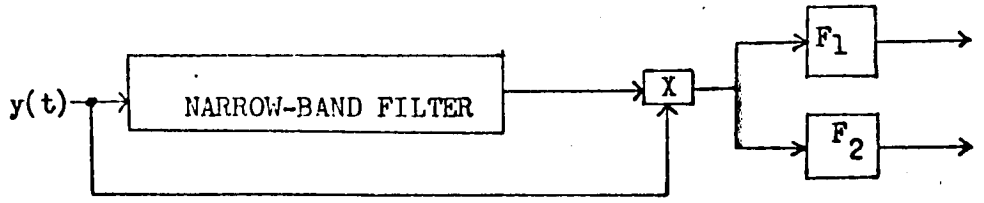

(b) NARROW-BAND FILTER CARRIER EXTRACTION

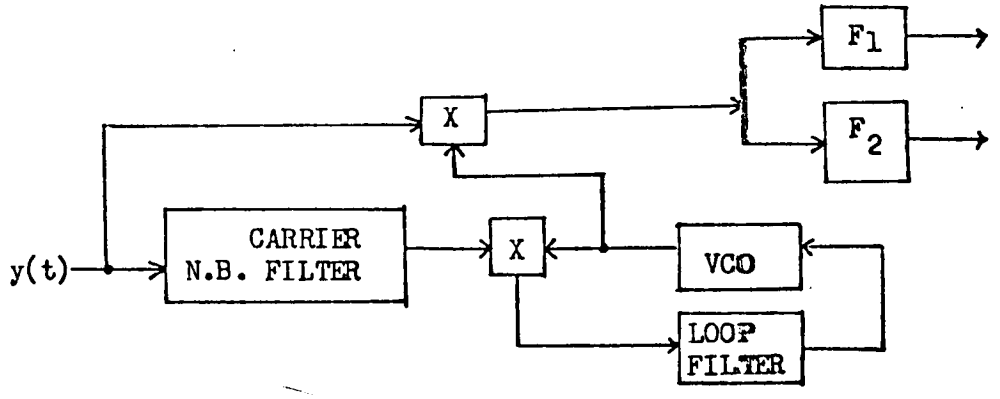

(c) PHASE-LOCKED-LOOP CARRIER EXTRACTION

Figure 6-2. Three Methods of IF Carrier Demodulation

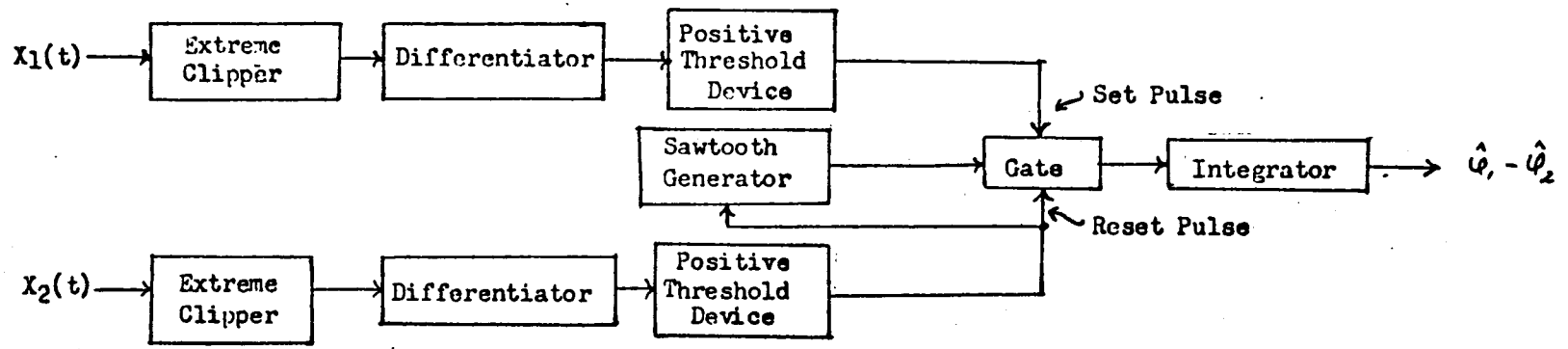

(1) ZERO CROSSING PHASE DETECTOR

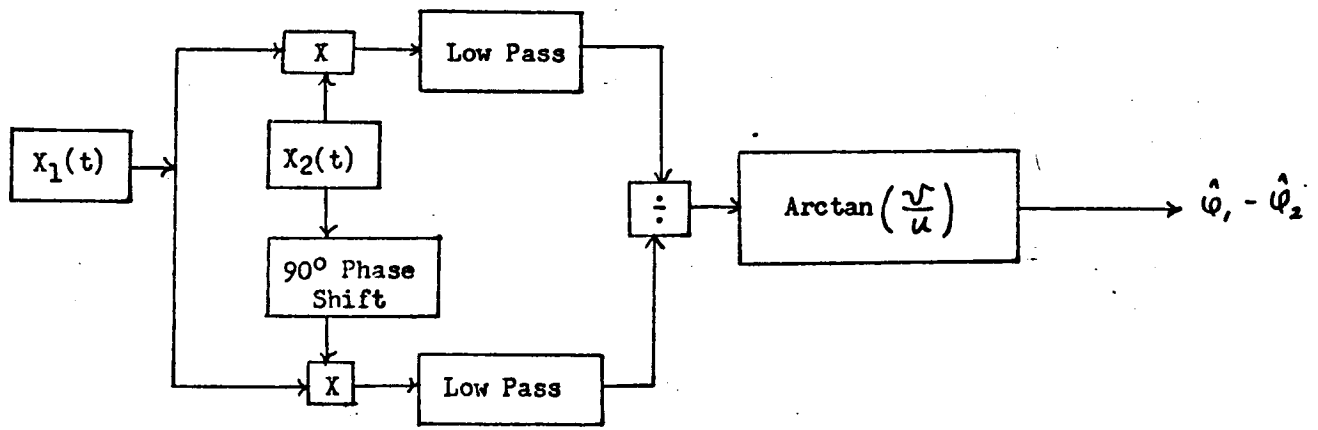

(2) QUADRATURE PHASE DETECTOR

Figure 6-3. Block Diagrams of Two Phase Detectors

$$- J_3(m) \left[\cos(\omega_c - 3\omega_1)t - \cos(\omega_c + 3\omega_1)t\right]$$

$$+ \ldots \qquad (2)$$

A pictorial view of the carrier and the significant sidebands for a modulation index, m, of 1.15 is shown in Figure 6-4. A vector representation of the carrier and the first two sidebands is shown in Figure 6-5.

The phasing of the sidebands (harmonics of the modulation frequency) are such that the instantaneous resultant of the composite signal is of a constant amplitude and hence independent of time. Bandwidth restriction in the predetection filtering results in an attenuation (and possible loss) and phase shift of the higher order sidebands resulting in phase and amplitude distortion. In this analysis we shall be concerned with only the case of total extinction of the n+1 order sidebands and no excess phase shift nor attenuation on the first n sidebands; i.e., ideal filtering. The end result

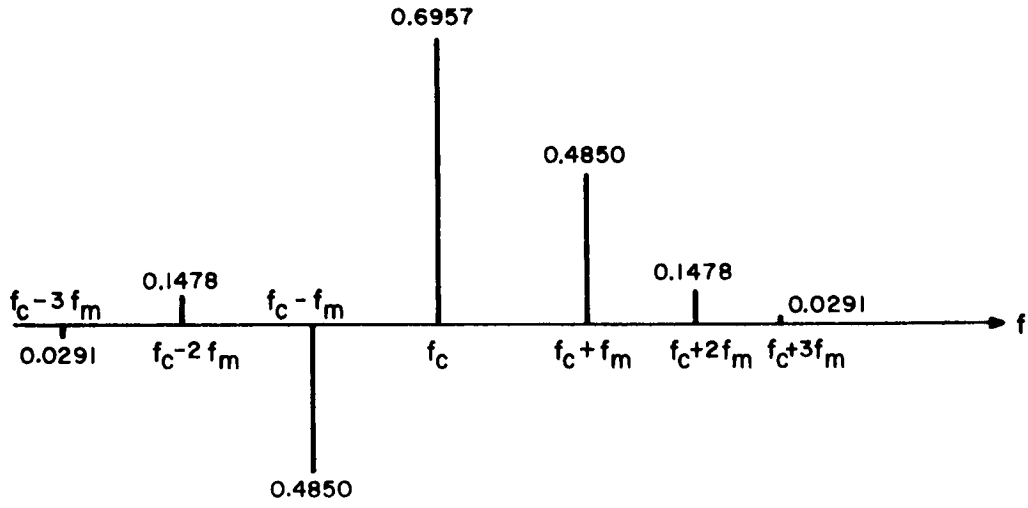

Figure 6-4. Sideband Distribution for an Angle-Modulated Carrier With m = 1.15

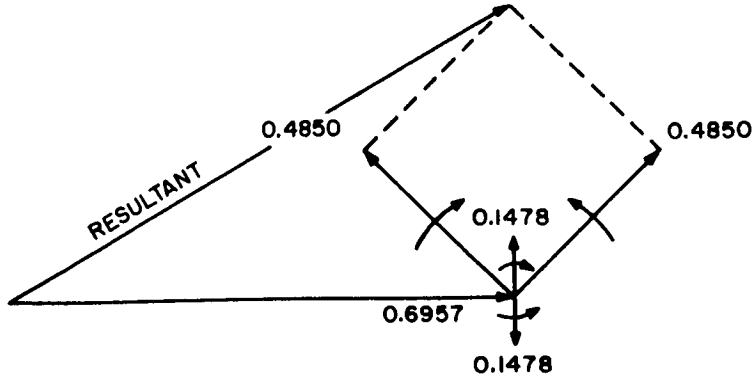

Figure 6-5. Vector Representation of Figure 6-4

in this type of filtering is that amplitude modulation is impressed on the angle modulated signal, resulting in a loss of power due to the conversion from angle modulation to amplitude modulation. The analysis is performed for a carrier and the first order sidebands only, then it is performed for a carrier and the first two order sidebands. Figure 6-6 pictorially represents the first case; i.e., first-order sidebands only.

As the angle modulation varies through one complete cycle, the resultant varies from a minimum (0.6957) to a maximum (1.1937) back through the minimum, the maximum, and then the minimum; that is, the envelope of the signal varies through a complete cycle for each cycle of modulation. The average value of the resultant is (1.1937 + 0.6957)/2 = 0.9447. The peak excursion about the average is 1.1937 - 0.9447 = 0.2490. The resulting amplitude modulation is (0.2490/2.9447) x 100% = 26.36%. The reduction in signal power because of the incidental AM amounts to approximately 5%.

If the predetection bandwidth is increased up to the point where the second order sidebands are included (pictorially shown in Figure 6-7) the resulting AM is approximately 2.8%, a reduction of almost 24%.

The reduction in signal power, in this case is about 0.2%

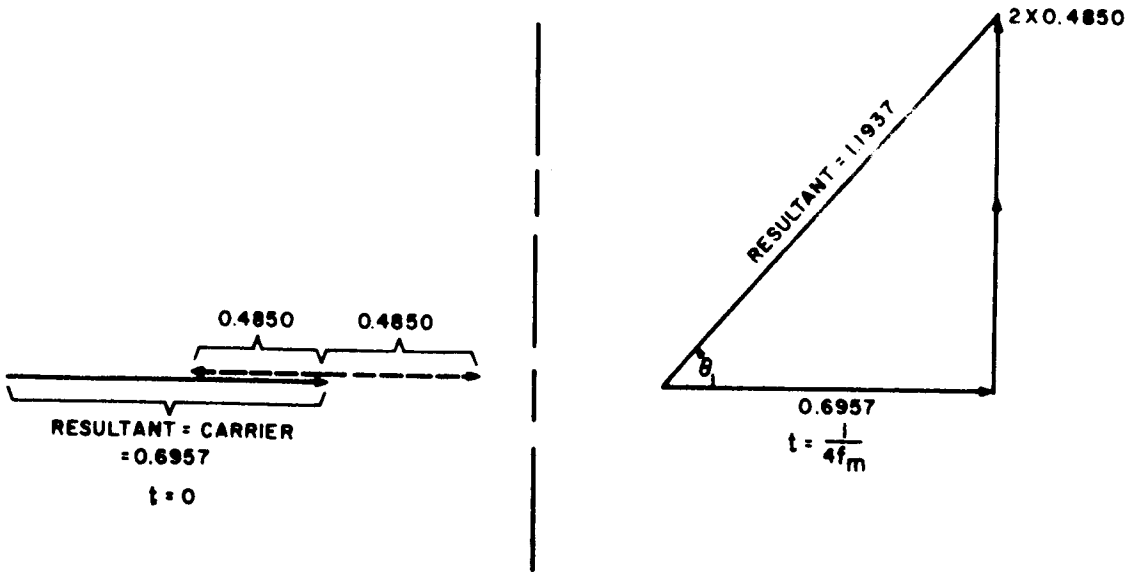

Figure 6-6. Resultant Signal Due to Carrier and First Order Sidebands for m = 1.15

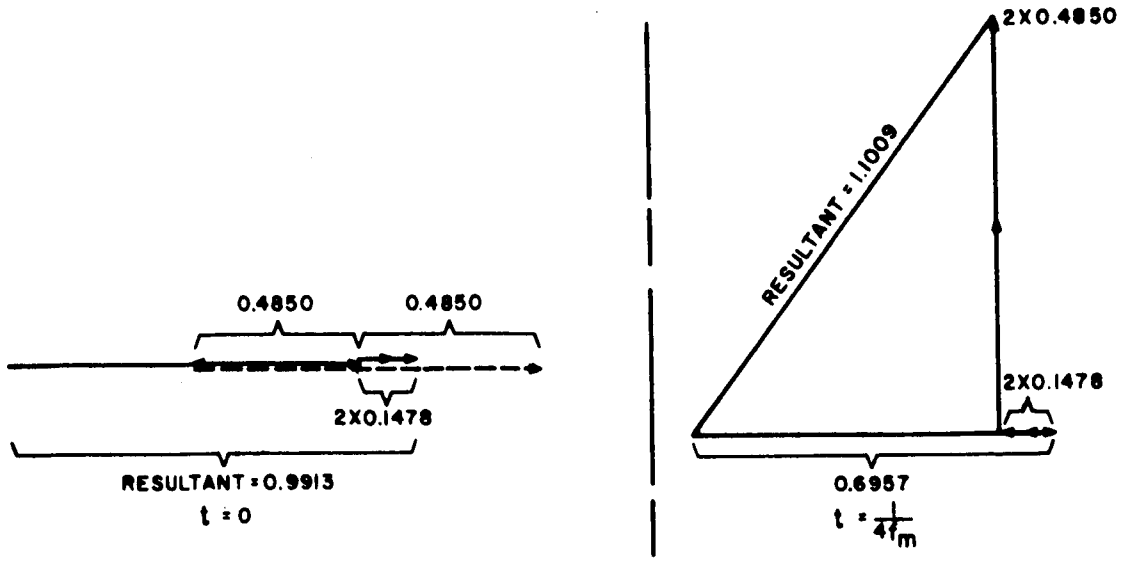

Figure 6-7. Resultant Signal Due to Carrier and First Two Order Sidebands for m = 1.15

6.2.1.2 TWO-TONE ANALYSIS

Corrington [6-3] shows that for the case of two-tone angle modulation the spectrum is given by:

$$f_c(t) = \sum_{k=-\infty}^{\infty} \sum_{\ell=-\infty}^{\infty} J_m(m_1)\, J_n(m_2) \sin(\omega_c + 2\pi k f_1 + 2\pi \ell f_2)t \qquad (3)$$

The resulting spectrum is now more complicated as can be seen from (3) and Figure 6-8.

Corrington further states: "Just as the maximum deviation occurs when D_1 [the deviation of the first signal] and D_2 [the deviation of the second signal] are in phase, the maximum bandwidth is given approximately by the sum of the two bandwidths that would be obtained with the two modulating tones used one at a time." (See p. 1016, Figure 6 of Ref. (6-3) for an example.) Since the coarse tone frequency is approximately 1/30 of the fine tone frequency, the bandwidth occupied by both signals is approximately 4% more than that required when only the fine tone is present. Therefore, the predetection bandwidth requirements analysis will proceed similar to the single-tone analysis except that the spectral components will be the product of two

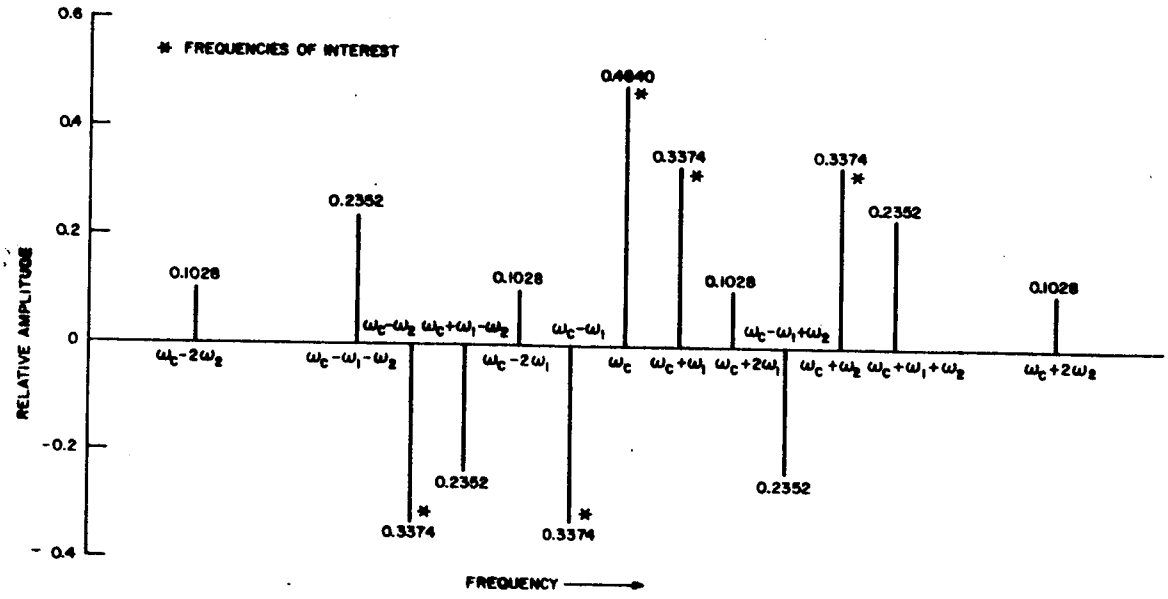

Figure 6-8. Two Tone Modulation Sidebands (Down to 3% Total Power) for $F_2 = 30\ F_1$, $m_1 = m_2 = 1.15$

Bessel terms instead of one. That is, the carrier amplitude is now given by $J_o(m_1)J_o(m_2)$, the coarse-frequency first-order-sideband amplitude by $J_1(m_1)J_o(m_2)$ and the fine-frequency first-order-sideband amplitude by $J_o(m_1)J_1(m_2)$. For $m_1 = m_2 = 1.15$, the above three terms become $J_o^2(1.15)$, $J_1(1.15) \times J_o(1.15)$, and $J_o(1.15) \times J_1(1.15)$.

The power lost by excluding all the terms that interact with the second harmonic of the fine frequency is less than 5%. If the second harmonic of the fine tone is allowed to interact with the carrier, with all significant harmonics of the coarse tone and with the fundamental of the fine tone, less than 1% of the total power is lost.

It is concluded that the power lost in the single-tone and in the two-tone case is very small even if the pre-detection bandwidth is only slightly wider than twice the fine tone frequency, and the loss is trivial if the pre-detection bandwidth is slightly wider than four times the fine frequency.

6.2.2 COMPARISON OF AM AND FM TONE MODULATION

6.2.2.1 SIGNAL POWER IN ONE TONE OF A TWO-TONE ANGLE MODULATION WAVE

The expression for the angle-modulated carrier wave with two-tone modulation is given by:

$$x(t) = \sum_{\ell=-\infty}^{\infty} \sum_{h=-\infty}^{\infty} J_{\ell}(m_r) J_n(m_s) \sin \left[(p + \ell r + ns)\, t\right]$$

where m_r is the phase-modulation index of the tone of frequency $r/2\pi$ Hz, and m_s is the pahse-modulation index of the tone of frequency $s/2\pi$ Hz. For $m_r=m_s=m$, the peak carrier voltage is $J_o^2(m)$ and the peak voltage of any of the first-order sidebands of one tone is $J_o(m) \times J_1(m)$ while the normalized power in the sideband is $J_o(m) \times J_1(m)^2$. Because of the method of demodulation, only the power in the first-order sidebands are utilized. Therefore, the total first-order power in a tone is $2\,[J_o(m)\, J_1(m)]^2$. The impedance level is assumed to be one ohm, resistive. This power is shown in the second column of Table 6-1 as a function of modulation index. Because the envelope of the RF signal is constant, the peak power or average power limitation of the transmitter does not limit the modulation index.

6.2.2.2 SIGNAL POWER IN ONE TONE OF A TWO-TONE AMPLITUDE MODULATED WAVE WITH AN AVERAGE-POWER LIMITATION IN THE TRANSMITTER

The expression for an amplitude-modulated carrier wave with two-tone modulation is given by:

$$\begin{aligned} X(t) &= a\left[1 + m_r \cos(rt) + m_s \cos(st)\right] \cos(pt) \\ &= a\cos(pt) + am_r \cos(pt)\cos(rt) + am_s \cos(pt)\cos(st) \\ &= a\cos(pt) + \frac{am_r}{2}\cos\left[(p-r)\,t\right] + \frac{am_r}{2}\cos\left[(p+r)\,t\right] \\ &\quad + \frac{am_s}{2}\cos\left[(p+s)\,t\right] + \frac{am_s}{2}\cos\left[(p+s)\,t\right] \end{aligned} \qquad (1)$$

The average power is:

$$P_{ar} = a^2 + 2\left(\frac{am_r}{2}\right)^2 + 2\left(\frac{am_s}{2}\right)^2 \qquad (2)$$

For $m_r = m_s = m$, and $P_{ar}\, e = 1$; $a = \dfrac{1}{\sqrt{1+m^2}}$

Substituting this value for a in (2), we obtain the power in one tone $P_{ta} = \dfrac{m^2}{2(1+m^2)}$

TABLE 6-1. MODULATION EFFICIENCIES

Modulation Index (m)	Sideband Power (mW)			Angle Mod. / Avg Pwr AM	Angle Mod. / Pk Pwr AM
	Angle-Modulation Tone-Power	Average-Power Limited AM	Peak-Power Limited AM		
0.1	4.954	4.950	3.472	1.0008	1.4268
0.2	19.406	19.230	10.204	1.0092	1.6118
0.3	42.036	41.284	17.578	1.0182	2.3914
0.4	70.866	68.965	24.691	1.0276	2.8701
0.5	103.418	99.999	31.250	1.0342	3.3094
0.6	136.732	132.352	37.190	1.0331	3.6766
0.7	168.100	164.429	42.534	1.0223	3.9521
0.8	194.830	195.121	47.337	0.9985	4.1158
0.9	214.858	223.756	51.657	0.9602	4.1593
1.0	226.818	250.000	55.555	0.9073	4.0828

The power in a tone for the average power limitation in the transmitter is shown in the third column of Table 6-1.

6.2.2.3 SIGNAL POWER IN ONE TONE OF A TWO-TONE AMPLITUDE MODULATED WAVE WITH PEAK-POWER LIMITATION IN THE TRANSMITTER

Repeating the expression for the two-tone amplitude-modulated signal:

$$X(t) = a\left[1 + m_r \cos(rt) + m_s \cos(st)\right] \cos(pt) \qquad (1)$$

The peak envelope voltage occur at $t = 0$ and is equal to $e_p = a(1+m_r+m_s)$; therefore, the peak power is $P_p = a^2(1+m_r+m_s)^2$ for $m_r = m_s = m$, and P_p normalized to unity, $a = 1/1 + 2m$.

Substituting this value for a in Equation (1), gives the power in one tone as

$$P_{tp} = \frac{1}{2}\left(\frac{m}{1+2m}\right)^2$$

A table of the power in a tone for the peak-power limitation in the transmitter is also shown in Table 6-1.

A comparison of narrow-band angle modulation with the average-power limited amplitude modulation and with the peak-power limited amplitude modulation, shown in the last two columns of Table 6-1. It can be seen that the narrow-band angle modulation has about the same signal-power content that the average-power limited amplitude modulated signal has, for the lower modulation indexes. For modulation indexes above, say, 0.8, the angle-modulation case becomes worse because of the increased power to the higher order sidebands.

In the comparison with the peak-power limited amplitude modulated signal, the angle-modulated signal becomes increasingly better as the modulation index increases, and improves by a factor of 4 (6 db) for a 100% amplitude modulated signal.

6.2.3 CARRIER NARROWBAND (N.B.) FILTER BANDWIDTH REQUIREMENTS

The purpose of this filter is to pass the carrier, while at the same time rejecting the modulation sidebands, to the carrier phase detector as shown in Figure 6-1. This filter must be compensated sufficiently for any carrier frequency shift due to user doppler and for all the frequency errors discussed in section 5.3.7. For a Mach 3 user aircraft with a nominal received signal at 1660 MHz, the doppler is about ±5 Hz and the maximum frequency error is 620 Hz, provided the first injection setting is calibrated once every 10 days. Therefore, the filter has to be at least 11.2 kHz wide (i.e., have a half-bandwidth of 5.6 kHz); it should be narrow enough to reject the first-order sidebands of the coarse tone modulation, which are separated by 10.0 kHz (in the case of a fine tone frequency of 300 kHz and a coarse tone frequency of 1/30 of the fine tone).

The shape-factor requirements are rather modest in that a 3-pole filter is all that is required to reject these first-order sidebands by 20 dB. The peak-to-valley ripple of the filter is about 0.1 dB. These requirements are easily met with a simple crystal filter.

6.2.4 RECEIVER DESCRIPTION (Figure 6-9)

6.2.4.1 RF STAGES

RF Preselector - The RF preselector is fixed tuned and broad enough to receive the signals from all the Phase Difference Navigation Satellites with little attenuation, while at the same time rejecting potential UHF telemetry and/or meteorological signals from other satellite carriers and also the user transmitter carrier frequencies. The insertion loss of the preselector is assumed to be less than 1 dB.

RF Amplifier - This amplifier consists of two transistor amplifier stages in a low-noise, high-gain, configuration. At 1600 MHz, each stage has a noise figure of about 3.5 dB and a power gain of greater than 6 dB. The receiver system noise figure can be made as low as 5 dB.

6.2.4.2 FIRST MIXER AND INJECTION CHAIN

First Mixer - Because of the low levels of the desired input signals (on the order of 0.1 microvolt) and the possibility of strong interference through the RF preselector, the first mixer must be designed to minimize intermodulation and crossmodulation products, thus minimizing the generation of spurious signals.

An analysis leading to the selection of the IF frequency and the type injection (high-side or low-side) will be required to predict the location of the unavoidable spurious responses.

Local Oscillator - The local oscillator must meet the long term and short term stability requirements of the navigation system as shown in section 6.3.7. Since UHF telemetry and tracking signals from all "visible" satellites can be present at the first mixer, the oscillator must be designed to minimize harmonic and spurious response.

Multiplier-Buffer - The multiplier-buffer transforms the local oscillator frequency to the proper injection frequency. The filter following the multiplier effectively attenuates spurious responses and harmonics of the local oscillator to the levels commensurate with desired system performance and RFI requirements.

6.2.4.3 FIRST IF AND 2nd MIXER/INJECTION CHAIN

IF Filter - As stated previously, the UHF telemetry signals from all the "visible" satellites may be present at the output of the first mixer. The IF filter is required primarily to reject these signals. Since the RF bandwidth occupied by each modulated carrier is about 600 kHz with a guard band of about 200 kHz, the total IF bandwidth required is of the order of 1.5 MHz.

First IF - Gain distribution requirements are such that the IF will have a maximum gain of 50 dB, including the filter loss. Proper shielding and decoupling will exist among the stages to prevent regeneration. This gain can be realized from five transistor stages.

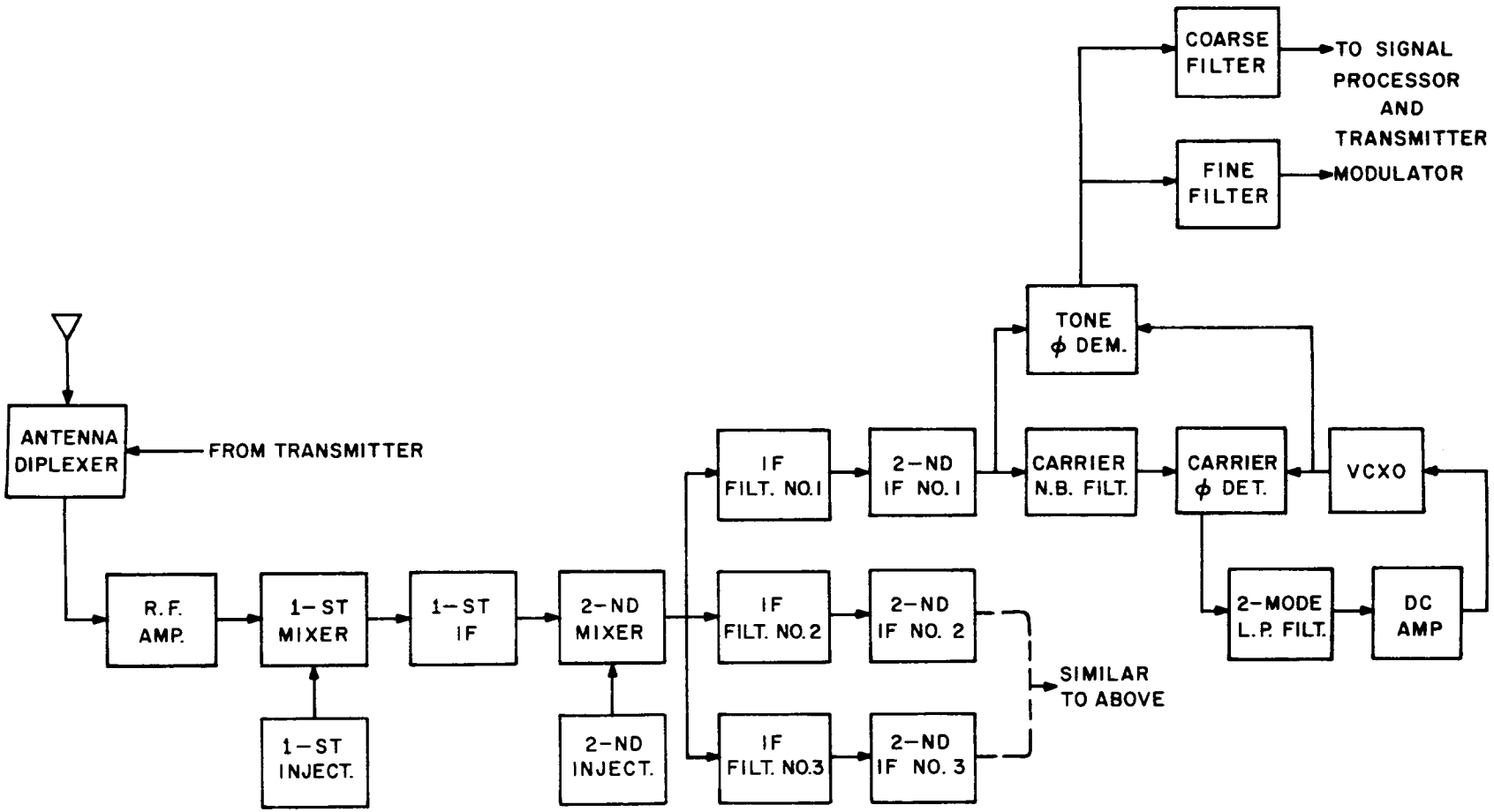

Figure 6-9. User Receiver (Functional Block Diagram)

The Second Mixer and Injection Chain - These circuits have no special requirements other than frequency conversion with a minimum of generated spuria. It is assumed that the short-term and long-term stabilities of the crystal oscillator are not compromised by the design of these circuits.

Channel Separation Filter - Assuming a small channel separation and a lumped-LC channel-separation filter, many filter sections may be required. For a 1 MHz separation and a -20 dB response, a 5-pole filter is needed. However, the required Q for each section is low, on the order of 20 to 30. The filter is assumed to have a linear phase and amplitude response.

6.2.4.4 SECOND IF AND LIMITER

A second frequency translation is incorporated into the receiver for two important reasons.

(a) To "break up" any potential high gain signal amplification at a single frequency, thus preventing possible regeneration amont the various stages. (The gain of the 2nd IF is around 60 dB.)

(b) To provide a low enough frequency for optimum phase detector operation. (Basically, the phase detector can be thought of as a synchronous switch that can be represented by a very low resistance (say, 50 ohms) in the "on" mode and a samll capacitor (say, 1 picofarad) in the "off" mode. At a 5 MHz switching frequency, the back-to-forward impedance ratio is approximately 1000. If this frequency is increased the impedance ratio decreases, resulting in a loss of efficiency.)

6.2.4.5 RANGE TONE DEMODULATION

Because of the relatively low satellite transmitter power, the high path loss due to the slant range, the large IF bandwidth required (on the order of 2 MHz), and the frequency of the fine-range tone; the predetection signal-to-noise ratio is low. In order to prevent a degradation of the signal-to-noise because of the "weak signal suppression effect" of a ν-law detector, coherent detection must be performed on the signal. In order to provide a coherent reference for the received signal, a highly stable voltage controlled crystal oscillator (VCXO) is phase-locked to the weak carrier. The noise bandwidth of the loop is narrow enought to ensure a carrier-to-noise ratio of at least 9 dB, and wide enough to maintain carrier lock during high vehicle-to-satellite accelerations.

Once carrier lock is obtained, the ranging tones are demodulated by multiplying the composite IF signal with the restored carrier. This multiplication occurs in the tone demodulator. Since the signal-to-noise ratio at the output of the tone demodulator is approximately the same as that at the input (quite low), filtering of the tone signals is required. The degree of filtering will result in a tone signal-to-noise ratio of at least 23 dB.

6.2.4.6 POWER SUPPLY

In addition to furnishing the required well regulated voltages with suitable open-circuit and short-circuit protection, the power supply must be free of low-level hum and random noise to prevent any possible phase modulation on the various VCXO's in the receiver. If phase modulation is present, unwanted sidebands will be generated that will distort the tone signals (introduce time delay) and worse, if of sufficient magnitude, prevent the phase-lock loop from closing.

6.2.5 CONTROL CENTER ACQUISITION OF RETURN-FIELD BURSTS

Since each user has a unique Doppler frequency offset (due to his relative motion with respect to the satellite field) the control center is required to perform a search-and-track operation every integration period (i.e., once every second). Because the RF signals emitted from each satellite are at nominal frequency (dynamically set by the control-center-to-satellite synchronization loop) only the user motion will cause a doppler shift. This shift can be as high as 5 kHz for a 1660 MHz carrier frequency and an aircraft velocity of Mach 3. However, once the user has been "in the system" for a while, his velocity is known fairly accurately so that the maximum incoming doppler uncertainty is very much less than 5 kHz.

In the search mode the VCO (voltage controlled oscillator) is stepped, in frequency, by the magnitude (and sign) of the expected doppler. The phase-locked loop will then "pull-in" the VCO until it locks to the incoming carrier. The pull in time is shown by Viterbi[6-4] to be a function of the initial frequency offset, the natural frequency of the loop, and the damping factor. In the case of a high-gain loop and a damping factor of 0.707, the pull-in time, T_p, is

$$T_p = 33.6 \frac{(\Delta f)^2}{(B_n)^3} \text{ seconds,}$$

Where Δf is the initial frequency offset and B_n is the two-sided noise bandwidth of the loop, as given in the link analysis. A plot of this equation is given in Figure 6-10 for initial frequency displacements of up to 1000 Hz and noise bandwidths of 25, 50, 100, and 500 Hz. In order not to degrade the signal-to-noise ratio by more than 1 dB, the pull-in time should be limited to no more than 26% of the integration time. (For a 1-second integration time the pull-in time should not exceed 0.26 second.)

In order to keep the pull-in time low, the loop should have a two-mode loop-bandwidth capability. That is, during the search the noise bandwidth should be as large as possible, compatible with loop minimum signal-to-noise requirements; and during tracking the noise bandwidth should be narrowed so that the coarse/fine resolution can be maintained. Richman [6-5] and Brooks [6-6] have analyzed two methods of mode switching. Both authors have taken experimental data to verify system performance.

6.3 CHANNEL CHARACTERIZATION

6.3.1 MATHEMATICAL CHANNEL MODELS

"Channel" as used here refers to the effects on transmitted signals from the time they leave the center ground station transmitter to the time they appear at the receiver IF

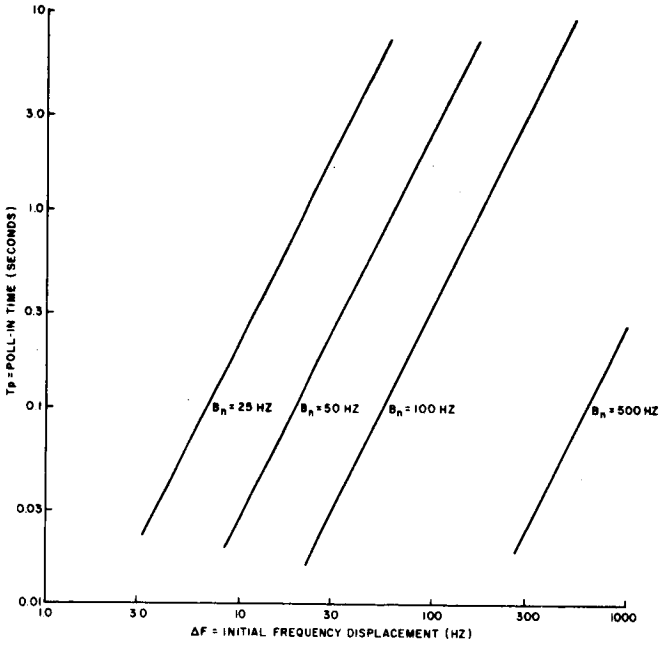

Figure 6-10. Pull-in Time vs Initial Frequency Offset as a Function of Carrier - Extraction Loop Noise - Bandwidth B_n

outputs. This definition implies a passive system. An active system would employ a user transponder. As shown in Figure 6-11, the "channel" includes the uplink transmission channel, the satellite receiver, signal processor and transmitter, the downlink transmission channel, and the user receiver front end. Implicit in this process are any effects on the received signals due to satellite and receiver motion. As indicated in Figure 6-11, the following signal notation will be used:

x = center transmitted signal

y_u = received signal and noise at the satellite uplink receiver front-end output

x_s = satellite transmitted signal

y = received signal and noise at the downlink user receiver IF output

For phase modulated signals,

$$x(t) = \sqrt{2P_T} \cos \left[\omega_c t + \theta(t) + \varphi_o\right] \tag{1}$$

For n tone modulation,

$$\theta(t) = \sum_{k=1}^{n} m_k \sin (\omega_k t + \alpha_k) \tag{2}$$

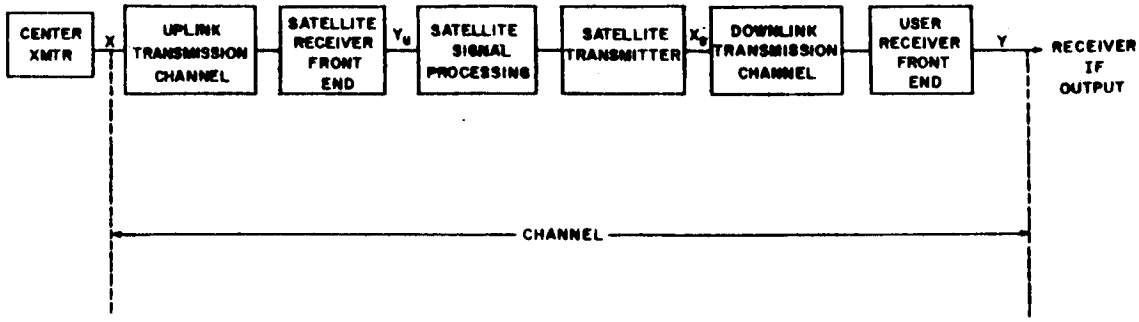

Figure 6-11. Channel Definition; Passive Mode

where

P_T = Transmitted signal power

ω_c = Carrier angular frequency

φ_o = Initial carrier phase (assumed to be a uniformly distributed random variable)

$\theta(t)$ = Tone modulation

m_k = Modulation index for the k-th tone

α_k = Initial phase of the k-th tone

Assuming that the uplink channel and the satellite receiver front-end can be modeled by a linear system, the satellite receiver front-end output will be of the form:

$$y_u(t) = \int_o^\infty A_u(\lambda, t)\, x(t - \lambda)\, d\lambda + n_u(t) \qquad (3)$$

where n_u represents uplink additive noise due to man-made interference, cosmic noise, and satellite receiver noise, and where $A_u(\lambda, t)$ is the unit impulse response function of the linear system model. The parameter λ is a memory variable, whereas

t represents real time. The dependence of A_u on t allows for time-variable effects due to Doppler shift, Faraday rotation, refraction, and receiver instability. The function A_u will be of the form

$$A_u(\lambda, t) = a_u(t)\ \delta\ [\lambda - \tau_u(t)] \tag{4}$$

where a_u describes the signal attenuation in the uplink, and the front end amplification. $\delta(u)$ represents a Dirac delta function, and τ_u represents a time variable delay of the form:

$$\tau_u(t) = \frac{r_u(t)}{C} + \tau_{uR}(t) + \tau_{uo}(t) \tag{5}$$

with

$r_u(t)$ = uplink slant range between the center and the moving satellite

C = speed of light

$\tau_{uR}(t)$ = change in transmission delay due to atmospheric refraction

$\tau_{uo}(t)$ = satellite uplink receiver front-end group-delay, assuming linear phase shift accross the frequency pass-band

Applying equations (1) and (4) to (3), the satellite receiver front-end output will be of the form:

$$y_u(t) = a_u(t)\ x\ [t - \tau_u(t)] + n_u(t) \tag{6}$$

where x is defined in (1).

If the satellite signal processing and transmitter is assumed to be linear, the transmitted satellite signal will be of the form:

$$x_s(t) = A_s \left\{ a_u(t)\ x\ [t - \tau_u(t) - \tau_s(t)] + n_u(t) \right\} \tag{7}$$

where A_s represents the satellite transmitter amplification factor, and $\tau_s(t)$ represents signal delay due to the satellite signal processing and the satellite transmitter power amplifier. Note that while the physical processes of frequency translation are strictly nonlinear, their effects on signal and noise can be regarded as linear. For simplicity, therefore, the satellite frequency translation will be ignored except for its contribution to the signal delay τ_s.

If the satellite signal processor employs an automatic gain control (AGC), the transmitted satellite signal can be approximated for analytical purposes by:[6-57]

$$x_s(t) = B_s \left\{ \frac{a_u(t)\ x\ [t - \tau_u(t) - \tau_s(t)] + n_u(t)}{\left[\int_{t - \tau_c}^{t} y_u^{\,2}(t')\ dt' \right]^{1/2}} \right\} \tag{8}$$

where T_c represents the AGC time constant.

If the satellite signal processor employs a bandpass limiter (hard-limiting satellite repeater), the transmitted satellite signal will be of the form[6-7]

$$x_s(t) = C_s \frac{a_u(t) \times \left[t - \tau_u(t) - \tau_s(t)\right] + n_u(t)}{\sqrt{\left[I_{cu}(t) + a_u \cos\left\{\theta(t - \tau_u - \tau_s) + \varphi\right]^2 + \left[I_{su}(t) + a_u \sin\left\{\theta(t - \tau_u - \tau_s) + \varphi_o\right]^2}} \quad (9)$$

where I_{cu} and I_{su} represent the inphase and quadrature components of the additive noise n_u. That is,

$$n_u(t) = I_{cu}(t) \cos(\omega_c t) - I_{su}(t) \sin(\omega_c t)$$

The downlink transmission channel can be modeled in a similar manner. Similarly to (3), the user receiver front-end output can be denoted by:

$$y(t) = \int_o^\infty A_d(\lambda, t)\, x_s(t - \lambda)\, d\lambda + n_d(t) \quad (10)$$

where n_d denotes downlink additive noise due to man-made interference, cosmic noise, and user receiver front-end noise; and where A_d represents the unit impulse response function of a linear system model of the downlink transmission channel and user receiver front end. This function will be more complicated than A_u since it must also account for: (1) frequency offsets between the received IF frequency and the user receiver IF frequency due to oscillator instability, and (2) multipath-fading signals due to one or more earth reflections to an aircraft receiver.

The general mathematical model is:

$$A_d(\lambda, t) = A_d(t) \cos(\Delta\omega t + \varphi)\, \delta(\lambda - \tau_d(t)) + \sum_{i=1}^{n} a_i(t) \cos\left[\Delta\omega_i t + \varphi_i\right] \delta\left[\lambda - \tau_i(t)\right] \quad (11)$$

The first term represents the direct component. The second term represents the multipath components.

$a_d(t)$ = Downlink signal attenuation

$\Delta\omega$ = Frequency offset due to oscillator drift

φ = Phase shift due to oscillator drift

τ_d = Time-delay of the direct component on the downlink

$a_i(t)$ = Amplitude of the i-th earth reflected signal.

$\Delta\omega_i$ = Frequency offset of i-th earth reflected signal.

φ_i = Phase shift of the i-th earth reflected signal.

$\tau_i(t)$ = Time delay of the i-th earth -reflected signal.

The direct component contains the desired time delay information. Similarly to equation (5),

$$\tau_d(t) = \frac{r_d(t)}{C} + \tau_{dR}(t) + \tau_{do}(t) \tag{12}$$

with

$r_d(t)$ = Downlink slant range between the moving satellite and a possibly moving receiver

$\tau_{dR}(t)$ = Change in transmission delay due to atmospheric refraction

$\tau_{do}(t)$ = Downlink receiver front end group-delay, assuming linear phase-shift across the receiver pass-band

Applying (11) to (10)

$$y(t) = a_d(t) \cos(\Delta\omega t + \varphi)\, x_s\left[t - \tau_d(t)\right] + \sum_{i=1}^{n} a_i(t) \cos\left[\Delta\omega_i t + \varphi_i\right]\, x_s\left[t - \tau_i(t)\right] + n_d(t) \tag{13}$$

Assuming a linear satellite repeater, x_s is given in (7). Applying (7) to (13),

$$y(t) = y_D(t) + \epsilon(t) \tag{14}$$

where

$$y_D(t) = A_s a_u(t) a_d(t) \cos(\Delta\omega t + \varphi)\, x\left[t - \tau(t) - \Delta(t)\right] \tag{15}$$

$$\tau(t) + \Delta(t) = \tau_u(t) + \tau_s(t) + \tau_d(t) \tag{16}$$

$$\tau(t) = \frac{r_u(t) + r_d(t)}{C} \tag{17}$$

$$\Delta(t) = \left[\tau_{uR}(t) + \tau_{dR}(t)\right] + \left[\tau_{uo}(t) + \tau_s(t) + \tau_{do}(t)\right] \tag{18}$$

The quantity τ contains the desired time delay information. The quantity $\Delta(t)$ consists of the uplink and downlink delay error due atmospheric refraction, and time delay errors generated in the satellite and user receiver equipment. Assuming that the systematic components of these equipment errors have been cancelled out by

means of an appropriate calibration process, the equipment induced delays in (18) can be interpreted as the residual errors caused by equipment and environmental instabilities. Similarly, the atmospheric refraction delays can be interpreted as residual errors after corrections have been made using predicted mean values.

Applying (7) to (13), the noise term in (14) is:

$$\epsilon(t) = A_s \sum_{i=1}^{n} a_i(t) \cos\left[\Delta\omega_i t + \varphi_i\right] a_u\left[t - \tau_i(t)\right] \times \left[t - \tau_u(t) - \tau_s(t) - \tau_i(t)\right]$$

$$+ A_s \sum_{i=1}^{n} a_i(t) \cos\left(\Delta\omega_i t + \varphi_i\right) n_u\left[t - \tau_i(t)\right]$$

$$+ A_s\, a_d(t) \cos\left(\Delta\omega t + \varphi\right) n_u\left[t - \tau_d(t)\right] + n_d(t) \qquad (19)$$

For analytical simplicity, three special cases will be considered in the analysis of system performance.

Model 1: No Multipath

Model 2: One reflection

Model 3: A large number of reflections

Since the retransmitted uplink noise components will have much smaller spectral density then the downlink noise, and assuming slowly varying $a_u(t)$,

Model 1: $\epsilon(t) \approx n_d(t)$

Model 2: $\epsilon(t) \approx A_s\, a_1(t) \cos\left(\Delta\omega_1 t + \varphi_1\right) a_u(t) \times \left[t - \tau(t) - \Delta(t) - \Delta_1(t)\right] + n_d(t)$

Model 3: $\epsilon(t) \approx A_s a_u(t) \sum_{i=1}^{n} a_i(t) \cos\left(\Delta\omega_i t + \varphi_i\right) \times \left[t - \tau(t) - \Delta(t) - \Delta_i(t)\right] + n_d(t) \qquad (20)$

The Δ_i are the differential delays between the direct and the reflected components.

For synchronous satellites, an aircraft receiver, and a smooth reflecting earth surface, the differential delay will be[6-8]

$$\Delta_1 \approx \frac{S/C}{\cos\varphi} \left[1 + \frac{Q\cos(\theta+\varphi) - R\cos\varphi}{M}\right] \tag{21}$$

where

R = Earth's radius $\approx$ 3960 miles

Q $\approx$ 6.5 R

M = Distance of the satellite to the tangent point to the earth directly below the aircraft

S = Aircraft altitude

θ = Aircraft latitude

φ = Angle between the reflected ray and the local vertical

Satellite elevation angle

These delays correspond to distances at least as large as the aircraft altitude. Therefore, for most cases of interest the earth-reflected components must be regarded as noise, since the desired range delay information has been destroyed by the reflection process.

Reference [6-8] also gives a formula for the differential doppler rate. Assuming an aircraft receiver flying due north and level,

$$\delta f = \frac{2SQ^2 V (R\cos\theta - Q) f_c \sin\theta}{M^3 (R+S) C} \tag{22}$$

where V is the aircraft speed. Figure 2 of Reference [6-8] gives Δ_1 and δf as a function of aircraft latitude for V equal to 600 miles per hour, a 30,000 feet altitude, and a 300 MHz carrier frequency f_c. At 150 MHz, the differential doppler will be halved. From this Figure 2, the maximum differential doppler frequency is seen to be about 0.4 Hz. This occurs at a latitude of about 70°. For a southern direction, the sign of δf is reversed. For an east-west direction the differential doppler will be less.

Expressions for the satellite doppler shift and doppler rate as seen from a stationary user are also given in Section 6.3.8. It is shown there that the 24-hour polar satellite contribution to the doppler shift and doppler rate at 1.66 GHz are less than 3311 Hz and 2.96 Hz/sec, respectively.

Applying the definition of x(t) in (1) to the expression for y_D in (15) and ϵ in (20), assuming Model 2, and writing $\Delta\omega_1$ and φ_1 as frequency and phase offsets on the carrier, the desired and undesired signals are:

$$y_D(t) = A(t)\cos\left[(\omega_c + \Delta\omega)(t - \tau - \Delta) + \theta(t - \tau - \Delta) + \varphi_o + \varphi\right]$$

$$\epsilon(t) = n_d(t) + A_1(t) \cos \left[(\omega_c + \Delta\omega)\ (t - \Delta - \Delta_1) + \theta\ (t - \tau - \Delta - \Delta_1) + \varphi_o + \varphi\right] \tag{23}$$

where

$$A(t) = \sqrt{2P_\tau}\ A_s\ a_u(t)\ a_d(t)$$

$$A_1(t) = \sqrt{2P_\tau}\ A_s\ a_u(t)\ a_1(t)$$

The complex multipath coefficient:

$$\rho = \frac{a_d}{a_1}\ e^{-j\ \Delta_1\ \omega}$$

determines the phasing and relative amplitudes of the direct and reflected components at angular frequency ω.

Model 3 corresponds to diffuse scattering. A frequently used diffuse scattering model employs a Gaussian process in describing the statistical properties of the sum of scattered components. This assumption will now be examined for the representation in equation (20).

Suppose x(t) is a unit amplitude sinusoid of frequency ω_o and random phase φ_o. It follows from (20) that the multipath scattered components will be:

$$\epsilon_r(t) = A_s\ a_u(t) \sum_{i=1}^{n} a_i(t) \cos\left[\Delta\omega_i t + \varphi_i\right] \cos\left[\omega_o\ (t - \tau - \Delta - \Delta_i) + \varphi_o\right] \tag{24}$$

Writing the function in terms of inphase and quadrature components about ω_o,

$$\epsilon_r(t) = I_{cr}(t) \cos(\omega_o t) + I_{sr}(t) \sin(\omega_o t) \tag{25}$$

where

$$I_{cr}(t) = A_s\ a_u(t) \sum_{i=1}^{n} a_i(t) \cos(\Delta\omega_i t + \varphi_i) \cos\left[\omega_o\ (\tau + \Delta + \Delta_i) + \varphi_o\right]$$

$$I_{sr}(t) = A_s\ a_u(t) \sum_{i=1}^{n} a_i(t) \sin(\Delta\omega_i t + \varphi_i) \sin\left[\omega_o\ (\tau + \Delta + \Delta_i) + \varphi_o\right] \tag{26}$$

Assume that the Δ_i are statistically independent random variables, and the φ_o and φ are independent uniformly distributed random variables over the interval $(0,\ 2\pi)$.

For sufficiently large n, it follows from the central limit theorem of probability theory that I_{cr} and I_{sr} will be normally distributed for any t, provided that their first two moments are finite. From the above assumptions, I_{cr}, and I_{sr} have zero mean value, are mutually uncorrelated, and have the same autocovariance function:

$$\begin{aligned}\psi_r(t - t') &= < I_{cr}(t)\, I_{cr}(t') > \\ &= < I_{sr}(t)\, I_{sr}(t') > \\ &= \frac{A_s^2\, a_u(t)\, a_u(t')}{4} \sum_{i=1}^{n} a_i(t)\, a_i(t') \cos\left[\Delta\omega_i(t - t')\right] \end{aligned} \tag{27}$$

It follows that I_{cr} and I_{sr} are non-stationary random processes as long as a_u and a_i are deterministic time variable quantities. If however a_u and a_i are stationary random processes,

$$\psi_r(t - t') = \frac{A_s^2 \psi_u(t - t')}{4} \sum_{i=1}^{n} \psi_i(t - t') \cos\left[\Delta\omega_i(t - t')\right] \tag{28}$$

where

$$\psi_u(t - t') = < a_u(t)\, a_u(t') >;\ \psi_i(t - t') = < a_i(t)\, a_i(t') >$$

Now, I_{cr} and I_{sr} are wide-sense stationary. Note also that the above autocorrelation functions are frequency independent. The assumptions have led to the so-called "non-frequency-selective fading" model. It follows that if the transmitted signal x(t) can be represented by an algebraic sum of single-frequency components, as is the case for the tone-modulated carrier defined by Equations (1) and (2), then each frequency component will have inphase and quadrature components with the same autocorrelation function, and therefore the same power spectrum. The bandwidth B_r of this power spectrum is the so-called fading bandwidth.

The variance

$$\begin{aligned}\sigma_r^2 &= \sigma^2\left[\epsilon_r(t)\right] \\ &= < \epsilon_r^2(t) > \\ &= \psi_r(o) \end{aligned} \tag{29}$$

is the average power of the random component. The fading ratio

$$\gamma = \frac{A_s a_u a_d}{\sigma_r} \tag{30}$$

is a measure of the relative contributions of the two components.

The above analysis can also be done for the AGC satellite repeater and the hard-limiting satellite repeater by applying equations (8) and (9). Because of the complexity of this analysis, the approach to be taken here will be to perform the linear repeater analysis, and then make estimates of any losses or gains due to employing a nonlinear repeater. For high satellite receiver input signal-to-noise ratios, one would expect a gain due to the nonlinearity.[6-9] For low signal-to-noise ratios, one expects losses in signal-to-noise ratio of the order of 1 dB in the presence of white noise interference. The worst case is a 6 dB loss, when the dominant source of interference is at the carrier frequency.[6-10] This is unlikely in a nonjamming environment. In the case of the use of the satellite repeater for multiple access, such an effect might occur due to co-channel interference. This represents a constraint on the multiple-access signal design.

In the case of an active system employing a transponder from the user receiver back through the satellite to the center receiver, the return channel is similar to that described in Figure 6-1, with the user and center interchanged. Instead of the user transmitting back a noiseless signal, it transmits back a noisy signal which is further corrupted by the return transmission channel. However, since the center receiver is ground-based, and can use a narrow-beam satellite tracking receiving antenna, there will be no multipath. Therefore channel Model 1 is applicable for a retransmission channel.

6.3.2 EFFECTS OF THE IONOSPHERE AND TROPOSPHERE

6.3.2.1 INTRODUCTION AND SUMMARY

The principal effect of the ionosphere and troposphere upon the Phase Difference Navigation Satellite system is to increase the effective propagation path length between the satellite and near-earth terminal. The effect of this incremental path length, may be partially removed by utilizing what is known of the state of the ionosphere and troposphere and a priori information as to the position of the earth terminal (particularly as it affects the elevation angle of the satellite relative to the earth terminal). In the hyperbolic and relative navigation modes, in which more than one propagation path is involved, there will be partial cancellation of the effect.

Ionosphere - At UHF the incremental path length, ΔL, due to the ionosphere is

$$\Delta L = \frac{135\, N_T\, Q(\varphi)}{f^2}$$

where

ΔL = incremental path length in feet

f = carrier frequency

N_T = "total electron content" of the ionosphere. Number of free electrons in a vertical column of one square meter (10.76 square feet) cross-section through the ionosphere

Q = "obliquity factor", a function of elevation angle, φ, of the satellite.

For a carrier frequency of 1.6 GHz and vertical propagation, the average value of ΔL is 1.6 meters (5.25 feet) but may vary by at least a factor of 10 in either direction about this value due to variations in N_T. For horizontal propagation the obliquity factor (which is unity at 90° elevation angle) is between approximately 2.4 and 4.2 depending upon the distribution of electron density with altitude. Because of the high alititude of the base of the ionosphere, approximately 100 km (62 miles), the obliquity factor does not fall off very rapidly with increasing elevation angle.

It is possible to postulate a crude mathematical model of the variation of the average value of N_T with smoothed sunspot number, local time, season and latitude based upon the measurements that have been made. The uncertainty in N_T at a particular time and place would then be about ±30% of this average. This uncertainty would include the ±20% day-to-day variation which has been experimentally observed, the uncertainty in smoothed sunspot number (which at the time of use is a predicted quantity), and the uncertainty in the model itself. Furthermore, at any one time there will be a random spatial variation of N_T due to the presence of irregularities in the ionosphere. This variation is in the order of ±5% with a correlation length of a few kilometers.

It is not possible on the basis of the experimental measurements of N_T which have been reported nor on the basis of existing physical theory to give a satisfactory statistical description of the temporal and spatial fluctuations of N_T. The percentage variations, and the correlation length due to irregularities given in the preceding paragraph are very crude estimates. It is unfortunate that the experimenters do not report the standard deviations of their data. From those published plots of average values that include plotted data points, it is estimated that the percentages given above represent something between the one- and two-sigma values.

Other effects of the ionosphere are discussed in this section and shown to be negligible at 1.6 GHz.

Troposphere - The incremental path length due to the troposphere is, in comparison to that due to the ionosphere, well predictable. That is, the variation of incremental path length is less than 5.1 meters (16.7 feet) for elevation angles greater than 6° and less than 2.5 meters (8.2 feet) for elevation angles greater than 10°. The short term fluctuation of path length is less than a few inches rms with an effective bandwidth of less than one hertz.

6.3.2.2 IONOSPHERIC EFFECTS

6.3.2.2.1 INDEX OF REFRACTION

For frequencies greater than the critical frequency, the real part, μ, of the index of refraction of the ionosphere is given by the following approximation to the Appleton-Hartree formula:(6-11)

$$\mu^2 = 1 - \frac{X}{1 - \frac{1}{2}\left[Y_T^2/(1-x)\right] \pm \left\{\frac{1}{4}\left[Y_T^4/(1-x^2)\right] + Y_L^2\right\}^{1/2}} \qquad (1)$$

where

$X = \omega_N^2/\omega^2$

$Y_T = \omega_T/\omega$

$Y_L = \omega_L/\omega$

ω = angular frequency of a radio wave

$\omega_N = \sqrt{Ne^2/\epsilon_o m}$ = angular plasma frequency

$\omega_T = \omega_H \sin\theta$

$\omega_L = \omega_H \cos\theta$

N = number density of free electrons

e = charge on an electron

ϵ_o = electric permittivity of free space

m = mass of an electron

$\omega_H = \mu_o He/m$ = angular gyro frequency of an electron

θ = angle between wave normal and geomagnetic field

μ_o = magnetic permittivity of free space

H = geomagnetic field intensity

The ± indicates that μ is double valued. The (+) refers to the ordinary and the (-) to the extradordinary wave.

For the present application (i.e., with a carrier frequency $\omega/2\pi$ of 1.6 GHz), Equation (1) may be considerably simplified. First, the X term may be eliminated from the denominator since $X=(\omega_N/\omega)^2$ and an exceptionally high value of the plasma frequency $\omega_N/2\pi$ would be 14 MHz. Hence, for a carrier frequency of 1.6 GHz

$$X < 10^{-4}$$

Equation (1) then reduces to

$$\mu^2 = 1 - \frac{X}{1 - \frac{1}{2} Y_T^2 \pm \left[\frac{1}{4} Y_T^4 + Y_L^2\right]^{1/2}} \tag{2}$$

Further simplification may be effected by noting that $\omega_H/2\pi$ is of the order of 1.6 MHz and hence from the preceding definitions of terms, for $\omega/2\pi$ of 1.6 GHz,

$$\frac{1}{2} Y_T^2 \pm \left[\frac{1}{4} Y_T^4 + Y_L^2\right]^{1/2} < 10^{-3}$$

By considering this quantity negligible in comparison to unity, Equation (2) is simplified to

$$\mu^2 \approx 1 - X \tag{3}$$

Since $X < 10^{-4}$, the following final simplification may be made,

$$\mu \approx 1 - X/2$$
$$\approx 1 - bN/\omega^2 \tag{4}$$

where

$$b = e^2/2\epsilon_o m = 1.6 \times 10^3 \text{ (MKS)} \tag{5}$$

The deviation of the index of refraction from unity $\Delta\mu = 1 - \mu$ is then

$$\Delta\mu = b \frac{N}{\omega^2} \tag{6}$$

Note that the index of refraction of the ionosphere is less than unity, corresponding to a phase velocity greater than the free space value.

Phase-Path Length - The effective phase path length, P, through the ionosphere is

$$P = \int \mu \, ds \tag{7}$$

where the integral is taken along the ray path. However, at S-band, taking the integral along the straight line path between the two terminals, even for small elevation angles, introduces only a lower order effect on P.

The difference, $\Delta L'$, between the phase path length and the geometric, free space, path length is then

$$\Delta L' = \int (\mu - 1)\, ds = - \int \Delta\mu\, ds$$

$$= - \frac{b}{\omega^2} \int N\, ds \qquad (8)$$

The quantity

$$N_T = \int_{\text{vert. column}} N\, ds$$

where the integration is over a vertical path through the ionosphere, N_T is referred to as the "total electron content" or "column density" (units of electrons per square meter) of the ionosphere. Equation (8) may now be written as

$$\Delta L' = - \frac{bN_T Q}{\omega^2} \qquad (9)$$

where Q is the "obliquity factor" which for relatively high elevation angles of the satellite relative to the terminal on the earth is equal to the cosecant of the elevation angle.

Modulation Path-Length - Although the ionosphere shortens the effective path for a pure sinusoidal signal, the medium is dispersive in such a way as to increase the effective path length of the modulation. As in a filter the time delay of the output modulation is

$$\tau = - \frac{d\varphi(\omega)}{d\omega} \qquad (10)$$

where φ is the phase advance.

From (9)

$$\varphi = \frac{\omega}{c} \cdot \frac{bN_T Q}{\omega^2} \qquad (11)$$

Hence, from (10)

$$\tau = \frac{bN_T Q}{c\omega^2}$$

and therefore, the incremental modulation path length, ΔL, is

$$\Delta L = c\tau = \frac{bN_T Q}{\omega^2} \qquad (12)$$

or the negative of that for the carrier.

6.3.2.2.2 INCREMENTAL PATH LENGTH

The most important effect of the ionosphere upon this system is the increase in effective modulation path length, ΔL, which it introduces between the satellite and the user. This effect is only partially removable due to the imperfect predictability of the ionosphere. Furthermore, the effect is not completely self compensating in the measurement of modulation phase differences between signals received at the user from several satellites.

In Equation (12), ΔL was shown to be

$$\Delta L = \frac{bQN_T}{\omega^2}$$

Since b and ω are known, the uncertainty in ΔL is due to the uncertain in Q, the obliquity factor, and in N_T, the total number of electrons in a vertical column of unit cross-sectional area through the ionosphere. These last two quantities will now be discussed.

6.3.2.2.2.1 OBLIQUITY FACTOR

The obliquity factor, Q, may be defined as

$$Q = \frac{1}{N_T} \int N(s)\, ds \qquad (13)$$

where the integral is along a straight line path connecting user and satellite. The ray bending at 1.6 GHz is negligible. If it is assumed that the electron density is spherically stratified (i.e., N = N(h) where h is altitude), then the integral in Equation (13) could be evaluated as follows:

The relationship between differential path length and differential altitude traversed by the ray is given by:

$$ds = \frac{dh}{\sin \varphi_i} \tag{14}$$

as may be seen from Figure 6-12.

From the law of sines,

$$\frac{\left(\sin \frac{\pi}{2} - \varphi_i\right)}{\left(\sin \frac{\pi}{2} + \varphi\right)} = \frac{a}{a + h} \tag{15}$$

or

$$\frac{\cos \varphi_i}{\cos \varphi} = \frac{a}{a + h} \tag{16}$$

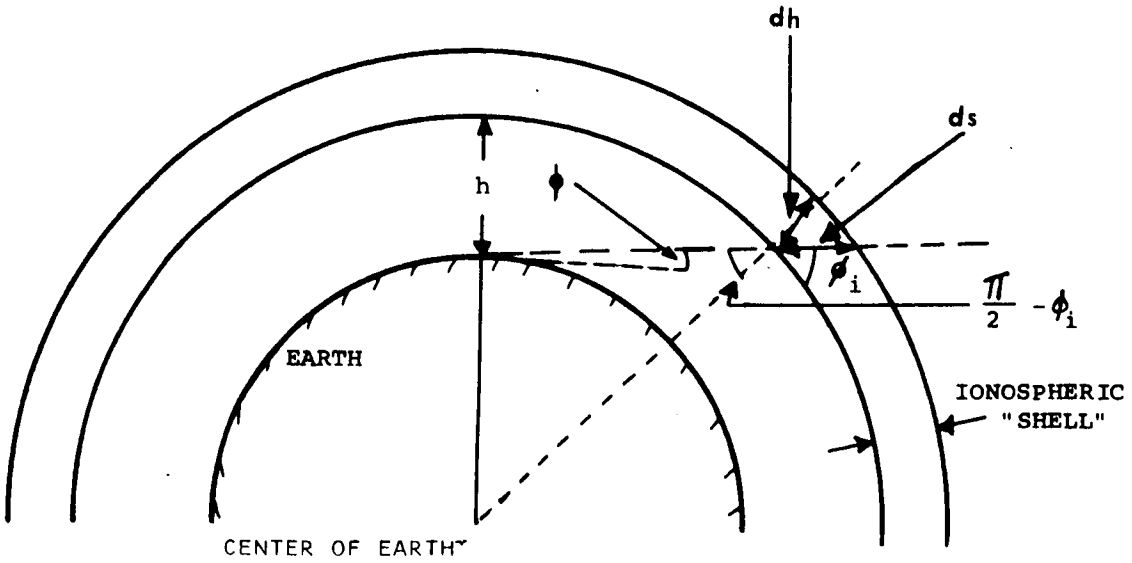

Figure 6-12. Obliquity Factor Geometry

From which

$$\sin \varphi_i = \sqrt{1 - \left(\frac{a}{a+h}\right)^2 \cos^2 \varphi} \tag{17}$$

Hence, from (13), (14) and (17)

$$Q = \frac{1}{N_T} \int_{h\,(user)}^{h\,(satellite)} \frac{N(h)\ dh}{\sqrt{1 - \left(\frac{1}{1 + h/a}\right)^2 \cos^2 \varphi}} \tag{18}$$

The detailed ionospheric profile N(h) is a function of many parameters, principally time of day, sunspot number, season and latitude. In addition to these determinable parameters, the ionosphere is strongly influenced by large day-to-day variations in the solar emission of ultraviolet, x-rays, and charged particles (this last called the "solar wind"). Furthermore, there are inhomegeneities in the ionosphere which produce variations in N_T of plus or minus a few percent. Nevertheless, the ionospheric profile does have a characteristic shape[6-12] as shown in Figure 6-13. The base of the ionosphere is at approximately 100 km (62.1 miles) at night and approximately 80 km (49.7 miles) during the day. The average height of the peak is approximately 350 km (218 miles) but may vary between the extremes of 200 and 500 km (124 and 311 miles). The columnar electron content above the peak varies from about twice to more than six times the content below the peak.

A theoretical N(h) profile was derived by Chapman[6-12] in 1931:

$$N(Z) = N_m \exp\left[\frac{1}{2}\left(1 - Z - \sec \chi\ e^{-Z}\right)\right] \tag{19}$$

where

$$Z = \frac{h - h_m}{H} \tag{19a}$$

h_m = height of maximum ionization density

H = "scale height"

χ = solar zenith angle

N_m = maximum electron density

The Chapman distribution is based on a highly simplified physical model, which is known to differ greatly from the true situation. Nevertheless, the Chapman distribution agrees surprisingly well with the measured profiles. It should be noted that Equation (19) is a single peaked function, whereas the actual ionospheric profile has several "layers" (D, E, F_1, F_2 in order of increasing altitude) which generally

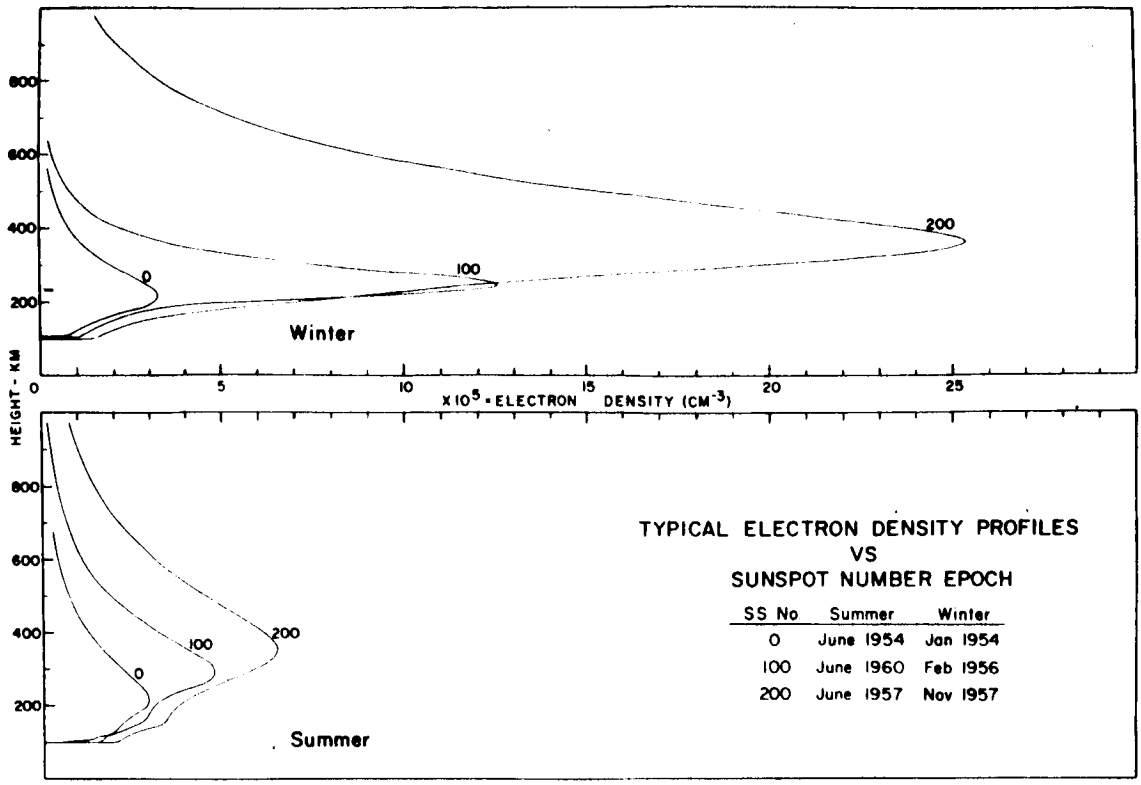

Figure 6-13. Solar Cycle Changes in Noon N(h) Profiles (From Ref. 6-12) (After J.W. Wright, 1962, Dependence of the Ionospheric F Region on the Solar Cycle, Nature 194, 461.)

(though not always) correspond to distinct peaks. The F region, which at times appears as two layers F_1 and F_2, represents most of the total electron content of the ionosphere. Excepting twilight conditions, the total ionospheric profile appears to be reasonably close to a Chapman model.(6-13)

The integral in Equation (18) with N(h) as given in Equation (19) will not be evaluated in this report. It is instructive, however, to consider the variation of Q with elevation angle for an idealized model consisting of the ionosphere concentrated into a thin spherical shell at the altitude of the peak of N(h). This form of approximation has been used(6-14, 6-115) in the evaluation of N_T from measurements of the Faraday rotation of satellite signals. The determination of N_T involved the evaluation of $\int$ NM ds

where M is a magnetic factor varying slowly with h. It was found(6-14) that using the value of M at 350 km (218 miles) was an optimal choice for elevation angles greater than 50°. In Figure 6-14, the obliquity factor versus elevation angle is plotted for such a shell model with shell altitude, h_o, of 350 km (218 miles) representing the average and 200 km (124 miles) and 500 km (311 miles) representing extremes, for the altitude of the F_1 or F_2 peak.

Millman(6-16) using two representative N(h) profiles, one for day and one for night, plots range error versus target altitude for 0°, 5° and 20° elevation angles at 400 MHz. The ratio of range error at 0° to that at 20° for a target at infinite altitude

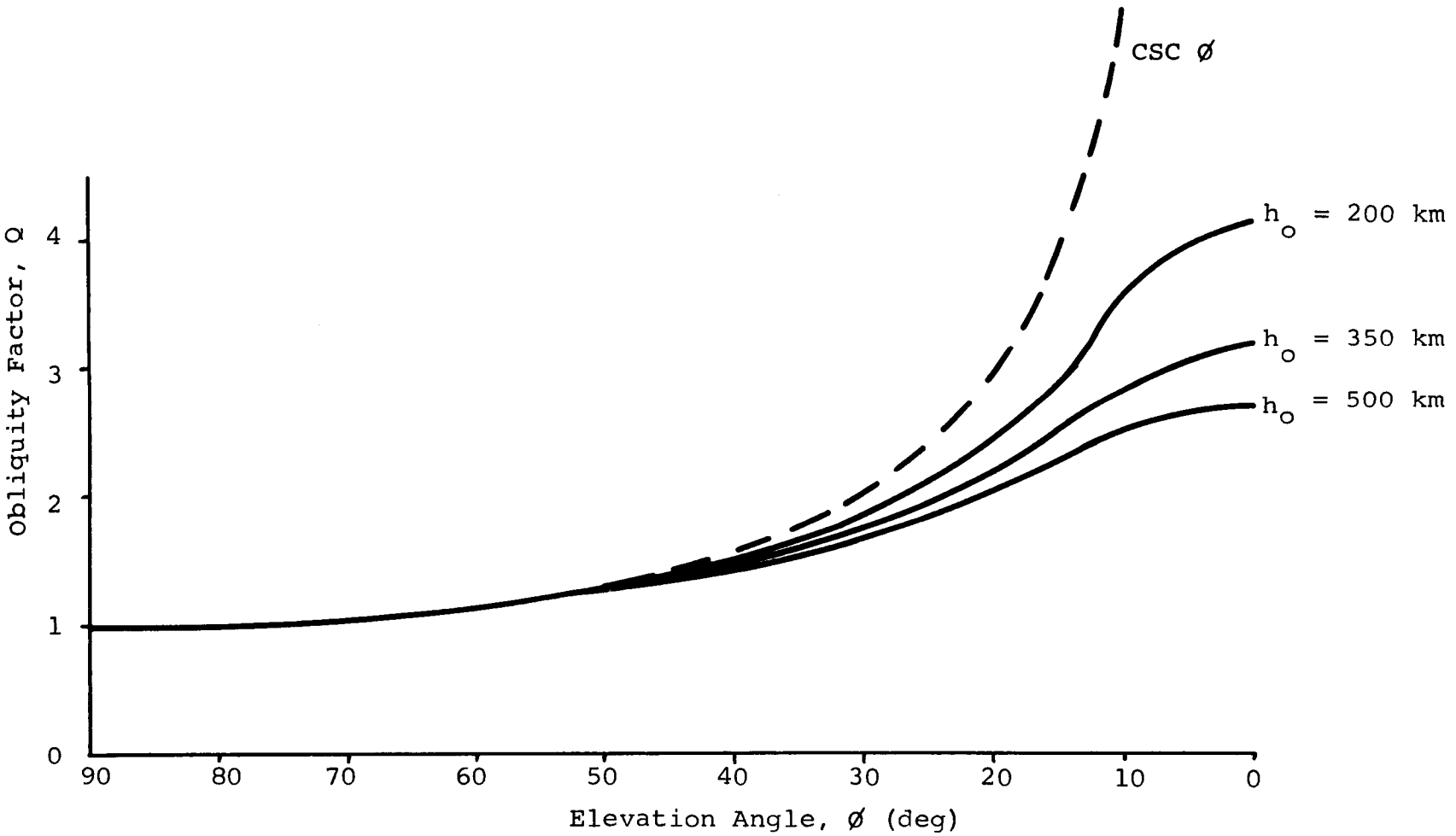

Figure 6-14. Obliquity Factor Versus Elevation Angle for Shell Model Ionosphere at Altitude h_o

should be equal to the ratio of obliquity factors at these angles. For Millman's curves this range error ratio is 1.46 (day) and 1.50 (night), which is in good agreement with the corresponding obliquity factor ratio of 1.43, using the shell model with an h_o of 350 km (218 miles); for h_o of 200 and 500 km (124 and 311 miles), the ratios are 1.31 and 1.69 respectively.

For high elevation angles the obliquity factor is approximately equal to the cosecant of the elevation angle, corresponding to a planar ionosphere, and is independent of the ionospheric profile. For elevation angles greater than 15° the uncertainty in Q should be less than ±10%, without a priori knowledge of the ionospheric profile.

If one assumes a Chapman distribution, the ability to eliminate the uncertainty in the obliquity factor is a function of one's ability either to measure or to predict both the scale height H (Equation 19a) and the height of the ionization peak.

Assuming a Chapman distribution the obliquity factor is a function of the scale height H (see Equations 19 and 19a) and h_m as well as elevation angle.

Smyth Research Associates(6-17) based their calculation of Q upon an analytically more convenient form of density profile than the Chapman distribution. They used a parabolic distribution below the peak and a hyperbolic secant form above the peak, or more specifically

$$N/N_{max} = 1 - (1 - \sigma)^2 \quad \text{for} \quad 0 \leq \sigma \leq 1$$

$$= \operatorname{sech} \frac{\pi}{4} (\sigma - 1) \quad \text{for} \quad \sigma > 1$$

where

$\sigma = h - h_b/Y_m$

h_b = altitude of base of distribution

Y_m = base to peak altitude difference

The equivalent of Q versus elevation angle was plotted for h_b = 200 and 250 km (124 and 155 miles) and Y_m = 100 and 150 km (62.1 and 93.2 miles). The four combinations of values of h_b and Y_m which correspond to distribution peaks at 300, 350 and 400 km (186, 218 and 249 miles) yield plots of Q which have approximately the same form as in Figure 6-14. The values of Q at zero elevation angle are between 2.7 and 3.0.

The uncertainty in the obliquity factor, for low elevation angles should be reducible by utilization of a Chapman model, or a physically more realistic model (see Reference 6-14 for a description of a "diffusion transport layer" above the peak and Chapman distribution below), and predictions of the parameters of the model. Predictions of the height of the peak density, h_m, and the peak density, N_m, are both used in the monthly "Ionospheric Predictions" published by ESSA(6-18, -19, -20).

For a Chapman distribution, the scale height is [6-21]

$$H = 1/4.133 \ N_T/N_m$$

The ratio N_T/N_m is designated in the literature as the "slab thickness", τ, of the ionosphere. Some studies[6-13, -14, -22, -23, -24, -25] have been conducted of the variation of τ.

Further investigations would be necessary to determine some quantitative description of the predictability of Q, such as the variance of Q about its predicted value.

6.3.2.2.2.2 TOTAL ELECTRON CONTENT

The total electron content, N_T, varies about its approximate mean of 10^{17} m^{-2} "by at least a factor of ten in each direction[6-11]. The principal variations of N_T are with sunspot number, time of day, season and latitude. In addition, there are day-to-day fluctuations, simultaneous spatial variations due to ionosphere irregularities, and short term (in the order of minutes) variations due to motion of the irregularities.

Seasonal and Sunspot Variations - Yeh and Swenson[6-14] have combined their observational data with that of several other observers to produce the empirical curves of Figure 6-15. These curves show the mid-day, mid-latitude dependence of N_T on smoothed sunspot number for the solstices and equinoxes. A more detailed picture of the seasonal variation of N_T is given in Figure 6-16 (from Yeh and Swenson). It would seem reasonable to expect that N_T would decrease from summer through the equinox to winter, following the intensity of solar irradiation (as does the diurnal variation). The fact that N_T does not follow such a pattern is referred to as the "seasonal anomaly". It should be noted that the data upon which these curves are based were obtained from satellites at altitudes of approximately 1000 km (621 miles). The total electron content up to synchronous altitude is approximately 10% greater than that up to 1000 km (according to Dr. Lawrence of ITSA, formerly the CRPL).[6-26]

The smoothed sunspot number, $\bar{R}$, is a running yearly average (six months ahead and six months behind) of a linear function of the number of spots and groups of spots observable[6-12]. $\bar{R}$ is roughly periodic with a period of approximately 11 years with maxima in the range 50 to 200 and minima in the range 0 to 10. Recent observed and predicted values of $\bar{R}$ are shown in Table 6-2 and Figure 6-17 which are reprinted from Reference 6-20.

Diurnal Variation - The diurnal variation of N_T is illustrated by the curves of Figures 6-18 through 6-21 (from Reference 6-27) which were made by monitoring radiation from synchronous altitude (Early Bird) at mid-latitude (Hamilton, Mass. and Greenbank, W. Va.). This general form of diurnal variation appears to occur (with the exception of the solstices in the polar regions) for all seasons, latitudes and sunspot numbers. The ratio of afternoon peak to pre-dawn minimum at mid-latitudes has been found to vary with sunspot number from about 3:1 at $\bar{R} = 10$ (Ref. 6-28) to 10:1 at $\bar{R} \approx 170$ (Ref. 6-21). Further evidence of this dependence of diurnal range upon $\bar{R}$ is given in Reference 6-24.

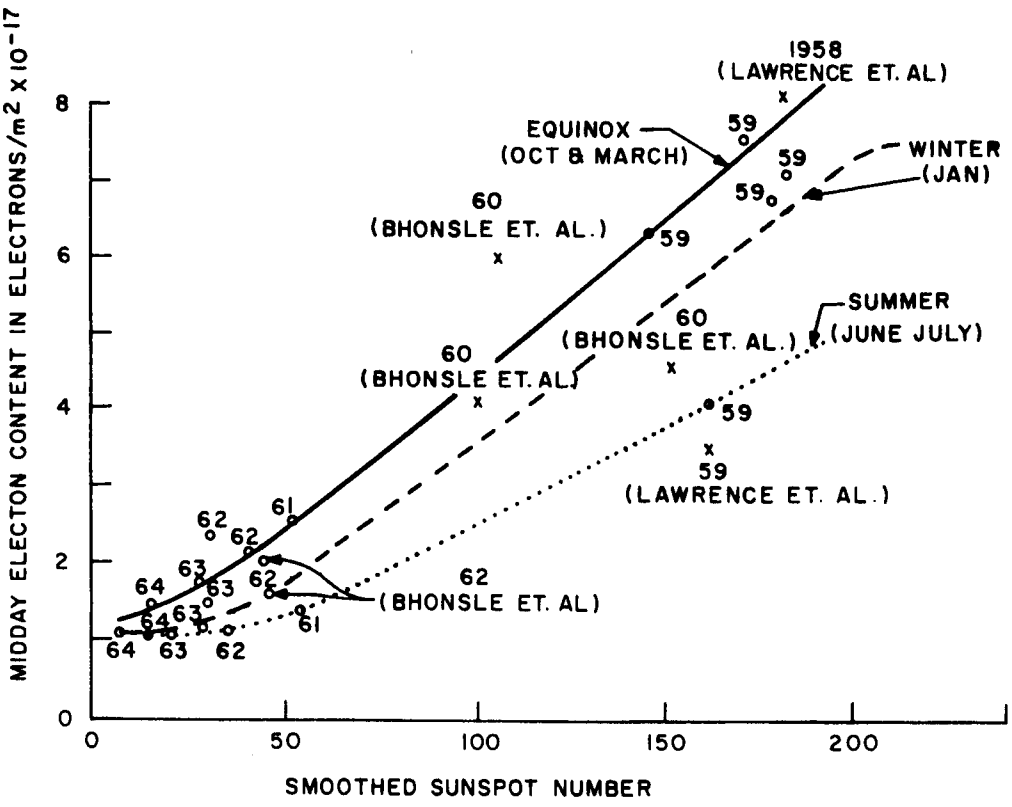

Figure 6-15. Sunspot Dependence of Midday Electron Content. (Present Values are Shown by Dots for Years 1961-1964. Values Obtained Earlier at the Univ. of Illinois are Also Shown as Dots for Years 1958-1959 (Yeh and Swenson, 1961.) Values Obtained by Other Authors are as Shown. (From Reference 6-14)

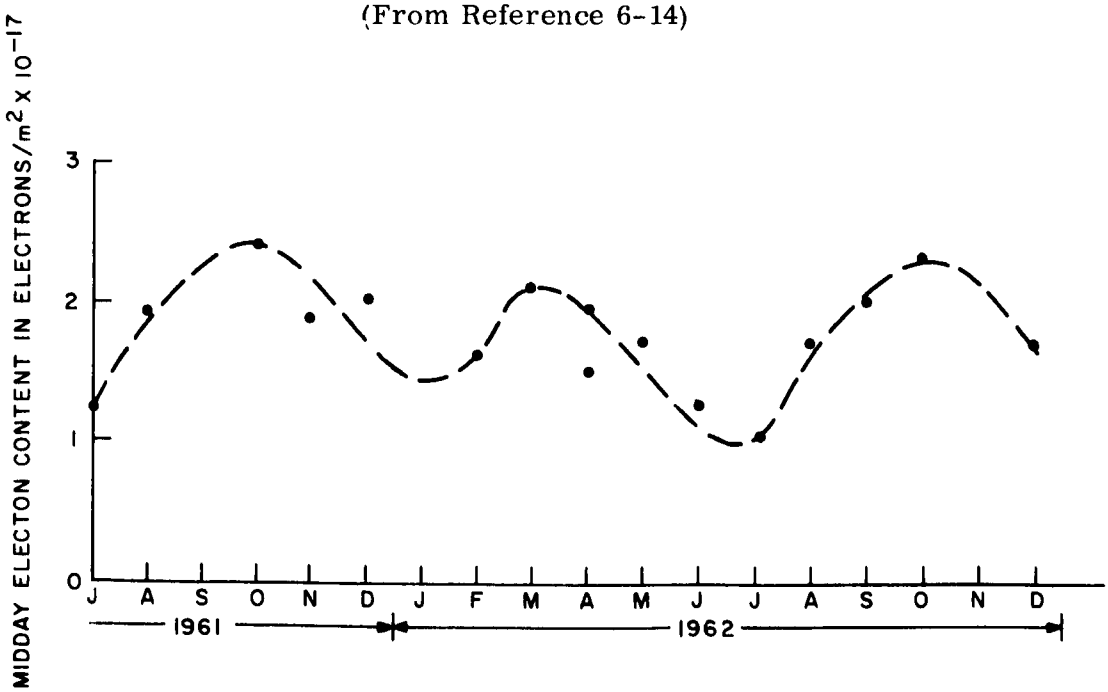

Figure 6-16. Seasonal Variation of Midday Electron Content, July 1961 to December 1962.

TABLE 6-2. OBSERVED AND PREDICTED ZURICH SMOOTHED SUNSPOT NUMBERS

(Reprinted from Ref. 6-20)

Month	Jan	Feb	Mar	Apr	May	Jun	Jul	Aug	Sep	Oct	Nov	Dec
1958	199	201	201	197	191	187	185	185	184	182	181	180
	(150)	(150)	(150)	(150)	(150)	(150)	(150)	(150)	(150)	(150)	(150)	(150)
1959	179	177	174	169	165	161	156	151	146	141	137	132
	(150)	(150)	(150)	(150)	(146)	(143)	(141)	(142)	(141)	(139)	(137)	(137)
1960	129	125	122	120	117	114	109	102	98	93	88	84
	(136)	(135)	(133)	(130)	(125)	(120)	(118)	(115)	(110)	(108)	(105)	(100)
1961	80	75	69	64	60	56	53	52	52	51	50	49
	(100)	(90)	(90)	(90)	(85)	(85)	(80)	(75)	(70)	(70)	(65)	(60)
1962	45	42	40	39	39	38	37	35	33	31	30	30
	(60)	(50)	(48)	(45)	(42)	(37)	(34)	(31)	(29)	(28)	(27)	(34)
1963	29	30	30	29	29	28	28	27	27	26	24	21
	(31)	(28)	(26)	(25)	(25)	(25)	(23)	(21)	(20)	(18)	(18)	(17)
1964	20	18	15	13	11	10	10	10	10	10	10	11
	(17)	(17)	(17)	(17)	(17)	(17)	(17)	(17)	(17)	(17)	(17)	(17)
1965	12	12	13	14	15	15	15	16	17	19	22	24
	(15)	(16)	(16)	(16)	(15)	(17)	(21)	(29)	(22)	(22)	(26)	(29)
1966	27	31	34	36	40	43						
	(33)	(37)	(40)	(47)	(50)	(52)	(55)	(58)	(59)	(65)	(68)	(71)
1967												
	(77)	(82)	(85)	(87)	(88)	(90)						

Note: Final numbers are listed through June 1965, the succeeding values being based on provisional data. The predicted numbers, in parenthesis, are not always exactly the same as the McNish-Lincoln figures used in Figure 6-17.

The diurnal range is evidently a function of latitude also as may be seen from Figures 6-22, 6-23, and 6-24 which show N_T as a function of local time and latitude. From these figures it may be seen that the diurnal range tends to increase with decreasing latitude. For equatorial latitudes, measurements at Nairobi[6-22] (which is at 1.32° S. Lat. and is 10.5°S. of the magnetic-dip equator) showed a diurnal range of 12:1 during a period when $\bar{R}$ was approximately 11. On the other hand, measurements at Huancayo Peru[6-23] at 12.03° S. Lat. showed a diurnal range of approximately 8:1 during a period when $\bar{R}$ was approximately 52. Because most of the measurements of N_T have been made at mid-latitude, information on the behavior of N_T near the equator is very limited.

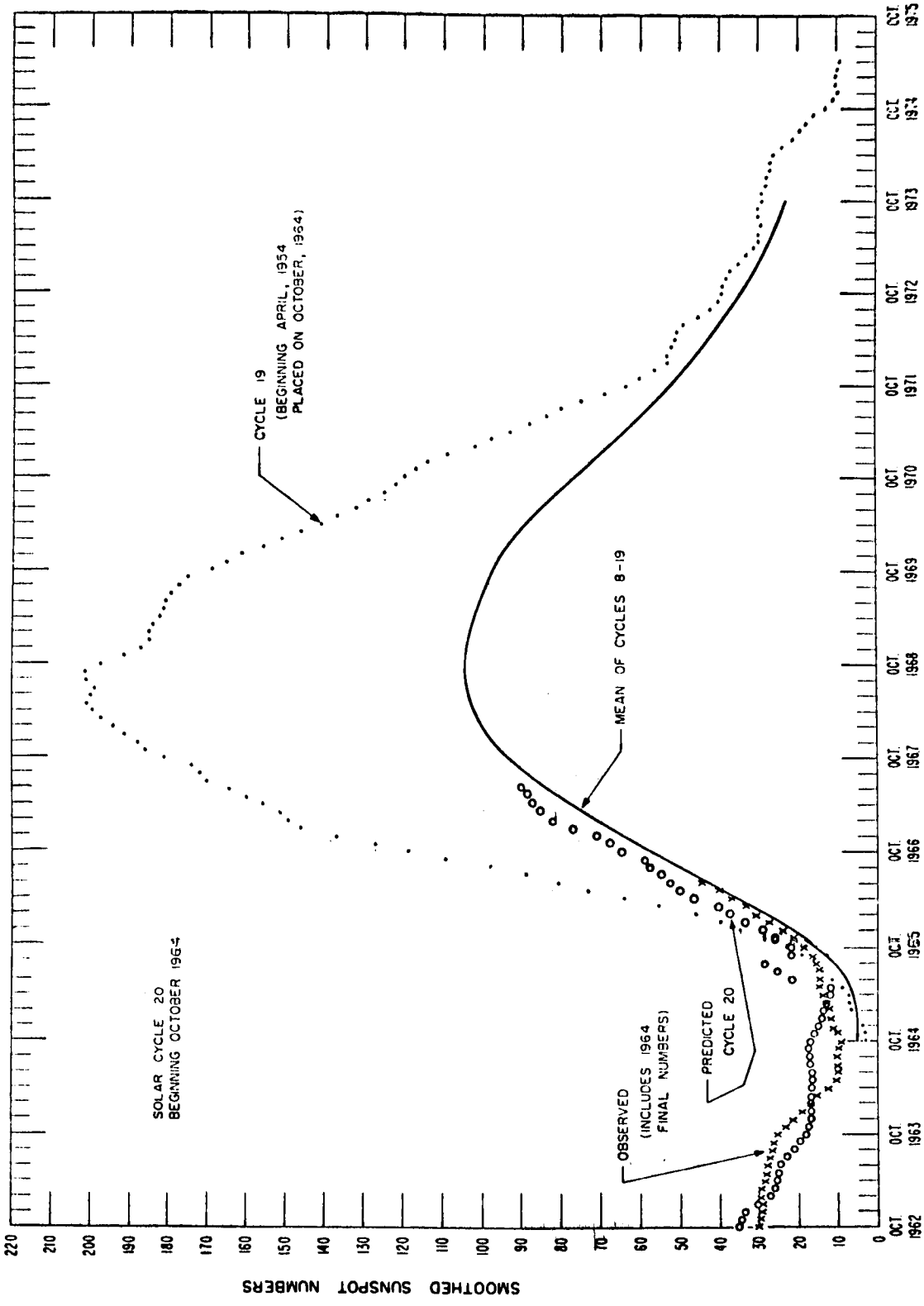

Figure 6-17. Predicted and Observed Sunspot Numbers (From Ref. 6-20)

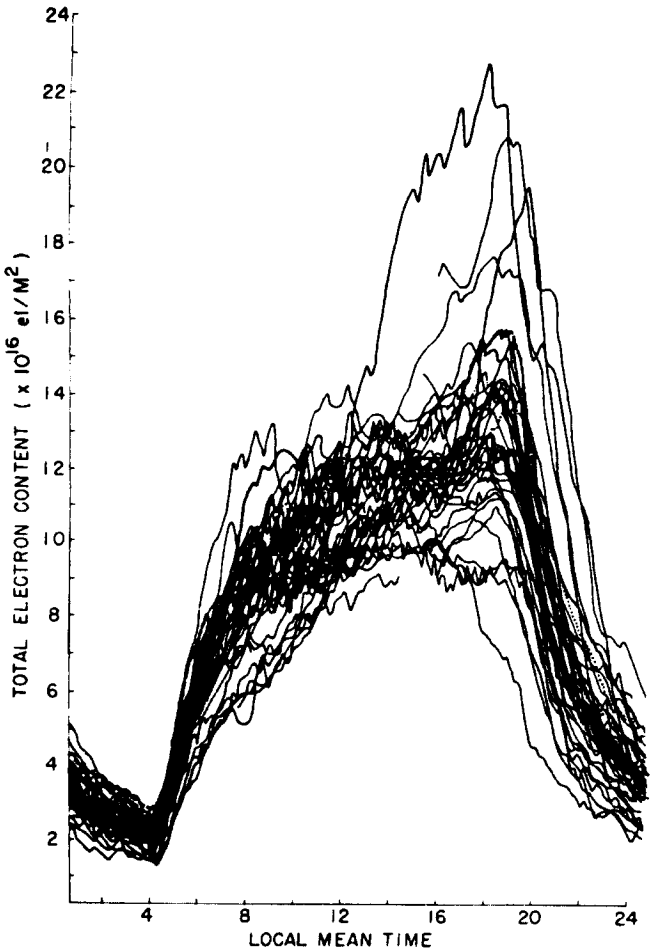

Figure 6-18. Total Electron Content May - June 1965, Local Noon at Center (From Ref. 6-27)

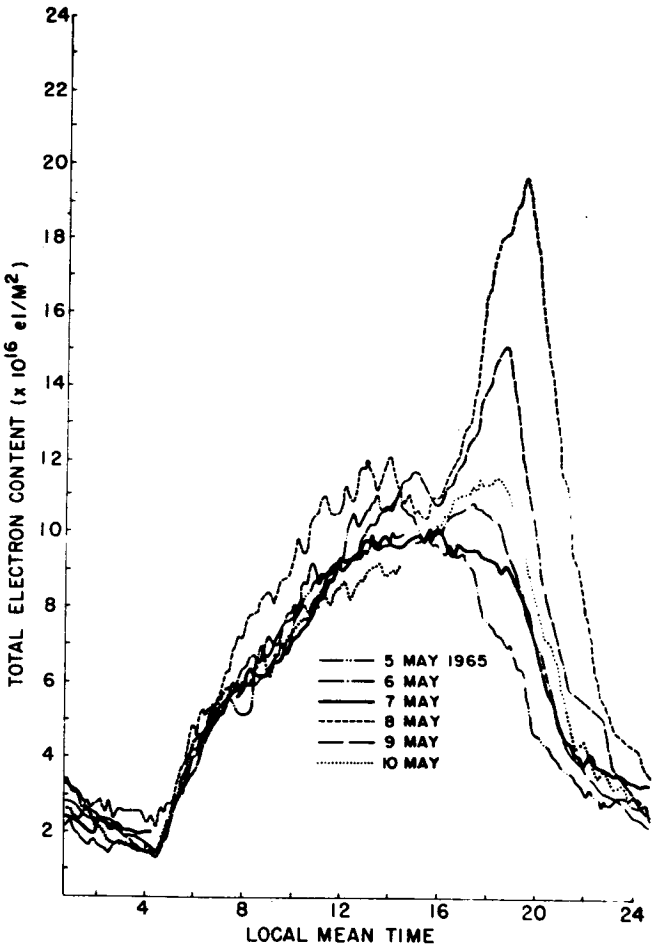

Figure 6-19. Total Electron Content - 5 May to 10 May 1965 (From Ref. 6-27)

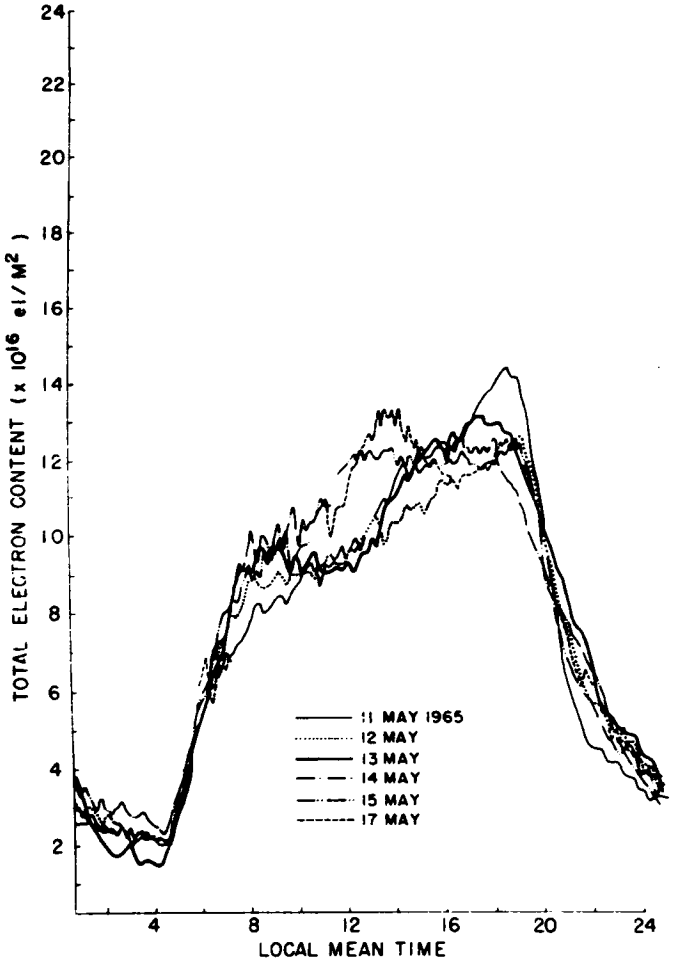

Figure 6-20. Total Electron Content - 11 May to 17 May 1965 (From Ref. 6-27)

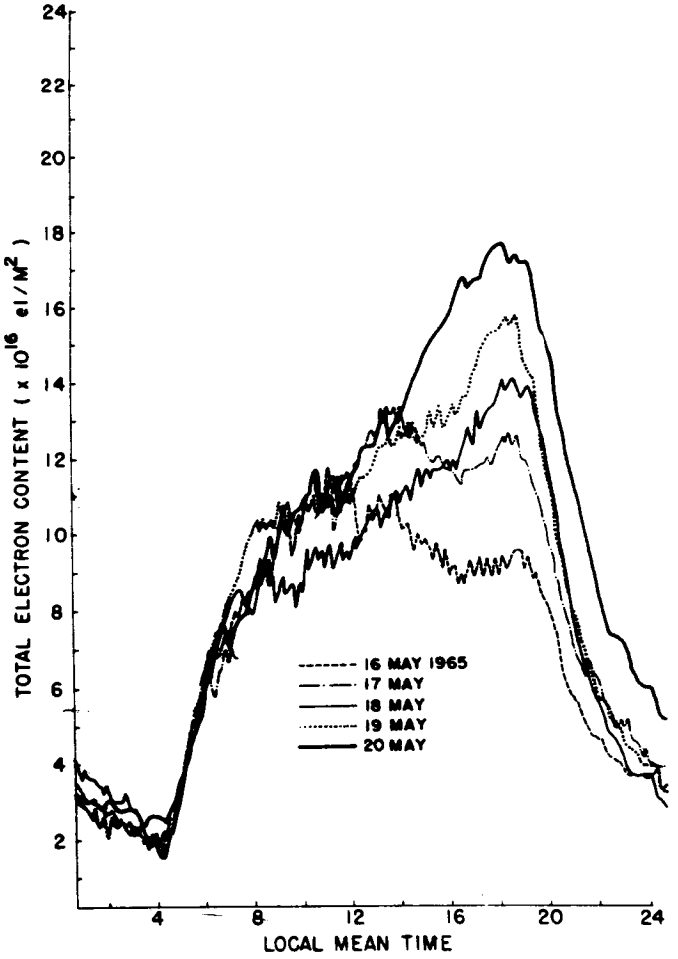

Figure 6-21. Total Electron Content - 16 May to 20 May 1965 (From Ref. 6-27)

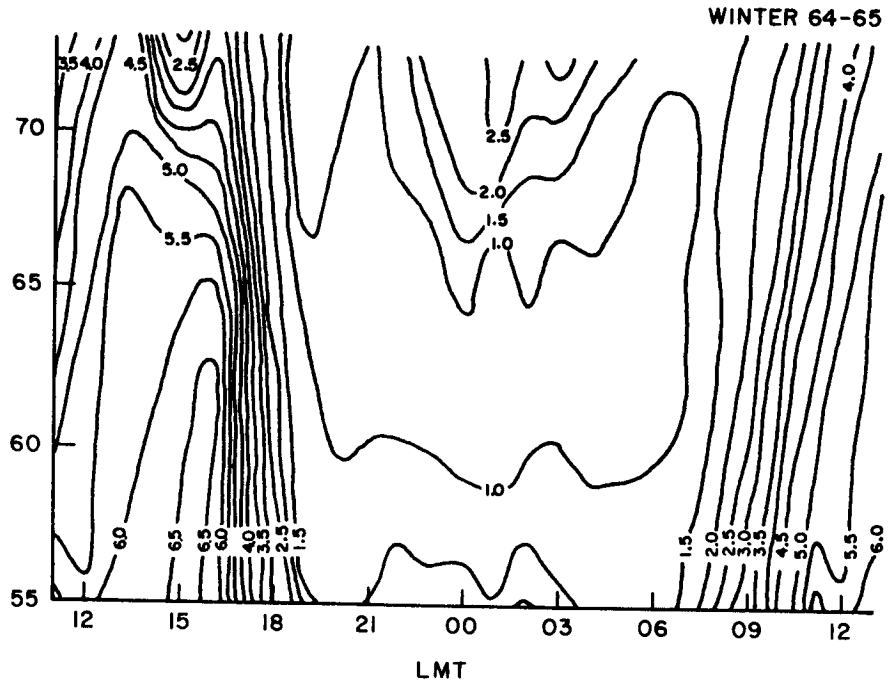

Figure 6-22. Latitudinal and Diurnal Variations of the Ionospheric Electron Content Near the Auroral Zone During Winter 1964-65. Units are 10^{-16} Electrons/m^2 (From Ref. 6-25)

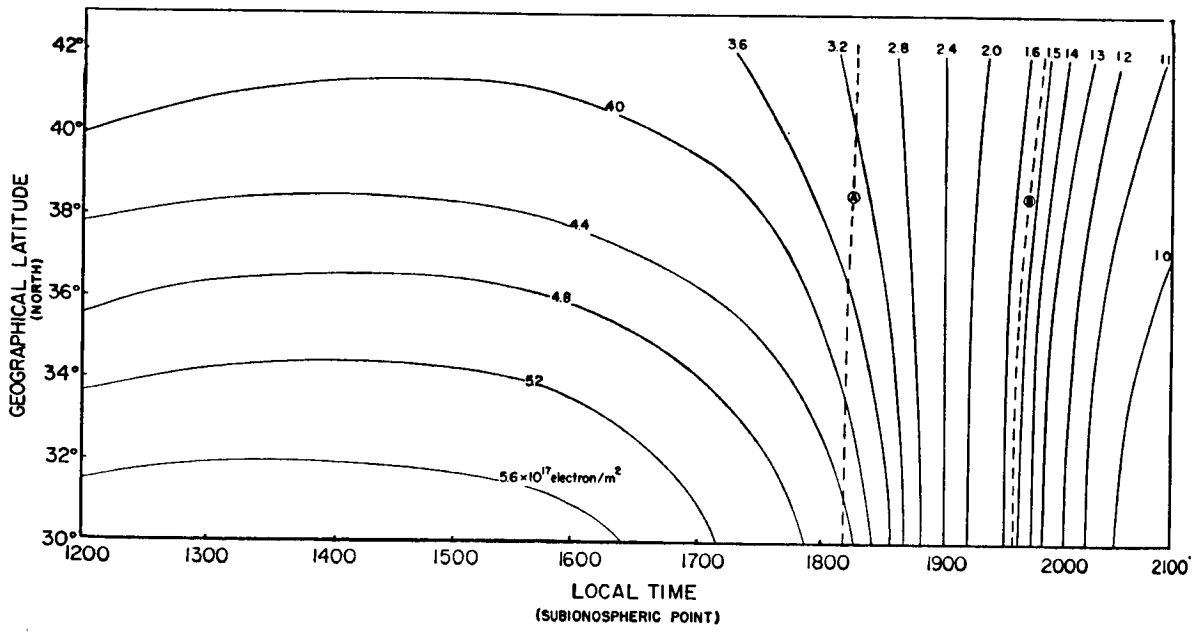

Figure 6-23. Smoothed Curves of Constant $\int N\,dh$ Derived from Measurements on Quiet Days During Sept. and Oct. 1960. Curve A Represents Sunset at Sea Level and Curve B Sunset at Height h = 400 Km for 12 Sept. 1960

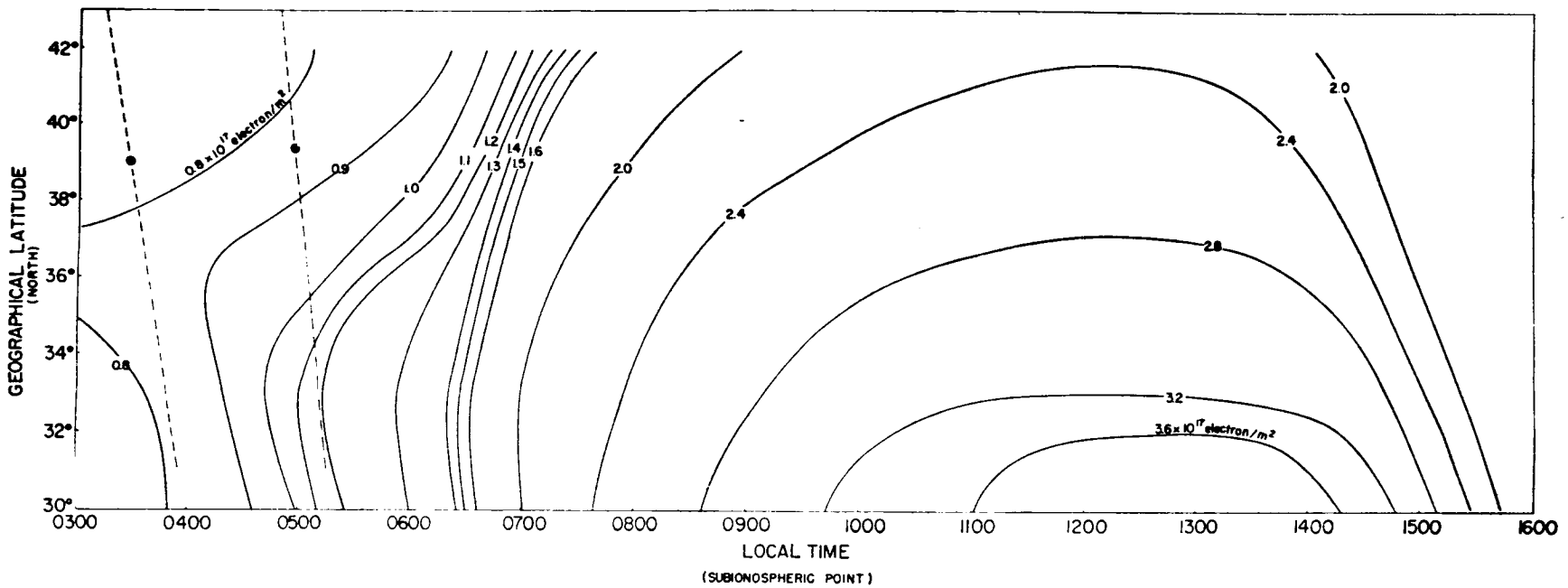

Figure 6-24. Smoothed Curves of Constant $\int N\,dh$ Derived from Measurements on Quiet Days During July and August 1960. Curve A Represents Sunrise at Sea Level and Curve B Sunrise at Height h = 400 Km for 29 July 1960

Latitudinal Variation - Observations of N_T have been made predominantly at mid-latitudes. Nevertheless, there appears to be a trend of decreasing N_T away from the equator. Observations close to the equator at Nairobi(6-22) and Huancayo(6-23) indicate a daytime peak approximately twice that at mid-latitude. Bhonsle et al(6-13) show a decrease of about 20% in daytime peak from 40°N to 45°N. The results of Liszka(6-25) in Figure (6-22) show the latitudinal and diurnal variations between 55°N and 72.5°N. This figure shows a decrease of N_T with latitude during the day and a minimum of N_T between 62°N and 70°N occurring at night. Figures 6-23 and 6-24 from Reference 6-29, covering the latitude range from 30°N to 42°N, show the same general features (without the night time latitudinal dip).

Day-To-Day-Variations - Bhonsle, daRosa and Garriott(6-13) referring to the day-to-day and pass-to-pass variations (of Transit 4A) report: "...there is scatter in the values of N_T on the order of ±20%...". F. deMendonca reports(6-29) day-to-day variations at given latitudes at a given hour in magnetically quiet periods were about ±15% from the mean. "However, it was also observed that there were less frequent magnetically quiet days in which N_T varied as much as ±50% from the average." Ross(6-30) reports: "there are day-to-day variations in electron content which may be as large as ± 20% from the mean."

The numbers quoted above agree roughly with the variation shown in Figure 6-18. Referring to that figure, at 19 hours LMT, excluding the four highest and the one lowest record, the spread in N_T is about ± 28%.

Spatial Variations Due to Irregularities - The existence of irregularities or clouds in the ionosphere has been known since 1946. They were first discovered by noting that the scintillation of radio stars as observed at separated locations were not correlated. This scintillation is caused by the horizontal variations in electron density, and hence by variations in the electromagnetic "thickness" of the ionosphere, acting to produce spatial phase variations which then result in amplitude variations at the ground receiver. This is similar to the action of a diffraction grating. Since their discovery, the irregularities have been studied by means of (1) their effect on stellar and solar radio emission and on lunar radar echoes; and (2) more recently through the scintillation of satellite signals and the direct measurement of N_T using orbiting and synchronous satellites.

Ideally, for the purposes of the Phase Difference Navigation Satellite System, one would like to have a description of the spatial fluctuation of N_T from its mean value in the form of a two-dimensional* auto-covariance function whose parameters would be known functions of local time, latitude, season, sunspot number and magnetic activity. Unfortunately, the available information falls far short of this ideal for reasons of the quantity and form of the data taken, the extent to which the data has been analyzed, and the interests of the experimental investigators. The investigators are interested in, among other things, the irregularities in the ionosphere as distinct

*Two-dimensional since there is good evidence that the irregularities are elongated along the earth's magnetic field.

from the irregularity of the ionosphere. This distinction is more than a semantic one. When records of N_T are obtained over many passes of an orbiting satellite, only those passes are evaluated which exhibit large variations of N_T during the pass. Numerical conclusions are then derived about the individual irregularities;[6-31] for example, the size, deviation in N_T at the center, and the horizontal gradient at the edge. It is interesting to note that the published sample N_T profiles of these selected passes do not appear as a set of clearly isolated peaks against a smooth background, but rather like a noise process. Two such examples are shown in Figures 6-25 and 6-26. The studies of irregularities through the spatial and temporal patterns of scintillation of stellar and satellite radiation sources have also concentrated upon the irregularities as distinguished from the irregularity of the ionosphere.

From an examination of the published literature and telephone conversations with people directly involved with ionosphere research (R. G. Merrill of ITSA; E. R. Schmerling, Chief Ionospheric Physics, NASA; J. AArons and J. A. Klobuchar of AFCRL), it appears that the correlation distance is several kilometers and the standard deviation is a few percent (less than five) of the average value of N_T (at the given local time, season, etc.) The most significant irregularities are close to the altitude centroid of the electron density; i.e., about 350 km (218 miles) altitude.

6.3.2.2.2.3 SUMMARY OF IONOSPHERIC PATH LENGTH ERRORS

In this subsection, several phase difference navigation modes of operation will be discussed in terms of their associated path length errors. Curves and examples of these errors will be given for the cases which include and exclude correction of the path length errors to the extent possible from a priori knowledge of the state of the ionosphere and position of the user.

The model assumed for the variation of the ionosphere is as follows: There is a predictable variation (with sunspot number, time of day, season and latitude) of total electron content, N_T, from 10^{16} to 10^{18} (with a nominal value of 10^{17}) electrons per square meter.

There is an uncertainty in the predicted value of N_T of ±30% due to day-to-day variations (± 20%); uncertainty in sunspot number (which at the time of its utilization is itself a predicted quantity); uncertainty in the parameters upon which the prediction is based, such as local time and latitude; and uncertainty in the prediction model itself. Furthermore, it is assumed that the spatial variation of N_T at any given time is ± 5% due to irregularities. The bounds of the uncertainty in obliquity factor will be those corresponding to the shell model of the ionosphere at heights of 200 km (124 miles) and 500 km (311 miles) as shown in Figure 6-14. The nominal obliquity factor will be for a shell at a height of 350 km (218 miles).

Circular Mode - In this mode, where range measurements are made from each of two satellites, the significant errors are in the path length itself (as distinguished from the hyperbolic and relative navigation modes in which the error is in the difference between two path lengths is significant). In Figure 6-27, this uncorrected error is plotted versus elevation angle. The upper and lower curves show the effective bounds

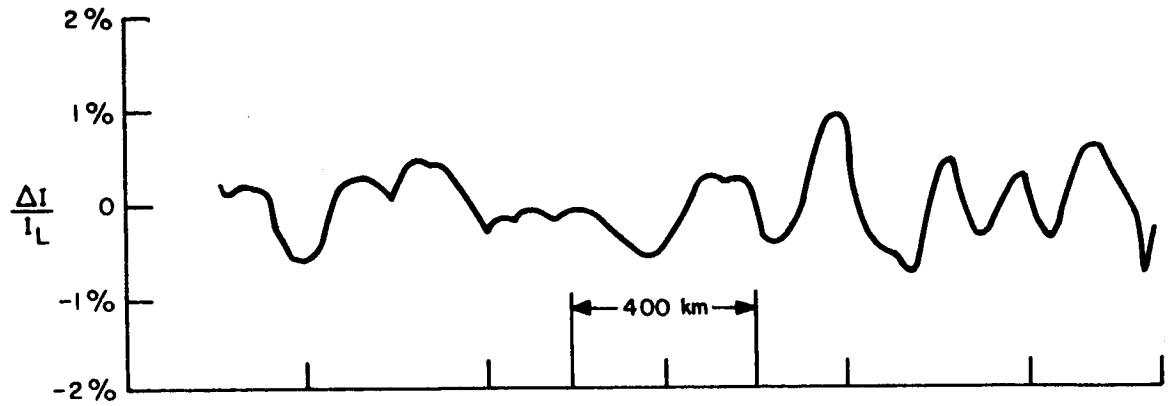

Figure 6-25. Irregularities in Subsatellite Ionospheric Electrical Content, 0830 m.s.t., 4 Sept. 1958 (From Ref. 6-32)

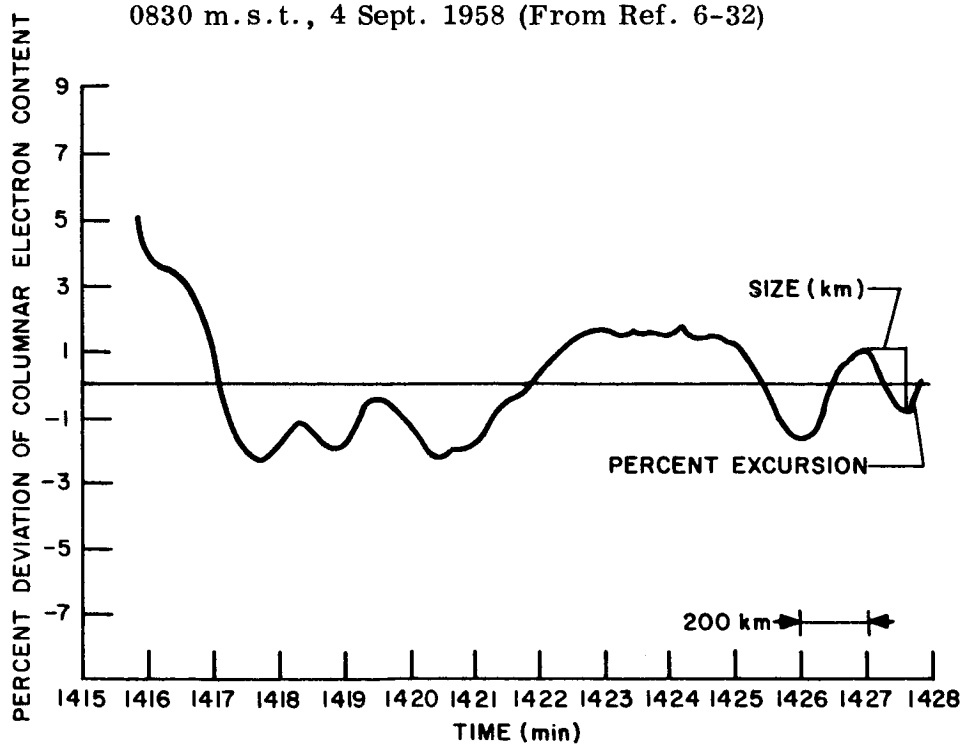

Figure 6-26. The Percent Deviations of Columnar Electron Content as a Function of Time in Minutes. Note the Quasi-Sinusoidal Variations Produced by Large-Scale Irregularities in the Columnar Electron Content (From Ref. 6-31)

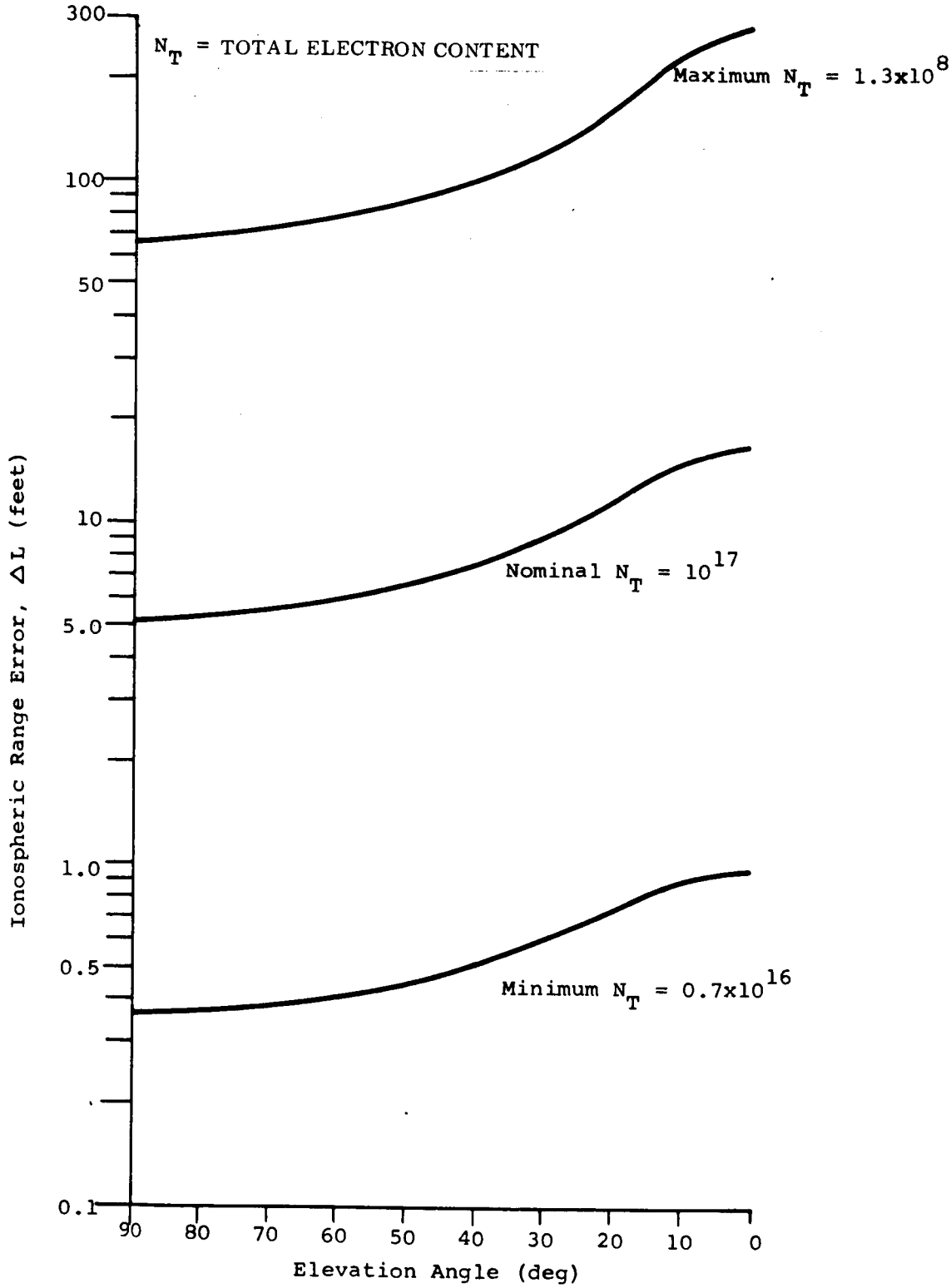

Figure 6-27. Ionospheric Range Error Versus Elevation Angle for No Correction

on the range error. For the upper curve the value of N_T used is 1.3×10^{18} corresponding to the maximum of the range of prediction (10^{18}) and a worst case variation of 30% above that value. The obliquity factor used for the upper curve is the worst case model of Figure 6-14, (h_o = 200 km). For the lower curve N_T is 0.7×10^{16} corresponding to the minimum of the range of prediction 10^{16} and a variation of 30% below the predictable value. The obliquity factor used corresponds to an ionospheric shell at 500 km (311 miles). The center curve corresponds to the nominal N_T of 10^{17} and the nominal obliquity factor (for h_o = 350 km).

In Figure 6-28, there is plotted the "peak" range error, $\delta(\Delta L)$, after using the a priori knowledge of the ionosphere and position of the user. This peak error is given by

$$\delta(\Delta L) = \left|(\Delta L_v \pm .3\Delta L_v)(Q \pm \delta Q) - Q\Delta L_v\right|_{\max}$$

$$= \Delta L_v (.3Q + 1.3\delta Q)$$

where δQ is the peak uncertainty in Q and ΔL_v is the difference between effective and free-space path-length for the satellite at the zenith. $\delta(\Delta L)$ is plotted in Figure 6-28 for ΔL_v corresponding to values of N_T of 10^{16}, 10^{17}, and 10^{18}.

Hyperbolic Mode - In this case the significant error is in the difference between path lengths from the user to each of two pairs of satellites. Generally there will be cancellation of the range errors in this mode when the elevation angles of the two satellites are comparable. As a worst case example of range difference error using prediction, consider satellite one to be on the horizon and satellite two to be at the zenith. For an ionospheric shell at 350 km (218 miles) height, the points at which the two propagation paths intersect the ionosphere may be shown to subtend 18.55° at the center of the earth. To determine the relative magnitudes of N_T at these two points, consider a latitudinal variation model which satisfies the condition that N_T at mid-latitude (45°) is half that at the equator, and N_T at the pole is half that at 45°. One model that satisfies these conditions is an exponential form for the latitudinal factor

$$F(\theta) = e^{-0.0154\theta}$$

Where θ is latitude in degrees. Therefore, for the two ionospheric intersections separated by 18.55° along a N-S great circle, the minimum ratio of the values of N_T is 0.75. A smaller ratio may be obtained for an equivalent local time (longitudinal) separation but only near the diurnal minimum, which would not be consistent with the worst case conditions assumed in this example.

The range difference error may be written as

$$\delta D = (Q_1 + \delta Q_1)(\Delta L_{v1} - k_1 \Delta L_{v1}) - (Q_2 + \delta Q_2)(\Delta L_{v2} + k_2 \Delta L_{v2})$$

$$-(Q_1 \Delta L_{v1} - Q_2 \Delta L_{v2})$$

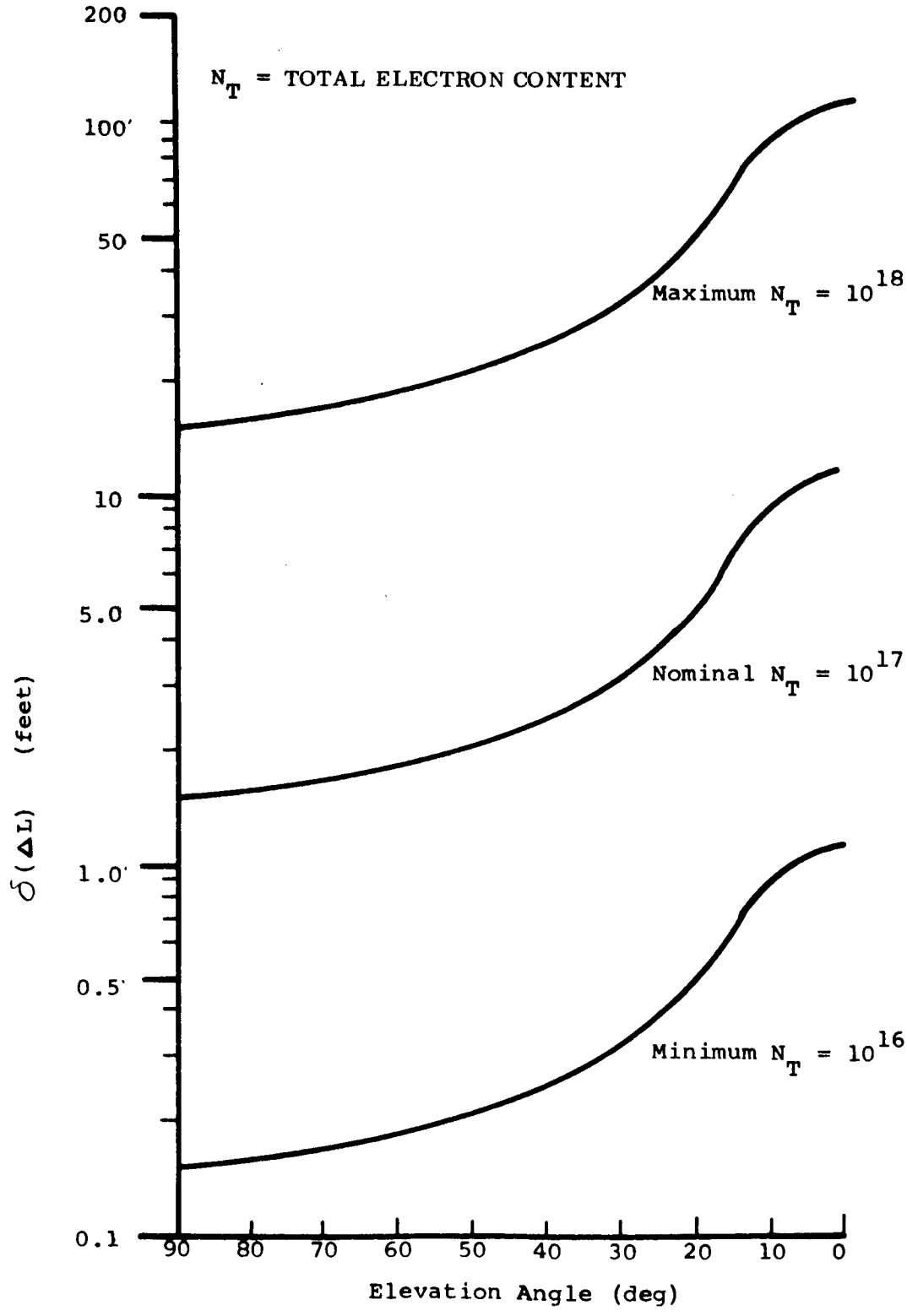

Figure 6-28. Ionospheric Range Error Versus Elevation Angle With Correction

where

δD = range difference error

Q_1 = predicted obliquity factor for satellite one (on horizon)

= 3.5 (see Figure 6-14)

Q_2 = predicted obliquity factor for satellite two (at zenith)

= 1.0

δQ_1 = uncertainty in Q_1

= 0.95

δQ_2 = uncertainty in Q_2

= 0.0

ΔL_{v1} = path length increase for vertical propagation through "point" at which signal from satellite one intersects ionosphere.

= 52.5 ft (corresponding to $N_T = 10^{18}$)

ΔL_{v2} = equivalent of ΔL_{v1} but for satellite two.

= 52.5 ft x (latitudinal factor .75)

= 39.4 ft

k_1 = uncertainty factor in ΔL_{v1}

= day-to-day etc. uncertainty + irregularity uncertainty

= 0.3 + 0.05

k_2 = uncertainty factor in ΔL_{v2}

= 0.3 - 0.05

Therefore

δD = 35.4 meters (116 ft)

Relative Navigation Mode - In this mode the elevation angles of the satellite are approximately equal at the two receivers. If the elevation angles are equal, the range difference error is caused by the ionospheric irregularity. It is assumed that there is (1) a +5% irregularity in N_T along one path, (2) a -5% irregularity along the other, (3) a satellite on the horizon with a worst case obliquity factor of 4.1, and (4) an average value of N_T of 1.3×10^{18} which corresponds to the peak of the prediction range and a peak (+30%) of the day-to-day, etc. fluctuation. The maximum error with no correction (none is possible in this case) is then approximately 8.24 meters (27 feet).

6.3.2.2.3 SCINTILLATIONS AND OTHER EFFECTS

6.3.2.2.3.1 SCINTILLATIONS

At 1.6 GHz, amplitude scintillation should be nonexistent except for relatively low elevation angles at which the scintillation should be small. This is because of the ratio of the Fresnel-zone radius to the scale size of the ionospheric irregularities. The Fresnel-zone radius is given by $\sqrt{Z\lambda}$ where Z is the distance from the diffracting surface to the receiver.

For a receiver at sea level, the Fresnel-zone radius corresponding to vertical reception and an effective ionospheric height of 350 km (218 miles) is 256 meters (840 feet). For horizontal reception the zone radius is 616 meters (2020 feet). The correlation or scale size of the irregularities is several kilometers horizontally but smaller vertically. Hence, for near horizontal reception, the Fresnel-zone radius and the size of the irregularities viewed "end on" could become comparable. This has been confirmed experimentally. At 915 MHz, power fluctuations at low elevation angles were between 3% and 5% but most of the time below 10%. (6-33) Scintillations have also been observed up to 3 GHz at low elevation angles. (6-34)

The phase scintillation rate at 1.6 GHz should be of the same order as the amplitude or power scintillation rate encountered at much lower frequencies. The scintillation rate from radio stars is 0.5 to 8 scintillations per minute. For a synchronous satellite, the rate should be about half these rates since the rotation of the earth is not involved. (6-26) For a satellite in a 24-hour polar orbit, the rate should be multiplied by a maximum factor of 2.

Frequency Shift Due To Receiver Motion - The preceding discussion of scintillation assumed a stationary receiver. Assuming now that the ionospheric irregularities are not drifting and that the satellite is stationary, the maximum frequency shift due to receiver motion along may be estimated as follows. An extreme value of the gradient of N_T is 7×10^{16} electrons per square meter in 50 km (31 miles). (6-35) This corresponds to a change in effective path length between receiver and satellite of 1.12 meters (3.68 feet) or 5.6 wavelengths at 1.6 GHz in 50 km (31 miles). An SST flying at 3340 km/hr (1800 knots) moves 50 km (31 miles) in about 50 seconds. The maximum frequency shift at the aircraft with such a gradient between itself and the satellite would be approximately 0.11 Hz.

6.3.2.2.3.2 OTHER IONOSPHERIC EFFECTS

In addition to incremental pathlength and scintillation there are other ionospheric effects which are small for a carrier frequency of 1.6 GHz. These effects are listed in Table 6-3, together with their ranges of values. The spread in values is due to the direct proportionality of these effects with N_TQ, the effective total electron content. N_T has a total variation of two orders of magnitude, and Q varies between unity and approximately 3.14 for vertical and horizontal propagation respectively. Wedge refraction refers to bending of the rays due to horizontal gradients in the electron density and hence in the index of refraction of the ionospheric. Frequency change refers to a shift in the carrier frequency from non-synchronous satellites due to a

TABLE 6-3. OTHER IONOSPHERIC EFFECTS

Effect	Average Value	Range
Wedge Refraction (rad)	1.56×10^{-7}	1.56×10^{-8} to 4.90×10^{-6}
Frequency Change (Hz)	0.375	0.0375 to 3.75
Differential Phase Path Length (mm)	1.56	0.156 to 49
Polarization Rotation (rad)	0.025	0.0025 to .785
Absorption (during Polar-cap Absorption Event) (dB)	0.0039	0.00039 to 0.122

change in the effective thickness of the ionosphere (equivalent to a changing obliquity factor and no irregularity in N_T). This effect has been calculated for a satellite at an altitude of 1000 km (621 miles). Differential phase path length refers to the difference in effective path length between the ordinary and extraordinary waves. This is the equivalent length of the Faraday or polarization rotation. A detailed discussion of all these effects may be found in Reference 6-11.

6.3.2.3 TROPOSPHERIC EFFECTS

The troposphere, as well as the ionosphere, increases the effective propagation path length between a satellite and a point near the surface of the earth. The refractivity of the ionosphere N, which is defined as

$$N = (n-1) \times 10^6$$

where n is the index of refraction. N is independent of frequency in the troposphere over the range of 100 MHz to 10 GHz and is related to the atmospheric variables by(6-35)

$$N = 77.6 \frac{P}{T} + 3.73 \times 10^5 \frac{e}{T^2}$$

where

P = total atmospheric pressure in millibars

e = water-vapor pressure in millibars

T = temperature in degrees Kelvin

6.3.2.3.1 INCREMENTAL PATH LENGTH

The Central Radio Propagation Laboratory of the National Bureau of Standards developed and adopted for prediction of refraction phenomena a particular model of the troposphere called the CRPL Exponential Reference Atmosphere.(6-36) This

model is based on the finding that the refractivity at high altitudes is well correlated with the refractivity at the surface of the earth. A ray-tracing program using this model was conducted by NBS. From the tabulated results of that program(6-36) Figure 6-29 was plotted showing the incremental path length (difference between effective path length and free space path length) for two extremes of surface refractivity versus elevation angle. It may be seen from the figure that the difference in incremental path length between the two extremes falls off very rapidly with increasing elevation angle and is less than eight feet for elevation angles greater than 10°. Hence, with a priori knowledge of the approximate elevation angle of the satellite, this refraction bias may be greatly reduced. With knowledge of the temperature, barometric pressure and humidity at the receiver, the bias may be reduced even further.

For a terminal which is not at sea level the incremental path length due to the troposphere may be determined from the tables in Reference 6-36. Incremental path length is tabulated for the transmitter at various altitudes. Hence, for a receiver at altitude h and a transmitter on a satellite well above the troposphere, first the incremental path is determined from infinity to sea level. Next determine the incremental path length from h to sea level, and then subtract the latter from the former.

6.3.2.3.2 FLUCTUATIONS

Fluctuations about the average effective path length may be expected due to the presence of inhomegeneities in the troposphere. This problem has been treated theoretically by Muchmore and Wheelon(6-37) who derived the following expression for the variance of this fluctuation:

$$\sigma_L^2 = 2 \ell_o L \sigma_N^2 \times 10^{12}$$

where

σ_L^2 = mean-square deviation of propagation path length

ℓ_o = scale-length or correlation size of inhomegeneities

L_2 = average propagation path length

σ_N^2 = mean-square deviation of refractivity

Representative values of ℓ_o and σ_N^2 are 60.1 meters (200 feet) and unity respectively. For a path length of 485 km (262 nmi) corresponding to horizontal propagation through a 18.5 km (10 nmi) thick troposphere σ_L is approximately .76 cm (0.3 inch). Measurements were made of the path length fluctuation on the island of Nauri in the Hawaiian Islands by the NBS.(6-37) An extreme fluctuation measured was $\sigma_L^2 = 10$ cm^2 (1.55^2) over a propagation path of 249 km (155 miles) coinciding with a variance of refractivity of $\sigma_N^2 = 25$. This would correspond to a path length horizontally through

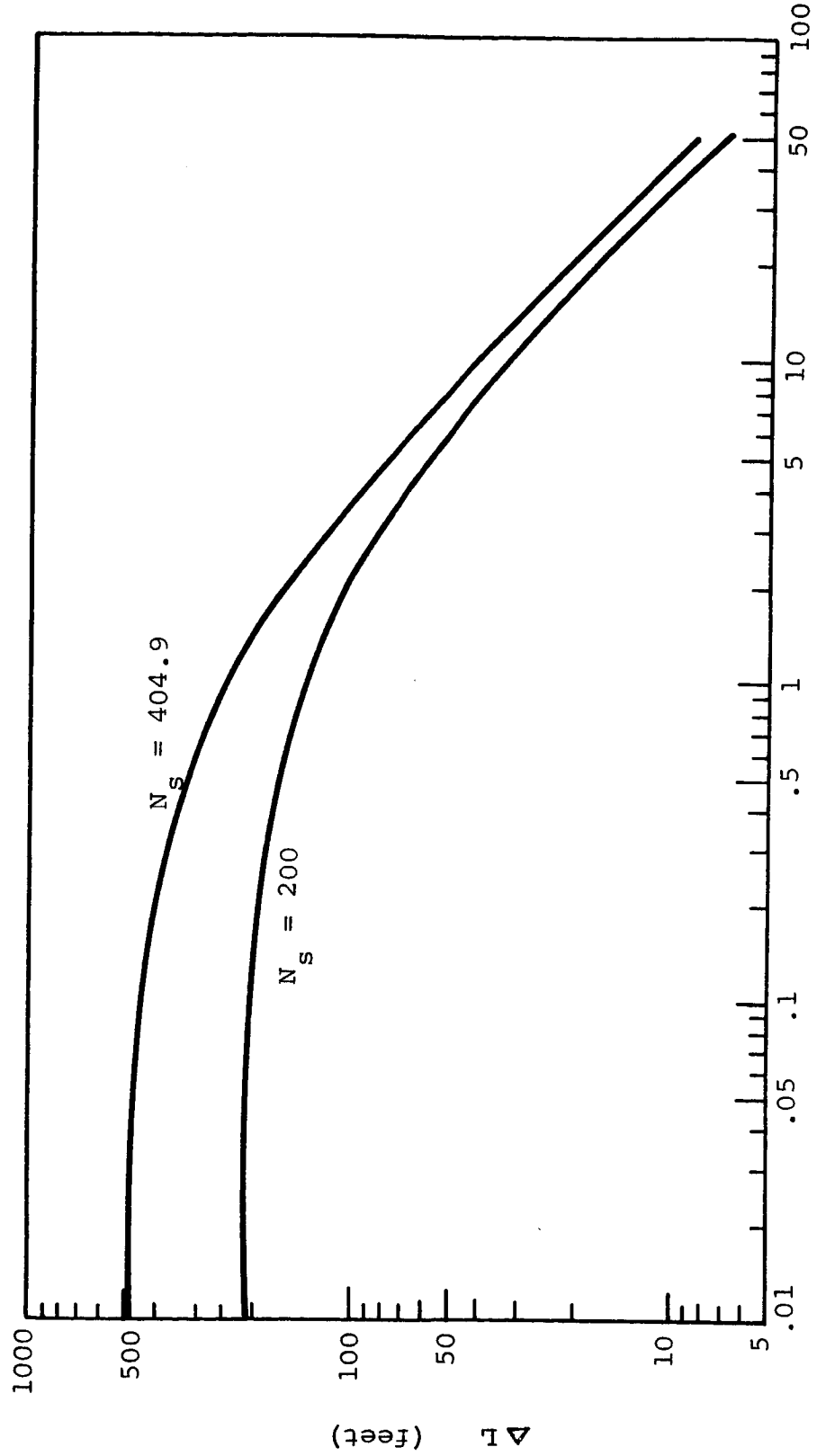

Figure 6-29. Tropospheric Range Error at Sea Level Versus Elevation Angle for Two Extremes of Sea Level Refractivity, N_s

the entire troposphere of 14.2 cm (5.6 inches), assuming from the Wheelon formula that σ_L^2 is proportional to L.

Measurements of the power spectra of the incremental path length indicate that the bandwidth of the fluctuations is well below one hertz, decreasing exponentially by approximately 20 dB from 0.1 to 1.0 hertz[6-38].

6.3.2.4 REFERENCES

In addition to references 6-11 through 6-38 (see Section 7), the following references were also consulted in writing Section 6.3.2.

(1) S. L. Solomon, "Variations in the Total Electron Content of the Ionosphere at Mid-Latitudes During Quiet Sun Conditions," Scientific Report No. 256, Ionospheric Research Laboratory, Penn. State Univ., College of Engr. Dept. of Electrical Engr. NASA Grant NsG-114-61, Nov. 30, 1965.

(2) O. K. Garriott, F. deMendonsa, "A Comparison of Methods Used for Obtaining Electron Content from Satellite Observations," Journ. of Geophys. Res., Vol. 68, No. 17, Sept. 1, 1963, pp. 4917-4927.

(3) T. R. Tyagi, Y. V. Somayajulu, "Some Results of Electronic Content Measurements at Delhi from Faraday Fading of S-66 Transmissions," Radio Science, Vol. 1, No. 10, Oct. 1966, pp. 1125-1130.

(4) A. A. Grann, J. D. Kolesar, W. J. Ross, "Some Geophysical Measurements Using Extended Range Observations of a Beacon Satellite," In "Space Research VI, Proceedings of the Sixth International Space Science Symposium. Mar Del Plata May 11-19, 1965, Organized by Committee on Space Research - COSPAR," Edited by R. L. Smith-Rose. Spartan Books, Washington, Macmillan and Co., Ltd. London 1966.

6.3.3 MULTIPATH PROPAGATION

6.3.3.1 INTRODUCTION

Due to reflections from the surface of the earth, the navigating user vehicle will receive two signals: (1) a direct signal from the satellite and (2) a signal reflected from the surface of the earth. For propagation over sea water the amount of signal reflected is large and therefore the operation of the receiving equipment may be impaired. To prevent this from happening sufficient directivity must be introduced in the radiation pattern of the receiving antenna so that at the expected direction for the arrival of the multipath component an attenuation is introduced; thus we can discriminate between the direct signal and the multipath component. If the reflecting surface is smooth and at rest, the so-called specular reflection condition results in which the power in the multipath component is comparable to the power in the direct ray. In Figure 6-30 the geometry in question is presented, where

h_a: user height

SR: slant range

ψ : angle of incidence

α : elevation angle of the satellite

β : incoming angle for the reflected signal

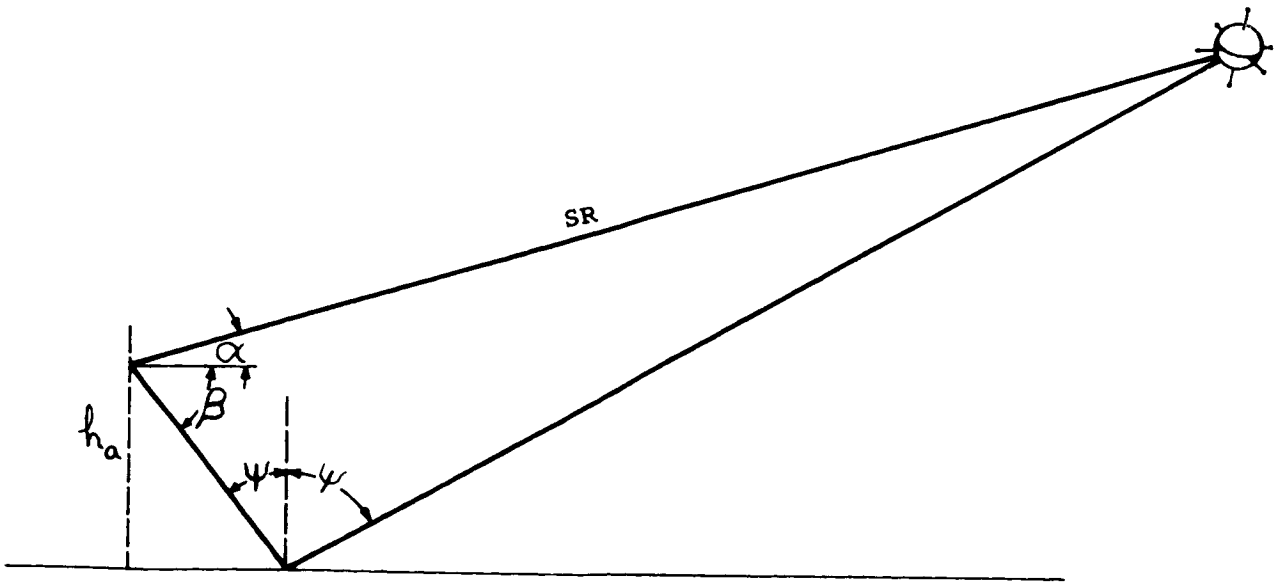

Figure 6-30. Multipath Geometry

For synchronous satellites:

$$SR > 36200 \text{ km } (22,500.0 \text{ miles})$$

and for typical aircraft users

$$0 \leq h_a \leq 32.2 \text{ km } (20 \text{ miles}).$$

Because $h_a << SR$, it is easy to show, using a mirror source for the reflected ray, that $\alpha = \beta$. Thus the angular separation between the direct and the reflected rays is equal to 2α. At the proposed L-band navigation frequency ($\lambda \approx 18.7$ cm), the occurrence of a smooth sea surface, as defined by the Rayleigh criterion, is indeed very rare, if not impossible. Thus the normal mechanism is that of scattering from a rough surface which results in diffuse scattering. Here we are concerned with the amount of energy scattered in a given direction by a large number of elementary surfaces whose orientations are random. This subject is treated in great detail by Beckmann and Spizzichino [6-39] and has recently been reviewed and amplified by Staras [6-40]. What follows is an adaptation of Staras' work to the Phase Difference Navigation system configuration. Our purpose is to determine the defining parameters of the appropriate Rayleigh distribution; namely, the mean value and the time rate of change of the scattered signal. The major assumptions for the mathematical description of the scattering phenomena are as follows:

(1) The surface undulations can be described by a two dimensional Gaussian distribution.

(2) The rms bump height is large compared to the wavelength.

(3) The rms slope of the surface is fairly small.

(4) The autocorrelation of the surface fluctuations is an analytic function.

(5) The Kirchoff-Huygens approximation is valid.

(6) Shadowing of one part of the surface by another is unimportant.

(7) Multiple scattering is also unimportant.

The last three assumptions are very good if one accepts the earlier assumption that the rms slope of the surface is small.

6.3.3.2 THE AVERAGE SCATTERED POWER

We begin by writing the following fundamental formula

$$\langle P_s \rangle = \int P_o \, dS \qquad (1)$$

where $\langle P_s \rangle$ represents the average scattered power from the earth's surface while P_o represents the average scattered power per unit area of surface. P_o is well-known in the literature, and from Equation (10), sec. 12.4.1 of Reference 6-39, it is given by (with minor changes in notation)

$$P_o = \frac{D|R|^2}{4\pi} \frac{r^2}{r_1^2 r_2^2} \frac{\cot^2 \beta o}{\cos^4 \beta} \exp -\left(\frac{\tan^2 \beta}{\tan^2 \beta_o}\right) \qquad (2)$$

where $\beta_o = \frac{2\sigma}{T}$ ($\approx$ rms slope of surface undulations)

$$\tan^2 \beta = \frac{\sin^2 \theta_1 + \sin^2 \theta_2 - 2 \sin \theta_1 \sin \theta_2 \cos \varphi}{(\cos \theta_1 + \cos \theta_2)^2}$$

D = divergence factor for scattering from a curved surface
R = Fresnel reflection coefficient for a plane surface

The angles and distances in the above formulas are indicated in Figure 6-31, while σ is the rms bump height and T is the correlation length of the surface fluctuations. D and R are known in terms of the geometrical and electrical properties of the reflecting surface respectively:

$$R_v = \frac{Y^2 \cos \psi - \sqrt{(Y^2 - \sin^2 \psi)}}{Y^2 \cos \psi + \sqrt{(Y^2 - \sin^2 \psi)}}$$

$$R_h = \frac{\cos \psi - \sqrt{(Y^2 - \sin^2 \psi)}}{\cos \psi + \sqrt{(Y^2 - \sin^2 \psi)}}$$

$$D = \left[1 + \frac{2r_1 r_2}{a(r_1 + r_2) \cos \psi}\right]^{-1/2} \left[1 + \frac{2r_1 r_2}{a(r_1 + r_2)}\right]^{-1/2}$$

where $R_v = R_h = R$ for vertical and horizontal polarization

$$Y^2 = \epsilon_1 - j (60 \lambda \sigma_e)$$

ϵ_1 = relative dielectric constant of reflecting medium

λ = incident wavelength

ψ = local angle of incidence

a = radius of earth

σ_e = electric conductivity of reflecting medium

It is probably because (2) above is such a complicated looking function that (1) has not been evaluated in the prior literature.

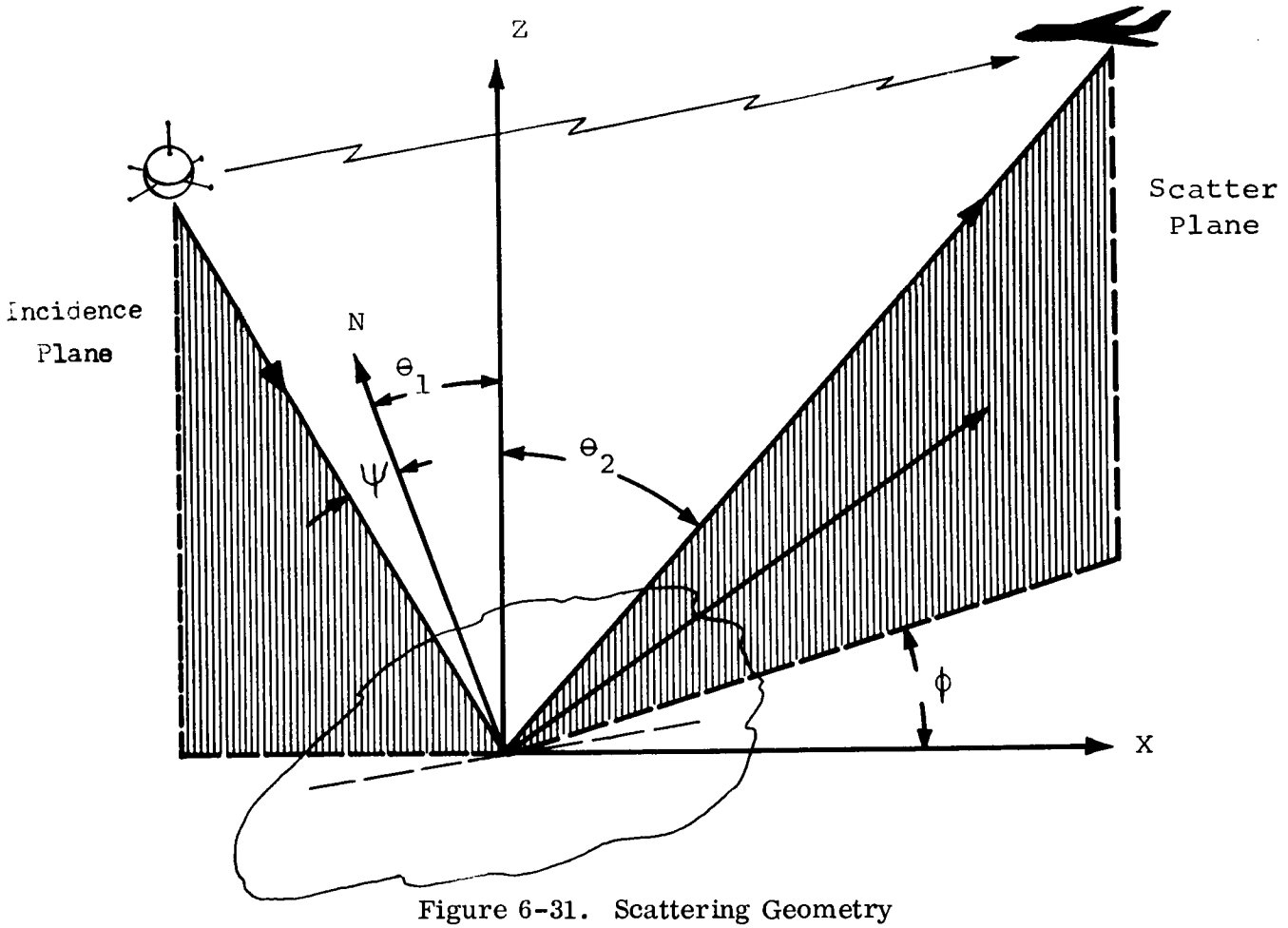

Figure 6-31. Scattering Geometry

We evaluate (1) by writing

$$\langle P_s \rangle = a^2 \int_0^{\pi} \int_0^{2\pi} P_o \sin\theta \, d\theta \, d\varphi \qquad (3)$$

where 'a' is the radius of the earth and a, θ, φ are the spherical coordinates of an arbitrary scattering surface on the earth's surface. Since P_o is such a complicated function, an exact closed-form solution is not possible. However, if the parameter $\tan\beta_o$ ($\sim$ rms slope of the rough surface) is sufficiently small, the "method of steepest descent" can be used (Ref. 6-41). The procedure requires the finding of the stationary points of $\tan^2\beta$. Mathematically, we must obtain the simultaneous solutions of

$$\frac{\partial \tan^2\beta}{\partial \theta} = 0 \qquad \frac{\partial \tan^2\beta}{\partial \phi} = 0 \qquad (4)$$

The solution to the first of the equations in (4) is quite direct, i.e., $\varphi = 0$. Physically, this means that the stationary point lies in the great circle plane containing the transmitter and receiver, a very reasonable result. The second of the equations in (4) becomes

$$\frac{\partial}{\partial\theta} \left(\frac{\sin\theta_1 - \sin\theta_2}{\cos\theta_1 + \cos\theta_2} \right)^2 = 0 \qquad (5)$$

With the aid of Figure 6-32, we obtain (assuming the synchronous satellite is extremely far away relative to all other distances)

$$\theta_2 = \Theta - \theta$$

$$r_1^2 = a^2 + (a+h)^2 - 2a(a+h)\cos\theta \approx h^2 + (1+h/a)a^2\theta^2 \quad (6)$$

$$\sin(\theta_1 - \theta) \approx \frac{a\theta}{\sqrt{h^2 + (1+h/a)a^2\theta^2}} = \frac{\theta}{\sqrt{(h/a)^2 + (1+h/a)\theta^2}}$$

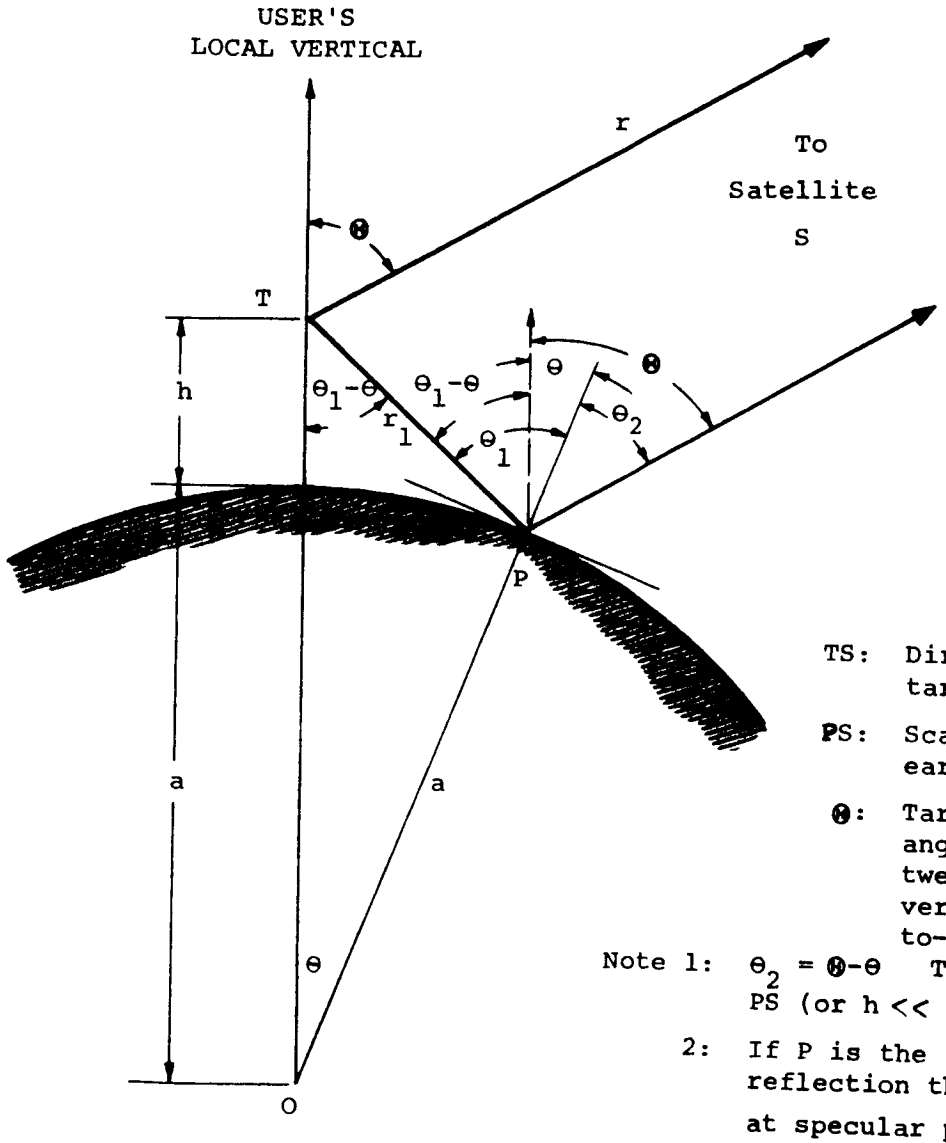

Definitions

TS: Direct ray from target to satellite.

PS: Scattered ray from earth to satellite.

Θ: Target's aspect angle, or angle between target's local vertical and target-to-satellite line.

Note 1: $\theta_2 = \Theta - \theta$ TS is parallel to PS (or $h << r$).

2: If P is the point of specular reflection then $\theta_2 = \theta_1$ at specular point $\theta = \theta_S$

Figure 6-32. Multipath Geometry

Here θ has been defined as the angle between the target's local vertical and the line from target to satellite; it may be called the "target aspect angle." The last two equations in (6) are very good approximations for $h/a = H \leq 0.1$. Solving (5) with the help of (6), we obtain the physically significant result that $\theta_1 = \theta_2$ at the stationary point; i.e., the most important contribution to the average scattered power comes from a region surrounding the specular point. The "method of steepest descent" requires only that we know P_o fairly accurately in the neighborhood of the specular point where $f(\equiv \tan^2 \beta)$ is given by

$$f \approx \frac{\phi^2}{4} \tan^2 (\Theta - \theta_s) + \left(1 + \frac{H^2}{2B}\right) (\theta - \theta_s)^2 \qquad (7)$$

In (7), θ_s is the value of θ at the stationary point and

$$B = \sqrt{H^2 + H\theta_s^2} \qquad \left[H^2 + (1 + H)\,\theta_s^2\right]$$

The value of θ_s can be computed from the following transcendental equation

$$\sin (\Theta - 2\theta_s) = \frac{\theta_s}{\sqrt{\left(\frac{h}{a}\right)^2 + (1+h/a)\theta_s^2}}$$

This equation was obtained from the fact that for specular reflection

$$\theta_1 = \theta_2$$

$$\theta = \theta_s$$

and by evaluating the third equation of (6) at $\theta = \theta_s$ and substituting the result of the first equation of (6).

Examination of (2) and (7) shows that the size of the effective region around the specular point which contributes most to the average scattered power is not determined by Fresnel zone considerations (as it is for a smooth surface) but rather by the rms slope of the surface undulations. Using the method of steepest descent as outlined in Reference 6-41, we obtain after some manipulation

$$\frac{\langle P_s \rangle}{P_d} = D^2 \left|R\right|^2 Q \qquad (8)$$

where

$$Q = \frac{\theta_s}{\left[H^2 + (1+H)\theta_s^2\right]} \frac{1}{\tan (\Theta - \theta_s)\; 2\left(1 + \frac{H^2}{2B}\right)}$$

$$= \frac{\tan (\Theta - 2\theta_s)}{\tan (\Theta - \theta_s)} \left[1 + \frac{2\theta_s}{\sin (\Theta - 2\theta_s) \cos (\Theta - 2\theta_s)} H \tan^2 (\Theta - 2\theta_s)\right]^{-1}$$

It is to be explicitly noted that D and R in (8) are to be evaluated at the specular point just as Q is, and that one must use R_h for the horizontally polarized wave and R_V for the vertically polarized wave.

Figure 6-33 describes graphically the following: (1) for a wide range of the angle θ, the average scattered power is comparable to the power in the direct signal; (2) only near the grazing angle is there substantial discrimination against the ground scattered signal; and (3) the scattered signal falls with increasing altitude of the target vehicle. It should be noted, however, that because the ground scattered signal is Rayleigh distributed it can quite frequently be larger than the direct signal even though its average value is somewhat lower. Fluctuations of 10 dB, 15 dB and even 20 dB can occur quite frequently. The details of the statistical characteristics of a direct signal added to a Rayleigh distributed signal can be found in several places in the literature, in particular see Norton et al. (6-42)

The expression given in (8) has been computed for sea water and land reflection characteristics and for two heights of interest; 8.05 km (5 miles) and 24.2 km (15 miles). These plots are given in Figure 6-33.

It is interesting to note from Figure 6-33 that near the grazing angle (where user antenna directivity cannot easily be used to discriminate against the ground scattered signal) the scattering phenomenon itself discriminates against the ground scattered signal. At the higher elevation angles, however, the ground scattered signal would normally be quite large according to the figures, and antenna directivity on the user vehicle would be needed to discriminate against ground reflections.

6.3.3.3 THE FADING RATE

The previous discussion restricted itself to the question of the depth of fading that is to be expected for typical Phase Difference Navigation geometries. We now undertake to evaluate the fading rate to be expected. To understand the concept of fading rate as it applies to this situation, it should be recognized that the ground scattered signal consists of a sum of rays with random relative phase. These rays produce a lobe pattern in the space above the earth, and as the user vehicle travels it traverses this lobe pattern and is thereby subjected to a time varying signal. It is the purpose of this subsection to obtain an estimate of the typical rate at which the signal is varying. Of course, the fading is a statistical phenomenon and does not occur at one frequency. We will, therefore, be evaluating the bandwidth of the ground scattered signal.

Actually, the scattered signal will also be beating against the direct signal. But for almost all geometrical situations, the direct signal will lie somewhere within the band of the ground scattered signal so that the beat frequencies between the direct signal and the ground scattered signal will also tend to lie somewhere within the same fading bandwidth. (Since in general the direct signal does not lie at the exact center of the fading band of the ground scattered signal, there is some broadening of the fading bandwidth. However, this broadening may be ignored because of the bandwidth itself cannot be determined very precisely.)

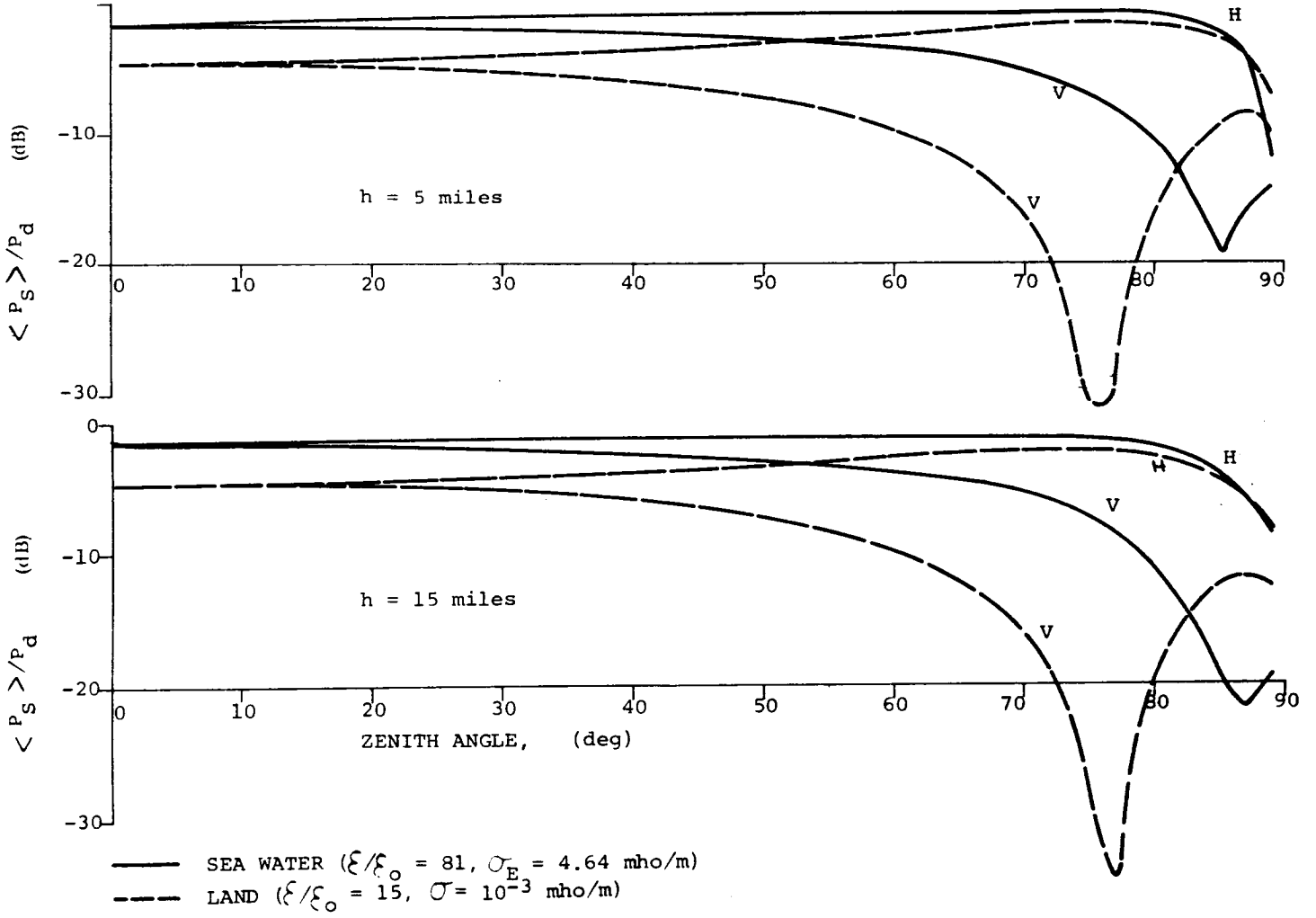

Figure 6-33. Average Scattered Power as a Function of Zenith Angle

The Fundamental Formula - It is well known in the theory of random functions that the power spectral density and the time autocorrelation function are Fourier transforms of each other. Therefore, knowing one implies the other. We will here derive and then compute the time autocorrelation function $C(\tau)$ of the complex envelope of the random ground scattered signal E(t). The relation is

$$C(\tau) = \langle E(t)\, E^*(t+\tau) \rangle \tag{9}$$

where $\langle\ \rangle$ denotes an ensemble average of the quantity inside the brackets and the asterisk denotes the complex conjugate. For the sake of simplicity, we will characterize E(t) by a sum of independent phasors (rays) with random relative phase:

$$E(t) = \sum_i E_i \exp(j\varphi_i) \tag{10}$$

From (10)

$$\langle E(t)E^*(t)\rangle = \sum_i E_i^2 \tag{11}$$

Equation (11) is the analogue of (1) with E_i^2 corresponding to $P_o\, dS$. At $t + \tau$, we have

$$E(t+\tau) = \sum_i E_i \exp j(\varphi_i + \Delta_{\varphi_i}) \tag{12}$$

where $\Delta\varphi_i$ is a systematic (not random) phase change introduced by the motion of the target vehicle. Applying (9) to (10) and (12) yields

$$\langle E(t)\, E^*(t+\tau)\rangle = \sum_i E_i^2 \exp(-j\Delta_{\varphi_i}) \tag{13a}$$

If one used continuous functions instead of discrete variables, the above would become

$$C(\tau) = \langle E(t)\, E^*(t+\tau)\rangle = \int P_o \exp\left[-jk(R_o - R_n)\right] ds \tag{13b}$$

where $R_o - R_n$ is the change in path length (in a time τ) of the target vehicle from an element of the scattering surface, and R is the wave number. It is assumed that the synchronous satellite's position from the scattering surface does not change in the period τ.

Evaluation of the Correlation Function - It can be shown that the normalized autocorrelation function of the complex envelope E(t) is given by $R(\tau) = C(\tau)/C(0)$ so that multiplicative constants need not be considered in the expression (13b) for $C(\tau)$. It is sufficient, therefore, to write [see (2) and (7)]

$$P_o \approx \exp - \frac{T^2}{4\sigma^2}\left[\frac{\varphi^2}{4}\tan^2(\Theta - \theta_s) + \left(1 + \frac{H^2}{2B}\right)(\theta - \theta_s)^2\right] \tag{14}$$

We evaluate $R_o - R_n$ with the aid of Figure 6-34, and note two cases:

$$\text{Case 1: } R_o - R_n \approx s \sin(\theta_1 - \theta)\cos\varphi \quad \text{(x-z plane)} \tag{15a}$$

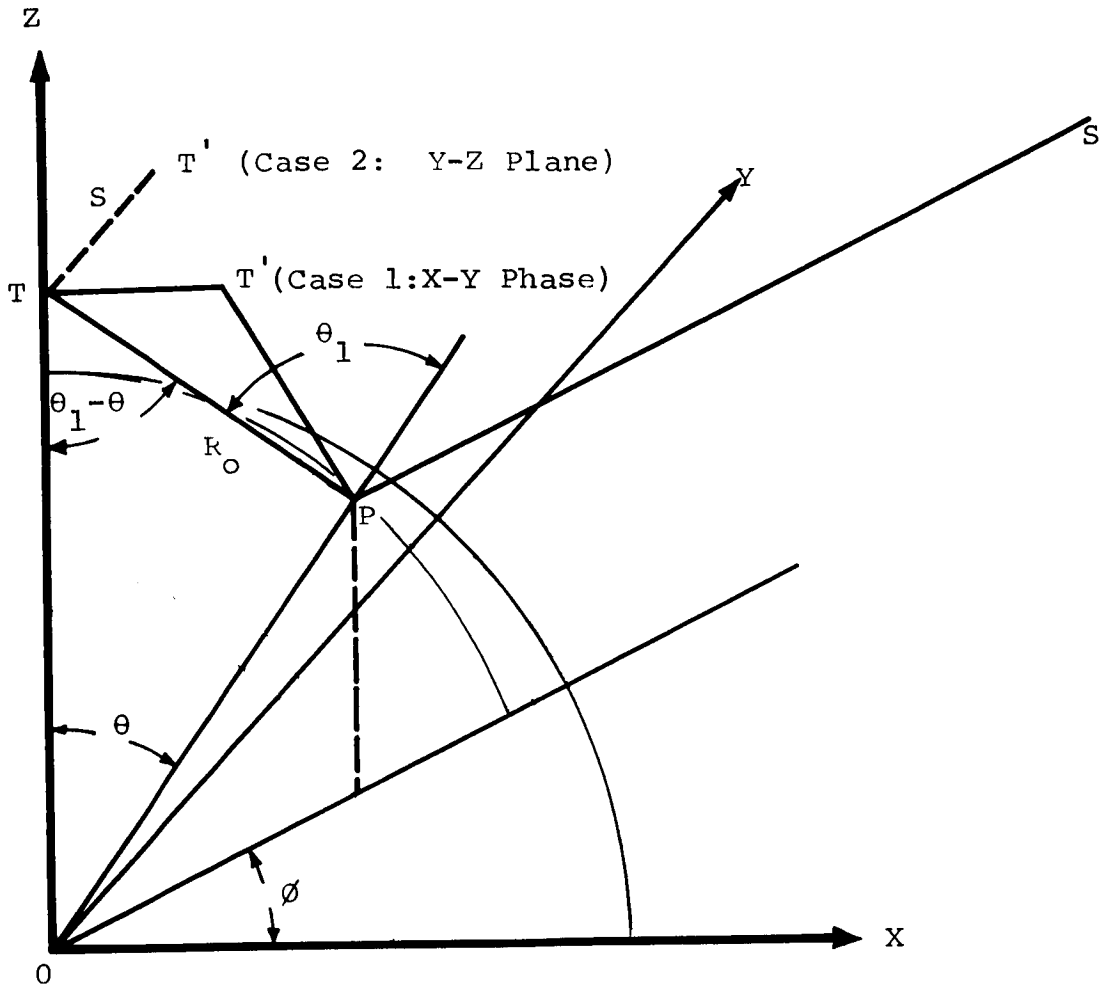

0 : Center of earth

T : Initial target position (defines Z axis)

S : Satellite (in X-Z plane)

T' : Target position after time τ; T' may be in X-Z plane (Case 1) or Y-Z plane (Case 2)

P : Position of a general scattering element for both T, T' ; Phase spherical coordinates a, θ, ø.

Figure 6-34. Geometry for Calculation of Fading Bandwidth

or

$$\text{Case 2: } R_o - R_n \approx s \sin(\theta_1 - \theta) \sin\varphi \text{ (y-z plane)} \qquad (15b)$$

In the above, $s = v\tau$ where v (≈ 0.4 km/sec for jet airplanes) is the velocity of the user vehicle relative to the earth. Equation (15a) applies to the case where the user vehicle velocity vector TT' lies in the great circle plane (x-z plane) containing the user vehicle and the synchronous satellite, while (15b) applies to the case where the user vehicle velocity is perpendicular to the great circle plane in question. Fron (14), it is to be observed that P_o is substantially different from zero only when φ is near zero (perhaps on the order of $\pm 10°$); therefore, $\cos\varphi \approx 1$ and $\sin\varphi \approx \varphi$. With these approximations, inserting (14) and (15a) into (13b) yields for the case of target velocity in the x-z plane,

$$C(\tau) \approx \int \exp\left[-jkv\tau \sin(\theta_1 - \theta)\right] \exp\left[-\frac{T^2}{4\sigma^2}\left(1 + \frac{H^2}{2B}\right)(\theta - \theta_s)^2\right] d\theta \qquad (16)$$

Since the integrand in (16) is appreciably different from zero only near $\theta = \theta_s$, we expand $\sin(\theta_1 - \theta)$ around $\theta = \theta_s$.

$$\sin(\theta_1 - \theta) \approx \frac{\theta}{\sqrt{H^2 + (1+H)\theta^2}}$$

$$\approx \frac{\theta_s}{\sqrt{H^2 + (1+H)\theta_s^2}} + \frac{H^2(\theta - \theta_s)}{\left[H^2 + (1+H)\theta_s^2\right]^{3/2}} \qquad (17)$$

Inserting (17) in (16) and integrating yields

$$R(\tau) \approx \exp -\left\{\frac{kv\tau\sigma}{T} \cdot \frac{H^2}{\left[H^2 + (1+H)\theta_s^2\right]^{3/2}\left[1 + \frac{H^2}{2B}\right]}\right\}^2 \qquad (18)$$

which can be rewritten as

$$R(\tau) = \exp -2(\pi\tau\sigma_F)^2 \qquad (19)$$

where

$$\sigma_F = \frac{kv\sigma}{\sqrt{2\pi}} \cdot \frac{H^2}{\left[H^2 + (1+H)\theta_s^2\right]^{3/2}\left[1 + \frac{H^2}{2B}\right]} \qquad (20)$$

Taking the Fourier transform of R(t) we obtain the power spectrum G(f) which is given by:

$$G(f) = \frac{1}{\sigma_F \sqrt{2\pi}} \exp \left[- \frac{f^2}{2 \sigma_F^2} \right] \tag{21}$$

Using (21) we can now define the half power fading bandwidth B_F such that:

$$G\left(\frac{Bf}{2}\right) = \frac{1}{\sigma_F \sqrt{2\pi}} \exp \left[- \frac{B_F^2}{8\sigma_F^2} \right] = \frac{0.5}{\sigma_F \sqrt{2\pi}} \tag{22}$$

from where

$$B_F = 2\sqrt{2 \ln 2} \quad \sigma_F \tag{23}$$

For the case where the target vehicle orbit is perpendicular to the great circle plane, we substitute (14) and (15b) into (13b) and obtain

$$R(\tau) \approx \int \exp \left[-jkv \tau \sin A\theta \right] \exp \left[- \frac{T^2}{4\sigma} [\tan^2 B] \theta^2 \right] d\theta$$

$$\approx \exp - \left\{ 2 \, kv \tau \, \frac{\sigma}{T} \, \frac{\sin A}{\tan B} \right\}^2 \tag{24}$$

where

$$A \equiv \Theta - 2\theta_s, \; B \equiv \Theta - \theta_s \; .$$

which can be rewritten as

$$R(t) = \exp \left[-2(\pi \, t \, \sigma_F')^2 \right] \tag{25}$$

where

$$\sigma_F' = \frac{\sqrt{2}}{\pi} \, kvt \, \frac{\sigma}{T} \, \frac{\sin A}{\tan B} \tag{26}$$

Taking the Fourier transform of (25) and defining the fading bandwidth as in (22) we obtain

$$B_F' = 2\sqrt{2 \ln 2} \; \sigma_F' \tag{27}$$

Formulas (23) and (27) have been computed as a function of the zenith angle Θ for two different user heights, 5 and 15 miles, v = 600 mph, and λ = 0.187 meters. The sea state assumed is moderate roughness, where

$$\frac{T}{2\sigma} = 15$$

The corresponding fading bandwidths are shown in Figure 6-35.

Variation of Delays - As has been shown earlier most of the scattered energy comes from the region around the specular point. From Fermat's principle we infer that the energy scattered from the specular point will exhibit minimum delay. For energy scattered from other areas the delays are larger.

We would like to obtain an upper bound for the delays. This becomes in part a matter of definition. We shall look for the resulting delays where P_o, the scattered power, given in Eqn. (14) is equal to 0.5 of its peak value.

Thus from Eqn. (14)

$$\frac{T^2}{4\sigma^2}\left[\frac{\varphi^2}{4}\tan^2(\Theta - \theta_s) + \left(1 + \frac{H^2}{2B}\right)(\theta - \theta_s)^2\right] = \ln 2$$

This is an elliptic equation in φ and θ, with center at $\theta = \theta_s$, $\varphi = 0$. Everything else is fixed. Extremium points of this ellipse are found when

$$\varphi = 0 \text{ for which } \theta = \theta_s \pm \sqrt{\frac{\frac{\ln 2}{T^2/4\sigma^2}}{1 + \frac{H^2}{2B}}}$$

and when

$$\theta = \theta_s \text{ for which } \varphi = \pm \frac{2\sqrt{\ln 2}\left(\frac{2\sigma}{T}\right)}{\tan(\theta - \theta_s)}$$

Because we are primarily interested in low elevation angles (0 to 15°), where the antenna will have less discrimination to multipath than for high elevation angles, the values of φ obtained when $\theta = \theta_s$ are very small as compared to the results of θ when $\varphi = 0$. Thus knowing the extremium values for θ we can compute the delay Δt with the aid of Figure 6-36 where Δt can be computed from

$$\Delta t = \frac{r_1}{C}\left[1 - \cos(180 - \Theta - \theta_1 + \theta)\right]$$

and

$$r_1 = a\sqrt{H^2 + \theta^2}\,(1 + H) \qquad H = h/a$$

C: velocity of light

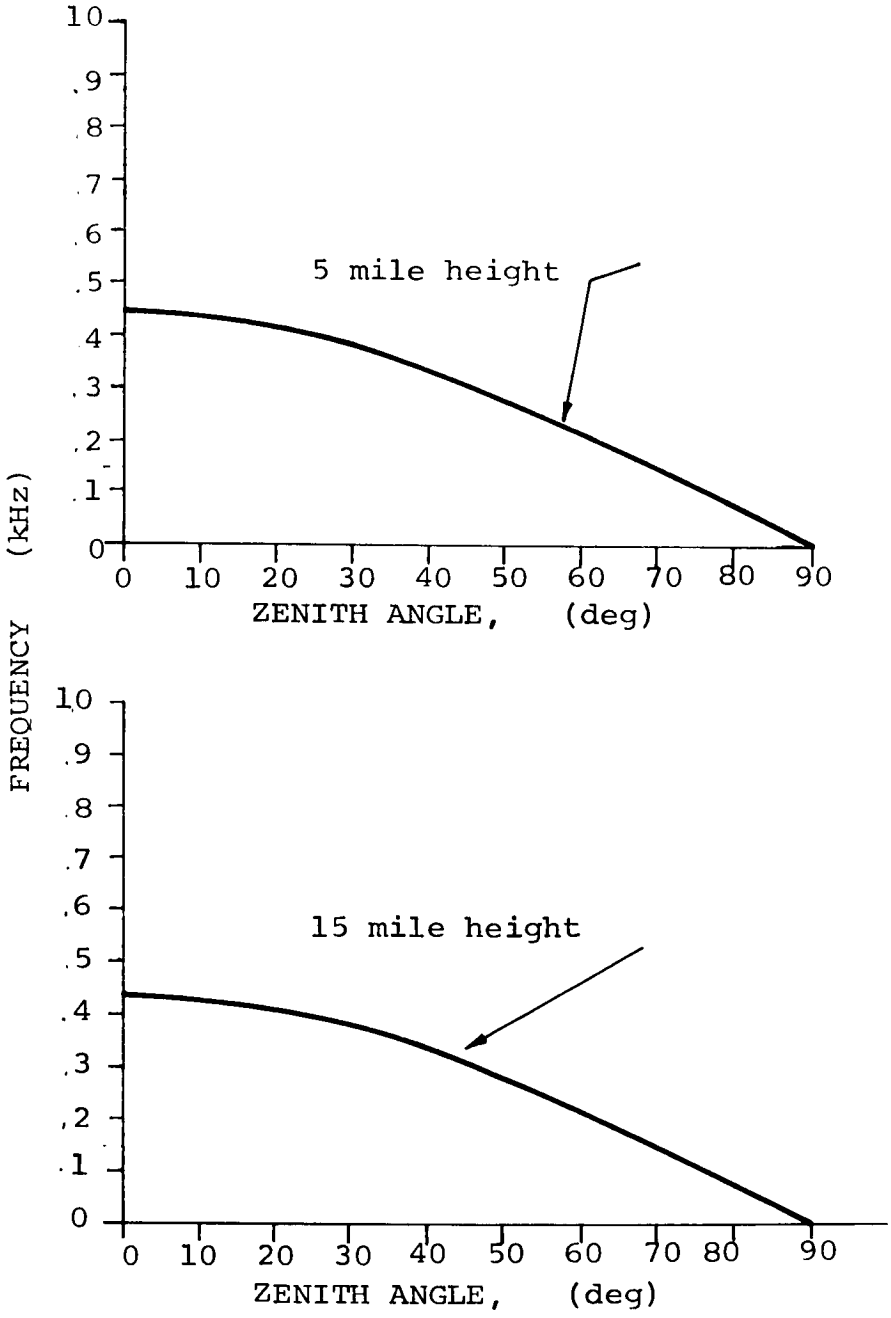

Figure 6-35. Typical Fading Bandwidth of Scattered Signal for Cases 1 and 2

Θ : zenith angle

$$\theta_1 = \theta + \arcsin\left(\frac{a}{r_1}\sin\theta\right)$$

Actually there are two values of Δt corresponding to each of the values of θ previously computed. The upperbound for the delay is now appropriately chosen. Figure 6-36 shows the variation of Δt_{min} and Δt_{max} as a function of the elevation angle for heights of 5 and 15 miles.

6.3.4 ANTENNA

The receiving antenna to be employed for navigational purposes must have the following characteristics.

(1) Conical sector beam of about 160°, with very low sidelobes.

(2) Circularly polarized.

(3) 10% Impedance bandwidth (VSWR < 2.0).

(4) Low pattern degradation within the frequency band.

(5) Multipath rejection capability as required by the receiver.

(6) Small size.

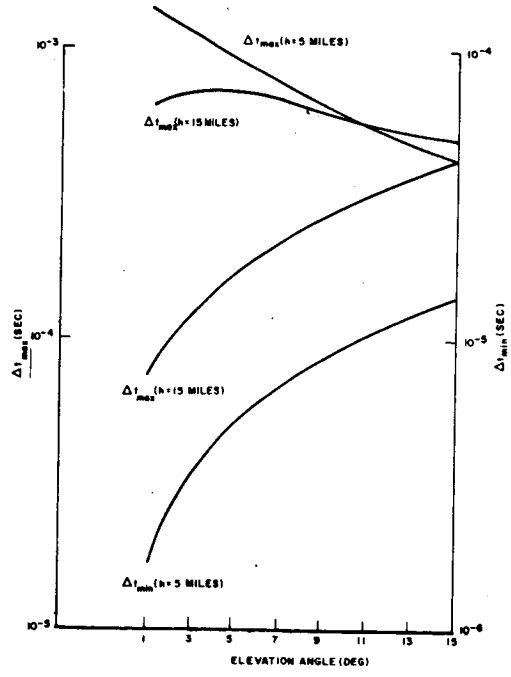

Figure 6-36. Δt_{max} and Δt_{min} Vs Elevation Angle

Furthermore, the shape of the antenna should be suitable for mounting on supersonic aircrafts, as well as on subsonic aircraft and ships at sea.

Initial considerations indicate the supersonic antenna design to be the most worthy of consideration given the fact that antennas fitting the desired properties have been available for a number of years for fixed station use. It is reasonable to assume that aerodynamic considerations will not tolerate any protrusions in the structure of a supersonic aircraft. Immediately, the selection of antennas is narrowed to a slot type or dipole structure that can be contained below a nearly-flush mounted fairing. An important aspect of the design is the selection of a low loss dielectric material capable of withstanding the mechanical and thermal conditions on the skin of the supersonic aircraft.

Circularly polarized antennas for aircraft use are now being designed by various companies. These antennas, being designed for operation in the VHF band, are to be tested with the ATS satellite series. At this frequency ($\simeq$ 136 MHz) the problem is much more severe due to the considerable longer wavelength (about 10 times longer than L-band) and the requirement of a reasonably compact device. Most of the model work has been performed at 1/10 scale, and neglecting fuselage effects, this information and experience is readily applicable to the L-band design problem.

In Figure 6-37 a schematic is shown of a possible configuration for circular polarization that involves four slots, consisting of two pairs at right angles, 90° out of phase. Each pair has a separation of approximately $\lambda/2$; the slot length is less than λ. Figure 6-38 is a schematic of two dipoles in a turnstile configuration, in quadrature phasing, to obtain circular polarization. To reduce the gain and broaden the resulting beam, the dipoles are bent down a certain angle, which is determined experimentally. The object is to bring the sharply decreasing part of the main lobe as close as possible to the horizon at the expense of a dimple at the zenith angle. This is acceptable as long as it is not more than about -3 dB from the maximum, or whatever the system margin may safely tolerate.

Figure 6-39 shows a typical pattern that can be expected for the turnstile antenna, when mounted on a large aircraft like the Boeing 707. It is reasonable to expect the sidelobes below the horizon to be more than 20 dB down.

If the first zero of the pattern, as measured from the zenith, falls below the horizon, one has to consider the slope of the pattern skirt, which determines the amount of multipath discrimination. For a direct ray arriving at an elevation angle α, above the horizon, it has been shown that the multipath components arrive at angles around α degrees below the horizon. (See section 6.3.3.1 and 6.3.3.2). We describe the multipath discrimination capability of the antenna by $M_d\alpha$ where M_d is the average discrimination introduced by the antenna when the direct ray arrives at α degrees above the horizon and the multipath component α degrees below the horizon. M_d is given in dB/degree.

Unfortunately, one cannot theoretically predict the patterns of these antennas when mounted on the aircraft. It becomes impossible to include the significant effects of the wings, tail structure, tapering fuselage, etc.

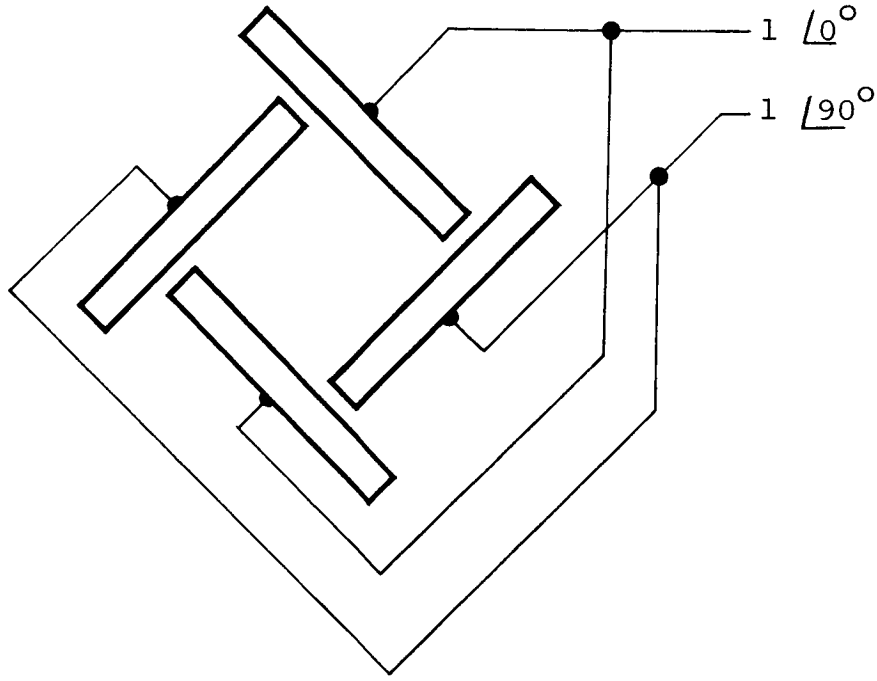

Figure 6-37. Four-Slot Configurations

It is conceivable that a pattern could be designed with a broader beamwidth; however, it would have to be developed experimentally.

For the pattern given in Figure 6-39, if the first zero were to fall 10° below the horizon with a relative voltage level of 0.1, the multipath discrimination is $M_d = \frac{1}{10}$ 20 log 0.66/0.1 = 1.64 dB/degree of elevation angle.

Where 0.66 is the relative voltage at 10° above the horizon (at 20° above the horizon in Figure 6-39).

For the purpose of illustration as to the kind of patterns that can be expected from a circularly polarized antenna on the surface of a large cylinder, we can make use of the expressions for the pattern of axial electric and magnetic dipoles near cylindrical structures. This subject has been treated by Wait [6-43] in an extensive way.

The far field radiation pattern of an axial electric dipole located at $\varphi = 0, \rho = \rho_o$ (see Figure 6-40) is given by

$$E_\theta \propto \sin\theta \sum_{m=0}^{\infty} \epsilon_m \cos m\varphi \, e^{jm\pi/2} \left[J_m(k\rho_o \sin\theta) - H_m^{(2)}(k\rho_o \sin\theta) \frac{J_m(ka\sin\theta)}{H_m^{(2)}(ka\sin\theta)} \right]$$

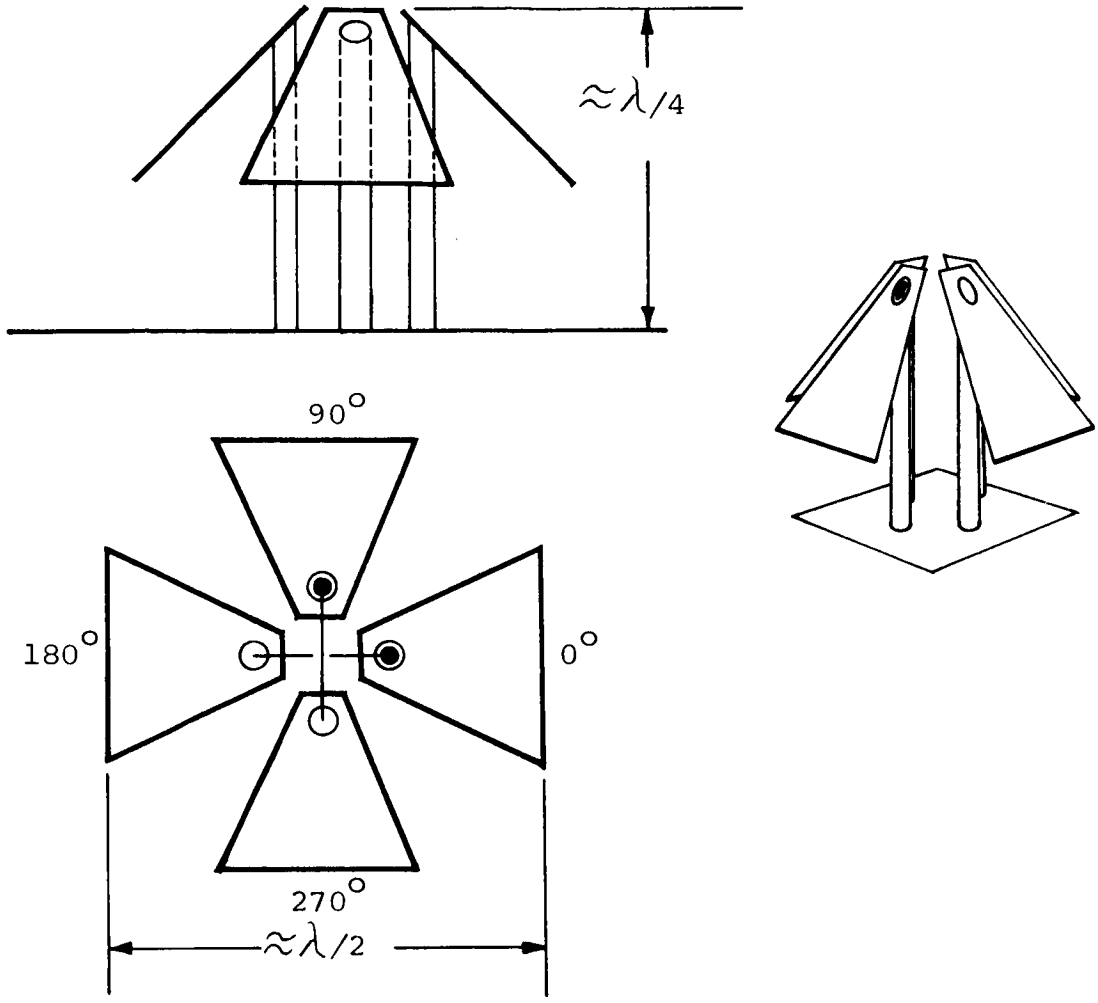

Figure 6-38. Turnstile Dipole Array

This pattern for E_θ has been computed in Figure 6-41 for the case of an axial dipole $\lambda/4$ above a cylinder of radius a. For the diameters of interest, the resulting 3-dB beamwidth is too narrow (about 80°) for a proper system utilization. This particular plane and polarization requires further study. The pattern of a half wave narrow slot is given by

$$E_\theta \propto \frac{\cos\left[\pi/2 \cos\theta\right]}{\sin^2\theta} \sum_{m=o}^{\infty} \frac{\epsilon_m j^m \cos m\varphi}{H_m^{(2)'}(ka \sin\theta)}$$

This last equation is plotted in Figure 6-42 for $\theta = 90°$ as a function of φ and values of ka = 100, 150, 200. It is of importance to notice that the 3-dB width is 90° in all patterns. From 80° to 100°, in the largest cylinder, there is a 6 dB drop in gain. This results in an average multipath discrimination of 0.6 dB/degree. Here we now

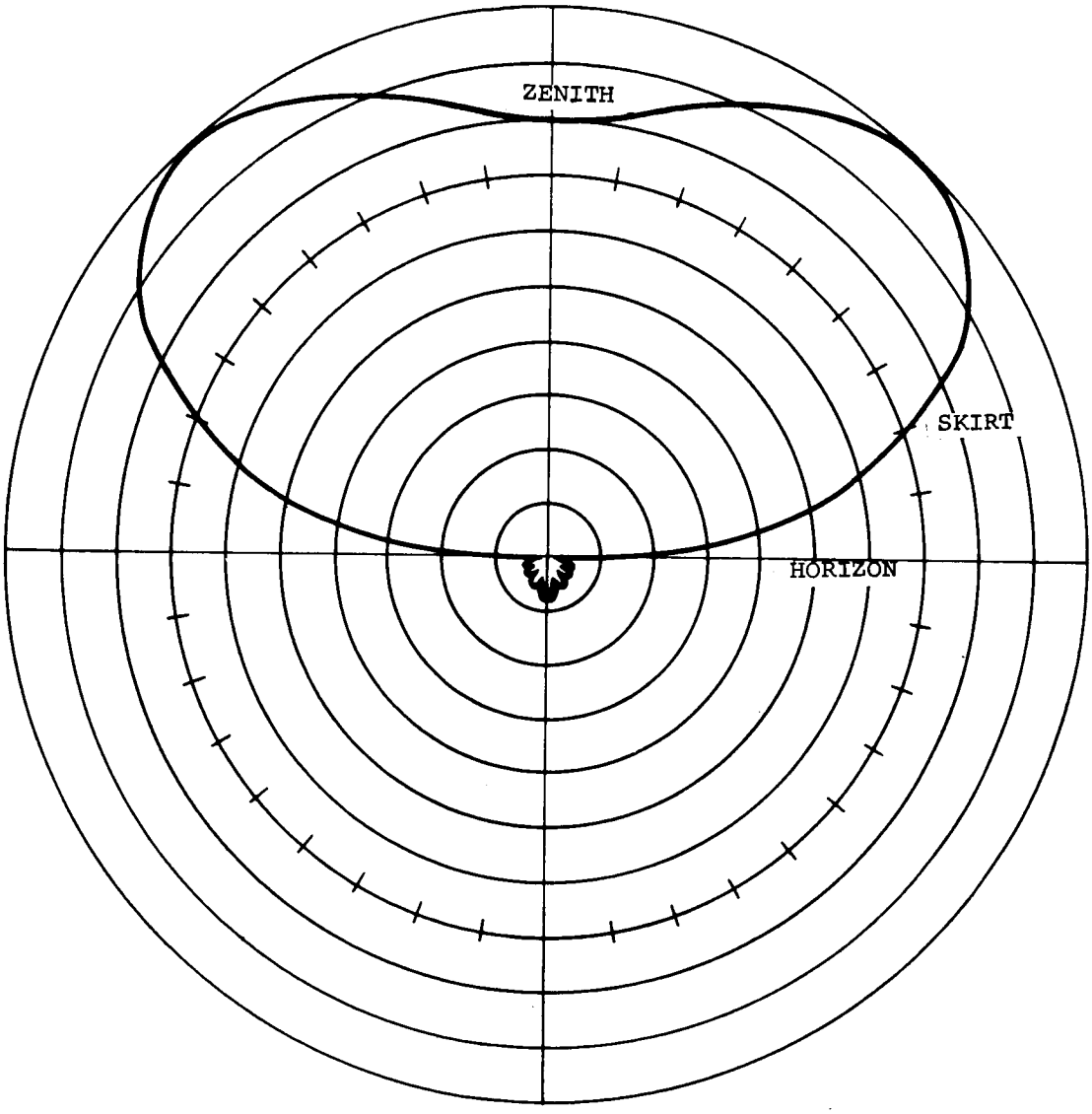

Figure 6-39. Typical Radiation Pattern from the Turnstile Antenna for Either Polarization and Any Plane

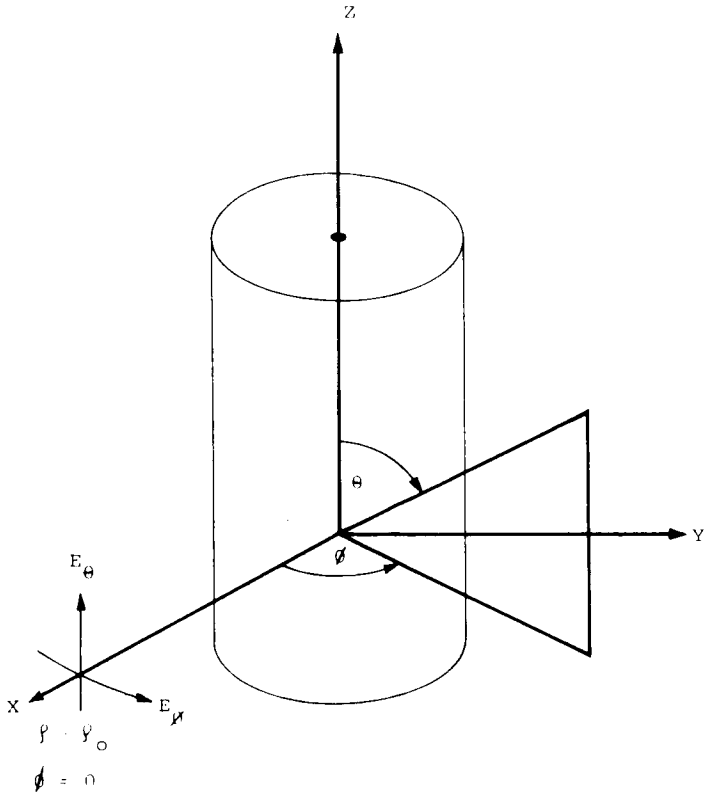

Figure 6-40. Spherical Coordinate System

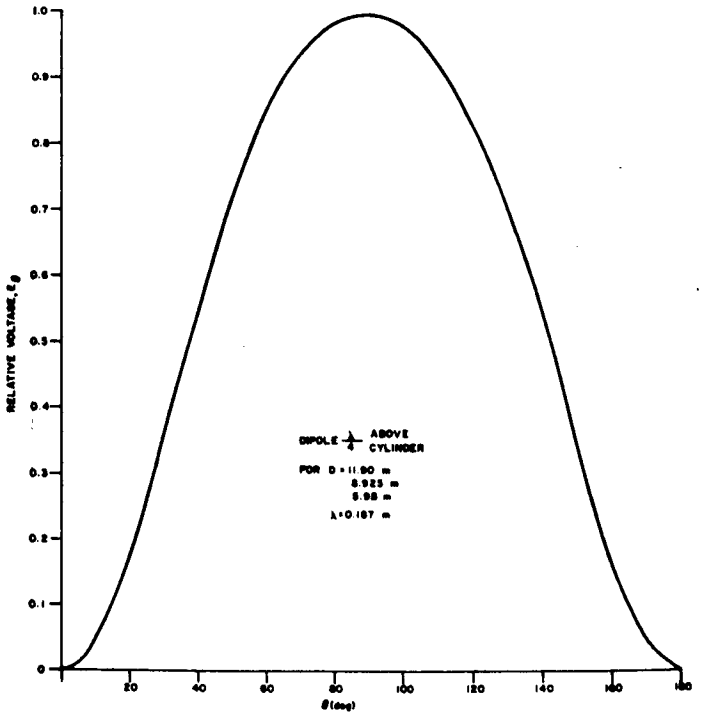

Figure 6-41. E_o Pattern for $\varphi = 0°$

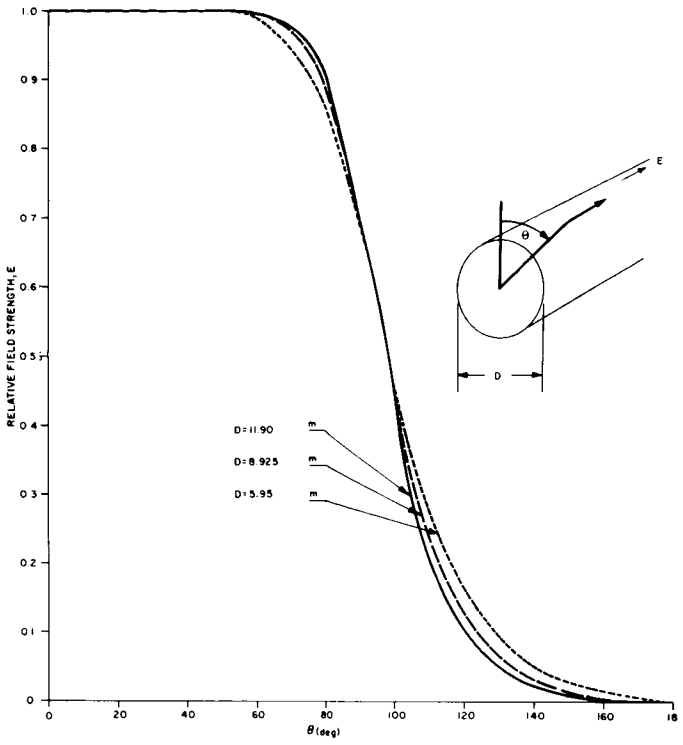

Figure 6-42. Relative Voltage Pattern for an Axial Dipole on a Cylinder (λ = 0.187 m)

have two probable values for the multipath discrimination: 0.6 and 1.64 dB/degree of elevation angle. It does not appear unreasonable to expect a value of about 1 dB/degree for a typical receiver multipath discrimination of 10 dB. This will impose a system limitation of 10° above the horizon for all measurements. Of course, the medium itself provides some multipath discrimination near the horizon. Inspection of Figure 6-33 indicates that the vertical polarization is essentially lost in all cases for elevation angles less than 15° (i.e., zenith angle greater than 75°). This already results in a 3 dB loss in the multipath component. For the horizontal component, the least discrimination results at lower altitudes. Table 6-4 shows the result of using the worst case values given in Figure 6-33 adding the 3-dB loss of the vertical polarization plus an antenna discrimination of 1 dB/degree.

Table 6-4 shows that the worst case occurs at an elevation angle of 3° and a rejection capability of 9.7 dB. It should be pointed out that our model assumes the antenna to be ideal in the sense that in the upper hemisphere the antenna is circularly polarized everywhere. For an antenna configuration as shown in Figure 6-38, it appears it will be primarily vertically polarized for low elevation angles, in which case the average signal level is down 3 dB. For this case, taking the worst case for the multipath component as shown in Figure 6-33 and adding a 1 dB/degree of antenna discrimination we obtain the results shown in Table 6-5.

TABLE 6-4. MULTIPATH REJECTION—CIRCULAR POLARIZATION

Elev. Angle (deg)	P_m/P_d (dB)	Loss of Vert. pol. (dB)	Ant. Discrimination (dB)	Total Disc. (dB)
1	7.1	3.0	1.0	11.1
2	5.0	3.0	2.0	10.0
3	3.7	3.0	3.0	9.7
4	2.9	3.0	4.0	9.9
5	2.1	3.0	5.0	10.1
6	1.75	3.0	6.0	10.75
7	1.47	3.0	7.0	11.47
8	1.3	3.0	8.0	12.3
9	1.11	3.0	9.0	13.11
10	1.0	3.0	10.0	14.0
11	0.9	3.0	11.0	14.9
12	0.9	3.0	12.0	15.93
13	0.84	3.0	13.0	16.84
14	0.80	3.0	14.0	17.80
15	0.80	3.0	15.0	18.80

TABLE 6-5. MULTIPATH REJECTION—VERTICAL POLARIZATION

Elev. Angle (deg)	Ant. Discrimination (dB)	$<P_m>_v/P_{dv}$ (dB)	Total Disc. (dB)
1	1	14.0	15.0
2	2	14.9	16.9
3	3	16.0	19.0
4	4	18.0	22.0
5	5	18.8	23.8
6	6	17.6	23.6
7	7	15.5	22.5
8	8	13.7	21.7
9	9	12.	21.0
10	10	10.7	20.7
11	11	9.6	20.0
12	12	8.8	20.8
13	13	8.1	21.1
14	14	7.6	21.6
15	15	6.98	21.98

These results are much more optimistic than those shown in Table 6-4. In either case the results are encouraging as to the performance of the system.

6.3.5 TRANSMISSION LOSS

6.3.5.1 FREE SPACE ATTENUATION

Free space path attenuation α is given by

$$\alpha = 37 + 20 \log f + 20 \log d$$

where f is in MHz with a range of 1540 MHz to 1660 MHz, and d is the distance in miles; d varies from 22,300 miles for an overhead satellite to 26,250 miles for a satellite on the horizon.

$$\text{Minimum attenuation} = \alpha_{min} = 37 + 20 \log 1540 + 20 \log 22{,}300$$

$$\alpha_{min} \approx 188 \text{ dB}$$

$$\text{Maximum attenuation} = \alpha_{max} = 37 + 20 \log 1660 + 20 \log 26{,}250$$

$$\alpha_{max} \approx 190 \text{ dB}$$

The variation of free space path loss due to carrier frequency and the range variations is only 2 dB. For the purpose of the analysis, we will assume the worst case attenuation applies; i.e., $\alpha = \alpha_{max} = 190$ dB.

6.3.5.2 ANTENNA POLARIZATION LOSS

Because of the geometry involved (satellite-to-earth or earth-to-satellite), the maximum polarization loss (assuming all antennas are circularly polarized with the correct sense) will be 3 dB. This occurs when one field of the linear polarizations (e.g., horizontal or vertical) is reduced to near zero, e.g., when the satellite is low on the horizon.

6.3.5.3 TRANSMISSION LINE AND COUPLER LOSSES

The insertion loss of any passive networks such as transmission lines, antenna couplers, preselectors, etc., attenuates the signal by the magnitude of the loss. The combined transmission line and coupler losses are expected to be less than 2.0 dB.

6.3.5.4 ATTENUATION OF SIGNAL DUE TO SNOW AND/OR RAIN ON RADOME

It is desired to determine the degradation of the received signal during a period of heavy rain (or snow). Furthermore, it is desired to determine the additional degradation that a radome over the antenna will contribute.

Experimental data [6-44] taken at Andover, Maine, by Bell Telephone Laboratory and Communications Satellite Corporation personnel on transmissions received from the Early Bird satellite, transmitting at a frequency of approximately 4000 MHz indicate that the carrier-to-noise degradation during a heavy rain can exceed 6 dB. Further measurements taken by Bell Telephone Laboratory personnel [6-45] on the radio source Cassiopeia A, at a frequency of 4000 MHz, indicated transmission degradations as high as 8 dB.

Using an analysis similar to Blevis [6-46] (who utilized equations developed by Leaderman and Turner[6-47]) in conjunction with rainfall data[6-48] and the value of the dielectric constant of water[6-49] at UHF, the average expected attenuation due to rainfall will be 0.5 dB; there is a 1% probability that the attenuation will exceed 2.5 dB during any five-minute period during the next 25 years. The above values of attenuation are for rainfall rates of one inch/hour, and 12 inches/hour on a 30-foot radome, the radome covering a 20-foot antenna. Without a radome, the worst case attenuation would be less than 0.5 dB.

It is felt that the only equipment that would be affected by the rain-radome consideration would be at the ground control center. The reasoning is as follows:

(1) For general field use, boats, ships, and trucks will not require a radome.

(2) High-performance aircraft, such as SST's or conventional jets, which require a radome will, however, usually fly above the rain.

(3) Low-performance aircraft will generally have small antennas (viz. less than 2 feet in diameter) and hence small radomes. (For a 3-foot radome the worst-case attenuation will be 0.6 dB — a relatively small value.)

6.3.6 NOISE SOURCES

6.3.6.1 NON-TERRESTRIAL NOISE SOURCES

6.3.6.1.1 SUN NOISE TEMPERATURE, T_s (See Reference 6-50, Equation 10)

$$\frac{T_s}{290} = \frac{675}{f} \left\{ 1 + \frac{1}{2.3} \sin \left[2 \frac{\log 6(f - 0.1)}{2.3} \right] \right\}$$

where f is in GHz;

for f = 1.54 GHz

$$T_s = \frac{1.96 \times 10^5}{1.54} \left[1 + \frac{1}{2.3} \sin \left(2 \frac{\log 9.18}{2.3} \right) \right]$$

$$T_s = 1.27 \times 10^5 \, (1 + 0.435 \sin 2.73 \times 0.963)$$

$$T_s = 1.54 \times 10^5 {}^\circ\text{K}.$$

Since the sun subtends an angle of approximately 0.5° as seen at the surface of the earth, antennas with a beamwidth of 0.5° or less (an ideal antenna with an infinite cutoff at beamwidth edge) will effectively see the full 1.54×10^5°K sun temperature. For beamwidths greater than 0.5° the antenna temperature is decreased by the square of the beamwidth with respect to the sun's diameter, i.e.,

$$T_a = T_s \left(\frac{0.5}{\theta} \right)^2 \quad ; \quad \text{(See Reference 6-50, Equation 11a)}$$

where θ equals the plane angle beamwidth of the antenna in degrees. Table 6-6 illustrates the effect of the antenna beamwidth on system noise figure, F_{dB}, for a receiver noise figure F_{cc}, of 5 dB. In the table, T_e (°K) is the sum of the antenna and the receiver noise temperatures, and ΔF_{dB} is the increase of the system noise figure over the receiver noise figure of 5 dB. As an example, an antenna with a 3° beamwidth pointed at the sun will cause a system noise figure of 12.5 dB, an increase of 7.5 dB over the receiver noise figure of 5 dB.

TABLE 6-6. SYSTEM NOISE FIGURE*

θ (deg)	T_a (°K)	T_e (°K)	F-1	F	F_{dB}	ΔF_{dB}
0.5	1.54×10^5	1.55×10^5	534.0	535.0	27.3	22.3
1.0	3.85×10^4	3.91×10^4	135.0	136.0	21.3	16.3
1.5	1.71×10^4	1.77×10^4	61.0	62.0	17.9	12.9
2.0	9.63×10^3	10.26×10^3	35.4	36.4	15.6	10.6
2.5	6.16×10^3	6.79×10^3	23.4	24.4	13.9	8.9
3.0	4.28×10^3	4.91×10^3	16.9	17.9	12.5	7.5
5	1.54×10^3	2.17×10^3	7.48	8.48	9.3	4.3
10	385.0	1012.0	3.48	4.48	6.5	1.5
15	171.0	798.0	2.75	3.75	5.7	0.7
20	96.3	723.3	2.49	3.49	5.4	0.4
25	61.3	688.3	2.39	3.39	5.4	0.3
50	15.4	642.4	2.21	3.21	5.1	0.1

*Based on F_{cc} = 5 dB → 316°K, and T_{cc} = 627°K.

6.3.6.1.2 GALACTIC NOISE

Galactic noise comprises noise contributions from (1) the galactic center, (2) background or the isotropic effect, and (3) discrete sources. The noise from the Galactic center is summarized in Table 6-7. The isotropic contribution [6-50] is 1°K at 1200 MHz. The more intense discrete galactic noise sources [6-51] are listed in Table 6-8.

TABLE 6-7. ANTENNA TEMPERATURE IN DIRECTION OF GALACTIC CENTER AT 1200 MHz

Antenna	Calculated (°K)	Observed (°K)
2°.8	18.7	17.0
Infinitely Narrow	34.0	-

TABLE 6-8. NOISE SOURCE INTENSITY, S, IN WATTS PER SQUARE FOOT PER Hz

Source	200 Hz	1000 MHz	3000 MHz	1500 MHz
Cassiopeia A	10^{-23}	3×10^{-24}	10^{-24}	2×10^{-24}
Cygnus A	10^{-23}	10^{-24}	7×10^{-25}	9×10^{-25}
Tarus A	10^{-24}	10^{-24}	10^{-24}	10^{-24}
Virgo A	10^{-24}	3×10^{-25}	10^{-25}	2×10^{-25}

The noise source power density is

$$P_d = SA_e$$

where

P_d = Discrete source noise power density (watts/Hz)

S = Discrete source intensity (watts/ft^2/Hz)

A_e = Effective area of the antenna in square feet; for a 20-foot diameter antenna, A_e = 314 square feet.

The discrete source noise power density is converted to an effective antenna temperature, T_{ad}, by

$$T_{ad} = \frac{P_d}{k}$$, where k = Boltzman's Constant = 1.38×10^{-23} joules/°K

The effective antenna temperatures for the discrete galactic noise sources shown in Table 6-8 for 1500 MHz are shown in Table 6-9 (for a 20-foot diameter antenna).

TABLE 6-9. EFFECTIVE ANTENNA TEMPERATURES

Source	Intensity	Power Density	T_{ad}
Cassiopeia A	2×10^{-24}	6.28×10^{-22}	45.5 °K
Cygnus A	9×10^{-25}	2.83×10^{-22}	20.5 °K
Tarus A	10^{-24}	3.14×10^{-22}	22.8 °K
Virgo A	2×10^{-25}	6.28×10^{-23}	4.55 °K

It is to be noted that all the above galactic noise sources have a negligible contribution to the total system noise and hence can be ignored.

6.3.6.2 TERRESTRIAL NOISE SOURCES

The major terrestrial noise source is the antenna minor lobes. The increase in effective antenna noise temperature due to minor lobe pickup is directly related to (1) the gain of the minor lobe as compared to the main lobe, and (2) the temperature of the medium in which the lobe is directed.

The relationship is[6-53]

$$T_{\text{minor lobes}} = \sum_{k=1}^{n} \gamma_k \delta_k T_k$$

where

γ_k = total fractional attenuation of the k minor lobe compared with the main lobe

δ_k = total fractional absorption of the reflected, scattered, and transmitted minor lobe in a medium whose temperature is T_k

For example, if the minor lobe is looking at the earth, $T_k = 290°K$, and the $\gamma_k \delta_k$ is -10 dB, $T_{\text{minor lobe}} = 29°K$.

6.3.7 EQUIPMENT TIME-DELAY ERRORS

6.3.7.1 OSCILLATOR STABILITY REQUIREMENTS

6.3.7.1.1 CONTROL CENTER

All frequencies (carrier, intermediate, coarse and fine tones, etc.) are derived from a common source, a cesium beam standard. The published accuracy of a standard such as the "Hewlett-Packard* 5060A Cesium Beam Frequency Standard" is $\pm 2 \times 10^{-11}$. The total fractional frequency drift for the life of the cesium beam tube is 1 part in 10^{11}. At 1660 MHz the total frequency error is about 0.05 Hz. This offset can be ignored.

6.3.7.1.2 SATELLITE TRANSPONDER

A glance at Figure 6-43 showing a simplified block diagram of the satellite transponder with suitable labels shows that the frequency error in oscillator No. 1 is effectively cancelled out by the process of subtraction and then addition in the transponder. The remaining error is ϵ_2, the error on the sidestep oscillator. Since the frequency of the sidestep oscillator is at least an order of magnitude lower than the RF frequencies the error, ϵ_2, is proportionally lower than the error on the first injection oscillator ϵ_1. For example, if Δf is 50 MHz and has a temperature compensated (no oven required) crystal oscillator such as the F15-CO-3 model made by Frequency Electronics, Inc. the frequency offset ϵ_2 at the end of a year would be 250 Hz maximum. This value represents an offset of 0.01% when compared to the satellite IF bandwidth which is on the order of several megahertz.

*Where a manufacturer's name and model are given, they are given only as representative examples of the state-of-the-art, and not as an endorsement of the product.

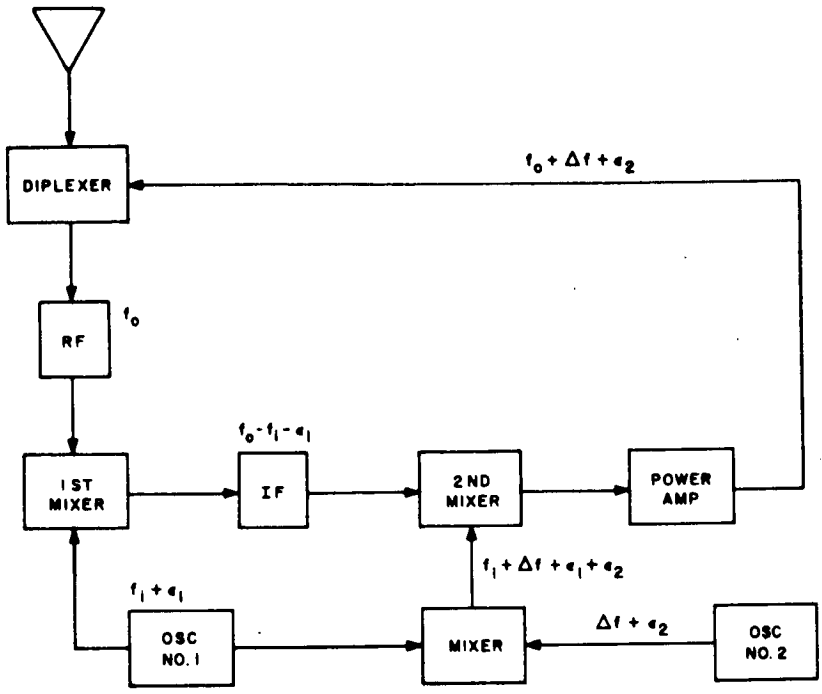

f_o = Received Signal frequency

f_i = Nominal Injection frequency

ϵ_1 = The frequency error on f_i

Δf = The sidestep frequency

ϵ_2 = The frequency error on Δf

$f_o + \Delta f$ = The nominal transmitted frequency

Figure 6-43. Satellite Transponder

6.3.7.1.3 USER RECEIVER

The prime source of frequency error in the user receiver is the first injection oscillator. This oscillator has the highest, internally generated, frequency in the receiver, of the order of 1300 MHz. However, the user is at liberty to calibrate or adjust the frequency# of this oscillator by tuning in one of the equatorial synchronous satellites (at a time of no relative motion between the user and the satellite). He does this by first disabling the automatic sweep of the carrier-lock loop and adjusts the first injection oscillator frequency control (over a limited range) until it is within the pull-in range of the carrier-lock loop. The frequency error is then less than 100 Hz.

#In the case of coherent injection, (i.e., the first and second injection oscillators are locked to a multiple of the VCO), only the VCO need be adjusted (Automatic sweep disabled).

If the mission is in the order of 6 hours (the time for a conventional jet to fly across the North Atlantic from New York to London), the frequency drift will be on the order of 17 Hz. This value is arrived at in the following way. It is assumed that a fast stabilization oscillator such as the FE4M model made by Frequency Electronics, Inc. is used in conjunction with a multiplier chain to derive the desired injection frequency. It is further assumed that the oscillator was initially turned on, allowed to warm up for 10 minutes, and then set. From the published warmup curve of the oscillator and the published 24-hour stability curve, the frequency error is expected to be approximately 1 part in 10^8 for an 8-hour period resulting in a frequency error of 16.6 Hz at a carrier frequency of 1660 MHz. It is assumed that the oscillator is loosely coupled to the multiplier chain so that no "frequency pulling" of the oscillator occurs.

The second injection oscillator# operates at a frequency of the order of 200 MHz so that it is expected that the frequency accuracy at the end of a year will be of the order of 200 Hz. This value is well within the tuning range of the first injection oscillator (± 2 kHz minimum) and the sweep range of the carrier-lock VCO (± 10 kHz).

The optimum frequency for the carrier VCO is in the 10 to 30 MHz range. 10 MHz is about the lowest practical frequency because of the high order sideband components on the fine frequency tone (which can extend ± 3 MHz), while 30 MHz is the highest practical frequency for fundamental mode AT cut crystals; the frequency deviation of the oscillator is inversely proportional to the square of the mode (e.g., a 3rd mode crystal can be pulled only 1/9 that of a fundamental mode crystal).

The worst case frequency drift for a crystal VCO is 5 parts in 10^6 for a year which is the published value for a model FE 20-VPC-10P made by Frequency Electronics, Inc. This results in a frequency drift of 150 Hz for a 30-MHz VCO.

It has been shown that the total frequency offset (at the input to the user demodulator) of the received signal has a worse case value of 467 Hz. This value represents the accumulated frequency error of the control center, satellite, and the user at the end of a year of operation and with the user calibrating his first injection oscillator once a day. If this oscillator is set once every 10 days the frequency error becomes 620 Hz. This also represents a worst case.

6.3.7.2 FILTER TIME DELAY STABILITY

The temperature drift of the components in a filter network can cause time delays that will appear as range errors in the measurement system, thus adding to the uncertainty in the position determination.

The following assumptions are made about the nature of the filter.

(1) The filter consists of n identical, isolated, synchronously-tuned RLC tank circuits.

#In the case of coherent injection, (i.e., the first and second injection oscillators are locked to a multiple of the VCO), only the VCO need be adjusted (Automatic sweep disabled).

(2) Any shift in center frequency, hence shift in phase or time delay, is caused only by temperature fluctuations.

(3) The phase shift of the filter is n times that of a single stage, i.e., all shift the same way.

(4) The parts-per-million change in the reactance of the tank circuit is the residual of both the individual ppm of each reactor due to incomplete temperature compensation, TC.

A schematic of a single section tank circuit is shown in Figure 6-44. In the actual configuration there are n circuits in cascade between the generator and load. In the circuit shown, R_g is the source driving resistance (reactive component tuned out) and R_L is the load resistance. For maximum power transfer, R_g equals the parallel combination of R_L and the resistors representing the loss in the reactors.

$$R_P = \frac{R_g R_L}{R_g + R_L}$$

In the S-plane, we can write the following equation for the circuit of Figure 6-44.

$$E_{OUT}(S) = I_{IN}(S) \frac{1}{\frac{1}{R_p} + \frac{1}{LS} + CS} \qquad (1)$$

simplifying (1) and noting

$$I_{IN}(S) = \frac{E_{IN}(S)}{R_g}$$

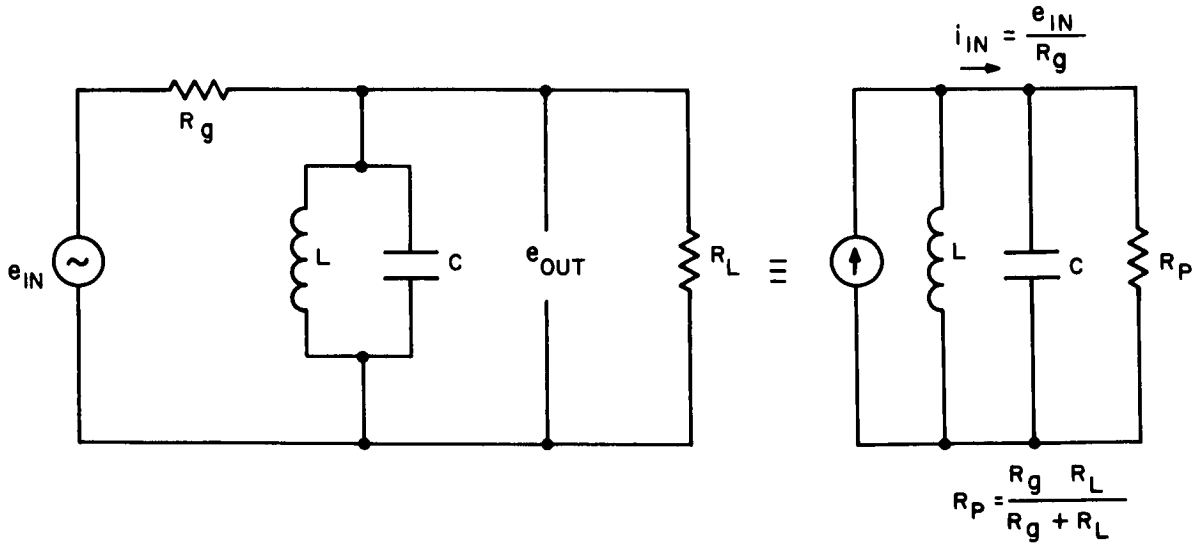

Figure 6-44. Single-Pole Tuned Circuit

we can write

$$\frac{E_{OUT}(S)}{E_{IN}(S)} = \frac{1}{R_g C}\left[\frac{S}{S^2 + \frac{S}{R_p C} + \frac{1}{LC}}\right] \tag{2}$$

Now let

$$a = \frac{1}{R_g C}$$

$$o = \frac{1}{\sqrt{LC}} \tag{3}$$

$$Q = \frac{\omega_o L}{R_p}$$

Upon substituting (3) in (2), we obtain:

$$\frac{E_{OUT}(S)}{E_{IN}(S)} = \frac{aS}{S^2 + \omega_o QS + \omega_o{}^2} \tag{4}$$

In equation (4) let $S = j\omega$, and define

$$\frac{E_{OUT}(j\omega)}{E_{IN}(j\omega)} = H(j\omega)$$

We obtain

$$H(j\omega) = \frac{a\omega^2 Q\omega_o + ja\omega(\omega_o{}^2 - \omega^2)}{(\omega_o{}^2 - \omega^2)^2 + (Q\omega_o\omega)^2}$$

which can be written as either

$$H(\omega) = X(\omega) + jY(\omega)$$

or

$$H(\omega) = A(\omega)e^{i\theta(\omega)}$$

where

$$A(\omega) = \sqrt{\left[X(\omega)\right]^2 + \left[Y(\omega)\right]^2}$$

and

$$\theta_e = \arctan \frac{Y(\omega)}{X(\omega)} \tag{5}$$

Restricting the analysis to $\theta_e(\omega)$ only and letting

$$\omega = \omega_o + \Delta\omega$$

we can simplify (5) to

$$\theta_e = \arctan - \left[\left(\frac{(2\omega_o + \Delta\omega)\,\Delta\omega}{(\omega_o + \Delta\omega)\,\omega_o Q}\right)\right] \tag{6}$$

Under the assumption of a narrow band system ($\Delta\omega << \omega_o$), Eq. (6) can be simplified to

$$\theta_e = \arctan\left[\frac{-2\Delta\omega}{Q\omega_o}\right]$$

As previously defined

$$\omega_o = \frac{1}{\sqrt{LC}}$$

and taking the logarithmic derivative with respect to L and C

$$\frac{d\omega_o}{\omega_o} = \frac{1}{2}\left(\frac{dL}{L} + \frac{dC}{C}\right)$$

Let $d\omega_o = \Delta\omega$, $\frac{dL}{L} = L_L$ and $\frac{dC}{C} = C_C$

where L_L and C_C are the changes in L and C per unit of L and C.

$$\theta_e = \text{Arctan} \quad \frac{(L_L + C_C)}{Q}$$

and since $Q = \frac{f_o}{B_3}$ where B_3 is the 3-db bandwidth in Hz. Then,

$$\theta_e = \arctan\left[\frac{B_3}{f_o}(L_L + C_C)\right] \tag{7}$$

assuming in (7) that

$$\epsilon \Delta T = L_L + C_C$$

where ϵ is the total change in $L_L + C_C$ per degree centigrade and

ΔT is the temperature change in degrees centigrade.

$$\theta_e = \arctan \left[\frac{B_3}{f_o} \epsilon \Delta T \right] \tag{8}$$

Equation (8) is plotted in Figure 6-45 as a function of ΔT and bandwidth.

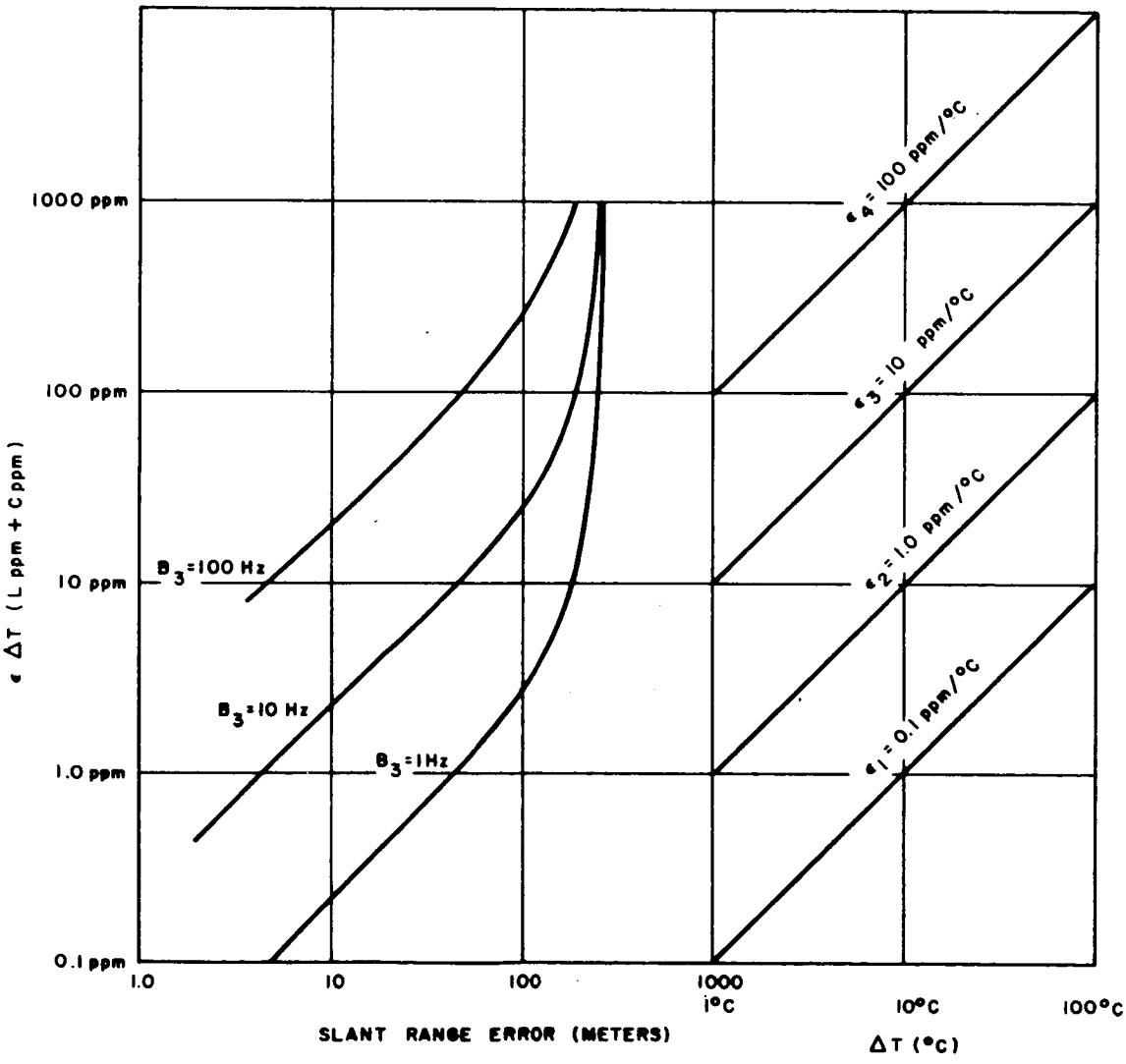

Figure 6-45. Slant Range Error vs 3 dB Bandwidth and Temperature at a Tone Frequency of 300 kHz

6.3.8 DOPPLER, AND DOPPLER RATE EFFECTS

The design of the receiver requires the knowledge of the maximum expected doppler and its rate of change. It is intuitively obvious that the maximum doppler in the system will be generated when use is made of the polar satellites. To study such a configuration assume a satellite at the (spherical coordinates) point $(a, \theta_s, 0°)$ and the user at $(a_u, 90°, \varphi_u)$, where a and a_u are the respective heights of the satellite and user (assumed to be stationary) relative to the center of the earth; θ_s is the complement of the elevation angle; and φ_u is the user azimuthal angle.

It should be noted that the indicated coordinates are completely general. Any other configuration can be reduced to the given one by a rotation of axis. In cartesian coordinates the satellite and user position vectors are given by:

$$\vec{R}_s = a\left[\sin\theta_s\,\hat{x} + \cos\theta_s\,\hat{z}\right]$$

$$\vec{R}_u = a_u\left[\cos\varphi_u\,\hat{x} + \sin\varphi_u\,\hat{y}\right]$$

The velocity of the satellite V_r relative to the rotating earth is given by:

$$\vec{V}_r = \vec{V}_s - \left(\vec{\omega} \times \vec{R}_s\right)$$

where $\vec{V}_s$ is the velocity relative to the inertial system,

$\vec{\omega}$ is the angular rotation of the earth, and

$\vec{R}_s$ is the position vector of the satellite

For a 24 hour satellite in polar orbit

$$\vec{V}_s = \omega a\hat{\theta} \text{ where } \omega = 7.95 \times 10^{-5} \text{ rad/sec}$$

$$\vec{V}_s = \omega a\left[\hat{x}\cos\theta_s - \hat{z}\sin\theta_s\right]$$

$$\vec{\omega} = \omega\hat{z}$$

$$\vec{\omega} \times \vec{R}_s = \left[+\omega a \sin\theta_s\, y\right]$$

Thus V_r is given by

$$\vec{V}_r = \omega a\left[\hat{x}\ (\cos\theta_s) + y\ (-\sin\theta_s) - \hat{z}\ (\sin\theta_s)\right]$$

The normalized vector between satellite and user is given by:

$$\frac{\vec{R}_u - \vec{R}_s}{\left|\vec{R}_u - \vec{R}_s\right|} = \frac{\hat{x}\left[-a \sin\theta_s + a_u \cos\varphi_u\right] + \hat{y}\left[a_u \sin\varphi_u\right] + \hat{z}\left[-a\cos\theta_s\right]}{\sqrt{a^2 + a_u^2 - 2aa_u \sin\theta_s \cos\varphi_u}}$$

Then the velocity in the direction of the user is given by:

$$V_d = \vec{V}_r \cdot \frac{\vec{R}_u - \vec{R}_s}{\left|\vec{R}_u - \vec{R}_s\right|} = \frac{\omega a a_u \cos(\theta_s + \varphi_u)}{\sqrt{a^2 + a_u^2 - 2a a_u \sin\theta_s \cos\varphi_u}}$$

The resulting doppler shift is given by

$$(\Delta f)_{\text{doppler}} = \frac{f_o}{C} \cdot \frac{\omega a a_u \cos(\theta_s + \varphi_u)}{\sqrt{a^2 + a_u^2 - 2aa_u \sin\theta_s \cos\varphi_u}}$$

where f_o is the transmitted frequency and C is the velocity of light. An upper bound for this expression is of the form

$$(\Delta f_d)_{\substack{\text{upper}\\\text{bound}}} = \frac{f_o}{C}\omega a_u \left(1 + \frac{a_u}{a}\right)$$

for

$$a_u = 3965 \text{ miles}$$

$$a = 26{,}250 \text{ miles}$$

$$f_o = 1.66 \times 10^9 \text{ Hz}$$

$$C = 186{,}280 \text{ miles}$$

$$(\Delta f_d)_{\substack{\text{upper}\\\text{bound}}} = 3311 \text{ Hz}$$

The acceleration is given by:

$$\vec{a}_r = \vec{a}_s - 2\vec{\omega} \times \vec{V}_s - \vec{\omega} \times (\vec{\omega} \times \vec{R}_s)$$

where

$\vec{a}_s = \omega^2 ar$ is the centrifugal acceleration in the inertial system of reference

$= \omega^2 a \sin\theta_s \hat{x} + \cos\theta_s z$

$\vec{a}_r$ is the acceleration relative to the user on the earth.

Evaluating the cross products we obtain

$$\vec{a}_r = \omega^2 a \left[+2 \sin\theta_s \hat{x} - 2 \cos\theta_s y + \cos\theta_s \hat{z} \right]$$

the acceleration in the direction of the user is given by

$$a_d = \vec{a}_r \cdot \frac{\left(\vec{R}_u - \vec{R}_s\right)}{\left(\vec{R}_s - \vec{R}_u\right)} = \frac{a^2 \omega^2 \left[2 \frac{a_u}{a} \sin(\theta_s - \varphi_u) - \sin^2\theta_s - 1 \right]}{\sqrt{a^2 + a_u^2 - 2aa_u \sin\theta_s \cos\varphi_u}}$$

The resulting doppler rate is given by

$$\left| \Delta \dot{f}_o \right| = \frac{f_o}{C} \frac{a^2 \omega^2 \left[2 \frac{a_u}{a} \sin(\theta_s - \varphi_u) - \sin^2\theta_s - 1 \right]}{\sqrt{a^2 + a_u^2 - 2a_u a \sin\theta_s \cos\varphi_u}}$$

An upper bound for this expression is given by:

$$\left| \Delta \dot{f}_o \right| = \frac{2f_o}{C} a\omega^2$$

for

$a_u = 3965$ miles

$a = 26250$ miles

$C = 186280$ miles

$f_o = 1.66 \times 10^9$ Hz

$$\left| \Delta \dot{f}_o \right| = 2.96 \text{ Hz/sec}$$

6.3.9 SAMPLE LINK CALCULATIONS

Forward Path - Values for forward-path paremeters are tabulated below:

	Value
CONTROL CENTER	
Transmitter power (dBW)	20.0
Antenna coupling losses (dB)	1.5
Antenna gain (dB)	37.0
Rain and snow attenuation (dB)	0.2
Effective radiated power, ERP (dBW)	55.8
PROPAGATION	
Path loss (dB)	190.0
Atmosphere & ionosphere attenuation (dB)	0.5
SATELLITE	
Antenna gain (dB)	17.5
Antenna polarization loss (dB)	1.5
Antenna coupling loss (dB)	1.0
Received RF power (dB)	-120.2
SATELLITE NOISE POWER	
Receiver noise figure (dB)	5.0
Receiver noise temperature (°K)	917.0
Effective sun temperature (°K)	0
Total galactic noise temperature (°K)	2.0
Effective earth temperature (°K)	133.0
Total noise temperature (°K)	1052.0
System noise figure (dB)	5.6
Noise density (dBW/Hz)	-198.4
Satellite noise bandwidth (MHz)	2.0
Satellite noise power (dBW)	-135.4
RF power/noise (dB)	15.2
*Transmitter power (dBW)	16.0
Antenna coupling loss (dB)	1.0
Antenna gain (dB)	17.5
ERP (dBW)	32.5
Effective radiated noise, ERN, (dBW)	17.3

*See Subsection 6.3.10

	Value
PROPAGATION	
Path loss (dB)	190.0
Atmospheric & ionospheric atten. (dB)	0.5
USER	
Antenna gain (dB)	2.0
Antenna polarization loss (dB)	1.5
Antenna coupling loss (dB)	2.0
Received RF power (dB)	-159.5
USER NOISE POWER	
Receiver noise figure (dB)	5.0
Receiver noise temp. (°K)	917.0
Total galactic noise temp. (°K)	2.0
Effective sun temp. (°K)	2.0
Total noise temp. (°K)	921.0
System noise figure (dB)	5.0
Noise density (dBW/Hz)	-199.0
Received noise from satellite (dBW)	-174.7
Received noise density (dBW/Hz)	-237.7
Total noise density (dBW/Hz)	-199.0
Predetection noise bandwidth (MHz)	2.0
Predetection noise power (dBW)	-136.0
RF power/noise (dB)	-23.5
Carrier/noise @ m_p = 1.15 (dB)	-29.9
Postdetection carrier noise bandwidth (Hz)	100.0
Reference carrier/noise (dB)	10.1
Tone noise bandwidth (Hz)	4.0
Tone signal/noise (dB)	24.1
SELF-NAVIGATION MODE	
*Tone noise bandwidth (Hz)	1.0
Tone signal/noise (dB)	30.1

*In active mode user tone-bandwidth is much larger (4-times) than control center tone-bandwidth so that the integration time (reciprocal of the tone-bandwidth) is predominately determined by the control center. In the case where the user wants his position (either in the active or passive mode), the effective bandwidth of the user's navigation equipment is 1 Hz.

Return Path - Values for return-path parameters are tabulated below:

	Value
USER	
Transmitter power (dBW)	(10w)
	10.0
Antenna gain (dB)	2.0
Antenna coupling losses (dB)	2.0
ERP (dBW)	10.0
*Effective radiated noise density (dBW/Hz)	29.5
PROPAGATION	
Path loss (dB)	190.0
Atmospheric & Ionospheric atten. (dB)	0.5
SATELLITE	
Antenna gain (dB)	17.5
Antenna polarization loss (dB)	1.5
Antenna coupling loss (dB)	1.0
Received RF power (dBW)	-165.0
Satellite Noise Power	
Noise density (same as forward path) (dBW/Hz)	-198.4
#Received noise density from user (dBW/Hz)	-204.5
Combined noise density (dBW/Hz)	-197.4
Effective noise power (dBW)	-135.4
Received RF power/noise (dB)	-29.6
Transmitter power (dBW)	(10w)
	10.0
Antenna coupling losses (dB)	1.0
Antenna gain (dB)	17.5
ERP (dBW)	-3.1
ERN (dBW)	26.5
PROPAGATION	
Path loss (dB)	190.0
Atmospheric & ionospheric atten. (dB)	0.5
CONTROL CENTER	
Antenna gain (dB)	37.0
Antenna polarization loss (dB)	1.5
Antenna coupling loss (dB)	1.0
Received RF power (dBW)	-159.1

*Retransmitted noise in a ± 1 Hz bandwidth about the carrier and about each tone sideband.

#Only affects the demodulated signal at the control center, since the noise is narrowbanded.

	Value
*CONTROL CENTER NOISE POWER	
System noise figure (dB)	5.0
System noise density (dBW/Hz)	-199.0
Received noise density from satellite (dBW/Hz)	-195.5
Total noise density (dBW/Hz)	-193.9
RF Power/total noise density (dBW/Hz)	34.8
Postdetection carrier noise bandwidth (Hz)	25.0
Reference carrier/noise (dB)	11.4
Tone noise bandwidth (Hz)	1.0
#Tone signal/noise (dB)	25.4
EFFECT OF SUN	
Receiver noise figure (dB)	5.0
Receiver noise temperature (°K)	917.0
Solar noise temperature (°K)	2570.0
Received noise temp. from satellite (°K)	2100.0
Total noise temperature (°K)	5587.0
System equivalent noise figure (dB)	12.8
Total noise density (dBW/Hz)	191.2
Increase in noise due to sun (dB)	2.7
Demodulated carrier/noise (dB)	8.7
Tone signal/noise (dB)	22.7

6.3.10 SATELLITE TRANSMITTER OUTPUT POWER

RCA is currently producing an all solid-state transmitting equipment for the LEM-Apollo program that is capable of delivering 1/2 watt into an antenna at a frequency of 9.6 GHz. An intermediate step in the multiplier chain, producing this signal, delivers a power of 5.5 watts at a frequency of 1.2 GHz. This equipment has been in production since 1965. Since then the state-of-the art has improved to the extent that a single-stage transistor amplifier produces this power level instead of the usual high-level VHF transistor power amplifier followed by several diode multipliers. Discussion with solid-state transmitter design engineers indicates that by the 1968-70 era transistors will be capable of delivering at least 10 watts of RF power in the 1 to 2 GHz frequency range. It is expected that these units will have a power gain of 5 to 6 db at an efficiency of 50 to 55%. By coupling four of these transistors (as shown in Figure 6-46) with suitable low-loss hybrid adders (less than 0.1 dB) a 40-watt RF power level can be obtained.

*This section excludes the effect of the control center antenna pointing directly at the sun which occurs at the spring and fall equinoxes for about a 4-day period with the maximum duration during any one day about 8 minutes.

#It is desirable that the signal-to-noise of the coarse tone be about 23 dB; thus, the correct cycle of the fine tone (30 times the coarse tone frequency) can be resolved in the coarse tone measurement with a confidence (probability) of 96% (two-sigma value).

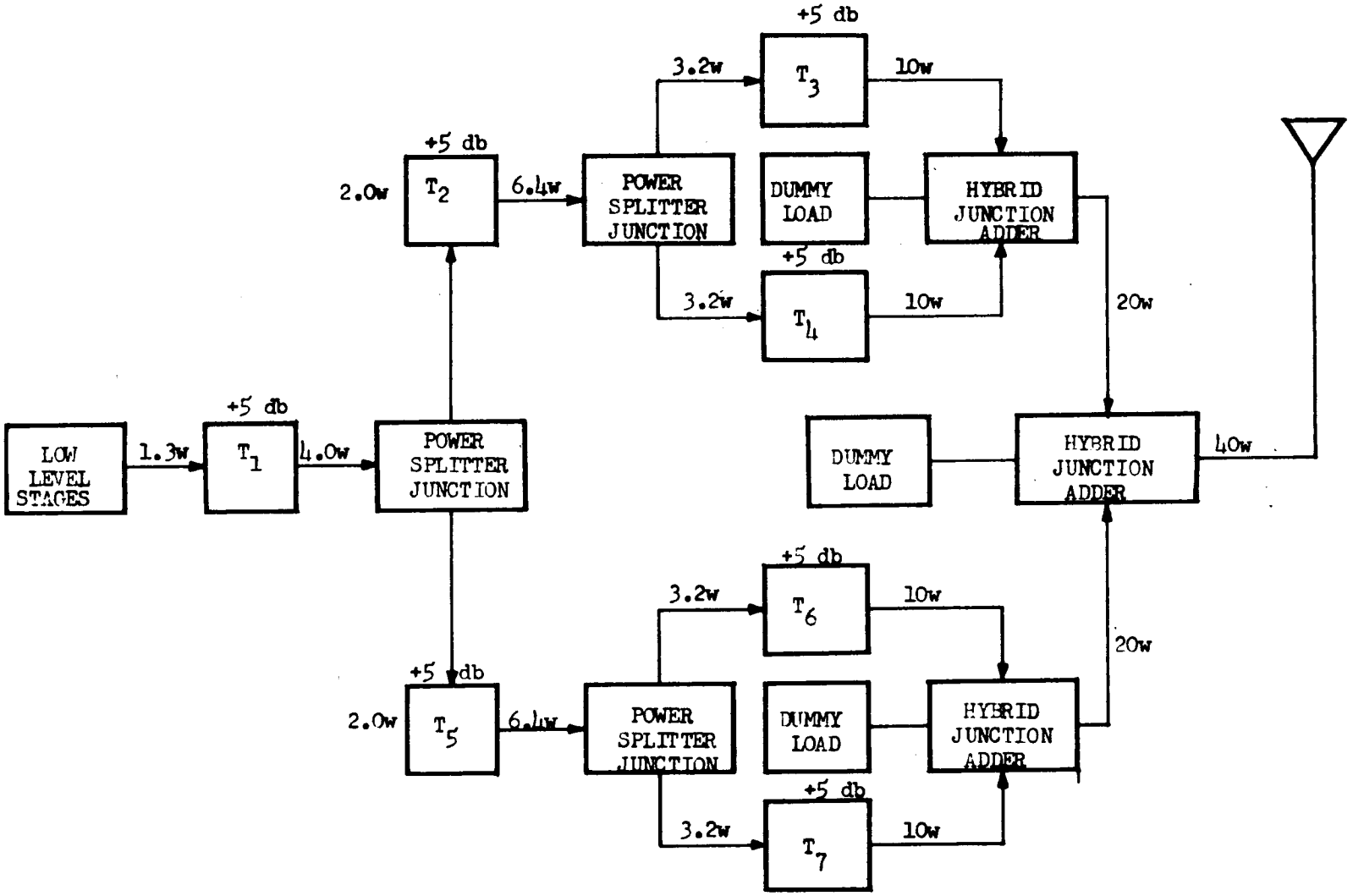

Figure 6-46. Illustrative L-Band, Solid State 40-Watt Power Amplifier

With the assumption that each of the stages are operating at an efficiency of 50%, the total DC power required is approximately 98 watts, resulting in an overall efficiency of 41%.

The above analysis pertains to the satellite power transmitted to the field. In the return link (i.e., from the satellite to the control center) the transmitter power is on the order of 10 watts so that a single power amplifier stage can be used to excite the antenna (see Figure 6-47). The total DC power required in this case is approximately 24 watts, also at an overall efficiency of 41%.

6.3.11 DATA LINK REQUIREMENTS

In the air-traffic-control mode of navigation, the user must transpond a burst of the field signals back up to the satellite, and hence to the control center. In order to prevent satellite power saturation, strong signal capture effects, or adverse intermodulation products from being generated in the satellite, the users will be interrogated in a serial (roll-call) manner; i.e., Time Division Multiplex will be incorporated. In the simplest form the control center will transmit a data link message which will consist of a synchronization signal and an address (to designate the user). In order to simplify the user equipment, while at the same time operating with a fairly good (low) probability of error, a modulation technique such as a differentially coherent phase-shift keyed binary system should be utilized. The address must be long enough to contain the whole active-user population and some margin. For example, a 16-bit address will handle up to 65,536 subscribers; adding one more bit will double the number of subscribers. Upon receiving the data link signal and after an accurately known and fixed time delay, the user will retransmit his own address (preceded, or course, with the synchronization pattern) and a burst of the remodulated field signal.

Because of the inherent error detection present when the returned address is compared with the initially transmitted address, at the control center, the bit-error probability requirement is modest (on the order of 10^{-3}). The reasoning behind this

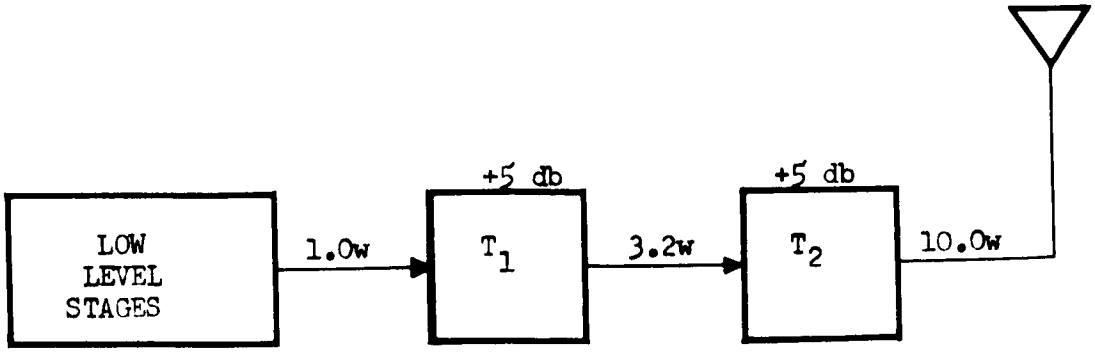

Figure 6-47. L-Band Solid State 10-Watt Power Amplifier

statement is as follows. Assume that an address that was to be processed by subscriber A had an error in one of the time slots so that aircraft B processed the address and sends a burst of the field signal along with the address B. In order for an error to be made, at the control center an error must occur in the B address in the same time slot as the error in the A address, i.e. the B address is received as an A address. The probability of this occuring $p_{e_B} \times p_{e_{cc}}$, where P_{e_B} is the probability of error at the B subscriber and $P_{e_{cc}}$ is the probability of error at the control center.

For example, for $p_{e_B} \times p_{e_{cc}} = 10^{-7}$, an address duration of 0.1 second, and 16 bits per address, the mean-time-to-error, at the control center, is 17.4 hours.

The RF power requirements for the data link signal are quite modest. In fact, if the RF frequency is in the same band as the ranging signal (i.e., 1540 to 1660 MHz), the control-center-to-user link would be identical to the ranging link. A glance at the forward-path link analysis (Section 5.39) shows that the user received power, from the satellite, is -159.5 dBW, while the total noise spectral density (two-sided) is -199.0 dBW/Hz. If the address is 16 binary bits in length and the synchronization is 4 binary bits in length, the whole message is 20 bits. This message is transmitted in 0.1 second, resulting in a bit duration of 5 milliseconds. The signal energy is, therefore -185.6 dBJ (J = joule). The one-sided noise spectral density is -196.0 dBW/Hz. Therefore the energy contrast, E/N_o is 13.5 dB. Lawton[6-52] shows that the error probability, p_e, for a differentially coherent phase-shift keyed binary signal is $p_e = 1/2\ e^{-E/N_o}$ so that given an E/N_o of 22.4 (13.5 db) the bit error probability is at $p_{e_B} \sim 10^{-10}$. This error probability is quite good for the simple system described above.

The average transmitter power required by the user to retransmit the data link signal back to the control center is quite modest, since the transmitter need be on only 0.1 second in any 3-minute interval (worst case). A glance at the return path link analysis (Section 5.3.9) shows that if the user transmitter had a peak power output of 25 watts for 0.1 second (presently obtainable from fairly small ceramic-and-metal planar triodes and pulsed-Gunn oscillators),[6-53] the received power at the satellite would be -161.0 dBW (-165.0+4.0). The ERP of the satellite would then be 0.9 dBW so that the power received at the control center becomes -155.1 dBW. In the absence of solar noise E/N_o would be 12.8 dB, resulting in a bit error probability of 2.7×10^{-6} (worst case calculations).

During the time of satellite conjunction with the sun (for a control center situated on the equator, solar interference occurs a few days before and after the spring equinox and the Autumn Equinoxes), the noise spectral density of the control center receiver increases as much as 2.7 dB in the worst case, resulting in an E/N_o of 10.1 dB leading to a bit error probability of 4.1×10^{-5}. However, this magnitude of the error probability only lasts for approximately 7 minutes in the worst case.*

*The angular diameter of the sun is assumed to be 0.53° and the 3 dB beamwidth of the control center antenna 3.86°. Furthermore, it is assumed that the angular response (gain) behaves identically to a single-pole filter.

6.3.12 CHANNEL CAPACITY - TRAFFIC CONTROL MODE

To make maximum use of a channel when addressing and receiving transponded tones from a number of users, it is desirable to have a time division multiplexing sequence at the Ground Control Center that is as close to continuous as the equipment will allow. However, if this interval is relatively short, say on the order of 0.10 second, it is possible to receive signals from two or more users simultaneously. To avoid this, a time delay can be included between each new address which equals the time difference of propagation between the closest and furthest user from each satellite. The returned signals, then, would be in the same order as the roll call initiated at the G.C.C. Figure 6-48 shows the geometry involved in this simple approach in avoiding traffic jamming or interference. For a satellite at synchronous altitude, S = 22,300 miles and F = 27,000 miles. The propagation time difference interval ($\Delta\tau$) becomes .0505 second. This represents the worst case and can be reduced if the traffic density warrants by having a computer frequently determine the value of $\Delta\tau$ based on prior data on the approximate location of all users.

Adding the maximum likely value of $\Delta\tau$ to the time required for an individual address and tone interval (the system equipment, in particular that of satellite effective radiated power and user receiver sensitivity will determine tone integration time requirements) provides an approximate indication of the traffic capacity per channel. Figure 6-49 shows the number of position determinations per hour which are possible on a non-interference basis versus the time required for a "burst" interval. An average burst interval of 0.5 second provides sufficient traffic capacity in a single channel to meet the 1975 anticipated requirement of 6500 fixes/hour. This goal is entirely achievable by 1975 even with current state-of-the-art developments.

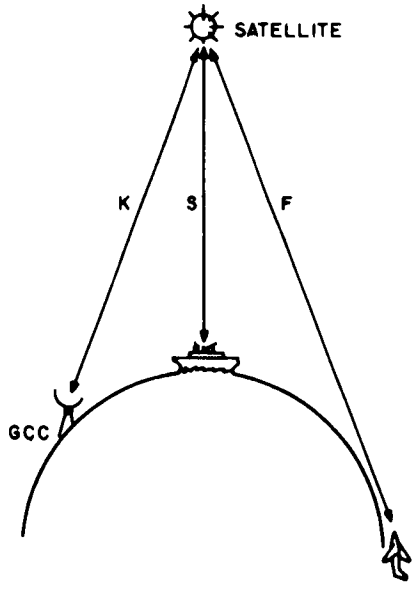

ASSUMPTIONS AND CONDITIONS:

1. Distance from GCC to Satellite is Fixed (K)
2. Distance from Satellite to Closest User (F) (Located Directly Under Satellite)
3. Distance from Satellite to Farthest User (F) (Located at Horizon Relative to Satellite)

Shortest Propagation Path = $2(K + S)$

Longest Propagation Path = $2(K + F)$

Maximum Propagation Path Difference = $2(F - S)$

Propagation Time Interval ($\Delta\tau$) = $\frac{2(F - S)}{C}$

where C = RF Propagation Velocity

Figure 6-48. Traffic Control Geometry

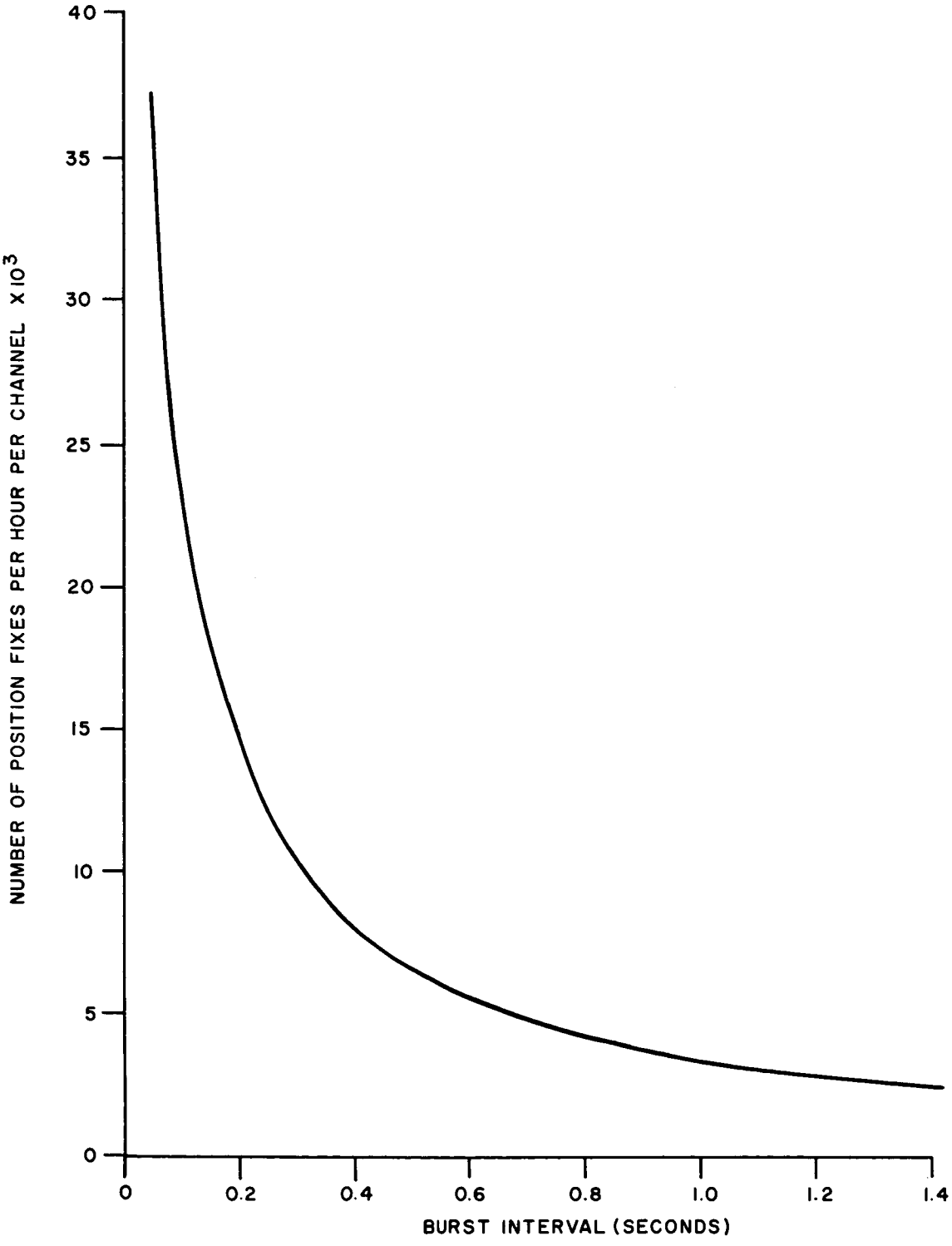

Figure 6-49. Channel Traffic Capacity on Non-Interference Basis Vs Average Burst Interval of Address and Tone Signals

6.4 MATHEMATICAL ANALYSIS OF PHASE MEASUREMENT ERRORS

6.4.1 INTRODUCTION

Subsection 6.2 describes three methods of carrier demodulation: (1) homodyne detection, (2) narrow-band filter carrier extraction and (3) phase-locked loop carrier extraction. Subsection 6.3-1 describes three channel models: (1) white noise, (2) one specular reflection plus white noise, and (3) multiple reflections (diffuse multipath) plus white noise. This corresponds to nine possible cases for analysis, as summarized in Table 6-10. The nine cases are denoted by the symbols C_{ij} in Table 6-10. Numbers of the section and/or appendixes containing the corresponding analysis are written in parenthesis below each case symbol. The analysis consists of tracing the signal and noise waveforms through the IF demodulator, the tone filters and the phase comparator. Expressions are derived for these waveforms, for the tone-filter output signal-to-noise ratios, and for the phase error. The phase error is expressible as an arctangent of a set of normally distributed random variables. Therefore, the phase error statistics can be estimated using a digital computer by calculating a large set of phase errors using random number generation. It has been found that for the cases in Table 6-10 the phase error distributions are approximately normally distributed. Therefore, calculations of the mean and standard deviation of the phase errors are sufficient for their characterization. These quantities have been calculated as a function of the signal-processing parameters and the channel parameters. The results are expressed in terms of phase error in radians, and range error in meters for fine tone frequencies equal to 100 kHz, 300 kHz, and 1MHz, and coarse tone frequencies equal to 3.125 kHz, 9.375 kHz and 31.25 kHz.

TABLE 6-10. SUMMARY OF SITUATIONS ANALYZED

Receiver Demodulator / Channel		Known Carrier Frequency Ideal Homodyne Detector	Narrow-Band Filter Carrier Extraction	Phase-Locked Loop Carrier Extraction
Model No. 1	White Noise	C_{11} (6A)*	C_{12} (6B)*	C_{13} #(6.4.2 & 6C)*
Model No. 2	One Reflection + White Noise	C_{21} (6D)*	C_{22} (6E)*	C_{23} (6D)*
Model No. 3	Multiple Reflections + White Noise	C_{31} #(5.4.3 & 6F)*	C_{32} (6G)*	C_{33} #(5.4.3 & 6F)*

*Appendix containing details on this case.
#Section containing details on this case.

6.4.2 PHASE-LOCK-LOOP CARRIER DEMODULATION WITH WHITE NOISE (C_{13})

6.4.2.1 LINEARIZED PHASE-LOCK LOOP MODEL

This section is concerned with a phase-lock receiving system subject to four independent sources of error: (1) thermal noise, (2) local oscillator instabilities, (3) fading, and (4) continuous wave interference. The following paragraphs contain details of the manner in which a linearized model of the loop is obtained and the effect on the output of the four error sources mentioned above.

A typical phase-lock system is shown in Figure 6-50. It comprises a phase-lock loop preceded by k reference oscillators. The phase-lock loop consists of a multiplier, a linear time-invariant filter with transfer function F(s), and a voltage controlled oscillator (VCO) with quiescent radian frequency ω_o. The input $s_1(t)$ to the system is the sum of a desired signal

$$\sqrt{2}\, A \sin\left(\omega_c t + \theta_1(t)\right) \quad ,$$

thermal noise

$$\sqrt{2}\left[I_1(t) \cos \omega_c t - I_2(t) \sin \omega_c t\right] \quad ,$$

a noise-like signal

$$\sqrt{2}\left[n_1(t) \cos \omega_c t - n_2(t) \sin \omega_c t\right]$$

due to scattering, and continuous wave interference

$$\sqrt{2}\, B \sin\left[\omega_c t + \theta_2(t)\right] \quad .$$

Here ω_c represents the carrier radian frequency, $\theta_1(t)$ the phase of the desired signal, A^2 the power of the received signal, $\theta_2(t)$ the instantaneous phase of the continuous wave interference relative to the carrier radian frequency, and B^2 the power of the continuous wave interference. In addition, we assume $I_1(t)$, $I_2(t)$, $n_1(t)$ and $n_2(t)$

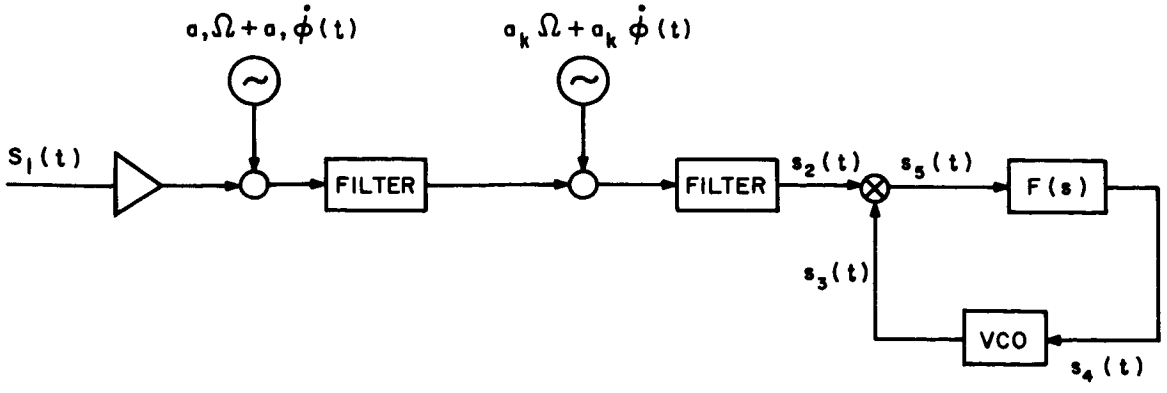

Figure 6-50. Typical Phase-Lock Receiving System

to be independent, zero-mean, stationary, gaussian random processes. In particular, $I_1(t)$ and $I_2(t)$ each have a flat power density spectrum of magnitude N_1 watts/Hz for $|\omega| \leq \pi W$ and zero magnitude for all other radian frequencies ω. We assume that the bandwidth W_1 is much greater than the bandwidth of the combination of filter and VCO in the phase-lock loop. The processes $n_1(t)$ and $n_2(t)$ each have a flat power density spectrum of magnitude N_2 watts/Hz for $|\omega| \leq \pi W_2$ and zero for all other ω. However, W_2 may be comparable to the bandwidth of the combination of loop filter and VCO.

Oscillator Instabilities - The local reference frequencies are derived from a single master oscillator operating at a nominal radian frequency Ω. Due to thermal effects, there is a deviation of the master oscillator frequency about Ω. This deviation is represented by [6-54] a zero mean, stationary, gaussian, random process $\dot{\varphi}(t)$. The two sided power density spectrum of $\dot{\varphi}(t)$ is assumed to be of magnitude N_3 watts/Hz for $|\omega| \leq W_1$ and of zero magnitude [6-55] for all other radian frequencies ω. Letting a_i (i=1, ...k) be the multiplication factor applied to the master oscillator frequency to obtain the i-th local reference frequency, the latter can be represented by $a_i [\Omega + \dot{\varphi}(t)]$. Setting $a = \sum_{i-1}^{k} a_i$ and assuming that $\omega_o = \omega_c - a\Omega$, the input $s_2(t)$ to the phase-lock loop is:

$$
\begin{aligned}
s_2(t) = & \sqrt{2}\ A \sin\left[\omega_o t + \theta_1(t) - a\varphi(t)\right] \\
& + \sqrt{2}\left\{n_1(t)\cos\left[\omega_o t - a\varphi(t)\right] - n_2(t)\sin\left[\omega_o t - a\varphi(t)\right]\right\} \\
& + \sqrt{2}\left\{I_1(t)\cos\left[\omega_o t - a\varphi(t)\right] - I_2(t)\sin\left[\omega_o t - a\varphi(t)\right]\right\} \\
& + \sqrt{2}\ B \sin\left[\omega_o t + \theta_2(t) - a\varphi(t)\right]
\end{aligned}
$$

This is analogous to the representation of oscillator instabilities used by Develet in reference [6-54].

Since W_1 is large compared to the bandwidth of the combination of loop filter and VCO, this is tantamount to the assumption that the power density spectrum of $\dot{\varphi}(t)$ is white; $1/N_3$ corresponds to the coherence time of the master oscillator [6-54, 6-55]. Typical coherence times are 36 seconds for a K band reflex klystron and 10^{14} seconds for a low frequency precision oscillator using a very excellent quartz crystal [6-55].

The VCO output $s_3(t)$ can be represented in the form

$$s_3(t) = \sqrt{2}\ K_1 \cos\left[\omega_o t + \theta_3(t) + \varphi_o(t)\right]$$

where K_1 is a constant of proportionality, $\dot{\varphi}_o(t)$ represents the frequency instability of the VCO due to thermal effects, and $\dot{\theta}_3(t)$ is proportional to the voltage applied to the VCO, i.e.,

$$\dot{\theta}_3(t) = K_2\, s_4(t)$$

where $s_4(t)$ is the output of the loop filter. $\dot{\varphi}_o(t)$ is here assumed to be a zero mean, stationary, gaussian, random process having a flat power density spectrum of magnitude N_4 watts/hertz for $|\omega| \leq \pi W_1$ and zero magnitude for all other radian frequencies ω.

Model of Phase-Lock Loop (Figure 6-54) - Neglecting terms in $2\omega_o$ which are suppressed by the combination of loop filter and VCO, the output of the loop multiplier is

$$s_5(t) = K_1 \left\{ A \sin\left[\theta_1(t) - a\,\varphi(t) - \theta_3(t) - \varphi_o(t)\right] + B \sin\left[\theta_2(t) - a\,\varphi(t) - \theta_3(t) - \varphi_o(t)\right] \right\} + n_3(t) + I_3(t)$$

where

$$n_3(t) = n_1(t) \cos\left[a\,\varphi(t) + \theta_3(t) + \varphi_o(t)\right] + n_2(t) \sin\left[a\,\varphi(t) + \theta_3(t) - \varphi_o(t)\right]$$

$$I_3(t) = I_1(t) \cos\left[a\,\varphi(t) + \theta_3(t) + \varphi_o(t)\right] + I_2(t) \sin\left[a\,\varphi(t) + \theta_3(t) + \varphi_o(t)\right]$$

Thus, the phase-lock loop can be represented by the block diagram of Figure 6-51 in which K represents the loop gain AK_1K_2.

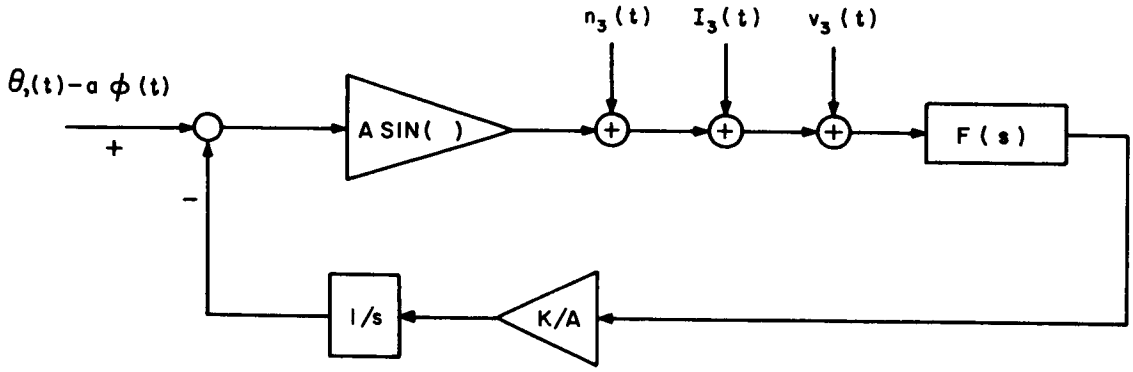

Figure 6-51. Model of Phase-Lock Loop

The most commonly used phase-lock loop is the so-called second order loop. The order of a loop is determined by the transfer function F(s). In the case of a second order loop

$$F(s) = \frac{s + \tau}{s}$$

This transfer function can be realized by the filter of Figure 6-52 when $R_1 >> R_2$ (See reference 6-56, p. 21.) In particular $\tau = (R_2 C)^{-1}$.

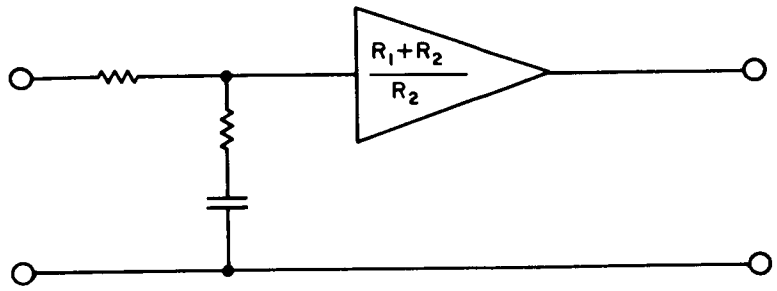

Figure 6-52. Filter for Second Order Loop

Modified Model of Phase-Lock Loop - Since the bandwidth of the combination of filter and VCO is much less than the bandwidth of the thermal noise, $I_3(t)$ in Figure 6-51 can be replaced by a stationary, zero mean, gaussian random process I(t) having the same power density spectrum as either $I_1(t)$ or $I_2(t)$. In addition, with a view to obtaining an upper bound on the deleterious effect of fading, we replace $n_3(t)$ by a stationary, zero mean, gaussian random process having a power density spectrum which is twice the spectrum of either $n_1(t)$ or $n_2(t)$, namely,

$$n(t) = n_1(t) - n_2(t)$$

The reasoning behind this is that $| \sin [a\varphi(t) + \theta_2(t) + \varphi_0(t)] |$ and $| \cos [a\varphi(t) + \theta_3(t) + \varphi_0(t)] |$ cannot exceed 1. (Arguments of this type have been used by Viterbi (reference 6-56, p. 33) to obtain simplified models of a phase-lock loop subjected to undesired modulation.) Similarly, we replace $\sin [\theta_2 - 2\varphi - \theta_3 - \varphi_0]$ by the unit step function u(t). With these modifications, the model of the phase-lock loop appears as shown in Figure 6-53.

Linear Model of Phase-Lock Loop - Under the assumption that the angle $\theta_1(t) - a\varphi(t) - \theta_3(t) - \varphi_0(t)$ is small, $\sin [\theta_1 - a\varphi - \theta_3 - \varphi_0] \approx \theta_1(t) - a\varphi(t) - \theta_3(t) - \varphi_0(t)$, and the model of Figure 5.4-6 can be linearized as shown in Figure 6-54. Hereafter, we shall restrict ourselves to the linear model of Figure 6-54 and the case in which F(s) has the form

$$F(s) = \frac{s + \tau}{s}$$

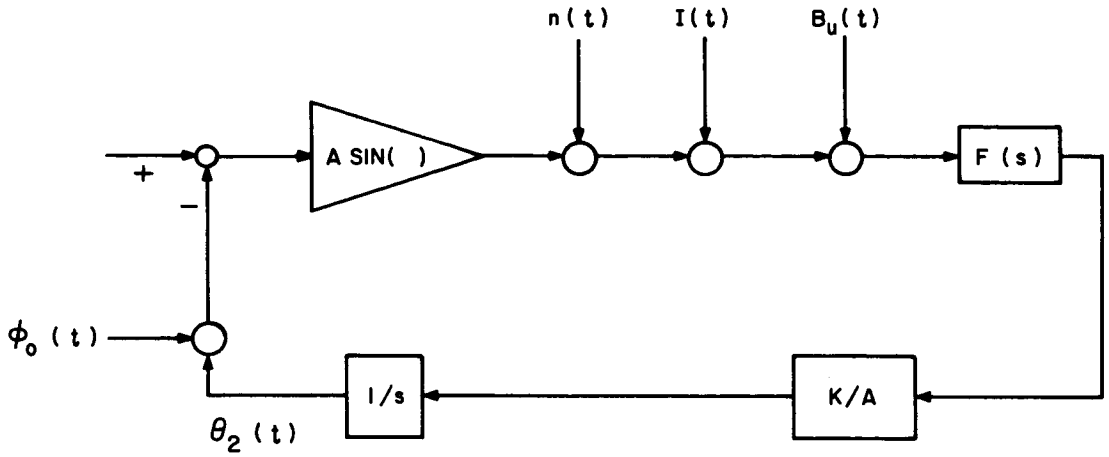

Figure 6-53. Modified Model of Phase-Lock Loop

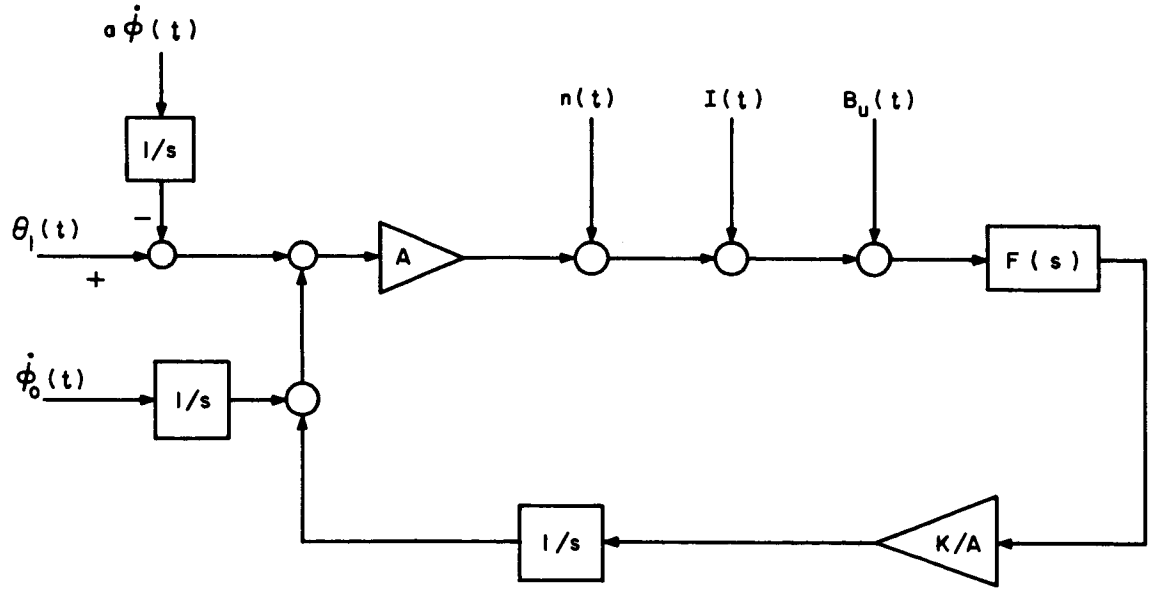

Figure 6-54. Linear Model of Phase-Lock Loop

Acceleration and Velocity Errors - Suppose that starting at time t = 0, the receiver experiences a constant acceleration in a radial direction either away from or toward the satellite. In other words, starting at t = 0, the radial velocity of the receiver relative to the satellite is of the form Rt + v where R and v are constants. Then the change in frequency due to the Doppler effect is

$$\theta_1(t) = \frac{\omega_c}{C}(Rt + v)$$

where C is the velocity of light and, as before, ω_c represents the carrier radian frequency transmitted from the satellite. The corresponding LaPlace transform of $\theta_1(t)$ is $\omega_c (R/S_3 + v/s^2)/C$. Hence, even in the absence of thermal noise, fading, oscillator instabilities, and continuous wave interference, the phase-lock loop will experience an error in the steady state of magnitude $\omega_c R/CK\tau$.

Here $S^2 (S^2 + K_s + K\tau)^{-1}$ represents the ratio of the transform of $\theta_1(t) - \theta_3(t)$ to the transform of $\theta_1(t)$, and we have applied the Final Value Theorem to obtain the steady state error, $\lim_{t\to\infty} [\theta_1(t) - \theta_3(t)]$.

Error due to Local Oscillator Instabilities - The ratio of the transform of $\theta_1 - a\varphi - \theta_3 - \varphi_0$ to the transform of $\theta_1 - a\varphi - \varphi_0$ is $S^2 (S^2 + KS + K\tau)^{-1}$. In other words, the oscillator instabilities $a\varphi$ and φ_0 cause an error in addition to the error (e.g., the acceleration error) caused by the form of the input phase θ_1. Referring to Figure 6-54, it is easy to see that the former error can be represented as a zero mean, stationary, gaussian random process with power density spectrum of magnitude

$$\frac{aN_3 + N_4}{2\pi} \left| \frac{j\omega}{(j\omega)^2 + Kj\omega + K\tau} \right|^2$$

for $|\omega| \leq \pi W_1$ and magnitude 0 elsewhere. Since the bandwidth of the combination of VCO and loop filter is much less than W_1, the variance of this process is approximately

$$\frac{aN_3 + N_4}{2\pi} \int_0^\infty \left| \frac{j\omega}{(j\omega)^2 + Kj\omega + K\tau} \right|^2 d\omega$$

Error due to Thermal Noise, Fading, and Continuous Wave Interference - Referring to Figure 6-54, the ratio of the transform of $-\theta_3$ to the transform of any one of I(t), n(t), and Bu(t) is $-(KS + K\tau) \div A(S^2 + KS + K\tau)$. From this, the contribution of the thermal noise, fading, and continuous wave interference to the overall error can be

determined. In particular, the errors caused by the thermal noise and fading are zero mean gaussian processes with density specutrums $S_1(\omega)$ and $S_2(\omega)$, respectively where

$$S_1(\omega) = \frac{N_1}{2\pi A^2} \left| \frac{Kj\omega + K\tau}{(j\omega)^2 + Kj\omega + K\tau} \right|^2 \quad ; \quad |\omega| \leq \pi W_1$$

$$= 0 \qquad \text{otherwise}$$

and

$$S_2(\omega) = \frac{N_2}{\pi A^2} \left| \frac{kj\omega + K\tau}{(j\omega)^2 + Kj\omega + K\tau} \right|^2 \quad ; \quad |\omega| \leq \pi W_2$$

$$= 0 \qquad \text{otherwise}$$

Thus, the variance of the error process due to fading is

$$\int_0^{W_2} S_2(\omega)\, d\omega$$

Since, W_1 is assumed to be much greater than the bandwidth of the combination of loop filter and VCO, the variance of the error process due to thermal noise is approximately the product of N_1/A^2 and the so-called loop noise bandwidth

$$\frac{1}{2\pi}\int_0^{\infty} \left| \frac{Kj\omega + K\tau}{(j\omega)^2 + Kj\omega + K\tau} \right|^2 d\omega = \frac{K + \tau}{4}$$

Finally, using the Final Value Theorem for LaPlace transforms, the steady state error due to the continuous wave interference is

$$\lim_{S \to o} \frac{S}{A} \left| \frac{KS + K\tau}{S^2 + KS + K\tau} \right| \frac{B}{S} = -\frac{B}{A}$$

6.4.2.2 RECEIVER PERFORMANCE ANALYSIS

The IF output signal and noise is:

$$y(t) \approx y_D(t) + n_d(t) \tag{1}$$

where

$$y_D(t) = A(t) \cos\left[(\omega_c + \Delta\omega)(t - \tau - \Delta) + \theta(t - \tau - \Delta) + \varphi_o + \varphi \right] \tag{2}$$

and where $\Delta\omega$ and φ represent unknown carrier frequency and phase.

As shown in Figure 6-2c, the IF signal and noise is passed through a carrier narrow-band filter which rejects the FM Carrier sidebands. The width of this filter is determined by the maximum expected frequency uncertainty. This width is assumed to be small enough so that no FM signal sideband appear at the filter output (Filter bandwidth less than twice the lowest tone frequency sideband) as discussed in Section 6.2.3. The purpose of the phase-locked loop is to extract a signal of frequency $f_c + \Delta f$ from the carrier narrow band filter output signal and noise for use in IF output carrier demodulation. If carrier side-bands were present, there would be a possibility of locking-in on one of these sidebands. This would result in a loss of signal at the tone-filter output.

Assuming loop-filter output signal-to-noise ratio greater than 10 dB, the phase-locked loop (PLL) voltage controlled oscillator (VCO) output will be of the form

$$r(t) = \sin\left[(\omega_c + \Delta\omega)\, t + \Delta\theta(t) + \theta_o\right] \tag{3}$$

where

$$\theta_o = \varphi + \varphi - (\omega_c + \Delta\omega)(\tau + \Delta) \tag{4}$$

and where $\Delta\theta(t)$ represents phase jitter which is approximately a Gaussian random process with zero mean value and variance

$$\sigma^2_{\Delta_\theta} = \frac{1}{2\rho_L} \quad ; \quad \rho_L = \frac{W_{IF}}{B_L}\left(\frac{C}{N}\right)_{IF} \tag{5}$$

Referring again to Figure 6-2c, the VCO output and the IF output are processed in a product detector with low-frequency signal output

$$\begin{aligned} z(t) &= 2\,LF\left\{ y_D(t) \sin\left[(\omega_c + \Delta\omega)\, t + \Delta\theta(t) + \theta_o\right]\right\} \\ &= A(t) \sin\left\{\Delta\theta(t) - \theta(t - \tau - \Delta)\right\} \end{aligned} \tag{6}$$

The difference from the homodyne detector signal output arises from the phase-jitter component $\Delta\theta(t)$.

Writing z(t) in terms of the first harmonics of its tone frequency components with $\alpha_j = 0$, and ignoring all other components,

$$\begin{aligned} z(t) &= A\left[\sin\Delta\theta\cos\theta(t-\tau-\Delta) - \cos\Delta\theta\sin\theta(t-\tau-\Delta)\right] \\ &= z_1(t) + z_2(t) \end{aligned} \tag{7}$$

where

$$z_j(t) = 2A\cos(\Delta\theta)\, J_o(m_k) J_1(m_j) \sin\left[\omega_j(t-\tau-\Delta)\right] \tag{8}$$

since in the neighborhood of the tone frequencies,

$$\left\{ \begin{array}{l} \sin\theta = -2 \sum_{j+k=1}^{2} J_o(m_k) J_1(m_j) \sin \omega_j (t-\tau-\Delta) \\ \cos\theta = 0 \end{array} \right. \tag{9}$$

envelope modulation. The $\Delta\theta$ term is due to the PLL phase jitter. As in Appendix 6A, this assumes unity gain tone filters, and slowly-varying envelope and time-delay.

The corresponding noise low-frequency component will be:

$$n(t) = 2\,LF \left\{ n_d(t) \sin \left[(\omega_c + \Delta\omega)\, t + \Delta\theta(t) + \theta_o \right] \right\} \tag{10}$$

Expanding n(t) as in equations (9) and (10) on pages 6A-2 and 6A-3

$$\begin{aligned} n(t) &= I_{cd}(t) \sin \left[\Delta\omega t + \Delta\theta(t) + \theta_o \right] \\ &\quad - I_{sd}(t) \cos \left[\Delta\omega t + \Delta\theta(t) + \theta_o \right] \end{aligned} \tag{11}$$

where θ_o is the same as in equation (11) on page 6A-3. Therefore, the only difference from equation (10) on page 6A-3 is the phase jitter term. To calculate the auto-correlation function of (11) exactly, one would have to consider the possible statistical dependence of the phase jitter and the noise in phase and quadrature components since the phase jitter is caused by this noise. However this statistical dependence is not easily accounted for.

Assuming the phase jitter and the input noise are uncorrelated, the auto-correlation function of n(t) can be written:

$$\begin{aligned} \psi_n(\tau) &= \langle n(t)\, n(t+\tau) \rangle \\ &= 2\, \psi_{I_{cd}}(\tau)\, \varphi_c(\tau) \end{aligned} \tag{12}$$

where

$$\begin{aligned} \psi_c(\tau) &= \langle \cos \left[\Delta\omega t + \Delta\theta(t) + \theta_o \right] \cos \left[\Delta\omega (t+\tau) + \Delta\theta(t+\tau) + \theta_o \right] \rangle \\ &= \langle \sin \left[\Delta\omega t + \Delta\theta(t) + \theta_o \right] \sin \left[\Delta\omega (t+\tau) + \Delta\theta(t+\tau) + \theta_o \right] \rangle \end{aligned}$$

and

$$\begin{aligned} \psi_{I_{cd}}(\tau) &= \langle I_{cd}(t)\, I_{cd}(t+\tau) \rangle \\ &= \langle I_{sd}(t)\, I_{sd}(t+\tau) \rangle \end{aligned} \tag{13}$$

Expanding the cosine product,

$$\psi_c(\tau) = \frac{1}{2} < \cos \left\{ \Delta\omega\tau + \Delta\theta(t) - \Delta\theta(t+\tau) \right\} > \tag{14}$$

The sum frequency term will go to zero if we assume θ_o is a uniformly distributed random phase angle.

Expanding the cosine in (4),

$$\psi_c(\tau) = \frac{1}{2} \left\{ \cos(\Delta\omega\tau) < \cos[\Delta\theta(t) - \Delta\theta(t+\tau)] > \right. \\ \left. - \sin(\Delta\omega\tau) < \sin[\Delta\theta(t) - \Delta\theta(t+\tau)] > \right\} \tag{15}$$

The ensemble averages can be evaluated by applying the known expression for the characteristic function of a normal distribution with zero mean and variance σ^2:

$$< e^{juX} > = e^{-u^2\sigma^2/2} \tag{16}$$

Therefore

$$\begin{cases} < \cos X > e^{-\sigma^2/2} \\ < \sin X > o \end{cases} \tag{17}$$

Letting

$$X = \Delta\theta(t) - \Delta\theta(t+\tau) \tag{18}$$

the variance is

$$\begin{aligned} \sigma^2 &= < [\Delta\theta(t) - \Delta\theta(t+\tau)]^2 > \\ &= 2[<(\Delta\theta)^2> - <\Delta\theta(t)\,\Delta\theta(t+\tau)>] \\ &= 2\sigma^2_{\Delta\theta}[1 - \rho_{\Delta\theta}(\tau)] \end{aligned} \tag{19}$$

For large signal-to-noise ratios,

$$\sigma^2_{\Delta\theta} = \frac{1}{2\rho_L} \tag{20}$$

where ρ_L is the loop filter output signal-to-noise ratio. The function $\rho_{\Delta\theta}(\tau)$ is the normalized auto-correlation function of $\Delta\theta$. This function is determined by the transfer function of the loop filter.

Applying (20) to (19),

$$\sigma^2 = \frac{1}{2\rho_L}[1 - \rho_{\Delta\theta}(\tau)] \tag{21}$$

Applying (21) and (17) to (15),

$$\psi_c(\tau) = \frac{1}{2}\cos(\Delta\omega\tau)\ \exp\left\{-\frac{1}{2\rho_L}\left[1-\rho_{\Delta\theta}(\tau)\right]\right\} \tag{22}$$

For large ρ_L,

$$\psi_c(\tau) = \frac{1}{2}\cos(\Delta\omega\tau)\left\{1-\frac{1}{2\rho_L}\left[1-\rho_{\Delta\theta}(\tau)\right]\right\} \tag{23}$$

Applying (23) to (22), the desired noise auto-correlation function is:

$$\psi_n(\tau) = \psi_{I_{cd}}(\tau)\cos(\Delta\omega\tau)\left[\left(1-\frac{1}{2\rho_L}\right)+\frac{\rho_{\Delta\theta}(\tau)}{2\rho_L}\right] \tag{24}$$

For large loop filter output signal-to-noise ratios, it is evident that (24) reduces to the function derived in C11 for the homodyne detector. The second term involves the phase jitter auto-correlation function. The normalized power spectrum of $\Delta\theta$ is:

$$S_{\Delta\theta}(f) = \frac{|H_L(f)|^2}{\int_{-\infty}^{\infty}|H_L(f)|^2\,df} \tag{25}$$

where $H_L(f)$ is the transfer function of the loop filter. The power spectrum corresponding to the product of the normalized correlation function by the cosine of $\Delta\omega\tau$ is:

$$G_c(f) = \frac{1}{2}\left[S_{\Delta\theta}(f-\Delta f) + S_{\Delta\theta}(f+\Delta f)\right] \tag{26}$$

This can be seen by taking the Fourier cosine transform of the product, expanding the product of cosine functions in the integrand, and then applying the Fourier cosine transform relation between the power spectrum and the auto-correlation function.

The power spectrum corresponding to

$$g(\tau) = \psi_{I_{cd}}(\tau)\,\rho_{\Delta\theta}(\tau)\cos(\Delta\omega\tau) \tag{27}$$

is therefore

$$G_g(f) = \int_{-\infty}^{\infty} G_{I_{cd}}(f')\,G_c(f-f')\,df' \tag{28}$$

From the assumtion that I_{cd} has a rectangular power spectrum,

$$G_g(f) = 2N_o \int_{\frac{-W_{IF}}{2}}^{\frac{W_{IF}}{2}} G_c(f-f')\ df' \tag{29}$$

Making the change of variable $u - f - f'$,

$$G_g(f) = 2N_o \int_{f-\frac{W_{IF}}{2}}^{f+\frac{W_{IF}}{2}} G_c(u)\ du \tag{30}$$

The spectral density at the tone frequency f_j is therefore:

$$G_g(f_j) = N_o \int_{f_j-\frac{W_{IF}}{2}}^{f_j+\frac{W_{IF}}{2}} [S_{\Delta\theta}(f-\Delta f) + S_{\Delta\theta}(f+\Delta f)]\ df$$

$$= N_o \int_{f_j-\frac{W_{IF}}{2}-\Delta f}^{f_j+\frac{W_{IF}}{2}-\Delta f} S_{\Delta\theta}(u)\ du + \int_{f_j-\frac{W_{IF}}{2}+\Delta f}^{f_j+\frac{W_{IF}}{2}+\Delta f} S_{\Delta\theta}(u)\ du \tag{31}$$

Assuming $W_{IF}/2 - f_j - \Delta f$ is much greater than the loop filter bandwidth,

$$G_g(f_j) \approx 2N_o \int_{-\infty}^{\infty} S_{\Delta\theta}(f)\ df = 2N_o \tag{32}$$

In other words, the detailed shape of a sufficiently narrow loop filter is of no consequence.

It follows that the noise output power for the tone filter will be 4 $N_o W_{oj}$, which is the same as in the homodyne detector case. The analysis has shown that the error is of the order of the reciprocal of the square of the loop-filter output signal-to-noise ratio.

Calculating the tone filter output signal power from (8), and applying (17),

$$S_j = A^2 J_o^{\,2}(M_k)\, J_1^{\,2}(M_j)\left[1+e^{-1/\rho_L}\right] \tag{33}$$

It follows that the tone filter output signal-to-noise ratio is:

$$\left(\frac{S}{N}\right)_{oj} = \frac{A^2 J_o^{\,2}(M_k)\, J_1^{\,2}(M_j)\left[1+e^{-1/\rho_L}\right]}{4 N_o W_{oj}} \tag{34}$$

The IF output carrier-to-noise ratio is:

$$\left(\frac{C}{N}\right)_{IF} = \frac{A^2(t)}{4 N_o W_{IF}} \tag{35}$$

Therefore,

$$\left(\frac{S}{N}\right)_{oj} = J_o^{\,2}(M_k)\, J_1^{\,2}(M_j)\left(\frac{W_{IF}}{W_{oj}}\right)\left[1+e^{-1/\rho_L}\right]\left(\frac{C}{N}\right)_{IF} \tag{36}$$

This agrees with equation (15) on Page 6A-4 for sufficiently large loop filter output signal-to-noise ratio.

Appendix 6C contains an analysis of this case C_{13} with a quadrature phase detector at the tone filter output. It is shown that for large tone filter output signal-to-noise ratios the mean phase error is approximately zero, and the variance approximately equal to the reciprocal of twice the tone filter output S/N as in equation (25) (on Page 6A-6.

Equation (34) of Page 6C-7 gives an expression for the phase error in a single measurement. For d_j equal to zero, this expression reduces to:

$$\delta_j = \arctan\left\{\frac{I_c}{\cos\Delta\theta\sqrt{2\left(\frac{S}{N}\right)_{oj}} + I_s}\right\} \tag{37}$$

As the loop filter output signal-to-noise ratio increases, cos $\Delta\theta$ will be close to unity with high probability. Therefore (37) approaches equation (47) on Page 6A-13.

6.4.3 DIFFUSE MULTIPATH EFFECTS WITH PHASE-LOCK LOOP CARRIER EXTRACTION (C_{33} and C_{31})

This analysis refers specifically to case C_{33}. However when the VCO phase jitter goes to zero, this case reduces to C_{31}, on the assumption of carrier synchronization.

Assuming a complex transmitted signal corresponding to equation (1), Section 6.3.1, the transmitted signal can be written:

$$x(t) = \sqrt{P_T} \exp \left\{ j \left[\omega_c t + \theta(t) + \varphi_o \right] \right\} \tag{1}$$

Assuming a complex channel unit impulse response function corresponding to (11) of Section 6.3.1, the channel unit impulse response function can be written:

$$\begin{aligned} A(\lambda, t) &= a_D \exp\left[j \left(\Delta \omega t + \varphi \right) \right] \delta(\lambda - \tau - \Delta) \\ &+ \sum_{i=1}^{n} a_i \exp\left[j \left(\Delta \omega_i t + \varphi_i \right) \right] \delta(\lambda - \tau - \Delta - \Delta_i) \end{aligned} \tag{2}$$

The corresponding real received signal is:

$$\begin{aligned} z_{IF}(t) &= R_e \left[\int_{-\infty}^{\infty} A(\lambda, t)\, x(t - \lambda)\, d\lambda \right] \\ &= z_D(t) + z_r(t) \end{aligned} \tag{3}$$

where

$$z_D(t) = A_D \cos \left[(\omega_c + \pm \omega) t + \theta(t - \tau - \Delta) + \theta_o \right] \tag{4}$$

and

$$z_r(t) = \sum_{i=1}^{n} a_i \cos \left[(\omega_c + \Delta\omega_i) t + \theta(t - \tau - \Delta - \Delta_i) + \theta_i \right] \tag{5}$$

where

$$\begin{cases} \theta_o = \varphi + \varphi_o - \omega_c (\tau + \Delta) \\ \theta_i = \varphi_i + \varphi_o - \omega_c (\tau + \Delta - \Delta_i) \end{cases} \tag{6}$$

Writing

$$\Delta\omega_i = \Delta\omega + \delta\omega_i \tag{7}$$

$$z_r(t) = \sum_{i=1}^{n} a_i \cos \left[(\omega_c + \Delta\omega) t + \theta(t - \tau - \Delta - \Delta_i) + \delta\omega_i t + \theta_i \right] \tag{8}$$

The direct component can be written:

$$z_D(t) = I_{CD}(t) \cos [(\omega_c + \Delta\omega) t] - I_{SD}(t) \sin [(\omega_c + \Delta\omega) t] \quad (9)$$

where

$$\begin{cases} I_{CD}(t) = A_D \cos [\theta (t - \tau - \Delta) + \theta_o] \\ I_{SD}(t) = A_D \sin [\theta (t - \tau - \Delta) + \theta_o] \end{cases} \quad (10)$$

Similarly, the random component can be written

$$z_r(t) = I_{cr}(t) \cos [(\omega_c + \Delta\omega) t] - I_{sr}(t) \sin [(\omega_c + \Delta\omega) t] \quad (11)$$

where

$$\begin{cases} I_{cr}(t) = \sum_i a_i \cos [\theta (t - \tau - \Delta - \Delta_i) + \delta\omega_i t + \theta_i] \\ I_{sr}(t) = \sum_i a_i \sin [\theta (t - \tau - \Delta - \Delta_i) + \delta\omega_i t + \theta_i] \end{cases} \quad (12)$$

For the assumed two-tone modulation, it can be shown that:

$$\begin{aligned} \cos [\theta(t)] = & \left[J_o(m_1) + 2 \sum_{n_1=1}^{\infty} J_{2n_1}(m_1) \cos (2n_1 \omega_1 t + 2n_1 \alpha_1) \right] \\ & \times \left[J_o(m_2) + 2 \sum_{n_2=1}^{\infty} J_{2n_2}(m_2) \cos (2n_2 \omega_2 t + 2n_2 \alpha_2) \right] \\ & + \left[2 \sum_{n_1=0}^{\infty} J_{2n_1+1}(m_1) \sin \left\{ (2n_1 + 1) \omega_1 t + (2n_1 + 1) \alpha_1 \right\} \right] \\ & \times \left[2 \sum_{n_2=0}^{\infty} J_{2n_2+1}(m_2) \sin \left\{ (2n_2 + 1) \omega_2 t + (2n_2 + 1) \alpha_2 \right\} \right] \end{aligned} \quad (13.1)$$

$$\sin[\theta(t)] = \left\{ 2\sum_{n_1=0}^{\infty} J_{2n_1+1}(m_1) \sin[(2n_1+1)\omega_1 t + (2n_1+1)\alpha_1] \right\}$$

$$\times \left\{ J_o(m_2) + \sum_{n_2=1}^{\infty} J_{2n_2}(m_2) \cos[2n_2\omega_2 t + 2n_2\alpha_2] \right\}$$

$$+ \left\{ J_o(m_1) + 2\sum_{n_1=1}^{\infty} J_{2n_1}(m_1) \cos[2n_1\omega_1 t + 2n_1\alpha_1] \right\}$$

$$\times \left\{ 2\sum_{n_2=0}^{\infty} J_{2n_2+1}(m_2) \sin[(2n_2+1)\omega_2 t + (2n_2+1)\alpha_2] \right\} \quad (13.2)$$

Expanding the cosine and sine functions in (12),

$$I_{cr}(t) = \sum_{i=1}^{n} a_i \left\{ \cos[\theta(t-\tau-\Delta-\Delta_i)] \cos(\delta\omega_i t + \theta_i) \right.$$
$$\left. - \sin[\theta(t-\tau-\Delta-\Delta_i)] \sin(\delta\omega_i t + \theta_i) \right\}$$

$$I_{sr}(t) = \sum_{i=1}^{n} a_i \left\{ \sin[\theta(t-\tau-\Delta-\Delta_i] \cos(\delta\omega_i t + \theta_i) \right.$$
$$\left. + \cos[\theta(t-\tau-\Delta-\Delta_i)] \sin(\delta\omega_i t + \theta_i) \right\} \quad (14)$$

The direct signal z_D in (4) can also be expanded in this fashion. Therefore

$$I_{cD}(t) = A_D \left\{ \cos\theta_o \cos[\theta(t-\tau-\Delta)] - \sin\theta_o \sin[\theta(t-\tau-\Delta)] \right\}$$

$$I_{sD}(t) = A_D \left\{ \sin\theta_o \cos[\theta(t-\tau-\Delta)] - \cos\theta_o \sin[\theta(t-\tau-\Delta)] \right\} \quad (15)$$

The purpose of all this is to determine the phase-lock loop (PLL) input direct signal and multipath signal, as well as later on determining the tone filter output signals. Since the carrier narrow-band filter at the PLL input rejects all side-bands, it follows from (13), that we can assume that

$$\cos[\theta(t)] = J_o(m_1) J_o(m_2) \; ; \; \sin[\theta(t)] = 0 \quad (16)$$

in determining the PLL inputs. From (15), we can write

$$\begin{cases} I_{cD_o}(t) = A_D \cos\theta_o \, J_o(m_1) \, J_o(m_2) \\ I_{sD_o}(t) = A_D \sin\theta_o \, J_o(m_1) \, J_o(m_2) \end{cases} \tag{17}$$

Applying this to (9), the direct signal at the PLL input is:

$$z_{D_o}(t) = A_D \, J_o(m_1) \, J_o(m_2) \cos\left[(\omega_c + \Delta\omega)\, t + \theta_o\right] \tag{18}$$

Applying this to (14), the inphase and quadrature components of the multipath signal at the PLL input is:

$$\begin{cases} I_{cr_o}(t) = J_o(m_1) \, J_o(m_2) \sum_{i=1}^{n} a_i \cos(\delta\omega_i t + \theta_i) \\ I_{sr_o}(t) = J_o(m_1) \, J_o(m_2) \sum_{i=1}^{n} a_i \sin(\delta\omega_i t + \theta_i) \end{cases} \tag{19}$$

Applying this to (11), the random signal component at the PLL input is:

$$z_{r_o}(t) = J_o(m_1) \, J_o(m_2) \sum_{i=1}^{n} a_i \cos\left[(\omega_c + \Delta\omega_i)\, t + \theta_i\right] \tag{20}$$

where $\Delta\omega_i$ is related to $\delta\omega_i$ and $\Delta\omega$ in (7).

On the assumption that a_i and θ_i are statistically independent identically distributed random amplitude and phase, and that n is large, it follows that z_{r_o} can be described by a Gaussian random process. Assuming θ_i to be uniformly distributed on the interval $(o, 2\pi)$, z_{r_o} will have zero mean. The variance of this random component is:

$$\sigma_{r_o}^2 = 1/2 \, J_o^2(m_1) \, J_o^2(m_2) \sum_{j=1}^{n} < a_j^2 > \tag{21}$$

Substituting for the Bessel function coefficients in (20) by applying (21), and then employing (7),

$$z_{r_o}(t) = \sum_{i=1}^{n} b_i \cos\left[(\omega_c + \Delta\omega)\, t + \delta\omega_i t + \theta_i\right] \tag{22}$$

where

$$b_i = \frac{\sqrt{2\ a_i}}{\left[\sum_j \langle a_j^2 \rangle\right]^{1/2}} \tag{23}$$

In general, the b_i and θ_i will be time variable. This time-variability, and the presence of the $\delta\omega_i$ results in a broadening of the bandwidth of the random function z_{r_o}. The power spectrum of z_{r_o} is the so-called fading spectrum. The bandwidth B_r of this power spectrum will be referred to as the "fading rate". The ratio

$$F_r = \frac{B_r}{W_o} \tag{24}$$

equals the fading bandwidth divided by a filter bandwidth W_o. Therefore F_r will be referred to as the "relative fading-rate". When F_r is much less than unity, we have the so-called slow-fading case. When F_r is greater than unity, we have the so-called "fast fading" case. The remaining situation will be referred to here as "intermediate" fading.

For large signal-to-random noise ratios, which is the usual case of interest in a precision navigation system, the multipath will be the dominant source of interference at the output of the phase-lock loop filter, or at the tone filter output. Therefore, for simplicity, the random noise will be ignored in the initial analysis. Later on, it will be included.

The total signal at the phase-lock loop input is:

$$z_o(t) = z_{D_o}(t) + z_{r_o}(t) \tag{25}$$

From the above,

$$z_o(t) = I_{co}(t)\cos[(\omega_c + \Delta\omega)t] - I_{so}(t)\sin[(\omega_c + \Delta\omega)t] \tag{26}$$

where

$$\begin{cases} I_{co}(t) = I_{cD_o}(t) + I_{cr_o}(t) \\ I_{so}(t) = I_{sD_o}(t) + I_{sr_o}(t) \end{cases} \tag{27}$$

From (17) and (22),

$$\begin{cases} I_{co}(t) = A_D \cos\theta_o\, J_o(m_1)\, J_o(m_2) + \sigma_{ro} \sum_i b_i \cos(\delta\omega_i t + \theta_i) \\ I_{so}(t) = A_D \sin\theta_o\, J_o(m_1)\, J_o(m_2) + \sigma_{ro} \sum_i b_i \sin(\delta\omega_i t + \theta_i) \end{cases} \tag{28}$$

Another key parameter is γ , the ratio of the amplitude of the direct signal component to the standard deviation of the random component. Applying (21),

$$\gamma = \frac{A_D J_o(m_1) J_o(m_2)}{\sigma_{ro}}$$

$$= \frac{A_D \sqrt{2}}{\left[\sum_j \langle a_j^2 \rangle\right]^{1/2}} \tag{29}$$

Applying this to (28),

$$\begin{cases} I_{co}(t) = \sigma_{r_o} [\gamma \cos\theta_o + \sum_i b_i \cos(\delta\omega_i t + \theta_i)] \\ I_{so}(t) = \sigma_{r_o} [\gamma \sin\theta_o + \sum_i b_i \sin(\delta\omega_i t + \theta_i)] \end{cases} \tag{30}$$

Applying (23) and the assumption that the θ_i are uniformly distributed random phases defined on (o, 2π), the variances and covariances of the random components of (30) are:

$$\begin{cases} \langle I_{cr_o}^2 \rangle = \langle I_{sr_o}^2 \rangle = \sigma_{r_o}^2 \\ \langle I_{cr_o} I_{sr_o} \rangle = 0 \end{cases} \tag{31}$$

Therefore,

$$\begin{cases} \langle I_{co}^2 \rangle = \sigma_{r_o}^2 [\gamma^2 \cos^2\theta_o + 1] \\ \langle I_{so}^2 \rangle = \sigma_{r_o}^2 [\gamma^2 \sin^2\theta_o + 1] \\ \langle I_{co} I_{so} \rangle = \frac{\gamma^2}{2} \sigma_{r_o}^2 \sin 2\theta_o \end{cases} \tag{32}$$

Applying (31) and (32) in calculating the mean-square-value of z_o in (26), and ignoring second harmonic terms,

$$P_o = \langle z_o^2 \rangle = \sigma_{r_o}^2 (1 + \frac{\gamma^2}{2}) \tag{33}$$

It follows that

$$\frac{\gamma^2}{2} = \frac{\text{average power of direct component}}{\text{average power of random component}} \tag{34}$$

Since P_o will be determined from the link calculations for a given receiving antenna,

$$\sigma_{r_o}^2 = \frac{P_o}{1 + \gamma^2/2} \tag{35}$$

On the assumption that random noise is negligible, $\gamma^2/2$ represents the loop filter output signal-to-noise ratio.

The analysis will now be divided into the three categories described in (24):

(a) Slow Fading

(b) Fast Fading

(c) Intermediate Fading

6.4.3.1 SLOW FADING

In this case, the frequency offsets $\delta\omega_i$ must be negligible, whereas b_i and θ_i must be very slowly variable. Let

$$\begin{cases} I_{cF} = \sum_i b_i \cos\theta_i \\ I_{sF} = \sum_i b_i \sin\theta_i \end{cases} \tag{36}$$

These quantities will be independent normal random variables with zero mean and variance

$$\langle I_{cF}^2 \rangle = \langle I_{sF}^2 \rangle = 1; \quad (\langle I_{cF} I_{sF} \rangle = 0) \tag{37}$$

This can be seen by applying (23) in calculating the mean-square-values of the b_i.

$$\begin{cases} \langle I_{cF}^2 \rangle = \sum_i \sum_j \langle b_i b_j \rangle \langle \cos\theta_i \cos\theta_j \rangle \\ \langle I_{sF}^2 \rangle = \sum_i \sum_j \langle b_i b_j \rangle \langle \sin\theta_i \sin\theta_j \rangle \\ \langle I_{cF} I_{sF} \rangle = \sum_i \sum_j \langle b_i b_j \rangle \langle \sin\theta_i \cos\theta_j \rangle \end{cases} \tag{38}$$

From the definition of the θ_i in (6),

$$\begin{cases} \theta_i = b + \omega_c \Delta_i + \varphi_i \\ b = \varphi_o - \omega_c (\tau + \Delta) \end{cases} \tag{39}$$

φ_o is an arbitrary phase shift on the transmitted carrier. φ_i is a carrier phase-shift for the i-th multipath component. $\omega_c (\tau + \Delta)$ is a phase shift due to the signal transmission delay τ, and the aggregate of equipment delays occurring at the satellite relay and in the receiver. The phase shifts φ_i also include any atmospheric refraction effects. In general, the phase shifts will be statistically dependent. However, if it is assumed that b is a uniformly distributed random phase angle defined on the interval $(0,2\pi)$,

$$\langle \cos \theta_i \cos \theta_j \rangle = \langle \sin \theta_i \sin \theta_j \rangle$$

$$= 1/2 \langle \cos [\omega_c (\Delta_i - \Delta_j) + (\varphi_i - \varphi_j)] \rangle \tag{40}$$

$$\langle \sin \theta_i \cos \theta_j \rangle = 1/2 \langle \sin [\omega_c (\Delta_i - \Delta_j) + (\varphi_i - \varphi_j)] \rangle \tag{41}$$

If it is assumed that the phase differences $\varphi_i - \varphi_j$ are uniformly distributed on $(0, 2\pi)$, it follows that

$$\langle \cos \theta_i \cos \theta_j \rangle = \langle \sin \theta_i \sin \theta_j \rangle$$

$$= 1/2 \, \delta_{ij} \tag{42}$$

$$\langle \sin \theta_i \cos \theta_j \rangle = 0 \tag{43}$$

where δ_{ij} is a Kronecker delta function. Applying (42) and (43) to (38) and applying (23) gives the results stated in (37).

On the assumption of a linear PLL model, the VCO output will be of the form:

$$r(t) = \sin [(\omega_c + \Delta\omega) t + \beta] \tag{44}$$

where β represents the phase angle of the signal plus noise. From (30) and (36),

$$\beta = \text{Arctan} \left\{ \frac{\gamma \sin \theta_o + I_{sF}}{\gamma \cos \theta_o + I_{cF}} \right\} \tag{45}$$

where θ_o is defined in equation (6). The next step is to determine the demodulator output components in the vicinity of the tone frequencies. From (3) and (44), the low-frequency components of the product demodulator output are:

$$y(t) = 2LF \left\{ r(t) \, z_{IF}(t) \right\}$$

$$= y_D(t) + y_r(t) \tag{46}$$

where

$$y_D(t) = 2LF\left\{r(t)\, z_D(t)\right\} \tag{47}$$

$$y_r(t) = 2LF\left\{r(t)\, z_r(t)\right\} \tag{48}$$

From (4) and (44),

$$y_D(t) = 2LF\left\{\sin\left[(\omega_c + \Delta\omega)t + \beta\right] A_D \cos\left[(\omega_c + \Delta\omega)t + \theta(t - \tau - \Delta) + \theta_o\right]\right\}$$

$$= A_D \sin\left[\theta(t - \tau - \Delta) + \theta_o - \beta\right. \tag{49}$$

From (5), (7) and (44),

$$y_r(t) = 2LF\left\{\sin\left[\omega_c + \Delta\omega)t + \beta\right] \sum_i a_i \cos\left[(\omega_c + \Delta\omega_i)t\right.\right.$$

$$\left.\left. + \theta(t - \tau - \Delta - \Delta_i) + \theta_i\right]\right\}$$

$$= \sum_i a_i \sin\left[\delta\omega_i t + \theta(t - \tau - \Delta - \Delta_i) + \theta_i - \beta\right] \tag{50}$$

The next step is to pick out the tone frequency components. This can be determined from equations (13). For tone frequency ω_j,

$$\begin{cases}\cos[\theta(t)] = 0 \\ \sin[\theta(t)] = 2J_o(m_k)\, J_1(m_j) \sin(\omega_j t + \alpha_j);\ j \neq k = 1, 2\end{cases} \tag{51}$$

Applying (51) to (49), and letting α_j equal zero,

$$y_{Dj}(t) = 2A_D \cos(\beta - \theta_o)\, J_o(m_k)\, J_1(m_j) \sin\left[\omega_j(t - \tau - \Delta)\right]\ j \neq k = 1,2 \tag{52}$$

Applying (51) to (50), when the fading is not fast,

$$y_{rj}(t) = 2J_o(m_k)\, J_1(m_j) \sum_i a_i \cos\left[\beta - \theta_i - \delta\omega_i t\right] \sin\left[\omega_j(t - \tau - \Delta - \Delta_i)\right] \tag{53}$$

The tone filter output signal plus interference will therefore be

$$y_j(t) = y_{Dj}(t) + y_{rj}(t) \tag{54}$$

For tone ω_1,

$$y_1(t) = 2J_o(m_2)\, J_1(m_1)\ \left\{A_D \cos(\beta - \theta_o) \sin\left[\omega_1(t - \tau - \Delta)\right]\right.$$

$$\left. + \sum_i a_i \cos\left[\beta - \theta_i - \delta\omega_i t\right] \sin\left[\omega_i(t - \tau - \Delta - \Delta_i\right]\right\} \tag{55}$$

Combining (23) and (29),

$$a_i = \frac{A_D}{\gamma} \; b_i \tag{56}$$

From (29),

$$\frac{A_D}{\gamma} = \frac{\sigma_{ro}}{J_o(m_1)\, J_o(m_2)} \tag{57}$$

Applying (56) and (57) to (55), and simplifying,

$$y_1(t) = \sigma_{ro} \frac{2J_1(m_1)}{J_o(m_1)} \left\{ \begin{array}{l} \gamma \cos(\beta - \theta_o) \sin[\omega_1 (t - \tau - \Delta)] \\ \\ + \sum_i b_i \cos(\beta - \theta_i - \delta\omega_i t) \sin[\omega_1 (t - \tau - \Delta - \Delta_i)] \end{array} \right\} \tag{58}$$

This expression is applicable for any fading rate. For slow fading, $\delta\omega_i$ equals zero, so that

$$y_1(t) = \sigma_{ro} \frac{2\, J_1(m_1)}{J_o(m_1)} \left\{ \begin{array}{l} \gamma \cos(\beta - \theta_o) \sin x \\ + \cos\beta \, [I_{cFc} \sin x - I_{cFs} \cos x] \\ + \sin\beta \, [I_{sFc} \sin x - I_{sFs} \cos x] \end{array} \right\} \tag{59}$$

where $x = \omega_1 (t - \tau - \Delta)$; $\varphi_{i1} = \omega_1 \Delta_i$

$$\left\{ \begin{array}{l} I_{sFs} = \sum_i b_i \sin\theta_i \sin\varphi_{i1} \\ I_{sFc} = \sum_i b_i \sin\theta_i \cos\varphi_{i1} \\ I_{cFc} = \sum_i b_i \cos\theta_i \cos\varphi_{i1} \\ I_{cFs} = \sum_i b_i \cos\theta_i \sin\varphi_{i1} \end{array} \right. \tag{60}$$

For sufficiently small $\omega_1 \Delta_i$, from (36),

$$I_{sFs} \approx 0 \qquad I_{cFc} \approx I_{cF}$$

$$I_{sFc} \approx I_{sF} \qquad I_{cFs} \approx 0$$

However, this will not generally be the case. Assuming that the ω_{i1} are statistically independent uniformly distributed random variables defined on the interval $(o, 2\pi)$, we can invoke the central limit theorem as before. Also, the various random variables in (60) have zero mean, variance equal to one half, and are mutually uncorrelated. Furthermore, these random variables are mutually uncorrelated with I_{cF} and I_{sF} in (36).

Writing $y_1(t)$ in terms of inphase and quadrature components about sin x and cos x,

$$y_1(t) = \sigma_{ro} \frac{2J_1(m_1)}{J_o(m_1)} \left\{ X_c \cos x + X_s \sin x \right\}$$

$$\begin{cases} X_c = -I_{cFs} \cos \beta - I_{sFs} \sin \beta \\ X_s = I_{sFc} \sin \beta + I_{cFc} \cos \beta + \gamma \cos(\beta - \theta_o) \\ \quad = (\gamma \sin \theta_o + I_{sFc}) \sin \beta + (\gamma \cos \theta_o + I_{cFc}) \cos \beta \end{cases} \tag{61}$$

The function y_1 can be written in the form

$$y_1 = E \sin(x + \delta) \tag{62}$$

where

$$\delta = \text{Arctan} \left(\frac{X_c}{X_s} \right) \tag{63}$$

represents the multipath phase error. From (45),

$$\begin{cases} \text{Sin } \beta = \dfrac{\gamma \sin \theta_o + I_{sF}}{[\gamma^2 + R_F^2 + 2\gamma R_F \cos(\omega_F - \theta_o)]^{1/2}} \\ \cos \beta = \dfrac{\gamma \cos \theta_o + I_{cF}}{[\gamma^2 + R_F^2 + 2\gamma R_F \cos(\omega_F - \theta_o)]^{1/2}} \end{cases} \tag{64}$$

where

$$\begin{cases} I_{cF} = R_F \cos \omega_F \\ I_{sF} = R_F \sin \omega_F \end{cases} \tag{65}$$

Applying (64) to (61) and (63),

$$\delta = \text{Arctan} \left\{ \frac{-I_{cFs}(\gamma \cos \theta_o + I_{cF}) - I_{sFs}(\gamma \sin \theta_o + I_{sF})}{(\gamma \sin \theta_o + I_{sFc})(\gamma \sin \theta_o + I_{sF}) + (\gamma \cos \theta_o + I_{cFc})(\gamma \cos \theta_o + I_{cF})} \right\} \tag{66}$$

For computational purposes it is convenient to write:

$$\delta = \text{Arctan}\left\{\frac{x_1 \cos\theta + x_2 \sin\theta + 1/\gamma\,(x_1y_1 + x_2y_2)}{\gamma + (y_2 + x_3)\sin\theta + (y_1 + x_4)\cos\theta + 1/\gamma(y_2x_3 + y_1x_4)}\right\} \qquad (67)$$

$$x_1 = -I_{cFs} \qquad x_3 = I_{sFc} \qquad y_1 = I_{cF} \qquad \theta = \theta_o$$

$$x_2 = -I_{sFs} \qquad x_4 = I_{cFc} \qquad y_2 = I_{sF}$$

where the x_i are mutually independent normal random variables with zero mean and variance equal to 1/2. The y_i are mutually independent normal random variables with zero mean and unit variance. The random variable θ is uniformly distributed on the interval $(o, 2\pi)$. Because of the complexity of the expression for the phase error in (66), the mean, standard deviation and distribution function of δ can most conveniently be determined by means of the "Monte Carlo" method, using a digital computer. The computer takes sets of random samples of the x_i, y_i and θ, and computes a value of the phase error δ for each set of samples. From these repeated sets of samples, the mean, standard deviation, and distribution function can be estimated for each value of the fading ratio γ.

As γ becomes large, the denominator of (67) approaches γ, whereas the numerator will be normally distributed with zero mean and variance equal to one-half. Therefore for large γ, the error will be approximately normally distributed with zero mean and variance equal to the reciprocal of twice the square of γ.

The slow-fading analysis will now be generalized to include the additive noise. From (26), the signal and noise at the phase-lock loop input is:

$$y_o(t) = z_o(t) + n_o(t)$$

where n(t) represents band limited white noise at the carrier narrow-band filter output. From (30) and (36), the inphase and quadrature components at the loop filter output will be:

$$I_{cyL} = \sigma_{ro}\left[\gamma\cos\theta_o + I_{cF}\right] + \sigma_L I_{cL}$$

$$I_{syL} = \sigma_{ro}\left[\gamma\sin\theta_o + I_{sF}\right] + \sigma_L I_{sL} \qquad (68)$$

where I_{cL} and I_{sL} are mutually independent zero mean, unit variance normally distributed random variables. The quantity σ_L^2 is the variance of the loop filter output noise. Therefore

$$\sigma_L^2 = 2N_oB_L \qquad (69)$$

where N_o is the white noise spectral density, and B_L is the loop filter bandwidth. The loop filter output is:

$$y_L(t) = I_{cyL}\cos\left[(\omega_c + \Delta\omega)\,t\right] - I_{syL}\sin\left[(\omega_c + \Delta\omega)\,t\right] \qquad (70)$$

The phase angle of the loop filter output signal plus noise is:

$$\beta^* = \text{Arctan}\left\{\frac{I_{syL}}{I_{cyL}}\right\}$$

$$= \text{Arctan}\left\{\begin{matrix}\sin\theta_o + \dfrac{I_{SF}}{\gamma} + r_L\, I_{sL} \\ \cos\theta_o + \dfrac{I_{cF}}{\gamma} + r_L\, I_{cL}\end{matrix}\right\} \tag{71}$$

where

$$r_L = \frac{\sigma L}{\gamma \sigma_{ro}}$$

$$= \frac{1}{\sqrt{2\rho_{DL}}} \tag{72}$$

where ρ_{DL} is the ratio of the average power of the direct signal component to the average random noise power at the loop filter output.

On the assumption of large signal-to-white noise power ratios, the parameter r_L will be much less than unity. Expanding (71) in a MacLaurin series in r_L, and retaining only the linear terms,

$$\beta^* \approx \beta + \Delta\theta_F \tag{73}$$

where β is given in (45),

$$\Delta\theta_F = r_L \left[\frac{I_{cL}\left(\cos\theta_o + \dfrac{I_{cF}}{\gamma}\right) - I_{sL}\left(\sin\theta_o + \dfrac{I_{sF}}{\gamma}\right)}{1 + \left(\dfrac{1}{\gamma^2}\, I_{cF}^{\,2} + I_{sF}^{\,2}\right) + \dfrac{2}{\gamma}\left(I_{cF}\cos\theta_o + I_{sF}\sin\theta_o\right)}\right] \tag{74}$$

For any given observation of the fading, it follows from (68) and (70) that the signal-to-random noise power ratio is:

$$Y = \frac{\sigma_{ro}^{\,2} R_F^{\,2}}{2\sigma_L^{\,2}} = \frac{\rho_{DL} R_F^{\,2}}{\gamma^2} \tag{75}$$

$$R_F^{\,2} = (\gamma\cos\theta_o + I_{cF})^2 + (\gamma\sin\theta_o + I_{sF})^2 \tag{76}$$

The mean value of Y equals $P_o/2\sigma_L^{\,2}$, where P_o is the total IF signal power defined in (35). Assuming the linear model for the phase-lock loop will be applicable when the signal-to-noise ratio exceeds 10 dB, it is useful to calculate the probability p of this being the case.

$$p = P_r \left\{ Y > 10 \right\}$$
$$= P_r \left\{ R_F > \gamma \sqrt{\frac{10}{\rho_{DL}}} \right\} \tag{77}$$

The distribution function of R_F is the well-tabulated Q-function. Therefore

$$p = Q\left(\gamma, \gamma \sqrt{\frac{10}{\rho_{DL}}} \right) \tag{78}$$

where

$$Q(\gamma, \beta) = \int_{\beta}^{\infty} v\, e^{-1/2(v^2 + \gamma^2)} I_o(\gamma v)\, dv$$

For large γ, this distribution can be approximated by a normal distribution with a mean γ and unit variance. Therefore

$$p = P_r \left\{ R_F - \gamma > \gamma \left[\sqrt{\frac{10}{\rho_{DL}}} - 1 \right] \right\}$$
$$\approx \Phi \left\{ \gamma \left[1 - \sqrt{\frac{10}{\rho_{DL}}} \right] \right\} \tag{79}$$

where $\Phi(z)$ is the standardized normal distribution function. When $\gamma^2/2$ equals 10, and $\rho_{DL} = 250$, $p \approx 0.9999$. It is clear from (79) that for large loop filter output direct signal-to-random noise ratios, this probability will be close to unity for values of γ greater than 3. It is concluded that for the cases of interest, the linear loop model is reasonable. Therefore, the VCO output will be of the form:

$$r(t) = \sin\left[(\omega_c + \Delta\omega)\, t + \beta^* \right]; \quad \beta^* \approx \beta + \Delta\theta_F \tag{80}$$

where β and $\Delta\theta_F$ are defined in (45) and (74) respectively.

Adding the IF noise to the IF signal in (3), the IF signal plus noise is

$$y_{IF}(t) = z_D(t) + z_r(t) + n_{IF}(t) \tag{81}$$

Similarly to (46), the low-frequency components of the product demodulator output are:

$$y(t) = 2LF \left\{ r(t)\, y_{IF}(t) \right\}$$
$$= y_D(t) + y_r(t) + y_n(t) \tag{82}$$

where

$$\begin{cases} y_D(t) = 2LF \left\{ r(t)\, z_D(t) \right\} \\ y_r(t) = 2LF \left\{ r(t)\, z_r(t) \right\} \\ y_n(t) = 2LF \left\{ r(t)\, n_{IF}(t) \right\} \end{cases} \tag{83}$$

From (4) and (80),

$$y_D(t) = -A_D \sin [\theta (t - \tau - \Delta) + \theta_o - \beta^*]; \beta^* \approx \beta + \Delta\theta_F \quad (84)$$

From (5) and (80),

$$y_r(t) = -\sum_i a_i \sin [\delta\omega_i t + \theta (t - \tau - \Delta - \Delta_i) + \theta_i - \beta^*] \quad (85)$$

Writing

$$n_{IF}(t) = R_{IF}(t) \cos [\omega_c t + \varphi_{IF}(t)] \quad (86)$$

$$\begin{aligned} y_n(t) &= 2LF \left\{ R_{IF}(t) \cos [\omega_c t + \varphi_{IF}(t)] \sin [(\omega_c + \Delta\omega) t + \beta^*] \right\} \\ &= R_{IF}(t) \sin [\Delta\omega t + \beta^* - \varphi_{IF}(t)] \\ &= I_{cIF}(t) \sin (\Delta\omega t + \beta^*) - I_{sIF}(t) \cos (\Delta\omega t + \beta^*) \end{aligned} \quad (87)$$

The autocorrelation function of this noise function assuming mutual independence of β^* and the inphase and quadrature components of y_n is:

$$\begin{aligned} \langle y_n(t)\, y_n(t+\tau) \rangle &= \psi_{cIF}(\tau) \langle \cos [\Delta\omega\tau + \beta^*(t) - \beta^*(t+\tau)] \rangle \\ &\approx \psi_{cIF}(\tau) \cos (\Delta\omega\tau) \end{aligned} \quad (88)$$

where ψ_{cIF} is the common autocorrelation function of I_{cIF} and I_{sIF}. The argument behind the approximation in (88) is that β^* has a much narrower bandwidth than the IF bandwidth. Therefore, over the significant range of variation of ψ_{cIF}, β^* cannot vary by much.

The power spectrum corresponding to (88) has been calculated on page 6A-**3**. A sketch of the power spectrum is given there. It is concluded that as long as the frequency offset Δf is much smaller than the IF bandwidth W_{IF}, the noise spectral density near the tone frequencies will be $2N_o$. Therefore the average noise power at the output of the j-th tone filter is:

$$\sigma_j^2 = 4N_o W_{oj} \quad (89)$$

Applying (51) to (49), as in deriving (52), the j-th tone filter output desired signal is:

$$y_{Dj}(t) = 2A_D \cos (\beta^* - \theta_o) J_o(m_k) J_1(m_j) \sin [\omega_j (t - \tau - \Delta)] \; j \neq k = 1,2 \quad (90)$$

Similarly, the random signal component of the j-th tone filter output when the fading is not fast is:

$$y_{rj}(t) = 2J_o(m_k) J_1(m_j) \sum_i a_i \cos [\beta^* - \theta_i - \delta\omega_i t] \sin [\omega_j (t - \tau - \Delta - \Delta_i)] \quad (91)$$

Denote the noise output of the j-th tone filter by

$$n_j(t) = \sigma_j \left[I_{cj} \cos \omega_j (t - \tau - \Delta) - I_{sj} \sin \omega_j (t - \tau - \Delta) \right] \tag{92}$$

The tone filter output will therefore be:

$$y_j(t) = y_{D_j}(t) + y_{r_j}(t) + n_j(t) \tag{93}$$

For tone ω_1, applying (56), (57), (90) - (92)

$$y_1(t) = 2\sigma_{ro} \frac{J_1(m_1)}{J_o(m_1)} \left\{ \gamma \cos(\beta^* - \theta_o) \sin[\omega_1 (t - \tau - \Delta)] + \sum_i b_i \cos(\beta^* - \theta_i - \delta\omega_i t) \sin[\omega_1 (t - \tau - \Delta - \Delta_i)] + \frac{\gamma}{\sqrt{2\rho_1}} [I_{c1} \cos \omega_1 (t - \tau - \Delta) - I_{s1} \sin \omega_1 (t - \tau - \Delta)] \right\} \tag{94}$$

where

$$\rho_1 = \frac{2A_D^2 J_o^2(m_1) J_1^2(m_2)}{\sigma_1^2} \quad ; \quad \sigma_1^2 = 4N_o W_{o1}$$

$$= \frac{2W_{IF}}{W_{o1}} J_o^2(m_2) J_1^2(m_1) \left(\frac{c}{N}\right)_{IF} \tag{95}$$

is the desired signal carrier-to-random noise power ratio at the tone filter output.

By writing y_1 in the form of inphase and quadrature components about $x = \omega_1 (t - \tau - \Delta)$,

$$y_1(t) = A_c \cos x + A_s \sin x. \tag{96}$$

It follows that

$$y_1 = E \sin(x + \delta) \tag{97}$$

where δ represents the phase error due to multipath and noise. Therefore

$$\delta = \text{Arctan} \left\{ \frac{A_c}{A_s} \right\} \tag{98}$$

since

$$\begin{cases} \sin\delta = \dfrac{A_c}{E} \qquad ; E^2 = A_c^{\,2} + A_s^{\,2} \\ \cos\delta = \dfrac{A_s}{E} \end{cases} \tag{99}$$

From (94),

$$\begin{cases} A_c = 2\sigma_{ro}\, \dfrac{J_1(m_1)}{J_o(m_1)} \left\{ \dfrac{\gamma I_{c1}}{\sqrt{2\rho_1}} - \sum_i b_i \cos(\beta^* - \theta_i - \delta\omega_i t)\sin\varphi_{i1} \right\} \\ A_s = 2\sigma_{ro}\, \dfrac{J_1(m_1)}{J_o(m_1)} \left\{ \dfrac{-\gamma I_{s1}}{\sqrt{2\rho_1}} + \sum_i b_i \cos(\beta^* - \theta_i - \delta\omega_i t)\cos\varphi_{i1} + \gamma\cos(\beta^* - \theta_o) \right\} \end{cases} \tag{100}$$

where

$$\varphi_{i1} = \omega_1 \Delta_i$$

as defined in (60).

In the special case of slow-fading, $\delta\omega_i = 0$. Therefore, the cosine function in the expression for the random component becomes

$$\cos(\beta^* - \theta_i) = \cos\beta^* \cos\theta_i + \sin\beta^* \sin\theta_i \tag{101}$$

Applying (60) and (101)

$$\begin{cases} \sum_i b_i \cos(\beta^* - \theta_i)\sin\varphi_{i1} = I_{cFs}\cos\beta^* + I_{sFs}\sin\beta^* \\ \sum_i b_i \cos(\beta^* - \theta_i)\cos\varphi_{i1} = I_{cFc}\cos\beta^* + I_{sFc}\sin\beta^* \end{cases} \tag{102}$$

From (71),

$$\sin \beta^* = \frac{1}{D}\left[\sin \theta_o + \frac{I_{sF}}{\gamma} + r_L I_{sL}\right]$$

$$\cos \beta^* = \frac{1}{D}\left[\cos \theta_o + \frac{I_{cF}}{\gamma} + r_L I_{cL}\right]$$

$$D^2 = \left(\sin \theta_o + \frac{I_{sF}}{\gamma} + r_L I_{sL}\right)^2 + \left(\cos \theta_o + \frac{I_{cF}}{\gamma} + r_L I_{cL}\right)^2 \qquad (103)$$

Applying (100), (102) and (103) to (98) gives the phase error due to slow multipath fading and random noise:

$$\delta = \text{Arctan}\left\{\frac{\frac{\gamma y_3}{\sqrt{2\rho_1}} + (X_1 \cos \beta^* + X_2 \sin \beta^*)}{\frac{\gamma y_4}{\sqrt{2\rho_1}} + \left[(\gamma \cos \theta + X_4)\cos \beta^* + (\gamma \sin \theta + X_3)\sin \beta^*\right]}\right\}$$

$$\sin \beta^* = \frac{1}{D}\left(\sin \theta + \frac{y_2}{\gamma} + r_L y_5\right) \quad ; r_L = \frac{1}{\sqrt{\rho_{DL}}}$$

$$\cos \beta^* = \frac{1}{D}\left(\cos \theta + \frac{y_1}{\gamma} + r_L y_6\right)$$

$$D^2 = \left(\sin \theta + \frac{y_2}{\gamma} + r_L y_5\right)^2 + \left(\cos \theta + \frac{y_1}{\gamma} + r_L y_6\right)^2$$

$$\begin{array}{lll} X_1 = I_{cFs} & y_1 = I_{cF} & y_5 = I_{sL} \\ X_2 = I_{sFs} & y_2 = I_{sF} & y_6 = I_{cL} \\ X_3 = I_{sFc} & y_3 = I_{c1} & \theta = \theta_o \\ X_4 = I_{cFc} & y_4 = I_{s1} & \end{array} \qquad (104)$$

This general formula for the phase error has not required any assumption about the underlying distributions of the x_i and y_i up to this point. It is reasonable, however, to assume that the y_i are normally distributed with zero mean, unit variance and mutually independent. Not so with the x_i defined in equation (60), due to their dependence upon the product of the angular tone frequency ω_1 and the differential multipath delays Δ_i. The minimum value of Δ_i is given by the formula for the specular differential delay given in Equation (21) of Section 6.3.1. The maximum value of delay can be calculated from the geometry of the satellite, aircraft receiver and reflecting surfaces. From (60) and (104),

$$\begin{cases} X_1 = - \sum_i b_i \cos\theta_i \sin(\omega_1 \Delta_i) \\ X_2 = - \sum_i b_i \sin\theta_i \sin(\omega_1 \Delta_i) \\ X_3 = \sum_i b_i \sin\theta_i \cos(\omega_1 \Delta_i) \\ X_4 = \sum_i b_i \cos\theta_i \cos(\omega_1 \Delta_i) \end{cases} \tag{105}$$

From the central limit theorem, it is reasonable to assume that the x_i are normally distributed. It is necessary, however, to determine their mean values and their covariance matrix. On the assumption that the θ_i are uniformly distributed over $(0, 2\pi)$, and mutually independent, it is not clear whether the x_i will have zero mean, since from the definition of the θ_i in equation (6), the θ_i and Δ_i are functionally related. Calculating the required mean values and applying (6), with

$$a_i = \varphi_i + \varphi_o - \omega_c (\tau + \Delta),$$

$$< \cos\theta_i \sin(\omega_1 \Delta_i) > = < \cos(a_i + \omega_c \Delta_i) \sin(\omega_1 \Delta_i) > \tag{106}$$

Assuming that the a_i are uniformly distributed on $(0, 2\pi)$, it follows that the above mean value is zero, as well as similar terms in (105). Therefore, the assumption that the x_i have zero mean appears to be reasonable. Calculating the variance of x_1

$$\sigma^2(X_1) = \langle X_1^2 \rangle$$

$$= \sum_i \langle b_i^2 \rangle \langle \cos^2 \theta_i \sin^2 (\omega_1 \Delta_i) \rangle \tag{107}$$

where

$$\langle \cos^2 \theta_i \sin^2 (\omega_1 \Delta_i) \rangle = \frac{1}{4} \langle [1 + \cos (2 a_i + 2 \omega_c \Delta_i)] [1 - \cos (2 \omega_1 \Delta_i)] \rangle$$

$$= \frac{1}{4} [1 - \langle \cos (2 \omega_1 \Delta) \rangle] \tag{108}$$

if we invoke the assumption that the a_i are uniformly distributed on $(0, 2\pi)$, and that the Δ_i are all identically distributed. Applying this and (23) to (107),

$$\sigma^2(X_1) = \frac{1}{2} \left[1 - \langle \cos (2\omega_1 \Delta) \rangle\right] \tag{109}$$

Similarly,

$$\sigma^2(X_2) = \sigma^2(X_1) \tag{110}$$

$$\sigma^2(X_3) = \sigma^2(X_4) = \frac{1}{2} \left[1 + \langle \cos (2\omega_1 \Delta) \rangle\right] \tag{111}$$

On the assumption that Δ is uniformly distributed on the interval $(\Delta_{min}, \Delta_{max})$,

$$C_1 = \langle \cos (2\omega_1 \Delta) \rangle = \frac{\sin \omega_1 (\Delta_{max} - \Delta_{min})}{\omega_1 (\Delta_{max} - \Delta_{min})} \cos \omega_1 (\Delta_{max} + \Delta_{min}) \tag{112}$$

The covariances of x_i and x_j are:

$$\begin{cases} \langle X_1 X_2 \rangle = \langle X_3 X_4 \rangle = \langle X_1 X_3 \rangle = \langle X_2 X_4 \rangle = 0 \\ \langle X_1 X_4 \rangle = \langle X_2 X_3 \rangle = -\frac{1}{2} \langle \sin (2 \omega_1 \Delta) \rangle \end{cases} \tag{113}$$

where

$$S_1 = \langle \sin (2\omega_1 \Delta) \rangle = \frac{\sin \omega_1 (\Delta_{max} - \Delta_{min})}{\omega_1 (\Delta_{max} - \Delta_{min})} \sin \omega_1 (\Delta_{max} + \Delta_{min}) \tag{114}$$

The resulting covariance matrix is:

$$\sum = \left\| < X_i X_j > \right\| = \begin{bmatrix} \frac{1}{2}(1 - C_1) & 0 & 0 & -\frac{S_1}{2} \\ 0 & \frac{1}{2}(1-C_1) & \frac{-S_1}{2} & 0 \\ 0 & \frac{-S_1}{2} & \frac{1}{2}(1 + C_1) & 0 \\ \frac{-S_1}{2} & 0 & 0 & \frac{1}{2}(1+C_1) \end{bmatrix} \quad (115)$$

Once minimum and maximum delays are specified, then the joint distribution of the x_i is uniquely determined by a quadrivariate normal distribution with zero mean and the above covariance matrix.

Another model for the distribution of the x_i can be obtained on the assumption that all the Δ_i are equal to a common value Δ_1

Then (105) becomes

$$\begin{cases} X_1 = -\sin(\omega_1 \Delta_1)\, y_1 \\ X_2 = -\sin(\omega_1 \Delta_1)\, y_2 \\ X_3 = \cos(\omega_1 \Delta_1)\, y_2 \\ X_4 = \cos(\omega_1 \Delta_1)\, y_1 \end{cases} \qquad \begin{cases} y_1 = I_{cF} \\ y_2 = I_{sF} \end{cases} \quad (116)$$

This case corresponds to the previous model if we let $\Delta_{min} = \Delta_{max} = \Delta_1$. The covariance matrix of the x_i in (116) reduces to (115) in this case with $(1 - C_1)/2$ replaced by $\sin^2(\omega_1 \Delta_1)$, $(1 + C_1)/2$ replaced by $\cos^2(\omega_1 \Delta_1)$ and S_1 replaced by $\sin(2\omega_1 \Delta_1)$. Assuming $\omega_1 \Delta_1$ to be uniformly distributed, the matrix becomes diagonal with variances equal to one-half.

6.4.3.2 FAST FADING

In the intermediate fading case the statistics of the random component will be unaffected by the phase-lock loop filter and the bandpass tone filters. Therefore, the phase measurement error statistics will be basically the same as for slow fading. In the fast fading case, the random component will be reduced in magnitude since the loop and tone filters will reduce the effective random noise power. For a variety of fading spectra, the direct-signal power to multipath power ratio will be multiplied by the relative fading rate F_r, when this ratio is greater than unity. This assumes that the loop filter and tone filter bandwidths are identical. When this is not the case the reduction of the random component by the differing filter bandwidths must be taken into account.

The normalized autocorrelation function of the inphase and quadrature components of the fading carrier can be approximated by the function

$$C(\tau) = \exp - \left[\frac{4\pi\ V\sigma T \sin\alpha}{\lambda T}\right]^2 \tag{117}$$

where

- V = aircraft speed
- α = satellite elevation angle
- λ = carrier wavelength
- σ = standard deviation of the terrain or ocean wave elevation about its mean value
- T = correlation distance of the terrain or ocean wave elevation

This is discussed in detail in the section on multipath effects (6.3.3). Defining the fading rate to be the half power point bandwidth B_F of the fading power spectrum (Fourier transform of (117)),

$$B_F = 8\sqrt{\ell n\ 2}\ \left[\frac{V\sigma\ \sin\alpha}{\lambda T}\right] \tag{118}$$

Assuming

$$T/\sigma = 15\sqrt{2}\ ,$$

$$B_F \approx \frac{0.3\ V \sin\alpha}{\lambda} \tag{119}$$

Assuming a carrier frequency of 1.6 GH_Z, $\lambda = 0.187$ meters. Assuming V = 600 miles per hour, or 268 meters per second, the fading rate becomes

$$B_F \approx 430 \sin \alpha \quad \text{Hz} \tag{120}$$

Assuming a maximum elevation angle of 15 degrees, the maximum value of B_F will be about 110 Hz. The minimum filter bandwidth of interest is 1.0 Hz. This results in the largest range of relative fading rates; i.e., from zero to 110.

The expression for the phase error will now be derived for the fast fading case. Adding the additive noise term to equations (25) - (27) the signal plus noise at the phase-lock loop input will be

$$\begin{aligned} y_o(t) &= z_o(t) + n_o(t) \\ &= I_{co}(t) \cos\left[(\omega_c + \Delta\omega)t\right] - I_{so}(t) \sin\left[(\omega_c + \Delta\omega)t\right] \end{aligned} \tag{121}$$

Adding the noise terms in (28),

$$\begin{cases} I_{co}(t) = A_D \cos\theta_o J_o(m_1) J_o(m_2) + \sigma_{ro} I_{cF}(t) + \sigma_{no} I_{c\,no}(t) \\ I_{so}(t) = A_D \sin\theta_o J_o(m_1) J_o(m_2) + \sigma_{ro} I_{sF}(t) + \sigma_{no} I_{s\,no}(t) \end{cases} \tag{122}$$

The functions I_{CF} and I_{SF} are assumed to be independent identically distributed Gaussian processes with zero mean and normalized correlation function given in (117). The corresponding normalized power spectral density is of the form:

$$S_F(f) = \frac{1}{\sigma_F \sqrt{2\pi}} e^{-\frac{f^2}{2\sigma_F^2}} \tag{123}$$

The Fourier transform of this function is

$$C(\tau) = \exp - \left[2(\pi \tau \sigma_F)^2\right] \tag{124}$$

Comparing coefficients in (117) and (124),

$$\sigma_F = \frac{2\sqrt{2}\,\sigma V \sin\alpha}{\tau \lambda} \tag{125}$$

The corresponding half power point bandwidth B_F of the power spectrum is

$$B_F = 2\sqrt{2\ \ell n\ 2}\ \ \sigma_F \tag{126}$$

Therefore, the fading rate B_F is as given in (118). The functions I_{cno} and I_{sno} are independent zero mean Gaussian noise processes with spectral density 2No.

The signal plus noise in (121) is processed in the narrow-band loop filter of bandwidth B_L. Assume that this loop filter has transfer function

$$H(f) = \begin{cases} 1\ ; & |\ f - f_c\ | \leq \dfrac{B_L}{2} \\ 0\ ; & \text{otherwise} \end{cases} \tag{127}$$

The response of this filter to the random signal component will be a Gaussian process with zero mean and power spectrum

$$S_{FL}(f) = \begin{cases} S_F(f - f_c)\ ; & |\ f - f_c\ | \leq \dfrac{B_L}{2} \\ 0\ ; & \text{otherwise} \end{cases} \tag{128}$$

Therefore, the variance of the random component of the loop filter output will be

$$\sigma_{rL}^2 = \sigma_{ro}^2 \int_{\frac{-B_L}{2}}^{\frac{B_L}{2}} S_F(f)\ df \tag{129}$$

From (123) and (129)

$$\sigma_{rL}^2 = \sigma_{ro}^2 \left[2\Phi\ (\frac{B_L}{2\sigma_F}) - 1 \right] \tag{130}$$

where Φ (z) is the standardized normal distribution function

$$\Phi\ (z) = \int_{-\infty}^{z} \frac{1}{\sqrt{2\pi}} e^{-X^2/2}\ dx \tag{131}$$

From (126),

$$\frac{B_L}{2\sigma_F} \equiv \sqrt{2\,\ell n\,2}\ \frac{B_L}{B_F} \approx 1.1774\ \frac{B_L}{B_F} \tag{132}$$

The fading ratio at the loop filter output can be defined to be:

$$\gamma_L = \frac{A_D\, J_o(m_1)\, J_o(m_2)}{\sigma_{rL}} \tag{133}$$

Relating this to the value of γ at the loop filter input as defined in (29),

$$\gamma_L = \gamma\, g\left(\frac{B_L}{B_F}\right) \tag{134}$$

where

$$g\left(\frac{B_L}{B_F}\right) = \left[2\,\Phi\left(\sqrt{2\,\ell n\,2}\ \frac{B_L}{B_F}\right) - 1\right]^{-\frac{1}{2}} \tag{135}$$

When B_L is much larger than B_F, this quantity approaches unity. When B_L is much smaller than B_F, the approximation

$$2\,\Phi(z) - 1 \approx z\sqrt{\frac{2}{\pi}} \tag{136}$$

can be used to show that

$$\frac{\gamma_L}{\gamma} = g\left(\frac{B_L}{B_F}\right) \approx \left(\frac{1}{2}\sqrt{\frac{\pi}{\ell n\,2}}\right)^{\frac{1}{2}} \left(\frac{B_F}{B_L}\right)^{\frac{1}{2}}$$

$$\approx (F_{rL})^{\frac{1}{2}}\ ;\ F_{rL} = \frac{B_F}{B_L} \tag{137}$$

where F_{rL} refers to the relative fading rate corresponding to the loop filter. Therefore, for large relative fading rates

$$\frac{\gamma_L^2}{2} \approx F_{rL}\ \frac{\gamma^2}{2} \tag{138}$$

so that γ_L becomes very large in the fast fading case.

Figure 6-55 contains a graph of the quantity

$$20 \log_{10} \frac{\gamma_L}{\gamma} = -10 \log_{10} \left[2\Phi \left(\sqrt{\frac{2 \ln 2}{Fr}} \right) - 1 \right] \tag{139}$$

This quantity describes the decibel increase in signal-to-multipath ratio as the relative fading rate increases. For very fast fading, it follows from (137) that this increase is given by

$$20 \log_{10} \frac{\gamma_L}{\gamma} \approx 10 \log_{10} Fr \tag{140}$$

At the loop filter output, the inphase and quadrature components of the signal plus noise can be written

$$I_{cyL} = A_D \cos \theta_o J_o(m_1) J_o(m_2) + \sigma_{rL} I_{CFL}(t) + \sigma_L I_{cL}(t) \tag{141}$$

$$I_{syL} = A_D \sin \theta_o J_o(m_1) J_o(m_2) + \sigma_{rL} I_{SFL}(t) + \sigma_L I_{sL}(t) \tag{142}$$

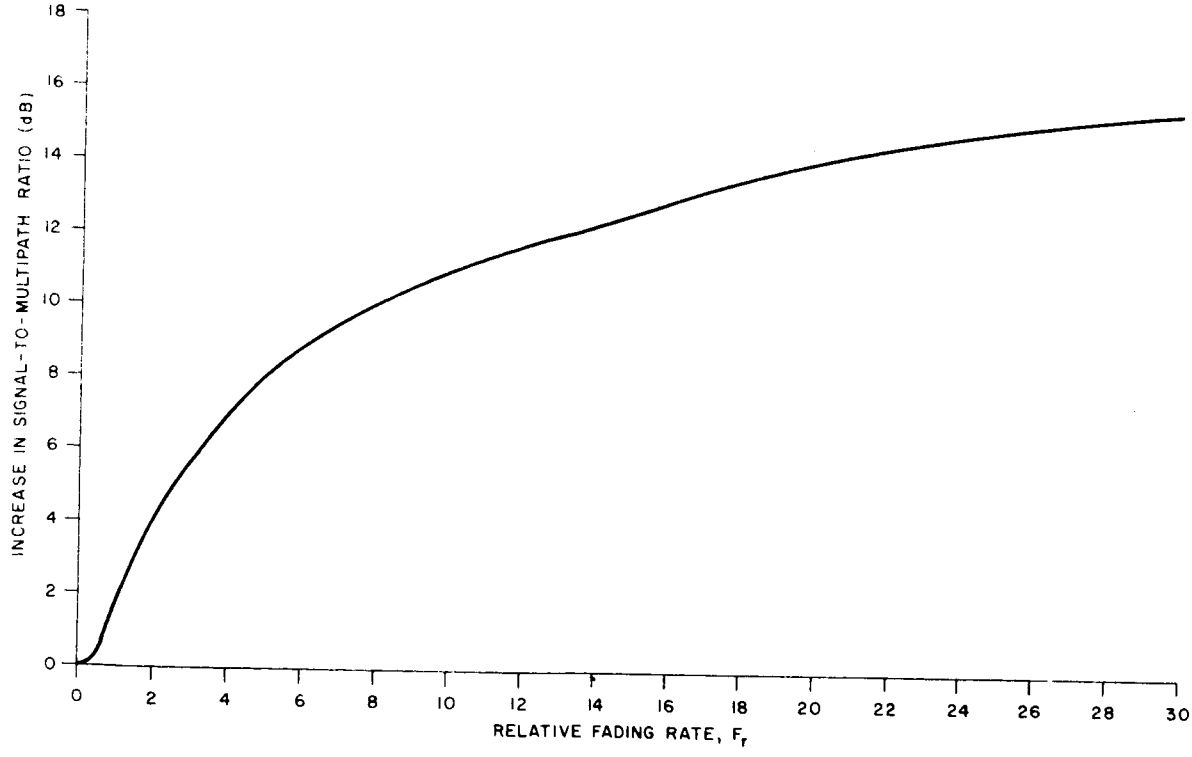

Figure 6-55. Increase in Signal-to Multipath Ratio (Fading Ratio) in dB vs Relative Fading Rate

Applying (133),

$$I_{cy_L} = \sigma_{rL}\left[\gamma_L \cos\theta_o + I_{CFL}\right] + \sigma_L I_{CL}$$

$$I_{sy_L} = \sigma_{rL}\left[\gamma_L \sin\theta_o + I_{SFL}\right] + \sigma_L I_{SL} \qquad (143)$$

This is similar to (68), with the exception of the above-described effects of filtering on the random component of the phase-lock loop input signal.

The phase angle of the loop filter output signal plus noise is:

$$\beta^* = \text{Arctan}\left\{\frac{I_{sy_L}}{I_{cy_L}}\right\}$$

$$= \text{Arctan}\left\{\frac{\sin\theta_o + \frac{1}{\gamma_L} I_{SFL} + r_L I_{SL}}{\cos\theta_o + \frac{1}{\gamma_L} I_{CFL} + r_L I_{CL}}\right\} \qquad (144)$$

where

$$r_L = \frac{\sigma_L}{\gamma_L \sigma_{rL}} \qquad (145)$$

Applying (130) and (133),

$$r_L = \frac{\sigma_L}{A_D J_o(M_1) J_o(M_2)} = \frac{1}{\sqrt{2\rho_{DL}}} \qquad (146)$$

Where ρ_{DL} represents the direct signal to random noise ratio at the loop filter output. In the slow fading case, the random signal component was lumped together with the direct signal component for purposes of calculating the loop filter output signal-to-noise ratio. This is reasonable since slow fading implies very slowly varying envelope and phase compared with the loop bandwidth. Therefore, the loop will be capable of tracking the phase of the algebraic sum of the direct and the random signal components in the presence of relatively weak random noise. Equations (78) and (79) give formulae for the probability that the loop filter output signal-to-noise ratio will exceed 10 db in the presence of noise and slow fading.

In the fast fading case, the random signal component at the loop filter output will be a random noise with bandwidth equal to the loop bandwidth. Therefore, in considering

the loop filter output signal-to-noise ratio, the random component must be lumped together with the random noise. Therefore, the loop filter output signal-to-noise ratio will be:

$$\delta_L = \frac{A_D^2 J_o^2(M_1) J_o^2(M_2)}{2\left[\sigma_{rL}^2 + \sigma_L^2\right]} = \frac{\rho_{DL}}{1 + \frac{\sigma_{rL}^2}{\sigma_L^2}} \tag{147}$$

From equation (72),

$$\frac{\sigma_{ro}^2}{\sigma_L^2} = \frac{2\,\delta_{DL}}{\gamma^2} \tag{148}$$

From (130) and (135)

$$\sigma_{rL}^2 = \frac{\sigma_{ro}^2}{g^2\left(\frac{1}{F_{rL}}\right)} \tag{149}$$

Therefore,

$$\frac{\sigma_{rL}^2}{\sigma_L^2} = \frac{\sigma_{ro}^2}{\sigma_L^2\, g^2\left(\frac{1}{F_{rL}}\right)} = \frac{2\,\rho_{DL}}{\gamma^2 g^2\left(\frac{1}{F_{rL}}\right)} \tag{150}$$

Applying (150) to (147),

$$\rho_L = \frac{\rho_{DL}}{1 + \frac{2\rho_{DL}}{\gamma^2 g^2\left(\frac{1}{F_{rL}}\right)}} \tag{151}$$

For very fast fading, it follows from (137) that,

$$\rho_L \approx \frac{\rho_{DL}}{1 + \frac{2\rho_{DL}\, BL}{\gamma^2 B_F}} \tag{152}$$

For example, when $\gamma^2/2$ equals 10, B_F equals $4B_L$, and ρ_{DL} equals 250, the denominator of (152) equals 6.25, which corresponds to an 8 db loss in signal-to-noise ratio. This is tolerable, however, since the next loop filter output signal-to-noise ratio will be about +16 db. In general, the denominator of (151) represents a signal-to-noise ratio degradation factor. If we impose the requirement that ρ_L must exceed 10, it follows from (151) that:

$$\rho_{DL} > \frac{10}{1 - \frac{20}{\gamma^2 g^2 \left(\frac{1}{F_{rL}}\right)}} \tag{153}$$

For example, if γ^2 equal to 20, it follows from (135) that

$$\rho_{DL} > \frac{5}{1 - \Phi\,(1.1774\, \frac{B_L}{B_F})} \tag{154}$$

Figure 6-56 contains a graph of this minimum value of ρ_{DL} as a function of the relative fading rate F_r. Even for a relative fading rate of unity the minimum required value of ρ_{DL} is only about +15 db. As the relative fading rate increases, the minimum value approaches +10 db since the multipath becomes insignificant. The curve is not plotted for relative fading rates less than unity, since the definition of the loop filter output signal-to-noise ratio in (151) is questionable for slow and intermediate fading.

Assuming the linear PLL model, the VCO output will be of the form

$$r(t) = \sin\left[(\omega_c + \Delta\omega)t + \beta^*\right] \tag{155}$$

where β^* is defined in (144). From here on the analysis is similar to that given in equations (81) to (104), with the exception that account has to be taken of the filtering action on the random signal component when the tone filter bandwidths W_{oj} are narrower than the fading bandwidth B_F. The term of interest corresponding to the j-th tone is given in (94). The function

$$y_{r1}(t) = 2\sigma_{ro}\, \frac{J_1(M_1)}{J_o(M_1)} \sum_i b_i \cos(\beta^* - \theta_i - \delta\,\omega_i t) \sin(x - \omega_1 \Delta_i) \tag{156}$$

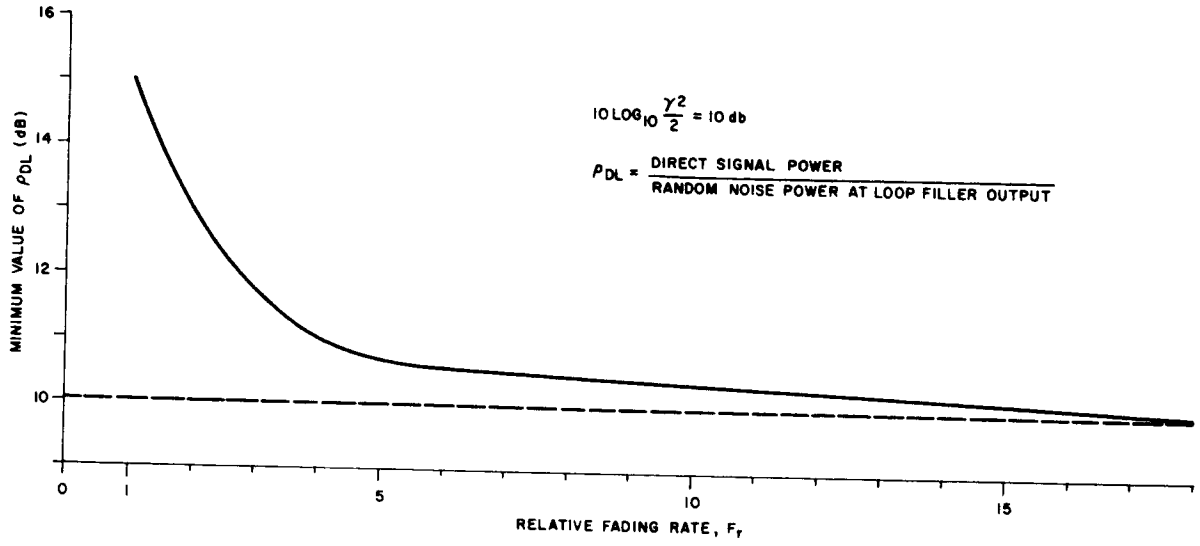

Figure 6-56. Minimum Value of Loop Filter Output Signal-to-Noise Ratio (Sol) Vs Relative Fading Rate

constitutes the portion of the product-demodulator output corresponding to the random signal component in the vicinity of tone frequency ω_1. The quantity B* is as defined in (144). Writing this in terms of inphase and quadrature components about $x = \omega_1$

$$y_{r1}(t) = A_{cr} \cos x + A_{sr} \sin x \tag{157}$$

where

$$\begin{cases} A_{cr} = -2\sigma_{ro} \dfrac{J_1(M_1)}{J_o(M_1)} \left[J_{CFS} \cos \beta^* + J_{SFS} \sin \beta^* \right] \\ A_{sr} = 2\sigma_{ro} \dfrac{J_1(M_1)}{J_o(M_1)} \left[J_{CFC} \cos \beta^* + J_{SFC} \sin \beta^* \right] \end{cases} \tag{158}$$

where

$$\begin{cases} J_{CFS} = \sum_i b_i \cos(\delta\omega_i t + \theta_i) \sin(\omega_1 \Delta_i) \\ J_{SFS} = \sum_i b_i \sin(\delta\omega_i t + \theta_i) \sin(\omega_1 \Delta_i) \\ J_{CFC} = \sum_i b_i \cos(\delta\omega_i t + \theta_i) \cos(\omega_1 \Delta_i) \\ J_{SFC} = \sum_i b_i \sin(\delta\omega_i t + \theta_i) \cos(\omega_1 \Delta_i) \end{cases} \tag{159}$$

When we were dealing with the fading carrier at the PLL input, the random functions involved were

$$\begin{cases} I_{CF} = \sum_i b_i \cos(\delta\omega_i t + \theta_i) \\ I_{SF} = \sum_i b_i \sin(\delta\omega_i t + \theta_i) \end{cases} \tag{160}$$

This can be seen from equation (30), and was employed in equation (122). The autocorrelation function in (117) refers to these functions. The problem is to relate the autocorrelation functions of the random functions in (159) to the correlation function in (117). This can be done provided we assume the differential delays in (159) to be independent and identically distributed. Calculating the autocorrelation function of I_{CF} and I_{SF} provides the identities:

$$\begin{aligned} C(t - t') &= \langle I_{CF}(t)\, I_{CF}(t') \rangle \\ &= \langle I_{SF}(t)\, I_{SF}(t') \rangle \\ &= \sum_i \sum_j \langle b_i(t)\, b_j(t') \cos\left[\delta\omega_i t + \theta_i(t)\right] \cos\left[\delta\omega_j t' + \theta_j(t')\right] \rangle \\ &= \sum_i \sum_j \langle b_i(t)\, b_j(t') \sin\left[\delta\omega_i t + \theta_i(t)\right] \sin\left[\delta\omega_j t' + \theta_j(t')\right] \rangle \end{aligned} \tag{161}$$

The identical distribution assumption imples that

$$\begin{cases} < \sin \omega_1 \Delta_i(t) \sin \omega_1 \Delta_i(t') > = R_{ss}(t - t') \\ < \cos \omega_1 \Delta_i(t) \cos \omega_1 \Delta_i(t') > = R_{cc}(t - t') \end{cases} \tag{162}$$

Assuming the b_i, $\Delta\omega_i$ and θ_i to be mutually independent, and assuming $a_i = \theta_i - \omega_c \Delta_i$ to be uniformly distributed as in (106) implies that the off-diagonal terms are of no consequence in (161). Therefore, the off-diagonal terms can also be ignored in calculating the autocorrelation functions of the random functions in (159). From the above,

$$\begin{aligned} < J_{CFS}(t)\, J_{CFS}(t + \tau) > &= < J_{SFS}(t)\, J_{SFS}(t + \tau) > \\ &= R_{ss}(\tau)\, C(\tau) \\ < J_{CFC}(t)\, J_{CFC}(t + \tau) > &= < J_{SFC}(t)\, J_{SFC}(t + \tau) > \\ &= R_{cc}(\tau)\, C(\tau) \end{aligned} \tag{163}$$

From (108) and (111)

$$\begin{aligned} R_{ss}(o) &= \frac{1}{2}(1 - C_1) \\ R_{cc}(o) &= \frac{1}{2}(1 + C_1) \end{aligned} \tag{164}$$

where C_1 is defined in (112). If we assume that the bandwidth of the time variations of the differential delays is much narrower than the bandwidth corresponding to $C(\tau)$, the correlation time of R_{cc} and R_{ss} will be much longer than that of $C(\tau)$. Then the correlation functions R_{cc} and R_{ss} in (163) can be replaced by their maximum values given in (164).

In order to calculate the variance of the random component after passage through the tone filter, it is necessary to calculate the power spectrum of the random component at the input, given in (158).

This requires calculating the autocorrelation functions of A_{cr} and A_{sr} in (158) and their cross-correlation functions. From (158)

$$\begin{cases} < A_{cr}(t)\, A_{cr}(t') > = 4\sigma_{ro}^2 \left[\dfrac{J_1(M_1)}{J_o(M_1)}\right]^2 \psi_{cc}(t, t') \\ < A_{sr}(t)\, A_{sr}(t') > = 4\sigma_{ro}^2 \left[\dfrac{J_1(M_1)}{J_o(M_1)}\right]^2 \psi_{ss}(t, t') \\ < A_{cr}(t)\, A_{sr}(t') > = -4\sigma_{ro}^2 \left[\dfrac{J_1(M_1)}{J_o(M_1)}\right]^2 \psi_{cs}(t, t') \\ < A_{sr}(t)\, A_{cr}(t') > = -4\sigma_{ro}^2 \left[\dfrac{J_1(M_1)}{J_o(M_1)}\right]^2 \psi_{sc}(t, t') \end{cases} \tag{165}$$

where

$$\psi_{cc}(t, t') = R_{ss}(\tau)\, C(\tau) < \cos \beta^*(t) \cos \beta^*(t') > ; \quad \tau = t - t'$$

$$+ R_{ss}(\tau)\, C(\tau) < \sin \beta^*(t) \sin \beta^*(t') >$$

$$+ < J_{CFS}(t)\, J_{SFS}(t') > < \cos \beta^*(t) \sin \beta^*(t') >$$

$$+ < J_{SFS}(t)\, J_{CFS}(t') > < \sin \beta^*(t) \sin \beta^*(t') > \qquad (166)$$

Similar expressions can be written for the other correlation functions in (165). Before doing this, it is useful to evaluate the correlation functions involving β^*. Since (71) and (144) are of the same form, β^* can be approximated for large γ by applying (73) and (74). Therefore,

$$\beta^* \approx \theta_o + \Delta\theta \qquad (167)$$

where

$$\Delta\theta = r_L \left[I_{CL} \cos \theta_o - I_{SL} \sin \theta_o \right] \qquad (168)$$

with r_L given in (146). The phase jitter $\Delta\theta$ is normally distributed with zero mean and variance

$$\sigma^2(\Delta\theta) = r_L^2$$

$$= \frac{1}{2\rho_{DL}} \qquad (169)$$

regardless of θ_o, which can be assumed to be uniformly distributed on $(-\pi \cdot \pi)$. The autocorrelation function of $\Delta\theta$ is:

$$R_{\Delta\theta}(\tau) = r_L^2 \operatorname{sinc}(B_L \tau) \qquad (170)$$

where B_L is the loop filter bandwidth. The required moments of β^* in (166) can be evaluated by applying the expression for the characteristic function of a normally distributed random variable with mean m and variance σ^2.

$$< e^{iuX} > = e^{imu}\, e^{-\frac{\sigma^2 u^2}{2}} \qquad (171)$$

Therefore,

$$\begin{cases} < \cos uX > = e^{-\frac{\sigma^2 u^2}{2}} \cos(mu) \\ < \sin uX > = e^{-\frac{\sigma^2 u^2}{2}} \sin(mu) \end{cases} \qquad (172)$$

Evaluating the moments involving β^* in (166), by applying (167) - (172),

$$< \cos \beta^*(t) \cos \beta^*(t') > \approx \frac{1}{2} \left\{ \begin{array}{l} < \cos \left[\Delta\theta(t) - \Delta\theta(t')\right] > \\ + < \cos \left[\Delta\theta(t) + \Delta\theta(t') + 2\theta_o\right] > \end{array} \right\} \quad (173)$$

The term involving θ_o goes to zero because of the uniform distribution of θ_o. The difference in $\Delta\theta$ at the times t and t' is normally distributed with zero mean and variance:

$$\begin{aligned} \sigma^2 &= \sigma^2 \left[\Delta\theta(t) - \Delta\theta(t')\right] \\ &= 2\sigma^2 (\Delta\theta) - 2R_{\Delta\theta}(\tau) \; ; \tau = t - t' \\ &= \frac{1}{\rho_{DL}} \left[1 - \text{sinc}\,(B_L \tau)\right] \end{aligned} \quad (174)$$

Therefore

$$< \cos \beta^*(t) \cos \beta^*(t') > \approx \frac{1}{2} \exp - \left\{ \frac{1}{2\rho_{DL}} \left[1 - \text{sinc}\,(B_L \tau)\right] \right\} \quad (175)$$

Using the same manipulation, it can be shown that

$$< \sin \beta^*(t) \sin \beta^*(t') > = < \cos \beta^*(t) \cos \beta^*(t') > \quad (176)$$

Similarly,

$$\left\{ \begin{array}{l} < \cos \beta^*(t) \sin \beta^*(t') > \approx \frac{1}{2} \left\{ \begin{array}{l} < \sin \left[\Delta\theta(t) + \Delta\theta(t') + 2\theta_o\right] > \\ - < \sin \left[\Delta\theta(t) - \Delta\theta(t')\right] > \end{array} \right\} \\ \qquad\qquad = 0 \\ < \sin \beta^*(t) \cos \beta^*(t') > = 0 \end{array} \right. \quad (177)$$

The term with θ_o goes to zero because of the uniform distribution of θ_o and by applying (172) in calculating the sine of a zero mean normal random variable.

Therefore,

$$\psi_{cc}(t, t - \tau) = R_{ss}(\tau)\, C(\tau) \exp - \left\{ \frac{1}{2\rho_{DL}} \left[1 - \text{sinc}\,(B_L \tau)\right] \right\} \quad (178)$$

Assuming large ρ_{DL} and replacing R_{SS} by its maximum value using (164),

$$\begin{aligned} \psi_{cc}(\tau) &\approx \frac{1}{2} (1 - C_1)\, C(\tau) \left\{ 1 - \frac{1}{2\rho_{DL}} \left[1 - \text{sinc}\,(B_L \tau)\right] \right\} \\ &\approx \frac{1}{2} (1 - C_1)\, C(\tau) \end{aligned} \quad (179)$$

In a similar manner, it can be shown that

$$\psi_{ss}(\tau) \approx \frac{1}{2}\,(1 + C_1)\,C(\tau) \tag{180}$$

The first cross correlation function in (165) is

$$\psi_{cs}(t,\, t') = < J_{CFS}(t)\, J_{CFC}(t') > < \cos \beta^*(t) \cos \beta^*(t') >$$

$$+ < J_{SFS}(t)\, J_{SFC}(t') > < \sin \beta^*(t) \sin \beta^*(t') > \tag{181}$$

The sine and cosine cross products are zero. From (159) and (161)

$$\begin{cases} < J_{CFS}(t)\, J_{CFC}(t') > = C(\tau)\, R_{sc}(\tau) \\ < J_{SFS}(t)\, J_{SFC}(t') > = C(\tau)\, R_{sc}(\tau) \end{cases} \tag{182}$$

where

$$R_{sc}(\tau) = < \sin \omega_1 \Delta_i(t) \cos \omega_1 \Delta_i(t') > \tag{183}$$

From (114),

$$R_{sc}(o) = \frac{S_1}{2} \tag{184}$$

Therefore,

$$\psi_{cs}(\tau) \approx \frac{S_1}{2} \exp - \left\{ \frac{1}{2\rho_{DL}} \left[1 - \operatorname{sinc} (B_L \tau) \right] \right\}$$

$$\approx \frac{S_1}{2}\, C(\tau) \tag{185}$$

The second cross correlation function in (165) is

$$\psi_{sc}(\tau) = < J_{CFC}(t)\, J_{CFS}(t') > < \cos \beta^*(t) \cos \beta^*(t') >$$

$$+ < J_{SFC}(t)\, J_{SFS}(t') > < \sin \beta^*(t) \sin \beta^*(t') > \tag{186}$$

From (159) and (161)

$$< J_{CFC}(t)\, J_{CFS}(t') > = R_{cs}(\tau)\, C(\tau)$$

$$= < J_{SFC}(t)\, J_{SFS}(t') > \tag{187}$$

where

$$R_{cs}(\tau) = < \cos \omega_1 \Delta_i(t) \sin \omega_1 \Delta_i(t - \tau) > \tag{188}$$

Therefore, as in (186)

$$\psi_{sc}(\tau) \approx \frac{S_1}{2} \; C(\tau) \tag{189}$$

These results can be used to calculate the autocorrelation function of $y_{r1}(t)$ in (157).

$$\psi_{y_{r1}}(t, t') = \langle A_{cr} A_{cr}' \rangle \cos x \cos x' + \langle A_{sr} A_{sr}' \rangle \sin x \sin x'$$

$$+ \langle A_{cr} A_{sr}' \rangle \cos x \sin x' + \langle A_{sr} A_{cr}' \rangle \sin x \cos x' \tag{190}$$

Applying (165), (179), (180), (186), and (188) to (190),

$$\psi_{y_{r1}}(t, t') = 2\sigma_{ro}^2 \left[\frac{J_1(M_1)}{J_o(M_1)}\right]^2 C(t - t') \left[\cos \omega_1 (t - t') - C_1 \cos (x + x')\right]$$

$$- S_1 \sin (x + x') \tag{191}$$

where

$$x + x' = W_1 \; (t + t') - 2(\tau + \Delta) \tag{192}$$

The terms C_1 and S_1 result in a random component in the vicinity of the tone frequency which is nonstationary. The remainder of the analysis will assume C_1 and S_1 to be negligible.

Let us check the ratio γ_1, of the amplitude of the direct component in (94) to the standard deviation of the random component whose covariance function is given in (191).

$$\gamma_1 = \frac{2\gamma\sigma_{ro} \cos(\beta^* - \theta_o)}{\sqrt{2}\;\sigma_{ro}}$$

$$= \sqrt{2}\;\gamma \cos(\beta^* - \theta_o) \tag{193}$$

where $\beta^* - \theta_o$ is the instantaneous phase error at the VCO output. Approximating $\cos(\beta^* - \theta_o)$ by applying (144) for large γ_L and small r_L,

$$\cos(\beta^* - \theta_o) \approx 1 + \Delta\theta \tag{194}$$

where $\Delta\theta$ is defined in (168). It is normally distributed with zero mean and variance equal to the reciprocal twice the loop filter output direct signal power to random noise power. Therefore, for large signal-to-noise ratios and large γ, (193) reduces to

$$\gamma_1 \approx \sqrt{2}\,\gamma \tag{195}$$

The factor $\sqrt{2}$ is due to the fact that when C_1 and S_1 are zero, the variances of the J variables in (159) are equal to one-half. The random variability of the Δ_i results

in this variance reduction as compared with the I_{CF} and I_{SF} variables in (160) which describe the carrier fading which have variance equal to unity.

Equation (191) with C_1 and S_1 equal to zero establishes that the normalized power spectrum of the random component at the tone filter input is the same as that given in (117). From (135),

$$\frac{\gamma_o}{\gamma_1} = \left[2\,\Phi\left(\sqrt{2\ln 2}\ \frac{W_{01}}{B_F}\right) - 1 \right]^{-1/2} \quad ; \quad \sqrt{2\ln 2} \approx 1.774 \tag{196}$$

where W_{01} is the tone filter output bandwidth, and γ_o is the ratio of the signal amplitude to the standard deviation of the random component at the tone filter output. The parameter

$$F_{r1} = \frac{B_F}{W_{01}} \tag{197}$$

refers to the relative fading rate at the tone filter output. Figure 6-55 can be used to determine the increase in signal-to-multipath ratio as the tone filter output relative fading rate increases.

We are now in a position to write an expression for the phase measurement error in the fast fading case. The formula will be similar to (104). There are 2 basic changes. (1) The formula for β^* is given in (144). It differs from the expression for β^* in (71) in that γ is replaced by γ_L, where γ_L / γ is defined in (135) as a function of relative fading rate. (2) The random component at the tone filter output has a different variance, as described by γ_o and γ_1 in (195) and (196).

The tone filter output corresponding to the random component is of the form

$$y_{r10} = A_{cr1} \cos x + A_{sr1} \sin x \tag{198}$$

where

$$A_{cr1} = \sigma_{r1} I_{cr1} \ ; \ A_{sr1} = \sigma_{r1} I_{sr1} \tag{199}$$

where I_{cr1} and I_{sr1} are independent zero-mean stationary Gaussian processes with unit variance. As in (130) and (132), and from (191)

$$\sigma_{r1}^2 = 2\sigma_{ro}^2 \left[2\,\Phi\left(\sqrt{2\ln 2}\ \frac{W_{o1}}{B_F}\right) - 1 \right] \cdot \left[\frac{J_1(M_1)}{J_o(M_1)}\right]^2 \tag{200}$$

Replacing the terms involving the random component in (100) with those in (199), the inphase and quadrature components in (96) are of the form

$$\begin{cases} A_c = 2\sigma_{ro} \dfrac{J_1(M_1)}{J_o(M_1)} \left\{ \dfrac{\gamma I_{c1}}{\sqrt{2\rho_1}} + h(F_{r1})\, I_{cr1} \right\} \\ A_s = 2\sigma_{ro} \dfrac{J_1(M_1)}{J_o(M_1)} \left\{ \dfrac{-\gamma I_{s1}}{\sqrt{2\rho_1}} + h(F_{r1})\, I_{sr1} + \gamma \cos(\beta^* - \theta_o) \right\} \end{cases} \tag{201}$$

where

$$h(F_{r1}) = \sqrt{2} \left[2\,\Phi\left(\frac{2 \ln 2}{F_{r1}}\right) - 1 \right]^{1/2} \tag{202}$$

For large signal-to-noise ratios, $\cos(\beta^* - \theta_o)$ will be close to unity.

The corresponding phase error is therefore:

$$\delta = \text{Arctan} \left\{ \frac{\dfrac{z_1}{\sqrt{2\rho_1}} + \dfrac{1}{\gamma} h(F_{r1}) z_2}{1 + \dfrac{z_3}{\sqrt{2\rho_1}} + \dfrac{1}{\gamma} h(F_{r1})\, z_4} \right\} \tag{203}$$

6.4.3.3 INTERMEDIATE FADING

The main difficulty in handling this case is in deriving a quantitative measure of when the phase-lock loop can be linearized for analysis purposes. Equation (78) describes the probability of having a loop filter output signal-to-noise ratio greater than 10 dB for the slow fading case. This equation involves lumping the multipath signal together with the direct component since it will have very slowly varying envelope and phase. In the fast fading case, the random component is similar to white noise insofar as loop performance is concerned. Intermediate fading corresponds to the transtion region between these two cases. A conservative approach is to lump the random component in with white noise, and to calculate the probability p that this signal-to-noise ratio will exceed 10 dB. The approach used will be to calculate the signal-to-noise ratio at the loop filter output averaging over the random noise. This gives the conditional signal-to-noise ratio for a given value of the fading. The probability p is based on the distribution function of this conditional signal-to-noise ratio.

From (142), the loop filter output signal plus noise is

$$y_L(t) = I_{cyL}\cos(\omega_o t) - I_{syL}\sin(\omega_o t) \tag{204}$$

In the absence of noise, it follows from (143) that

$$y_L(t) = \sigma_{rL}\gamma_L\cos(\omega_o t + \theta_o) \tag{205}$$

Therefore the average signal power is:

$$S = \frac{\sigma_{rL}^2\,\gamma_L^2}{2} \tag{206}$$

In the absence of signal,

$$y_L(t) = E_L\cos(\omega_o t + \varphi_L) \tag{207}$$

where

$$\begin{cases} E_L^2 = (\sigma_{rL}I_{CFL} + \sigma_L I_{CL})^2 + (\sigma_{rL}I_{SFL} + \sigma_L I_{SL})^2 \\ \varphi_L = \text{Arctan}\left\{\dfrac{\sigma_{rL}I_{SFL} + \sigma_L I_{SL}}{\sigma_{rL}I_{CFL} + \sigma_L I_{CL}}\right\} \end{cases} \tag{208}$$

The conditional noise power can be defined to:

$$N = \frac{1}{2}\langle E_L^2\rangle = \frac{1}{2}\left(\sigma_{rL}^2 R_{FL}^2 + 2\sigma_L^2\right) \tag{209}$$

where

$$R_{FL}^2 = I_{CFL}^2 + I_{SFL}^2 \tag{210}$$

The quantity R_{FL} has probability density

$$p_{FL}(x) = xe^{-x^{2/2}} \tag{211}$$

Combining (206) and (209) gives the conditional signal-to-noise ratio at the loop filter output for given values of the fading envelope R_{FL} at the loop filter output:

$$y = \frac{S}{N}$$

$$= \frac{\gamma_L^2 \sigma_{rL}^2}{\sigma_{rL}^2 R_{FL}^2 + 2\sigma_L^2}$$

$$= \frac{\gamma_L^2}{R_{FL}^2 + 2\gamma_L^2 \gamma_L^2} = \frac{\gamma_L^2}{R_{FL}^2 + \gamma_L^2 / \rho_{DL}} \tag{212}$$

Calculating the probability p that Y exceeds 10,

$$p = P_r \left\{ R_{FL} < \frac{\gamma_L}{\sqrt{10}} \left[1 - \frac{10}{\rho_{DL}} \right]^{\frac{1}{2}} \right\} \tag{213}$$

Applying (211),

$$p = 1 - \exp - \left[\frac{\gamma_L^2}{20} \left(1 - \frac{10}{\rho_{DL}} \right) \right] \tag{214}$$

where γ_L is related to γ and the relative fading rate F_{rL} in equation (137). This formula shows that for sufficiently large ρ_{DL} and γ_L, the probability of linear phase-lock-loop operation will be close to unity.

Assuming linear loop operation, equation (203) can be used for computing the phase error distribution in the intermediate fading case.

Appendix 6D contains a similar analysis of the phase errors using a nonselective fading model which assumes that the differential multipath delays are negligible. This results in smaller phase errors than in the above analysis which assumes random differential multipath delays. This is demonstrated in Figure 6-57 which contains

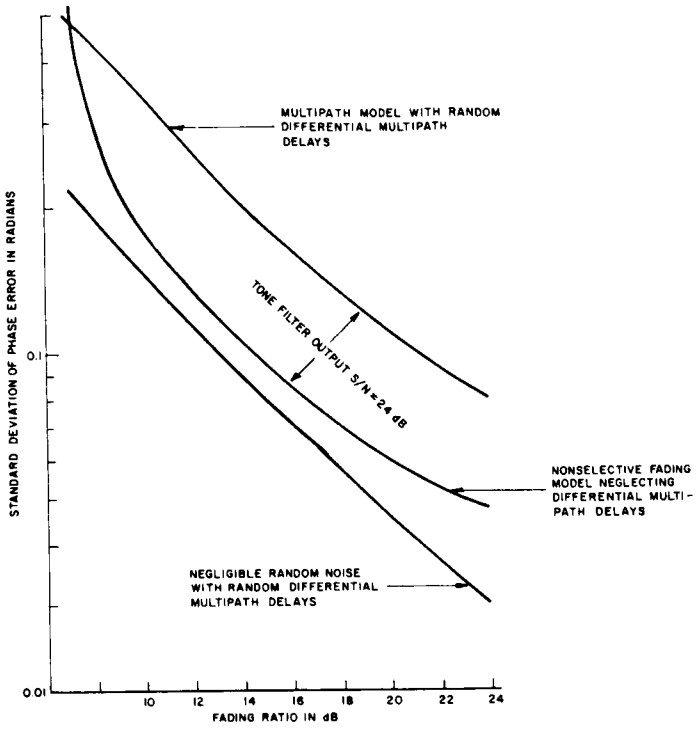

Figure 6-57. Standard Deviation of Phase Error vs Fading Ratio (C_{33})

graphs of the standard deviation of phase error as a function of the fading (multipath) ratio for both models, assuming a 24 dB desired signal-to-random noise ratio at the tone filter output. Comparison of these curves with a curve which assumes the random noise to be negligible shows the significant contribution of the multipath to the phase error. The question to be answered is which multipath model is more valid for the the satellite navigation system of interest. Figure 6-36 contains graphs of the minimum differential delay Δ min and the maximum differential delay Δ max for satellite elevation angles from 1° to 15°, and aircraft altitudes of 5 miles and 15 miles. Table 6-11 gives the extreme values at the 1° and 5° elevation angles. The smallest value of Δ max- Δ min in Table 6-11 is about 400 μsec. This determines a range of possible random phases. When the product of the tone frequency and this range exceeds unity, the assumed uniformly distributed random phase distribution is reasonable.

This implies that the assumption is reasonable for tone frequencies greater than the reciprocal of the differential-delay range. For the above 400 μsec range, which refers to a 15° elevation angle and a 5 mile aircraft altitude, the assumption is valid for tone frequencies greater than 2.5 kHz.

Estimates of the distribution function of the phase error have been made by applying equation (203) using 100 phase error computations for each of a set of values of relative fading rate, fading ratio, and tone filter output signal-to-noise ratio. Figures 6-58 and 6-59 contain graphs of some of these distribution functions plotted on normal

TABLE 6-11. MINIMUM AND MAXIMUM DIFFERENTIAL MULTIPATH DELAYS FOR 1° AND 15° SATELLITE ELEVATION ANGLES: 5 MILE AND 15 MILE AIRCRAFT ALTITUDES

Aircraft Altitude (miles)	Elev. (deg)	Differential Multipath Delays (Seconds)	
		Δ_{min}	Δ_{max}
5	1	1.7	1400
	15	14	415
	10	7.4	620
15	15	40	490

probability graph paper. The approximate linearity of the graphs for both slow fading ($F_r = 0.$) and fast fading ($F_r = 32$) for fading ratios from 10 to 25 dB demonstrates that the phase error distrubutions are approximately normal. It is shown in Section 6.3 that a smallest fading ratio of about 10 dB occurs at elevation angles between 2° and 4.5°, whereas the fading ratio is about 19 dB at a 15° elevation angle. Therefore, the computations have covered the range of fading ratios of interest.

Tables 6-12 through 6-15 contain lists of the estimates of the mean, m, and standard deviation, σ, of the phase error in radians for relative fading rates $F_r = 0$, 0.5, 1, 2, 4, 8, 16, 32; fading ratios 10, 15, 20, 25 dB, and tone-filter output signal-to-noise ratios equal to 15, 20, 24 and 30 dB. These phase errors have been converted to range errors and are tabulated in the summary given in Section 6.6. Improved estimates of these means and standard deviations can be obtained by using larger sample sizes. However, by plotting smoothed curves as a function of the various parameters, the estimation sampling error can be reduced.

Figure 6-60 shows the dependence of the mean and standard deviation of the phase error on the relative fading rate for a 10 dB fading ratio, and tone filter output signal-to-noise ratios equal to 15, 20, 24, 30. Figures 6-61 to 6-67 contain corresponding graphs as a function of the fading ratio for different fading rates and tone filter output signal-to-noise ratios. Figures 6-68 to 6-71 contain graphs of the mean and standard deviation of the phase error as a function of tone filter output signal-to-noise ratio for different fading rates, and fading ratios. Figure 6-72 shows the variation of the fading ratio with satellite elevation angles as calculated in Section 6.3.3. This curve, and the curve in Figure 6-55, in conjunction with the previous curves can be used to show the dependence of the phase errors on satellite elevation angle. This is shown in Figure 6-73 for a 300 Hz tone filter, and in Figure 6-74 for a 10 Hz filter. As the elevation angle increases, the mean phase error approaches zero, and the standard deviation approaches a limiting value determined by the signal-to-random noise ratio at the tone filter output.

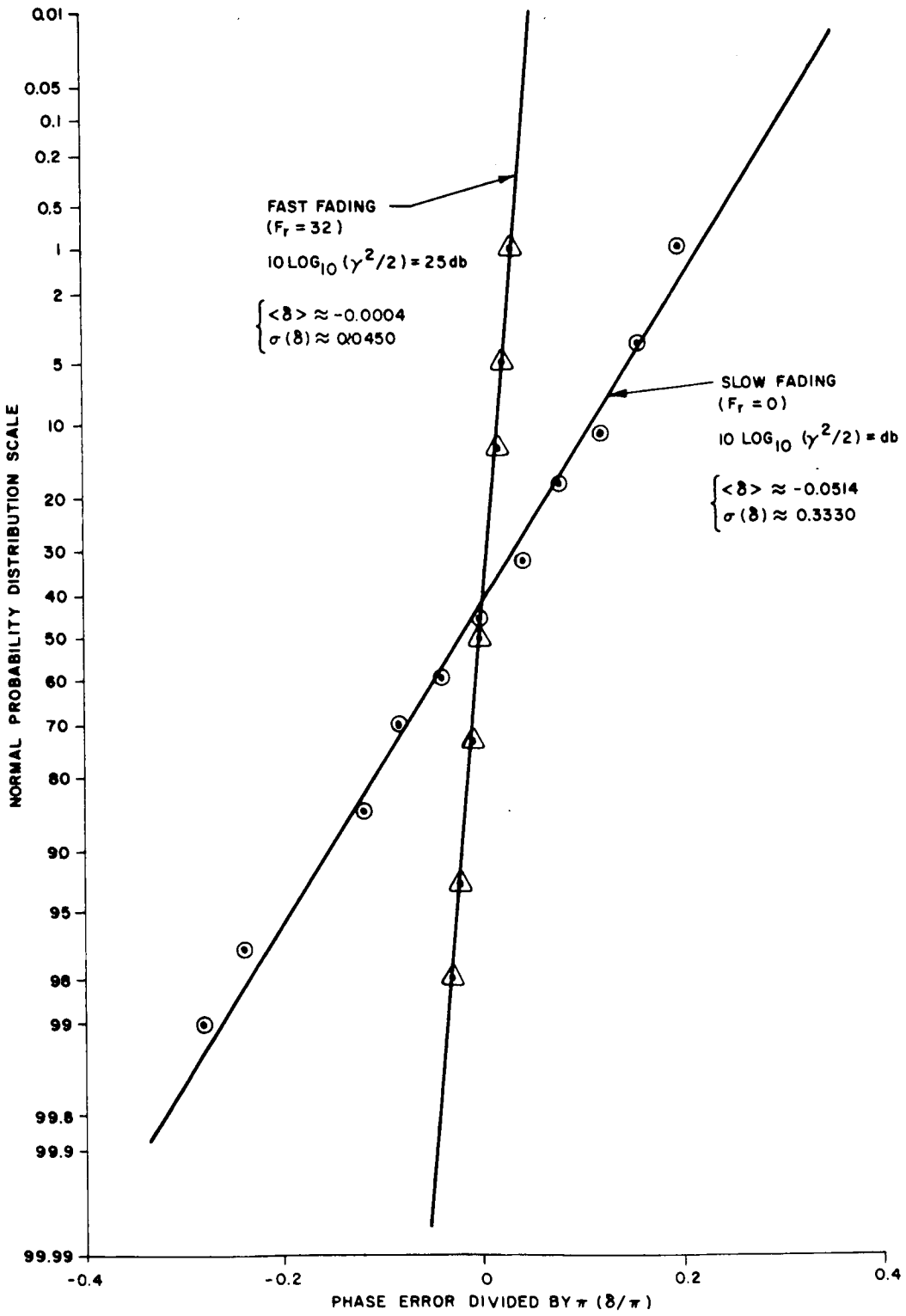

Figure 6-58. Probability Distribution Function of Phase Error Relative Fading Rate = 0, 32; Fading Ratio = 10, 25 dB

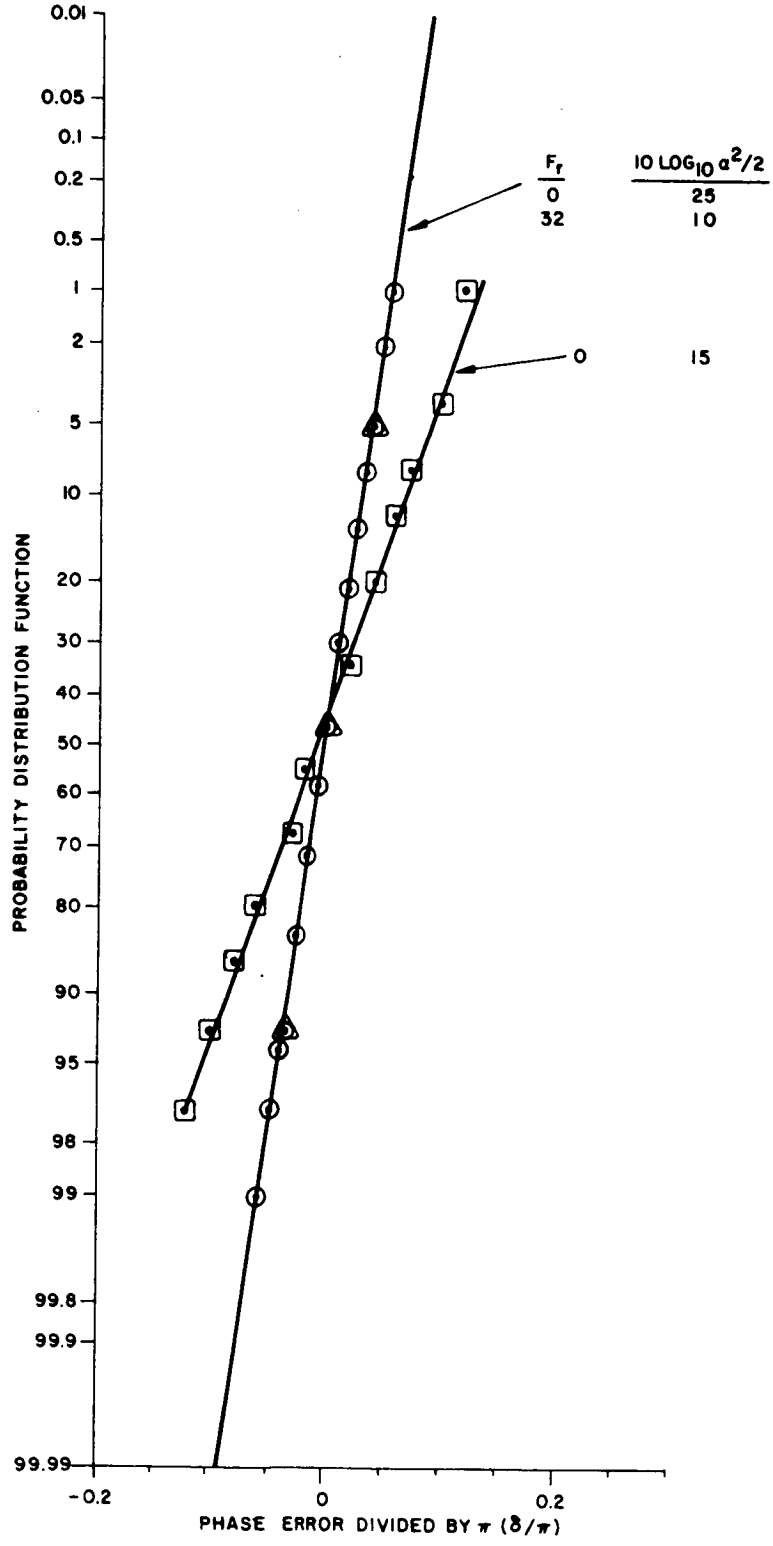

Figure 6-59. Distribution Function of Phase Error; Relative Fading Rate = 0, 32; Fading Ratio = 10, 25 dB

TABLE 6-12. MEAN AND STANDARD DEVIATION OF PHASE ERROR IN RADIANS VS. FADING RATIO AND RELATIVE FADING RATE; TONE FILTER OUTPUT S/N = 15 dB

(Upper entry = mean, m

lower entry = standard deviation, σ)

F_r \ $\frac{\nu^2}{2}$ in db	10	15	20	25
0	m = -0.0480 σ = 0.3640	-0.0242 0.2328	-0.0116 0.1690	-0.0050 0.1414
0.5	-0.0476 0.3610	-0.0238 0.2312	-0.0114 0.1682	-0.0048 0.1412
1	-0.0410 0.3244	-0.0204 0.2128	-0.0096 0.1600	-0.0038 0.1378
2	-0.0296 0.2626	-0.0146 0.1828	-0.0066 0.1470	-0.0022 0.1328
4	-0.0200 0.2104	-0.0094 0.1588	-0.0038 0.1374	-0.0008 0.1292
8	-0.0128 0.1750	-0.0056 0.1438	-0.0018 0.1316	-0.0004 0.1272
16	-0.0080 0.1530	-0.0030 0.1352	-0.0002 0.1284	-0.0012 0.1260
32	-0.0046 0.1404	-0.0012 0.1304	-0.0008 0.1266	-0.0018 0.1254

TABLE 6-13. MEAN AND STANDARD DEVIATION OF PHASE ERROR IN RADIANS VS. FADING RATIO AND RELATIVE FADING RATE; TONE FILTER OUTPUT S/N = 20 dB

(Upper entry = mean, m

lower entry = Standard Deviation, σ)

F_r \ $\frac{\gamma^2}{2}$ in dB	10	15	20	25
0	m = -0.0504	-0.0262	-0.0134	-0.0066
	σ = 0.3404	0.2030	0.1296	0.0936
0.5	-0.0500	-0.0260	-0.0134	-0.0066
	0.3374	0.2012	0.1288	0.0934
1	-0.0432	-0.0224	-0.0114	-0.0056
	0.2998	0.1810	0.1184	0.0886
2	-0.0318	-0.0164	-0.0082	-0.0038
	0.2352	0.1464	0.1014	0.0814
4	-0.0220	-0.0112	-0.0054	-0.0024
	0.1780	0.1170	0.0880	0.0760
8	-0.0148	-0.0074	-0.0034	-0.0012
	0.1370	0.0970	0.0796	0.0730
16	-0.0098	-0.0048	-0.0020	-0.0004
	0.1094	0.0848	0.0748	0.0712
32	-0.0064	-0.0028	-0.0008	-0.0002
	0.0922	0.0778	0.0722	0.0702

TABLE 6-14. MEAN AND STANDARD DEVIATION OF PHASE ERROR IN RADIANS VS. FADING RATIO AND RELATIVE FADING RATE; TONE FILTER OUTPUT S/N = 24 dB

(Upper entry = mean, m

lower entry = Standard deviation, σ)

F_r \ $\frac{\gamma^2}{2}$ in dB	10	15	20	25
0	m = -0.0514	-0.0270	-0.0142	-0.0074
	σ = 0.3330	0.1936	0.1162	0.0756
0.5	-0.0510	-0.0268	-0.0140	-0.0074
	0.3300	0.1918	0.1154	0.0750
1	-0.0442	-0.0232	-0.0122	-0.0062
	0.2922	0.1708	0.1040	0.0694
2	-0.0326	-0.0172	-0.0090	-0.0046
	0.2266	0.1344	0.0848	0.0604
4	-0.0228	-0.0120	-0.0062	-0.0030
	0.1678	0.1024	0.0686	0.0532
8	-0.0156	-0.0080	-0.0040	-0.0018
	0.1242	0.0796	0.0580	0.0488
16	-0.0106	-0.0054	-0.0026	-0.0010
	0.0940	0.0646	0.0514	0.0464
32	-0.0070	-0.0036	-0.0016	-0.0004
	0.0738	0.0554	0.0478	0.0450

TABLE 6-15. MEAN AND STANDARD DEVIATION OF PHASE ERROR IN RADIANS VS. FADING RATIO AND RELATIVE FADING RATE; TONE FILTER OUTPUT S/N = 30 dB

(Upper entry = mean, m
lower entry = Standard Deviation, σ)

F_r \ $\frac{\gamma^2}{2}$ in dB	10	15	20	25
0	m = -0.0522	-0.0276	-0.0148	-0.0080
	σ = 0.3284	0.1882	0.1088	0.0644
0.5	-0.0518	-0.0274	-0.0146	-0.0078
	0.3256	0.1866	0.1078	0.0638
1	-0.0450	-0.0238	-0.0128	-0.0068
	0.2876	0.1650	0.0958	0.0574
2	-0.0334	-0.0178	-0.0096	-0.0050
	0.2216	0.1276	0.0748	0.0462
4	-0.0234	-0.0124	-0.0066	-0.0036
	0.1620	0.0940	0.0564	0.0368
8	-0.0162	-0.0086	-0.0046	-0.0024
	0.1170	0.0690	0.0432	0.0304
16	-0.0110	-0.0060	-0.0030	-0.0016
	0.0848	0.0516	0.0344	0.0266
32	-0.0076	-0.0040	-0.0020	-0.0010
	0.0624	0.0398	-0.0288	0.0242

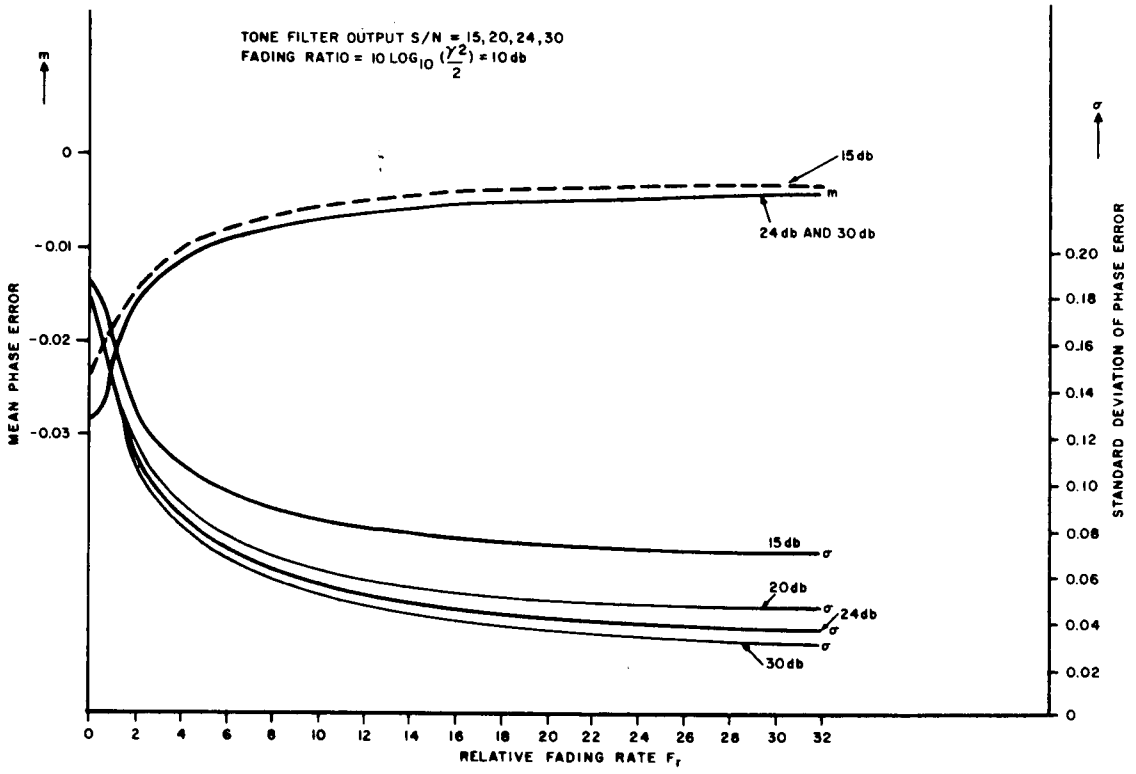

Figure 6-60. Mean and Standard Deviation of Phase Error vs. Relative Fading Rate

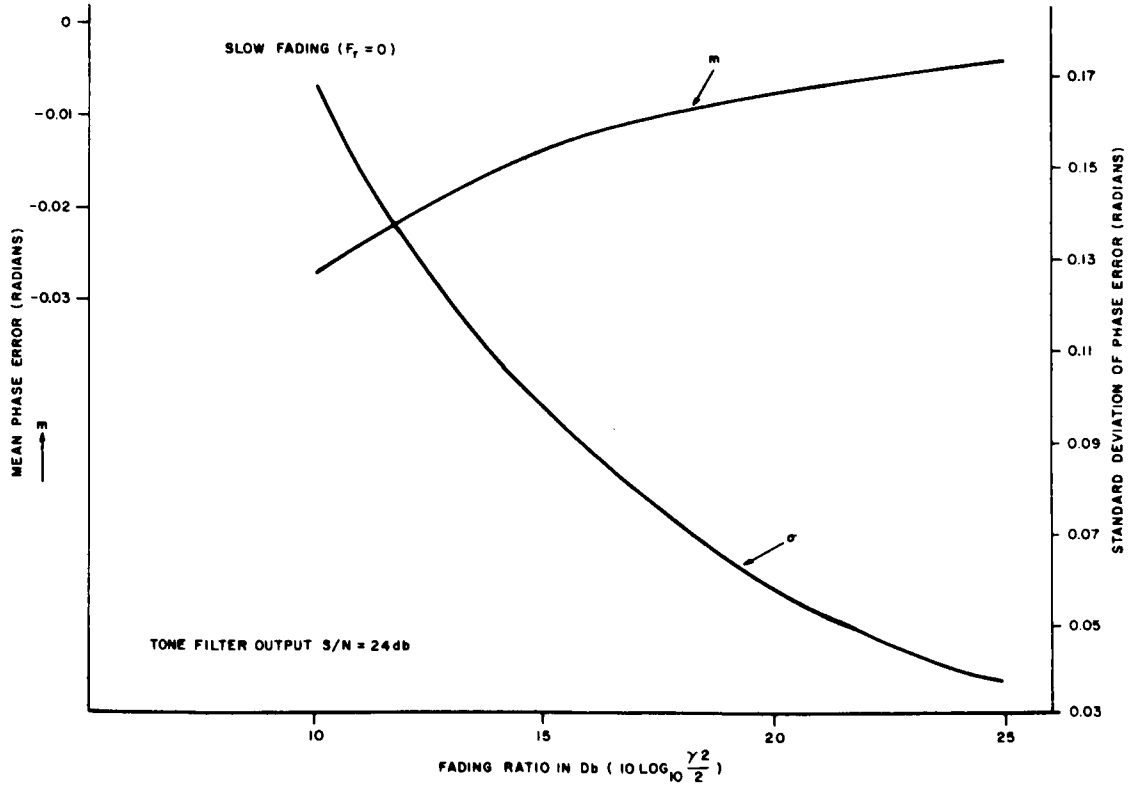

Figure 6-61. Mean and Standard Deviation of Phase Error vs. Fading Ratio, Tone Filter Output S/N = 24 dB

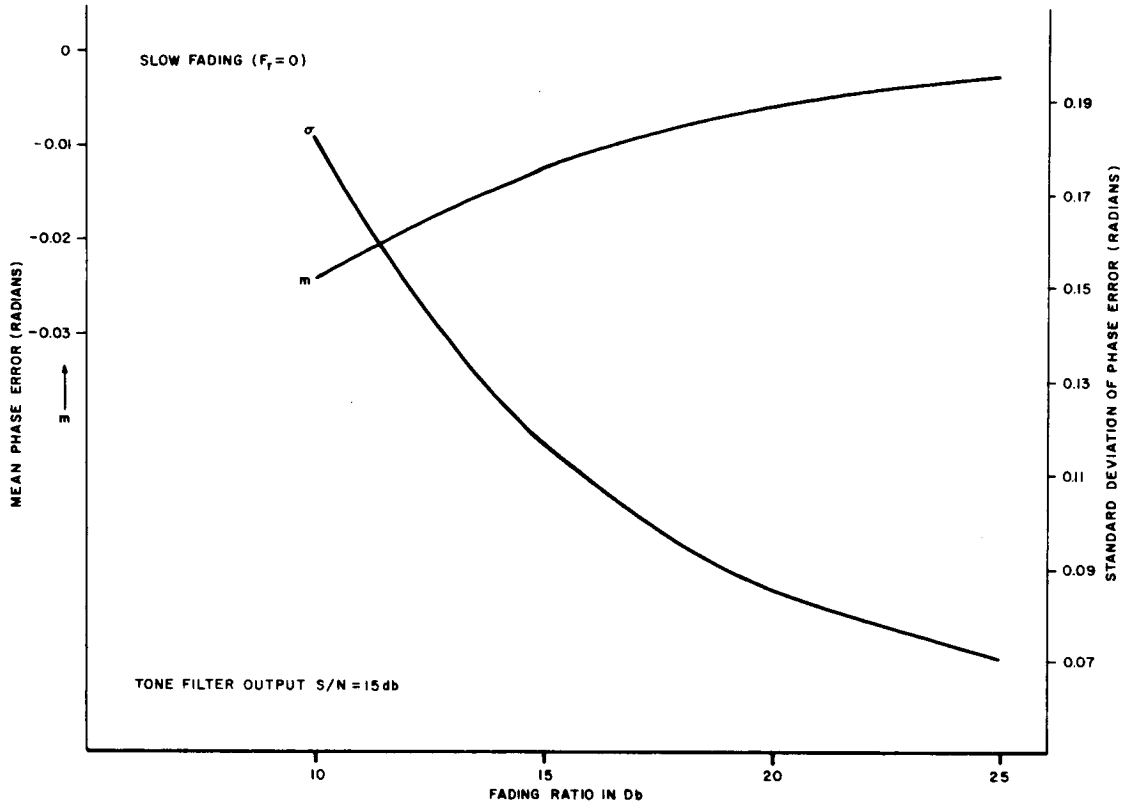

Figure 6-62. Mean and Standard Deviation of Phase Error vs. Fading Ratio, Tone Filter Output S/N = 15 dB

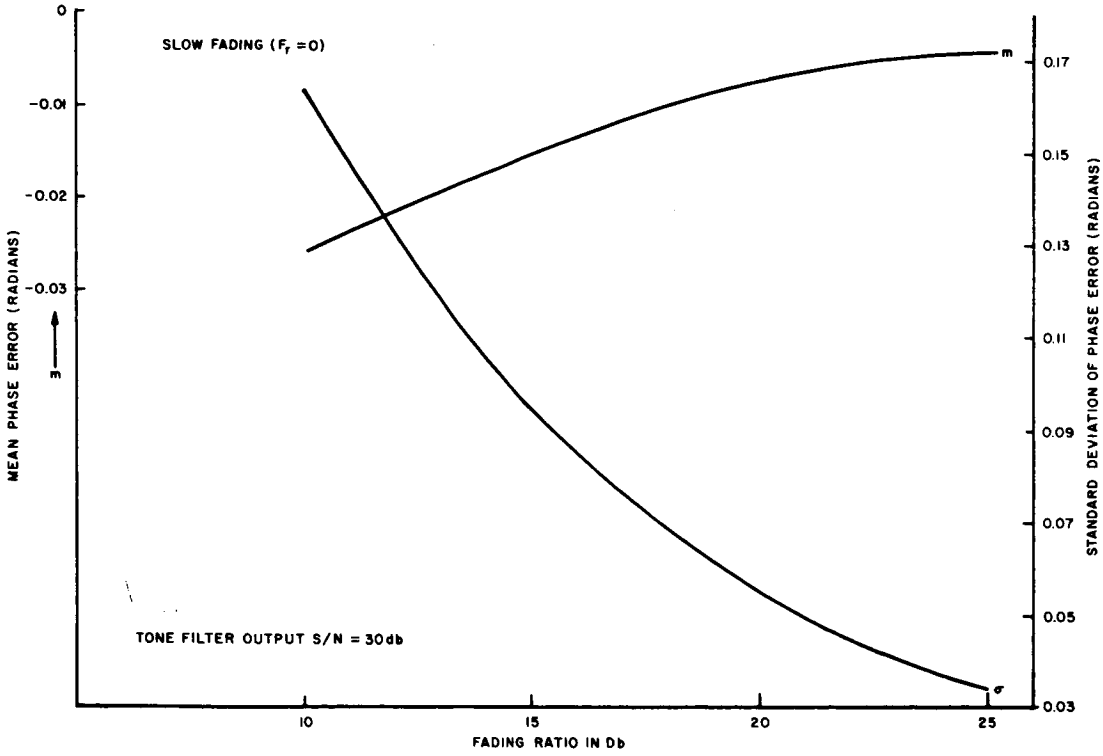

Figure 6-63. Mean and Standard Deviation of Phase Error vs. Fading Ratio, Tone Filter Output S/N = 30 dB

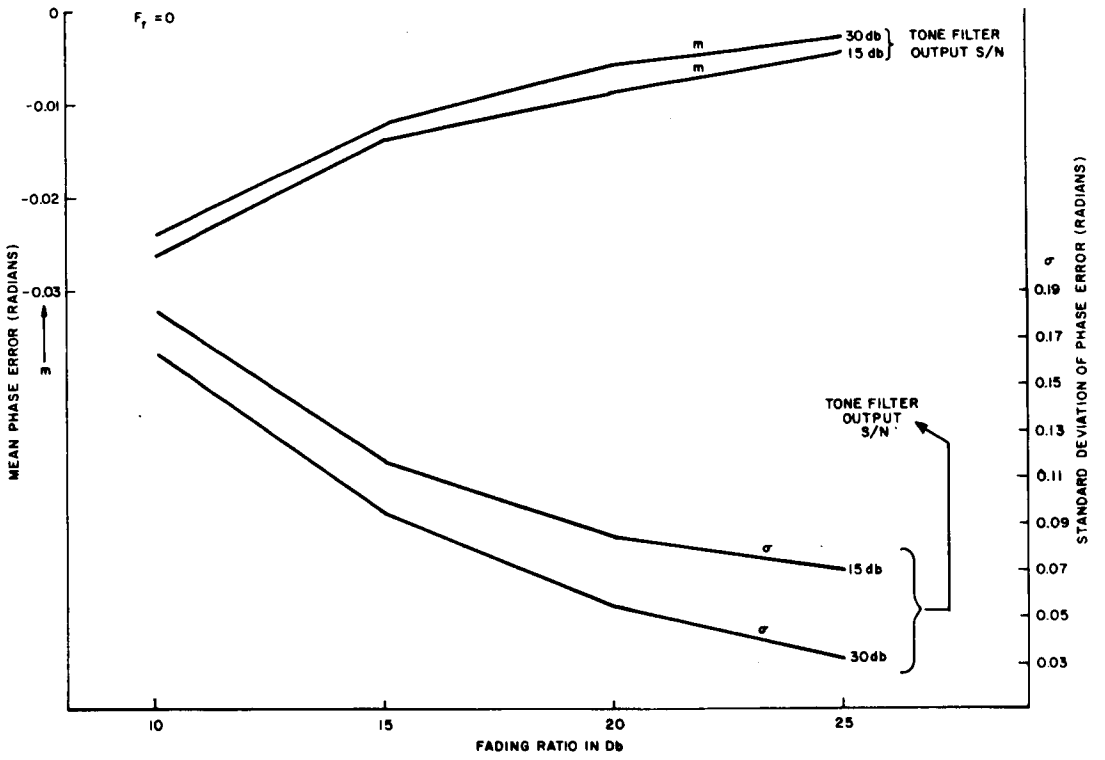

Figure 6-64. Mean and Standard Deviation of Phase Error vs. Fading Ratio, Tone Filter Output S/N = 15, 30 dB

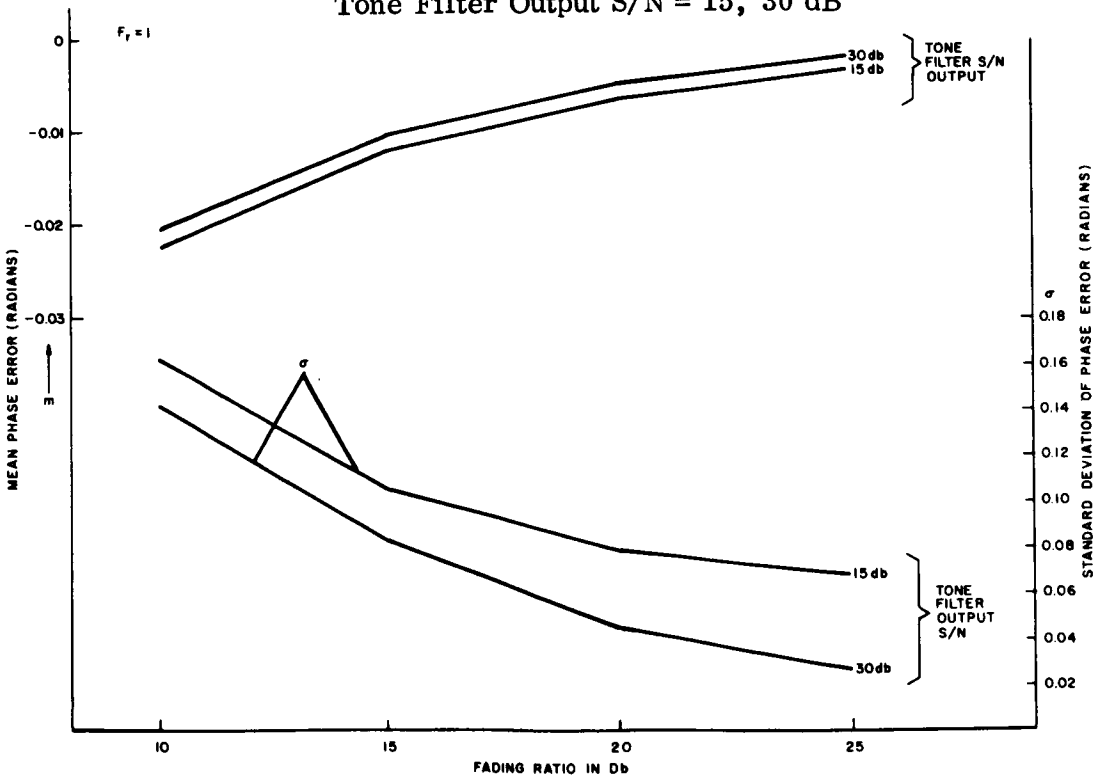

Figure 6-65. Mean and Standard Deviation of Phase Error vs. Fading Ratio, Relative Fading Rate = 1

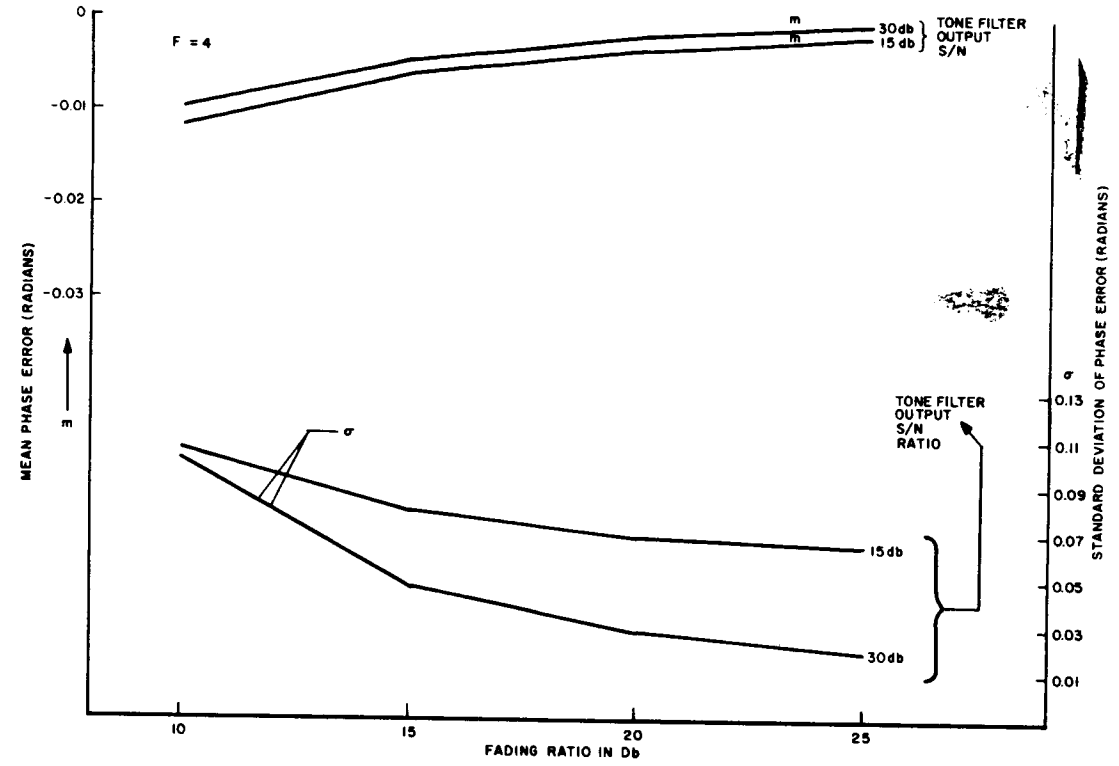

Figure 6-66. Mean and Standard Deviation of Phase Error vs. Fading Ratio, Relative Fading Rate = 4

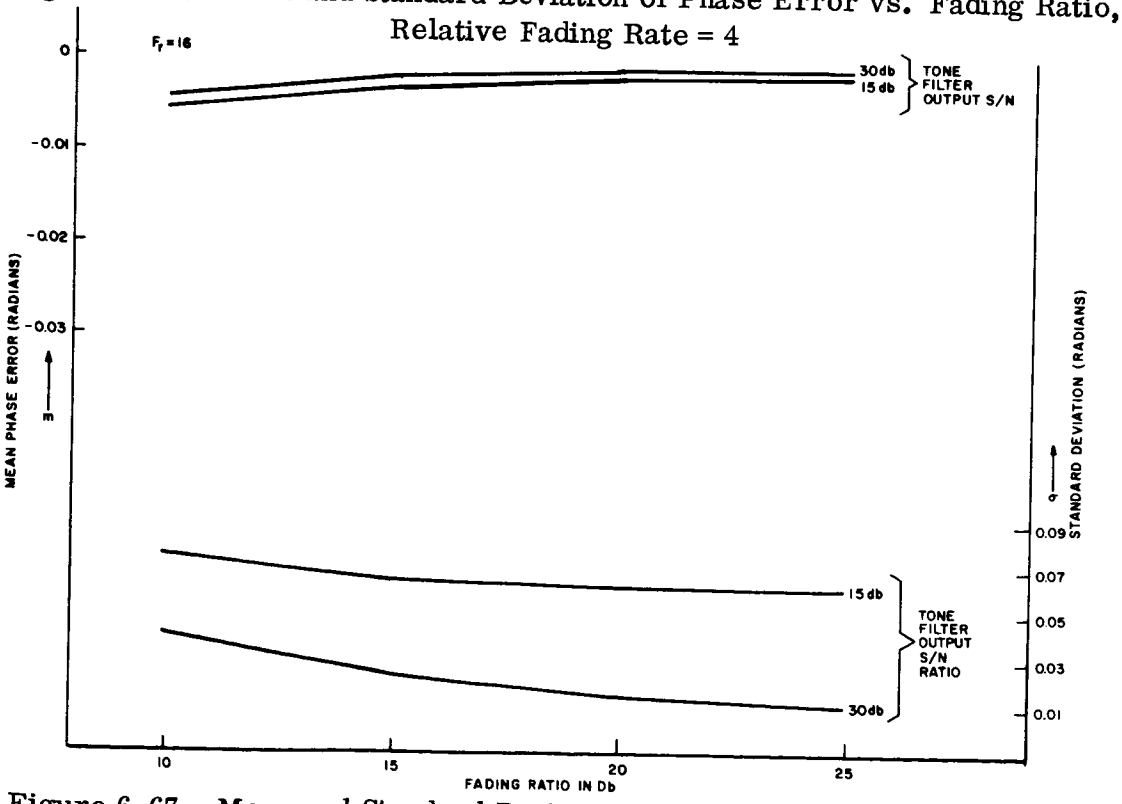

Figure 6-67. Mean and Standard Deviation of Phase Error vs. Fading Ratio, Relative Fading Rate = 16

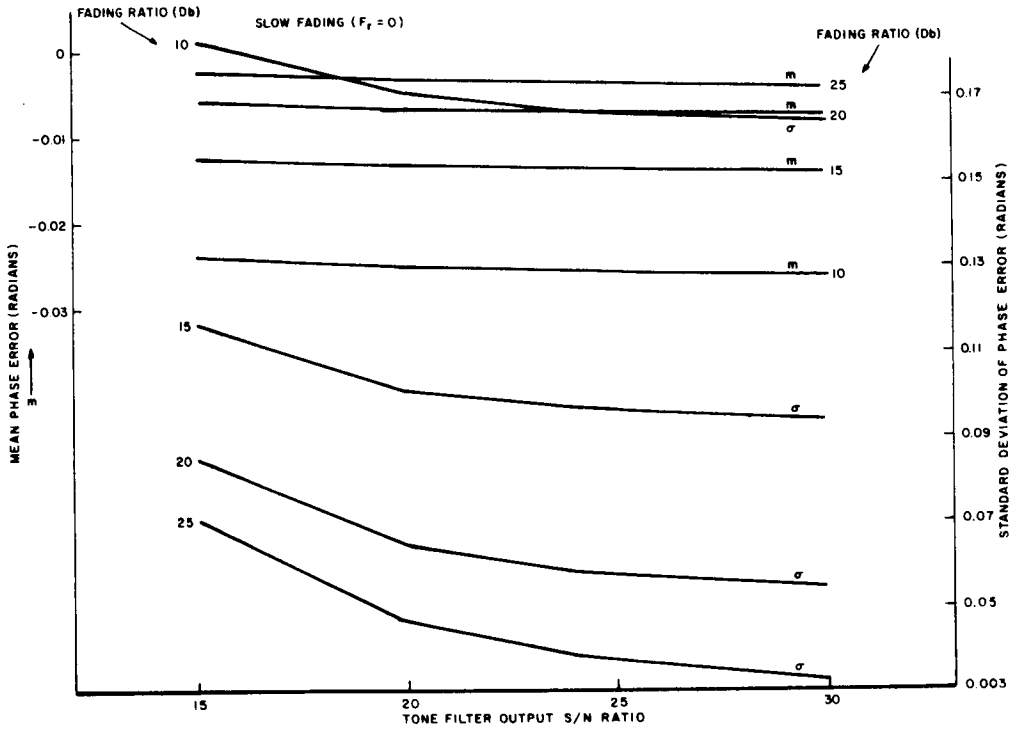

Figure 6-68. Mean and Standard Deviation of Phase Error vs. Tone Filter Output S/N

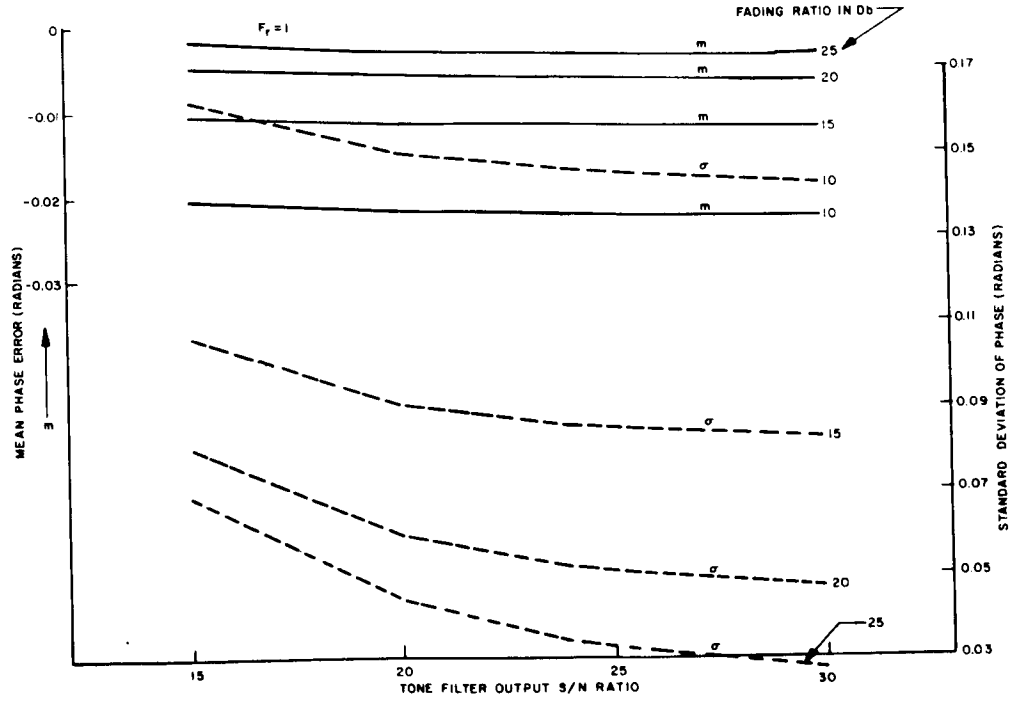

Figure 6-69. Mean and Standard Deviation of Phase Error vs. Fading Ratio, Relative Fading Rate = 1

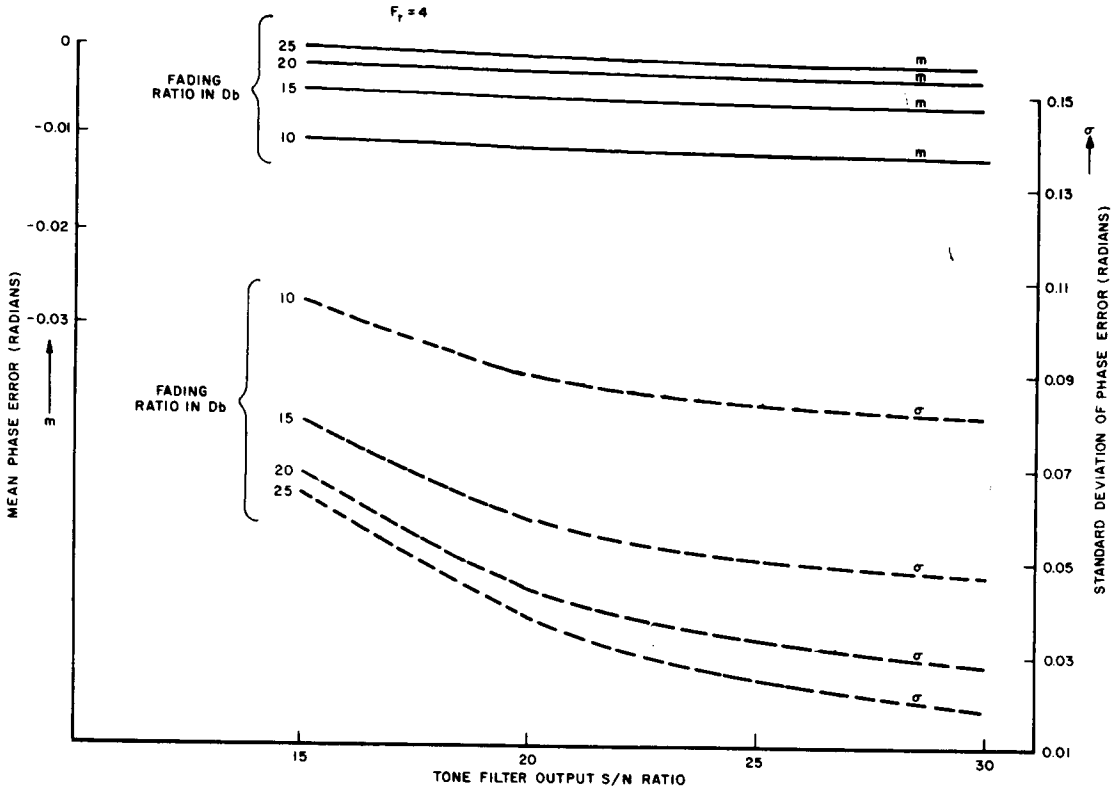

Figure 6-70. Mean and Standard Deviation of Phase Error vs. Tone Filter Output S/N, Relative Fading Rate = 4

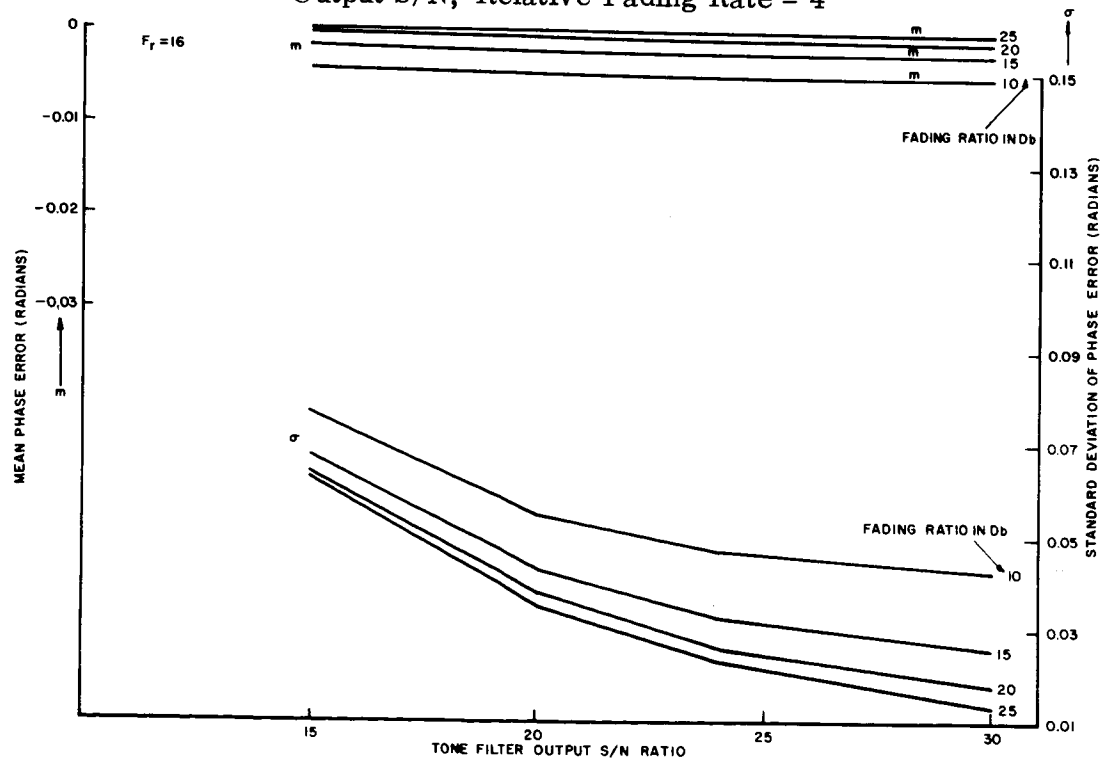

Figure 6-71. Mean and Standard Deviation of Phase Error vs. Tone Filter Output S/N, Relative Fading Rate = 16

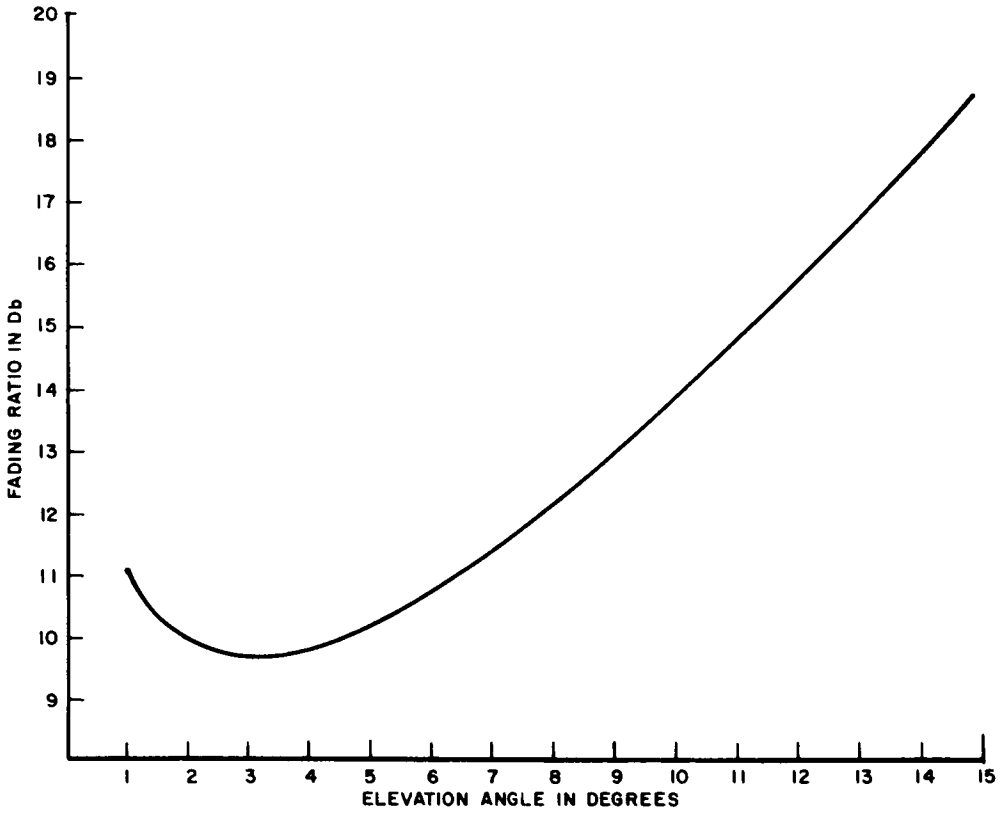

Figure 6-72. Fading Ratio vs. Elevation Angle

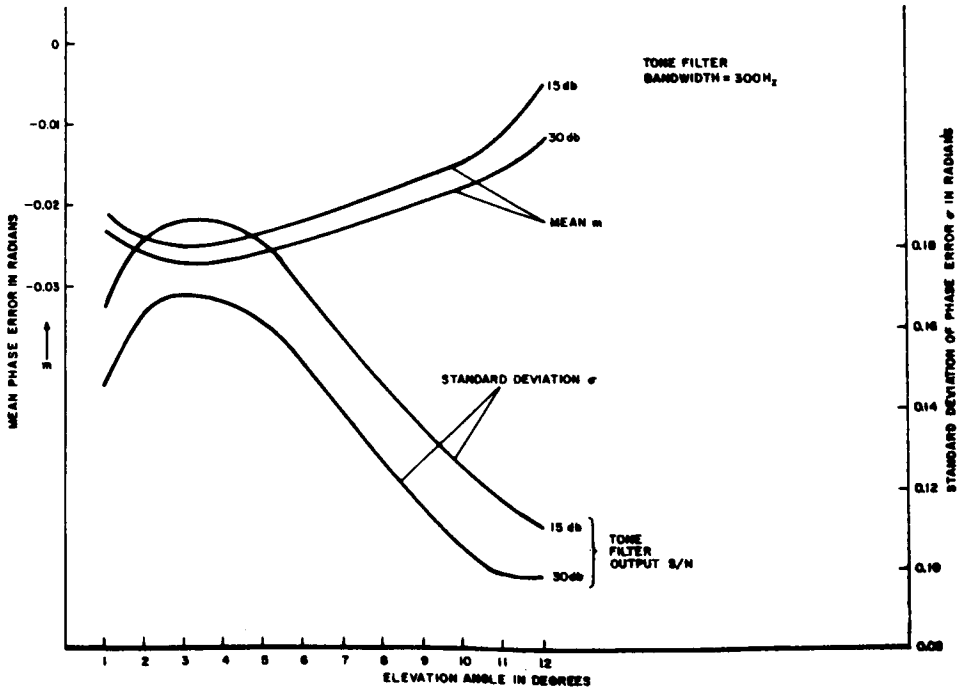

Figure 6-73. Mean and Standard Deviation of Phase Error vs. Elevation Angle, Tone Filter Output S/N = 15, 30 dB

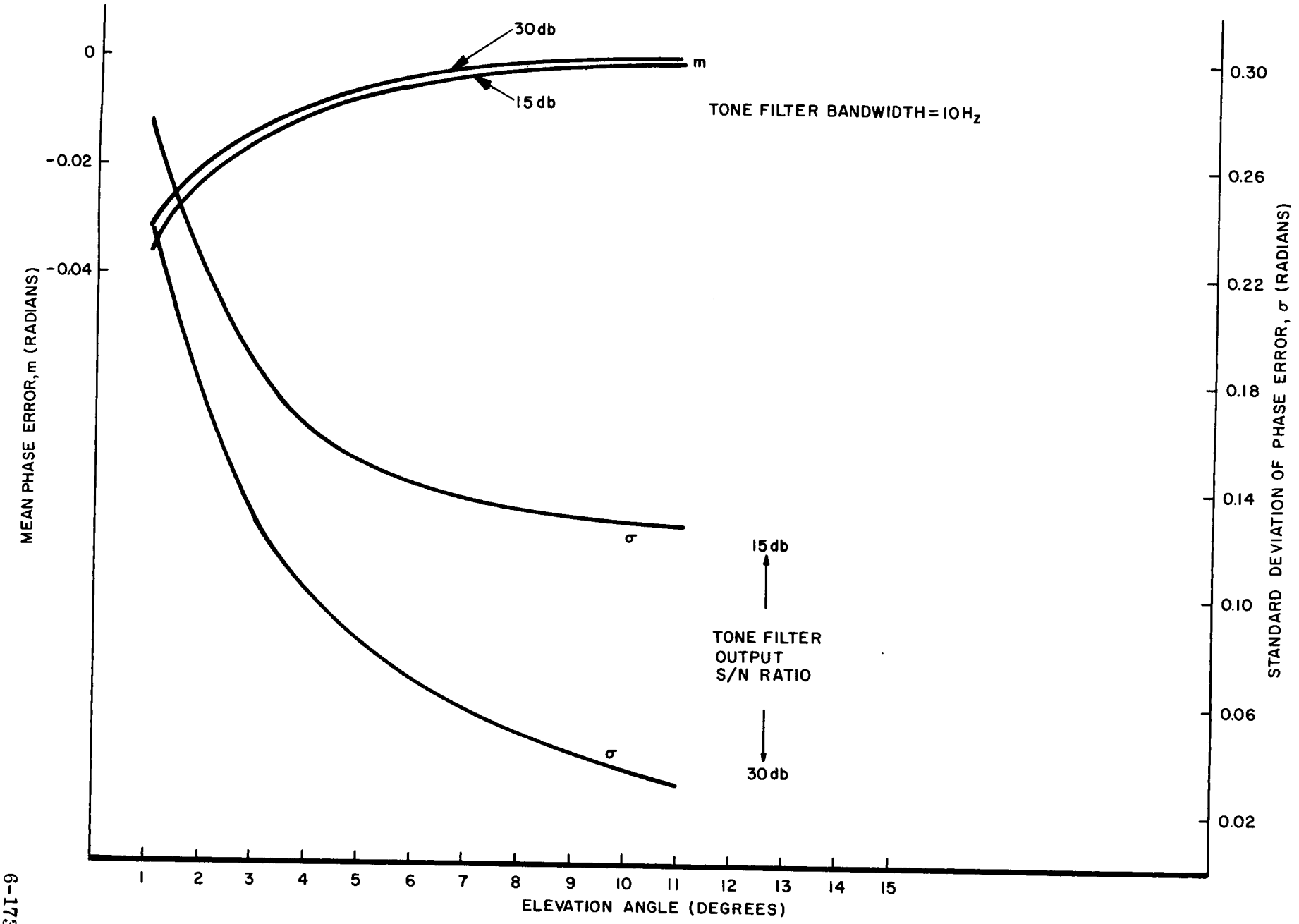

Figure 6-74. Mean and Standard Deviation of Phase Error vs. Elevation Angle

6.4.4 NOISE AND MULTIPATH SUMMARY

Formulae have been derived for the phase errors for each of the nine cases summarized in Table 6-10. The mean, standard deviation and probability distribution function of these phase errors have been estimated using a digital computer based on random samples of size 100. It has been found that the phase errors for signal-to-noise ratios greater than or equal to 10 dB are approximately normally distributed regardless of fading ratio and fading rate. Therefore, the mean and standard deviation of the phase error together with the normal distribution provide a complete description of the phase error statistics due to noise and multipath.

Tables 6-16 through 6-20 summarize the derived phase error formulae. Tables 6-21 to 6-44 contain sets of computed values of the mean and standard deviation of the range error in meters. Each table covers relative fading rates F_r equal to 0, 0.5, 1, 2, 4, 8, 16 and 32, and fading ratios corresponding to values of $10 \log_{10} (\gamma^2/2)$ equal to 10, 15, 20 and 25. As defined previously, the relative fading rate is the ratio of the half-power point bandwidth of the power spectrum of the random component of the received fading carrier to the bandwidth of the loop filter or tone filter. The fading ratio γ is defined to be the ratio of the amplitude of the direct component to the standard deviation of the random component. There are 24 tables in all, covering 4 tone filter output signal-to-noise ratios 15, 20, 24 and 30 dB and 6 tone frequencies: 3.125 kHz, 100 kHz, 9.375 kHz, 300 kHz, 31.25 kHz and 1 MHz. One can think of the 100 kHz, 300 kHz and 1 mHz frequencies as possible fine tones, and the frequencies 3.125 kHz, 9.375 kHz and 31.25 kHz as coarse tones of frequency equal to 1/32 of the fine tone frequency.

The computed values are based on formula C_{33} in Table 6-16. This formula assumes that the signal-to-noise ratio is large enough so that the contribution of the phase jitter at the VCO output will have a relatively small effect on the phase tone filter output signal phase. Table 6-19 contains more exact formulae which don't make this assumption. However, no computations have been made with them, since the analysis indicates that the assumption is reasonable for the large signal-to-noise ratios at which a precision navigation system must operate.

Comparison of the various phase error formulae in Table 6-16 should be helpful. For a white noise channel, the phase error formulae are all of the same form. Their statistical properties are determined by the normalized inphase and quadrature components of the tone filter output noise, I_c and I_S. For large tone filter output signal-to-noise ratios, the approximation $\text{Aratan}(x) \approx x$ can be used to show the phase errors to be approximately normally distributed.

Table 6-17 gives explicit formulae for the tone filter output S/N for each of the nine cases as a function of the tone modulation indices m_j, the ratio of the IF bandwidth W_{IF} to the j-th tone filter bandwidth W_{oj}, and the IF output carrier-to-noise power ratio $(C/N)_{IF}$. The output signal-to-noise ratio for the bandpass-filter extracted-carrier case contains a degradation factor K_j which depends upon the carrier-to-noise ratio ρ_B at the filter output, on the modulation indices, and on the ratio of the carrier extraction filter bandwidth W to the tone filter bandwidth W_{oj}.

TABLE 6-16. SUMMARY OF FORMULAE FOR PHASE ERRORS; CASES Cij

Channel \ Demodulator	Homodyne Detector (Assuming Carrier Frequency and Phase Synchronization)	Bandpass Filter Extracted Carrier	Phase-Lock Demodulator
White Noise	C_{11} $\text{Arctan}\left\{\frac{I_c}{\sqrt{2S_j}+I_s}\right\}$	C_{12} $\text{Arctan}\left\{\frac{I_c}{\sqrt{2(\frac{S}{N})_{oj}}+I_s}\right\}$	C_{13} $\text{Arctan}\left\{\frac{I_c}{\sqrt{2S_j}\cos\Delta\theta + I_s}\right\}$ I_c and I_s are normalized inphase and quadrature components of the tone filter output noise. They are independent and normal with unit variance.
One Specular Reflection + White Noise	C_{21} Same as C_{23} with VCO phase jitter equal to zero	C_{22} $\text{Arctan}\left\{\frac{I_c - U}{V + I_s}\right\}$ $U = \frac{1}{d}\left(R\cos\theta_{10} + R^2\right)\sin(\omega_j\Delta_1)$ $V = \frac{1}{d}\left[1 + R\cos\theta_{10} + (R\cos\theta_{10} + R^2)\cos(\omega_j\Delta_1)\right]$ $d = \frac{1+R}{\sqrt{2S_s}} + \frac{1}{\sqrt{S_o}}$	C_{23} $\text{Arctan}\left\{\frac{I_c - Rg_1\sqrt{2S_j}\sin(\omega_j\Delta_1)}{\sqrt{2S_j}\left[g_o + Rg_1\cos(\omega_j\Delta_1)\right] + I_s}\right\}$ $\begin{cases} g_1 = \frac{1}{D}\left[R\cos\Delta\theta + \cos(\Delta\theta - \theta_{10})\right] \\ g_o = \frac{1}{D}\left[\cos\Delta\theta + R\cos(\Delta\theta - \theta_{10})\right] \\ D = (1 + R^2 + 2R\cos\theta_{10})^{\frac{1}{2}};\ \theta_{10} = (\omega_c + \Delta\omega)\Delta_1 \end{cases}$
Diffuse Multipath + White Noise	C_{31} Same as C_{33} with zero phase jitter	C_{32} $\text{Arctan}\left\{\frac{I_c - X}{Y + I_s}\right\}$ $X = \frac{1}{\gamma L}\left(R\cos\theta_1 + \frac{\beta R R_o}{\gamma_j}\right)\sin\theta_2$ $Y = \frac{1}{L}\left[1 + \frac{\beta R_o\cos\theta_1}{\gamma_j} + \left(R\cos\theta_2 + \frac{RR_o\beta}{\gamma_j}\right)\frac{\cos\theta_2}{\gamma}\right]$ $L = \frac{1+\frac{\beta R_o}{\gamma_j}}{\sqrt{2S_s}} + \frac{1}{\sqrt{S_o}}$; $\beta = \sqrt{\frac{W}{B_F}}$ $\gamma_j = \gamma\left[H\left(\frac{\sqrt{2\ln 2}}{F_{rj}}\right)\right]^{-\frac{1}{2}}$	C_{33} (neglecting VCO phase jitter); (See Table 5.4-11 for more general formulae) $\text{Arctan}\left\{\frac{I_c + \frac{\sqrt{2S_j}}{\gamma}h(F_{rj})x}{\sqrt{2S_j} + I_s + \frac{\sqrt{2S_j}}{\gamma}h(F_{rj})y}\right\}$ $\begin{cases} h(F_{rj}) = \sqrt{2}\left[H\left(\frac{\sqrt{2\ln 2}}{F_{rj}}\right)\right]^{\frac{1}{2}} \\ H(z) = \int_{-z}^{z}\frac{1}{\sqrt{2\pi}}e^{-u^2/2}\,du \end{cases}$ x,y are independent normal random variables with zero mean and unit variance. F_{rj} = Relative Fading Rate = $\frac{B_F}{\omega_{oj}}$

TABLE 6-17. SUMMARY OF SIGNAL-TO-NOISE RATIO PARAMETERS USED IN TABLE

Channel \ Demodulator	Homodyne Detector (Assuming Carrier Frequency and phase Synchronization)	Bandpass Filter Extracted Carrier	Phase-Lock Demodulator
White Noise	C_{11} ρ_j defined as in C_{13}	C_{12} $\left(\frac{S}{N}\right)_{oj} = K_j \rho_j$ $K_j = \begin{cases} \left[1+\frac{1}{2\rho_B}+\frac{W}{W_{oj}}\left(J_0(m_k)J_1(m_j)\right)^2\right]^{-1}; \frac{W_{oj}}{W} \neq 1 \\ \left[1+\frac{1}{2\rho_B}+\left(J_0(m_k)J_1(m_j)\right)^2\right]^{-1}; \frac{W_{oj}}{W} \leq 1 \end{cases}$ ρ_B = Carrier-to-noise ratio at bandpass filter output	C_{13} $\rho_j = 2 J_0^2(m_k) J_1^2(m_j) \frac{W_{IF}}{W_{oj}} \left(\frac{C}{N}\right)_{IF}$ $k \neq j = 1, 2$
One Specular Reflection + White Noise	C_{21} ρ_j as in C_{23} $R = \frac{\text{Reflected Signal Amplitude}}{\text{Desired Signal Amplitude}}$	C_{22} $\rho_o = 2 K_j^* \rho_j$ K_j^* as in C_{12} with the 1 replaced by $1/1+R^2$ R as in C_{21} ρ_B as in C_{12} ρ_j as in C_{23}	C_{23} $\rho_j = 2 J_0^2(m_k) J_1^2(m_j) \frac{W_{IF}}{W_{oj}} \left(\frac{C}{N}\right)_{IF,o}$ $\left(\frac{C}{N}\right)_{IF,o}$ = Ratio of desired signal carrier power to random noise power at IF output. R, as in C_{21}
Diffuse Multipath + White Noise	C_{31} Same as C_{33}	C_{32} ρ_B as in C_{12} $\rho_o = 2 K_j' \rho_j$ K_j' as in C_{12} with the 1 replaced by $\left(1+\frac{R}{\gamma}\right)^{-2}$ R has p.d.f. $f(x) = x e^{-x^2/2}; x \geq 0$ γ as in C_{33} ρ_j as in C_{23}	C_{33} ρ_j, as in C_{23} $\gamma = \frac{\text{Amplitude of Direct Signal Component}}{\text{Standard Deviation of Diffuse Signal Component}}$

TABLE 6-18. SUMMARY OF FORMULAE FOR PHASE ERRORS, CASE C_{33}
NONSELECTIVE FADING, NEGLIGIBLE DIFFERENTIAL PHASE DELAYS

Slow Fading	$\text{Arctan}\left\{\dfrac{I_c - X}{Y\sqrt{2\rho_j} + I_s}\right\}$ $\begin{cases} X = \dfrac{\sqrt{2\rho_j}}{M}\left[\dfrac{R^2}{\gamma^2}\cos\Delta\theta + \dfrac{R}{\gamma}\cos(\Delta\theta - \theta_1)\right]\sin\theta_2 \\ Y = \dfrac{1}{M}\left\{\cos\Delta\theta + \dfrac{R}{\gamma}\cos(\Delta\theta - \theta_1) + \left[\dfrac{R^2}{\gamma^2}\cos\Delta\theta + \dfrac{R}{\gamma}\cos(\Delta\theta + \theta_1)\right]\cos\theta_2\right\} \\ M = \left(1 + \dfrac{R^2}{\gamma^2} + \dfrac{2R}{\gamma}\cos\theta_1\right)^{\frac{1}{2}} \end{cases}$
Intermediate and Fast Fading	$\text{Arctan}\left\{\dfrac{I_c - U}{V\sqrt{2\rho_j} + I_s}\right\}$ $\begin{cases} U = \dfrac{R}{\gamma_j}\sqrt{2\rho_j}\cos(\Delta\theta - \theta_1)\sin\theta_2 \\ V = \cos\Delta\theta + \dfrac{R}{\gamma_1}\cos(\Delta\theta - \theta_1)\cos\theta_2 \end{cases}$ For both cases: $\begin{cases} \theta_i \text{ are independent random phases} \\ R \text{ has p.d.f. } p(x) = xe^{-x^2/2} \\ \Delta\theta \text{ is normally distributed with zero mean, } \sigma^2_{\Delta\theta} = \dfrac{1}{2\rho_L} \\ \rho_L \text{ Loop Filter output S/N} \end{cases}$ $\gamma_j = \gamma\left[H\left(\dfrac{\sqrt{2k_2}}{F_{rj}}\right)\right]^{-\frac{1}{2}}$; $\rho_j = 2J_0^2(m_k)J_1^2(m_j)\dfrac{W_{IF}}{W_{oj}}\left(\dfrac{C}{N}\right)_{IF}$ $H(z) = \int_{-z}^{z}\dfrac{1}{\sqrt{2\pi}}e^{-\frac{x^2}{2}}dx$; $F_{rj} = \dfrac{B_F}{W_{oj}}$

TABLE 6-19. SUMMARY OF FORMULAE FOR PHASE ERRORS, CASE C_{33} RANDOM DIFFERENTIAL PHASE DELAYS

Slow Fading

$$\text{Arctan}\left\{\frac{I_c + X}{Y\sqrt{2\rho_j} + I_s}\right\}$$

$$X = \frac{\sqrt{2\rho_j}}{\gamma}\left(x_1 \cos\beta^* + x_2 \sin\beta^*\right)$$

$$Y = \left(\cos\theta + \frac{x_4}{\gamma}\right)\cos\beta^* + \left(\sin\theta + \frac{x_3}{\gamma}\right)\sin\beta^*$$

$\left\{\begin{array}{l} x_i \text{ are normal with zero mean, variance } 1/2 \\ y_i \text{ are normal with zero mean, unit variance} \\ \theta \text{ is a random phase angle} \end{array}\right.$

$$\sin\beta^* = \frac{1}{D}\left(\sin\theta + \frac{y_2}{\gamma} + r_L y_5\right) \quad ; \quad \cos\beta^* = \frac{1}{D}\left(\cos\theta + \frac{y_1}{\gamma} + r_L y_6\right)$$

$$D^2 = \left(\sin\theta + \frac{y_2}{\gamma} + r_L y_5\right)^2 + \left(\cos\theta + \frac{y_1}{\gamma} + r_L y_6\right)^2$$

$$r_L = \frac{1}{\sqrt{2\rho_{DL}}} \quad ; \quad \rho_j = 2 J_0^2(m_k) J_1^2(m_j) \frac{W_{IF}}{W_{oj}} \left(\frac{C}{N}\right)_{IF}$$

$$\rho_{DL} = 2 J_0^2(m_k) J_1^2(m_j) \frac{W_{IF}}{B_L} \left(\frac{C}{N}\right)_{IF}$$

Fast and Intermediate Fading

$$\text{Arctan}\left\{\frac{I_c + U}{V\sqrt{2\rho_j} + I_s}\right\}$$

$\left\{\begin{array}{l} U = \dfrac{\sqrt{2\rho_j}}{\gamma} h(F_{rj}) I_{cr} \\ V = \dfrac{1}{\gamma} h(F_{rj}) I_{sr} + \cos(\beta^* - \theta_0) \end{array}\right.$

$$\beta^* = \text{Arctan}\left\{\frac{\sin\theta_0 + \frac{1}{\gamma_L} I_{SFL} + r_L I_{SL}}{\cos\theta_0 + \frac{1}{\gamma_L} I_{CFL} + r_L I_{CL}}\right\}$$

I_{cr}, I_{sr}, I_C, I_S, I_{CFL}, I_{SFL}, I_{CL}, I_{SL} are all independent normal random variables with zero mean and unit variance.

θ_0 is uniformly distributed.

$$r_L = \frac{1}{\sqrt{2\rho_{DL}}}$$

$$\gamma_L = \gamma\left[H\left(\frac{\sqrt{2\ln 2}}{F_{rj}}\right)\right]^{-\frac{1}{2}}$$

$$H(z) = \int_{-z}^{z} \frac{1}{\sqrt{2\pi}} e^{-x^2/2}\,dx \quad ; \quad F_{rj} = \frac{B_L}{W_{oj}}$$

For large S/N: $\cos(\beta^* - \theta_0) \approx 1 + \Delta\theta$; $\Delta\theta$, normal with zero mean and variance $\sigma^2_{\Delta\theta} \approx \frac{1}{2\rho_{DL}}$

TABLE 6-20. CONDITIONS FOR LINEAR PHASE-LOCK LOOP OPERATION; CASE C_{33}

B_F = Fading Bandwidth B_L = Fading Bandwidth Slow Fading $B_F = 0$	Assume linear loop operation for loop filter output S/N greater than 10db $P = P_r\left\{\frac{S}{N}\,db > 10\right\} = Q\left(\gamma, \gamma\sqrt{\frac{10}{\rho_{DL}}}\right)$ (Marcum's Q-function) $\rho_{DL} = 2J_0^2(m_k)J_1^2(m_j)\frac{W_{IF}}{B_L}\left(\frac{C}{N}\right)_{IF}$
Intermediate Fading	$P = P_r\left\{\frac{S}{N}\,db > 10\right\} = 1 - exp - \left[\frac{\gamma_L^2}{20}\left(1 - \frac{10}{\rho_{DL}}\right)\right]$ $\gamma_L = \gamma\left[H\left(\sqrt{\frac{2\ln 2}{F_{rL}}}\right)\right]^{-\frac{1}{2}}$; $H(z) = \int_{-z}^{z}\frac{1}{\sqrt{2\pi}}e^{-\frac{x^2}{2}}dx$ $F_{rL} = \frac{\text{Fading Bandwidth}}{\text{Loop Filter Bandwidth}}$; $\gamma = \frac{\text{Desired Signal Carrier Amplitude}}{\text{Standard Deviation of Random Component}}$
Fast Fading B_F B_L	Multipath Treated as Random Noise , since it has larger bandwidth than loop filter. ρ_L = Loop Filter Output S/N $= \frac{\rho_{DL}}{1 + \frac{2\rho_{DL}}{\gamma^2}H\left(\sqrt{\frac{2\ln 2}{F_{rL}}}\right)}$ $H(z) = \int_{-z}^{z}\frac{1}{\sqrt{2\pi}}e^{-x^2/2}dx$; $F_{rL} = \frac{\text{Fading Bandwidth}}{\text{Loop Filter Bandwidth}}$

TABLE 6-21. MEAN AND STANDARD DEVIATION OF RANGE ERROR IN METERS VERSUS FADING RATIO, AND RELATIVE FADING RATE; TONE FILTER OUTPUT S/N = 15 db; TONE FREQUENCY = 3.125 kHz

$\frac{\sigma^2}{2}$ in db / F_r	10	15	20	25
0	m = -734 σ = 5560	-370 3560	-178 2580	-76 2160
0.5	-728 5520	-364 3540	-174 2560	-74 2160
1	-626 4960	-312 3240	-146 2440	-58 2100
2	-452 4020	-224 2800	-100 2240	-34 2020
4	-306 3220	-144 2420	-58 2100	-12 1980
8	-194 2680	-86 2200	-28 2000	6 1940
16	-122 2340	-46 2060	-4 1960	18 1920
32	-70 2140	-18 2000	12 1940	28 1920

TABLE 6-22. MEAN AND STANDARD DEVIATION OF RANGE ERROR IN METERS VERSUS FADING RATIO, AND RELATIVE FADING RATE; TONE FILTER OUTPUT S/N = 15 db; TONE FREQUENCY 9.375 kHz.

$\frac{r^2}{\bar{r}^2}$ in db. / F_r	10	15	20	25
0	m = -244 σ = 1854	-124 1186	-60 860	-26 720
0.5	-242 1838	-122 1178	-58 856	-24 720
1	-208 1652	-104 1084	-48 814	-20 702
2	-150 1338	-74 932	-34 748	-12 676
4	-102 1072	-48 808	-20 700	-4 658
8	-64 892	-28 732	-8 670	2 648
16	-40 780	-16 688	-1 654	6 642
32	-24 716	-6 664	4 644	8 638

TABLE 6-23. MEAN AND STANDARD DEVIATION OF RANGE ERROR IN METERS VERSUS FADING RATIO, AND RELATIVE FADING RATE; TONE FILTER OUTPUT S/N = 15 db; TONE FREQUENCY = 31.25 kHz

in db

F_r	10	15	20	25
0	m = -73.4	-37.0	-17.8	-7.6
	σ = 556	356	258	216
0.5	-72.8	-36.4	-17.4	-7.4
	552	354	256	216
1	-62.6	-31.2	-14.6	-5.8
	496	324	244	210
2	-45.2	-22.4	-10.0	-3.4
	402	280	224	202
4	-30.6	-14.4	-5.8	-1.22
	322	242	210	198
8	-19.4	-8.6	-2.8	0.62
	268	220	200	194
16	-12.2	-4.6	-0.30	1.84
	234	206	196	192
32	-7.0	-1.84	1.22	2.8
	214	200	194	192

TABLE 6-24. MEAN AND STANDARD DEVIATION OF RANGE ERROR IN METERS VERSUS FADING RATIO, AND RELATIVE FADING RATE; TONE FILTER OUTPUT S/N = 15 db; TONE FREQUENCY = 100 kHz.

$\frac{\chi^2}{\sigma^2}$ in db / F_r	10	15	20	25
0	m = -23.0 σ = 173.8	-11.56 111.2	-5.54 80.6	-2.38 67.6
0.5	-22.8 172.4	-11.36 110.4	-5.44 80.4	-2.30 67.4
1	-19.58 155.0	-9.74 101.6	-4.58 76.4	-1.82 65.8
2	-14.14 125.4	-6.98 87.2	-3.16 70.2	-1.06 63.4
4	-9.56 100.4	-4.48 75.8	-1.82 65.6	-0.38 61.6
8	-6.12 83.6	-2.68 68.6	-0.86 62.8	0.20 60.8
16	-3.82 73.0	-1.44 64.6	-0.10 61.4	0.58 60.2
32	-2.20 67.0	-0.58 62.2	0.38 60.4	0.86 59.8

TABLE 6-25. MEAN AND STANDARD DEVIATION OF RANGE ERROR IN METERS VERSUS FADING RATIO, AND RELATIVE FADING RATE; TONE FILTER OUTPUT S/N = 15 db; TONE FREQUENCY = 300 kHz.

σ_z^2 in db / F_r	10	15	20	25
0	m = -7.64 σ = 58.0	-3.86 37.0	-1.84 26.8	-0.80 22.4
0.5	-7.58 57.4	-3.78 36.8	-1.82 26.8	-0.76 22.4
1	-6.52 51.6	-3.24 33.8	-1.52 25.4	-0.60 22.0
2	-4.72 41.8	-2.32 29.2	-1.04 23.4	-0.36 21.2
4	-3.18 33.4	-1.50 25.2	-0.60 21.8	-0.12 20.6
8	-2.04 27.8	-0.88 22.8	-0.28 21.0	0.06 20.2
16	-1.28 24.4	-0.48 21.6	-0.04 20.4	0.20 20.0
32	-0.74 22.4	-0.20 20.8	0.12 20.2	0.28 19.8

TABLE 6-26. MEAN AND STANDARD DEVIATION OF RANGE ERROR IN METERS VERSUS FADING RATIO, AND RELATIVE FADING RATE; TONE FILTER OUTPUT S/N = 15 db; TONE FREQUENCY = 1 MHz.

$\frac{\gamma^2}{2}$ in db / F_r	10	15	20	25
0	m = -2.30 σ = 17.38	-1.156 11.12	-0.156 8.06	-0.238 6.76
0.5	-2.28 17.24	-1.136 11.04	-0.544 8.04	-0.230 6.74
1	-1.958 15.50	-0.974 10.16	-0.458 7.64	-0.182 6.58
2	-1.414 12.54	-0.698 8.72	-0.316 7.02	-0.106 6.34
4	-0.956 10.04	-0.448 7.58	-0.182 6.56	-0.038 6.16
8	-0.612 8.36	-0.268 6.86	-0.086 3.28	0.020 6.08
16	-0.382 7.30	-0.144 6.46	-0.010 6.14	0.058 6.02
32	-0.220 6.70	-0.058 6.22	0.038 6.04	0.086 5.98

TABLE 6-27. MEAN AND STANDARD DEVIATION OF RANGE ERROR IN METERS VERSUS FADING RATIO, AND RELATIVE FADING RATE; TONE FILTER OUTPUT. S/N = 20 db; TONE FREQUENCY = 3.125 kHz.

F_r \ $\frac{\gamma^2}{2}$ in db	10	15	20	25
0	m = -770 σ = 5200	-400 3100	-204 1980	-100 1440
0.5	-764 5160	-398 3080	-204 1960	-100 1420
1	-660 4580	-342 2760	-174 1800	-86 1360
2	-486 3600	-250 2240	-126 1540	-58 1240
4	-336 2720	-172 1780	-82 1340	-36 1160
8	-226 2100	-112 1480	-52 1220	-18 1120
16	-150 1680	-74 1300	-30 1140	-6 1080
32	-98 1400	-42 1180	-12 1100	-4 1080

TABLE 6-28. MEAN AND STANDARD DEVIATION OF RANGE ERROR IN METERS VERSUS FADING RATIO, AND RELATIVE FADING RATE; TONE FILTER OUTPUT S/N = 20 db; TONE FREQUENCY = 9.375 kHz.

F_r \ $\frac{\gamma^2}{2}$ in db.	10	15	20	25
0	m = -256 σ = 1734	-134 1034	-68 660	-34 476
0.5	-254 1718	-132 1024	-68 656	-34 476
1	-220 1526	-114 922	-58 604	-28 452
2	-162 1198	-84 746	-42 516	-20 414
4	-112 906	-58 596	-28 448	-12 388
8	-76 698	-38 494	-18 406	-6 372
16	-50 558	-24 432	-10 380	-2 362
32	-32 470	-14 396	-4 368	-1.0 358

TABLE 6-29. MEAN AND STANDARD DEVIATION OF RANGE ERROR IN METERS VERSUS FADING RATIO, AND RELATIVE FADING RATE; TONE FILTER OUTPUT S/N = 20 db; TONE FREQUENCY = 31.25 kHz.

F_r \ $\frac{\gamma^2}{2}$ in db.	10	15	20	25
0	m = -77.0 σ = 520	-40.0 310	-20.4 198	-10.0 144
0.5	-76.4 516	-39.8 308	-20.4 196	-10.0 142
1	-66.0 458	-34.2 276	-17.4 180	-8.6 136
2	-48.6 360	-25.0 224	-12.6	-5.8 124
4	-33.6 272	-17.2 178	-8.2 134	-3.6 116
8	-22.6 210	-11.2 148	-5.2 122	-1.84 112
16	-15.0 168	-7.4 130	-3.0 114	-0.60 108
32	-9.8 140	-4.2 118	-1.22 110	-0.30 108

TABLE 6-30. MEAN STANDARD DEVIATION OF RANGE ERROR IN METERS VERSUS RATIO, AND RELATIVE FADING RATE; TONE FILTER OUTPUT S/N = 20 db; TONE FREQUENCY = 100 kHz.

F_r \ $\frac{\gamma^2}{2}$ in db	10	15	20	25
0	m = -24.0 σ = 162.6	-12.52 97.0	-6.40 61.8	-3.16 44.6
0.5	-23.8 161.2	-12.42 96.0	-6.40 61.6	-3.16 44.6
1	-20.6 143.2	-10.70 86.4	-5.44 56.6	-2.68 42.4
2	-15.18 112.4	-7.84 70.0	-3.92 48.4	-1.82 38.8
4	-10.50 85.0	-5.34 55.8	-2.58 42.0	-1.14 36.2
8	-7.06 65.4	-3.54 46.4	-1.62 38.0	-0.58 34.8
16	-4.68 52.1	-2.30 40.4	-0.96 35.8	-0.20 34.0
32	-3.06 44.0	-1.34 37.2	-0.38 34.2	-0.10 33.6

TABLE 6-31. MEAN AND STANDARD DEVIATION OF RANGE ERROR IN METERS VERSUS FADING RATIO, AND RELATIVE FADING RATE; TONE FILTER OUTPUT S/N = 20 db; TONE FREQUENCY = 300 kHz.

F_r	$\frac{S}{N}$ in db 10	15	20	25
0	m = -8.02 σ = 54.2	-4.16 32.4	-2.14 20.6	-1.04 14.8
0.5	-7.96 53.8	-4.14 32.0	-2.14 20.4	-1.04 14.8
1	-5.88 47.8	-3.56 28.8	-1.82 18.84	-0.88 14.0
2	-5.06 37.4	-2.60 23.2	-1.30 16.2	-0.60 13.0
4	-3.50 28.4	-1.78 18.6	-0.86 14.0	-0.38 12.0
8	-2.36 21.8	-1.18 15.4	-0.54 12.6	-0.20 11.6
16	-1.56 17.4	-0.76 13.6	-0.32 12.0	-0.06 11.4
32	-1.02 14.6	-0.44 12.4	-0.12 11.4	-0.04 11.2

TABLE 6-32. MEAN AND STANDARD DEVIATION OF RANGE ERROR IN METERS VERSUS FADING RATIO, AND RELATIVE FADING RATE; TONE FILTER OUTPUT. S/N = 20 db; TONE FREQUENCY = 1 MHz.

F_r	$\frac{\gamma^2}{\Xi}$ in db 10	15	20	25
0	m = -2.40 = 16.26	-1.252 9.70	-0.640 6.18	-0.316 4.46
0.5	-2.38 16.12	-1.242 9.60	-0.640 6.16	-0.316 4.46
1	-2.06 14.32	-1.070 8.64	-0.544 5.66	-0.268 4.24
2	-1.518 11.24	-0.784 7.00	-0.392 4.84	-0.182 3.88
4	-1.050 8.50	-0.534 5.58	-0.258 4.20	-0.114 3.62
8	-0.706 6.54	-0.354 4.64	-0.162 3.80	-0.058 3.48
16	-0.468 5.22	-0.230 4.04	-0.096 3.58	-0.020 3.40
32	-0.306 4.40	-0.134 3.72	-0.038 3.44	-0.010 3.36

TABLE 6-33. MEAN AND STANDARD DEVIATION OF RANGE ERROR IN METERS VERSUS FADING RATIO, AND RELATIVE FADING RATE, TONE FILTER OUTPUT S/N = 24 dB; TONE FREQUENCY = 3.125 kHz

UPPER ENTRY = MEAN, M
LOWER ENTRY = STANDARD DEVIATION, σ

F_r \ $\frac{\lambda^2}{2}$ in db	10	15	20	25
0	-786 5080	-412 2960	-316 1780	-114 1160
0.5	-780 5040	-410 2940	-214 1760	-114 1140
1	-676 4460	-354 2600	-186 1580	- 94 1060
2	-498 3460	-262 2060	-138 1300	- 70 920
4	-348 2560	-184 1560	- 94 1040	- 46 820
8	-238 1900	-122 1220	- 62 880	- 28 740
16	-162 1440	- 82 980	- 40 789	- 16 700
32	-106 1120	- 56 840	- 24 740	- 6 680

TABLE 6-34. MEAN AND STANDARD DEVIATION OF RANGE ERROR IN METERS VERSUS FADING RATIO, AND RELATIVE FADING RATE; TONE FILTER OUTPUT S/N = 24 dB; TONE FREQUENCY = 9.375 kH_Z

UPPER ENTRY = MEAN, M
LOWER ENTRY = STANDARD DEVIATION, σ

F_r \ $\frac{\gamma^2}{2}$ in db	10	15	20	25
0	-262	-138	- 72	- 38
	1696	986	592	386
0.5	-230	-136	- 72	- 38
	1680	976	588	382
1	-226	-118	- 62	- 32
	1488	870	330	354
2	-166	- 88	- 46	- 24
	1154	684	432	308
4	-116	- 62	- 32	- 16
	854	522	350	270
8	- 80	- 40	- 20	- 10
	632	406	296	248
16	- 54	- 28	- 14	- 6
	478	330	262	236
32	- 36	- 18	- 8	- 2
	376	282	244	230

TABLE 6-35. MEAN AND STANDARD DEVIATION OF RANGE ERROR IN METERS VERSUS FADING RATIO, AND RELATIVE FADING RATE; TONE FILTER OUTPUT S/N = 24 dB; TONE FREQUENCY = 31.25 kH_z

UPPER ENTRY = MEAN, M
LOWER ENTRY = STANDARD DEVIATION, σ

F_r \ $\frac{\chi^2}{2}$ in db	10	15	20	25
0	-78.6 303	-41.2 296	-21.6 178	-11.4 116
0.5	-78.0 504	-41.0 294	-21.4 176	-11.4 114
1	-67.6 446	-35.4 260	-18.6 158	- 9.4 106
2	-49.8 346	-26.2 206	-13.8 130	- 7.0 92
4	-34.8 256	-18.4 156	- 9.4 104	- 4.8 82
8	-23.8 190	-12.2 122	- 6.2 88	- 2.8 74
16	-16.2 141	- 8.2 98	- 4.0 78	- 1.52 70
32	-10.6 112	- 5.6 84	- 2.4 74	- 0.62 68

TABLE 6-36. MEAN AND STANDARD DEVIATION OF RANGE ERROR IN METERS VERSUS FADING RATIO, AND RELATIVE FADING RATE; TONE FILTER OUTPUT S/N = 24 dB; TONE FREQUENCY = 100 kH_z

UPPER ENTRY = MEAN, M
LOWER ENTRY = STANDARD DEVIATION, σ

F_r \ $\frac{\gamma^2}{2}$ in db	10	15	20	25
0	-24.6 159.0	-12.90 92.4	-6.78 55.4	-3.54 36.0
0.5	-24.4 157.6	-12.80 91.6	-6.68 55.0	-3.54 35.8
1	-21.2 139.6	-11.08 81.6	-5.82 49.6	-2.96 33.2
2	-15.56 108.2	- 8.22 64.2	-4.30 40.4	-2.20 28.8
4	-10.88 80.2	- 5.72 48.8	-2.96 32.8	-1.44 25.4
8	- 7.44 59.2	- 3.82 38.0	-1.90 27.6	-0.86 23.2
16	- 5.06 44.8	- 2.58 30.8	-1.24 24.6	-0.48 22.2
32	- 3.34 35.2	- 1.72 26.4	-0.76 22.8	-0.20 21.4

TABLE 6-37. MEAN AND STANDARD DEVIATION OF RANGE ERROR IN METERS VERSUS FADING RATIO, AND RELATIVE FADING RATE; TONE FILTER OUTPUT S/N = 24 dB; TONE FREQUENCY = 300 kH_z

UPPER ENTRY = MEAN, M
LOWER ENTRY = STANDARD DEVIATION, σ

F_r \ $\frac{\lambda^2}{2}$ in db	10	15	20	25
0	-8.18 53.0	-4.30 30.8	-2.26 18.4	-1.08 12.0
0.5	-8.12 52.6	-4.26 30.6	-2.22 18.4	-1.18 12.0
1	-7.04 46.6	-3.70 27.2	-1.94 16.6	-0.98 11.0
2	-5.18 36.0	-2.74 21.4	-1.44 13.4	-0.74 9.6
4	-3.62 26.8	-1.90 16.2	-0.98 11.0	-0.48 8.4
8	-2.48 19.8	-1.28 12.6	-0.64 9.2	-0.28 7.8
16	-1.68 15.0	-0.86 10.2	-0.42 8.2	-0.16 7.4
32	-1.12 11.8	-0.58 8.8	-0.26 7.6	-0.06 7.2

TABLE 6-38. MEAN AND STANDARD DEVIATION OF RANGE ERROR IN METERS VERSUS FADING RATIO, AND RELATIVE FADING RATE; TONE FILTER OUTPUT S/N = 24 dB; TONE FREQUENCY = 1 MH_Z

UPPER ENTRY = MEAN, M
LOWER ENTRY = STANDARD DEVIATION, σ

F_r \ $\frac{\chi^2}{2}$ in db	10	15	20	25
0	-2.46 15.90	-1.290 9.24	-0.678 5.54	-0.354 3.60
0.5	-2.44 15.76	-1.280 9.16	0.668 5.50	-0.354 3.58
1	-2.12 13.96	-1.108 8.16	-0.582 4.96	-0.296 2.32
2	-1.556 10.82	-0.822 6.42	-0.430 4.04	-0.220 2.88
4	-1.088 8.02	-0.572 4.88	-0.296 3.28	-0.144 2.54
8	-0.744 5.92	-0.382 3.80	-0.190 2.76	-0.086 2.32
16	-0.506 4.48	-0.258 3.08	-0.124 2.46	-0.048 2.22
32	-0.334 3.52	-0.172 2.64	-0.076 2.28	-0.020 2.14

TABLE 6-39. MEAN AND STANDARD DEVIATION OF RANGE ERROR IN METERS VERSUS FADING RATIO, AND RELATIVE FADING RATE; TONE FILTER OUTPUT S/N = 30 dB; TONE FREQUENCY = 3.125 kHz.

$\frac{\gamma^2}{2}$ in db / F_r	10	15	20	25
0	m = -798 σ = 5020	-422 2880	-226 1660	-122 980
0.5	-792 4980	-418 2860	-224 1640	-120 980
1	-688 4400	-364 2520	-196 1460	-104 880
2	-510 2380	-272 1940	-146 1140	-76 700
4	-358 2480	-190 1440	-100 860	-56 560
8	-248 1780	-132 1060	-70 660	-36 460
16	-168 1300	-92 780	-46 520	-24 400
32	-116 960	-60 600	-30 440	-16 360

TABLE 6-40. MEAN AND STANDARD DEVIATION OF RANGE ERROR IN METERS VERSUS FADING RATIO, AND RELATIVE FADING RATE; TONE FILTER OUTPUT S/N - 30 dB; TONE FREQUENCY = 9.375 kHz.

$\frac{\gamma^2}{2}$ in db / F_r	10	15	20	25
0	m = -266 σ = 1672	-140 958	-76 554	-40 328
0.5	-264 1658	-140 950	-74 548	-40 324
1	-228 1464	-122 840	-64 488	-34 292
2	-170 1128	-90 650	-48 380	-26 236
4	-120 824	-64 478	-34 288	-18 188
8	-82 596	-44 352	-24 220	-12 154
16	-56 432	-30 262	-16 176	-8 136
32	-38 318	-20 202	-10 146	-4 124

TABLE 6-41. MEAN AND STANDARD DEVIATION OF RANGE ERROR IN METERS VERSUS FADING RATIO, AND RELATIVE FADING RATE; TONE FILTER OUTPUT S/N = 30 dB; TONE FREQUENCY - 31.25 kHz.

F_r \ σ_z^2 in db	10	15	20	25
0	m = -79.8	-42.2	-22.6	-12.2
	σ = 502	288	166	98
0.5	-79.2	-41.8	-22.4	-12.0
	498	286	164	98
1	-68.8	-36.4	-19.6	-10.4
	440	252	146	88
2	-51.0	-27.2	-14.6	-7.6
	338	194	114	70
4	-35.8	-19.0	-10.0	-5.6
	248	144	86	56
8	-34.8	-13.2	-7.0	-3.6
	178	106	66	46
16	-16.8	-9.2	-4.6	-2.4
	130	78	52	40
32	-11.6	-6.0	-3.0	-1.52
	96	60	44	36

TABLE 6-42. MEAN AND STANDARD DEVIATION OF RANGE ERROR IN METERS VERSUS FADING RATIO, AND RELATIVE FADING RATE; TONE FILTER OUTPUT S/N = 30 dB; TONE FREQUENCY = 100 kHz.

$\frac{\gamma^2}{2}$ in db / F_r	10	15	20	25
0	m = -25.0 σ = 156.8	-13.18 89.8	-7.06 52.0	-3.82 30.8
0.5	-24.8 155.4	-13.08 89.2	-6.96 51.4	-3.72 30.4
1	-31.4 137.4	-11.36 78.8	-6.12 45.8	-3.24 27.4
2	-15.94 105.8	-8.50 61.0	-4.58 35.6	-2.38 22.0
4	-11.18 77.4	-5.92 44.8	-3.16 27.0	-1.72 17.58
8	-7.74 55.8	-4.10 33.0	-2.20 20.6	-1.14 14.52
16	-5.26 40.4	-2.86 24.6	-1.44 16.42	-0.76 12.70
32	-3.62 29.8	-1.92 19.0	-0.96 13.76	-0.48 11.56

TABLE 6-43. MEAN AND STANDARD DEVIATION OF RANGE ERROR IN METERS VERSUS FADING RATIO, AND RELATIVE FADING RATE; TONE FILTER OUTPUT S/N = 30 dB; TONE FREQUENCY = 300 kHz.

$\frac{\gamma^2}{2}$ in db / F_r	10	15	25	25
0	m = -8.32 σ = 52.2	-4.40 30.0	-2.36 17.4	-1.28 10.2
0.5	-8.24 51.8	-4.36 29.6	-2.32 17.2	-1.24 10.2
1	-7.16 45.8	-3.78 26.2	-2.04 15.2	-1.08 9.2
2	-5.32 35.2	-2.84 20.4	-1.52 12.0	-0.80 7.4
4	-3.72 25.8	-1.98 15.0	-1.04 9.0	-0.58 5.8
8	-2.58 18.6	-1.36 11.0	-0.74 6.8	-0.38 4.8
16	-1.76 13.6	-0.96 8.2	-0.48 5.4	-0.26 4.2
32	-1.20	-0.64	-0.32	-0.16

TABLE 6-44. MEAN AND STANDARD DEVIATION OF RANGE ERROR IN METERS VERSUS FADING RATIO, AND RELATIVE FADING RATE; TONE FILTER OUTPUT S/N = 30 dB; TONE FREQUENCY = 1 MHz

$\frac{\gamma^2}{2}$ in db / F_r	10	15	20	25
0	m = -2.50 σ = 15.68	-1.318 8.98	-0.706 5.20	-0.382 3.08
0.5	-2.48 15.54	-1.308 8.92	-0.696 5.14	-0.372 3.04
1	-2.14 13.74	-1.136 7.88	-0.612 4.38	-0.324 2.74
2	-1.594 10.58	-0.850 6.10	-0.458 3.56	-0.238 2.20
4	-1.118 7.74	-0.592 4.48	-0.316 2.70	-0.172 1.758
8	-0.774 5.58	-0.410 3.30	-0.22- 2.06	-0.114 1.452
16	-0.526 4.04	-0.286 2.46	-0.144 1.642	-0.076 1.270
32	-0.362 2.98	-0.192 1.900	-.096 1.376	-0.048 1.156

The difference between the phase-lock demodulator phase error formula, and the other 2 white noise cases in Table 6-16 is embodied in the phase jitter term cos $\Delta\theta$. For large loop filter output signal-to-noise ratios ρ_L, this quantity has mean approximately equal to $1 - \frac{1}{4\rho_L}$, and variance approximately equal to $1/8\ \frac{2}{L}$. Therefore, its effect on the phase errors for large loop filter output signal-to-noise ratios must be small.

When there is a specular multipath component, the second row of Table 6-16 gives the appropriate phase error formulae. For the phase-lock demodulator, formula C_{32} gives the phase error as a function of ρ_j as defined in cell C_{23} of Table 6-17, in terms of the phase-lock loop VCO phase jitter $\Delta\theta$, in terms of the phase difference θ_{10} between the direct signal carrier and the specular reflection, and in terms of the multipath ratio R. The quantity R is the ratio of the amplitude of the reflected component to the amplitude of the direct component. The phase difference θ_{10} equals the product of the received IF carrier frequency, and the differential time delay Δ_1, between the direct and the reflected component. An explicit formula for Δ_1, is given in Section 6.3 as a function of aircraft velocity and the transmitter-receiver geometry. When the multipath ratio R goes to zero, phase error formula C_{23} reduces to formula C_{13} as one would expect.

Case C_{21} refers to an ideal situation when carrier frequency and phase synchronization is available, in which case, phase-error formula C_{21} corresponds to C_{23} with the VCO phase jitter taken to be zero. Phase error formula C_{22} is in the same form as C_{23}. The signal-to-noise ratio parameters ρ_B and ρ_O are defined in Table 6-17. The factor K_j^* reduces to K_j in formula C_{12}, when the multipath ratio R goes to zero.

In the diffuse multipath case, C_{31} corresponds to C_{33}, since the VCO phase jitter was neglected. As mentioned previously, Table 6-19 gives the corresponding formula for C_{33} when the phase jitter is not neglected. Formula C_{33} is based on a random distribution of differential multipath phase delays. Formula C_{32} is based on a non-selective fading model which assumes the differential multipath phase delays to be negligible. Table 6-18 summarizes the corresponding phase error formulae for this fading model. The quantities R and R_o in formula C_{32} are correlated Rayleigh random envelope variables with joint probability density

$$p(R, R_o) = \frac{R_o R}{1-r^2}\ I_o\left(\frac{rR_oR}{1-r^2}\right)\ \exp\left[-\frac{R_o^2 + R^2}{2(1-r^2)}\right]$$

When r equals unity, $R = R_o$. The correlation coefficient r can be approximated by:

$$r = \begin{cases} 1; W \geq B_F; W = \text{Filter Bandwidth} \\ \sqrt{\frac{W}{B_F}}\ ;\ W < B_F; B_F = \text{Fading Bandwidth} \end{cases}$$

The correlation coefficient r is between the normalized bandpass filter output fading envelope R_o, and normalized filter input fading envelope R. The signal-to-noise ratio ρ_o is defined in Table 6-17. The factor K_j' is a random variable depending upon the random fading envelope R. As γ approaches infinity, K_j' approaches in formula C_{12}.

Table 6-18 summarizes the phase error formula for case C_{33}, for slow fading and non-slow-fading for the nonselective fading model, assuming negligible differential phase delays. The quantity R is a Rayleigh distributed envelope variable. θ is the phase-lock loop VCO phase jitter I_c and I_s are normalized random noise inphase and quadrature components. The parameter ρ_j is the j^{-th} tone filter output S/N. γ refers to the fading ratio at the output of the carrier narrow band filter. As γ approaches infinity, the formulae in C_{33} reduce to that in C_{13}, as one would expect.

Table 6-19 summarizes a corresponding set of formulae assuming random differential multipath phase delays. It is believed that this model is more valid than the previous one. The computed phase errors from Table 6-19 are larger than those from Table 6-18. Therefore, the random phase model is more conservative. The quantities F_{rj} in Table 6-19 are the relative fading rates for the j^{-th} tone filter output. The quantity γ_L is the fading ratio corresponding to the loop filter output.

Table 6-20 summarizes the conditions employed in the analysis of case C_{33} for the assumption of the linear phase-lock loop model. It is based on a minimum of 10 dB signal-to-noise ratio at the loop filter output. In the slow and intermediate fading cases, formulae are given for the probability of having at least 10 dB loop filter output S/N. In the fast fading case, an expression is given for the loop filter output signal-to-noise ratio as a function of the fading ratio γ, and as a function of the relative fading rate F_{rL} at the loop filter output.

6.5 COMPARISON OF FOUR PHASE DETECTORS IN WHITE NOISE

The following four phase detectors have been analyzed: (1) positive-slope zero-crossing, (2) limiter-multiplier, (3) quadrature, and (4) product demodulator envelope division phase detector. Details of the analysis are presented in Appendix 6H.

The comparative analysis is made for a two-noisy-channel input to each phase detector. Under the assumption of additive noise, the phase difference between the two signal components can only be estimated. The mean and variance of the estimate of phase difference is obtained under the assumption of high signal-to-noise ratios on the inputs.

6.5.1 SUMMARY

The inputs to each phase detector are two noisy signals which can be denoted by:

$$x_1(t) = A_1 \cos(\omega_o t + \theta) + n_1(t)$$

$$x_2(t) = A_2 \cos(\omega_o t + \theta + \varphi) + n_2(t) \quad (1)$$

The difference between the two phase angles is defined to be $+\varphi$. Since additive white noise is present, the difference in phase angles can only be estimated. This estimate will be indicated by $\hat{\varphi}$.

Table 6-45 lists the expectation and variance of the estimate of phase difference for the four phase detectors and shows the block diagrams.

TABLE 6-45. MEAN (EXPECTATION) AND VARIANCE FOR FOUR PHASE DETECTORS

SCHEMATIC	EXPECTATION	VARIANCE
	POSITIVE SLOPE ZERO CROSSING	
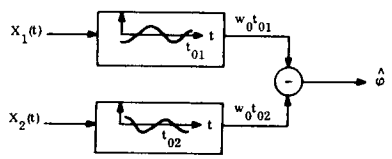	$\phi_{\text{mod}} \pm 2\pi$	Variance $\frac{1}{2}\left[\frac{1}{(S/N)_1} + \frac{1}{(S/N)_2}\right]$
	LIMITER - MULTIPLIER	
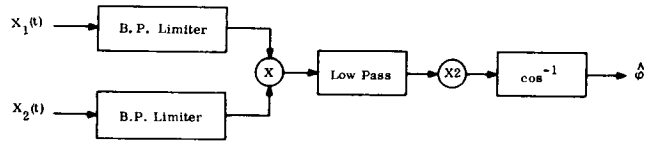	$\phi_{\text{mod}} \pm 2\pi + \frac{\tan\frac{\phi}{2}}{2}\left[\frac{1}{(S/N)_1} + \frac{1}{(S/N)_2}\right]$	$\frac{(\cos\phi - 1)^2\left[\frac{1}{(S/N)_1} + \frac{1}{(S/N)_2}\right]}{2\sin^2\phi - 2(\cos^2\phi + \cos\phi)\left[\frac{1}{(S/N)_1} + \frac{1}{(S/N)_2}\right]}$
	QUADRATURE	
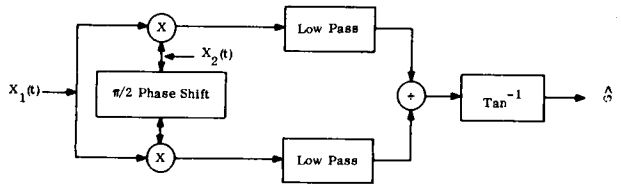	$\phi_{\text{mod}} \pm 2\pi$	$\frac{1}{2}\left[\frac{1}{(S/N)_1} + \frac{1}{(S/N)_2}\right]$
	PRODUCT - DEMODULATOR ENVELOPE DIVISION	
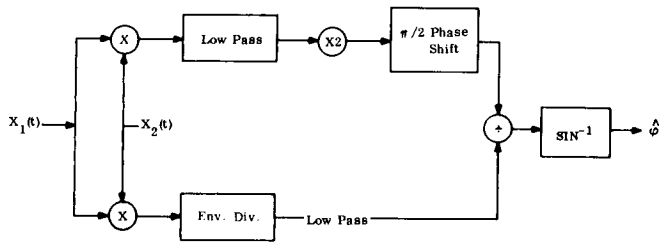	$\phi_{\text{mod}} \pm 2\pi \pm \frac{\tan}{2}\phi\left[\frac{1}{(S/N)_1} + \frac{1}{(S/N)_2}\right]$	$\frac{\tan^2\phi\left[\frac{1}{(S/N)_1} + \frac{1}{(S/N)_2}\right]}{2 + 2\tan^2\phi\left[\frac{1}{(S/N)_1} + \frac{1}{(S/N)_2}\right]}$

6.5.2 CONCLUSIONS

If we assume the existence of the variance, the Cramér-Rao inequality can be used in the parameter estimation process; i.e., it will yield a lower bound on the variance of $\hat{\phi}$, the estimate of the difference in phase angles. It can be shown that, if the estimate is unbiased, the minimum variance for the estimate of phase angle for a single noisy channel is one-half times the reciprocal of the signal-to-noise ratio.

If we assume the two inputs are uncorrelated (as they will be if they originate from two different satellites) and the estimates are unbiased, the minimum variance of $\hat{\varphi}$ is

$$\sigma^2_{\min}\ (\hat{\varphi}) = \frac{1}{2}\left[\frac{1}{(S/N)_1} + \frac{1}{(S/N)_2}\right] \tag{2}$$

The minimum variance is attained by both the positive-slope zero-crossing and quadrature phase detectors under the assumption of high signal-to-noise ratios.

The limiter-multiplier and product-demodulator envelope division phase detectors both break down for phase differences equal to an integer multiple of π.

We observe that in the limiter-multiplier phase detector, a phase shift of $\pi/2$ following the bandpass-limiter application to input $x_2(t)$ necessitates an arc-sine transformation in order to obtain the estimate $\hat{\phi}$. This may be more applicable for small $\hat{\phi}$.

6.6 SUMMARY AND ERROR BUDGET

The previous subsections have detailed all the error sources and explained the behavior of the errors as functions of many parameters.

In this section, all these errors will be combined into a single range error, for a representative set of parameters.

6.6.1 EQUIPMENT ERRORS*

The equipment errors can be predicted as follows:

I. Errors at the Control Center

A. Transmitter	Mean error (meters)	Standard deviation (meters)
1. Atomic reference	negligible	negligible
2. Tone modulator	negligible	negligible
3. Power amplifier	negligible	negligible
4. Antenna and coupler	negligible	negligible

*For certain items the errors are negligibly small, however the intent of including the items is to assure the reader that they have not been overlooked.

		Mean error (meters)	Standard deviation (meters)
B.	Receiver		
1.	Predetection filtering	negligible	negligible
2.	Injection oscillators	negligible	negligible
3.	Demodulator circuitry	negligible	1 meter
4.	Post-demodulator circuitry	negligible	1 meter

II. Errors at the Satellite Transponder

		Mean error (meters)	Standard deviation (meters)
1.	RF circuitry	negligible	negligible
2.	Injection sidestop oscillator	0.8 meter	negligible
3.	IF filters	0.8 meter	1.5 meters
4.	Power amplifier	negligible	negligible
5.	Antenna and coupler	negligible	negligible

III. Errors at the User

		Mean error (meters)	Standard deviation (meters)
A.	Receiver		
1.	Predetection filtering	negligible	negligible
2.	Injection oscillators	0.7 meter	negligible
3.	Demodulator circuitry	0.7 meter	2 meters
4.	Post-demodulation circuitry	1 meter	2 meters
B.	Transmitter		
1.	Modulator	1 meter	1 meter
2.	Power amplifier	negligible	negligible
3.	Antenna and Coupler	negligible	negligible

All these errors result in a combined one-way mean-square-error of 17.51 square meters. In an operational system this error could be reduced by calibration procedures.

6.6.2 ATMOSPHERIC REFRACTION ERRORS

As has been shown in Section 6.3.2, the atmospheric refraction range error is a function of the elevation angle of the satellite relative to the user. Depending upon the user sophistication, one can minimize the range error due to refraction by introducing corrections which depend upon: satellite elevation angle, user approximate position, time and date, solar activity, etc. Unfortunately, at present, we do not have sufficient

satellite-to-ground propagation data to construct a reasonable range error corrector. All indications are that such a corrector is possible and it is only a matter of time to accumulate sufficient data.

With the presently available data the curves of Figures 6-27 and 6-28 were prepared. These curves represent all conditions with the minimum and maximum electron content representing extreme values of the range error. When no corrections are made, the range error can vary from less than 1 foot to as much as 300 feet. With the corrections, the upper bound of the error can be reduced to less than 150 feet. The variation with elevation angle is due to the fact that at lower elevation angles the propagation path is much larger, as can be seen from Figure 6-12.

In lieu of a true statistical model, we construct a model on the observation that extreme values (Figures 6-27, 6-28) for the range error are symmetrically located on a logarithmic scale. Assuming the random process to be logarithmic normally distributed, and further assuming that the extreme values correspond to the 1% and 99% probability we can construct Table 6-46 with the values of range errors and the corresponding mean and standard deviation for the case of refraction errors with corrections as shown in Figure 6-28.

The tropospheric range error is shown in Figure 6-29. Here again, the data available is given in terms of extremes. However, with knowledge of the surface conditions, i.e. atmospheric pressure, water vapor and temperature, one can correct for it leaving an uncertainty of ±50' at 1° elevation angle. Table 6-47 shows the mean and standard deviation of the error after a correction has been applied. This correction is based on average surface conditions and could be further refined in an operational system. For this model the geometric mean of the two extremes was subtracted and assuming that the remaining error is uniformly distributed between the two extremes given, from where the mean and standard deviation were computed.

6.6.3 NOISE AND MULTIPATH ERRORS

The Link Analysis (Section 6.3.9) has shown that the S/N ratio at the output of the tone filter is 24 dB for an assumed fine tone frequency of 300 kHz and a filter bandwidth of 1 Hz. Now since the fading rate

$$F_r = \frac{\text{Multipath Fading Bandwidth}}{\text{Tone Filter Bandwidth}}$$

then for the intended filter with bandwidth of 1 Hz,

$$F_r = \text{Multipath Fading Bandwidth}$$

Table 6-37 shows the mean and rms errors in the phase measurement following this filter. The errors are given as a function of the fading rate Fr, and fading ratio $\gamma^2/2$ which is the ratio of direct signal strength to multipath signal strength. (Both the fading rate and fading ratio were shown in Section 6.3.3 to depend on the elevation angle at the user.)

These results allow the computation of Table 6-48 and Figure 6-75 which show the behavior of the mean standard deviation and rms errors in meters, as a function of the elevation angle. The table also displays the values of fading rate F_r, fading ratio $\gamma^2/2$, and the mean square error (MSE).

TABLE 6-46. CORRECTED IONOSPHERIC RANGE ERRORS IN METERS AT 1.6 GHz.

Elevation Angle (deg)	Max. Range Error (m)	Nominal Error (m)	Minimum Error (m)	Mean (m)	Std. Dev. (m)	MSE (m)
0	35	3.5	0.35	5.73	7.4	87.6
1	34	3.4	0.34	5.57	7.2	84.2
2	33.8	3.38	0.33	5.52	7.14	81.3
3	33.5	3.35	0.33	5.47	7.09	80.1
4	32.9	3.29	0.32	5.30	7.0	77.0
5	32.2	3.22	0.32	5.28	6.83	74.4
6	31.6	3.16	0.31	5.17	6.70	71.5
7	30.4	3.04	0.30	4.93	6.44	65.7
8	29.2	2.92	0.29	4.79	6.2	61.3
9	28.6	2.86	0.28	4.67	6.05	58.3
10	27.4	2.74	0.27	4.48	5.8	53.5
11	25.8	2.58	0.25	4.24	5.47	47.6
12	24.4	2.44	0.24	3.98	5.17	42.5
13	23.7	2.37	0.23	3.88	5.0	39.9
14	21.9	2.19	0.21	3.58	4.65	34.3
15	19.8	1.98	0.19	3.24	4.2	28.0

6.6.4 SATELLITE POSITION ERRORS

The computation of user position has been seen to depend on his (or the center's) knowledge of the satellites location at the time of fix. Goddard Space Flight Center has estimated that for communication type satellites at synchronous height, its existing network of tracking stations can achieve a 20-meter range measurement; and furthermore, that predictions made on the basis of these measurements about a week or so later, may be in error by 1 kilometer along the orbit.

Taking these estimates at face value, we make the following remarks with respect to the impact of this information on the SPOT system:

(1) The ATC-mode of SPOT operation contemplates a measurement on satellite position every few minutes or so, interlaced with its interrogations of the user field. The continuous freshness of this data is intended to preclude accumulating errors of prediction; that is, the ATC-mode will not predict satellite position (for more than about 10 minutes), it will measure it.

TABLE 6-47. CORRECTED TROPOSPHERIC RANGE ERRORS

Elevation (degrees)	Range Error Bounds (meters)					Range Error Mean and Standard Deviation for Uniformly Distributed Errors (Meters)		MSE (m^2)
	Uncorrected			Corrected				
	Max.	Min.	Geometric Mean	Max. (b)	Min. (a)	Mean $\left(\frac{b+a}{2}\right)$	Std. Dev. $\sqrt{\frac{(b-a)^2}{12}}$	
1	74.7	44.2	57.3	17.4	-13.1	2.1	8.8	81.8
2	48.8	32.0	39.3	9.5	- 7.3	1.1	4.9	25.20
3	36.6	25.0	30.2	6.4	- 5.2	0.6	3.4	11.46
4	29.0	20.0	24.0	4.9	- 4.0	0.5	2.6	6.96
5	23.0	17.0	20.0	3.4	- 2.7	0.3	1.8	3.31
6	20.0	15.0	17.0	2.7	- 2.4	0.15	1.5	2.25
7	17.0	13.0	15.0	2.1	- 1.8	0.15	1.2	1.44
8	15.0	12.0	13.0	2.1	- 1.5	0.30	1.1	1.21
9	13.0	11.0	12.0	1.5	- 1.2	0.15	0.80	0.65
10	12.0	10.0	11.0	1.2	- 0.91	0.15	0.61	0.38
11	11.0	8.8	10.0	1.2	- 1.2	0	0.61	0.37
12	10.0	8.2	8.8	1.2	- 0.61	0.30	0.52	0.36
13	9.4	7.6	8.5	0.91	- 0.91	0	0.52	0.27
14	8.8	7.3	7.9	0.91	- 0.61	0.15	0.43	0.20
15	8.2	6.7	7.3	0.91	- 0.61	0.15	0.43	0.20

TABLE 6-48. RANGE ERRORS DUE TO NOISE AND MULTIPATH*

Elev. Angle (deg)	$\gamma^2/2$ (dB)	F_r	Mean (m)	σ (m)	MSE (m^2)	RMS (m)
1	11.1	7.55	-2.4	19.5	386.01	19.64
2	10.0	15.2	-1.7	15.5	243.01	15.59
3	9.7	22.7	-1.5	14.0	198.25	14.08
4	9.9	30.4	-1.3	11.5	133.24	11.57
5	10.1	37.9	-1.0	10.5	111.25	10.54
6	10.75	45.5	-0.8	10.0	100.64	10.03
7	11.47	53.0	-0.7	8.5	72.74	8.52
8	12.3	60.5	-0.6	7.5	56.61	7.52
9	13.11	68.0	-0.35	7.3	53.41	7.30
10	14.0	75.5	-0.2	6.0	36.04	6.00
11	14.9	83.0	-0.15	5.8	33.66	5.80
12	15.93	90.5	-0.1	5.0	25.01	5.00
13	16.89	97.8	-0.05	5.0	25.00	5.00
14	17.80	105.0	-0.03	4.5	20.25	4.5
15	18.80	112.5	-0.01	4.3	18.49	4.3

*Based on the following conditions:
Tone frequency = 300 kHz
Tone filter Bw = 1 Hz
Output tone filter S/N = 24 dB
Assumptions for the multipath model are given in Sections 6.3.3 and 6.3.4.

(2) The satellite measurements in any region are made from a network of three fixed "users", perhaps unattended ground stations, which on command transpond their ambient field like any other active user. The center treats this data with an inverse of its usual equations, now computing the implied satellite position rather than user position. This procedure results in a real time process which generates satellite data matched to the geodetic base of the region, with respect to which the users are navigating.

(3) The service channel of each satellite carries the gross deghosting tone, time distribution signals, and orbital coefficients. These coefficients are intended for passive users who need recent data for precise navigation. Again, the orbital elements are updated perhaps every 10 minutes at the center, for promulgation into the field of passive users.

(4) There are approximately 1000 ten-minute intervals in a week during which a 15-meter measurement error grows into a 1000-meter prediction error. It is not unreasonable to assume that the rate of error accumulation is larger toward the end of that week than it is at the start of the week. Even so, a

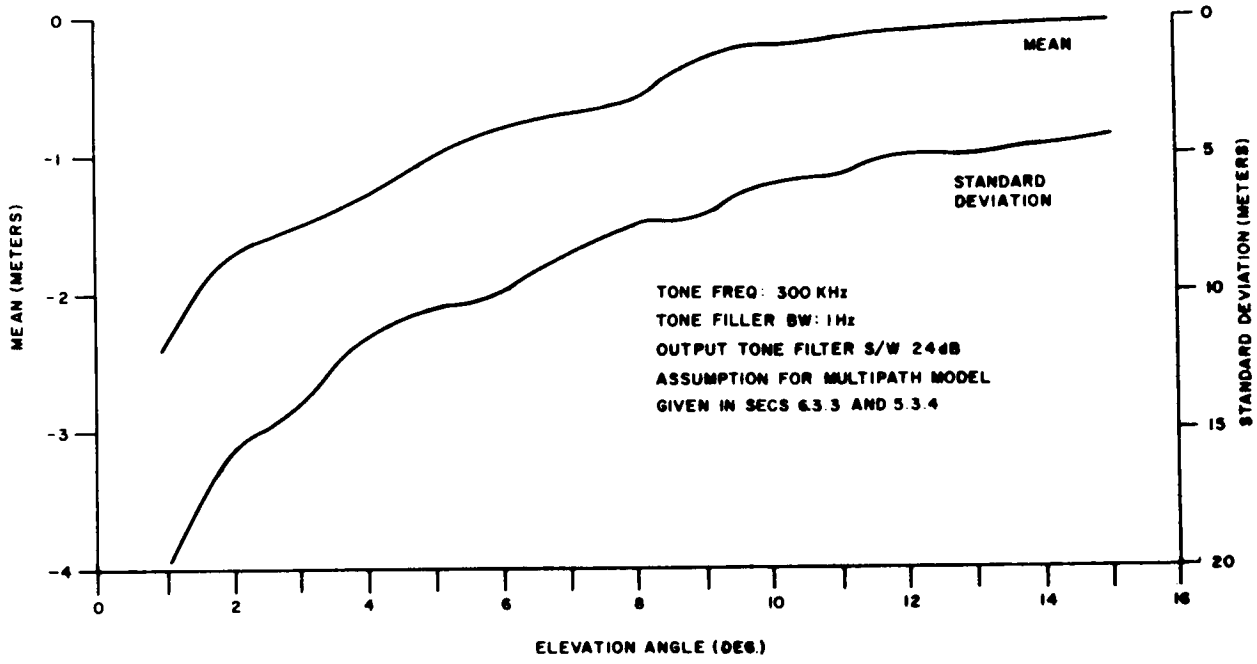

Figure 6-75. Mean and Standard Deviation of Range Error vs Elevation Angle

uniformly prorated rate of error shows a growth of about 1 meter in the first ten minutes after measurement. Hence it is estimated that a ten-minute updating interval is more than sufficient to keep the satellite tracking error in check.

(5) For relative navigation the situation is improved again, for it has been pointed out that satellite position errors tend to cancel, and that the cancellation is more efficient when the relative navigation domain is small compared to the range to the satellite. As an example, consider two points separated by 100 miles each viewing the same satellite about 20,000 miles away. If the satellite position is in error by 1 mile, the maximum error in the difference between the respective ranges is less than one foot. That is, all LOP's in the domain of flight will be translated by virtually the same amount, keeping their relative spacing intact.

6.7 POSITION ERROR SUMMARY

In the previous section a summary of range errors was derived. In this section, performance of the Phase Difference Navigation Satellite system is summarized for both a North Atlantic system and for a Global system. Preliminary conclusions are drawn concerning system performance when operating in a passive navigation mode, traffic control mode, and a relative navigation mode.

6.7.1 TOTAL RANGE ERRORS

Table 6-49 presents a summary of range errors including the effects of instrumentation drift, ionospheric refraction, tropospheric refraction, multipath, noise, and uncertainty in satellite ephemeris. Two cases of ionospheric refraction are considered including an optimistic assumption that ionospheric refraction range delay is distributed in a log-normal distribution and for a conservative assumption that refraction delays are normally distributed. Satellite ephemeris data is assumed to be derived from an external tracking system with the component of satellite position error along the range vector from satellite to user of 20 meters.

6.7.2 POSITION ERRORS

The range errors summarized in Table 6-49 result in horizontal errors in the position of the vehicle, to an extent determined by the relative geometry of vehicle and satellites. Depending on this geometry, the errors are amplified or attenuated, but in either case are referred to as Geometric Dilution of Precision (GDOP). In this view, GDOP is seen to provide error multiplication, and is not in itself a source of error; that is, GDOP does not generate error, it transforms it.

6.7.2.1 ERROR TRANSFORMATION

We have already seen GDOP factors in Section 5 whose inverses are called Fix Confidence Coefficients. These results were developed for a global system of satellites where the user was free to select the most suitable group of satellites for error optimization. Now we consider a situation where two navigation satellites are aloft, placed to favor traffic over the North Atlantic. This configuration may occur in the early stages of a deliberate evolutionary process toward a global system, either by placing two satellites in orbit there, or by seeding only the equatorial orbit, albeit with its full complement.

In this example the North Atlantic satellites are placed in near synchronous orbit above the equator at 10° WL and 70° WL respectively. The airplane is assumed to be flying at 6 nm, and using an antenna whose minimum elevation angle is 5°. The altimeter aboard has an rms height error of about 50 feet.

Figure 6-76 shows the results of parametric runs in the GDOP-program,varying the user's position in latitude and longitude throughout the North Atlantic region. The two cases shown in that figure refer to the assumption of a logarithemic normal distribution of refraction error on the one hand (Case A), and a conventional normal distribution on the other (Case B). While it is true that this figure has assumed a 60° separation between satellites, this is consistent with the standard spacing in the global discussions, and is not far from the optimum spacing indicated by parametric runs previously performed.

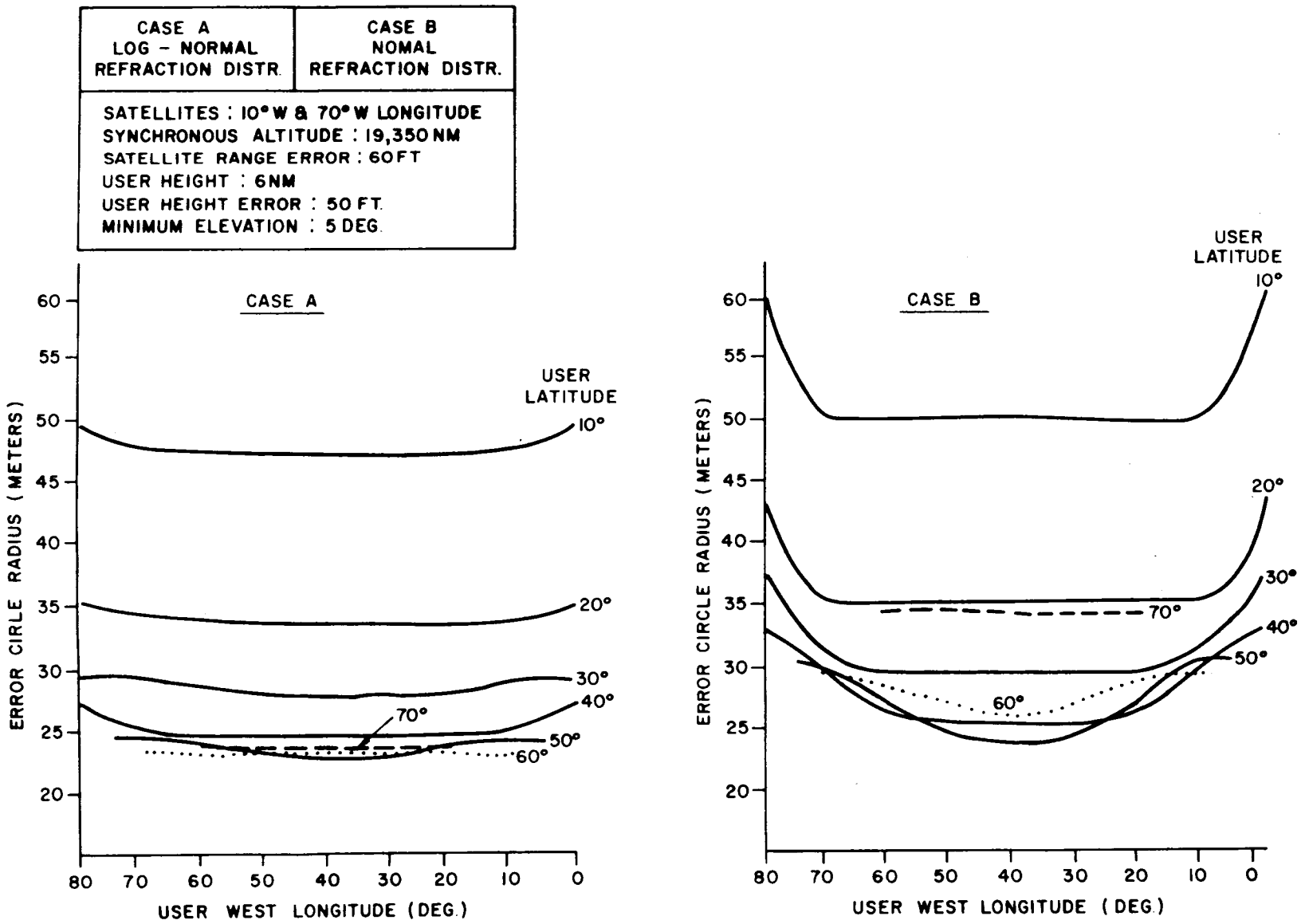

Figure 6-76. Position Error Summary

TABLE 6-49. RANGE ERROR SUMMARY

Elevation Angle (Deg)	Log-Normal Ionosphere Distribution (m^2)	Normal Ionosphere Distribution (m^2)	Troposphere (m^2)	Multipath/ Noise (m^2)	Equipment (m^2)	Satellite Range Error (m^2)	Total	
							Case A Log-Normal RMSE-m	Case B Normal RMSE-m
1	84.2	990.0	81.8	386.01	17.5	400	31.1	43.3
5	74.4	840.0	3.3	111.25	17.5	400	24.6	37.04
10	53.5	604.0	0.4	36.04	17.5	400	22.5	32.5
15	28.1	318.0	0.2	18.49	17.5	400	21.54	27.4
45	5.0	57.4	0	10.0	17.5	400	20.8	22.02
90	1.8	20.7	0	10.0	17.5	400	20.7	21.17

6.7.2.2 PASSIVE MODE

Figure 6-76 shows the behavior of the error circle radius in meters as a function of user longitude, for several latitudes. The radius is the geometric mean between the major and minor semi-axes of the characteristic error ellipse at each location of user.

The most striking feature of the plots is the minimal nature of the errors, even at low latitudes (10°) for the more pessimistic assumption of Case B, where it is less than 55 meters for virtually the full Atlantic reach. In the more heavily travelled lanes (40°, 50° and 60°), the plan-position errors are typically 30 meters or so, in Case B and about 25 meters in Case A.

Notice that the 5° antenna limitation asserts itself in restricting the longitudinal coverage at the higher latitudes, so that at 70° latitude the coverage extends from about 20° WL to 60° WL. Performance in terms of coverage falls off here, indicating the point at which global configurations are justified.

6.7.2.3 AIR TRAFFIC MODE AND RELATIVE NAVIGATION

The results of Figure 6-76 apply in substance to position determination at an ATC center. In Section 4.7 it was pointed out that although the GDOP for two-way navigation is twice as good for the same geometry as one-way (passive) navigation, the range errors are in the order of twice as high, resulting in a virtual stand-off in position error.

Relative navigation on the other hand is expected to result in subtantially reduced errors, especially because the more significant contributors to the range error such as satellite range error and refraction error, are precisely those components which tend to cancel in relative flight. Quantitative investigations of error cancellation in the relative mode are currently in progress. Results of these analyses will be reported in the final report.

Section 7

REFERENCES

The references cited throughout the main text in this document are listed below. References cited in the Appendixes are listed there.

2-1 RCA, "Proposal for Phase Difference Navigation Satellite Experiment Study," DS 105-526-6789, 20 April 1966.

3-1 Final Report of the Ad Hoc Joint Navigation Satellite Committee - May 1966.

3-2 "Predicated Operational Requirements for a Non-Military Traffic Coordination and Navigation Satellite System," NASA Contract No. NASw-809, Final Report, by James W. Campbell.

3-3 K. D. McDonald, et al., "Analysis and Technical Evaluation of Selected Navigation and Communication System Concepts for 1975," March 1966.

3-4 "A Statistical Analysis of the World's Merchant Fleets," December 31, 1964, U. S. Department of Commerce, Maritime Administration.

3-5 "Fishery Statistics of the United States - 1964," Statistical Digest No. 58, U. S. Department of the Interior, Bureau of Commercial Fisheries.

3-6 Personal Communication from Mr. A. Moody and Mr. A. Skaggs of the FAA, Washington, D. C. to Mr. M. Mitchell of RCA.

3-7 Personal Communication from Mr. Charles Kurz of the U. S. Department of Commerce, Maritime Administration, Washington, D. C. to Mr. M. Mitchell of RCA.

3-8 Personal Communication from Mr. Julius Rockwell and Mr. Charles Lyles of the U. S. Department of the Interior, Bureau of Commercial Fisheries, Washington, D. C. to Mr. M. Mitchell of RCA.

3-9 "SST's Time of Decision," Space/Aeronautics, September 1966, p. 22.

3-10 "Concorde Fare Forecast," Aviation Week and Space Technology, December 19, 1966, p. 25.

6-1 T. J. Goblick, Jr., "Navigation with High-Altitude Satellites: A Study of Ranging Errors," MIT Lincoln Laboratory, TN 1966-46, 26 August 1966.

6-2 M. I. Skolnick, Radar Systems, McGraw Hill, 1962, p. 467.

6-3 M. S. Corrington, "Variation of Bandwidth with Modulation Index in Frequency Modulation," Proc. IRE, Vol. 35, No. 10, October 1947, pp. 1013-1020.

6-4 A. J. Viterbi, "Acquisition and Tracking Behavior of Phase-Locked Loops," JPL External Publication, No. 673, July 14, 1959.

6-5 D. Richman, "The O. C. Quadricorrelator: A Two Mode Synchronization System," Hazeltine Report No. 7147, December 29, 1953.

6-6 R. R. Brooks, "Improving the Performance of a Phase Locked Loop Using a Nonlinear Filter and a Sawtooth Phase Comparator, M. S. Thesis, University of Penna., Moore School of Electrical Engineering, May 1964.

6-7 W. B. Davenport, W. L. Root, Random Signals and Noise, McGraw-Hill 1958.

6-8 F. E. Bond, H. F. Meyer, "Fading and Multipath Considerations in Aircraft/Satellite Communications Systems," AIAA, Communications Satellite Systems Conference, Washington, D. C., May 1966, Edited by R. B. Marsten, Academic Press, 1966.

6-9 W. B. Davenport, "Signal-to-Noise Ratios in Bandpass Limiters," J. App. Phys., 24 June 1953, pp. 720-727.

6-10 C. R. Cahn, "Note on Signal-to-Noise Ratios in Bandpass Limiters," IRE Transactions on Information Theory, January 1961, pp. 39-43.

6-11 R. S. Lawrence, C. G. Little, H. J. A. Chivers, "A Survey of Ionospheric Effects Upon Earth-Space Radio Propagation," Proc. IEEE, Jan. '64, pp. 4-27.

6-12 K. Davies, "Ionospheric Radio Propagation," NBS Monograph 80, April 1965.

6-13 R. V. Bhonsle, A. V. daRosa, O. K. Garriott, "Measurements of the Total Electron Content and the Equivalent Slab Thickness of the Mid-Latitude Ionosphere," Radio Science, Journal of Res, NBS/USNC-URSI, Vol. 69D, No. 7, July '65, pp. 929-936.

6-14 K. C. Yeh, B. J. Flaherty, "Ionospheric Electronic Content at Temperate Latitudes During the Declining Phase of the Sunspot Cycle," Journ. of Geophys. Res., Vol. 71, No. 19, Oct. 1, 1966, pp. 4557-4570.

6-15 K. C. Yeh, G. W. Swenson, Jr., "Ionospheric Electron Content and its Variations Deduced from Satellite Observations," Journ. of Geophys. Res., Vol. 66, No. 4, April '61, pp. 1061-1067.

6-16 G. H. Millman, "Atmospheric on Extraterrestrial Effects on Radio Wave Propagation," General Electric Report TISR61EMH29 (G. E. Technical Information Series), June '61.

6-17 Smyth Research Associates, "Tropospheric and Ionospheric Radar Refraction Effects," San Diego, Cal. (Anderson, Weisbrad, Morgan, Fouchs) ASTIA No. AD217406 (probably 1958).

6-18 "Ionospheric Predictions for September '65," Central Radio Propagation Laboratory, NBS No. 30, Issued June '65.

6-19 "Ionospheric Predictions for February '66," CRPL, NBS No. 35, Issued Nov. '65.

6-20 "Ionospheric Predictions for June '67," Institute for Telecommunications Science and Aeronomy (CRPL), ESSA, No. 51, Issued March '67.

6-21 R. S. Lawrence, D. J. Posakony, O. K. Garriott, S. C. Hall, "The Total Electron Content of the Ionosphere at Middle Latitudes near the Peak of the Solar Cycle," Journ. of Geophys. Res., Vol. 68, No. 7, April 1, 1963, pp. 1889-1898.

6-22 A. N. Hunter, A. R. Webster, R. F. Kelleher, P. E. Miall, "Diurnal Variation of Total Electron Content of the Ionosphere over Nairobi," Nature, letters to the editor, Vol. 206, May 29, 1965, pp. 920-921.

6-23 W. J. Ross, L. J. Blumle, "The Distribution of Ionization about the Magnetic Equator," pp. 84-87 in Proceedings of the International Conference on the Ionosphere 1962, Published by the Institute of Physics and the Physical Society, London 1963.

6-24 P. F. Checcacci, "Ionospheric Measurements by Means of the Early Bird Geostationary Satellite," Radio Science, Vol. 1, No. 10, Oct. '66, pp. 1154-1158.

6-25 L. Liszka, "Latitudinal and Diurnal Variations of the Ionospheric Electron Content Near the Auroral Zone in Winter, Radio Science, Vol. 1, No. 10, Oct. '66, pp. 1135-1137.

6-26 D. S. Bond, E. C. Hewitt, "Trip Report to the Institute for Telecommunication Sciences and Aeronomy (ITSA), Boulder, Colorado, January 12 and 13", AED Memorandum for File, Voice Broadcast Mission Study, 18 January 1967.

6-27 J. A. Klobuchar, H. E. Whitney, "Middle-Latitude Ionospheric Total Electron Content: Summer '65," Radio Science, Vol. 1, No. 10, Oct. '66, pp. 1171-1175.

6-28 K. H. Schmelovsky, "Seasonal Variations of Total Electron Content of the Ionosphere During Sunspot Minimum," In "Space Research VI, Proceedings of the Sixth International Space Science Symposium. Mar Del Plata May 11-19. 1965, Organized by Committee on Space Research - COSPAR," Edited by R. L. Smith-Rose. Spartan Books, Washington, Macmillan and Co., London 1966.

6-29 F. deMendonsa, "Ionospheric Electron Content and Variations Measured by Doppler Shifts in Satellite Transmissions," Journal of Geophys. Res., Vol. 67, No. 6, June '62, pp. 2315-2337.

6-30 W. J. Ross, "The Determination of Ionospheric Electron Content from Satellite Doppler Measurements," Journal of Geophys. Res., Vol. 65, No. 9, Sept. '60.

6-31 R. V. Bhonsle, "Diurnal Variation of Large-Scale Irregularities," Journ. of Geophys. Res., Vol. 71. No. 19, Oct. 1, 1966, pp. 4571-4577.

6-32 C. G. Little, R. S. Lawrence, "The Use of Polarization Fading of Satellite Signals to Study the Electron Content and Irregularities in the Ionosphere," Journ. of Res. of NBS-D. Radio Propagation Vol. 64D, No. 4, July-August 1960, pp. 335-345.

6-33 H. C. Ko, "Amplitude Scintillation of Radio Star," Proc. IRE, Vol. 48, No. 11, Nov. '60, pp. 1871-1880.

6-34 J. P. Castelli, J. Aarons, H. M. Silverman, "Ionospheric and Tropospheric Scintillations of a Radio Star at Zero to Five Degrees of Elevation," Journal of Atmospheric and Terrestrial Physics, 1964 Vol. 26, pp. 1197-1213.

6-35 B. R. Bean, G. D. Thayer, "Models of the Atmospheric Radio Refractive Index," Proc. IRE, Vol. 47, No. 5, May '59, pp. 741-755.

6-36 B. R. Bean, G. D. Thayer, "CRPL Exponential Reference Atmosphere, NBS Monograph 4, Oct. 29, 1959.

6-37 R. B. Muchmore, A. D. Wheelon, "Line-of-Sight Propagation Phenomena-I: Ray Treatment," Proc. IRE, Vol. 43, Oct, '55, pp. 1437-1449.

6-38 "Final Report on Phase Stability Studies of Ground-to-Ground Microwave Links," Lower Atmosphere Physics Section, Radio Propagation Engineering Division. NBS Report 6702, June 14, 1960.

6-39 P. Beckmann and A. Spizzichino, The Scattering of Electromagnetic Waves from Rough Surfaces, The MacMillan Co., New York (1963).

6-40 H. Staras: "Multipath Parameters," Internal Memo RCA-AED ODRN TM-5-79, Dec. 28/66.

6-41 H. and B. S. Jeffreys, Methods of Mathematical Physics, Cambridge University Press (1950), sec. 17.04, p. 503.

6-42 Norton, K. A. et al., "Probability Distribution of the Amplitude of a Constant Vector Plus a Rayleigh Distributed Vector," Proc. IRE, October 1955.

6-43 J. R. Wait, Electromagnetic Radiation from Cylindrical Structure, Pergamon Press, N. Y., 1959, pp. 27-28.

6-44 L. F. Gray, "Experimental Performance of the Early Bird Communications System," AIAA Communications Satellite Systems Conference, Washington, D. C., May 2-4, 1966, AIAA Paper No. 66-246.

6-45 A. J. Giger, "4-gc Transmission Degradation Due to Rain at the Andover, Maine, Satellite Station," BSTJ, September 1965, pp. 1528-1533.

6-46 B. C. Blevis, "Losses Due to Rain on Radomes and Antenna Reflecting Surfaces," IEEE Transactions on Antennas and Propagation, January 1965, pp. 175 and 176.

6-47 H. Leaderman and L. A. Turner, "Theory of the Reflection and Transmission of Electromagnetic Waves by Dielectric Materials, Radar Scanners and Radomes," Vol. 26, Rad. Lab. Series, McGraw Hill, 1948, Chapter 12.

6-48 "Climatic Extremes and a 500 Foot Radome," Aerospace Instr. Lab. AFCRL (Technical Report).

6-49 E. H. Grant, et al., "Dielectric Behavior of Water at Microwave Frequencies," The Journal of Chemical Physics, Vol. 26, No. 1, January 1957, pp. 156-161.

6-50 D. C. Hogg and W. W. Mumford, "The Effective Noise Temperature of the Sky," The Microwave Journal, March 1960, pp. 80-84.

6-51 O. M. Salati, "RFI in Satellite Communications Systems," Electronic Industries, April 1960, Table 1 (data interpolated for 1500 mc).

6-52 J. G. Lawton, "Comparison of Binary Data Transmission Systems," Proc. Second Nat'l Conf. on Military Electronics, 1958, p. 56, Fig. 2 and Appendix II (pp. 58-60).

6-53 R. Barber, "Solid-State Devices for Microwave Power Generation," IEEE 1967 Intn'l Solid-State Circuits Convention (U of Penna.), pp. 36-37 (Fig. 2).

6-54 J. A. Develet, "Fundamental Sensitivity Limitation for Second-Order Phase-Lock Loops," AD No. 416683, June, 1961.

6-55 W. A. Edson, "Noise in Oscillators," Proc. IRE, August, 1960.

6-56 A. J. Viterbi, Principles of Coherent Communication, McGraw-Hill, 1966.

6-57 B. M. Oliver, "Automatic Volume Control as a Feedback Problem," Proc. IRE, April 48, pp. 466-473.

APPENDIXES

1A New Technology Appendix

4A Glossary of Navigational Terms and Symbols

4B Position and Uncertainty: The General Solution

6A Homodyne Detector With White Noise (C_{11})

6B Extracted Carrier Demodulation With White Noise (C_{12})

6C Phase-Lock-Loop Carrier Demodulation With White Noise (C_{13}), and a Quadrature Phase Detector

6D Specular Reflection With Phase-Lock Loop Carrier Extraction (C_{23} and C_{21})

6E Extracted Carrier Demodulation With One Specular Reflection (C_{22})

6F Diffuse Multipath Effects With Phase-Lock Loop Carrier Extraction (C_{33} and C_{31}), Assuming Non-Selective Fading With Negligible Differential Multipath Delays

6G Extracted Carrier Demodulation With Diffuse Multipath (C_{32})

6H Comparison of Four Phase Detectors in the Presence of White Noise

Appendix 1A

NEW TECHNOLOGY APPENDIX

After a diligent review of the work performed under this contract, no new innovation, discovery, improvement or invention was made.

Appendix 4A

GLOSSARY OF NAVIGATIONAL TERMS AND SYMBOLS

A -

A double-summation of terms appearing in the general solution of the over-determined case. In particular

$$A = \sum_{i=1}^{N} \sum_{j=1}^{N} 2\Lambda_{ij} \sin \varphi_i \sin \varphi_j$$

A, B, C, etc:

Appearing as a prefix (e.g., A -), suffix (e.g., - A) or subscript (e.g., R_A), these symbols designate the readings and derived quantities associated with a circular-LOP, or a hyperbolic-LOP (i.e., LOP's involving one or two satellites) as the context makes clear.

A_1, A_2

Coefficients appearing in the computation formula for the image-point abscissa, in the baseplane. They mix the residuals linearly to produce x_I. In particular

$$A_1 = - \frac{L_A \cos \varphi_B}{\sin (\varphi_B - \varphi_A)} \quad , \quad A_2 = \frac{L_B \cos \varphi_A}{\sin (\varphi_B - \varphi_A)}$$

Active navigation: -

A system of navigation requiring transmission or retransmission of the navigation signal from the user vehicle, generally to a control center.

Absolute navigation:

A navigation process which generates the vehicle position in terms of a global coordinate system, such as latitude and longitude.

Absolute position:

A statement of position with respect to a global coordinate system, such as latitude and longitude. The absolute position of a vehicle may be derived from its relative position, if the absolute position of the basepoint is known.

Assignable bias, assigned bias:

That contribution to a particular type of bias for which a model exists, on the basis of which estimates may be made on the extent of the bias under actual or anticipated operating conditions.

ATC

Abbreviation for Air Traffic Control. ATC is a large-scale operational procedure whereby the individual flight paths of all participating vehicles in a designated volume of air space are coordinated.

ATC center:

The facilities from which control of the flight pattern in a designated air space is exercised. It generally houses the interrrogation, receiving, and computational facilities indigenous to an active navigation mode.

Automatic navigation:

A navigation procedure in which the input data is processed by computer to produce indications of position and/or velocity.

Azimuth:

The angle to a satellite or extraterrestial object, measured in the horizontal plane, clockwise from true north.

B

(a) A double-summation of terms appearing in the general solution of the overdetermined case, In particular

$$B = \sum_{i=1}^{N} \sum_{j=1}^{N} \Lambda_{ij} \sin (\varphi_i + \varphi_j)$$

(b) The bandwidth at a place given by $B = \lambda_c/G$ where λ_c is the wavelength of the coarse tone, and G is the gradient at the point.

B_1, B_2

Coefficients appearing in the computation formula for the image-point ordinate, in the baseplane. They mix the residuals linearly to produce y_1. In particular

$$B_1 = \frac{L_A \sin \varphi_B}{\sin (\varphi_B - \varphi_A)} \quad , \quad B_2 = - \frac{L_B \sin \varphi_A}{\sin (\varphi_B - \varphi_A)}$$

Back-up oscillator:

An atomic oscillator aboard the satellite, intended to activate automatically on failure of or interference with the ground excitation signal. In an ideal transfer to the satellite's internal oscillator, the navigation signal at the user is undisturbed in phase and frequency, hence the description "fail-soft".

Band

(a) The volume of space enclosed by two successive surfaces of position, each of which is assigned a cardinal number in the coarse-phase field. In hyperbolic system, the central plane hyperboloid is assigned zero, and coarse repetition

intervals are numbered from there. In a circular system, the satellite itself is assigned zero, and coarse-repetition intervals are numbered from that point. In a two-way system, coarse repetition intervals, and hence bands, are halved because of the phase-folding properties of such a system.

(b) The area on a designated surface, such as the earth or a horizontal plane, enclosed between two such SOP's.

Band number:

A serial number desingating the band. The band receives its designation from the algebraically lower number of its two bounding SOP's. See example under LOP-value. Band number is represented by the letter B.

Band-width:

(a) The conventional bandwidth of communications practice.

(b) The width of the band at the user, in the user plane, on the assumption that the user's gradient applies throughout the width. It is designated by the symbol B with appropriate subscripts and is given by $B = \lambda_c/G$ where λ_c is the wavelength of the coarse tone, and G is the gardient.

Base, basepoint:

The point of reference in a navigational situation. It is the point with respect to which LOP-residuals are generated, and from which the resulting LOP-offsets are laid out. In relative navigation, it is therefore the natural point to which the position of the vehicle is referred. In absolute navigation it is the temporary "assumed position: in a particular cycle of computation.

Base accrual:

In zero-start navigation, this is the increment in basepoint geometric accumulated at the basepoint since the start of flight from that point.

Base bias:

The amount by which the (real or conceptual) LOP-reading at a basepoint exceeds the LOP-geometric.

Base-chart:

A graphic aid to the manual navigator. The chart is a scale map of an area showing geographic and flight detail. It carries a compass rose suitable for laying bearing lines for LOP-offsets, and the LOP's are struck directly on the chart. The base chart corresponds more or less to the horizontal extent of the base domain.

Base domain:

The volume of space in the vicinity of a basepoint throughout which the LOP-family parameter values at the basepoint may be assumed to obtain, to give fixes of useful precision. Better precision may be developed by applying one

or more of the less-usual corrections. The horizontal extent of the base domain is generally represented by the base chart. Also, the geographic limits of usefulness of an LOP-almanac correspond to the base domain.

Base excess:

The amount by which the base bias exceeds the assigned bias at that point.

Base geometric:

The reading on an ideal LOP-meter at a basepoint, in the absence of all errors and disturbances.

Baseground:

The point on the local sphere vertically beneath (or above) the basepoint, along the geocentric radius.

Base-LOP:

Thr reading including geometric and bias, on an LOP-meter at the basepoint.

Baseplane:

The geometrically horizontal plane, through the basepoint; that is, the plane perpendicular to the radius from the earth's center.

Base prediction:

The assignable bias at the basepoint.

Bearing:

The angle to a point on or near the earth, measured in the horizontal plane, clockwise from true north.

Bias, bias error:

See long-term error.

Bias correction:

A correction intended to account for all or a particular part of the assignable bias in an LOP-reading.

Bias residual:

That part of a bias error which remains unaccounted for, or which arises in over-accounting for, by a bias correction.

C

A double-summation of terms appearing in the general solution of the over-determined case, In particular

$$C = \sum_{i=1}^{N} \sum_{j=1}^{N} 2\Lambda_{ij} \cos \varphi_i \cos \varphi_j$$

c

When the probability density function of a multi-dimensional normal distribution is written in such a way that the exponent may assume a zero value but no positive value for any arbitrary value of the variate-vector, then the exponent may be written in the form $-c^2/2$. In this formulation, c is an index on the equi-probability elliptical contours characterizing the distribution, and in particular, the Error Ellipse is designated by the value $c = 1$.

C_1, C_2

Coefficients appearing in the computation formula for the A-residual. They mix the image-point coordinates linearly to produce ΔP_A. In particular

$$C_1 = \frac{\sin \varphi_A}{L_A} \qquad C_2 = \frac{\cos \varphi_A}{L_A}$$

Calibratable bias:

In a navigation system, disturbing effects whose long-term mean is not zero; hence, they are accountable by adjusting the system instrumentation until they are tuned out; that is, until the long-term mean is zero. Operating systems are continuously monitored for these effects, and are assumed to be properly tuned in the discussions.

Calibrated system:

A system in which the calibratable bias has been removed.

Calibration:

The process of tuning out, or removing, the calibratable bias.

Carry-over, carry-over excess:

In circular passive navigation the excess advisories are referred to the virtual midnight resynchronization of the base-tone-LO. To accommodate navigators who set their LOP-meters previous to this resynchronization, who in other words are operating on a previous synchronization, it is necessary to announce the excess carried-over past midnight from the previous day. This is the carry-over, or carry-over excess. It is equal to the excess obtaining at the moment before the previous midnight (remembering that precisely at midnight, the excess goes to zero). A navigator then, who straddles one or more midnights on a single setting of his LOP-meters, adds all the applicable carry-overs to the current excess adivsory to compute his net excess.

Channel:

(a) The receiver circuitry associated with a particular carrier, from a single satellite.

(b) The receiver circuitry associated with a particular LOP, which sometimes involves two satellites.

(c) The receiver circuitry associated with the coarse-phase signal, or the fine-phase-signal.

Chart navigation:

A procedure for manual navigation which uses an LOP-chart as the basic device for finding the fix.

Circular navigation:

A navigation system using ranging measurements to two (or more) satellites, to develop circular arcs of position in the user's vicinity.

Clock:

A device on-board the vehicle, keeping accurate civil time, intended as a source of the time T to use in satellite position calculations, or to use as an entry into the LOP-almanac. It is reset or calibrated as necessary by time distribution signals, or reference to ground standards. It is not synonomous with the tone-LO, whose function is to key the vehicle into the phase field rather that pin-point the present position of the satellites.

Coarse tone:

The navigation signal intended for resolution of lane ambiguities in the user's position. The coarse-tone repetition interval subtends one band in the field, and its dimension is chosen to avoid operational ambiguities.

Common error:

Error components shared in magnitude and sense by two or more measurements, leading to correlation of errors. For example, the on-board tone-LO is a source of common error in circular navigation; refraction errors are shared to a greater or lesser extent by observations from near-by points; and satellite-ephemeris errors appear coherently in measurements from the same vicinity of time and/or space.

Confidence ellipse:

A pseudo-ellipse in the user's plane whose principal dimensions are the reciprocals of the corresponding dimensions of the error ellipse. It is the error ellipse which is the equal-probability contour in the multi-variable, planar, normal distribution, and whose analytic form is elliptical. The confidence ellipse on the other hand, while having the appearance of an ellipse is not an analytic ellipse (its equation being bi-quadratic rather than quadratic). However, its principal directions are the same as those of the associated error ellipse, and a computational convenience attaches to dealing with fix confidence as opposed to fix error, in that the confidence coefficients are virtually confined to the interval from zero to two.

Correction:

A deliberate offset in LOP-reading or related quantity, intended to compensate for a predictable bias error, geometric effect, or formula term.

Covariance:

Between two random variables, the expected value of the product of their deviations from their deviations from their respective means. That is,

$$\text{covar } (X, Y) = E\,(X - \mu_x)\ (Y - \mu_y)$$

Correlation coefficient:

Between two random variables, the ratio of their covariance to the product of their standard deviations. That is,

$$\rho = \frac{\text{covar } (x, y)}{\sigma_x \sigma_y}$$

Covariance matrix:

A square array displaying in the ij^{th} element the covariance of the i^{th} and j^{th} random variables.

Cross-handover:

In circular relative navigation, the procedure used when simultaneously changing the basepoint, as in crossover, and the satellite, as in handover.

Crossing angle:

The angle in the basepoint plane, between two LOP's. All other things being equal, the precision of the fix improves with the sharpness of crossing, that is LOP angles near 90° are preferred to shallow crossings.

Crossover:

In relative navigation, the procedure used to make the transition from one basepoint to another when the vehicle is about to leave the domain of the first and enter the domain of the second.

Curve bias; curve correction:

Curve bias is the error introduced into a fix by using straight-line LOP's, instead of their true analytic shape. Curve correction is a term or procedure designed to compensate for this error.

D

(a) A double-summation of terms appearing in the general solution of the overdetermined case. In particular

$$D = \sum_{i=1}^{N} \sum_{j=1}^{N} \Lambda_{ij} \cos (\varphi_i + \varphi_j)$$

(b) Line density. It is given by $D = 1000/L$.

d

The distance in the baseplane between a designated point in that plane and an LOP given by the context and/or a subscript.

D_1, D_2

Coefficients appearing in the computation formula for the B-residual. They mix the image-point coordinates linearly to produce ΔP_B. In particular

$$D_1 = \frac{\sin \varphi_B}{L_B} \qquad D_2 = \frac{\cos \varphi_B}{L_B}$$

Determined case:

The establishment of a fix by observing exactly two LOP's, when only plan-position is desired, or exactly three LOP's when it is desired to extract height information as well.

Direction bias; direction correction:

Direction bias is the error introduced into a fix by using the direction of gradient at the basepoint as the gradient direction throughout the basepoint locale. Direction correction is a term or procedure designed to compensate for this error.

E

Sometimes used in place of ϵ as elevation angle.

Elevation:

The angle between the horizontal plane at a point and the line-of-sight to a satellite or other distant body.

Elliptical navigation:

A hypothetical navigation system in which one or more LOP's are derived from a measurement which is proportional to the sum of the user's distances from two known locations. This situation may occur, for example, in an active system where the user returns a navigation signal via a satellite other than the one he received it from.

Ephemeris error:

The error in the satellite position due to the use of promulgation of imprefect orbital elements. The elements may be in error because of imperfect observations, computational or model approximations, or geodetic errors in the location of the stations in the tracking network.

Error ellipse:

The characteristic ellipse of uncertainty surrounding the nominal fix in the horizontal plane. It contains the true position about 39.3% of the time.

Error ellipsoid:

The characteristic ellipsoid of uncertainty surrounding the nominal fix. Its cross-section in the horizontal plane is the error ellipse; its semi-axis in the vertical direction is σ_h , the standard deviation in the height error.

Error transformation:

The behavior of errors in the observed measurement, as the measured quantities undergo processing to extract navigational information. The errors in phase transform into errors in position.

Exactly-determined case:

See determined case.

Excess:

The bias in the LOP-readings in a locality, over and above the assignable bias. In a circular passive system, the estimate of excess depends on the confidence in the stability of a tone-LO within the locality. For this reason excess advisories directed to circular passive navigators are arbitrarily set to zero excess at midnight, and all other bulletins during the day give accumulated excess from midnight. In effect this amounts to a resynchronization of the tone-LO at every midnight. In hyperbolic systems, the excess issued to hypersolic navigators is the full difference between the observed bias and the assignable bias.

Excess advisory:

A bulletin, broadcast or otherwise promulgated, which informs vehicles in the vicinity on the amount of local LOP-excess prevalent at the issue time of the bulletin. In some localities carrying important traffic, advisory bulletins may be issued on an hourly basis. See excess.

Excitation center:

One of several ground stations around the globe, which excites satellites in its domain with the navigation signal, for relay into the field of users.

f

A generic symbol representing fix confidence.

f_m

Average fix confidence at a fix. It is taken as the geometric mean between the maximum and minimum fix confidences, that is, $f_m = \sqrt{f_x f_n}$.

f_n

Minimum fix confidence at a fix.

f_x

Maximum fix confidence at a fix.

F

Coefficient which generates the image-foot correction in the baseplane. It multiplies h_f to produce the correction. In particular

$$F = (F_1^2 + F_2^2)^{1/2}$$

See also φ_F, F_1, F_2

F_1, F_2

Coefficients which generate the X, Y components of the image-foot correction in the baseplane. They multiply h_f to produce the respective component. In particular

$$F_1 = \frac{H_A \cos \varphi_A - H_B \cos \varphi_B}{H_A H_B \sin (\varphi_B - \varphi_A)} \quad , \quad F_2 = - \frac{H_A \sin \varphi_A - H_B \sin \varphi_B}{H_A H_B \sin (\varphi_B - \varphi_A)}$$

Fail-soft:

See back-up oscillator.

Field:

(a) The ubiquitous navigation signal surrounding the earth and extending into near-earth space.

(b) The ensemble of user's of the field signal.

Field signal:

See field, (a).

Fine tone:

The navigation signal intended for the precise determination of user position. The fine-tone repetition interval is called a lane, and an integral number of lanes are included in a band.

FI - offset:

Abbreviation for foot-image offset.

Fix:

(a) The process whereby the observed LOP-readings are reduced to a statement of position.

(b) The position resulting from that process.

Fix confidence:

A geometric figure of merit on the confidence associated with a particular fix. It is a function of the LOP-gradients and their relative directions in the base plan. It is represented by the symbol f , with appropriate subscripts, and is used to estimate the effect of error in the measured parameter on the plan-position, as follows:

$$\text{(estimated fix error)} = \frac{1}{f} \text{ (estimated parameter error)}$$

f is thus seen as a divider of input error, to produce output error; hence all other things being equal, higher f-values imply better performance.

Fix worksheet:

In manual relative navigation, a worksheet designed to aid the entry and processing of the LOP information, to produce a fix.

Foot, foot point:

The point at the foot of the perpendicular from the user to the baseplane.

Foot-image offset:

The line in the baseplane, from the foot to the image point. In the reverse sense, it is the image-foot correction.

Foot-pierce correction:

The line in the baseplane, from the foot to the pierce point. In developing a fix in relative navigation, the process may proceed from the image to the foot, to the pierce, to the ground-point. The transition from the foot to the pierce is the FP-correction. Frequently this correction is omitted, being small compared to the residual errors in the fix.

Formula error:

The error in the fix attributable to the use of formula or model simplification, such as neglecting higher-order terms in a power series under appropriate conditions.

FP-correction:

Abbreviation for foot-pierce correction.

Frequency synchronization:

The excitation of the system's satellites in such a way that the signals seem to originate within the satellite, generated by internal oscillators of standard tone frequencies.

g

(a) The symbol for the earth-central angle between two points donoted by the context and/or subscripts.

(b) The granularity; it is given by g = L/1000.

G

The symbol for the gradient of an LOP family.

GDOP

Abbreviation for: geometric dilution of precision.

Geometric:

When used as a noun, this refers to the value of an LOP at a point under ideal errorless conditions.

Geometric dilution of precision:

The amplification of observation error into position error due to poor gradient and/or crossing angles of the LOP's. Under some circumstances in hyperbolic navigation or two-way circular nagigation, the position error may be smaller than the error in the observed parameter. In either case, amplification or attenuation of error, the error transformation is referred to as GDOP.

Global elements:

The set of orbital elements for a satellite resulting from the weighted average of its orbital behavior as seen by all the regional networks which can view it. The use of such elements gives an average position of the satellite at any time, sufficiently precise for all but the more demanding navigation requirements. These situations employ the regional perturbations.

Gradient:

A measure of the maximum rate of change of the measured parameter, with respect to a displacement in the horizontal plane. It may be conveniently thought of as the linear density of LOP's in the vicinity of a point. If a lane (in a horizontal plane) is thought to be partitioned into a thousand parallel strips, called lines, the gradient may be given in lines per mile, or lines per kilometer. Since lines so defined have linear units associated with them (the width of a strip), the dimensionless quality of gradient is seen to be retained under this formulation.

Gradient bias; gradient correction:

Gradient bias is the error introduced into a fix by using the gradient at the basepoint as the gradient throughout the basepoint locale. Gradient correction is a term or procedure designed to compensate for this error.

Gradient direction:

The direction in the horizontal plane (usually given by a clockwise angle measured from true north), of the gradient of an LOP-family, in the sense of increasing LOP-value.

Granularity:

Arbitrarily, the thousandth part of a lane-width. It is synonomous with line (def. b.) and line-width, and is given by $g = L/1000$.

Ground point:

The point on the local sphere vertically beneath the user, along the geocentric radius.

Ground-range:

The distance along the local sphere, between the baseground and the ground point.

h

The vertical height of the user above the local sphere, along the geocentric radius.

h_f

The distance of the user above the baseplane, along the perpendicular to that plane.

h_p

The height of the user above the baseplane, along the geocentric radius.

H

The symbol for the height-sensitivity of an LOP-family.

H_b

The vertical height of the basepoint above the local sphere, along the geocentric radius.

H_{xy}

This symbol represents the hypothesis that the user is at some particular point x, y in the baseplane. It is used in the derivation, via Bayes' rule, of the multivariate, planar normal distribution describing the user's uncertainty in his determination.

Handover:

In relative navigation, the procedure used to make the transition from one satellite to another, when the vehicle is about to leave the domain of the first and enter the domain of the second; more particularly, the procedure in circular, relative navigation. Although this situation occurs in absolute navigation and hyperbolic relative navigation, the procedures then are much simplified, and do not need extensive detailing.

Height sensitivity:

The ratio of the vertical displacement at a point to the minimum horizontal displacement necessary to remain on the same SOP. Its direction and sense are the same as the gradient direction and sense.

Horizontal, horizontal plane:

Perpendicular to the geocentric radius to a point.

Hyperbolic navigation:

A navigation system using the range-difference to two satellites to generate a hyperboloid SOP. The intersection of this surface with a plane in the vicinity of the user results in a hyperbolic LOP. A second hyperbolic LOP, perhaps again using one of the original two satellites, results in a hyperbolic fix.

i, j

(a) Summation indices.

(b) Serialization indices.

IF-correction:

Abbreviation for image-foot correction.

Image, image point:

The point where a given image line intersects the baseplane.

Image correction nomograph:

A computational aid in manual navigation which is entered with a baseplane range (either pierce-range, or image-range) and altimeter height, and from which one exits with height above the baseplane.

Image-foot correction:

The line in the baseplane from the image to the foot point. In developing a fix in relative navigation, the process may proceed from the image, to the foot, to the pierce, to the ground-point. The transition from the image to the foot is the IF-correction.

Image ground:

The point where a given image line intersects the local sphere.

Image line:

The line of intersection, passing through the user, between two SOP's. All points on the image line will have the same pair of LOP-meter readings as did the user. All image lines between the same pair of SOP-families are parallel, more or less, over a base domain.

Image-pierce correction:

The line in the baseplane, from the image to the pierce point. In developing a fix in relative navigation the process may proceed from the image to the foot, to the pierce, to the ground-point. The transition from the image to the pierce is the IP-correction. It consists of the sum of the IF-correction and the FP-correction, and is frequently taken as virtually identical to the IF-correction, since the FP-correction is often omitted.

Image-range:

The distance in the baseplane from the basepoint to the image.

In-flight calibration:

A procedure for LOP-meter resetting (phase resynchronization of the tone-LO) in flight. It depends on the availability of redundant range information which might otherwise be used to statistically over-determine the fix. It is different from landmark reset, which does not depend on redundant information.

Initialization:

The procedure for setting the LOP-meters at the beginning of a flight or flight leg. It depends on the knowledge of the coordinates of the set point in the flight coordinate system.

Integration interval:

The effective time interval over which the incoming phase information is smoothed to produce an independent LOP-reading. It is approximately given by the reciprocal of the noise-bandwidth of the overall receiver-signal processing channel.

IP-correction:

Abbreviation for image-pierce correction.

Iteration, iterative process:

In a computation algorithm, the technique of successive approximations to a desired value by cycles of computation around a loop, which converge toward the desired value. The process is generally stopped, when two successive values of a variable at a judiciously chosen test-point in the loop show a difference less than a pre-set threshold.

j

See i, j.

ℓ

Distance in the baseplane measured perpendicular to a particular LOP-family. A small increment $\Delta \ell$ in ℓ, in the neighborhood of a point is used to measure line density (gradient) or height sensitivity.

L

The lane-width in the vicinity of a point. It is given by $L = \lambda_f/G$ where λ_f is the wave-length of the fine tone, and G is the gradient at the point.

λ

The longitude of the user, in an absolute designation.

Landmark reset:

A procedure for resetting LOP-meters enroute, based on the proximity of identifiable landmarks whose coordinates in the flight system are well-known. It is similar to initalization.

Lane:

(a) The volume of space enclosed by two successive surfaces of position, each of which is assigned a cardinal number in the fine-phase field. The phase difference between the two SOP's is one LOP-cycle.

(b) The area on a designated surface, such as the earth or a horizontal plane, enclosed between two such SOP's.

Lane number:

A serial number designating the lane. The lane receives its designation from the lower number of its two bounding SOP's. See example under LOP-value. Lane number is represented by the Greek letter Λ.

Lane width:

The width of the lane at the user, in the user plane, on the assumption that the user's gradient applies throughout the width. It is designated by the symbol L, with appropriate subscripts, and is given by $L = \lambda_f / G$ where λ_f is the fine-tone wavelength, and G is the gradient.

Line:

(a) A line of position (LOP).

(b) Arbitrarily, the thousandth part of a lane-width on a given surface. It is this use of line which is implied in such phrases as line density and lines per mile. (See also, granularity.)

Line density:

The linear density of lines in the vicinity of a point. It is given by $D = 1/g$; i.e., $D = 1000/L$.

Line number:

(a) A serial number designating the line. It is 1000 times the lane fraction. The line number is represented by the Greek letter λ.

(b) The LOP-value.

Line of position:

The intersection of a surface of position (SOP) with a surface containing a given point (such as the earth's surface, a horizontal plane, or a surface parallel to the earth). A pair of lines of position determine a fix in the given surface.

Line-width:

Synonym for granularity.

Local advisory:

See excess advisory.

Local excess:

See excess.

Local lane-width:

Same as lane-width.

Local radius:

The distance from the center of the earth to the local terrain at the user or other given point.

Local sphere:

The sphere whose radius is the local radius.

Long-term error:

(a) The resultant of those errors of zero mean which show significant auto-correlation for intervals of time in the order of an integration interval. In other words, only measurements spaced by many integration intervals (and for some errors, perhaps months) are independent with respect to the long-term error.

(b) Any of the components of the resultant long-term error.

LOP

Abbreviation for line of position.

LOP-almanac:

A chronological tabulation for a given base domain of LOP-parameters and coefficients. The LOP-almanac is intended for use by manual navigators who use the tabulated values, perhaps augmented by local advisories, in conjunction with appropriate worksheets, nomographs, and/or base-charts.

LOP-cycle:

The unit of indication on the LOP-meter. When the lane number on the LOP-meter changes by one, the meter has gone through one LOP-cycle. It is equal to one fine-tone repetition interval.

LOP-distance:

Same as measured parameter.

LOP-excess:

See excess.

LOP-family:

The ensemble of virtually parallel, straight, uniformly spaced lines resulting from the intersection of a given plane with successive surfaces of position.

LOP-family parameters, LOP-parameters:

In a given context, these phrases refer to some subset of the parameters: LOP-value P ; gradient G ; gradient direction φ ; height sensitivity H ; and lane-width L.

LOP-gradient:

See gradient.

LOP-meter:

An instrument, real or conceptual, at the point of phase comparison, which measures and displays and/or carries forward the actual LOP-number associated with the LOP passing through the position.

LOP-number:

The numerical designation of the line of position passing through a place. See LOP-value.

LOP-offset:

The distance in the baseplane between the basepoint and the LOP.

LOP-parameter:

See LOP-family parameters.

LOP-reading:

The indication, real or conceptual, on the LOP-meter.

LOP-timetable:

Same as LOP-almanac.

LOP topology:

A body of geometric and analytic statements concerning the properties of a set of LOP's constituting a navigational observation, sequence of observations, or collection of observations.

LOP-value:

The designation of the LOP associated with a given place. The full designation includes a band number, a lane number, and a line number. The band number appears first, followed by a colon. The lane number appears next, followed by a decimal point. The line number appears last. For example, 1421:02.167 designates line 167 in lane 02 of band 1421. The LOP-value is represented by the letter ρ . The full number is almost never needed. In many situations only the lane and line numbers are needed to carry all the information. In other cases only one or two band digits need be given.

Manual navigation:

A navigation procedure whereby the user finds his fix from the LOP-meter readings by means of the LOP-almanac, procedures, worksheets, nomographs, and/or base charts, as opposed to automatic navigation.

Measured parameter:

The observed parameter; in the circular mode this parameter is range, and in the hyperbolic mode it is range-difference.

Mixed mode fix:

A navigation fix in which both circular and hyperbolic LOP's are used.

Mixed system fix:

A navigation fix, the LOP's for which do not all originate in the same system. For example, a fix may consist of an LOP from a satellite system and an LOP from a VOR system.

Model error:

Same as formula error.

Motion error:

The component of error in the user's position due to the vehicle's position at the mid-time of the integration interval not being coincident with its time-average position during that interval. It is seen that for uniform motion during the interval, there is no discrepancy between these two positions, and hence no motion error. Also, when the motion is significantly non-uniform, some estimate of the discrepancy is generally available, which reduces the motion error. It is assumed that satellite motions are well-known so that non-uniformity in their motions may be accounted for.

Multipath error:

The error in LOP-value which results from phase shifts in the incoming tone signals due to delayed field signals arriving at the antenna simultaneously with the proper signal. These delayed signals are the result of reflection of the main field signal from local terrain or nearby objects.

Navigation:

(a) The process of estimating the position of the vehicle from the indications of the LOP-meter and various other environmental and orbital data, and computation aids. More generally, navigation may include the height of the vehicle, its velocity, and even its attitude in space. Frequently these latter quantities are available from instruments external to the plan-position finding system, but a fully-implemented phase system can develop these quantities as well.

(b) The FAA distinguishes between navigation as an on-board fixing process, and position-determination as a fixing process at a remote center, such as an ATC center.

Navigation mode:

Generally this refers to the selection of either the circular navigation mode, or the hyperbolic navigation mode.

Navigation signal:

(a) The coarse and/or fine tones which embody the position-finding information in the form of distinctive phases which characterize a given point in near-earth space.

(b) The total emanated tone-bearing signal, including the carrier as well as the tones.

Net point:

The geodetic location of a station in the tracking network.

$\mathcal{O}$

This symbol represents the collection of LOP's comprising the total observation of the user, on any fix. It is used in the derivation, via Bayes' rule, of the multi-variate, planar normal distribution describing the user's uncertainty in his determination.

One-way navigation:

Passive navigation, so called because the field signal travels only one-way with respect to the user - toward him.

Oscillator drift error:

(a) That component of LOP-reading error due to the drift of the tone-LO in frequency, thus accumulating phase error from the time of setting or resetting in-flight.

(b) In a fail-soft backup mode, where the field signal actually originates in the satellites, the error due to the asynchronous drifts among the various oscillators in the system.

(c) In a global system, where several ground stations are required to excite the total orbiting system, the error due to the asynchronous drifts among the various oscillators in the system.

Over-determined case:

The observation of more LOP's than are needed to extract a fix. In a system designed to get the most from such a situation, all information is treated statistically with appropriate weights, and a best estimate of fix is generated, frequently along with an estimate of the uncertainty ellipse surrounding the fix.

P

The LOP-value, in LOP-cycles. It has the form

$$P = B : \Lambda . \lambda$$

where B, Λ and λ are the band, lane, and line numbers respectively.

P'

The LOP-value at the basepoint. When subtracted from the observed value at the user, the result is the residual.

p

Symbol representing the measured parameter.

Passive navigation:

A navigation procedure which allows the user to estimate his fix with on-board facilities only; he does not need nor use external computation facilities.

PF-offset:

Abbreviation for pierce-foot offset.

Phase:

A generic word. In its usual context in navigation discussions it refers to the time delay between corresponding parts of congruent waveforms.

Phase field:

Same as field, def. (a).

Phase grid navigation:

A navigation application, wherein the user seeks to bring his vehicle to such a position, or series of positions, which make his LOP-meter readings compatible with a set of control LOP-values.

Phase synchronization:

The excitation of the system's satellites in such a way that the signals seem to originate within the satellite, generated by internal oscillators of standard tone phase.

Pierce, pierce point:

The point in the baseplane vertically beneath (or above) the user, along his geocentric radius.

Pierce-foot offset:

The line in the baseplane from the pierce to the foot point. In the reverse sense it is the foot-pierce correction.

Pierce-image offset:

The line in the baseplane, from the pierce to the image point. In the reverse sense it is the image-pierce correction.

Pierce-range:

The distance in the baseplane from the basepoint to the pierce-point.

PI-offset:

Abbreviation for pierce-image offset.

Plan-position:

The position of the user, either in a horizontal plane or on a surface parallel to the earth. It does not include height information.

Position determination:

(a) The process of finding the vehicle's position, based on the field signals.
(b) The FAA contrasts this phrase with navigation, definition b.

Predictable bias, predicted bias:

See assignable bias.

Principal dimensions:

The lengths of the semi-axes of the Error Ellipse, or Ellipsoid.

Principal directions:

The directions of the semi-axes of the Error Ellipse or Ellipsoid.

Proper residual:

The residual corrected as far as possible for assignable bias and excess.

r

The radius from the center of the earth to the local terrain at the basepoint.

R

The slant-range to a satellite.

Random error:

See short-term error.

Range:

Distance from one given point such as the user, to another such as a satellite.

Range circles:

The intersection of a family of concentric spheres with a plane or another spherical surface, like the earth. The resulting circles are loci of constant range from the common center of spheres. In circular navigation, the common center is the satellite.

Range difference:

The difference in the distances from a point such as the user, to two other points such as a pair of satellites.

Range-difference navigation:

See hyperbolic navigation.

RDN

Abbreviation for range-difference navigation.

Range-range navigation:

Circular navigation, so called because the user needs two ranges to make his fix.

Refraction; refraction bias, refraction error:

The result of several atmospheric processes, the net effect of which is to delay the field signal so that its transit time is longer than its freespace time for the same distance. The effect is significant at VHF, but becomes quite small at the upper frequencies in the UHF band. Much of the delay constitutes predictable error and depends on the season, time of day, user latitude, elevation angle and sun-spot number. Some of the error remains as random error and as refraction residue.

Region:

A more or less large area of the earth within which a tracking network operates in a geodetic frame, providing satellite ephemeris information for absolute navigation with respect to the same geodetic frame.

Regional geoid:

The geoid applicable to the Region within which a given set of tracking stations operate, and within which the user seeks an absolute position.

Regional perturbations:

A set of coefficients for a satellite, applicable to a given earth region, describing the satellite's deviations from the nominal positions given by the Global Elements. The use of such coefficients makes available to the user statements of satellite position specific to the geodesy of the region containing the tracking network. Where this is also the user's region, his navigation precision is improved.

Relative navigation:

A navigation process which generates the vehicle position in terms of a local coordinate system, such as ground range and bearing from a basepoint.

Relative position:

A statement of position with respect to a local coordinate system, such as ground range and bearing from a basepoint. The relative position of a vehicle may be derived from its absolute position, if the absolute position of the base is known.

Residual:

The residual ΔP is given by $\Delta P = P - P'$ (see P).

Residue:

The total error due to a particular source, less the estimate of the error. The residue is seen to be the excess of the error over the correction intended for it; also, if the correction is more than sufficient, the residue may be negative.

RRN

Abbreviation for range-range navigation.

Running fix:

A fix resulting from two (or more) LOP's which were not observed simultaneously. The motion of the vehicle between LOP-readings makes necessary a suitable procedure to estimate the position at some interpolated time (which is generally taken to coincide with the time of one of the observations).

Satellite ellipsoid:

The surface bounding the volume of uncertainty surrounding the stated position of a satellite.

Sense of correction, - error, - offset, - etc.

The terms correction, error, offset, etc. imply a vector originating on some source or reference point, and terminating at some destination point. In naming such terms, the convention is to name the reference first, then the terminal. For example, the image-foot correction is a line directed from the image to the foot. Where there is no ambiguity, the reference is often omitted, it being understood by the context. For example, image range is a line directed from the basepoint to the image-point, and the bearing of the image is the direction of this line, not its reverse.

Sensitivity bias; sensitivity correction:

Sensitivity bias is the error introduced into a fix by using the height sensitivity at the basepoint as the height sensitivity throughout the basepoint locale. Sensitivity correction is a term or procedure designed to compensate for this error.

Service Computation:

This term refers to the computation performed for the user, at a remote center. In this system the user does not carry his own navigation computer; instead he transmits the outputs of his phase comparators and altimeter reading to a service center for processing. The center then returns the results of computation in suitable form for on-board display.

Set Point:

A place at which the LOP-meters in a vehicle are set.

Shape bias; shape correction:

Shape bias is the error introduced into a fix by using some too-simplified model of earth figure in the vicinity of the fix. Shape correction is a term or procedure designed to compensate for this error.

Sheet:

A surface of position, so called because the field of surfaces in a region distant from the originating satellite resembles a field of more or less parallel planar sheets, which respond to the "winds" of refraction or other disturbing influences.

Sheet-warp model:

The various error phenomena disturbing a family of SOP's can be conceptualized as an effective wind blowing through the sheets of position, and distorting or warping them. For example, tone-LO drift may be thought of as a translation of the sheets without reorientation. Refraction generally warps the sheets in more or less complex ways which need model simplification to be tractable. The conceptual description of sheet behavior under the influence of various error winds is referred to sheet-warp model.

Short-term error:

The resultant or any of those errors of zero mean which show no significant auto-correlation for intervals in the order of one integration interval. Sometimes called random error.

Signal synchronization:

The excitation of the system's satellites in such a way that the signals seem to originate within the satellite, generated by internal oscillators of standard tone frequency and standard tone phase.

Signal-to-noise error:

The LOP-reading error attributed to the presence of noise in the communication channels.

SOP:

Abbreviation for surface-of-position.

Standard ellipsoid:

A geodetic model of the earth as an oblate spheroid, for use by navigators who seek better precision than is available on the standard sphere.

Standard sphere:

A simplified geodetic model of the earth as a sphere, sufficiently good for the large class of navigators who are content with fix precisions to a few miles.

Those navigators who seek better precision correct their findings to a standard ellipsoid, or regional geoid, or even to the local terrain.

Standard tone frequency:

The frequency of the tone (coarse or fine) at the standard tone generator.

Standard tone generator:

A real or conceptual standard oscillator and frequency synthesizer which generates coarse and fine tones whose frequencies are virtually invariant. As a consequence, the phases are also invariant and such a generator may be used as a reference for the navigation system.

Standard tone phase:

The phase of the tone (coarse or fine) at the standard tone generator.

Straight-line computation:

A computational procedure which allows the use of straight lines to represent the LOP's in the fix process, rather than the circles or hyperbolas as the case may be.

Surface of position:

Surfaces of equal phase indication. In a circular system, these are spheres around the satellite in question; in a hyperbolic system they are hyperboloid sheets with the two satellites as foci.

T:

The time of a fix. In LOP almanac tabulations, T is given in local standard time.

Terrain correction:

A correction beyond the regional geoid, for the variation therefrom in the locale of the user, when extreme precision of fix is required.

Time distribution:

A service of a fully implemented navigation system. The possibility of the global distribution of timing signals arises in the maintenance of synchronized precision standards at the excitation centers, coupled with a globally deployed orbital network.

Tone:

Either the coarse or the fine tone, the position-bearing signals on the rf carrier emanating from the satellites.

Tone-LO:

Abbreviation for tone-local oscillator.

Tone-local oscillator:

In passive circular navigation, the onboard reference tone generator, against which the incoming field signal is compared for phase, to derive the LOP-meter readings. Notice that the tone-LO is a device which keys the user into the phase field; it does not provide the civil time information necessary for pin-pointing the present position of the satellites; this latter is the task of the vehicle's clock.

Total error:

a) The discrepancy between the observed LOP-reading and the geometric at a point.

b) The discrepancy between the apparent position and the true position.

Tracking network, tracking stations:

The collection of stations in a region whose task it is to locate the satellites with precision, and provide data from which global elements and regional perturbations may be prepared.

Tuned system:

A navigation system in which all calibratable errors have been neutralized.

Two-way navigation:

A system of navigation in which the using vehicle transponds the ambient field signal to a remote computation center, where the fix is computed. So-called because the navigation signal travels two ways with respect to the user - toward and away from him.

Uncertainty ellipse:

See Error Ellipse.

User:

The navigator; the person who is assigned the task of finding the vehicle's position, or of causing it to be found. The user is considered to be aboard the vehicle in the navigation discussions. When the computation is done remotely, the user is the person aboard participating in the exchange of information.

User plane:

The horizontal plane through the vehicle.

Variable delay:

A device in the signal processing equipment onboard the vehicle, which allows the signal from the tone-LO to be phase-shifted over a coarse-tone cycle with respect to the incoming signal. This is the device which is used to set the LOP-meters at the start of a voyage and perhaps enroute.

Vertical:

The vertical at a point is taken to be along the geocentric radius.

VOR:

Very high frequency omnirange, a navigation system in widespread use in the United States, for commercial and private aviation. In its usual form a single VOR-determination gives a bearing line to a ground station.

Warp model:

Same as sheet-warp model.

X, X-Axis:

The abscissa, or axis of the abscissa, in the base plane. The positive X-direction is conventionally taken to the east of the basepoint.

X_f, Y_f:

The baseplane coordinates of the foot.

X_I, Y_I:

The baseplane coordinates of the image.

X_p, Y_p:

The baseplane coordinates of the pierce.

Y, Y-Axis:

The ordinate, or axis of the ordinate, in the baseplane. The positive Y-direction is conventionally taken to the north of the basepoint.

Zero-start navigation:

A relative navigation procedure in which the user sets his LOP-meters to zero at the start of his voyage. Subsequent fixes must take into account the LOP-accrual at the basepoint, as well as assignable bias and excess.

NUMBERS AND GREEK LETTERS

B	This symbol represents band number.
δ	The latitude of the user in an absolute designation.
ΔP	The symbol for residual.
δR	In a hyperbolic system, the range difference between the satellites associated with the LOP.
ϵ	The elevation angle of a satellite.
θ	a) The azimuth to a satellite; b) The bearing from the base to a designated point.

θ_F The bearing from the base to the foot.

θ_p The bearing from the base to the pierce.

λ The line number.

λ_c The wavelength of the coarse tone.

λ_f The wavelength of the fine tone.

λ_{ij} The ij^{th} element in the covariance matrix.

Λ a) The determinant of the covariance matrix among the LOP's in the total observation;
b) The lane number.

Λ_{ij} The cofactor of the ij^{th} element in the covariance matrix, among the LOP's in the total observation.

ρ a) The correlation coefficient relating the errors in two LOP's;
b) The range from the base to a designated point.

ρ_f The range from the base to the foot.

ρ_I The range from the base to the image.

ρ_p The range from the base to the pierce.

σ The generic symbol for standard deviation.

σ^2 The generic symbol for variance.

σ^2_{AB} The variance associated with the common error shared by the A- and B-LOP's.

σ_E, σ_E' The dimensions of the semi-axes of the Error Ellipse.

σ_h^2 The variance in the height measurement.

σ^2_{LOP} The variance in the error associated with an LOP.

σ^2_p The variance in the measured parameter.

σ^2_R The variance in the error associated with a particular range measurement.

Φ The direction, measured clockwise from north, of the gradient of an LOP-family.

Φ_E, Φ'_E The principal directions, measured clockwise from north, of the Error Ellipse.

Φ_F Bearing of foot from image in the baseplane. It gives the direction of the image-foot correction, and is given by

$$\varphi_F = \tan^{-1} \frac{F_1}{F_2}$$

See also, F, F_1, F_2

00A Read as: "Double-oh hundred advisory." This is the advisory issued at midnight, and which by convention announces a zero excess for circular navigation.

01A, 02A, etc.

Read as: "oh-one hundred advisory, oh-two hundred advisory, etc." These advisories are issued locally for a base domain, and promulgate the local excess as of the time of issue.

Appendix 4B

POSITION AND UNCERTAINTY: THE GENERAL SOLUTION

We address the problem of estimating the user's position when he has more than two LOP's, that is, he is over-determined. We will also find the size and direction of the uncertainty ellipse surrounding the estimated position (See Figure 4B-1).

The Baye's probability of the user being at (x, y) in the light of his observations is, from Figure 4B-1,

$$P_r(H_{xy}|\sigma) = \frac{P_r(\sigma|H_{xy})\ P_r(H_{xy})}{\sum_{\text{plane}} P_r(\sigma|H_{xy})}$$

whence

$$p_{H|\sigma}(H_{xy}|\sigma) = \frac{p_{\sigma|H}(\sigma|H_{xy})p_p(H_{xy})}{\iint_{\text{plane}} p_{\sigma|H}(\sigma|H_{xy})\,dx\,dy}$$

in which the $p_{(\ )}$ are density functions.

Now $p_{\sigma|H}(\sigma|H_{xy})$ is given by a joint multi-dimensional normal distribution, based on the variances and covariances among the several LOP's. $p_p(H_{xy})$ is the a priori joint two-dimensional normal distribution from previous or external information.

Then since the denominator $p_{H|\sigma}(H_{xy}|\sigma)$ is constant, and the numerator is the product of normal-form exponentials, $p_{H|\sigma}$ itself is normal and is given by:

$$p_{H|\sigma}(H_{xy}|\sigma) = \frac{1}{(2\pi)^{N/2}\Lambda^{1/2}} \exp\left[-\frac{1}{2}\left(\frac{1}{\Lambda}\sum_{i=1}^{N}\sum_{j=1}^{N}\Lambda_{ij}\,d_i\,d_j\right)\right]$$

which is a canonical formulation for joint multi-dimensional normal distributions, and in which d_i is the distance from (x,y) to the i^{th} LOP; $E[d_i] = 0$; $[\Lambda]$ is the covariance matrix for the joint observation; Λ is its determinant; and Λ_{ij} is the cofactor of the ij^{th} element. While the distribution is multi-dimensional, it is also planar in the sense that we consider the probability mass to be distributed in the x, y-plane (See Figure 4B-2).

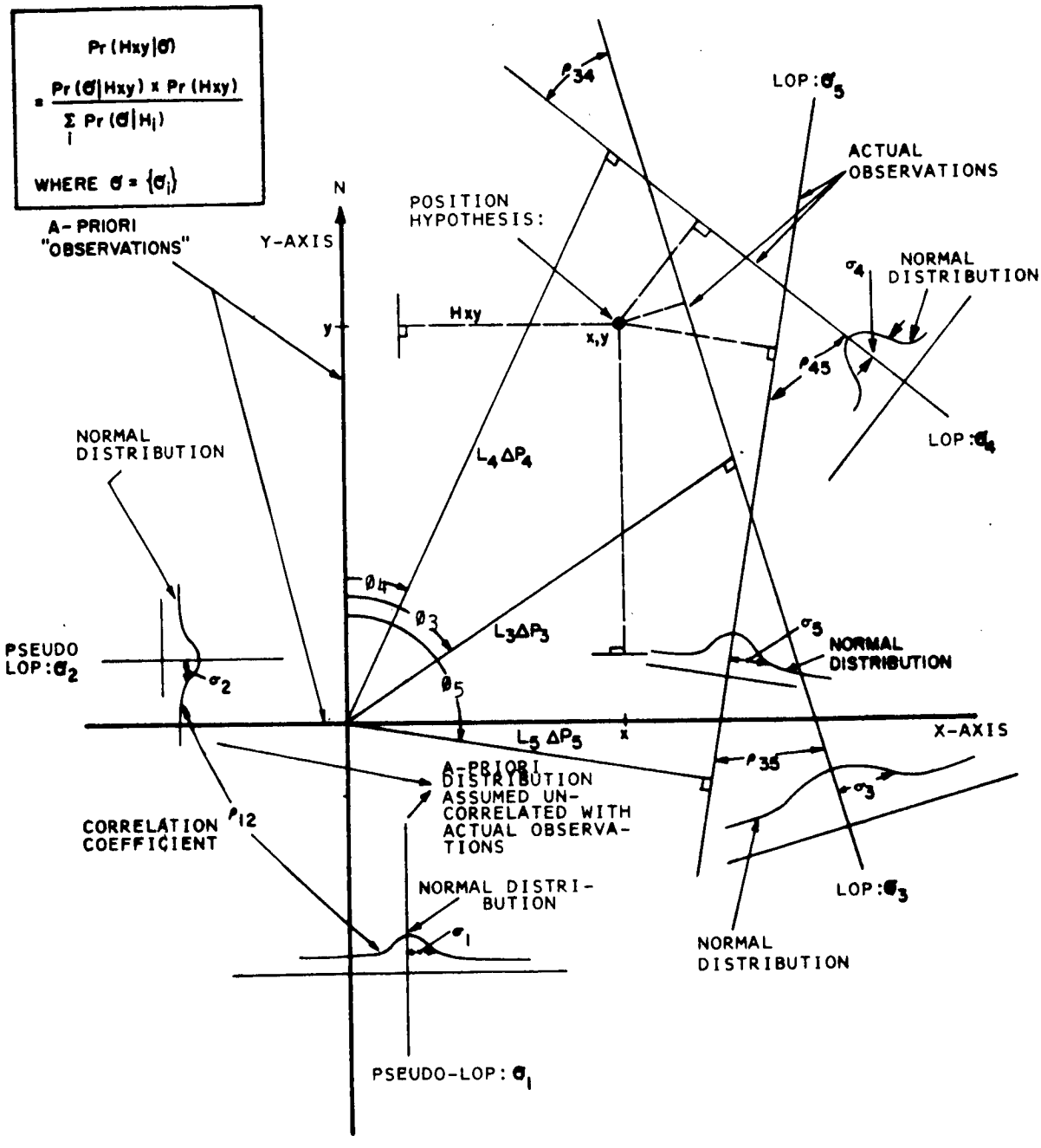

Figure 4B-1. Development of Multi-Dimensional, Planar Normal Distribution

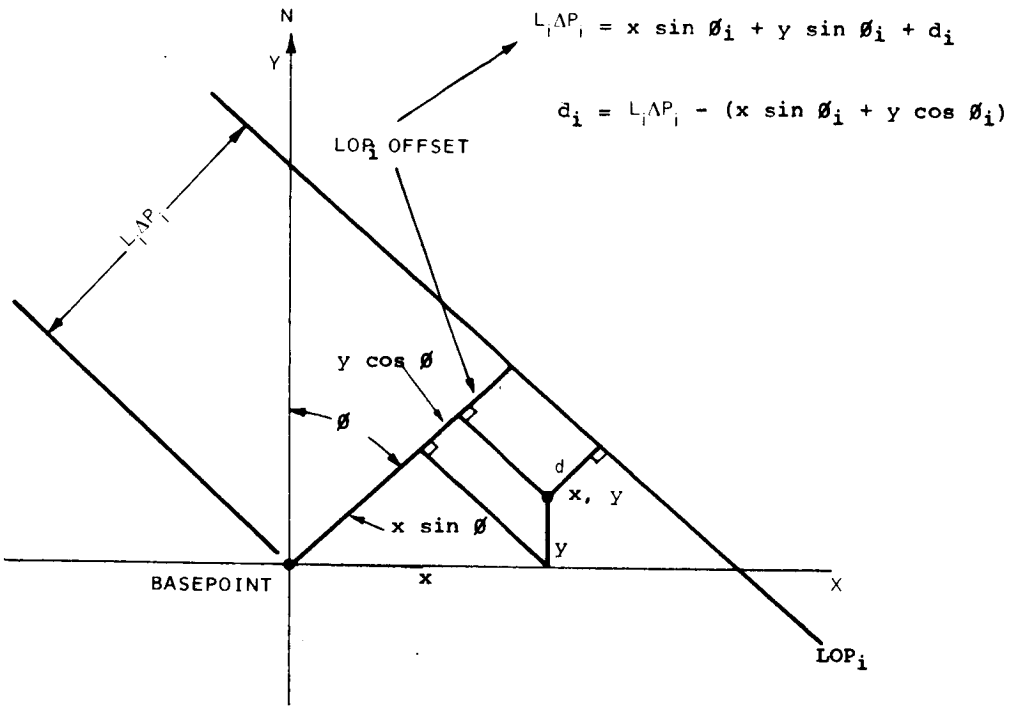

Figure 4B-2. Development of Displacement d_i of the General Point (x,y) from the i^{th} - LOP

$$[A] = \begin{bmatrix} \sigma_1^2 & \lambda_{12} & 0 \cdots 0 \\ \lambda_{21} & \sigma_2^2 & 0 \cdots 0 \\ 0 & 0 & \sigma_3^2 \quad \lambda_{34} \cdots \lambda_{3N} \\ \vdots & \vdots & \lambda_{43} \quad \sigma_4^2 \\ 0 & 0 & \lambda_{N3} \quad\quad \sigma_N^2 \end{bmatrix}$$

Covariance Matrix

$\lambda_{ij} = \sigma_i \sigma_j \rho_{ij}$

$\rho_{ii} = 1$

In the corvariance matrix the a priori distributions are represented as pseudo-observations and are assigned index numbers 1 and 2. The index numbers for the actual observations run from 3 to N. The zeros completing rows and columns 1 and 2 reflect the independence of the a priori information from the ensuing observations. The

λ_{ij} represent covariances. Where no dependable a priori information is available, the matrix consists only of actual observations (see Figures 4B-3 and 4B-4).

In a normal distribution the maximum liklihood point is co-located with the point of minimum variance. To find this point we focus attention on the exponent, and in particular on the factor in brackets:

$$c^2 = \frac{1}{\Lambda} \sum_{i=1}^{N} \sum_{j=1}^{N} \Lambda_{ij} \, d_i \, d_j$$

where c is an index on the family of equi-probability ellipses. The maximum liklihood point corresponds to the point of minimum c. Therefore we seek (x,y) such that

$$\left.\frac{\partial c^2}{\partial x}\right]_{x,y} = 0 \quad \text{and} \quad \left.\frac{\partial c^2}{\partial y}\right|_{x,y} = 0$$

The general terms are

$$\Lambda_{ij} \frac{\partial}{\partial x} \left[\frac{\Delta P_i}{G_i} - (x \sin\varphi_i + y \cos\varphi_i)\right] \left[\frac{\Delta P_j}{G_j} - (x \sin\varphi_j + y \cos\varphi_j)\right]$$

and

$$\Lambda_{ij} \frac{\partial}{\partial y} \left[\frac{\Delta P_i}{G_i} - (x \sin\varphi_i + y \cos\varphi_i)\right] \left[\frac{\Delta P_j}{G_j} - (x \sin\varphi_j + y \cos\varphi_j)\right]$$

whence

$$x_I \sum_i \sum_j 2\Lambda_{ij} \sin\varphi_i \sin\varphi_j + y_I \sum_i \sum_j \Lambda_{ij} \sin(\varphi_i + \varphi_j) =$$

$$\sum_i \sum_j \Lambda_{ij} \left(\frac{\Delta P_i}{G_i} \sin\varphi_j + \frac{\Delta P_j}{G_j} \sin\varphi_i\right)$$

and

$$x_I \sum_i \sum_j \Lambda_{ij} \sin(\varphi_i + \varphi_j) + y_I \sum_i \sum_j 2\Lambda_{ij} \cos\varphi_i \varphi_j = \sum_i \sum_j \Lambda_{ij} \left(\frac{\Delta P_i}{G_i} \cos\varphi_j + \frac{\Delta P_j}{G_j} \cos\varphi_i\right)$$

where x_I, y_I are the coordinates of the point of maximum liklihood.

MEASURED PARAMETER

P ≙ R, RANGE IN CIRC. NAV

P ≙ δR, RANGE DIFFERENCE IN HYP NAV

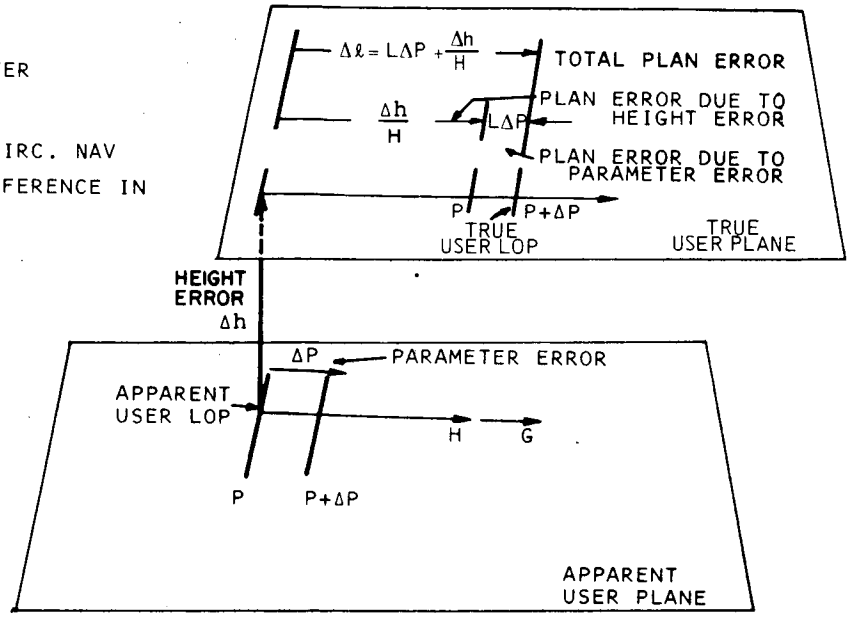

NOTE: ERRORS ARE DEFINED IN THE SENSE OF (TRUE-APPARENT), THAT IS THE QUANTITY WHICH WHEN ADDED VECTORIALLY TO THE APPARENT, GIVES THE TRUE

THE VARIANCE ASSOCIATED WITH THE LOP IS GIVEN BY

$$\sigma^2_{LOP} = \frac{\sigma_P^2}{G^2} + \frac{\sigma_h^2}{H^2}$$

(HEIGHT MEASUREMENT IS ASSUMED INDEPENDENT OF PARAMETER MEASUREMENT)

CIRCULAR NAVIGATION

$$\sigma^2_{LOP} = \frac{\sigma_R^2}{G^2} + \frac{\sigma_h^2}{H^2}$$

σ_R^2 :VARIANCE IN RANGE ERROR

σ_h^2 :VARIANCE IN HEIGHT ERROR

HYPERBOLIC NAVIGATION

$$\sigma^2_{LOP} = \frac{\sigma_{R_A}^2 + \sigma_{R_B}^2 - 2\rho\sigma_{R_A}\sigma_{R_B}}{G^2} + \frac{\sigma_h^2}{H^2}$$

$\sigma_{R_A}^2$:VARIANCE IN RANGE ERROR, SAT-A

$\sigma_{R_B}^2$:VARIANCE IN RANGE ERROR, SAT-B

ρ :CORRELATION COEFFICIENT BETWEEN RANGE ERRORS

σ_h^2 :VARIANCE IN HEIGHT ERROR

Figure 4B-3. LOP-Error Description

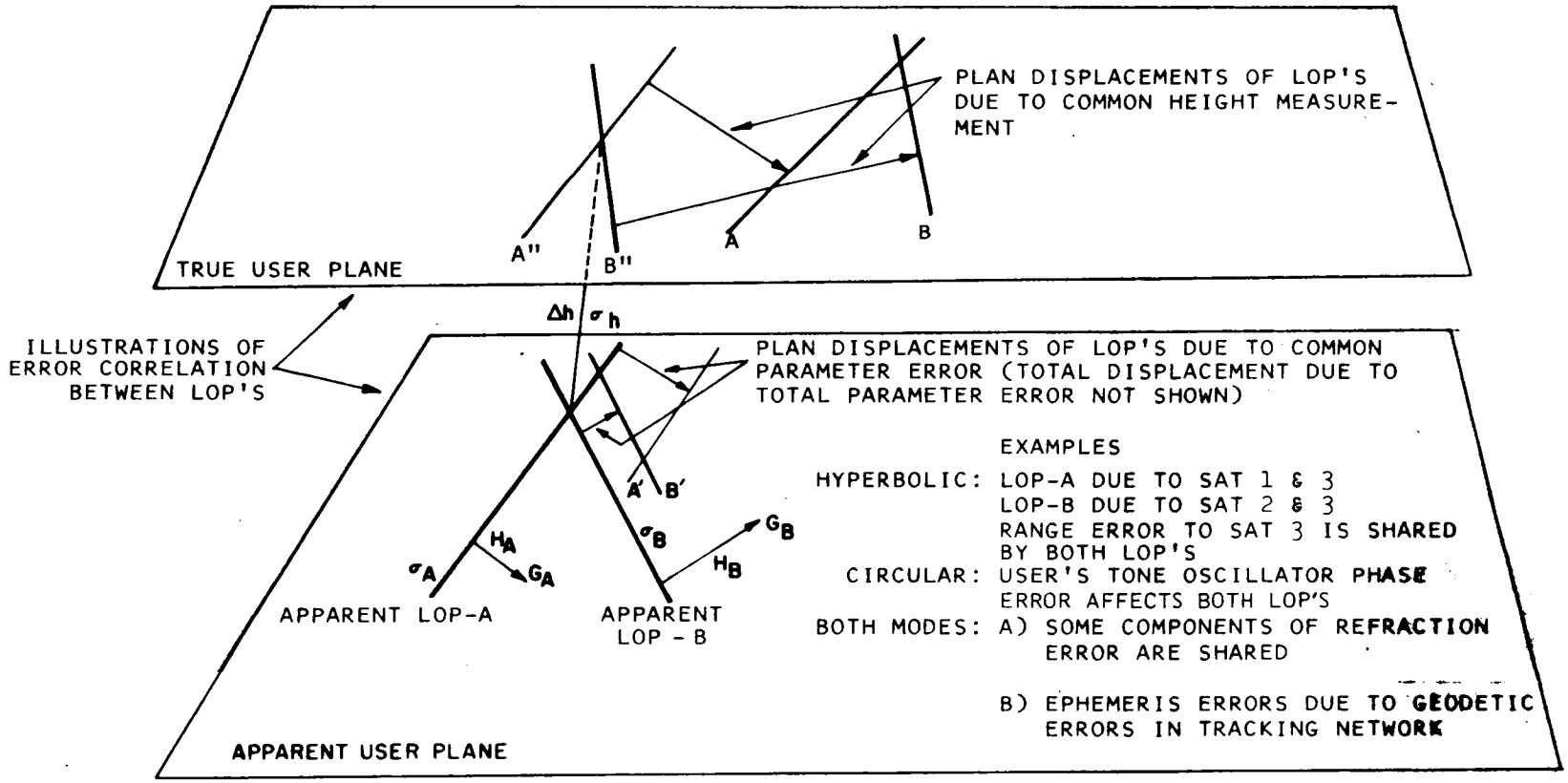

CORRELATION COEFFICIENT: $\rho = \frac{1}{\sigma_A \sigma_B}\left(\frac{\sigma_{AB}^2}{G_A G_B} + \frac{\sigma_h^2}{H_A H_B}\right)$

σ_A^2: VARIANCE IN LOP-A
σ_B^2: VARIANCE IN LOP-B
σ_h^2: VARIANCE IN HEIGHT ERROR

σ_{AB}^2: TOTAL VARIANCE IN THE COMMON ERROR COMPONENTS OF THE MEASURED PARAMETER. (I.E., RANGE IN CIRCULAR NAVIGATION; RANGE-DIFFERENCE IN HYPERBOLIC NAVIGATION)

Figure 4B-4. LOP Correlation Coefficient

If we let

$$A = 2\sum_i\sum_j \Lambda_{ij} \sin\varphi_i \sin\varphi_j \,, \quad B = \sum_i\sum_j \Lambda_{ij} \sin(\varphi_i + \varphi_j)$$

$$C = 2\sum_i\sum_j \Lambda_{ij} \cos\varphi_i \cos\varphi_j \,, \quad D = \sum_i\sum_j \Lambda_{ij} \cos(\varphi_i + \varphi_j)$$

then

$$x_I = \frac{\sqrt{C^2 + B^2}}{AC - B^2}\left[\sum_i \frac{\sum_j \Lambda_{ij} \sin\left(\varphi_j - \tan^{-1}\frac{B}{C}\right)}{G_i}\Delta P_i + \sum_j \frac{\Lambda_{ij} \sin\left(\varphi_i - \tan^{-1}\frac{B}{C}\right)}{G_j}\Delta P_j\right]$$

$$y_I = \frac{\sqrt{A^2 + B^2}}{AC - B^2}\left[\sum_i \frac{\sum_j \Lambda_{ij} \cos\left(\varphi_j + \tan^{-1}\frac{B}{A}\right)}{G_i}\Delta P_i + \sum_j \frac{\sum_i \Lambda_{ij} \cos\left(\varphi_i + \tan^{-1}\frac{B}{A}\right)}{G_j}\Delta P_j\right]$$

x_I, y_I is the best estimate of plan-position, and is the center of a family of parallel (i.e., common eccentricity) ellipses, which are contours of equal probability.

We now postulate a clockwise rotation of the x,y-axes through an angle φ, to some new position x', y'. Then in terms of the new coordinate system

$$c^2 = \frac{1}{\Lambda}\sum_i\sum_j \Lambda_{ij}\left[\frac{\Delta P_i}{G_i} - \left[x' \sin(\varphi_i - \varphi) + y' \cos(\varphi_i - \varphi)\right]\right] \times \left[\frac{\Delta P_j}{G_j} - \left[x' \sin(\varphi_j - \varphi) + y' \cos(\varphi_j - \varphi)\right]\right]$$

We seek the angles φ which would make the total crossproduct in x'y' vanish. This occurs when the coordinate axes are parallel to the principal axes, so that the values of φ gives the directions of the principal axes. The general crossproduct term is:

$$x'y' \Lambda_{ij} \sin(\varphi_i + \varphi_j - 2\varphi)$$

Hence we require that

$$\sum_i \sum_j \Lambda_{ij} \sin(\varphi_i + \varphi_j) \cos 2\varphi_E = \sum_i \sum_j \Lambda_{ij} \cos(\varphi_i + \varphi_j) \sin 2\varphi_E$$

whence

$$\varphi_E = \frac{1}{2} \tan^{-1} \frac{\sum_i \sum_j \Lambda_{ij} \sin(\varphi_i + \varphi_j)}{\sum_i \sum_j \Lambda_{ij} \cos(\varphi_i + \varphi_j)} = \frac{1}{2} \tan^{-1} \frac{B}{D}$$

and

$$\varphi'_E = \varphi_E - 90°$$

To find the principal dimensions of the error ellipse, we set up new axes x', y' with y' at a clockwise angle φ_E from y. The coefficients of $(x')^2$ and $(y')^2$ define the principal semi-axes.

$$\frac{1}{\Lambda} \sum_i \sum_j \Lambda_{ij} \left[\frac{\Delta P_i}{G_i} - x' \sin(\varphi_i - \varphi_E) - y' \cos(\varphi_i - \varphi_E) \right]$$

$$\times \left[\frac{\Delta P_j}{G_j} - x' \sin(\varphi_j - \varphi_E) - y' \cos(\varphi_j - \varphi_E) \right]$$

The coefficient of $(x')^2$ is:

$$\frac{1}{\Lambda} \sum_i \sum_j \Lambda_{ij} \sin(\varphi_i - \varphi_E) \sin(\varphi_j - \varphi_E)$$

The coefficient of $(y')^2$ is:

$$\frac{1}{\Lambda} \sum_i \sum_j \Lambda_{ij} \cos(\varphi_i - \varphi_E) \cos(\varphi_j - \varphi_E)$$

The principal semi-axes are then:

$$\sigma_E = \left[\frac{\Lambda}{\sum_i \sum_j \Lambda_{ij} \sin(\varphi_i - \varphi_E) \sin(\varphi_j - \varphi_E)} \right]^{1/2}$$

$$\sigma'_E = \left[\sum_i \sum_j \frac{\Lambda}{\Lambda_{ij} \cos(\varphi_i - \varphi_E) \cos(\varphi_j - \varphi_E)} \right]^{1/2}$$

See Figures 4B-5 and 4B-6.

In conclusion we make the following observations regarding this derivation:

1) The form of the density function in which the exponent can take on a zero value but no positive value we will refer to here as the standardized form. In general, the canonical form is not the standardized form when the function is viewed as a two-dimensional (although multi-variate) distribution.

2) In our procedure we need never actually find the standardized form: we can find our goals (x_E, y_E, φ_E, φ'_E, σ_E, σ'_E) in the working form.

3) Our procedure synthesizes a joint two-dimensional normal distribution from an original multi-dimensional distribution, where the several dimensions become merely variates in the plane. The resulting distribution is dimensionally reduced because it is, in effect, a conditional distribution; i.e., it is the distribution resulting from the superposition onto the set of observations of the additional constraint that all LOP's lie in the given plane.

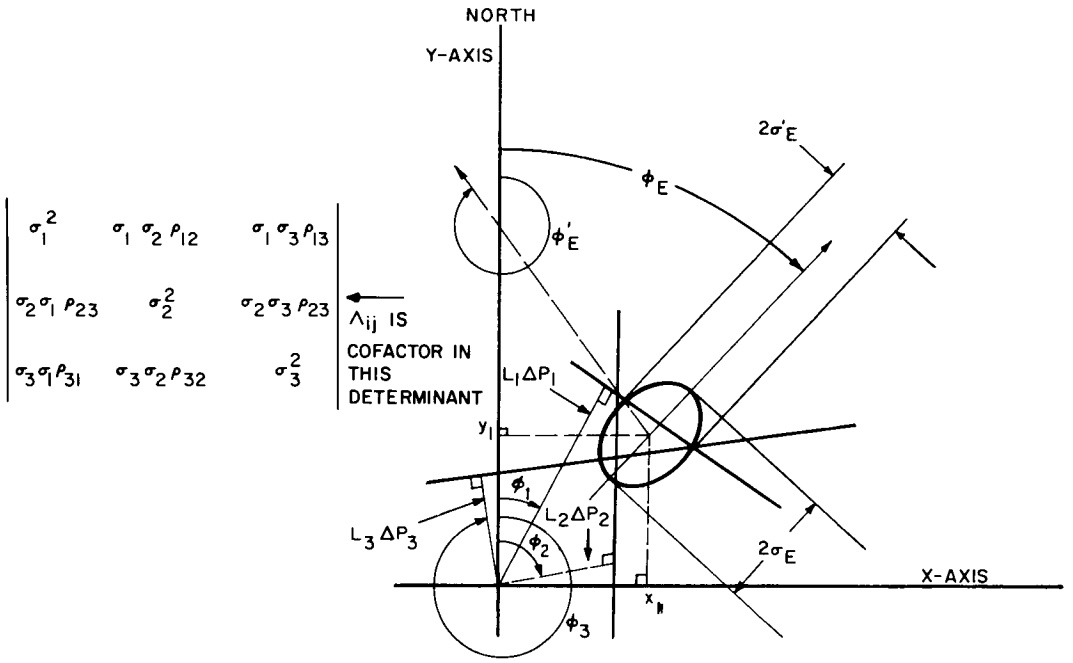

$$\begin{vmatrix} \sigma_1^2 & \sigma_1\sigma_2\rho_{12} & \sigma_1\sigma_3\rho_{13} \\ \sigma_2\sigma_1\rho_{23} & \sigma_2^2 & \sigma_2\sigma_3\rho_{23} \\ \sigma_3\sigma_1\rho_{31} & \sigma_3\sigma_2\rho_{32} & \sigma_3^2 \end{vmatrix} \leftarrow \Lambda_{ij} \text{ IS COFACTOR IN THIS DETERMINANT}$$

$$A = \sum_i \sum_j 2\Lambda_{ij} \sin\phi_i \sin\phi_j$$

$$B = \sum_i \sum_j \Lambda_{ij} \sin(\phi_i + \phi_j)$$

$$C = \sum_i \sum_j 2\Lambda_{ij} \cos\phi_i \cos\phi_j$$

$$D = \sum_i \sum_j \Lambda_{ij} \cos(\phi_i + \phi_j)$$

$$\phi_E = \frac{1}{2}\tan^{-1}\frac{B}{D}$$

$$\phi_E' = \phi_E - 90°$$

$$\sigma_E = \left[\frac{\Lambda}{\sum\sum \Lambda_{ij} \sin(\phi_i - \phi_E)\sin(\phi_j - \phi_E)}\right]^{\frac{1}{2}}$$

$$\sigma_E' = \left[\frac{\Lambda}{\sum\sum \Lambda_{ij} \cos(\phi_i - \phi_E)\sin(\phi_j - \phi_E)}\right]^{\frac{1}{2}}$$

$$x_I = \frac{\sqrt{C^2+B^2}}{AC-B^2}\left[\sum_i\left[\sum_j \Lambda_{ij}\sin\left(\phi_j - \tan^{-1}\frac{B}{C}\right)\right] L_i\Delta P_i + \sum_j\left[\sum_i \Lambda_{ij}\sin\left(\phi_i - \tan^{-1}\frac{B}{C}\right)\right] L_j\Delta P_j\right]$$

$$y_I = \frac{\sqrt{A^2+B^2}}{AC-B^2}\left[\sum_i\left[\sum_j \Lambda_{ij}\cos\left(\phi_j + \tan^{-1}\frac{B}{A}\right)\right] L_i\Delta P_i + \sum_j\left[\sum_i \Lambda_{ij}\cos\left(\phi_i + \tan^{-1}\frac{B}{A}\right)\right] L_j\Delta P_j\right]$$

Figure 4B-5. General Solution to the Over-Determined Fix

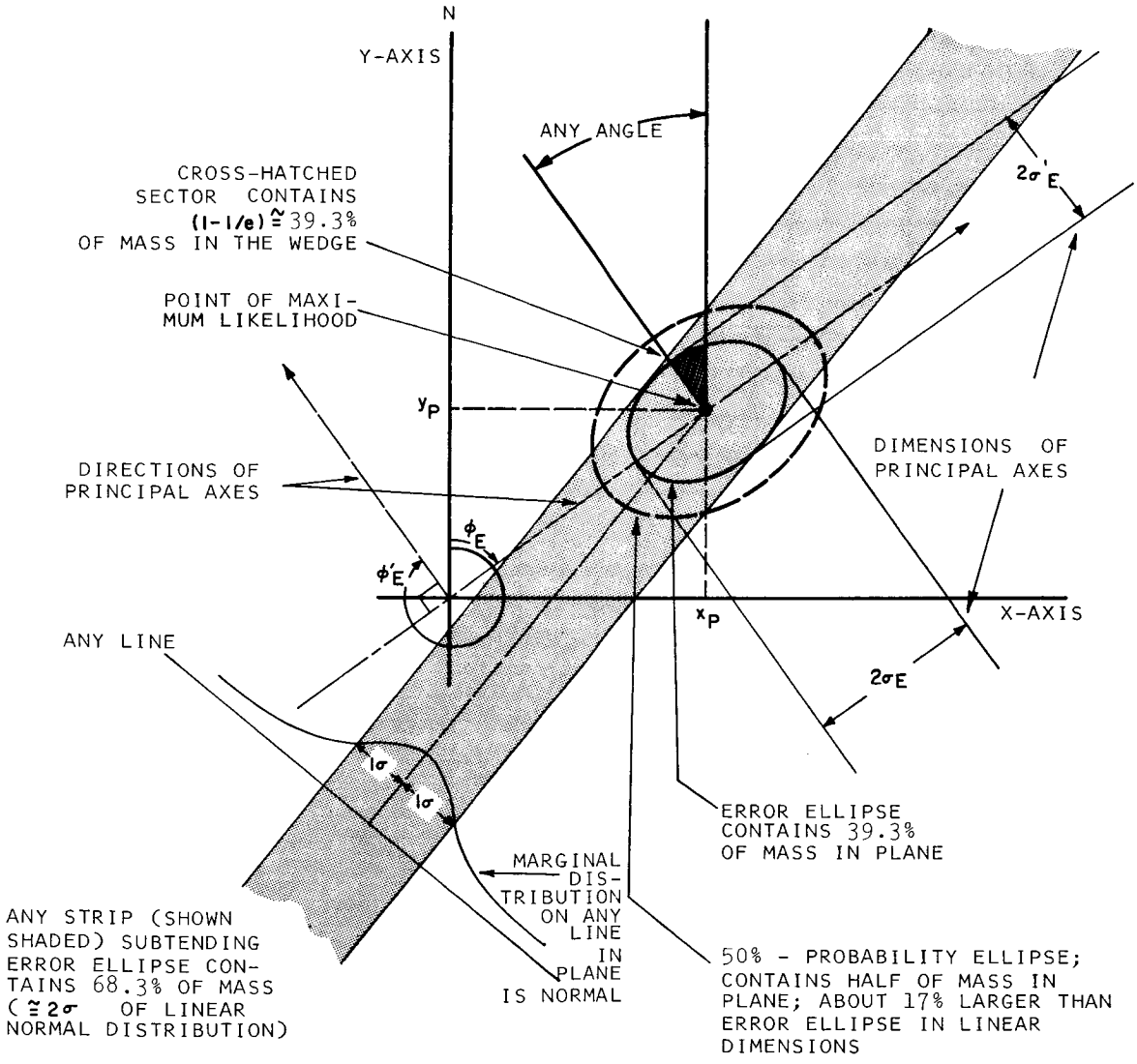

Figure 4B-6. Properties of the Error Ellipse

Appendix 6A

HOMODYNE DETECTOR WITH WHITE NOISE (C_{11})

This case is the easiest to analyze, and provides a lower bound on expected system measurement errors.

6A.1 GENERAL ANALYSIS

For Model 1, the IF output signal and noise is represented by

$$y(t) \approx y_D(t) + n_d(t) \tag{1}$$

where n_d represents the downlink noise, and

$$y_D(t) = A_s\, a_u(t)\, a_d(t) \cos\left[\Delta\omega t + \phi\right]\left[t - \tau(t) - \Delta(t)\right] \tag{2}$$

$\tau(t)$ represents the desired uplink and downlink transmission path time delay. $\Delta(t)$ represents the time delay error due to uplink and downlink atmospheric refraction and due to various equipment delays as described in **section 6.3, channel characterization.**

For a two-tone phase-modulated carrier,

$$\begin{cases} x(t) = \sqrt{2P_T}\cos\left[\omega_c t + \theta(t) + \phi_0\right] \\ \theta(t) = \sum_{k=1}^{2} m_k \sin\left(\omega_k t + \alpha_k\right) \end{cases} \tag{3}$$

Assuming that $\Delta\omega t + \varphi$ is due to a frequency and phase offset of the incoming IF signal relative to the receiver IF frequency, y_D can be replaced by

$$y_D(t) = A(t)\cos\left[(\omega_c+\Delta\omega)(t-\tau-\Delta) + \theta(t-\tau-\Delta) + \varphi_o + \varphi\right] \tag{4}$$

where $A(t)$ represents a slowly varying received signal envelope due to antenna fluctuations, Faraday rotation, and time variable transmission loss.

If the IF carrierphase and frequency are known, a homodyne detector can be used, with the resulting output signal component:

$$z(t) = 2\,LF\left\{ y_D(t)\sin\left[(\omega_c+\Delta\omega)(t-\tau-\Delta) + \varphi_o+\varphi\right]\right\}$$
$$= A(t)\sin\left[\theta(t-\tau-\Delta)\right] \tag{5}$$

The symbol LF $\{\ \}$ refers to the low frequency portion of the quantity in brackets. The tone filter output only involves low frequency components in the vicinity of the tone frequency.

The tone signal components of (5) are:

$$z(t) = 2A\sum_{j\neq k=1}^{2} J_0(m_k)J_1(m_j)\sin\left[\omega_j(t-\tau-\Delta)+\alpha_j\right] \tag{6}$$

where $J_n(m)$ are n-th order Bessel functions.

Taking $\alpha_1=\alpha_2=0$, the signal component of the j-th tone filter output is:

$$z_j(t) = 2AJ_0(m_k)J_1(m_j)\sin\left[\omega_j(t-\tau-\Delta)\right]\ ;\ j\neq k=1,2 \tag{7}$$

This assumes unity gain tone filters, and slowly varying envelope and time-delay. The homodyne detector noise output is

$$n(t) = 2\,LF\left\{ n_d(t)\sin\left[(\omega_c+\Delta\omega)(t-\tau-\Delta)+\varphi_o+\varphi\right]\right\} \tag{8}$$

where n_d is band-limited white noise with double-sided spectral density N_o and bandwidth W_{IF}, centered at ω_c. Therefore,

$$n_d(t) = I_{cd}(t)\cos(\omega_c t) - I_{sd}(t)\sin(\omega_c t) \tag{9}$$

Applying (9) to (8),

$$\eta(t) = I_{cd}(t)\sin[\Delta\omega t + \theta_0] - I_{sd}(t)\cos[\Delta\omega t + \theta_0] \tag{10}$$

where

$$\theta_0 = (\omega_c + \Delta\omega)(\tau + \Delta) + \varphi_1 + \varphi \tag{11}$$

is of no importance in determining the noise power spectrum. The covariance function of $\eta(t)$ is:

$$\psi_\eta(\tau) = \langle \eta(t)\,\eta(t+\tau)\rangle$$
$$= \psi_{I_{cd}}(t)\cos(\Delta\omega\tau) \tag{12}$$

where $\psi_{I_{cd}}$ represents the autocovariance function of the inphase component of I_{cd}. Assuming I_{cd} has a rectangular power spectrum on the interval $(-\frac{W_{IF}}{2}, \frac{W_{IF}}{2})$ the power spectrum corresponding to (12) consists of a sum of two rectangles of height N_0, one centered at $\Delta\omega$, and the other centered at $-\Delta\omega$. The resulting power spectrum is shown in Figure 6A-1.

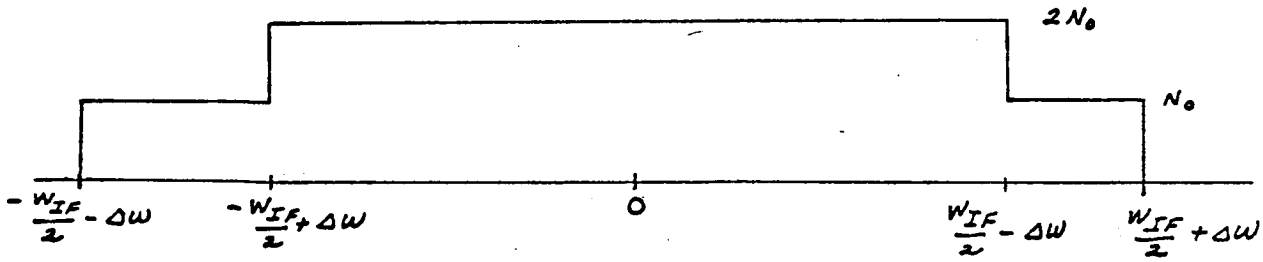

FIGURE 6A-1. Power Spectrum of Homodyne Detector Output Noise

As long as the tone frequencies f_1 and f_2 occur in the interval $(-\frac{W_{IF}}{2} + \Delta\omega, \frac{W_{IF}}{2} - \Delta\omega)$, which will be the usual case, the noise spectral density in the tone filter passbands will be $2\,N_0$. Therefore the noise power at the j-th tone filter output will be $4N_0W_{0j}$, where W_{0j} is the j-th tone filter output noise bandwidth. The analysis assumes double-sided spectra and filters throughout.

It follows from the above, and equation (7) that the j-th filter output signal-to-noise ratio will be:

$$\left(\frac{S}{N}\right)_{oj} = \frac{A^2 J_0^2(m_k)\, J_1^2(m_j)}{2 N_0 W_{oj}} \quad ; \; j \neq k = 1, 2 \tag{13}$$

This quantity can be related to the IF carrier-to-noise power ratio,

$$\left(\frac{C}{N}\right)_{IF} = \frac{A^2}{4 N_0 W_{IF}} \tag{14}$$

in which case,

$$\left(\frac{S}{N}\right)_{oj} = 2 J_0^2(m_k) J_1^2(m_j) \frac{W_{IF}}{W_{oj}} \left(\frac{C}{N}\right)_{IF} \tag{15}$$

Since the useful signal power for ranging purposes is contained in the tone sidebands, it is meaningful to relate the tone-filter output signal-to-noise ratio to the average power of the j-th tone frequency side-band at the IF output. The carrier and tone sideband components are:

$$y_D(t) = A J_0(m_1) J_0(m_2) \cos\left[(\omega_c + \Delta\omega)(t - \tau - \Delta) + \omega_0 + \varphi\right] - 2A \left[\sum_{j \neq k = 1}^{2} J_0(m_k) J_1(m_j) \sin\left[\omega_j (t - \tau - \Delta)\right]\right] \sin\left[(\omega_c + \Delta\omega)(t - \tau - \Delta) + \omega_0 + \varphi\right] \tag{16}$$

It follows that the j-th tone side-bands have average power

$$P_j = A^2 J_0^2(m_k) J_1^2(m_j) \tag{17}$$

Therefore the j-th tone side-band signal-to-noise ratio at the IF output will be

$$\left(\frac{S}{N}\right)_{IF,j} = \frac{A^2 J_0^2(m_k) J_1^2(m_j)}{2 N_0 W_{IF}} \tag{18}$$

Applying this to (13),

$$\left(\frac{S}{N}\right)_{oj} = \frac{W_{IF}}{W_{oj}} \left(\frac{S}{N}\right)_{IF,j} \tag{19}$$

A third signal-to-noise ratio of some interest is the total IF tone side-band signal-to-noise ratio

$$\left(\frac{S}{N}\right)_{IF} = \frac{A^2}{2N_0 W_{IF}} \left[J_0^2(m_1) J_1^2(m_2) + J_0^2(m_2) J_1^2(m_1)\right] \tag{20}$$

Applying this to (13),

$$\left(\frac{S}{N}\right)_{oj} = \left[\frac{J_0^2(m_k) J_1^2(m_j)}{J_0^2(m_1) J_1^2(m_2) + J_0^2(m_2) J_1^2(m_1)}\right] \frac{W_{IF}}{W_{oj}} \left(\frac{S}{N}\right)_{IF} \tag{21}$$

The most useful signal-to-noise ratio relationship, is (15), which gives the tone-filter output signal-to-noise ratio as a function of the carrier-to-noise ratio, which is the total received I.F. signal-to-noise ratio.

An important quantity in choosing the modulation index is the ratio of the sideband power to the carrier power. From (16), the tone of frequency ω_1 has amplitude $A J_0(m_2) J_1(m_1)$ after I.F. carrier demodulation. Therefore, the tone power to carrier power ratio is:

$$R_{1C} = \frac{J_0^2(m_2) J_1^2(m_1)}{J_0^2(m_1) J_0^2(m_2)} = \frac{J_1^2(m_1)}{J_0^2(m_1)} \tag{22}$$

Figure 6A-2 contains a plot of this quantity in decibels as a function of the modulation index m. When $m \approx 1.44$, the two powers are equal. This is a possible criterion for choice of m.

Denoting the j-th tone filter output for the ℓ-th I.F. by $y_{j\ell}$, it follows from (7) that

$$y_{j\ell}(t) = 2A J_0(m_k) J_1(m_j) A_\ell(t) \sin[\omega_j(t-\tau_\ell-\Delta_\ell)] + n_{j\ell}(t) \qquad (23)$$

τ_ℓ represents the true total path delay for the k-th satellite repeater channel. Δ_ℓ represents the corresponding total delay error. $n_{j\ell}$ represents the additive noise at the output of the j-th tone filter for the ℓ-th I.F.

When the phase comparison is made with an accurate local oscillator with output $\sin(\omega_j t)$, the phase detector output will be:

$$\phi_{j\ell} = \left\{ 2\pi f_j (\tau_\ell + \Delta_\ell) \right\}_{mod\, 2\pi} + \epsilon_{j\ell} \qquad (24)$$

Assuming large tone-filter output signal-to-noise ratio, $\epsilon_{j\ell}$ will be approximately normally distributed with zero mean and variance

$$\sigma^2_{j\ell} = \frac{1}{2\left(\frac{S}{N}\right)_{j\ell}} \qquad (25)$$

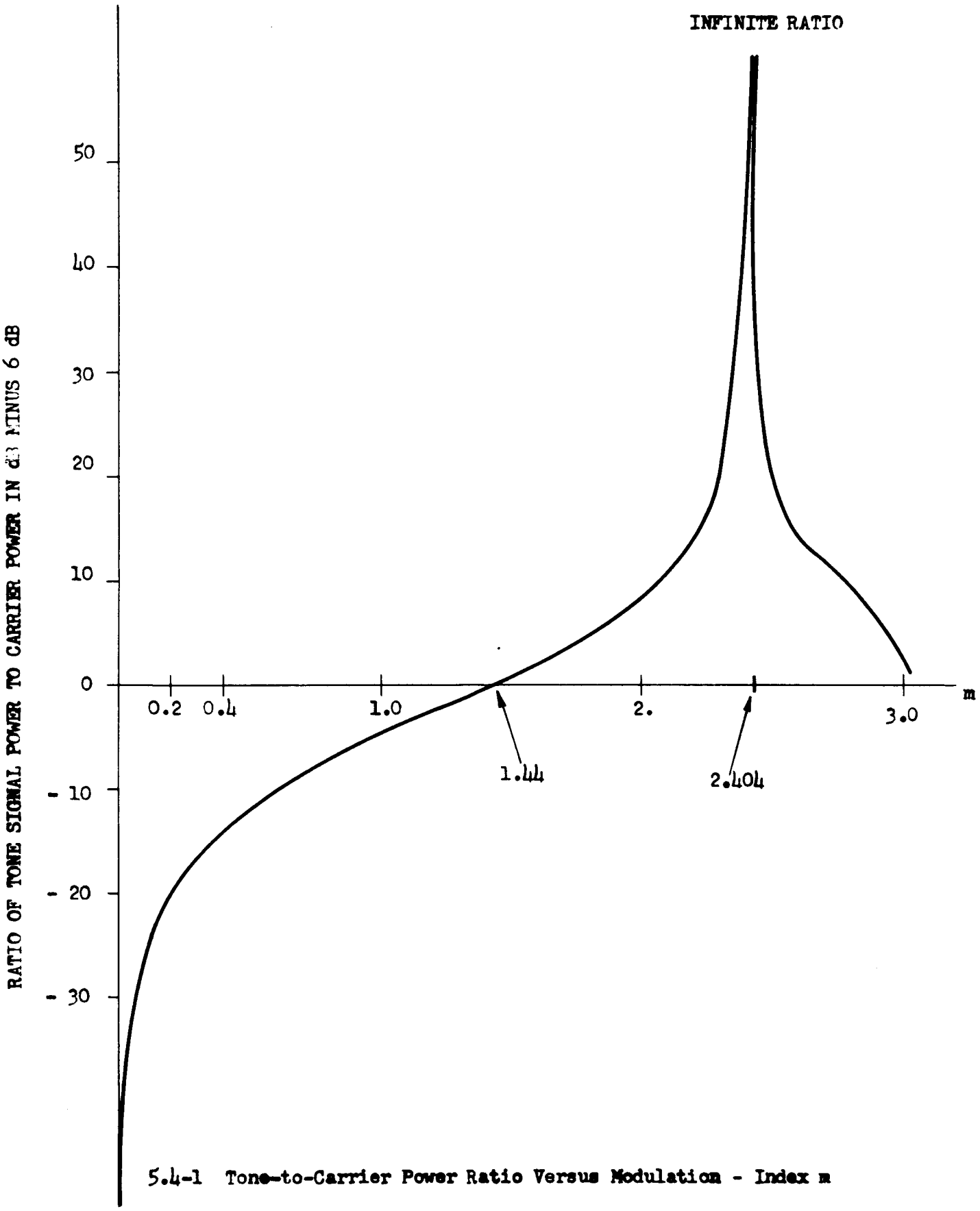

5.4-1 Tone-to-Carrier Power Ratio Versus Modulation - Index m

where $\left(\frac{S}{N}\right)_{j\ell}$ represents the tone filter output signal-to-noise ratio for the j-th tone frequency and the ℓ-th satellite.

From (24), the actual phase measurement error will be:

$$\Delta\phi_{j\ell} = \phi_{j\ell} - \left\{2\pi f_j \tau_\ell\right\}_{mod\,2\pi} \tag{26}$$

Assuming that $f_j\Delta_\ell$ is much less than unity,

$$\Delta\phi_{j\ell} = \omega_j\Delta_\ell + \epsilon_{j\ell} \tag{27}$$

The corresponding distance error is:

$$\Delta R_{j\ell} = \frac{c\,\Delta\phi_{j\ell}}{\omega_j} = c\Delta_\ell + \frac{c\,\epsilon_{j\ell}}{\omega_j} \tag{28}$$

For tone filter output signal-to-noise ratios greater than or equal to 10 db, the conditional probability distribution of $\Delta R_{j\ell}$ for given Δ_ℓ will be approximately normal with mean $c\Delta_\ell$ and standard deviation:

$$\sigma\left[\Delta R_{j\ell} \mid \Delta_\ell\right] = \frac{c}{\omega_j\sqrt{2\left(\frac{S}{N}\right)_{j\ell}}} \tag{29}$$

This expression is equivalent to σ_{min} in equation (5) of subsection 6.1, if we equate the tone filter output signal-to-noise ratio with the tone filter output signal-energy-to-noise spectral density. This is reasonable, since the tone filter can be regarded as an integrator with integration-time equal to the reciprocal of its bandwidth.

Figure 6A-3 contains a plot of the above standard deviation as a function of tone filter output signal-to-noise ratio for tone frequencies equal to 1 MHz and 31.25 KHz. For a 10 db output signal-to-noise ratio, the standard deviation is about 2.4 meters at 1 MHz, and about 68.5 meters at 31.25 KHz. For a 30 db output signal-to-noise ratio, the standard deviation is about .21 meters at 1 MHz and about 6.85 meters at 31.25 KHz.

If we average over the probability distribution of time-delay errors Δ_ℓ as well as that for the errors due to additive noise, $\epsilon_{j\ell}$, the mean and variance of $\Delta R_{j\ell}$ are:

$$b_{j\ell} = \langle \Delta R_{j\ell} \rangle = c \langle \Delta_\ell \rangle$$

$$D_{j\ell}^2 = c^2 \sigma^2(\Delta_\ell) + \frac{1}{2\left(\frac{S}{N}\right)_{j\ell}}$$

The coefficient of variation of the distance error is:

$$C_{j\ell} = \frac{D_{j\ell}}{b_{j\ell}} = \left[C_\ell^2 + \frac{1}{2c^2\left(\frac{S}{N}\right)_{j\ell}} \right]^{\frac{1}{2}} \approx C_\ell \qquad (30)$$

where

$$C_\ell = \frac{\sigma(\Delta_\ell)}{\langle \Delta_\ell \rangle} \qquad (31)$$

is the coefficient of variation of the total time-delay error. In other words, if the coefficient of variation of the total time-delay error is significantly different from zero, then the explicit dependence of the coefficient of variation of the distance error on tone-filter output signal-to-noise ratio and tone frequency disappears. There will be irreducible errors regardless of signal-to-noise ratio and tone frequency.

FIGURE 6A-3 - STANDARD DEVIATION OF RANGE ERROR VS. TONE FILTER OUTPUT S/N FOR CASE C_{11}

(TONE FREQUENCIES = 31.25 MH_z and 1 MH_z)

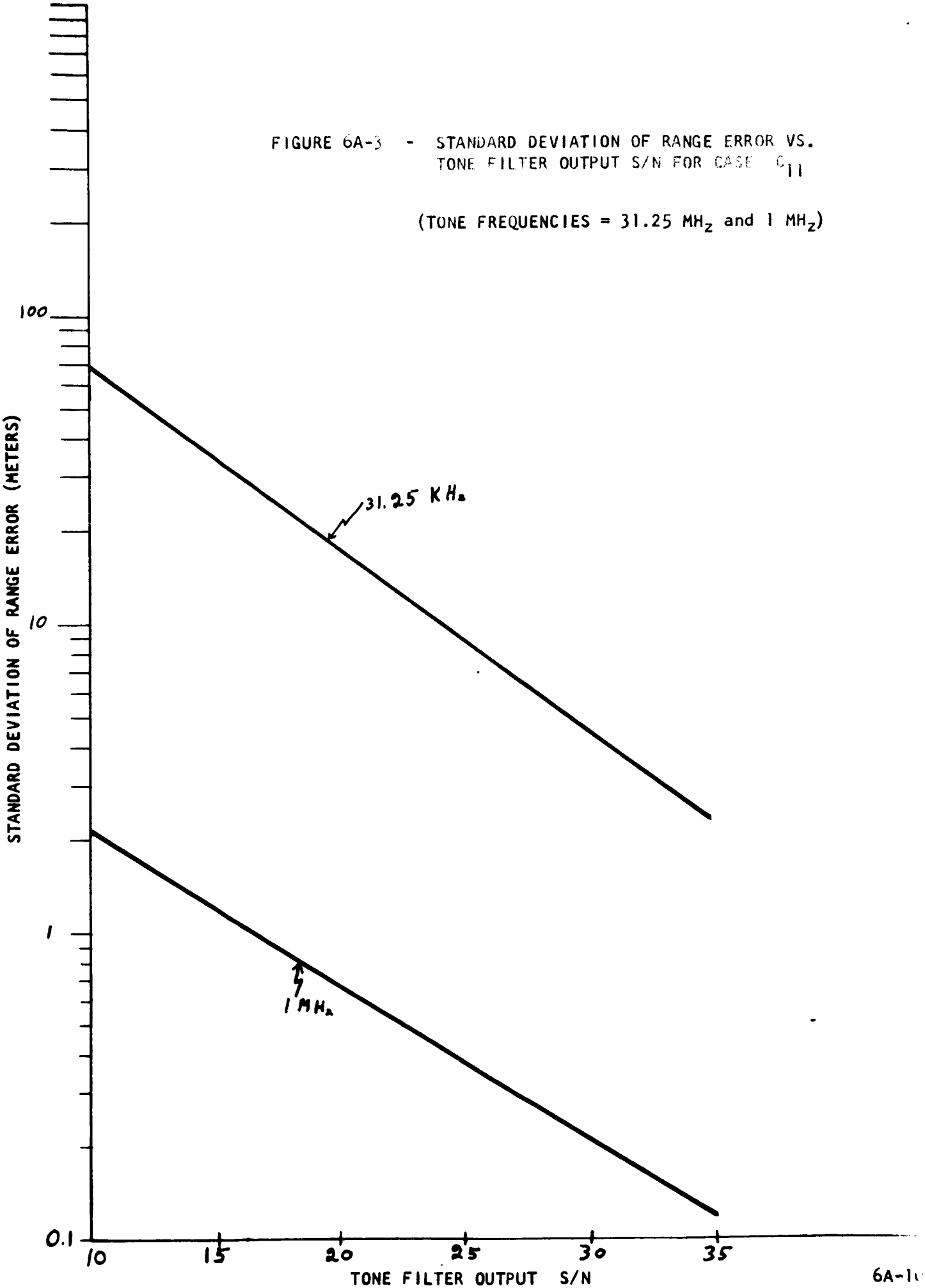

The validity of this is based on the correctness of (28) which assumes that

$$\Delta_\ell < \frac{\alpha}{f_j} \tag{32}$$

where α is a constant much less than unity. This implies that

$$c\Delta_\ell < \frac{\alpha c}{f_j} \tag{33}$$

Taking $\alpha = 0.1$, $c\Delta_\ell$ must be less than 960 meters for a tone frequency of 31.25 KHz, whereas $c\Delta_\ell$ must be less than 30 meters for a tone frequency of 1 MHz.

Section 6A.2 contains a more detailed signal and noise analysis, including small modulation index approximations. An analysis is given there of the performance of a zero-crossing phase detector. For large signal-to-noise ratios, it is shown that the phase measurement error statistics approach those of an ideal phase detector with standard deviation as given in equation (29).

When a phase comparison is made between two satellites, as in the relative navigation mode, it follows from (24) that the resulting phase difference for the j-th tone is:

$$\phi_{j1} - \phi_{j2} = \left\{ \omega_j(\tau_1+\Delta_1) \right\}_{mod\,2\pi} - \left\{ \omega_j(\tau_2+\Delta_2) \right\}_{mod\,2\pi} + \epsilon_{j1} - \epsilon_{j2} \tag{34}$$

Assuming $f_j\Delta_\ell$ to be less than unity as in (26), the resulting phase difference measurement error will be

$$\Delta\phi_{j1} - \Delta\phi_{j2} = \omega_j(\Delta_1 - \Delta_2) + \epsilon_{j1} - \epsilon_{j2} \tag{35}$$

The corresponding range difference error is:

$$\Delta R_{j1} - \Delta R_{j2} = c(\Delta_1 - \Delta_2) + \frac{c(\epsilon_{j1} - \epsilon_{j2})}{\omega_j} \tag{36}$$

This error has mean and standard deviation

$$\langle \Delta R_{j1} - \Delta R_{j2} \rangle = c \langle \Delta_1 - \Delta_2 \rangle$$

$$\sigma(\Delta R_{j1} - \Delta R_{j2}) = c \left\{ \sigma^2(\Delta_1 - \Delta_2) + \frac{1}{2 w_j^2} \left[\frac{1}{\left(\frac{S}{N}\right)_{j1}} + \frac{1}{\left(\frac{S}{N}\right)_{j2}} \right] \right\} \quad (37)$$

The time delay errors Δ_i should be mutually uncorrelated so that

$$\sigma^2(\Delta_1 - \Delta_2) = \sigma^2(\Delta_1) + \sigma^2(\Delta_2) \quad (38)$$

In an absolute navigation mode using 3 satellites, the errors are

$$\begin{cases} X = \Delta R_{j1} - \Delta R_{j2} \\ Y = \Delta R_{j3} - \Delta R_{j2} \end{cases} \quad (39)$$

The mean value and variance formulae are as in (37). Account has to be taken for the covariance between X and Y.

$$\sigma(X, Y) = \langle XY \rangle - \langle X \rangle \langle Y \rangle \quad (40)$$

From (39)

$$\sigma(X, Y) = \sigma^2(\Delta R_{j2}) \quad (41)$$

on the assumption that ΔR_{j1}, ΔR_{j2}, and ΔR_{j3} are mutually uncorrelated.

The product-moment correlation coefficient between X and Y is:

$$r_j = \frac{\sigma(X, Y)}{\sigma(X)\sigma(Y)}$$

$$= \frac{\sigma^2(\Delta R_{j2})}{\left\{ \left[\sigma^2(\Delta R_{j1}) + \sigma^2(\Delta R_{j2}) \right] \left[\sigma^2(\Delta R_{j3}) + \sigma^2(\Delta R_{j2}) \right] \right\}^{\frac{1}{2}}} \quad (42)$$

In the special case of equal variances, this correlation coefficient equals one-half.

In the Appendixes, the mean and standard deviation for a single range measurement will be calculated for the different cases summarized in Table 6-10. Given these quantities, the required means, standard deviations, and correlations for the relative and absolute navigation schemes can be calculated from the above formulae.

Exact phase error probability distributions for an ideal phase detector, can be obtained by applying equation (23). This can be done as follows. For simplicity, a single satellite transmission and tone frequency ω_1 will be considered. Writing the tone filter output signal plus noise in terms of inphase and quadrature components about $x = \omega_1 (t-\tau-\Delta)$,

$$y_1(t) = A_c \cos x + A_s \sin x \tag{43}$$

where

$$\begin{cases} A_c = \sigma I_c \\ A_s = 2A J_0(m_2) J_1(m_1) + \sigma I_s \end{cases} \tag{44}$$

where σ is the standard deviation of the tone filter output noise, and I_c, I_s are normalized inphase and quadrature components of this output noise. The signal plus noise y_1 in (43) can be written

$$y_1(t) = \sqrt{A_c^2 + A_s^2}\, \sin(x + \delta_1) \tag{45}$$

where

$$\delta_1 = \operatorname{Arctan}\left(\frac{A_c}{A_s}\right) = \operatorname{Arctan}\left[\frac{I_c}{\frac{2A}{\sigma} J_0(m_2) J_1(m_1) + I_s}\right] \tag{46}$$

represents the phase error. Applying (13) to (46),

$$\delta_j = \operatorname{Arctan}\left[\frac{I_c}{\sqrt{2\left(\frac{S}{N}\right)_{oj}} + I_s}\right] \tag{47}$$

where

$$\sigma^2 = 4 N_0 W_{oj} \tag{48}$$

For large signal-to-noise ratios,

$$\delta_j \approx \frac{I_c}{\sqrt{2\left(\frac{S}{N}\right)_{oj}}} \tag{49}$$

so that δ_j is normally distributed with zero mean and variance equal to the reciprocal of twice the tone filter output signal-to-noise ratio as stated in (29). As the signal-to-noise ratio approaches zero, the phase error distribution approaches a uniform distribution over $(0,2\pi)$, as one would expect.

6A2 Small Modulation Index

The IF output signal and noise is:

$$x(t) = s(t) + n(t) \tag{1}$$

where

$$s(t) = A\cos\left[\omega_0 t + \theta + m_1 \sin(\omega_1 t + \theta_1) + m_2 \sin(\omega_2 t + \theta_2)\right] \tag{2}$$

and

$$n(t) = I_c(t)\cos\omega_0 t - I_s(t)\sin\omega_0 t \tag{3}$$

It is possible to represent the signal term with in-phase and quadrature components by using a Bessel expansion

$$s(t) = A\left[I_{c\times D}(t)\cos(\omega_0 t + \theta) - I_{s\times D}(t)\sin(\omega_0 t + \theta)\right] \tag{4}$$

where the in-phase component is:

$$\begin{aligned} I_{c\times D}(t) = &\left[J_0(m_1) + 2\sum_{n_1=1}^{\infty} J_{2n_1}(m_1)\cos 2n_1(\omega_1 t + \theta_1)\right]\cdot \\ &\cdot\left[J_0(m_2) + 2\sum_{n_2=1}^{\infty} J_{2n_2}(m_2)\cos 2n_2(\omega_2 t + \theta_2)\right] \\ &-\left[2\sum_{n_1=0}^{\infty} J_{2n_1+1}(m_1)\sin(2n_1+1)(\omega_1 t + \theta_1)\right]\cdot \\ &\cdot\left[2\sum_{n_2=0}^{\infty} J_{2n_2+1}(m_2)\sin(2n_2+1)(\omega_2 t + \theta_2)\right] \end{aligned} \tag{5}$$

and the quadrature component is:

$$I_{SXD}(t) = \left[2\sum_{n_1=0}^{\infty} J_{2n_1+1}(m_1)\sin(2n_1+1)(\omega_1 t+\theta_1)\right]\cdot$$
$$\cdot\left[J_0(m_2)+2\sum_{n_2=1}^{\infty} J_{2n_2}(m_2)\cos\left[(2n_2)(\omega_2 t+\theta_2)\right]\right]$$
$$+\left[J_0(m_1)+2\sum_{n_2=1}^{\infty} J_{2n_1}(m_1)\cos\left[(2n_1)(\omega_1 t+\theta_1)\right]\right]\cdot$$
$$\cdot\left[2\sum_{n_2=0}^{\infty} J_{2n_2+1}(m_2)\sin\left[(2n_2+1)(\omega_2 t+\theta_2)\right]\right] \qquad (6)$$

It is possible to define a number of different input signal-to-noise ratios. The carrier-to-noise ratio is:

$$(C/N)_{IF} = A^2/4N_0 W_{IF} \qquad (7)$$

for a double-sided noise power spectrum with total noise power $2N_0 \cdot W_{IF}$. Another signal-to-noise ratio is the j-th tone sideband signal-to-noise ratio at the IF output:

$$(S/N)_{IF,j} = \frac{A^2\left[J_0(m_k)\,J_1(m_j)\right]^2}{2N_0 W_{IF}}, \qquad j \neq k = 1,2 \qquad (8)$$

which information is contained in the IF signal output quadrature term. For small modulation indices, (8) reduces to:

$$\left(\frac{S}{N}\right)_{IF,j} = \frac{A^2 m_j^2}{8N_0 W_{IF}}, \qquad m_j < 1/2 \qquad (9)$$

A third signal-to-noise ratio is the total IF-tone sideband signal-to-noise ratio:

$$\left(\frac{S}{N}\right)_{IF} = \frac{A^2\left[1 - J_o^2(m_1)J_o^2(m_2)\right]}{4N_o W_{IF}} \tag{10}$$

For small modulation indices, we cannot use Equation (10) because it takes into account all intermodulation frequencies in addition to f_1 and f_2 in which we are interested. Hence for small modulation indices, the total IF tone sideband signal-to-noise ratio is:

$$\left(\frac{S}{N}\right)_{IF} = \frac{A^2(m_1^2+m_2^2)}{8N_o W_{IF}}, \quad m_1, m_2 < 1/2 \tag{11}$$

Let the local oscillator output r(t) be described by:

$$r(t) = \sin(\omega_o t + \theta + \varphi) \tag{12}$$

where φ represents lag or advance of the L.O. output on the phase of the IF carrier. This output and the IF output are processed in a product detector with a low frequency output:

$$\begin{aligned} z(t) &= LF\left[x(t)\, r(t)\right] \\ &= \frac{A}{2}\left[I_{cxD}(t)\sin\varphi - I_{sxD}(t)\cos\varphi\right] + \frac{1}{2}\left[I_c(t)\sin(\theta+\varphi) - I_s(t)\cos(\theta+\varphi)\right] \end{aligned} \tag{13}$$

This signal plus noise is now passed through the tone filters F_1 and F_2 of width W_{o1} and W_{o2} (not necessarily equal) at frequencies $\pm f_1$ and $\pm f_2$, since we consider double-sided spectra.

We note that the desirable output is contained in the IF signal quadrature component. Denoting the tone filter output by $y_j(t)$, $j = 1, 2$ corresponding to the tones, we obtain

$$y_j(t) = -A J_0(m_k) J_1(m_j) \cos\varphi \sin(\omega_j t + \theta_j) + \frac{1}{2}\left[I_c(t) \sin(\theta+\varphi) - I_s(t) \cos(\theta+\varphi)\right] \; ; \; j = 1, 2 \tag{14}$$

We now want to relate the output signal-to-noise ratio to the input S/N ratio.

The signal power of the j-th tone filter output is:

$$S_{oj} = \left[A J_0(m_k) J_1(m_j) \cos\varphi\right]^2 / 2 \tag{15}$$

The noise power of this filter is:

$$N_{oj} = \frac{1}{4}(2N_0) 2 W_{oj} = N_0 W_{oj} \tag{16}$$

The output signal-to-noise ratio is thus:

$$\left(\frac{S}{N}\right)_{oj} = \frac{\left[A J_0(m_k) J_1(m_j) \cos\varphi\right]^2}{2 N_0 W_{oj}} \tag{17}$$

or alternately:

$$\left(\frac{S}{N}\right)_{oj} = \left(\frac{S}{N}\right)_{IF} \frac{2W_{IF}}{W_{oj}} \left[J_0(m_k) J_1(m_j)\right]^2 \cos^2\varphi$$

$$= \left(\frac{S}{N}\right)_{IF,j} \frac{W_{IF}}{W_{oj}} \cos^2\varphi$$

$$= \left(\frac{S}{N}\right)_{IF} \frac{2W_{IF}}{W_{oj}} \frac{\left[J_0(m_k) J_1(m_j)\right]^2 \cos^2\varphi}{\left[1 - J_0^2(m_1) J_0^2(m_2)\right]} \tag{18}$$

For small modulation indices, the corresponding relationships are:

$$\left(\frac{S}{N}\right)_{oj} = \left(\frac{S}{N}\right)_{IF} \frac{m_j^2}{2} \frac{W_{IF}}{W_{oj}} \cos^2\varphi$$

$$= \left(\frac{S}{N}\right)_{IF} \frac{W_{IF}}{W_{oj}} \cos^2\varphi$$

$$= \left(\frac{S}{N}\right)_{IF} \frac{W_{IF}}{W_{oj}} \frac{m_j^2}{m_1^2+m_2^2} \cos^2\varphi \qquad (19)$$

The tone filter output as described in Equation (14), together with either an L.O. output or another tone filter output as obtained from a second satellite and a different tone demodulator system, are processed in a phase detector.

6A.3 Performance of a Zero Crossing Phase Detector

Let the phase detector be an ideal zero-crossing phase detector, and let the two input signals with noise be:

$$H_1(t) = A_1 \cos(\omega_j t + \theta) + n_1(t) \quad ; \quad 1^{st} \text{ satellite}$$

$$H_2(t) = A_2 \cos(\omega_j t + \theta + \varphi) + n_2(t) \quad ; \quad 2^{nd} \text{ satellite} \qquad (20)$$

where A_1 and A_2 are of the form

$$A_i = A J_0(m_k) J_1(m_j) \cos\varphi \quad ; \text{ satellite } i$$

$$\theta = \theta_{j1} \quad ; \text{ first satellite}$$

$$\theta + \varphi = \theta_{j2} \quad ; \text{ second satellite}$$

$$\varphi = \theta_{j2} - \theta_{j1} \qquad (21)$$

$$n_j(t) = \text{Gaussian Noise}$$

Relative to Equation (13), if we let $H_2(t)$ represent also the L.O. A_2 would be equal to unity and $\theta + \phi$ equal to zero, as well as $n_2(t)$. This specialization will be introduced at the end of the analysis.

The zero-crossing measurement consists of calculating the time at which the waveform crosses the zero-axis. Due to the presence of noise, the zero-crossing times t_{oi} of $H_i(t)$ are not equal to the signal zero-crossing times, $t_o^{(i)}$.

Approximating the signal term by a straight line near a positive slope zero-crossing, we find that

$$t_{oi} = t_o^{(i)} - \frac{H_i(t_o^{(i)})}{H_i'(t_o^{(i)})} \tag{22}$$

The prime indicating differentiation with respect to time.

The error in choosing time t_{oi} instead of $t_o^{(i)}$ is

$$\varepsilon_i = \frac{H_i(t_o^{(i)})}{H_i'(t_o^{(i)})}$$

$$= \frac{n_i(t_o^{(i)})}{A_i\omega_j + n_i'(t_o^{(i)})}$$

$$\approx \frac{n_i(t_o^{(i)})}{A_i\omega_j} \tag{23}$$

for high signal-to-noise ratios on the inputs $H_i(t)$.

The estimate $\hat{\phi}$ of the phase difference ϕ is given by:

$$\hat{\phi} = \left[\omega_j (t_{oj} - t_{ok})\right]_{\text{mod} \pm 2\pi} \tag{24}$$

That is, if the quantity in brackets is negative, ϕ is defined module -2π, whereas if it is positive, ϕ is defined module $+2\pi$.

From (21) and (22)

$$\omega_j (t_{o1} - t_{o2}) = \omega_j (t_o^{(1)} - t_o^{(2)}) + \delta \tag{25}$$

where

$$\delta = \omega_j (-\varepsilon_1 + \varepsilon_2)$$
$$= \frac{n_1 (t_o^{(1)})}{A_1} - \frac{n_2 (t_o^{(2)})}{A_2} \tag{26}$$

for high signal-to-noise ratios.

In the absence of noise:

$$\left[\omega_j (t_o^{(1)} - t_o^{(2)}) \right]_{\text{mod} \pm \pi} \tag{27}$$

The conditions for positive slope signal zeros are:

$$\omega_j t_o^{(1)} + \theta = (2n_1\pi - \pi/2) \; ; \quad n_1 = 0, \pm 1, \pm 2, \ldots$$

$$\omega_j t_o^{(2)} + \theta + \varphi = (2n_2\pi - \pi/2) \; ; \quad n_2 = 0, \pm 1, \pm 2, \ldots \tag{28}$$

Therefore:

$$\omega_j (t_o^{(1)} - t_o^{(2)}) = 2(n_1 - n_2)\pi - \theta + \theta + \varphi \tag{29}$$

It follows from (26) and (28) that in the absence of noise

$$\hat{\varphi} = [2(n_1 - n_2)\pi + \varphi]_{\text{mod} \pm 2\pi}$$

$$= (\varphi)_{\text{mod} \pm 2\pi} \tag{30}$$

In the presence of noise

$$\hat{\varphi} = [\varphi + \delta]_{\text{mod} \pm 2\pi} \tag{31}$$

Since the original IF noise was assumed to be white noise with zero mean, the noise on the tone filter outputs is also white with zero mean and centered at f_1. Furthermore, these noises are uncorrelated because they are due to different channels. The variance of δ for high signal-to-noise ratios is:

$$\sigma_\delta^2 = E\left\{\left[\frac{r_1(t_0^{(1)})}{A_1} - \frac{r_2(t_0^{(2)})}{A_2}\right]^2\right\}$$

$$= \frac{N_1}{A_1^2} + \frac{N_2}{A_2^2}$$

$$= \frac{1}{2}\left[\frac{1}{(S/N)_{oj_1}} + \frac{1}{(S/N)_{oj_2}}\right] \tag{32}$$

relating the variance to the tone filter output signal-to-noise ratios of the i^{th} satellite, i = 1, 2.

From (30) the mean value of the phase estimate ϕ is given by:

$$E(\hat{\phi}) = \int_{-\infty}^{\infty} \frac{1}{\sigma\sqrt{2\pi}} \exp\left[-\frac{\delta^2}{2\sigma^2}\right] \cdot (\varphi + \delta)_{\text{mod} \pm 2\pi} \, d\delta \tag{33}$$

and $\sigma = \sigma_\delta$

It is straight forward to show that if we define

$$(\varphi)_{\text{mod} \pm 2\pi} = \varphi_0 \tag{34}$$

that

$$(\varphi + \delta)_{\text{mod} \pm 2\pi} = (\varphi_0 + \delta)_{\text{mod} \pm 2\pi} \tag{35}$$

Substituting y for $\varphi + \delta$ (or $\varphi_0 + \delta$) we can evaluate the integral in Equation (33).

$$E(\hat{\phi}) = \phi_0 + b(\varphi_0, \sigma) \tag{36}$$

where $b(\varphi_0, \sigma)$ represents a bias.

$$b(\varphi_0, \sigma) = 2\pi \sum_{n=1}^{\infty} \left[\Phi\left(\frac{2(n+1)\pi + \phi_0}{\sigma}\right) - \Phi\left(\frac{2n\pi + \phi_0}{\sigma}\right) - \Phi\left(\frac{\phi_0 - 2n\pi}{\sigma}\right) + \Phi\left(\frac{\phi_0 - (2n+1)\pi}{\sigma}\right) \right] \tag{37}$$

$$\Phi(x) = \frac{1}{\sqrt{2\pi}} \int_{-\infty}^{x} \exp\left[-\frac{t^2}{2}\right] dt \tag{38}$$

and φ is the largest integer less than or equal to $\left| \frac{3\sigma - \phi_0}{2\pi} \right|$

This bias is small when

$$|\varphi_0| < 2\pi - 3\sigma \tag{39}$$

or using Equation (32)

$$|\varphi_0| < 2\pi - 3\left[\frac{1}{2}\left(\frac{1}{\left(\frac{S}{N}\right)_{0_{J_1}}} + \frac{1}{\left(\frac{S}{N}\right)_{0_{J_2}}}\right)\right]^{1/2} \tag{40}$$

This amounts to writing

$$E(\hat{\varphi}) = \varphi_0 \tag{41}$$

and $$\hat{\phi} = \phi_0 + \delta \tag{42}$$

Under the assumption of high signal-to-noise ratio on the inputs and Equation (40)

$$\sigma^2(\hat{\phi}) = \sigma^2(\delta) \approx \frac{1}{2}\left[\frac{1}{\left(\frac{S}{N}\right)_{o_{j_1}}} + \frac{1}{\left(\frac{S}{N}\right)_{o_{j_2}}}\right] \tag{43}$$

In case $H_2(t)$ represented the L.O. output cos $\omega_j t$, the important equivalent relationships are:

phase estimate:

$$\hat{\theta} = [\theta + \delta]_{mod \pm 2\pi} \tag{31b}$$

$$\delta \approx \frac{n_1(t_0^{(1)})}{A_1} \tag{26b}$$

$$E(\hat{\theta}) = \hat{\theta} \tag{41b}$$

$$\sigma^2(\hat{\theta}) = \frac{1}{2}\left[\frac{1}{\left(\frac{S}{N}\right)_{o_{j_1}}}\right] \tag{43b}$$

for high signal-to-noise ratio on the input, and

$$|\theta_{mod \pm 2\pi}| < 2\pi - 3\left[\frac{1}{2\left(\frac{S}{N}\right)_{o_{j_1}}}\right]^{1/2} \tag{40b}$$

Appendix 6B

EXTRACTED CARRIER DEMODULATION WITH WHITE NOISE (C_{12})

6B.1 Summary

The I.F. output signal and noise is

$$y(t) = y_D(t) + n_d(t) \tag{1}$$

where

$$y_D(t) = A(t)\cos\left[(\omega_c + \Delta\omega)(t-\tau-\Delta) + \theta(t-\tau-\Delta) + \omega_o + \varphi\right] \tag{2}$$

The function $y(t)$ is processed in a narrow bandpass filter matched to the IF frequency followed by a 90 degree phase shifter. The resulting signal is

$$r(t) = A\,J_0(m_1)J_0(m_2)\sin\left[(\omega_c + \Delta\omega)(t-\tau-\Delta) + \omega_o + \varphi\right] + n_s(t) \tag{3}$$

The form of the carrier component is exactly as given in equation 16 on page 6A-4. The noise function $n_s(t)$ has bandwidth equal to the filter bandwidth W.

The demodulator output is expressed below as twice the low frequency portion of the product of the IF output in (1) and the extracted reference in (3).

$$z(t) = 2LF\left\{r(t)y(t)\right\} \tag{4}$$

This function is then processed in the tone filters. It is shown in Section 6B.2 that the j-th tone filter output is of the form:

$$y_j(t) = A\,J_0(m_k)J_1(m_j)\sin\left[\omega_j(t-\tau-\Delta)\right] + n_j(t) \tag{5}$$

where $n_j(t)$ is band-limited white noise of bandwidth W_{oj} and spectral density

$$N_j = A^2 N_0 W_{oj}\begin{cases} 1 + \frac{1}{2\rho_B} + \frac{W}{W_{oj}}\left[J_0(m_k)J_1(m_j)\right]^2 ; & W_{oj} \geq W \\ 1 + \frac{1}{2\rho_B} + \left[J_0(m_k)J_1(m_j)\right]^2 ; & W_{oj} \leq W \end{cases} \tag{6}$$

where

$$\rho_B = \frac{A^2}{4 N_0 W} \tag{7}$$

is the signal-to-noise ratio at the output of the carrier-extraction bandpass filter.

The signal-to-noise ratio at the output of the j-th tone-filter is therefore:

$$\left(\frac{S}{N}\right)_{oj} = 2 J_0^2(m_k) J_1^2(m_j) \frac{W_{IF}}{W_{oj}} \left(\frac{C}{N}\right)_{IF} \begin{cases} \left[1 + \frac{1}{2\rho_B} + \frac{W}{W_{oj}} \left(J_0(m_k) J_1(m_j)\right)^2\right]^{-1}; & W_{oj} \geq W \\ \left[1 + \frac{1}{2\rho_B} + \left(J_0(m_k) J_1(m_j)\right)^2\right]^{-1}; & W_{oj} \leq W \end{cases} \tag{8}$$

Since the statistics of the tone filter output noise will be Gaussian, the phase error distribution will be normally distributed for large signal-to-noise ratios with zero mean and variance

$$\sigma_j^2 = \frac{1}{2\left(\frac{S}{N}\right)_{oj}} \tag{9}$$

as in equation (25) on page 6A-6.

The case when the IF carrier is not bracketed by the narrow band filter is included in equation (8). In this case, ρ_B will equal zero, in which case the tone filter output signal-to-noise ratio will go to zero.

When ρ_B goes to infinity, and $\frac{W}{W_{oj}}$ goes to zero, equation (8) reduces to equation (15) on page 6A-4 as one would expect.

An exact expression for the phase error can be derived as in (46) on page 6A-13. The resulting formula for tone frequency ω_1 is:

$$\delta_1 = \text{Arctan}\left\{ \frac{I_c}{\frac{2A}{\sigma} J_0(m_2) J_1(m_1) + I_s} \right\} \tag{10}$$

where

$$\sigma_1^2 = 2N_1 W_{01} \quad . \tag{11}$$

where N_1 is given in (6). It follows from (5) that

$$\left(\frac{S}{N}\right)_{01} = \frac{A^2 J_0^2(m_2) J_1^2(m_1)}{4 N_0 W_{01}} \tag{12}$$

Therefore

$$\delta_1 = \text{Arc tan} \left\{ \frac{I_c}{\sqrt{2\left(\frac{S}{N}\right)_{01}} + I_s} \right\} \tag{13}$$

which is exactly the same form as (47) on page 6A-13.

6B.2 Detailed Analysis

The IF output signal plus noise is described by:

$$x(t) = A\cos\left[\omega_0 t + \theta + m_1 \sin(\omega_1 t + \theta_1) + m_2 \sin(\omega_2 t + \theta_2)\right] + n(t)$$

$$= A\left[I_{cxo}(t)\cos(\omega_0 t + \theta) - I_{sxo}(t)\sin(\omega_0 t + \theta)\right] + n(t) \qquad (1)$$

where x(t) is expressed as in Equation (4) on page 6A-15. The noise n(t) is band-limited and white with a double sided spectrum of width W_{IF} and total noise power $2N_0 W_{IF}$.

Let the output of the bandpass filter

$$r(t) = A\sin(\omega_0 t + \theta) + n_B(t) \qquad (2)$$

The noise term $n_B(t)$ is due to the IF noise, hence also white of width W, the width of the BPF. This output and the IF output are processed together in a low pass filter. The output

$$z(t) = LF\left[x(t)\, r(t)\right]$$

$$= \frac{A^2}{2}\left[-I_{sxo}(t)\right] + \varepsilon_{sxn}(t) + \varepsilon_{nxs}(t) + \varepsilon_{nxn}(t) \qquad (3)$$

where the last three terms describe different noises.

The first one is:

$$\varepsilon_{sxn}(t) = LF\left[x(t)\, n_B(t)\right]$$

$$= LF\left\{A\left[I_{cxo}(t)\cos(\omega_0 t + \theta) - I_{sxo}(t)\sin(\omega_0 t + \theta)\right]\left[I_{cB}(t)\cos\omega_0 t - I_{sB}(t)\sin\omega_0 t\right]\right\}$$

$$= \frac{A}{2}\left\{ I_{cxo}(t)\left[I_{cB}(t)\cos\theta + I_{sB}(t)\sin\theta \right] - I_{sxD}(t)\left[I_{cB}(t)\sin\theta - I_{sB}(t)\cos\theta \right] \right\} \quad (4)$$

We note from the Bessel expansion in equation (6) on page 6A-16 that only one term, at f_j, will be passed by the tone filters F_1 or F_2 at f_1 of f_2. Hence the tone filter output due to the signal-cross-noise noise term is

$$\varepsilon_{sxn,j}(t) = -A J_0(m_k) J_1(m_j)\left[I_{cB}(t)\sin\theta - I_{sB}(t)\cos\theta \right]\sin(\omega_j t + \theta_j) \quad (5)$$

$$j \neq k = 1, 2$$

The noise power of this term can be found via its autocorrelation function.

$$P_{sxn,j}(\tau) = \left[A J_0(m_k) J_1(m_j) \right]^2 \psi_0(\tau)\cos\frac{\omega_j \tau}{2} \quad (6)$$

where $\psi_0(\tau)$ is the autocorrelation function of the BPF noise, and we assumed that $I_{cB}(t)$ and $I_{sB}(t)$ are uncorrelated. Since this noise is due to the passage of IF noise by the bandpass filter, its power spectrum is of height $2N_0$ and width W. Hence the noise power of $\varepsilon_{sxn,j}$ is:

$$N_{sxn,j} = \left[A J_0(m_k) J_1(m_j) \right]^2 N_0 \begin{cases} W & W_{oj} > W \\ W_{oj} & W_{oj} < W \end{cases} \quad (7)$$

The next noise term is:

$$\varepsilon_{nxs}(t) = LF\left\{[I_c(t)\cos\omega_0 t - I_s(t)\sin\omega_0 t]A\sin(\omega_0 t+\theta)\right\}$$

$$= \frac{A}{2}[I_c(t)\sin\theta - I_s(t)\cos\theta] \tag{8}$$

Its autocorrelation function is:

$$R_{nx,s}(\tau) = \left(\frac{A}{2}\right)^2 \psi_{IF}(\tau) \tag{9}$$

where $\psi_{IF}(\tau)$ is the autocorrelation function of the IF noise which has bandwidth W_{IF}. If the tone filters F_1 and F_2 are such that

$$f_1 + \frac{W_{oj}}{2} < W_{IF}/2 \tag{10}$$

The noise power is:

$$N_{nxs,j} = A^2 N_o W_{oj} \tag{11}$$

The last noise term to consider is

$$\varepsilon_{nxn}(t) = LF[n(t)\, n_B(t)] \tag{12}$$

These noises are however correlated. A way to handle this is to write n(t) as the sum of three noises (Figure 6B-1).

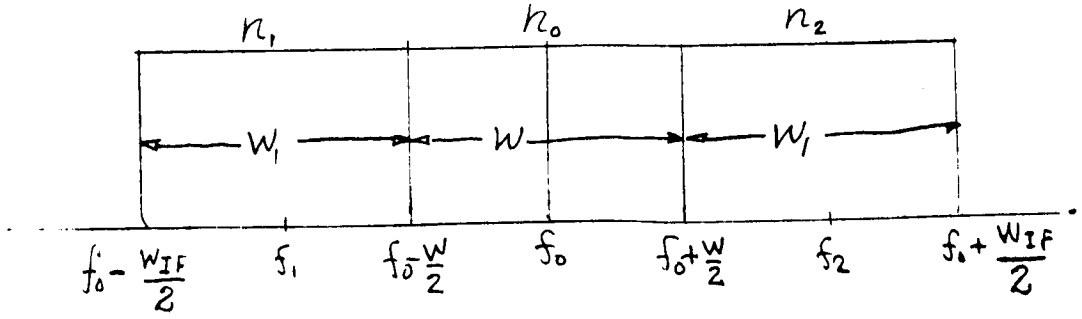

Figure 6B-1. Decomposition of the Power Spectrum of n(t)

for convenience we will call $n_B(t)$ now $n_o(t)$

Let

$$n(t) = n_1(t) + n_o(t) + n_2(t) \tag{13}$$

$$n_i(t) = I_c(t)\cos\omega_i t - I_s(t)\sin\omega_i t \quad ; \quad i = 0, 1, 2 \tag{14}$$

where f_i denote the mean frequencies

$$f_o = f_o$$

$$f_1 = f_o - \frac{1}{4}\left[W_{IF} + W\right]$$

$$f_2 = f_o + \frac{1}{4}\left[W_{IF} + W\right] \tag{15}$$

Since the power spectra of $n_i(t)$ are non-overlapping, they will be uncorrelated.

The bandwidths of $n_o(t)$ and $n_2(t)$ are both:

$$W_1 = \frac{W_{IF} - W}{4} \tag{16}$$

whereas the bandwidth of $n_1(t)$ is W as shown in Figure 6B-2. Applying (14) to (12):

$$\mathcal{E}_{n\times n}(t) = LF\left\{\left[n_1(t) + n_o(t) + n_2(t)\right] n_o(t)\right\}$$

$$= LF\left[n_o^2(t)\right] + LF\left[n_1(t) n_o(t)\right] + LF\left[n_2(t) + n_o(t)\right] \tag{17}$$

Now

$$LF\left[n_o^2(t)\right] = LF\left\{\left[I_{co}(t)\cos\omega_o t - I_{so}(t)\sin\omega_o t\right]^2\right\}$$

$$= \frac{1}{2}\left[I_{co}^2(t) + I_{so}^2(t)\right] \tag{18}$$

which has an autocorrelation function:

$$R_{n_o^2(t)}(\tau) = \frac{1}{4}\left\langle \left[I_{co}^2(t) I_{co}^2(t') + I_{co}^2(t) I_{so}^2(t') + I_{co}^2(t') I_{so}^2(t) + I_{so}^2(t) I_{so}^2(t') \right] \right\rangle \tag{19}$$

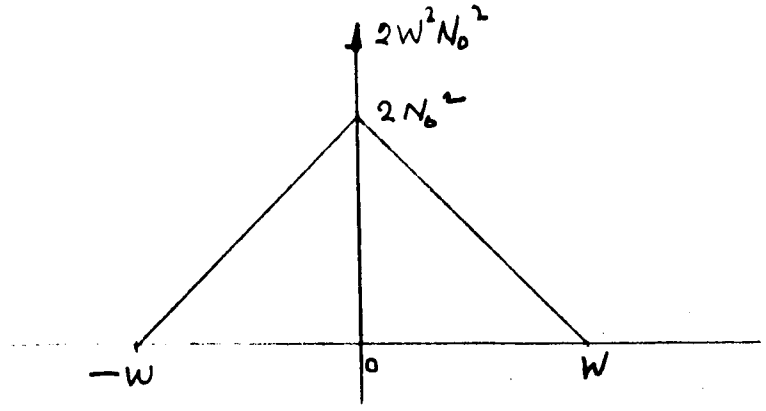

Figure 6B-2. Power Spectrum of LF $[n_o^2(t)]$

Applying (14)

$$LF\left[n_o(t)\, n_1(t)\right] = \frac{1}{2}\left[I_{co}(t)\, I_{c1}(t) + I_{so}(t)\, I_{s1}(t)\right]\cos(\omega_o - \omega_1)t$$
$$-\frac{1}{2}\left[I_{co}(t)\, I_{s1}(t) + I_{so}(t)\, I_{c1}(t)\right]\sin(\omega_o - \omega_1)t \tag{20}$$

Since the $I_{ci}(t)$ and $I_{si}(t)$ are mutually uncorrelated, the autocorrelation function of LF $[n_o(t)\ n_1(t)]$ is given by:

$$R_{n_o n_1}(\tau) = \frac{1}{2}\,\psi_o(\tau)\,\psi_1(\tau)\cos(\omega_o - \omega_1)\tau \tag{21}$$

The power spectrum corresponding to $\psi_o(\tau)\,\psi_1(\tau)$

$$g(f) = \int_{-\infty}^{\infty} g_1(u)\, g_o(f-u)\, du \tag{22}$$

where $g(f)$ is the power spectrum corresponding to $\psi_0(\tau)$, whereas $g_1(f)$ corresponds to $\psi_1(\tau)$. These power spectra are shown in Figure 6B-3.

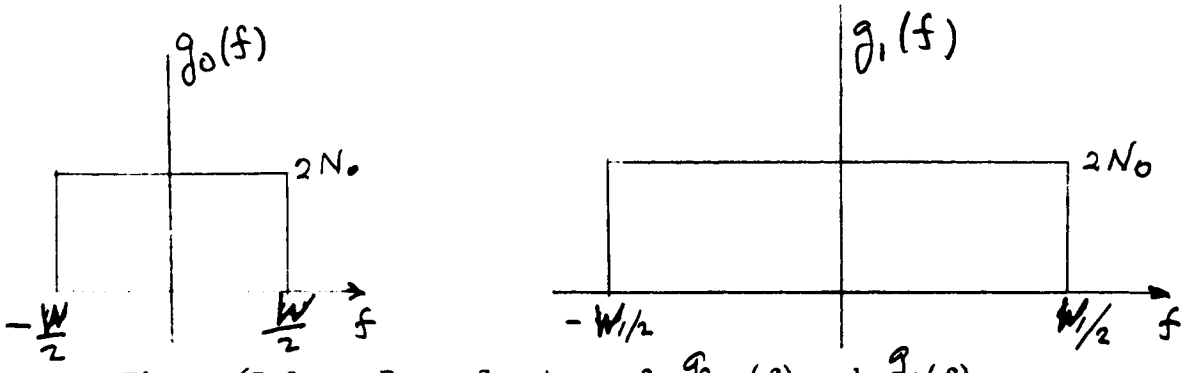

Figure 6B-3. Power Spectrum of $g_0(f)$ and $g_1(f)$

Hence

$$g(f) = 2N_0 \int_{-W_1/2}^{W_1/2} g_0(f-u)\,du$$

$$= 2N_0 \int_{f-\frac{W_1}{2}}^{f+\frac{W_1}{2}} g_0(\xi)\,d\xi$$

$$= 4N_0^2 \begin{cases} f + \dfrac{W+W_1}{2} & ; \quad -\dfrac{W+W_1}{2} < f < -\dfrac{W_1-W}{2} \\ W & ; \quad -\dfrac{W_1-W}{2} < f < \dfrac{W_1-W}{2} \\ -f + \dfrac{W+W_1}{2} & ; \quad \dfrac{W_1-W}{2} < f < \dfrac{W+W_1}{2} \end{cases} \qquad (23)$$

The power spectrum corresponding to $R_{n_0 n_1}(\tau)$ in (21) is obtained by translating the power spectrum $g(f)$ up and down by (f_0-f_1) and dividing by 4. Note that

$$f_0 - f_1 = \frac{1}{4}(W_{IF} + W) = \frac{1}{2}(W_{IF} - W_1)$$

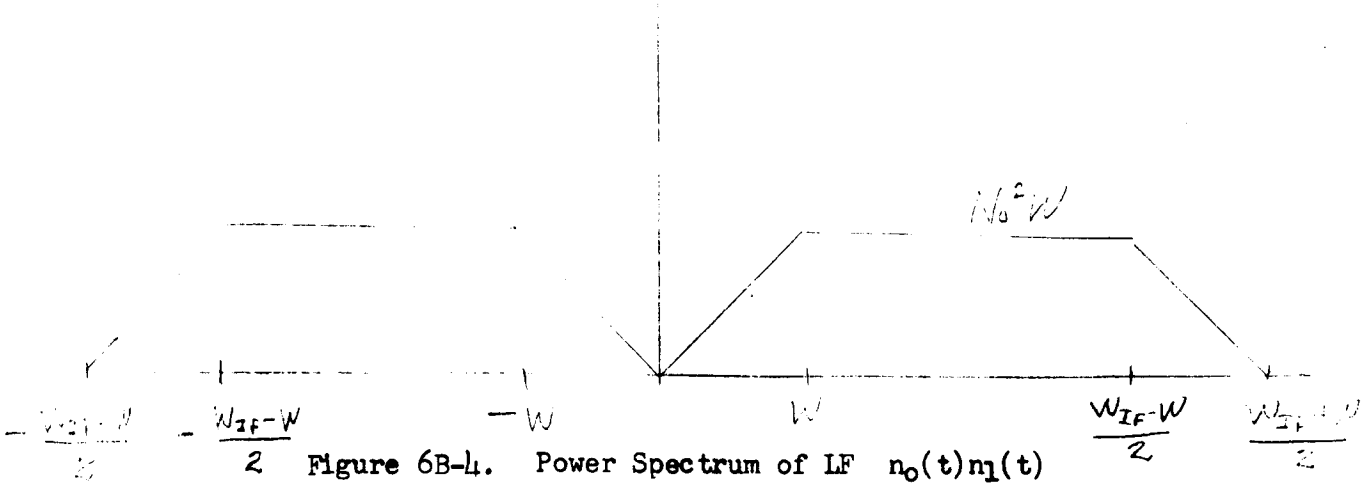

Figure 6B-4. Power Spectrum of LF $n_0(t)n_1(t)$

The analysis of LF $[n_0(t)n_2(t)]$ is as shown in Figure 6B-4 with f_1 replaced by f_2. It is simple to show that their spectra are identical.

If the filters F_j are such that

$$W < f_j - \frac{W_{oj}}{2} < f_j + \frac{W_{oj}}{2} < \frac{W_{IF}-W}{2} \tag{24}$$

the noise-cross-noise power is:

$$N_{n_0 n_j} = 2 N_0^2 W W_{oj} \tag{25}$$

The tone filter output can be found from (3), (5), (8) and (17)

$$y_j(t) = A \cos(m_j \sin \omega_j t) J_1(m_j) \sin(\omega_j t + \theta_j) + n_j(t) \tag{26}$$

and the noise $n_j(t)$ can be written with in-phase and quadrature terms about f_j as:

$$n_j(t) = I_{cj}(t) \cos \omega_j t - I_{sj}(t) \sin \omega_j t \tag{27}$$

of bandwidth W_{oj} and total noise power

$$N_j = (N_o W_{oj} A^2) \begin{cases} \left[1 + \frac{1}{2\rho_B} + \frac{W}{W_{oj}} \left[J_o(m_k)\, J_1(m_j)\right]^2\right] ; & W_{oj} > W \\ \left[1 + \frac{1}{2\rho_B} + \left[J_o(m_k)\, J_1(m_j)\right]^2\right] ; & W_{oj} < W \end{cases} \tag{28}$$

where

$$\rho_B = \frac{A^2}{4 N_o W} \tag{29}$$

The signal-to-noise ratio at the output of the bandpass filter.

The signal power is:

$$S_j = \frac{1}{2}\left[A\, J_o(m_k)\, J_1(m_j)\right]^2 \tag{30}$$

Then the output signal-to-noise ratio is:

$$\left(\frac{S}{N}\right)_{oj} = \frac{\left[A J_o(m_k)\, J_1(m_j)\right]^2}{2 N_o W_{oj}} \tag{30a}$$

$$= \left(\frac{C}{N}\right)_{IF} \frac{2W_{IF}}{W_{oj}} \left[J_o(m_k)\, J_1(m_j)\right]^2 \tag{30b}$$

$$= \left(\frac{S}{N}\right)_{IF,j} \frac{W_{IF}}{W_{oj}} \tag{30c}$$

$$\cdot \begin{cases} \left\{1 + \frac{1}{2\rho_B} + \frac{W}{W_{oj}} \left[J_o(m_k) J_1(m_j)\right]^2\right\}^{-1} ; & W_{oj} > W \\ \left\{1 + \frac{1}{2\rho_B} + \left[J_o(m_k) J_1(m_j)\right]^2\right\}^{-1} ; & W_{oj} < W \end{cases}$$

If we now process $y_j(t)$ given in Equation (26), with another equation just like it from a second satellite, or the output of a local oscillator, in a phase demodulation system in order to obtain an estimate of phase difference, we obtain the same results as before (Equ. 31*) because the tone filter outputs are comparable.

Hence, writing

$$H_1(t) = A_1^2 J_0(m_k) J_1(m_j) \sin(\omega_j t + \theta_j) + n_{j1}(t) \quad ; \ 1^{st} \text{ Satellite}$$

$$H_2(t) \begin{cases} = A_2^2 J_0(m_k) J_1(m_j) \sin(\omega_j t + \theta_j + \varphi) + n_{j2}(t) \ ; & 2^{nd} \text{ Satellite} \\ = \sin(\omega_j t) \ ; & L.O. \end{cases} \tag{31}$$

The estimate of phase difference is:

$$\hat{\varphi} = \left[\omega_0 (t_0^{(1)} - t_0^{(2)}) + \delta\right]_{mod \pm 2\pi} \tag{32}$$

The expected value of $\hat{\varphi}$ is:

$$E(\hat{\varphi}) = \varphi_{mod \pm 2\pi} + b(\varphi_0, \sigma) \tag{33}$$

where $b(\varphi_0, \sigma)$ is a bias (see Equation 37*) while the variance of $\hat{\varphi}$ is:

$$\sigma^2(\hat{\varphi}) \simeq \frac{1}{2}\left[\frac{1}{\left(\frac{S}{N}\right)_{oj1}} + \frac{1}{\left(\frac{S}{N}\right)_{oj2}}\right] \tag{34}$$

*pages 6A-23 and 6A-24.

for high signal-to-noise ratios on the input (i.e., large $\left(\frac{S}{N}\right)_{oji}$)

and

$$\left|\varphi_{mod} \pm 2\pi\right| < 2\pi - 3\left[\frac{1}{2\left(\frac{S}{N}\right)_{oj1}} + \frac{1}{2\left(\frac{S}{N}\right)_{oj2}}\right]^{\frac{1}{2}} \qquad (35)$$

Appendix 6C

PHASE-LOCK-LOOP CARRIER DEMODULATION WITH WHITE NOISE (C_{13}), AND A QUADRATURE PHASE DETECTOR

The IF output signal plus noise is:

$$x(t) = S(t) + n(t) \tag{1}$$

where

$$S(t) = A\cos\left[\omega_0 t + \theta + m_1 \sin(\omega_1 t + \theta_1) + m_2 \sin(\omega_2 t + \theta_2)\right] \tag{2}$$

and the double sided white noise is described by

$$n(t) = \bar{I}_c(t)\cos\omega_0 t - \bar{I}_s(t)\sin\omega_0 t \tag{3}$$

Representing x(t) with in-phase and quadrature components:

$$x(t) = A\left[I_{cxo}(t)\cos(\omega_0 t + \theta) - \bar{I}_{sxo}(t)\sin(\omega_0 t + \theta)\right] \tag{4}$$

where $I_{cxo}(t)$ and $I_{sxo}(t)$ are given in equations (5) and (6) on pages 6A-15 and 6A-16.

The reference signal r(t) which is extracted in the phase-locked loop is:

$$r(t) = \sin\left[\omega_0 t + \theta + \Delta\theta(t)\right] \tag{5}$$

where $\Delta\theta(t)$ represents phase jitter which is due to the IF noise. The signals x(t) and R(t) are processed in a low pass filter to yield:

$$z(t) = LF\,[x(t)\,r(t)]$$

$$= \frac{A}{2}\left[I_{cxo}(t)\,\sin\Delta\theta(t) - I_{sxo}(t)\,\cos\Delta\theta(t)\right] + \xi_{nx_A}(t) \tag{6}$$

The noise here is described by $\xi_{nx_A}(t)$

$$\xi_{nx_A}(t) = LF\,[n(t)\,r(t)]$$

$$= \frac{1}{2}\left\{ I_c(t)\,\sin[\theta + \Delta\theta(t)] - I_s(t)\,\cos[\theta + \Delta\theta(t)]\right\} \tag{7}$$

The tone filter outputs of the filters F_j of width W_{oj} centered at the tones $\pm f_j$, (we consider double sided spectra) are:

$$y_j(t) = -A\,J_0(m_k)\,J_1(m_j)\cos\Delta\theta(t)\,\sin(\omega_j t \pm \theta_j)$$

$$+ \frac{1}{2}\left\{ I_c(t)\,\sin[\theta + \Delta\theta t] - I_s(t)\cos[\theta + \Delta\theta(t)]\right\};\ j \neq k = 1, 2 \tag{8}$$

The difference from the homodyne detector output arises from the phase jitter component $\Delta\,\theta(t)$. We assume the phase jitter to be approximately a Gaussian random process with zero mean value and variance

$$\sigma_{\Delta\theta}^2 = \frac{1}{2\rho_L} \quad ; \quad \rho_L = \left(\frac{C}{N}\right)_{JF} \frac{W_{IF}}{B_L} \tag{9}$$

In order to then determine the output signal-to-noise ratio we need some results from statistics. The characteristic function of a normal distribution with zero mean and variance σ^2 is

$$\langle e^{jnx} \rangle = e^{-n^2\sigma^2/2} \tag{10}$$

Therefore

$$\langle \cos x \rangle = e^{-\sigma^2/2}$$

$$\langle \sin x \rangle = 0 \tag{11}$$

Letting $$X = \Delta\theta(t) \pm \Delta\theta(t') \tag{12}$$

the variance is

$$\sigma^2 = \langle [\Delta\theta(t) - \Delta\theta(t')]^2 \rangle$$

$$= 2\left\{ \langle [\Delta\theta(t)]^2 \rangle - \langle \Delta\theta(t)\Delta\theta(t') \rangle \right\}$$

$$= 2\sigma_{\Delta\theta}^2 [1 - \rho_{\Delta\theta}(\tau)] \tag{13}$$

where $\rho_{\Delta\theta}(\tau)$ is the normalized autocorrelation function of $\Delta\theta(t)$. This function is determined by the transfer function of the loop filter. Applying (14) and (13) to (12),

$$\langle \cos [\Delta\theta(t) - \Delta\theta(t')] \rangle = e^{-\sigma_{\Delta\theta}^2 [1 - \rho_{\Delta\theta}(\tau)]} \tag{14}$$

$$\approx 1 - \sigma_{\Delta\theta}^2 [1 - \rho_{\Delta\theta}(\tau)] \tag{15}$$

for high S/N ratios at the end of the loop filter, alternately, since $\sigma_{\Delta\theta}^2 = \frac{1}{2\rho_2}$ for small $\sigma_{\Delta\theta}^2$.

The noise power at the tone filter output can be obtained from the noise term of equation (8). It has an autocorrelation function

$$R(\tau) = \frac{1}{4} \psi(\tau) \langle \cos [\Delta\theta(t) - \Delta\theta(t')] \rangle \tag{16}$$

when $\psi(\tau)$ is the IF autocorrelation function and $\Delta\theta(t)$ and the IF noise are treated as independent variables, which is only an approximation since the statistical dependence is not easily accounted for. Using the result of (15), for the difference $\Delta\,\theta(t) - \Delta\,\theta(t')$ and combining this with (16), we have:

$$R(\tau) = \frac{1}{4}\,\psi(\tau)\exp\left\{-\frac{1}{2\rho_L}\left[1-\rho_{\Delta\theta}(\tau)\right]\right\}$$

$$\approx \frac{1}{4}\,\psi(\tau)\left\{1-\frac{1}{2\rho_L}\left[1-\rho_{\Delta\theta}(\tau)\right]\right\} \qquad (17)$$

This function reduces to the corresponding result for the homodyne detector for large loop filter signal-to-noise ratio. The normalized power spectrum of $\Delta\,\theta(t)$ is:

$$S_{\Delta\theta}(f) = \frac{|H_L(f)|^2}{\int_{-\infty}^{+\infty}|H_L(f)|^2\,df} \qquad (18)$$

where $H_L(f)$ is the loop transfer function. The power spectrum corresponding to

$$g(\tau) = \psi(\tau)\,\rho_{\Delta\theta}(\tau) \qquad (19)$$

is therefore

$$G_g(f) = \int_{-\infty}^{+\infty} G(z)\,S_{\Delta\theta}(f-z)\,dz \qquad (20)$$

where $G(z)$ is the power spectrum of the IF noise. From the assumption that this power spectrum is rectangular

(21)

$$G_q(f) = 2N_0 \int_{-W_{IF}/2}^{+W_{IF}/2} S_{\Delta\theta}(f-z)\,dz$$

$$= 2N_0 \int_{f-W_{IF}/2}^{f+W_{IF}/2} S_{\Delta\theta}(n)\,dn$$

The spectral density at the tone frequency $+f_j$ is therefore

$$G_q(f) = 2N_0 \int_{f_j-W_{IF}/2}^{f_j+W_{IF}/2} S_{\Delta\theta}(n)\,dn$$

$$\approx 2N_0 \int_{-\infty}^{+\infty} S_{\Delta\theta}(f)\,df \qquad (22)$$

$$= 2N_0$$

assuming that $(WIF/2)\pm f_j$ is much larger than the loop filter bandwidth so that the detailed shape of the loop filter is of no consequence. Combining (22), at $+f_j$, with the other term of Equation (20), we find that the noise power is

$$N_j \approx N_0 W_{oj}\left[1 - \frac{1}{2\rho_L}\right] + \frac{4 N_0 W_{oj}}{4 \cdot 2\rho_L}$$

$$= N_0 W_{oj}\left[1 - \frac{1}{\rho_L}\right] \qquad (23)$$

The signal power is found by using (11) in (8)

$$S_j = \frac{\left[A J_0(m_k) J_1(m_j)\right]^2 \left[1 + e^{-1/\rho_L}\right]}{4} \qquad (24)$$

The output signal-to-noise ratio is thus:

$$\left(\frac{S}{N}\right)_{oj} = \left(\frac{C}{N}\right)_{IF} \frac{W_{IF}}{W_{oj}} \left[J_0(m_k) J_1(m_j)\right]^2 \left[\frac{1 + e^{-1/\rho_L}}{1 - 1/\rho_L}\right]. \qquad (25)$$

for a carrier-to-noise ratio

$$\left(\frac{C}{N}\right)_{IF} = \frac{A^2}{4 N_0 W_{IF}} \qquad (26)$$

and large loop filter signal-to-noise ratio.

We will first describe the analysis for processing the tone-filter output $y_j(t)$ as given in Equation (8) with the output of a local oscillator in a phase detector. Renaming $y_j(t)$

$$H_1(t) = -A\, J_0(m_k)\, J_1(m_j) \cos \Delta\theta(t) \sin(\omega_j t + \theta_j) + n_1(t)$$
$$H_2(t) = \sin \omega_j t \tag{27}$$

Let

$$B = -A\, J_0(m_k)\, J_1(m_j) \tag{28}$$

and write $H_1(t)$ with in-phase and quadrature terms:

$$H_1(t) = \left[B \cos\Delta\theta(t) \sin\theta_j + I_c(t)\right] \cos\omega_j t + \left[B \cos\Delta\theta(t) \cos\theta_j - I_s(t)\right] \sin\omega_j t$$
$$= R \sin(\omega_j t + \alpha)$$
$$H_2(t) = \sin(\omega_j t) \tag{29}$$

$H_1(t)$ and $H_2(t)$ are processed together in a low pass filter. The output of the first one is

$$L_1(t) = LF\left[H_1(t)\quad H_2(t, \pi/2 \text{ Phase Shift})\right]$$
$$= \frac{R_1}{2} \sin\alpha \tag{30}$$

while the low frequency output of the second low pass filter is

$$L_2(t) = LF\left[H_1(t)\, H_2(t)\right]$$
$$= \frac{R_1}{2} \cos\alpha \tag{31}$$

These two signals are then passed through the divider and arc tangent filter. The estimate θ obtained at the end of this filter is:

$$\hat{\theta}_j = \text{Arctan}\left[\frac{L_1(t)}{L_2(t)}\right]$$

$$= \text{Arctan}\left[\tan\alpha\right] \tag{32}$$

If the $H_1(t)$ were noiseless, $\hat{\theta}_j$ would be

$$\hat{\theta}_j = \text{Arctan}\left[\frac{B_1 \cos\Delta\theta(t)\sin\theta_j}{B\cos\Delta\theta(t)\cos\theta_j}\right]$$

$$= \theta_j \bmod \pm 2\pi \tag{33}$$

In the presence of noise, we have to use the equation

$$\hat{\theta}_j = \text{Arctan}\left[\frac{B\cos\Delta\theta(t)\sin\theta_j + I_c(t)}{B\cos\Delta\theta(t)\cos\theta_j - I_j(t)}\right]$$

$$= \text{Arctan}\left[\frac{\cos\Delta\theta(t)\sin\theta_j + I_c(t)/\sqrt{2\rho}}{\cos\Delta\theta(t)\cos\theta_j - I_s(t)/\sqrt{2\rho}}\right] \tag{34}$$

where we normalized $I_c(t)$ and $I_s(t)$ to have variance equal to unity and $\rho = \frac{B^2}{2N}$, i.e., the signal-to-noise ratio on the tone filter output. We are interested in the mean of $\hat{\theta}_j$, $E(\hat{\theta}_j)$ and in variance $\sigma^2(\hat{\theta}_j)$.

The variables in the definition of θ_j are $\Delta\theta(t)$, $I_c(t)$ and $I_s(t)$. Let

$$\left.\begin{aligned} X_1 &= \Delta\theta(t) \\ X_2 &= I_c(t) \\ X_3 &= I_s(t) \end{aligned}\right\} \tag{35}$$

then $\langle \chi_i \rangle = 0$

$$\sigma^2(X_1) = \frac{1}{2\rho_L}$$

$$\sigma^2(X_2) = \sigma^2(\chi_3) = 1$$

(36)

and approximating $\hat{\theta}_j$ by a Taylor's series up to and including the quadratic terms

$$\hat{\theta}_j = f(X_1, X_2, X_3)$$

$$\approx f(0,0,0) + \sum_{i=1}^{3} X_i \left.\frac{\partial f}{\partial X_1}\right|_{\langle X_i \rangle} + \frac{1}{2}\sum_{i=1}^{3} \chi_i^2 \left.\frac{\partial^2 f}{\partial \chi_i^2}\right|_{\langle X_i \rangle} + \sum_{i \neq j}\sum X_i X_j \left.\frac{\partial^2 f}{\partial X_i \partial X_j}\right|_{\langle X_i \rangle} \quad (37)$$

Obviously

$$f(0,0,0) = \theta_j \bmod \pm 2\pi \quad (38)$$

and since $\langle X_i \rangle = 0$

$$E(\hat{\theta}_j) \approx \theta_j \bmod \pm 2\pi + \frac{1}{2}\sum \langle \chi_i^2 \rangle \left.\frac{\partial^2 \rho}{\partial \chi_i^2}\right|_{\langle X_i \rangle} \quad (39)$$

while

$$\sigma^2(\hat{\theta}_j) \approx \sum_{i=1}^{3} \sigma^2(X_i) \left(\left.\frac{\partial f}{\partial \chi_i}\right|_{\langle X_i \rangle} \right)^2 \quad (40)$$

The partials can be evaluated in a straightforward manner. In passing we note that

$$\frac{\partial f}{\partial \Delta\theta} = 0 \tag{41}$$

so $\Delta\ \theta$ does not contribute to the error of the measurement of θ_j; also the contributions of I_e and I_s cancel each other in the evaluation of $E(\hat{\theta}_j)$, so that:

$$E(\hat{\theta}_j) \approx \theta_j \bmod \pm 2\pi \tag{42}$$

up to and including the second partials. We find that the variance of our estimate $\hat{\theta}_j$ is:

$$\sigma^2(\hat{\theta}) \approx \sigma^2(I_s)\left(\left|\frac{\partial f}{\partial I_s}\right|\right)^2_{\langle x_i \rangle} + \sigma^2(I_c)\left(\left|\frac{\partial f}{\partial I_s}\right|\right)^2_{\langle x_i \rangle}$$

$$= \frac{1}{2\rho + 4 + 2/\rho}$$

$$\approx \frac{1}{2\rho}$$

$$= \frac{1}{2(S/N)_{oJ}} \tag{43}$$

so that the variance of the estimate $\hat{\theta}_j$ is proportional to the tone filter output signal-to-noise ratio.

We are now interested in processing the tone filter output $y_j(t)$, of equation (28), with the tone filter output of another signal derived from a second

satellite in order to obtain the difference between the two phase angles on the tones. The quadrature phase detector inputs are described by:

$$H_1(t) = -A_1 J_0(m_k) J_1(m_j) \cos \Delta\theta_1 \sin(\omega_j t + \theta_1) + n_1(t)$$

$$H_2(t) = -A_2 J_0(m_k) J_1(m_j) \cos \Delta\theta_2 \sin(\omega_j t + \theta_2) + n_2(t) \tag{44}$$

The quantities $\Delta\theta_1$ and $\Delta\theta_2$ are the phase jitters. They as well as the Gaussian noise functions $n_j(t)$ have zero mean, and all are mutually uncorrelated, while θ_1 and θ_2 are the phases of the j-th tone.

The functions H_1 and H_2 are multiplied in phase and in quadrature and the low frequency portion of each product extracted in a low pass filter. Then the second low pass filter output is divided by the first and the quotient is passed through an arc tangent transfer function to obtain an estimate of phase difference.

Writing H_1 and H_2 with in-phase and quadrature components:

$$\begin{aligned} H_1(t) &= [-A_1 J_0(m_k) J_1(m_j) \cos \Delta\theta_1 \sin\theta_1 + I_{c1}(t)] \cos \omega_j t \\ &\quad + [-A_1 J_0(m_k) J_1(m_j) \cos \Delta\theta_2 \cos\theta_1 - I_{s1}(t)] \sin \omega_j t \\ &= R_1 \sin(\omega_j t + \alpha_1) \end{aligned} \tag{45}$$

$$\begin{aligned} H_2(t) &= [-A_2 J_0(m_k) J_1(m_j) \cos \Delta\theta_2 \sin\theta_2 + I_{c2}(t)] \cos \omega_j t \\ &\quad + [-A_2 J_0(m_k) J_1(m_j) \cos \Delta\theta_2 \cos\theta_2 - I_{s2}(t)] \sin \omega_j t \\ &= R_2 \sin(\omega_j t + \alpha_2) \end{aligned} \tag{46}$$

If $L_1(t)$ is the product of H_1 and H_2 in-phase:

$$L_1(t) = \frac{R_1 R_2}{2} \cos(\alpha_1 - \alpha_2) \tag{47}$$

while $L_2(t)$ is the product of H_1 and H_2, where H_2 has been phase shifted by 90 degrees:

$$L_2(t) = \frac{R_1 R_2}{2} \sin(\alpha_1 - \alpha_2) \tag{48}$$

Dividing L_2 by L_1:

$$\frac{L_1(t)}{L_2(t)} = \tan(\alpha_1 - \alpha_2) \tag{49}$$

Our estimate of phase difference $\hat{\theta}_1 - \hat{\theta}_2$ of $\theta_1 - \theta_2$ is:

$$\widehat{\theta_1 - \theta_2} = \text{Arctan}\left[\tan(\alpha_1 - \alpha_2)\right] \tag{50}$$

Applying the expressions for α_1 and α_2 from (55) and (56):

$$\widehat{\theta_1 - \theta_2} = \text{Arctan}\left[\frac{\cos\Delta\theta_1 \cos\Delta\theta_2 \sin(\theta_1 - \theta_2) + \frac{\cos\Delta\theta_2}{\sqrt{2\rho_1}} I_{C1} - \frac{\cos\Delta\theta_1}{\sqrt{2\rho_2}} I_{C2} + \frac{I_{S1} I_{C2} - I_{C1} I_{S2}}{2\sqrt{\rho_1 \rho_2}}}{\cos\Delta\theta_1 \cos\Delta\theta_2 \cos(\theta_1 - \theta_2) - \frac{\cos\Delta\theta_2}{\sqrt{2\rho_1}} I_{S1} - \frac{\cos\Delta\theta_1}{\sqrt{2\rho_2}} I_{S2} + \frac{I_{C1} I_{C2} + I_{S1} I_{S2}}{2\sqrt{\rho_1 \rho_2}}}\right] \tag{51}$$

where the additive noise components have been normalized to have mean zero and variance unity, and

$$\rho_i = \frac{\left[-A_i J_0(m_k) J_1(m_j)\right]^2}{2N_i} \; ; \; i = 1, 2 \tag{52}$$

which is the STN tone filter output ratio, N_1 is the noise power of the additive white noise at the tone filter output.

In the absence of noise (61) reduces to:

$$\widehat{\theta_1 - \theta_2} = \text{Arctan}\left[\frac{\cos\Delta\theta_1 \cos\Delta\theta_2 \sin(\theta_1-\theta_2)}{\cos\Delta\theta_1 \cos\Delta\theta_2 \cos(\theta_1-\theta_2)}\right]$$

$$= (\theta_1-\theta_2)_{\text{mod}\pm 2\pi} \qquad (53)$$

In the presence of noise, we have to work from equation (61). Under the assumption that ρ_i are large, we will consider $\widehat{\theta_1 - \theta_2}$ as a function, f, of ρ_1 and ρ_2, and expand about ρ_1 and ρ_2 equal to zero.

$$\widehat{\theta_1-\theta_2} = (\theta_1-\theta_2)_{\text{mod}\pm 2\pi} + \sum_{i=1}^{2} \chi_i \left.\frac{\partial f}{\partial \chi_i}\right|_{\chi_i=0} + \frac{1}{2}\sum_{i=1}^{2} \chi_i^2 \left.\frac{\partial^2 f}{\partial \chi_i^2}\right|_{\chi_i=0} + \sum_{i\neq j=1}^{2}\sum \chi_i\chi_j \left.\frac{\partial^2 f}{\partial \chi_i \partial \chi_j}\right|_{\substack{\chi_i=0\\ \chi_j=0}} + \cdots \qquad (54)$$

where

$$\chi_i = \frac{1}{\sqrt{2\rho_i}} \quad ; \quad i = 1, 2 \qquad (55)$$

The expected value of $\widehat{\theta_1 - \theta_2}$ may be approximated by:

$$E(\widehat{\theta_1-\theta_2}) \approx (\theta_1-\theta_2)_{\text{mod}\pm 2\pi} + \sum \chi_i E\left(\left.\frac{\partial f}{\partial \chi_i}\right|_{\chi_i=0}\right) + \frac{1}{2}\sum_{i=1}^{2} \chi_i^2 E\left(\left.\frac{\partial^2 f}{\partial \chi_i}\right|_{\chi_i=0}\right) \qquad (56)$$

while the variance is:

$$\sigma^2(\theta_1-\theta_2) \approx \sum_{i=1}^{2} \chi_i^2 \left(\left.\frac{\partial f}{\partial \chi_i}\right|_{\chi_i=0}\right)^2 \qquad (57)$$

The partials can be evaluated in a straightforward manner

$$\left.\frac{\partial f}{\partial \chi_i}\right|_{\chi_i = 0} = \frac{I_{S1}\,\mathrm{Sin}(\theta_1 - \theta_2) + I_{C1}\,\mathrm{Cos}(\theta_1 - \theta_2)}{\mathrm{Cos}\ \Delta\theta_1} \tag{58}$$

while

$$\left.\frac{\partial f}{\partial \chi_2}\right|_{\chi_i = 0} = \frac{I_{S2}\,\mathrm{Sin}(\theta_1 - \theta_2) - I_{C2}\,\mathrm{Cos}(\theta_1 - \theta_2)}{\mathrm{Cos}\ \Delta\theta_2} \tag{59}$$

Combining these results with (56) and (57), we find that the expected value of $\theta_1 - \theta_2$ is:

$$E\,(\hat{\theta_1 - \theta_2}) \approx (\theta_1 - \theta_2)_{\mathrm{mod}\ \pm 2\pi} \tag{60}$$

i.e., the estimate is unbiased, while the variance is:

$$\sigma^2(\hat{\theta_1 - \theta_2}) \approx \frac{1}{2}\left[\frac{1}{(S/N)_{OJ1}} + \frac{1}{(S/N)_{OJ2}}\right] \tag{61}$$

where $(S/N)_{oji}$ is the signal-to-noise ratio at the j-th tone filter output of the i-th satellite.

Appendix 6D

SPECULAR REFLECTION WITH PHASE-LOCK LOOP CARRIER EXTRACTION (C_{23} and C_{21})

The analysis given below refers specifically to case C_{23}. However, on the assumption that the phase-lock loop VCO phase jitter goes to zero, the phase error formulae apply to case C_{21} on the assumption of carrier synchronization.

The IF output signal and noise is:

$$y(t) \approx y_D(t) + \epsilon(t) \tag{1}$$

where

$$y_D(t) = A(t)\cos[(\omega_c + \Delta\omega)(t-\tau-\Delta) + \theta(t-\tau-\Delta) + \omega_0 + \omega] \tag{2}$$

and

$$\epsilon(t) = n_d(t) + A_1(t)\cos[(\omega_c + \Delta\omega)(t-\tau-\Delta-\Delta_1) + \theta(t-\tau-\Delta-\Delta_1) + \omega_0 + \omega] \tag{3}$$

as described in **Section 6.3.1.**

As described in **Section 6.2 Figure 6-2** the IF output is passed through the carrier-narrow band filter, and then processed in a phase-locked-loop in order to extract the carrier frequency $f_c + \Delta f$. For sufficiently high loop filter output signal-to-noise ratios, the loop filter will lock in on the desired signal frequency with VCO output:

$$r(t) = \sin\left\{(\omega_c + \Delta\omega)t + \Delta\theta(t) + \phi(t)\right\} \tag{4}$$

The quantity $\Delta\theta$ is a zero mean Gaussian process with variance

$$\sigma_{\Delta\theta}^2 = \frac{1}{2\rho_L} \tag{5}$$

where $\phi(t)$ is the loop filter output signal-to-noise ratio. The function depends upon the multipath ratio, R, and the phase shifts of the direct and reflected components. The quantities ρ_L and ϕ will now be determined.

From the point of view of the demodulation process, the reflected signal can be considered to be a desired signal since the frequency offset δ_f will be small.

The PLL input desired signal is therefore of the form

$$S(t) = A\cos[(\omega_c + \Delta\omega)t + \theta_0] + A_1\cos[(\omega_c + \Delta\omega)t + \theta_1]$$

$$= E(t)\cos[(\omega_c + \Delta\omega)t + \phi(t)] \tag{6}$$

where

$$\phi t = \text{Arc}\tan\left[\frac{\sin\theta_0 + \frac{A_1}{A}\sin\theta_1}{\cos\theta_0 + \frac{A_1}{A}\cos\theta_1}\right] \tag{7}$$

From (2) and (3),

$$\begin{cases} \theta_0 = \theta_0 + \varphi - (\omega_c + \Delta\omega)(T + \Delta) \\ \theta_1 = \theta_0 + \varphi - (\omega_c + \Delta\omega)(T + \Delta + \Delta_1) \end{cases} \tag{8}$$

Approximating (7) for small A_1/A,

$$\phi(t) \simeq \theta_0 + \frac{A_1}{A}\sin\theta_{10}$$

$$\theta_{10} = \theta_0 - \theta_1$$

$$E(t) \simeq A\left\{1 + \frac{A_1}{A}\cos[\theta_1 + \theta_0]\right\} \tag{9}$$

where

$$\theta_0 = (\omega_c + \Delta\omega)\Delta_1 \tag{10}$$

To determine the loop filter output signal-to-noise ratio, let

$$\begin{cases} \left(\frac{C}{N}\right)_{IF,0} = \frac{A^2}{4N_0 W_{IF}} \\ \left(\frac{C}{N}\right)_{IF,1} = \frac{A_1^2}{4N_0 W_{IF}} \end{cases} \tag{11}$$

Then,

$$\rho_L = \frac{A^2 + A_1^2}{4N_0 B_L}$$

$$= \frac{W_{IF}}{B_L}\left[\left(\frac{C}{N}\right)_{IF,0} + \left(\frac{C}{N}\right)_{IF,1}\right] \tag{12}$$

Denoting the multipath ratio by $R = A_1/A$, one would expect that for loop filter output signal-to-noise ratios greater than 10 db, for small R, and δ_f the VCO output will be

$$r(t) = \sin\left[(\omega_c + \Delta\omega)t + \Delta\theta(t) + \theta_0 + R\sin\theta_{10}\right] \tag{12}$$

Referring to Figure 6-2C the low frequency portion of the product demodulator output will be

$$z(t) = 2LF\left\{y_D(t)\, r(t)\right\}$$

$$= A(t)\sin\left[\Delta\theta(t) + R\sin\theta_{10} - \theta(t-T-\Delta)\right] \tag{13}$$

Writing $z(t)$ in terms of the first harmonic of its tone frequency with $\alpha_i = 0$, and ignoring all other frequency components,

$$z(t) = A\left\{\sin[\Delta\theta + R\sin\theta_{10}]\cos\theta(t-T-\Delta) - \cos[\Delta\theta + R\sin\theta_{10}]\sin(\theta(t-T-\Delta))\right\}$$

$$= z_1(t) + z_2(t) \tag{14}$$

Retaining only the tone frequency terms,

$$z_j(t) = 2A\cos[\Delta\theta + R\sin\theta_{10}]\, J_0(m_k)\, J_1(m_j)\sin[\omega_j(t-T-\Delta)] \tag{15}$$

The noise will have 2 components at the tone filter outputs. One, due to the white noise with average power $4N_0W_{0j}$, the other due to the product of the VCO output and the reflected signal. The low frequency component of this product is:

$$n_1(t) = 2LF\left\{A\cos[(\omega_c + \Delta\omega)t + \theta(t-T-\Delta-\Delta_1) + \theta_1]\, r(t)\right\}$$

$$= A_1\sin\left[\Delta\theta + \phi - \theta(t-T-\Delta-\Delta_1) - \theta_1\right]$$

$$\approx A_1\sin\left[\Delta\theta + \theta_{10} + R\sin\theta_{10} - \theta(t-T-\Delta-\Delta_1)\right] \tag{16}$$

As in (14) and (15), it follows that the j-th tone filter output interference will be:

$$z_{ji}(t) = 2A_i \cos[\Delta\theta + R\sin\theta_0 + \theta_{i0}] J_0(m_k) J_i(m_j) \sin[\omega_j(t-T-\Delta)] \tag{17}$$

The mean-square value of the j-th tone filter output signal is:

$$\begin{aligned} \langle z_j^2 \rangle &= 2A^2 J_0^2(m_k) J_i^2(m_j) \langle \cos^2[\Delta\theta + R\sin\theta_{i0}] \rangle \\ &= A^2 J_0^2(m_k) J_i^2(m_j) [1 + \langle \cos(2\Delta\theta + 2R\sin\theta_{i0}) \rangle] \end{aligned} \tag{18}$$

Since

$$\langle \cos(2\Delta\theta + \chi) \rangle = \langle \cos 2\Delta\theta \rangle \langle \cos\chi \rangle - \langle \sin 2\Delta\theta \rangle \langle \sin\chi \rangle , \tag{19}$$

and since from (5) and equations 16 and 17 of C13,

$$\begin{cases} \langle \sin 2\Delta\theta \rangle = 0 \\ \langle \sin 2\Delta\theta \rangle = e^{-\frac{1}{\beta_L}} \end{cases} \tag{20}$$

it follows that

$$\langle \cos[2\Delta\theta + 2R\sin\theta_{i0}] \rangle = e^{-\frac{1}{\beta_L}} \langle \cos[2R\sin\theta_{i0}] \rangle \tag{21}$$

Assuming θ_{i0} to be a uniformly distributed random phase angle on the interval $(0,2\pi)$,

$$\begin{aligned} &\langle \cos[2R\sin\theta_{i0}] \rangle \\ &= \frac{1}{2\pi} \int_0^{2\pi} \cos[2R\sin\chi]\, d\chi \\ &= J_0(2R) \end{aligned} \tag{22}$$

Therefore,

$$\langle z_j^2 \rangle = A^2 J_0^2(m_k) J_i^2(m_j) [1 + e^{-\frac{1}{\beta_L}} J_0(2R)] \tag{23}$$

For small R,

$$J_0(2R) \approx 1 - R^2 \tag{24}$$

For large ρ_L,

$$e^{-\frac{1}{\rho_L}} \approx 1 - \frac{1}{\rho_L} \tag{25}$$

Therefore,

$$\langle z_j^2 \rangle \approx A^2 J_0^2(m_k) J_1^2(m_j) \left[2 - \frac{1}{\rho_L} - R^2\right] \tag{26}$$

Applying (17) and (20), the mean-square value of the j-th tone filter output interference is

$$\langle z_{j1}^2 \rangle = A_1^2 J_0^2(m_k) J_1^2(m_j) \left[1 + \langle \cos(2\Delta\theta + 2\theta_{10} + 2R\sin\theta_{10}) \rangle\right]$$

$$= A_1^2 J_0^2(m_k) J_1^2(m_j) \left[1 + e^{-\frac{1}{\rho_L}} \langle \cos(2\theta_{10} + 2R\sin\theta_{10} \rangle\right] \tag{27}$$

Assuming θ_{10} to be uniformly distributed,

$$\langle \cos(2\theta_{10} + 2R\sin\theta_{10}) \rangle = \frac{1}{2\pi} \int_0^{2\pi} \cos(2R\sin x + 2x)\, dx$$

$$= \frac{1}{\pi} \int_0^{\pi} \cos(2R\sin x + 2x)\, dx$$

$$= J_2(2R) \tag{28}$$

This involved applying identity 513-1C on p. 195 of **Reference** 6-39. Since $J_2(z) \approx \frac{z^2}{8}$ for small z, this term is negligible for small R.

Since from the point of view of phase measurement, the reflected component must be regarded as noise, the tone filter output signal-to-noise ratio is:

$$\left(\frac{S}{N}\right)_{oj} = \frac{A^2 J_0^2(m_k) J_1^2(m_j) \left[1 + e^{-\frac{1}{\rho_L}} J_0(2R)\right]}{4 N_0 W_{oj} + A_1^2 J_0^2(m_k) J_1^2(m_j) \left[1 + e^{-\frac{1}{\rho_L}} J_2(2R)\right]} \tag{29}$$

This quantity can be expressed in terms of the direct and reflected IF signal-to-noise ratios in (11). The resulting expression is:

$$\left(\frac{S}{N}\right)_{oj} = \frac{\left(\frac{C}{N}\right)_{IF,0}\left[1+e^{-\frac{1}{S_L}}J_0(2R)\right]}{\frac{W_{oj}}{W_{IF}}\left[J_0(m_k)J_1(m_j)\right]^{-2}+\left(\frac{C}{N}\right)_{IF,1}\left[1+e^{-\frac{1}{S_L}}J_2(2R)\right]} \qquad (30)$$

This reduces to equation (36) of Section 6.4.2.2 in the absence of a reflected signal.

The above analysis is based upon a linearized phase-lock loop model. Due to the presence of the interfering signal, the instantaneous signal-to-noise ratio can be reduced significantly. When this occurs, the linear loop model is no longer valid, phase lock can be lost, and the phase jitter can increase significantly. From (6) and (7), it is evident that the envelope of the sum of signals will be a minimum when cos (θ_{10}) equals -1. Defining the instantaneous signal-to-noise ratio at the loop filter output as:

$$\rho_L(t) = \frac{E^2(t)}{4N_0B_L} \qquad (31)$$

this quantity will be a minimum when E(t) is a minimum . Therefore,

$$Min\left[\rho_L(t)\right] = \frac{(A-A_1)^2}{4N_0B_L} = \frac{A^2}{4N_0B_L}(1-R)^2 \qquad (32)$$

The quantity ρ_L in (12) is the average value of $\rho_L(t)$.

When this minimum value of $\rho_L(t)$ goes below 10 db, the linear loop model becomes unacceptable. It is useful therefore to calculate this minimum signal-to-noise ratio for given signal-to-noise ratios.

$$\begin{cases} \chi = 10\log_{10}\dfrac{A^2}{4N_0B_L} \\ \chi_1 = 10\log_{10}\dfrac{A_1^2}{4N_0B_L} \end{cases} \qquad (33)$$

Solving for A and A_1, in (31) and applying (30), the minimum signal-to-noise ratio in db is:

$$10\log_{10}\left\{Min\left[S_L(t)\right]\right\} = 20\log_{10}\left\{\sqrt{\log_{10}^{-1}\left(\frac{\chi}{10}\right)} - \sqrt{\log_{10}^{-1}\left(\frac{\chi_1}{10}\right)}\right\} \tag{34}$$

For example, at VHF frequencies (150 MHz), it has been estimated that the largest expected value of R is about -5db, or $R \approx 0.56$. From (34), as long as the desired signal-to-noise ratio exceeds about 17 db, the above minimum signal-to-noise ratio will exceed 10 db, when $\chi = 24$, $\chi_1 = 19$. When χ = 24 db, the minimum instantaneous signal-to-noise ratio in (32) is about 17 db, or a 7 db maximum loss. The linear model assumption is reasonable for this example, but the small R assumption is not.

At L-band frequencies (1.6 GHz), it is estimated that the largest expected value of R is about -11 db, or $R \approx 0.28$. From (34), as long as the desired signal-to-noise ratio exceeds about 21 db, the above minimum signal-to-noise will exceed 10 db, when χ = 24, χ_1 = 13. For this case, the minimum instantaneous signal-to-noise ratio in (32) is about 21 db.

It should be pointed out that the single reflection model is applicable at VHF frequencies, whereas at L-band, the multiple reflection (diffuse scattering) models are more applicable.

It is desirable to generalize the analysis in equations (12) - (30) for arbitrary R. Another point which requires justification is the representation of the VCO output in (12) as

$$r(t) = \sin\left[(\omega_c + \Delta\omega)t + \Delta\theta(t) + \phi(t)\right] \tag{35}$$

The phase angle of the VCO output in the linear model should be equal to the phase angle of the signal plus noise at the loop filter output. This phase angle is:

$$\begin{cases} \beta(t) = \text{Arctan}\left\{\dfrac{\sin\theta_0 + R\sin\theta_1 + R_L I_{SL}(t)}{\cos\theta_0 + R\cos\theta_1 + R_L I_{CL}(t)}\right\} \\ R_L = \dfrac{\sigma_L}{A} \end{cases} \tag{36}$$

where σ_L is the standard deviation of the loop filter output random noise; I_{SL}, I_{CL} represent the normalized noise inphase and quadrature components. For the case of interest, R_L will be small e.g., the above value of +24 db corresponds to $R_L < 0.05$.

Regarding $\beta(t)$ as a function of R_L, and expanding it in a MacLaurin series for small R_L,

$$\beta(t) \approx \beta(t)\Big|_{R_L=0} + R_L \frac{\partial\beta}{\partial R_L}\Big|_{R_L=0} \tag{37}$$

From (33) and (7)

$$\beta(t)\Big|_{R_L=0} = \phi(t) \tag{38}$$

and

$$\Delta\theta(t) = R_L \frac{\partial\beta}{\partial R_L}\Big|_{R_L=0} = R_L\left\{\frac{I_{SL}[\cos\theta_0 + R\cos\theta_1] - I_{CL}[\sin\theta_0 + R\sin\theta_1]}{1 + R^2 + 2\cos(\theta_{10})}\right\} \tag{39}$$

For sufficiently small R,

$$\Delta\theta(t) \approx R_L\left[I_{SL}(t)\cos\theta_0 - I_{CL}(t)\sin\theta_0\right] \tag{40}$$

In this case, $\Delta\theta$ is normally distributed with zero mean, and variance

$$\sigma_{\Delta\theta}^2 = \frac{\sigma_L^2}{A^2} = \frac{1}{\frac{2W_{IF}}{B_L}\left(\frac{C}{N}\right)_{IF,0}} \tag{41}$$

when one applies the definitions in (11). Therefore, (35) is a valid representation when R_L is small. However, the statistics of $\Delta\theta$ change when R is not small.

The low-frequency portion of the product demodulator output is proportional to:

$$z(t) = A(t)\sin\left[\Delta\theta + \phi - \theta_0 - \theta(t-T-\Delta)\right] \tag{42}$$

As in (14),

$$z(t) = A\left\{\sin[\Delta\theta+\phi-\theta_0]\cos\theta(t-T-\Delta) - \cos[\Delta\theta+\phi-\theta_0]\sin\theta(t-T-\Delta)\right\} = z_1(t) + z_2(t). \tag{43}$$

Retaining only the tone frequency terms,

$$z_j(t) = 2A\cos[\Delta\theta+\phi-\theta_0]J_0(m_k)J_1(m_j)\sin[w_j(t-T-\Delta)] \tag{44}$$

The expression for $\Delta\theta$ in (39) can be simplified by noting from (7) that

$$\Delta\theta(t) = \frac{\sigma_L}{E(t)}\left\{I_{CL}\cos\phi - I_{SL}\sin\phi\right\} \tag{45}$$

For any time t, and regarding θ_0 to be fixed, $\Delta\theta$ will be normally distributed with zero mean and variance

$$\sigma^2(\Delta\theta) = \frac{\sigma_L^2}{E^2(t)} \tag{46}$$

The mean-square value of z_j for slowly varying T and Δ is

$$\langle z_{ij}^2 \rangle = A^2 J_0^2(m_k) J_1^2(m_j) \left[1 + \langle \cos(2\Delta\theta + 2\phi - 2\theta_0) \rangle \right] \tag{47}$$

Expanding the cosine term, and averaging over the random noise distribution,

$$\langle \cos[2\Delta\theta + 2\phi - 2\theta_0] \rangle_n$$

$$= \langle \cos[2\Delta\theta(t)] \rangle \cos[2\phi(t) - 2\theta_0] - \langle \sin[2\Delta\theta(t)] \rangle \sin[2\phi(t) - 2\theta_0] \tag{48}$$

Since $\Delta\theta$ is normally distributed with zero mean,

$$\begin{cases} \langle \cos(2\Delta\theta) \rangle \exp[-2\sigma^2(\Delta\theta)] \\ \langle \sin(2\Delta\theta) \rangle = 0 \end{cases} \tag{49}$$

From (46),

$$2\sigma^2(\Delta\theta) = \frac{2\sigma_L^2}{A^2} \left[1 + R^2 + 2R\cos\theta_{10} \right]^{-\frac{1}{2}} \tag{50}$$

From (7),

$$\cos\phi = \frac{\cos\theta_0 + R\cos\theta_1}{\left[1 + R^2 + 2R\cos\theta_{10} \right]^{1/2}}$$

$$\sin\phi = \frac{\sin\theta_0 + R\sin\theta_1}{\left[1 + R^2 + 2R\cos\theta_{10} \right]^{1/2}} \tag{51}$$

It follows from (51) that

$$\cos[2\phi - 2\theta_0] = \frac{1 + R^2\cos(2\theta_{10}) + 2R\cos\theta_{10}}{1 + R^2 + 2R\cos\theta_{10}} \tag{52}$$

Applying (49) to (48),

$$\langle \cos(2\Delta\theta + 2\phi - 2\theta_0)\rangle = \exp[-2\sigma^2(\Delta\theta)] \cdot \cos[2\phi - 2\theta_0]$$
$$\approx \cos[2\phi - 2\theta_0] \tag{53}$$

for large loop filter output signal-to-noise ratios. Therefore the desired mean value can be approximated by averaging $\cos(2\phi - 2\theta_0)$ in (52) over a uniform distribution for the phase angle θ_{10}. This average involves three integrals:

$$I_1 = \frac{1}{2\pi}\int_0^{2\pi} \frac{dx}{1+R^2+2R\cos x}$$

$$I_2 = \frac{1}{2\pi}\int_0^{2\pi} \frac{\cos(2x)\,dx}{1+R^2+2R\cos x}$$

$$I_3 = \frac{1}{2\pi}\int_0^{2\pi} \frac{\cos x\,dx}{1+R^2+2R\cos x} \tag{54}$$

The integral I_1 is given in Reference 1, (see page 6D-23)page 99,Eg.44b as

$$I_1 = \frac{1}{|1-R^2|} \quad ; \quad |R| \neq 1 \tag{55}$$

The integral I_3 is given in Reference 1, page 100,Eg, 45a and 45b as:

$$I_3 = \begin{cases} \dfrac{-R}{1-R^2} & ; \ |R|<1 \\ -\dfrac{1}{R(R^2-1)} & ; \ |R|>1 \end{cases} \tag{56}$$

The integral I_2 can be evaluated by applying identity 3.451, No. 4, page 162 of Reference 5:

$$I_4 = \frac{1}{2\pi}\int_0^{2\pi} \frac{\cos^2 x\,dx}{1+R^2+2R\cos x}$$
$$= \begin{cases} \dfrac{1+R^2}{2(1-R^2)} & ; \ R^2<1 \\ \dfrac{R^2+1}{2R^2(R^2-1)} & ; \ R^2>1 \end{cases} \tag{57}$$

From the identity:

$$\cos 2x = 2\cos^2 x - 1 \tag{58}$$

it follows that

$$I_2 = 2I_4 - I_1 \tag{59}$$

For the case of interest R is a positive number less than unity. Therefore, applying (55) and (57) to (59),

$$I_2 = \frac{R^2}{1-R^2} \tag{60}$$

Applying (55), (56) and (54) to the mean value of the function in (52),

$$\langle \cos(2\Delta\theta + 2\phi - 2\theta_0)\rangle \approx \langle \cos(2\phi - 2\theta_0)\rangle = 1 - R^2 \tag{61}$$

Applying this to (47), gives an approximate expression for the j-th tone signal power under the assumption that the direct signal to white noise ratio at the output of the loop filter is large enough for the mean of cos ($2\Delta\theta$) in (49) to be close to unity. Since this mean is an exponential function, it must be positive and less than or equal to unity. Therefore, the approximation in (61) gives an upper bound on the output signal power. On the other extreme, a lower bound can be obtained by setting the exponential function equal to zero. From (47) and (61), the ratio of the upper bound to the lower bound equals $2-R^2$. Therefore the decibel error in employing (61) must be less than $10 \log_{10}(2-R^2)$. Taking a worst case of $10 \log_{10} R^2$ equal to -5 db, this corresponds to a maximum error of about 2.3 db.

A more accurate lower bound can be calculated by expanding the exponential in (50). For large signal-to-noise ratios, retaining just the linear terms should be adequate. Therefore, applying (50), (52), and (61),

$$\langle \cos(2\Delta\theta + 2\phi - 2\theta_0)\rangle \approx \langle \cos(2\phi - 2\theta_0)\rangle - \frac{2\sigma_L^2}{A^2}\left\langle (1+R^2+2R\cos\chi)^{-\frac{1}{2}} \cos(2\phi - 2\theta_0)\right\rangle$$

$$= 1 - R^2 - \frac{2\sigma_L^2}{A^2}\left\langle \frac{1+R^2\cos 2\chi + 2R\cos\chi}{[1+R^2+2R\cos\chi]^{3/2}}\right\rangle$$

$$= 1 - R^2 - \frac{2\sigma_L^2}{A^2}\left\langle (1+R^2+2R\cos\chi)^{-1/2}\right\rangle \qquad (62)$$

From an identity in Reference 2

$$\left\langle [1+R^2+2R\cos\chi]^{-\frac{1}{2}}\right\rangle = \frac{1}{2\pi}\int_0^{2\pi} \frac{d\chi}{[1+R^2+2R\cos\chi]^{1/2}}$$

$$= \frac{2}{\pi} K(R); \quad 0 < R < 1 \qquad (63)$$

The function K is the complete elliptic integral of the first kind:

$$K(R) = \int_0^{\pi/2} \frac{du}{\sqrt{1 - R^2 \sin^2 u}} \qquad (64)$$

A useful table of K(R) as a function of R^2 is given in Reference 3 , p. 91. Taking the largest decibel value of R to be -5 db, $R^2 \approx 0.31$. From Reference 4 $K \approx 1.72$, so that $\frac{2K}{\pi} \approx 1.1$. For a loop filter output signal-to-noise ratio of +24 db, $\frac{2\sigma_L^2}{A^2} \approx .004$. Therefore, $\left(\frac{2\sigma_L^2}{A^2}\right)\frac{2K}{\pi} \approx .0044$, so that for the case of interest the lower bound is very close to the upper bound $1 - R^2$. Equation (61) is reasonable. Applying (61) to (47), the average signal power is:

$$\langle z_j^2 \rangle \approx A^2 J_0^2(m_k) J_1^2(m_j)[2 - R^2] \qquad (65)$$

The j-th tone filter output will be of the form

$$y_j(t) = z_j(t) + z_{j1}(t) + \epsilon_j(t) \tag{66}$$

where z_j represents the desired signal, as given in equation (44), z_{j1} is due to the reflected signal, and ϵ_j is due to the white noise. ϵ_j is normally distributed with zero mean and variance $4N_0W_{bj}$. The expression for z_{j1} can be derived by applying the expression for the reflected signal in (3) and the VCO output signal in (35). The low frequency portion of the product demodulator output is:

$$z_1(t) = 2LF\left\{A_1 \cos[(\omega_c + \Delta\omega)(t-T-\Delta-\Delta_1)+\theta(t-T-\Delta-\Delta_1)+\varphi_0+\varphi]\, r(t)\right\}$$

$$= A_1 \cos[\theta(t-T-\Delta-\Delta_1) + \theta_1 - \Delta\theta - \phi] \tag{67}$$

where

$$\theta_1 = \varphi_0 + \varphi - (\omega_c + \Delta\omega)[T + \Delta + \Delta_1] \tag{68}$$

As in (17), the interference components at the j-th tone filter outputs are:

$$z_{j1}(t) = 2A_1 \cos[\Delta\theta + \phi - \theta_1] J_0(m_k) J_1(m_j) \sin[\omega_j(t-T-\Delta-\Delta_1)] \tag{69}$$

The mean-square-value of this undesired signal is:

$$\langle z_{j1}^2 \rangle = A_1^2 J_0^2(m_k) J_1^2(m_j)[1 + \langle \cos(2\Delta\theta + 2\phi - 2\theta_1)\rangle] \tag{70}$$

Expanding the cosine term, and averaging over the random noise distribution,

$$\langle \cos(2\Delta\theta + 2\phi - 2\theta_1)\rangle_n = \langle \cos(2\Delta\theta)\rangle \cos(2\phi - 2\theta_1)$$

$$- \langle \sin(2\Delta\theta)\rangle \sin(2\phi - 2\theta_1) \tag{71}$$

Applying (49),

$$\langle \cos(2\Delta\theta + 2\phi - 2\theta_1)\rangle = \exp[-2\sigma^2(\Delta\theta)]\cos(2\phi - 2\theta_1) \tag{72}$$

where $\sigma^2(\Delta\theta)$ is given in (50). From (51),

$$\begin{cases} \cos 2\phi = \dfrac{\cos 2\theta_0 + 2R\cos(\theta_0+\theta_1) + R^2\cos 2\theta_1}{1 + R^2 + 2R\cos\theta_{10}} \\ \sin 2\phi = \dfrac{\sin 2\theta_0 + 2R\sin(\theta_0+\theta_1) + R^2\sin 2\theta_1}{1 + R^2 + 2R\cos\theta_{10}} \end{cases} \tag{73}$$

where $\theta_{10} = \theta_0 - \theta_1$. Therefore,

$$\cos(2\phi - 2\theta_1) = \frac{R^2 + 2R\cos\theta_{10} + \cos 2\theta_{10}}{1 + R^2 + 2R\cos\theta_{10}} \tag{74}$$

Approximating the exponential in (72) for large desired signal-to-random noise ratios and averaging over a uniform distribution for θ_{10},

$$\langle \cos(2\Delta\theta + 2\phi - 2\theta_1)\rangle \approx \langle \cos(2\phi - 2\theta_1)\rangle - \frac{2\sigma_1^2}{A^2}\left\langle \left\{(1+R^2+2R\cos\theta_{10})^{-\frac{1}{2}}\cos(2\phi - 2\theta_1)\right\}\right\rangle \tag{75}$$

will enable the evaluation of the undesired signal power in (70). Applying (54) - (57), and (59), and assuming R less than unity,

$$\begin{aligned} \langle \cos(2\phi - 2\theta_1)\rangle &= R^2 I_1 + I_2 + 2RI_3 \\ &= R^2 I_1 + 2I_4 - I_1 + 2RI_3 \\ &= \frac{R^2 - 1}{1 - R^2} + \frac{2(1+R^2)}{2(1-R^2)} - \frac{2R^2}{1-R^2} = 0 \end{aligned} \tag{76}$$

The other term in (75) is:

$$\left\langle \frac{\cos 2\theta_{10} + R^2 + 2R\cos 2\theta_{10}}{[1 + R^2 + 2R\cos\theta_{10}]} \right\rangle \leq \left\langle (1 + R^2 + 2R\cos\theta_{10})^{-1/2} \right\rangle = \frac{2}{\pi} k(R) \tag{77}$$

Applying (63). As discussed previously for the worst case of $R^2 = 0.31$, $\frac{2K}{\pi} \approx 1.1$.

Therefore, for large signal-to-noise ratios,

$$\langle \cos(2\Delta\theta + 2\phi - 2\theta_1) \rangle \approx 0 \tag{78}$$

Therefore, from (70),

$$\langle z_{j1}^2 \rangle \approx A_1^2 J_0^2(m_k) J_1^2(m_j) \tag{79}$$

Therefore, the total undesired signal and noise power at the tone filter output is:

$$N_j \approx 4 N_0 W_{oj} + A_1^2 J_0^2(m_k) J_1^2(m_j) \tag{80}$$

Applying (65) and (80), the tone filter output signal-to-noise ratio is:

$$\left(\frac{S}{N}\right)_{oj} = \frac{A_1 J_0^2(m_k) J_1^2(m_j) (2 - R^2)}{4 N_0 W_{oj} + A_1^2 J_0^2(m_k) J_1^2(m_j)} \tag{81}$$

Applying (11),

$$\left(\frac{S}{N}\right)_{oj} = \frac{(2 - R^2)\left(\frac{C}{N}\right)_{IF,0}}{\frac{W_{oj}}{W_{IF}}\left[J_0(m_k) J_1(m_j)\right]^{-2} + \left(\frac{C}{N}\right)_{IF,1}} \tag{82}$$

For the cases of interest, W_{oj} is much less than W_{IF}. Therefore,

$$\begin{aligned} \left(\frac{S}{N}\right)_{oj} &\approx (2 - R^2) \frac{\left(\frac{C}{N}\right)_{IF,0}}{\left(\frac{C}{N}\right)_{IF,1}} \\ &= (2 - R^2) \frac{1}{R^2} \\ &= \frac{2}{R^2} - 1 \end{aligned} \tag{83}$$

whenever,

$$\frac{W_{oj}}{W_{IF}} << \left[J_0(m_k)\, J_1(m_j) \right]^2 \left(\frac{C}{N}\right)_{IF,1} \qquad (84)$$

Since

$$\left(\frac{C}{N}\right)_{IF,1} = R^2 \left(\frac{C}{N}\right)_{IF,0} \qquad (85)$$

a useful form for (84) is:

$$\left(\frac{S}{N}\right)_{oj} = \frac{(2-R^2)\left(\frac{C}{N}\right)_{IF,0}}{\frac{W_{oj}}{W_{IF}\left[J_0(m_k)\, J_1(m_j)\right]^2} + R^2\left(\frac{C}{N}\right)_{IF,0}} \qquad (86)$$

It is evident from this equation that when R^2 is non-zero, $\left(\frac{S}{N}\right)_{oj}$ approaches the expression in (83) for sufficiently large $\left(\frac{C}{N}\right)_{IF,0}$.

In order to complete the analysis, it is necessary to calculate the mean and the variance of the phase-comparison measurement. The mean will determine the bias errors. The variance will determine the measurement precision.

Writing the j-th tone filter output signal and noise in terms of inphase and quadrature components about $\omega_j(t-\tau-\Delta)$,

$$y_j(t) = 2 J_0(m_k)\, J_1(m_j) \left\{ I_{cj}(t) \cos[\omega_j(t-\tau-\Delta)] - I_{sj}(t) \sin[\omega_j(t-\tau-\Delta)] \right\} \qquad (87)$$

where

$$I_{cj}(t) = -A_1 \sin(\omega_j \Delta_1) \cos(\Delta\theta + \phi - \theta_1)$$

$$I_{sj}(t) = -A \cos(\Delta\theta + \phi - \theta_0) - A_1 \cos(\omega_j \Delta_1) \cos(\Delta\theta + \phi - \theta_1) \qquad (88)$$

Therefore

$$y_j(t) = E_j(t)\cos[\omega_j(t-T-\Delta) + \delta_j(t)] \tag{89}$$

where

$$\delta_j(t) = \text{Arctan}\left\{\frac{I_{sj}(t)}{I_{cj}(t)}\right\} \tag{90}$$

Assuming an ideal phase detector, the function $\delta_j(t)$ represents the instantaneous phase error due to multipath on the assumption of high signal-to-random noise ratio. Applying (90),

$$\frac{I_{sj}(t)}{I_{cj}(t)} = \frac{1}{R}F_j(t) + G_j(t) \tag{91}$$

where

$$\begin{cases} F_j(t) = \dfrac{\cos[\Delta\theta + \phi - \theta_0]}{\sin(\omega_j\Delta_1)\cos(\Delta\theta + \phi - \theta_1)} \\ G_j(t) = \cot(\omega_j\Delta_1) \end{cases} \tag{92}$$

and

$$\begin{cases} \theta_0 = \varphi_0 + \varphi - (\omega_c + \Delta\omega)(T + \Delta) \\ \theta_1 = \varphi_0 + \varphi - (\omega_c + \Delta\omega)(T + \Delta + \Delta_1) \end{cases} \tag{93}$$

so that

$$\begin{aligned} \theta_{10} &= \theta_0 - \theta_1 \\ &= (\omega_c + \Delta\omega)\Delta_1 \end{aligned} \tag{94}$$

For large signal-to-random noise ratios, the term can be ignored, so that:

$$F_j(t) \simeq \frac{\cos[\phi - \theta_0]}{\sin(\omega_j\Delta_1)\cos(\phi - \theta_1)} \tag{95}$$

This can be simplified by applying (51), so that when $\Delta\theta$ is negligible,

$$F_j = \frac{1 + R\cos\theta_{10}}{\sin(\omega_j \Delta_1)\cos(\phi - \theta_1)} \tag{96}$$

Since in the absence of multipath, the tone filter output signal in (89) should reduce to

$$y_j(t) = E_j(t)\sin[\omega_j(t - T - \Delta)] \tag{97}$$

it is natural to write (89) in terms of a sine function rather than cosine. This can be done by noting that

$$y_j(t) = -E_j(t)\sin\left[\omega_j(t-T-\Delta) + \delta_j - \frac{3\pi}{2}\right] \tag{98}$$

The mean phase-measurement error due to multipath is therefore $\delta_j - \frac{\pi}{2}$. Applying (90), (92) and (96),

$$\begin{aligned}\Delta\phi_j &= \delta_j - \frac{\pi}{2} \\ &= \text{Arctan}\left\{\cot(\omega_j\Delta_1) + \frac{\frac{1}{R} + \cos[(\omega_c + \Delta\omega)\Delta_1]}{R\cos[(\omega_c+\Delta\omega)\Delta_1]\sin(\omega_j\Delta_1)}\right\} - \frac{\pi}{2}\end{aligned} \tag{99}$$

When Δ_1, or R equals zero, δ_j equals Arctan (∞), which is a multiple valued function equal to $\pm\frac{\pi}{2}, \pm\frac{3\pi}{2}, \pm\frac{5\pi}{2}$, etc. If we take the first quadrant value, $\frac{\pi}{2}$, then $\Delta\phi_j$ equals zero as it should. Converting to a range error,

$$\Delta R_j = \frac{c\,\Delta\phi_j}{2\pi f_j} \tag{100}$$

This quantity is an estimate of the mean range error due to multipath.

In order to calculate the variance of the phase error, the noise phase-jitter term in the expression Fj(t) in (92) can no longer be ignored. Applying (51) to (92) as was done in deriving (96),

$$F_j(t) = \frac{(1+R\cos\theta_{10})\cos\Delta\theta + R\sin\theta_{10}\sin\Delta\theta}{\sin(\omega_j\cdot\Delta_1)\left[(R+\cos\theta_{10})\cos\Delta\theta - \cos\theta_{10}\sin\Delta\theta\right]} \tag{101}$$

When $\Delta\theta$ is not taken to be zero, the counterpart of the phase error in (99) can be determined by applying (90) - (92) to (101) to give

$$\Delta\phi_j = \text{Arctan}\left\{\cot(\omega_j\Delta_1) + \frac{\frac{1}{R}\cos\Delta\theta + \cos(\Delta\theta-\theta_{10})}{\sin(\omega_j\cdot\Delta_1)\left[R\cos\Delta\theta + \cos(\Delta\theta+\theta_{10})\right]}\right\} - \frac{\pi}{2} \tag{102}$$

For large signal-to-noise ratios, the variance of this phase error can be approximated by means of the formula:

$$\sigma^2(\Delta\phi_j) \approx \left[\frac{\partial\,\Delta\phi_j}{\partial\,\Delta\theta}\bigg|_{\Delta\theta=0}\right]^2 \sigma^2(\Delta\theta) \tag{103}$$

The variance of $\Delta\theta$ is

$$\sigma^2(\Delta\theta) \approx \frac{1}{2\rho_L} \tag{104}$$

where ρ_L represents the phase-lock loop filter desired output signal-to-random noise ratio

$$\rho_L = \frac{A^2}{4N_0B_L} \tag{105}$$

It follows that the standard-deviation of the phase error is given by:

$$\sigma(\Delta\phi_j) \approx \frac{g_j}{\sqrt{2\rho_L}} \tag{106}$$

where

$$\begin{cases} g_j = \dfrac{|\sin(\omega_j \Delta_1)| \cdot |(R+\frac{1}{R})\sin\theta_{10} + \sin(2\theta_{10})|}{(R+\cos\theta_{10})^2 \sin^2(\omega_j\Delta_1) + [(R+\cos\theta_{10})\cos(\omega_j\Delta_1) + \frac{1}{R} + \cos\theta_{10}]^2} \\ \theta_{10} = (\omega_c + \Delta\omega)\Delta_1 \end{cases} \tag{107}$$

The corresponding standard deviation of the range measurement is:

$$\sigma(\Delta R_j) \approx \frac{c\, g_j}{2\pi f_j \sqrt{2 S_L}} \tag{108}$$

The expression gj in (107) goes to zero as the differential multipath delay Δ_1, and/or the multipath amplitude ratio R goes to zero.

Finally, it is necessary to show what happens when we don't neglect the additive noise $\epsilon_j(t)$ in (87). This noise is Gaussian with zero mean and variance

$$\sigma_j^2 = 4 N_0 W_{oj} \tag{109}$$

Denoting the inphase and quadrature components of this noise by $\sigma_j I_c$ and $\sigma_j I_s$, the signal plus noise corresponding to (87) can be written

$$y_j(t) = A_c \cos[\omega_j(t-\tau-\Delta)] + A_s \sin[\omega_j(t-\tau-\Delta)] \tag{110}$$

where

$$\begin{cases} A_c = -2A_1 J_0(m_k) J_1(m_j) \sin\omega_j\Delta_1 \cos(\Delta\theta+\phi-\theta_1) + \sigma_j I_c \\ A_s = 2 J_0(m_k) J_1(m_j)[A\cos(\Delta\theta+\phi-\theta_2) + A_1\cos(\omega_j\Delta_1)\cos(\Delta\theta+\phi-\theta_1) + \sigma_j I_s] \end{cases} \tag{111}$$

Therefore

$$y_j(t) = e_j \sin[\omega_j(t-\tau-\Delta) + \delta_j] \tag{112}$$

where

$$\delta_j = \text{Arctan}\left\{\frac{A_c}{A_s}\right\}$$

$$= \text{Arctan}\left\{\frac{-R\sin(\omega_j\Delta_1)\cos(\Delta\theta+\phi-\theta_1) + \frac{I_c}{\sqrt{2\rho_j}}}{\cos(\Delta\theta+\phi-\theta_0)+R\cos(\omega_j\Delta_1)\cos(\Delta\theta+\phi-\theta_1)+\frac{I_s}{\sqrt{2\rho_j}}}\right\} \tag{113}$$

where

$$\rho_j = \frac{2A^2 J_0^2(m_R)\, J_1^2(m_j)}{\sigma_j^2} \tag{114}$$

represents the average power of the j-th tone divided by the random noise power. The random variables I_c and I_s are independent and normally distributed with zero mean and unit variance. For large loop filter output signal-to-noise ratios, $\Delta\theta$ is normally distributed with zero mean and variance $\frac{1}{2}\rho_L$, where ρ_L is the loop output signal-to-random noise power ratio. From (51)

$$\cos(\Delta\theta+\phi-\theta_1) = \frac{R\cos\Delta\theta + \cos(\Delta\theta-\theta_{10})}{[1+R^2+2R\cos\theta_{10}]^{1/2}}$$

$$\cos(\Delta\theta+\phi-\theta_0) = \frac{\cos\Delta\theta + R\cos(\Delta\theta-\theta_{10})}{[1+R^2+2R\cos\theta_{10}]^{1/2}} \tag{115}$$

where $\theta_{10} = \theta_0 - \theta_1 = (\omega_L+\Delta\omega)\Delta_1$. Therefore the phase error depends upon three random variables, on the differential IF phase delay θ_{10} and on the differential tone phase delay $\omega_j\Delta_1$.

The easiest way to handle the analysis from here on in is to estimate the phase error probability distribution using a general digital computer. Sample phase errors are determined by means of random number generation.

Table 6D-1 gives a set of range measurement bias errors calculated from equation (102). The underlying assumptions are given in the table. For these assumptions, the mean range error calculated from (113) and (115) does not differ significantly from the errors in Table 6D-1. For small R, and large signal-to-noise, equation (113) reduces to the expression for the phase error derived in Section 5.4.2. Figure 6D-1 gives the standard deviation of the range error for the 2 tone frequencies in Table 6D-1.

Relating ρ_j to the desired signal carrier-to-noise ratio,

$$\rho_j = \frac{2 W_{IF}}{W_{oj}} J_o^2(m_k) J_1^2(m_j) \left(\frac{C}{N}\right)_{IF,O} \quad (116)$$

which is exactly the same as the tone filter output signal-to-noise ratio in Appendix 6A.

REFERENCES

1. W. Grobner and N. Hofreiter, Integral Tables, Part 2, Springler-Verlag, 1958
2. F. S. Gradshteyn and I. M. Ryzhik, Tables of Integrals, Series, and Products
3. "Handbook of Mathematical Functions...." AMS 55, NBS, Washington, D.C. 1964
4. W. A. Edson, "Noise in Oscillators", Proc. IRE, August 1960

TABLE 6D-1 RANGE MEASUREMENT BIAS ERRORS* FOR A SPECULAR MULTIPATH CHANNEL

Ratio of Reflected to Direct Component (db)	Range Measurement Bias Errors (meters)		Ratio of Reflected to Direct Component (db)	Range Measurement Bias Errors (meters)	
	f_1 = 200 Hz (Coarse tone)	f_2 = 6.4kHz (Fine tone)		f_1=200 Hz (Coarse tone)	f_2 = 6.4kHz (Fine tone)
-5	641	612	-16	31	30
-6	468	449	-17	23	23
-7	347	335	-18	17	17
-8	261	252	-19	12	12
-9	198	192	-20	9	9
-10	151	146	-21	6	6
-11	116	112	-22	4	4
-12	89	86	-23	2	2
-13	68	66	-24	1	1
-14	52	51	-25	0	0
-15	40	39			

*The assumptions used in deriving these errors are listed below:

1. Large signal-to-random noise power ratios
2. Equal tone and loop filter bandwidths
3. Tone filter output desired signal-to-random noise ratio = +24 db
4. Ideal phase detector
5. Phase jitter at the output of the phase lock loop VCO equals the phase of the loop input signal plus interference plus noise (linear loop model)
6. IF frequency f_c = 68 kHz
7. Input signal frequency offset
8. Differential multipath delay = 10 usec

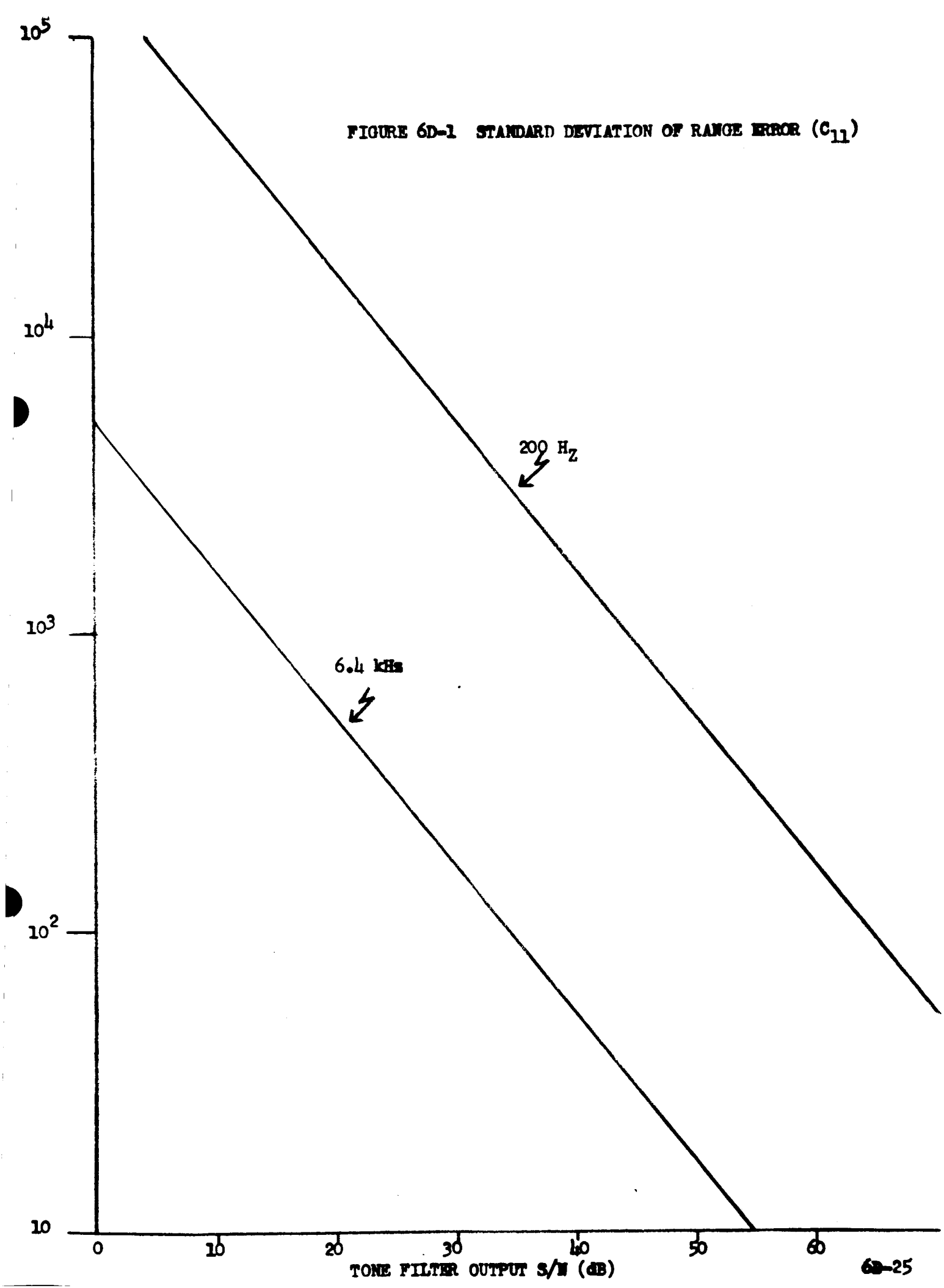

FIGURE 6D-1 STANDARD DEVIATION OF RANGE ERROR (C_{11})

Appendix 6E

EXTRACTED CARRIER DEMODULATION WITH ONE SPECULAR REFLECTION (C_{22})

The IF output plus noise is given by

$$x(t) = s(t) + s_R(t) + n(t) \tag{1}$$

where the direct and reflected components are given by

$$\left.\begin{aligned} s(t) &= A\cos\left\{\omega_0(at+b)+\theta+\sum_{j=1}^{2} m_j \sin[\omega_j(at+b)+\theta_j]\right\} \\ s_R(t) &= A_1\cos\left\{\omega_0(a_1t+b_1)+\theta_R+\sum_{j=1}^{2} m_j \sin[\omega_j(a_1t+b_1)+\theta_{jR}]\right\} \end{aligned}\right\} \tag{2}$$

while $n(t)$ is double sided white noise of bandwidth ω_{IF}, the IF bandwidth and spectral density N_0. It can be shown that $n(t)$ may be written with in phase and quadrature component about the carrier of the direct signal by:

$$n(t) = I_c\cos\left[(\omega_0+\Delta\omega)t\right] - I_s \sin\left[(\omega_0+\Delta\omega)t\right] \tag{3}$$

using the relationships

$$a = 1 + \frac{\Delta\omega}{\omega_0} \tag{4}$$

An analogous expression holds for the reflected component. The quantity b is given by:

$$b = \frac{\Delta\theta}{\omega_0} + a\,\Delta\tau \tag{5}$$

representing phase and time delays due to the medium.. Both signal terms can be expressed with in-phase and quadrature components as:

$$\begin{aligned} s(t) &= A\left\{I_{c\times D}(t)\cos\left[(\omega_0+\Delta\omega)t+\bar{\theta}_1\right] - I_{s\times D}(t)\sin\left[(\omega_0+\Delta\omega)t+\bar{\theta}_1\right]\right. \\ s_R(t) &= A_1\left\{I_{c\times R}(t)\cos\left[(\omega_0+\Delta\omega_1)t+\bar{\theta}_2\right] - I_{s\times R}(t)\sin\left[(\omega_0+\Delta\omega_1)t+\bar{\theta}_2\right]\right. \end{aligned} \tag{6}$$

using (4.) and defining

$$\begin{aligned} \bar{\theta}_1 &= \theta + \omega_0 b \\ \bar{\theta}_2 &= \theta_R + \omega_0 b_1 \end{aligned} \tag{7}$$

$$I_{cxb}(t) = \left\{ J_0(m_1) + 2\sum_{n_1=1}^{\infty} J_{2n_1}(m_1) \cos 2n_1 \left[\omega_1(at+b) + \theta_1\right] \right\} \cdot$$

$$\cdot \left\{ J_0(m_2) + 2\sum_{n_2=1}^{\infty} J_{2n_2}(m_2) \cos 2n_2 \left[\omega_2(at+b) + \theta_2\right] \right\}$$

$$- \left\{ 2\sum_{n_1=0}^{\infty} J_{2n_1+1}(m_1) \sin(2n_1+1) \cdot \left[\omega_1(at+b) + \theta_1\right] \right\} \cdot \qquad (8)$$

$$\cdot \left\{ 2\sum_{n_2=0}^{\infty} J_{2n_2+1}(m_2) \sin(2n_2+1) \cdot \left[\omega_2(at+b) + \theta_2\right] \right\}$$

$$I_{sxb}(t) = \left\{ J_0(m_1) + 2\sum_{n_1=1}^{\infty} J_{2n_1}(m_1) \cos 2n_1 \cdot \left[\omega_1(at+b) + \theta_1\right] \right\} \cdot$$

$$\cdot \left\{ 2\sum_{n_2=0}^{\infty} J_{2n_2+1}(m_1) \sin(2n_2+1) \left[\omega_2(at+b) + \theta_2\right] \right\}$$

$$+ \left\{ J_0(m_2) + 2\sum_{n_2=1}^{\infty} J_{2n_2}(m_2) \sin 2n_2 \left[\omega_2(at+b) + \theta_2\right] \right\} \cdot \qquad (9)$$

$$\cdot \left\{ 2\sum_{n_1=0}^{\infty} J_{2n_1}(m_1) \cos(2n_1+1) \left[\omega_1(at+b) + \theta_1\right] \right\}$$

where $J_s(x)$ are the Bessel function of order s in the variable x. Like expressions are valid for the reflected component involving the arguments $\omega_j(a_1 t + b_1) + \theta_{jR}$.

The IF output $X(t)$ is passed through a carrier narrow band filter, which rejects the modulation, so that the input to the bandpass filter (BPF) is given by:

$$d(t) = A\cos\left[(\omega_0 + \Delta\omega)t + \bar{\theta}_1\right] + A_R \cos\left[(\omega_0 + \Delta\omega)t + \bar{\theta}_2\right] + n_0(t) \qquad (10)$$

The output of the BPF is:

$$r(t) = A\sin\left[(\omega_0 + \Delta\omega)t + \bar{\theta}_1\right] + \varepsilon(t) \qquad (11)$$

where $\varepsilon(t)$ describes the noise which includes the reflected component because of its interfering nature in the tone and phase demodulation process. The noise $\varepsilon(t)$ is:

$$\mathcal{E}(t) = n_R(t) + n_B(t)$$

$$n_R(t) = A_1 \sin\left[(\omega_0 + \Delta\omega)t + \frac{\bar{\theta}}{2}\right] \qquad (12)$$

$$n_B(t) = I_{CB}\sin(\omega_0 + \Delta\omega)t - I_{SB}\cos(\omega_0 + \Delta\omega)t$$

where I_{CB} and I_{SB} are derived from the IF components . The BPF output signal-to-noise ratio is:

$$\rho_B = \frac{A^2/2}{A_R^2/2 + 2N_0W} \qquad (13)$$

The extracted reference $r(t)$ is processed together with the IF output in a product detector and the low frequency portion is:

$$z(t) = LF[x(t)\,r(t)]$$

$$= -\frac{A^2}{2}I_{SxD} + \mathcal{E}_{Sxn}(t) + \mathcal{E}_{nxS}(t) + \mathcal{E}_{nxn}(t) \qquad (14)$$

where the last three terms describe noise and signal intermodulation products.

When $z(t)$ is passed through the tone filters f_j which are centered at the tones $\pm f_j$, and are of bandwidth w_{oj} , the tone filter output is:

$$y_j(t) = -A^2 J_0(m_k) J_1(m_j)\sin[\omega_j t + \eta_j] + n_{Sxn,j}(t) + n_{nxs,j}(t) + n_{nxn,j}(t) \qquad (15)$$

$$j \neq k = 1, 2$$

The three noise terms are of course derived from the corresponding noise terms of (14). We also made the approximation

$$\omega_j a = \omega_j\left[1 + \frac{4\omega}{\omega_0}\right] \approx \omega_j \qquad (16)$$

for direct and reflected components and defined by

$$\eta_j = \omega_j b + \theta_j \qquad (17)$$

$$\eta_{jR} = \omega_j b_R + \theta_{jR}$$

The noise term $n_{sxn,j}(t)$ is derived from $\varepsilon_{sxn,j}(t)$.

$$\begin{aligned}\varepsilon_{sxn}(t) &= LF\left[s(t)\varepsilon(t)\right] \\ &= LF\left[s(t)n_R(t)\right] + LF\left[s(t)n_B(t)\right] \\ &= \frac{AA_1}{2}\Big\{I_{cxD}(t)\sin\left[(\Delta\omega_1-\Delta\omega)t+\bar{\theta}_2-\bar{\theta}_1\right] \\ &\qquad -I_{sxD}(t)\cos\left[(\Delta\omega_1-\Delta\omega)t+\bar{\theta}_2-\bar{\theta}_1\right] \\ &\quad + \frac{A}{2}\Big\{I_{cxD}(t)\left[I_{cB}\sin(\bar{\theta}_1)-I_{sB}\cos\bar{\theta}_1\right] \\ &\qquad -I_{sxD}(t)\left[I_{cB}\cos(\bar{\theta}_1)-I_{sB}\sin\bar{\theta}_1\right]\Big\}\end{aligned} \tag{18}$$

If we define

$$\begin{aligned}\theta_{21} &= (\Delta\omega_1-\Delta\omega)t+\bar{\theta}_2) \\ \theta_{10} &= \bar{\theta}_1-\theta_{21}\end{aligned} \tag{19}$$

and assume that the tone filters are so narrow that all harmonies and intermodulation frequencies are rejected, as before,

$$\begin{aligned}n_{sxn,j}(t) &= -AA_1J_0(m_k)J_1(m_j)\cos\theta_{10}\sin(\omega_jt+\eta_j) \qquad j\neq k=i,2 \\ &\quad -AJ_0(m_k)J_1(m_j)\left[I_{cB}\cos\bar{\theta}_1-I_{sB}\sin\bar{\theta}_1\right]\sin(\omega_jt+\eta_j)\end{aligned} \tag{20}$$

The second tone filter output noise term is:

$$\begin{aligned}n_{nxs,j}(t) &= -AA_1J_0(m_k)J_1(m_j)\cos\theta_{10}\sin(\omega_jt+\eta_{jR}) \\ &\quad +\frac{A}{2}\left[I_c\sin\bar{\theta}_1-I_s\cos\bar{\theta}_1\right]\end{aligned} \tag{21}$$

of course I_c and I_s now have bandwidth W_{oj} of the tone filter. The last noise term at the filter output is:

$$\begin{aligned}n_{nxn,j}(t) &= -A_1^2J_0(m_k)J_1(m_j)\sin(\omega_jt+\eta_{jR}) \\ &\quad +\frac{A_1}{2}\left[I_c\sin\theta_{21}-I_s\cos\theta_{21}\right]+LF\left[n(t)n_B(t)\right] \\ &\quad -A_1J_0(m_k)J_1(m_j)\sin(\omega_jt+\eta_{jR})\left[I_{cB}\cos\theta_{21}-I_{sB}\sin\theta_{21}\right]\end{aligned} \tag{22}$$

where $LF\left[n(t)n_B(t)\right]$ has been analyzed in C_{12}. It is white noise with power

$$2N_0^2WW_{oj}$$

We can express $y_j(t)$ with in-phase and quadrature components of the desired tone and phase angle which are part of the modulation on the direct signal. We first collect all elements which make up the tone filter output $y_j(t)$, eqns (15), (20), (21) and (22):

$$y_j(t) = -A^2 J_0(m_k) J_1(m_j) \left\{ \left[1 + R\cos\theta_{10} + \frac{I_{cB}\cos\bar{\theta}_1 - I_{sB}\sin\bar{\theta}_1}{A} \right] \sin(\omega_j t + \eta_j) \right.$$

$$\left. + \left[R\cos\theta_{10} + R^2 + R\,\frac{I_{cB}\cos\theta_{21} - I_{sB}\sin\theta_{21}}{A} \right] \sin(\omega_j t + \eta_{jR}) \right\} \qquad (23)$$

$$+ \frac{A}{2}\left[I_c \sin\bar{\theta}_1 - I_s \cos\bar{\theta}_1 \right] + \frac{A_1}{2}\left[I_c \sin\theta_{21} - I_s \cos\theta_{21} \right] + LF\left[n(t)\, n_0(t) \right]$$

where we defined

$$R = A_1/A \qquad (24)$$

Since

$$\frac{I_{cB}\cos\bar{\theta}_1 - I_{sB}\sin\bar{\theta}_1}{A} \sin(\omega_j t + \eta_j) \qquad (25)$$

is stationary white noise centered at ω_j, we can replace this term by:

$$\frac{1}{\sqrt{2\rho_B}} \left[I_{cT}\cos(\omega_j t + \eta_j) - I_{sT}\sin(\omega_j t + \eta_j) \right] \qquad (26)$$

where

$$\rho_B = \frac{A^2}{4 N_0 W} \qquad (27)$$

without changing its statistics, and where I_{cT} and I_{sT} are normalized in-phase and quadrature components. We can do the same with

$$R\,\frac{I_{cB}\cos\theta_{21} - I_{sB}\sin\theta_{21}}{A} \sin\left[\omega_j t + \eta_{jR} \right] \qquad (28)$$

which becomes

$$\frac{R}{\sqrt{2\rho_B}}\left[I_{cT}\cos(\omega_j t+\eta_j)-I_{sT}\sin(\omega_j t+\eta_j)\right] \tag{29}$$

If we apply the same technique to the last three term of (22), defining

$$\rho_2=\frac{N}{S}=\left[\frac{(1+R)N_0 w_{0j}^2}{A^2 J_0^2(m_k)J_1^2(m_j)}+\frac{N_0^2 W w_{0j}^2}{A_0^4 J_0^2(m_k)J_1^2(m_j)}\right] \tag{30}$$

we can write

$$\frac{A}{2}\left[I_c\sin\bar{\theta}_1-I_s\cos\bar{\theta}_1\right]+\frac{A_1}{2}\left[I_c\sin\theta_{21}-I_s\cos\theta_{21}\right]+LF\left[n(t)\,n_0(t)\right]=$$

$$=\sqrt{\rho_2}\,A^2 J_0(m_k)\,J_1(m_j)\left[I_{cj}\cos(\omega_j t+\eta_j)-I_{sT}\sin(\omega_j t+\eta_j)\right] \tag{31}$$

Hence

$$y_j(t)=I_{cj}\cos[\omega_j t+\eta_j]-I_{sj}\sin[\omega_j t+\eta_j] \tag{32}$$

$$=E_j\cos[\omega_j t+\eta_j-\delta]$$

where

$$I_{sj}(t)=-A^2 J_0(m_k)J_1(m_j)\left\{1+R\cos\theta_{10}+\left[R\cos\theta_0+R^2\right]\cos(\eta_{jR}-\eta_j)+\left[\frac{1+R}{\sqrt{2\rho_B}}+\sqrt{\rho_2}\right]I_{sT}\right\}$$

$$I_{cj}(t)=-A^2 J_0(m_k)J_1(m_j)\left\{\left[R\cos\theta_{10}+R^2\right]\sin[\eta_{jR}-\eta_j]-\left[\frac{1+R}{\sqrt{2\rho_B}}+\frac{1}{\sqrt{\rho_2}}\right]I_{cT}\right\} \tag{33}$$

We prefer to write $y_j(t)$ with a sine rather than a cosine in eq (31). If we add and subtract $\pi/2$:

$$y_j(t)=E_j\sin\left[\omega_j t+\eta_j-(\delta-\pi/2)\right] \tag{34}$$

where the instantaneous phase error due to the reflected component and additive noise is:

$$\delta-\pi/2=\tan^{-1}\frac{I_{sj}}{I_{cj}}-\pi/2$$

$$= \tan^{-1}\left\{ \frac{1+R\cos\theta_{20}+\left[R\cos\theta_{10}+R^2\right]\cos(\eta_{jk}-\eta_j)+\left[\frac{1+R}{\sqrt{2\rho_B}}+\sqrt{\rho_2}\right]I_{ST}}{\left[R\cos\theta_{10}+R^2\right]\sin\left[\eta_{jR}-\eta_j\right]-\left[\frac{1+R}{\sqrt{2\rho_B}}+\sqrt{\rho_2}\right]I_{CT}} \right\} - \frac{\pi}{2}$$

$\eta_{jR}-\eta_j = \omega_j \Delta_1$; $\theta_{10} = (\omega_c + \Delta\omega)\Delta_1$ (Notation of Section 5.4.4)

(35)

I_{CT} and I_{ST} are normally distributed with zero mean and **unit variance,**

$$\rho_B = \frac{A^2}{4N_0 W} \tag{36}$$

which is the signal-to-additive noise power at the BPF output

$$\rho_2 = \frac{1}{2\rho_T}\left(\frac{1}{2\rho_B^3} + 1+R^2\right) \tag{37}$$

where we defined

$$\rho_T = \frac{A^2 J_0^2(m_k) J_1^2(m_j)}{2N_0 W_{0j}} \tag{38}$$

which is signal-to-additive noise at the tone filter output.

The function δ has been analyzed on the computer in order to determine its mean and variance. Figures 6E-1 and 6E-2 contain graphs of the mean and the standard deviation of the phase error versus the multipath ratio R computed from equation (35), on the assumption that $\eta_{jR}-\eta_j$ and θ_{10} are independent uniformly distributed random variables defined on the interval $[0, 2\pi]$ Note that ρ_2 is a noise-to-signal ratio while all others are the usual signal-to-noise ratios.

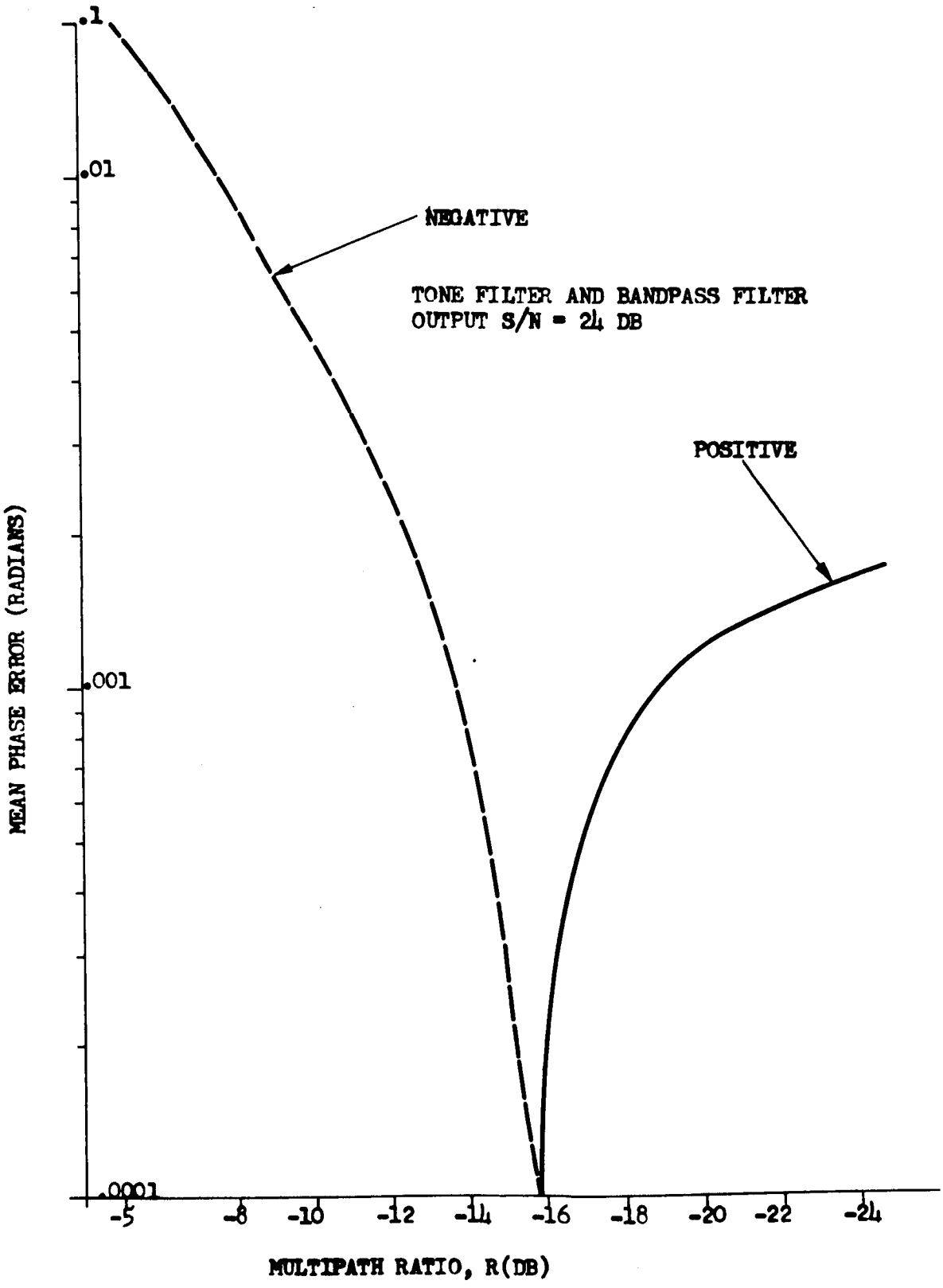

FIGURE 6E-1 MEAN PHASE ERROR VS. MULTIPATH RATIO

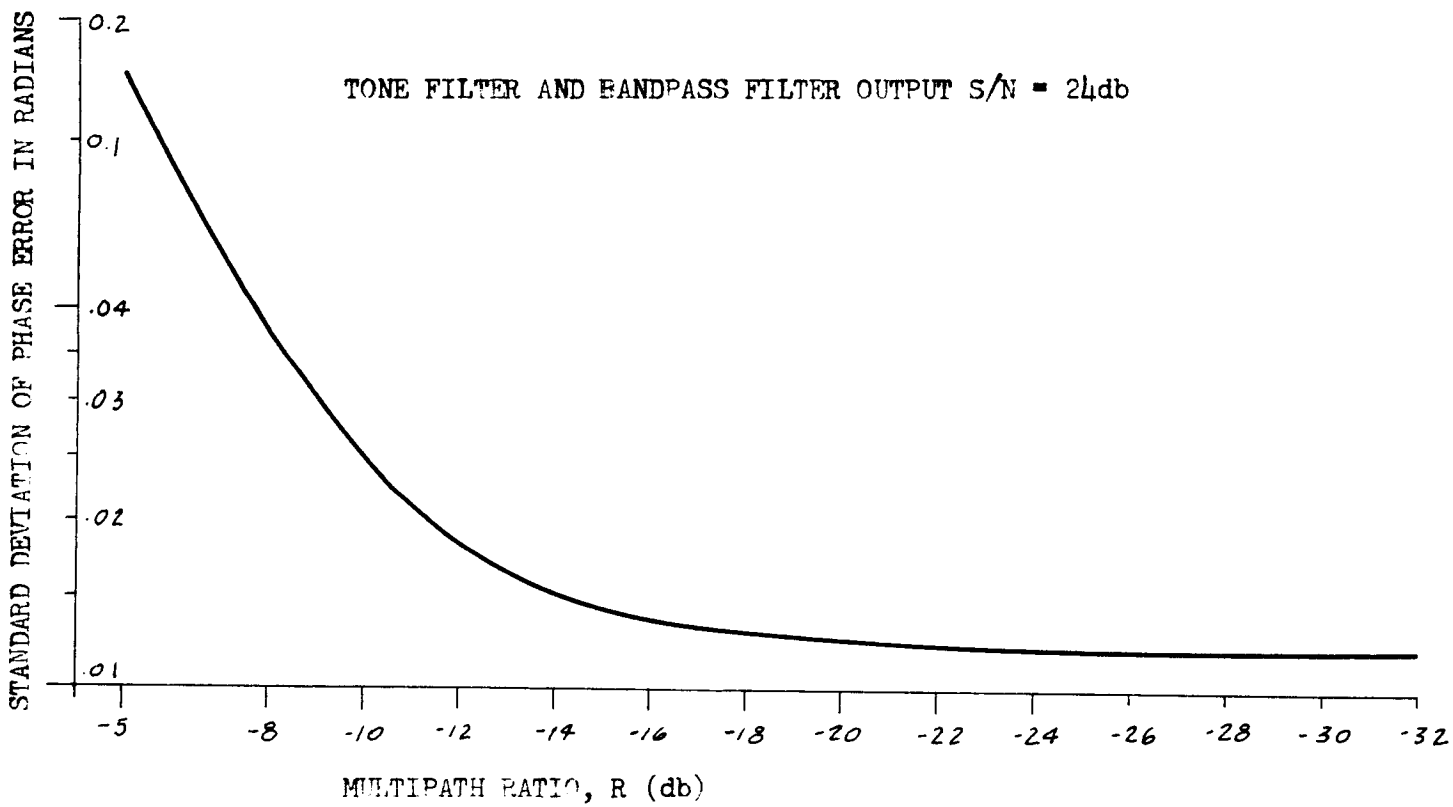

FIGURE 6E-2 STANDARD DEVIATION OF PHASE ERROR VS. MULTIPATH RATIO

Appendix 6F

DIFFUSE MULTIPATH EFFECTS WITH PHASE-LOCK LOOP CARRIER EXTRACTION, (C_{33} AND C_{31}), ASSUMING NON-SELECTIVE FADING WITH NEGLIGIBLE DIFFERENTIAL MULTIPATH DELAYS

6F.1 GENERAL FORMULATION

The IF output signal plus noise is:

$$\chi(t) = S_D(t) + S_R(t) \tag{1}$$

where the direct signal is described by:

$$S_D(t) = \alpha \cos\left\{\omega_0(at+b) + \theta + \sum_{j=1}^{2} m_j \sin\left[\omega_j(at+b) + \theta_{jD}\right]\right\} \tag{2}$$

and the random component is:

$$S_R(t) = R(t)\cos\left[\omega_0 t + \zeta(t) + \sum_{j=1}^{2} m_j \sin(\omega_j t + \theta_{jR})\right] \tag{3}$$

$R(t)$ and $\zeta(t)$ representing envelope and phase functions. Assuming that the scattered components can be described by a Gaussian process, $R(t)$ and $\zeta(t)$ correspond to the envelope and phase of such a process where $R(t)$ is Raleigh distributed and $\zeta(t)$ is uniformly distributed over the interval $[0, 2\pi]$ The additive white noise is stationary. It can be written with in-phase and quadrature components about the IF carrier of the direct signal:

$$n(t) = I_c(t)\cos(\omega_0 + \Delta\omega)t - I_s(t)\sin(\omega_0 + \Delta\omega)t \tag{4}$$

Using the relation

$$a = 1 + \frac{\Delta\omega}{\omega_0} \tag{5}$$

i.e., the frequency shift due to the medium; the quantity b describes phase and time delay

$$b = \frac{\Delta\theta}{\omega_0} + a\Delta\gamma \tag{6}$$

All power spectra will be considered to be double-sided. If the spectral density of $n(t)$ is N_0, and the IF bandwidth is W_{IF} the additive noise has average power

$$N_n = 2 N_0 W_{IF} \tag{7}$$

Since the random component interferes with demodulation process we will consider it to be noise. We will define the random component to have average power

$$N_r = \sigma_F^2 \tag{8}$$

A useful parameter is the ratio of the amplitude of the direct received signal to the standard deviation of the random component. Denoting this parameter by γ

$$\gamma = \frac{\alpha}{\sigma_F} \tag{9}$$

It is now possible to relate the random noise power to the total received power. Letting P_0 be the total received power

$$P_0 = \frac{\alpha^2}{2} + \sigma_F^2$$

$$= \sigma_F^2 \left(\frac{\gamma^2}{2} + 1 \right) \tag{10}$$

or

$$\sigma_F^2 = \frac{P_0}{\left(\frac{\gamma^2}{2} + 1 \right)} \tag{11}$$

The carrier-to-noise ratio is then:

$$\left(\frac{C}{N} \right)_{IF} = \frac{\gamma^2}{\frac{4 N_0 W_{IF}}{P_0 \left(\frac{\gamma^2}{2} + 1 \right)} + 2} \tag{12}$$

It will be convenient to express the direct and random component with in-phase and quadrature components.

The direct signal can be written as:

$$S_D(t)=\alpha\left\{ I_{cxD}(t)\cos\left[(\omega_0+\Delta\omega)t+\theta_1\right]-I_{sxD}(t)\sin\left[(\omega_0+\Delta\omega)t+\theta_1\right]\right. \tag{13}$$

where

$$\theta_1 = \omega_0 b+\theta \tag{14}$$

and

$$I_{cxD}(t)=\left\{J_0(m_1)+2\sum_{n_1=1}^{\infty}J_{2n_1}(m_1)\cos 2n_1\left[\omega_1(at+b)+\theta_{D1}\right]\right\}\cdot$$

$$\cdot\left\{J_0(m_2)+2\sum_{n_2=1}^{\infty}J_{2n_2}(m_2)\cos 2n_2\left[a_2(at+b)+\theta_{D2}\right]\right\}$$

$$-2\left\{\sum_{n_1=0}^{\infty}J_{2n_1+1}(m_1)\sin\left[(2n_1+1)(\omega_1[at+b]+\theta_{D1})\right]\right\}\cdot$$

$$\cdot\left\{2\sum_{n_2=0}^{\infty}J_{2n_2+1}(m_2)\sin\left[(2n_2+1)(\omega_2[at+b]+\theta_{D2})\right]\right\} \tag{15}$$

$$I_{sxD}=\left\{2\sum_{n_1=0}^{\infty}J_{2n_1+1}(m_1)\sin\left[(2n_1+1)(\omega_1[at+b]+\theta_{D1})\right]\right\}\cdot$$

$$\cdot\left\{J_0(m_2)+2\sum_{n_2=1}^{\infty}J_{2n_2}(m_2)\cos\left[(2n_2)(\omega_2[at+b]+\theta_{D2})\right]\right\}$$

$$+\left\{J_0(m_1)+2\sum_{n_1=1}^{\infty}J_{2n_1}(m_1)\cos\left[(2n_1)(\omega_1[at+b]+\theta_{D1}\right]\right\}\cdot$$

$$\left\{2\sum_{n_2=0}^{\infty}J_{2n_2+1}(m_2)\sin\left[(2n_2+1)(\omega_2(at+b)+\theta_{D2}\right]\right\} \tag{16}$$

where $J_s(x)$ is the Bessel function of order s in the variable x

The random component assumes the form:

$$= R(t) - R(t) \left\{ I_{C \times R}(t) \cos\left[\omega_0 t + \zeta(t)\right] - I_{S \times R}(t) \sin\left[\omega_0 t + \zeta(t)\right] \right\} \quad (17)$$

where

$$I_{C \times R}(t) = \left\{ J_0(m_1) + 2 \sum_{n_1=0}^{\infty} J_{2n_1}(m_1) \cos\left[2n_1(\omega_1 t + \theta_{1R})\right] \right\} \cdot$$

$$\cdot \left\{ J_0(m_2) + 2 \sum_{n_2=0}^{\infty} J_{2n_2}(m_2) \cos\left[2n_2(\omega_2 t + \theta_{2D})\right] \right\}$$

$$- \left\{ 2 \sum_{n_1=0}^{\infty} J_{2n_1}(m_1) \sin\left[(2n_1+1)(\omega_1 t + \theta_{1R})\right] \right\} \quad (18)$$

$$\cdot \left\{ 2 \sum_{n_2=0}^{\infty} J_{2n_2}(m_2) \sin\left[(2n_2+1)(\omega_2 t + \theta_{2R})\right] \right\}$$

$$I_{SxR}(t) = \left[2 \sum_{n_1=0}^{\infty} J_{2n_1+1}(m_1) \sin(2n_1+1)(\omega_1 t + \theta_{1R})\right]$$

$$\times \left[J_0(m_2) + 2 \sum_{n_2=1}^{\infty} J_{2n_2}(m_2) \cos 2n_2(\omega_2 t + \theta_{2R})\right]$$

$$+ \left[J_0(m_1) + 2 \sum_{n_1=1}^{\infty} J_{2n_1}(m_1) \cos 2n_1(\omega_1 t + \theta_{1R})\right]$$

$$\times \left[2 \sum_{n_2=0}^{\infty} J_{2n_2+1}(m_2) \sin 2n_2(\omega_2 t + \theta_{2R})\right] \qquad (19)$$

Equations (18) and (19) are identical to (15) and (16) except for the arguments of the sines and cosines.

We now have to consider the random component. Let

$$I_{CF}(t) = R(t) \cos \varphi(t)$$
$$I_{SF}(t) = R(t) \sin \varphi(t) \qquad (20)$$

The power spectrum of $I_{CF}(t)$ is called the fading spectrum. Its bandwidth β_F is a measure of the fading rate.

We will consider three cases:

(A) Slow fading, $\beta_F = 0$

(B) Fast fading, $\beta_F > B_L$

where B_L is the bandwidth of the PLL

(C) Intermediate fading $0 < \beta_F < B_L$

The IF output signal plus noise is passed through a narrow band carrier extraction filter, so that the signal plus noise entering the PLL can be described by:

$$d(t) = \alpha \cos\left[\omega_0 (at+b) + \theta_1\right] + R(t)\cos\left[\omega_0 t + \beta(t)\right] + n_0(t) \tag{21}$$

where $n_0(t)$ is the additive white noise, now limited by the PLL bandwidth B_L.

If we assume that no signal energy is lost in the PLL, nor any energy removed from the random component as would be for a fast fading random component, the PLL output signal-to-noise ratio would be:

$$\rho_L = \frac{\alpha^2/2}{R^2(t)/2 + 2N_0 B_L} \tag{22}$$

Introducing the definition of γ, eq. (9), ρ_L may be expressed as

$$\rho_L = \frac{\gamma^2}{\left[R^2(t) + 4N_0 B_L\right]/\sigma_F^2} \tag{23}$$

where the envelope of the random component is normalized by replacing $R(t)$ by $R(t)/\sigma_f$. The probability distribution of the normalized $R(t)$ is

$$p(R) = R\, e^{-R^2/2} \tag{24}$$

which is the Raleigh distribution. We can use the information in eqs. (23), (24) to determine the probability that the PLL will lock up and remain so.

Defining

$$Y = \frac{1}{\rho_L} = \frac{R^2(t) + \beta^2}{\gamma^2} \tag{25}$$

where

$$\beta = \frac{4 N_0 B_L}{\sigma_F^2} \tag{26}$$

The requirement that the signal-to-noise ratio at the output of the PLL exceeds a db (e.g. a = 10), implies that

$$\begin{aligned} P_r(10\log_{10} Y \le -a\ dB) &= P_r(.434 \ln Y \le -a/10) \\ &= P_r\left(Y \le \exp\left(-\frac{a}{.434}\right)\right) \\ &= P_r\left(R^2(t) \le \gamma^2 \exp\left(-\frac{a}{.434}\right) - \beta^2\right) \\ &= \int_0^{\left[\gamma^2 \exp(-a/.434) - \beta^2\right]^{1/2}} R \exp(-R^2/2)\, dR \\ &= 1 - \exp\left\{\frac{-1}{2}\left[\gamma^2 \exp\left(-\frac{a}{.434}\right) - \beta^2\right]\right\} \end{aligned} \tag{27}$$

If β defined by (26) is small, and if $\gamma^2/2$, the power ratio of direct to random component is 10 db,

$$Pr(10\log_{10} P_2 > 10\ dB) = .63 \tag{28}$$

which is an optimistic estimate because β has been neglected. However, the random component for typical cases may exceed the white noise power by at least 14 db so that the effect of β is indeed very small.

If $\frac{\gamma^2}{2} = 15$, the probability that P_L exceeds 10 db is about .96.

When the bandwidth of the fading signal is appreciably larger than the bandwidth of the PLL, it is straightforward to show that

$$Pr[10\log_{10} P_L > a\ dB] = 1 - \exp\left\{-\frac{1}{2}\left[\gamma^2 \frac{B_F}{B} \exp\left(-\frac{a}{.434}\right) - \beta^2 \frac{B_F}{B_L}\right]\right\} \tag{29}$$

Letting a be equal to 10 db, and $\gamma^2/2$ be equal to 10, then if the fading bandwidth is twice the loop filter bandwidth

$$Pr[10\log_{10} P_L > 10\ dB] \approx .96 \tag{30}$$

The slow fading will be analyzed first, and except for a small introduction, the analysis for fast and intermediate fading will be combined.

6F.2 SLOW FADING

Slow fading means that the random component has a power spectrum consisting of two spikes at $\pm f_0$ of height $\sigma = \sigma^2/2$, for a double sided power spectrum.

From the point of view of extracting a reference signal in the PLL, the slowly varying random component can be regarded as a desired signal. The PLL will lock onto the algebraic vector sum of the direct and random component, which varies slowly with time.

The instantaneous PLL output S/N ratio is given by:

$$\rho_L = \frac{\alpha^2/2 + \sigma_F^2}{2N_0 B_L} = \frac{P_0}{2N_0 B_L} \tag{31}$$

The PLL input function is given in (21)

$$\begin{aligned} d(t) &= \alpha \cos\left[(\omega_0 + \Delta\omega)t + \theta_1\right] + R(t)\cos\left[\omega_0 t + \zeta(t)\right] + n_0(t) \\ &= \left\{\alpha\cos\theta_1 + R(t)\cos\left[\zeta(t) - \Delta\omega t\right] + I_{c0}(t)\right\}\cos\left[(\omega_0+\Delta\omega)t\right] \\ &\quad - \left\{\alpha\sin\theta_1 + R(t)\sin\left(\zeta(t) - \Delta\omega t\right) + I_{s0}(t)\right\}\sin\left[(\omega_0+\Delta\omega)t\right] \\ &= E(t)\cos\left[(\omega_0+\Delta\omega)t + \beta(t)\right] \end{aligned} \tag{32}$$

in polar form. We now observe that for slow fading $\Delta\omega$ must be negligible, so that we may write

$$d(t) = E(t)\cos\left[\omega_0 t + \beta(t)\right] \tag{33}$$

where $\beta(t)$ describes the total phase angle due to the direct signal, random component and additive noise.

The amplitude $E(t)$ can be approximated by:

$$E(t) = \alpha \left\{ 1 + \delta^2(t) + 2S \cos\theta_{10} \right\}^{1/2} \tag{34}$$

where $S(t) = \dfrac{R(t)/\sigma}{\gamma}$

$$\theta_2 = S(t)$$

$$\theta_1 = \omega_0 t + \theta$$

$$\theta_{10} = \theta_1 - \theta_2 \tag{35}$$

The fading model here resembles closely the fading model employed in case C_{23}, except that the constant R has been replaced by the time variable S(t).

The phase angle $\beta(t)$ in equation (33) is:

$$\beta(t) = \text{Arctan}\left[\frac{\sin\theta_1 + R\sin\theta_2 + R_L I_{SL}(t)}{\cos\theta_1 + R\cos\theta_2 + R_L I_{CL}(t)}\right] \tag{36}$$

where

$$R_L = \sigma_L/\alpha$$

σ_L is the standard deviation of the loop filter output random noise, I_{CL} and I_{SL} are the normalized in-phase and quadrature components. Since R_L is small we can expand in a MacLaurin series about $R_L = 0$.

$$\beta(t) = \beta(t)\Big|_{R_L=0} + R_L \frac{\partial\beta(t)}{\partial R_L}\Big|_{R_L=0} \tag{37}$$

If we then identify the phase angle $\phi(t)$ and phase jitter $\Delta\theta(t)$ of the desired PLL output

$$r(t) = \sin[\omega_0 t + \Delta\theta(t) + \phi(t)] \tag{38}$$

with these first two terms we find that

$$\sin\phi(t) = \frac{\sin\theta_1 + S\sin\theta_2}{[1+S^2+2S\cos\theta_{10}]^{1/2}}$$

$$\cos\phi(t) = \frac{\cos\theta_1 + S\cos\theta_2}{[1+S^2+2S\cos\theta_{10}]^{1/2}} \tag{39}$$

and

$$\Delta\theta(t) = K_L\left[\frac{I_{SL}\cos\phi - I_{CL}\sin\phi}{(1+S^2+2S\cos\theta_{10})^{1/2}}\right] \tag{40}$$

The change from cosine in the PLL input $d(t)$, (33), to the sine of the desired output, (38), is due to the VCO.

The extracted reference $r(t)$ is processed together with the IF output in a low pass product detector yielding

$$z(t) = LF[x(t)y(t)]$$

$$= \frac{A}{2}\left[I_{CXD}(t)\sin(\Delta\theta+\phi-\theta_1) - I_{SXD}(t)\cos(\Delta\theta+\phi-\theta_1)\right] + \varepsilon_{nxs} \tag{41}$$

where ε_{nxs} describes the noise.

The function $\zeta(t)$ is then passed through the tone filters F_j of width W_{oj} centered at $\pm f_j$, resulting in the tone filter output

$$y_j(t) = -\alpha J_0(m_k) J_1(m_j) \cos[\Delta\theta + \phi - \theta_1] \sin[\omega_j(at+b) + \theta_{jD}] + n_j(t) \quad (42)$$

where $n_j(t)$ is derived from $\epsilon_{nxs}(t)$, and only the quadrature term of the signal component of $\zeta(t)$ produces an output provided the filters W_{oj} are narrow enough to reject all harmonics and intermodulation frequencies.

The function $n_j(t)$ is:

$$n_j(t) = -R(t) J_0(m_k) J_1(m_j) \cos[\Delta\theta + \phi - \theta_2] \sin[\omega_j t + \theta_{jR}] + \frac{1}{2}[I_c(t)\sin(\Delta\theta+\phi) - I_s(t)\cos(\Delta\theta+\phi)] \quad (43)$$

From equation (115) of Appendix 6D, expressions for $\cos(\Delta\theta+\phi-\theta_1)$ and $\cos(\Delta\theta+\phi-\theta_2)$ are obtained. Combining these with (43) and substituting into (42) we find that the tone filter output is described by:

$$y_j(t) = -\alpha J_0(m_k) J_1(m_j) \left[\frac{\cos\Delta\theta + S\cos(\Delta\theta - \theta_{10})}{(1+S^2+2S\cos\theta_{10})^{1/2}} \sin(\omega_j t + \eta_1) + \frac{S^2\cos\Delta\theta + S\cos(\Delta\theta+\theta_{10})}{(1+S^2+2S\cos\theta_{10})^{1/2}} \sin(\omega_j t + \eta_2) \right] + [I_{cT}\cos\omega_j t - I_{sT}\sin\omega_j t] \; ; \quad j \neq k = 1, 2 \quad (44)$$

under the approximation:

$$\omega_j a = \omega_j \left[1 + \frac{\Delta\omega}{\omega_0}\right] \approx \omega_j \quad (45)$$

and definitions:

$$\eta_1 = \omega_g b + \theta_{gD}$$

$$\eta_2 = \theta_{gR} \tag{46}$$

The additive noise represented by the last two terms is derived from the IF noise. It has noise power $N_o W_{ag}$. As before we determine the tone filter output S/N ratio. Let $f(t)$ represent the signal term of $y_g(t)$; its mean square value is:

$$\langle f^2(t)\rangle = \frac{[\alpha J_0(m_R) J_1(m_g)]^2}{4} \left\langle \frac{\left\{ \begin{array}{l} 1 + \cos 2\Delta\theta \left[1 + 2S\cos\theta_{1D} + S^2 \cos 2\theta_{2D} \right] \\ + \sin 2\Delta\theta \left[S^2 \sin 2\theta_{1D} + 2S \sin\theta_{1D} \right] \end{array} \right\}}{1 + S^2 + 2S\cos\theta_{1D}} \right\rangle \tag{47}$$

Since $\Delta\theta(t)$ has zero mean, and if we assume that θ_{2D} is uniformly distributed over $(0, 2\pi)$

$$\langle f^2(t)\rangle = \frac{[\alpha J_0(m_R) J_1(m_g)]^2}{4} \begin{cases} \langle 2 - S^2(t) \rangle & ; \; S<1 \\ 1 & S>1 \end{cases} \tag{48}$$

Now $S = (R/\sigma)/\gamma$ has a normalized Raleigh distribution.

$$\langle S^2(t)\rangle = \langle R^2(t)/\sigma^2 \rangle / \gamma^2$$

$$= \frac{2}{\gamma^2}\left[1 - e^{-\frac{1}{2\sigma^2}} \left(1 + \frac{1}{2\sigma^2} \right) \right] \tag{49}$$

Hence

$$\langle f^2(t)\rangle = \frac{[\alpha J_0(m_k) J_1(m_j)]^2}{4} \begin{cases} 2\cdot\frac{2}{\gamma^2}\left[1-e^{-\frac{1}{2\sigma^2}}\left(1+\frac{1}{2\sigma^2}\right)\right] & S<1 \\ 1 & S>1 \end{cases} \quad (50)$$

We can find the noise power due to the random component in a similar manner.

If $g(t)$ describes this function, its mean square value is given by

$$\langle g^2(t)\rangle = \frac{[\alpha J_0(m_k) J_1(m_j)]^2}{2} \left\langle \frac{[S^2\cos\theta_{10} + S\cos(\Delta\theta+\theta_{10})]^2}{1+S^2+2S\cos\theta_{10}} \right\rangle \quad (51)$$

$$= \frac{[\alpha J_0(m_k) J_1(m_1)]^2}{4} \begin{cases} \langle S^2\rangle & ; S<1 \\ \left\langle S^2\left[1+\frac{S^2-1}{S^2}\right]\right\rangle & ; S>1 \end{cases} \quad (52)$$

$$= \frac{[\alpha J_0(m_k) J_1(m_j)]^2}{4} \begin{cases} \frac{2}{\gamma^2}\left[1-e^{-\frac{1}{2\sigma^2}}\left(1+\frac{1}{2\sigma^2}\right)\right]; & S<1 \\ \frac{4}{\gamma^2}\left[1-e^{-\frac{1}{2\sigma^2}}\left(1+\frac{1}{2\sigma^2}\right)\right]; & S>1 \end{cases} \quad (53)$$

The tone filter output signal-to-noise ratio is:

$$\left(\frac{S}{N}\right)_{oj} = \frac{[\alpha J_0(m_k) J_1(m_j)]^2\left\{1-\frac{1}{\gamma^2}\left[1-e^{-\frac{1}{2\sigma^2}}\left(1+\frac{1}{2\sigma^2}\right)\right]\right\}}{2\left\{N_0 W_{oj} + \frac{[\alpha J_0(m_k) J_1(m_j)]^2}{2\gamma^2}\left[1-e^{-\frac{1}{2\sigma^2}}\left(1+\frac{1}{2\sigma^2}\right)\right]\right\}}; \quad S<1$$

$$= \frac{[\alpha J_0(m_k) J_1(m_j)]^2}{4\left\{N_0 W_{oj} + \frac{[\alpha J_0(m_k) J_1(m_j)]^2}{\gamma^2}\left[1-e^{-\frac{1}{2\sigma^2}}\left(1+\frac{1}{2\sigma^2}\right)\right]\right\}}; \quad S>1 \quad (54)$$

Define the following two input signal-to-noise ratios

$$\left(\frac{C}{N}\right)_1 = \frac{\alpha^2}{4N_0 W_{IF}}$$

$$\left(\frac{C}{N}\right)_2 = \frac{\alpha^2}{4\gamma^2 N_0 W_{IF}} \quad (55)$$

The tone filter output signal-to-noise ratio can be written as

$$\left(\frac{S}{N}\right)_{oj} = \left[J_0(m_k)J_1(m_j)\right]^2\left(\frac{C}{N}\right)_1 \cdot$$

$$\cdot \begin{cases} \dfrac{1-\frac{1}{\gamma^2}\left[1-\exp\left(-\frac{1}{2\sigma^2}\right)\left(1+\frac{1}{2\sigma^2}\right)\right]}{\frac{\omega_{oj}}{2W_{IF}}+\left[J_0(m_k)J_1(m_j)\right]^2\left[1-\exp\left(-\frac{1}{2\sigma^2}\right)\left(1+\frac{1}{2\sigma^2}\right)\left(\frac{C}{N}\right)_2\right.} & j \le 21 \\ \dfrac{1}{\frac{\omega_{oj}}{W_{IF}}+\left[J_0(m_k)J_1(m_j)\right]^2\left[1-\exp\left(-\frac{1}{2\sigma^2}\right)\left(1+\frac{1}{2\sigma^2}\right)\left(\frac{C}{N}\right)_2\right.} & \end{cases} \quad (56)$$

The tone filter output $y_j(t)$ is processed together with the output of a local oscillator in a quadrature phase detector in order to obtain an estimate of the phase angle η_1 on the direct signal f_j-th tone filter output. This output is:

$$y_j(t) = -\alpha J_0(m_k)J_1(m_j)\left[\frac{\left[\cos\Delta\theta + S\cos(\Delta\theta-\theta_{10})\right]\sin(\omega_j t+\eta_1)+\left[S^2\cos\Delta\theta+S\cos(\Delta\theta+\theta_{10})\right]\sin(\omega_j t+\eta_2)}{(1+S^2+2S\cos\theta_{10})^{1/2}}\right]$$

$$+ I_{cj}\cos\omega_j t - I_{sj}\sin\omega_j t \quad (57)$$

If we write $y_j(t)$ with in-phase and quadrature components of $(\omega_j t+\eta_1)$

$$y_j(t) = I_{cj}(t)\cos(\omega_j t+\eta_1) + I_{sj}(t)\sin(\omega_j t+\eta_1)$$
$$= E_j(t)\cos\left[\omega_j t+\eta_1-\delta\right]$$

$$I_{cj}(t) = -\alpha J_0(m_k)J_1(m_j)\left\{\frac{\left[S^2\cos\Delta\theta+S\cos(\Delta\theta+\theta_{10})\right]\sin(\eta_2-\eta_1)}{1+S^2+2S\cos\theta_{10}} - \frac{I_{cT}(t)}{\alpha J_0(m_k)J_1(m_j)}\right\} \quad (58)$$

$$I_{sj}(t) = -\alpha J_0(m_k)J_1(m_j)\left\{\frac{\cos\Delta\theta+S\cos(\Delta\theta-\theta_{10})+\left[S^2\cos\Delta\theta+S\cos(\Delta\theta+\theta_{10})\right]\cos(\eta_2-\eta_1)}{1+S^2+2S\cos\theta_{10}}\right.$$

$$\left. + \frac{I_{sT}(t)}{\alpha J_0(m_k)J_1(m_j)}\right\} \quad (59)$$

and the instantaneous phase error due to the random component and additive noise is described by:

$$\delta(t) = \text{Arctan}\left[\frac{I_{sj}(t)}{I_{cj}(t)}\right]$$

$$= \text{Arctan}\left[\frac{\cos\Delta\theta + S\cos(\Delta\theta - \theta_{10}) + [S^2\cos\Delta\theta + S\cos(\Delta\theta - \theta_{10})]\cos(\eta_2 - \eta_1) + \frac{I_{sj0}}{\sqrt{2\rho}}(1+S^2+2S\cos\theta_{10})^{1/2}}{[S^2\cos\Delta\theta + S\cos(\Delta\theta - \theta_{10})]\sin(\eta_2 - \eta_1) - \frac{I_{cj0}}{\sqrt{2\rho}}(1+S^2+2S\cos\theta_{10})^{1/2}}\right] \quad (60)$$

where the in phase and quadrature additive noise components have been normalized. Expressing S in terms of R as before,

$$S = \frac{R/\sigma}{\gamma} \quad (61)$$

the phase error becomes

$$\delta(t) = \text{Arctan}\left\{\frac{\cos\Delta\theta + \frac{R}{\gamma}\cos[\Delta\theta - \theta_{10}] + \left[\frac{R^2}{\gamma^2}\cos\Delta\theta + \frac{R}{\gamma}\cos(\Delta\theta + \theta_{10})\right]\cos(\eta_2 - \eta_1) + \frac{I_{sj0}}{\sqrt{2\rho}}\left(1 + \frac{R^2}{\gamma^2} + \frac{2R}{\gamma}\cos\theta_{10}\right)^{1/2}}{\left[\frac{R^2}{\gamma^2}\cos\Delta\theta + \frac{R}{\gamma}\cos(\Delta\theta + \theta_{10})\right]\sin(\eta_2 - \eta_1) - \frac{I_{cj0}}{\sqrt{2\rho}}\left(1 + \frac{R^2}{\gamma^2} + \frac{2R}{\gamma}\cos\theta_{10}\right)^{1/2}}\right\} \quad (62)$$

where R is distributed according to

$$P(R)\,dR = Re^{-\frac{R^2}{2}}\,dR \quad (63)$$

The quantity ρ is defined by

$$\rho = \frac{\alpha^2[J_0(m_k)\,J_1(m_j)]^2}{2N_0 W_{oj}} \quad (64)$$

which describes the direct signal tone filter output power to the additive noise power.

Because $\delta(t)$ is of such a complicated form, its distribution, expected value and standard deviation can best be found by computer simulation, treating θ_{10}

and $\eta_2 - \eta_1$ as uniformly distributed random variables over the interval $[0, 2\pi]$, while $\Delta\theta(t)$ is normally distributed with zero mean and variance equal to the reciprocal of twice the loop filter output S/N.

6F.3 FAST AND INTERMEDIATE FADING

Since fast and intermediate fading can be treated mathematically in much the same manner we will combine the two analyses, making only a few introductory comments to each one separately.

The effect of the PLL is, that it will pass the direct signal component, reduce the bandwidth of the random component from B_F to B_L, i.e., to the bandwidth of the loop and also reduce the bandwidth of the additive white noise to B_L. For fast fading, the signal-to-noise ratio at the output of the PLL is:

$$\rho_L = \frac{\gamma^2}{\frac{4 N_0 B_L}{P_0/(\frac{\gamma^2}{2}+1)} + \frac{2 B_L}{B_F}} \tag{65}$$

The power ratio, $\gamma^2/2$, of direct to random component can be obtained from (50). Assuming that ρ_L should exceed 10 db for the loop to remain locked

$$\frac{\gamma^2}{2} > \frac{\frac{P_0}{2 N_0 B_L} + 1}{\frac{P_0}{20 N_0 B_L} - 1} \tag{66}$$

The corresponding instantaneous PLL output signal-to-noise ratio for intermediate fading is:

$$\rho_L = \frac{\gamma^2}{\frac{4 N_0 B_L}{P_0 (\frac{\gamma^2}{2}+1)} + 1} \tag{67}$$

Hence the instantaneous power ratio $\frac{\gamma^2}{2}$ should be

$$\frac{\gamma^2}{2} > \frac{\frac{P_o}{2N_o B_L} + 1}{\frac{P_o}{2N_o B_L} + 1} \qquad (68)$$

for the loop to remain locked.

The analyses for fast and intermediate fading will be combined from this point on.

The carrier narrow band filter output is:

$$d(t) = \alpha \cos[(\omega_o + \Delta\omega)t + \theta_1] + R(t)\cos[\omega_o t + \rho(t)] + n_o(t) \qquad (69)$$

Expressing the sum of the white noise and the random signal component, as in-phase and quadrature terms about the IF carrier,

$$d(t) = \alpha \cos[(\omega_o + \Delta\omega)t + \theta_1] + \varepsilon(t)$$

$$\varepsilon(t) = n_o(t) + S_R(t)$$

$$= [I_c(t) + I_{CF_1}(t)]\cos(\omega_o + \Delta\omega)t - [I_s(t) + I_{SF_1}(t)]\sin(\omega_o + \Delta\omega)t \qquad (70)$$

where

$$I_{CF_1}(t) = R(t)\cos[\rho(t) - \Delta\omega t]$$

$$= R(t)\cos\theta_2$$

$$I_{SF_1}(t) = R(t)\sin\theta_2$$

$$\theta_2 = \rho(t) - \Delta\omega t \qquad (71)$$

The subscript 1 is introduced to distinguish these random components from the ones defined earlier, (20).

The signal $d(t)$ looks like the noisy channel model considered in Appendix 6C, except that the noise is now time dependent.

Let the PLL reference output signal be

$$r(t) = \sin\left[(\omega_0 + \Delta\omega)t + \Delta\theta(t) + \theta_1\right] \tag{72}$$

where $\Delta\theta(t)$ represents PLL phase jitter due to random noise. It will be approximately Gaussian distributed with zero mean and variance

$$\sigma^2(\Delta\theta) \approx \frac{1}{2\rho_L} \tag{73}$$

where the PLL output S/N is given by (65) or (67) depending upon the fading rate of the random component.

The IF output will be processed together with the reference signal in a low-pass filter. If we denote the function so obtained by $z(t)$,

$$\begin{aligned} z(t) &= LF\left[x(t)\,r(t)\right] \\ &= \frac{\alpha}{2}\left\{I_{cxD}(t)\sin\Delta\theta(t) - I_{sxD}(t)\cos\Delta\theta(t)\right\} + \varepsilon_{nxr}(t) \end{aligned} \tag{74}$$

where the noise is described by $\varepsilon_{nxr}(t)$

$$\begin{aligned} \varepsilon_{nxr}(t) &= LF\left\{\left[S_R(t) + n(t)\right]r(t)\right\} \\ &= \frac{R(t)}{2}\left\{I_{cxR}(t)\sin(\Delta\theta - \theta_{10}) - I_{sxR}(t)\cos(\Delta\theta - \theta_{10})\right\} \\ &\quad + \frac{1}{2}\left[I_c(t)\cos\omega_j t - I_s(t)\sin\omega_j t\right] \end{aligned} \tag{75}$$

The low-pass filter output is passed through the tone filters F_j of bandwidths W_{oj} centered at If_j, $j=1,2,\cdots$, to yield

$$\begin{aligned} y_j(t) = &-\alpha J_0(m_k) J_1(m_j) \cos\Delta\theta(t) \sin[\omega_j(at+b)+\theta_{jD}] \\ &- R(t) J_0(m_k) J_1(m_j) \cos[\Delta\theta(t)-\theta_{10}] \sin(\omega_j t+\theta_{jR}) \\ &+ I_{cj}\cos\omega_j t - I_{sj}\sin\omega_j t \quad ; j\neq k=1,2, \end{aligned} \tag{76}$$

where the tone filter output derived from the additive IF noise has total noise power $N_o W_{oj}$, and is expanded about the tone frequency.

Let

$$\begin{cases} \eta_1 = \omega_j b + \theta_{jD} \\ \eta_2 = \theta_{jR} \end{cases} \tag{77}$$

and approximate

$$\begin{aligned} \omega_j a &= \omega_j\left(1+\frac{\Delta\omega}{\omega_0}\right) \\ &\approx \omega_j \end{aligned} \tag{78}$$

The j-th tone filter output can be denoted by:

$$\begin{aligned} y_j(t) = &-\alpha J_0(m_k) J_1(m_j) \cos\Delta\theta(t) \sin(\omega_j t+\eta_1) \\ &- \alpha J_0(m_k) J_1(m_j) S \cos\Delta\theta(t) \sin(\omega_j t+\eta_2) \\ &+ I_{cj}\cos\omega_j t - I_{sj}\sin\omega_j t \end{aligned} \tag{79}$$

The signal power of $y_j(t)$ is:

$$\begin{aligned} S_j &= \frac{[\alpha J_0(m_k) J_1(m_j)]^2}{} \langle \cos^2\Delta\theta(t)\rangle \\ &= \frac{[\alpha J_0(m_k)^2 J_1(m_j)]^2}{4}\left[1+\langle\cos 2\Delta\theta(t)\rangle\right] \end{aligned} \tag{80}$$

Since $\Delta\theta(t)$ is normally distributed with zero mean and variance $\sigma^2_{\Delta\theta}$

$$\langle \cos 2\Delta\theta(t) \rangle = e^{-1/\rho_L} \tag{81}$$

where ρ_L is given by (66) or (67)

Hence

$$S_j = \frac{[\alpha J_0(m_k) J_1(m_j)]^2}{4} \left[1 + e^{-1/\rho_L}\right] \tag{82}$$

$$\approx \frac{[\alpha J_0(m_k) J_1(m_j)]^2}{4} \left[2 - 1/\rho_L\right] \tag{83}$$

for large ρ_L .

The noise power due to the random component is:

$$N_{R,j} = \frac{[\alpha J_0(m_k) J_1(m_j)]^2}{2} \langle S^2 \cos^2[\Delta\theta(t) - \theta_{10}] \rangle$$

$$= \frac{[\alpha J_0(m_k) J_1(m_j)]^2}{4} \langle S^2 \rangle \tag{84}$$

If the correlation between $\Delta\theta$ and θ_{10} is small.

From (32) we find that

$$N_{R,j} = \frac{[\alpha J_0(m_k) J_1(m_j)]^2}{4} \left[1 - e^{-1/2\sigma^2}\left(1 + 1/2\sigma^2\right)\right] \tag{85}$$

Hence the tone filter output S/N ratio is:

$$\left(\frac{S}{N}\right)_{oj} = \frac{\left[J_0(m_R)J_1(m_j)\right]^2\left[1+e^{-1/2\sigma^2}\right]\left(\frac{C}{N}\right)_1}{\frac{W_{oj}}{W_{Ij}} + 2\left[J_0(m_R)J_1(m_j)\right]^2\left[1-e^{-1/2\sigma^2}\left(1+1/2\sigma^2\right)\right]\left(\frac{C}{N}\right)_2}$$

(86)

where $\left(\frac{C}{N}\right)_1$ and $\left(\frac{C}{N}\right)_2$ are defined in (55)

We now want to obtain an estimate of the phase angle η_1 on the tone filter output $y_j(t)$ of eq. (61).

Writing $y_j(t)$ with in-phase and quadrature components of $\omega_j(t)+\eta_1$

$$y_j(t) = I_{cj}(t)\cos(\omega_j t+\eta_1) + I_{sj}(t)\sin(\omega_j t+\eta_1)$$
$$= E_j(t)\cos(\omega_j t+\eta_1-\delta)$$

(87)

where

$$I_{cj}(t) = -\alpha J_0(m_R)J_1(m_j)\left[S\cos(\Delta\theta-\theta_{10})\sin(\eta_2-\eta_1) - \frac{I_{cT}(t)}{\alpha J_0(m_R)J_1(m_j)}\right]$$

$$I_{sj}(t) = -\alpha J_0(m_R)J_1(m_j)\left[S\cos(\Delta\theta-\theta_{10})\cos(\eta_2-\eta_1) + \cos\Delta\theta(t) + \frac{I_{sT}(t)}{\alpha J_0(m_R)J_1(m_j)}\right] \quad (88)$$

and

$$\delta(t) = \tan^{-1}\frac{I_{sj}(t)}{I_{cj}(t)}$$

$$= \tan^{-1}\left[\frac{\cos\Delta\theta(t)+S\cos(\Delta\theta-\theta_{10})\cos(\eta_2-\eta_1)+\frac{I_{sTo}}{\sqrt{2}\sigma}}{S\cos(\Delta\theta-\theta_{10})\sin(\eta_2-\eta_1)-\frac{I_{cTo}}{\sqrt{2}\sigma}}\right] \quad (89)$$

Where ρ is the direct component tone filter output signal power to additive noise power,

$$\rho = \frac{\left[\alpha J_0(m_R)J_1(m_j)\right]^2}{2N_0 W_{oj}} \quad (90)$$

The function $\delta(t)$ is the instantaneous phase error due to the random component and additive noise. I_{CTD} and I_{STD} are normalized additive noise components.

In the absence of noise

$$\delta(t) = Arctan(\infty) = \pi/2 \tag{91}$$

However (87) should reduce to (79) in the absence of noise. If we consider the absence of noise as a limiting process, in which random component and additive noise go to zero slowly, we find that

$$\delta(t) = -\frac{\pi}{2} \tag{92}$$

Considering now $\delta(t)$ of eq. (71), we write

$$\delta(t) = Arctan\left(\frac{Cos\,\Delta\theta(t) + \frac{R}{\gamma}Cos(\Delta\theta - \theta_{10})\,Cos(\eta_2 - \eta_1) + \frac{I_{SjD}}{\sqrt{2\rho}}}{\frac{R}{\gamma}Cos(\Delta\theta - \theta_{10})\,Sin(\eta_2 - \eta_1) - \frac{I_{CjD}}{\sqrt{2\rho}}}\right) \tag{93}$$

where

$$S = \frac{R/\sigma}{\gamma} \tag{94}$$

γ must be increased as a function of fading rate in accordance with Figure 6-55. R has probability density

$$P(R) = R e^{-R^2/2} \tag{95}$$

Hence R has expected value, and variance

$$E(R) = \sqrt{\pi/2} \quad ; \quad \sigma^2(R) = 2 - \frac{\pi}{2} \tag{96}$$

If S and $1/\sqrt{2\rho}$ are small, we can expand $\delta(t)$ in a MacLaurin series about S and $1/\sqrt{2\rho}$ equal to zero:

$$\delta(t) = \text{Arctan}(\infty) + S\left.\frac{\partial \delta}{\partial S}\right| + \left.\frac{1}{\sqrt{2\rho}}\,\frac{\partial \delta}{\partial 1/\sqrt{2\rho}}\right| + \cdots$$

$$S, \frac{1}{\sqrt{2\rho}} = 0 \qquad S, \frac{1}{\sqrt{2\rho}} = 0 \qquad (97)$$

The expected value of $\delta(t)$ is then

$$E[\delta(t)] \simeq \text{Arctan}(\infty) + E\left(S\,\frac{\partial \delta}{\partial S}\right) + E\left(\frac{1}{\sqrt{2\rho}}\,\frac{\partial \delta}{\partial 1/\sqrt{2\rho}}\right)$$

$$= \text{Arctan}(\infty) - \sqrt{\frac{\pi}{2}}\,\cos\theta_{10}\,\sin(\eta_2 - \eta_1) \qquad (98)$$

If we can assume that θ_{10} is uniformly distributed over the interval $(0, 2\pi)$

$$E[\delta(t)] \simeq \text{Arctan}(\infty) = \frac{\pi}{2} \qquad (99)$$

Therefore to obtain the phase error, $\frac{\pi}{2}$ must be subtracted from δ in (93). This answer is due to the choice of a cosine rather than a sine in eq. (87). We find that the variance of $\delta(t)$ is:

$$\sigma^2(\delta) \simeq \frac{2 - \pi/2}{\gamma^2}\,\sin^2(\eta_2 - \eta_1)\cos^2\theta_{10} + \frac{1}{2\rho} \qquad (100)$$

where ρ is the direct signal tone filter output power to additive noise power. Again, if $\eta_2 - \eta_1$ and θ_{10} are uniformly distributed over $[0, 2\pi]$

$$\sigma^2(\delta) \simeq \frac{2 - \frac{\pi}{2}}{4\gamma^2} + \frac{1}{2\rho}$$

$$\simeq \frac{1}{2\rho} \qquad (101)$$

for large γ .

Figures 6F-1 and 6F-2 contain plots of the mean and standard deviation of the phase error as a function of the fading ratio for a tone filter output signal-to-noise ratio of 24 db in the slow fading case. Figures 6F-3 and 6F-4 give the corresponding mean and standard deviation of the range error.

FIG. 1

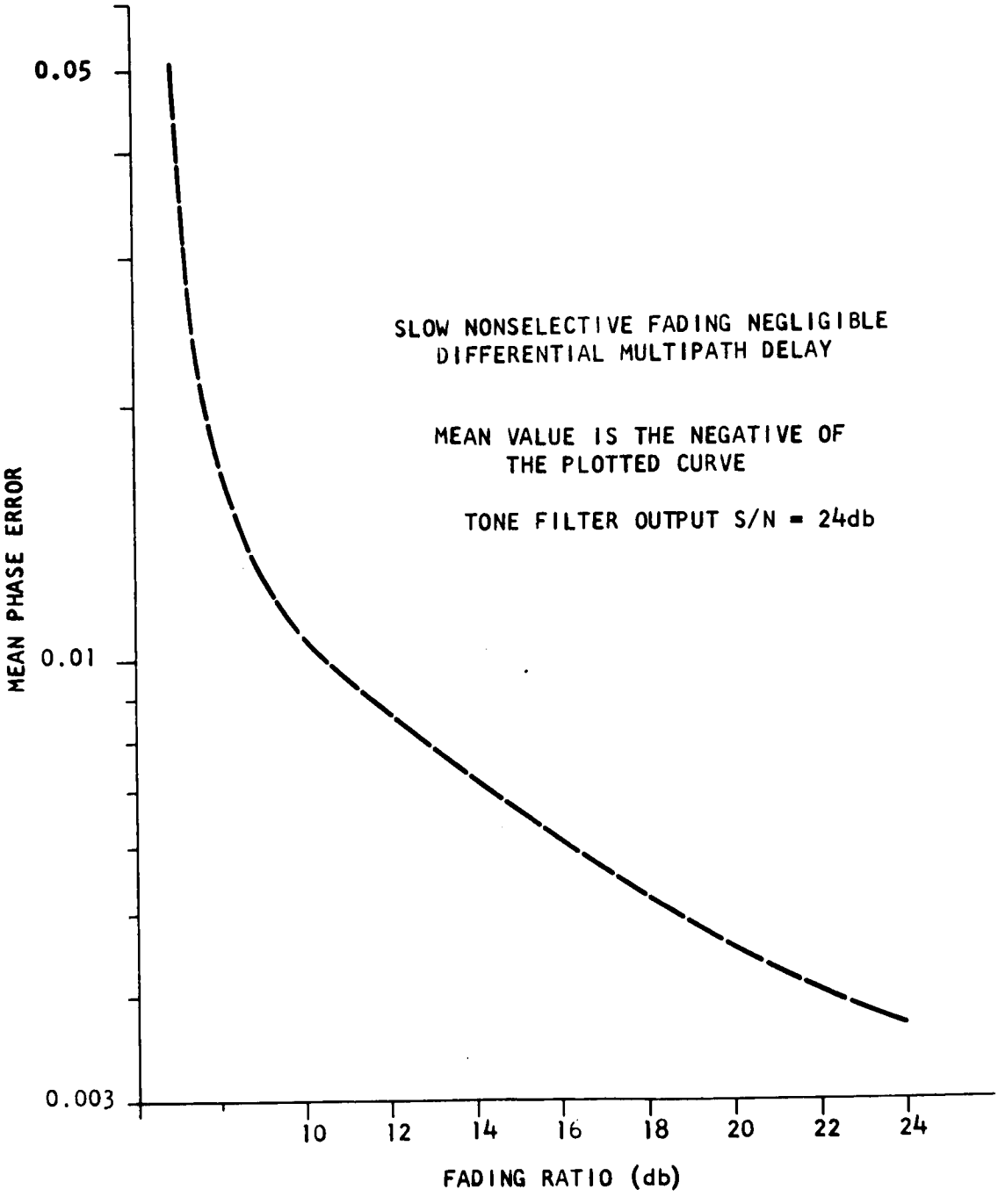

FIGURE 6F-1 - MEAN PHASE ERROR VS. FADING RATIO, SLOW FADING

FIG. 2

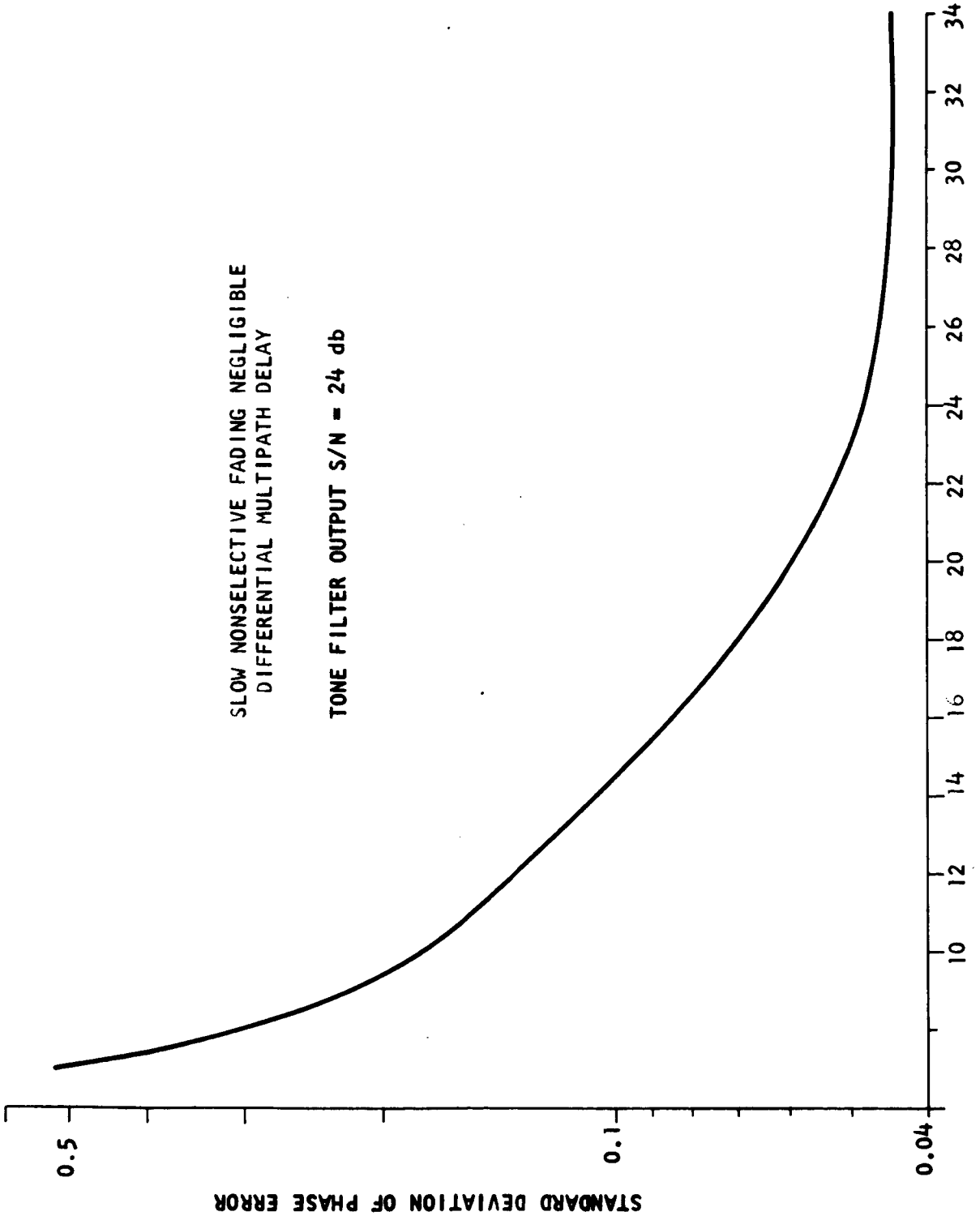

FIGURE 6F-2 - STANDARD DEVIATION OF PHASE ERROR VS. FADING RATIO

FIGURE 6F-3 - MEAN RANGE ERROR VS. FADING RATIO, SLOW NONSELECTIVE FADING, NEGLIGIBLE DIFFERENTIAL MULTIPATH DELAY

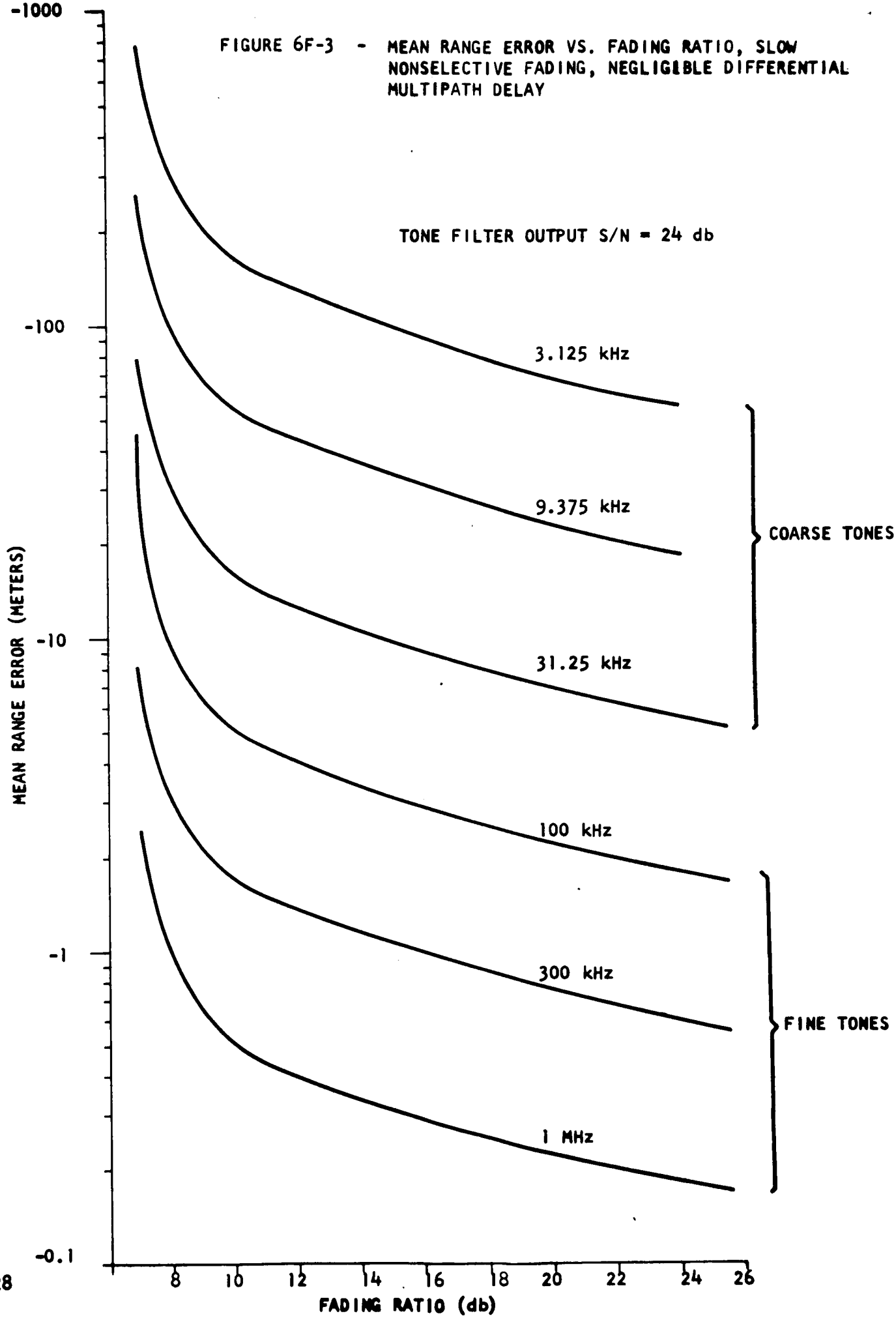

FIGURE 6F-4. STANDARD DEVIATION OF RANGE ERROR VS. FADING RATIO, SLOW NONSELECTIVE FADING, NEGLIGIBLE DIFFERENTIAL MULTIPATH DELAY

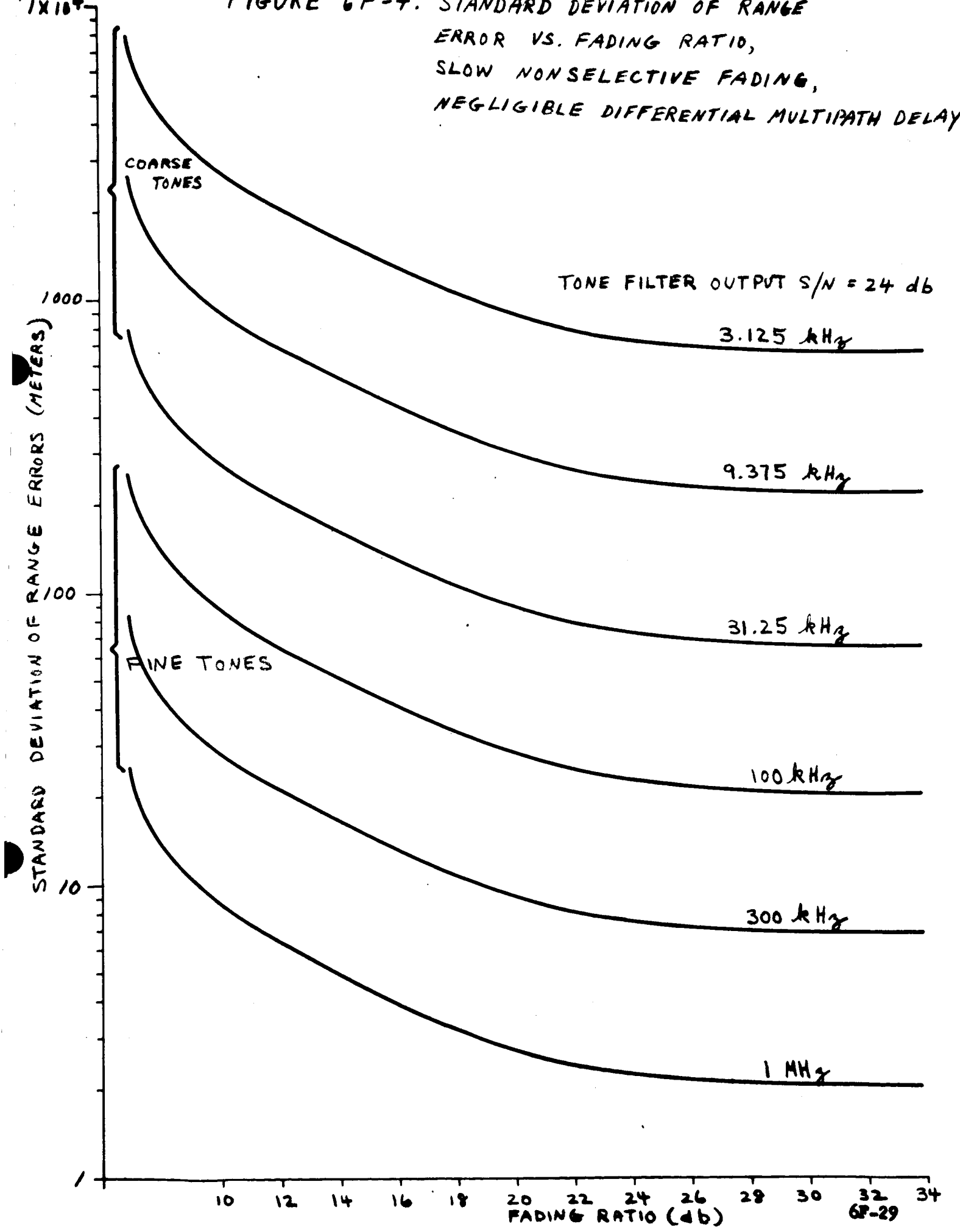

EXTRACTED CARRIER DEMODULATION WITH DIFFUSE MULTIPATH (C_{32})

The IF output signal plus noise is given by:

$$x(t) = S_D(t) + S_R(t) + n(t) \tag{1}$$

where the direct signal is:

$$S_D(t) = \alpha \cos\left\{\omega_0(at+b) + \theta + \sum_{j=1}^{2} m_j \sin\left[\omega_j(at+b) + \theta_{jD}\right]\right\} \tag{2}$$

and the random component is:

$$S_R(t) = R(t)\cos\left[\omega_0 t + \zeta(t) + \sum_{j=1}^{2} m_j \sin(\omega_j t + \theta_{jR})\right] \tag{3}$$

$R(t)$ and $\zeta(t)$ representing envelope and phase functions. Assuming that the scattered components can be described by a Gaussian process, $R(t)$ which is Raleigh distributed corresponds to the envelope of such a process, while $\zeta(t)$ which is uniformly distributed over $(0, 2\pi)$ corresponds to the phase.

The additive white noise $n(t)$ is stationary. It can be written with in-phase and quadrature components about the direct signal's IF carrier:

$$n(t) = I_c(t)\cos(\omega_0 + \Delta\omega)t - I_j(t)\sin(\omega_0 + \Delta\omega)t \tag{4}$$

using the relation

$$a = 1 + \frac{\Delta\omega}{\omega_0} \tag{5}$$

which describes the frequency offset due to the medium. We have the following relationship for phase and time delays:

$$b = \frac{\Delta\theta}{\omega_0} + a\Delta\tau \tag{6}$$

If we consider all spectra to be double sided, the random IF noise power is

$$N_n = 2N_0 W_{IF} \tag{7}$$

where N_0 is the spectral density and W_{IF} is the IF bandwidth.

The random component has power

$$N_R = \sigma_F^2 \tag{8}$$

by definition.

A useful parameter is the ratio of the amplitude of the direct received signal to the standard deviation of the random component. Denoting this parameter by γ:

$$\gamma = \frac{\alpha}{\sigma_F} \tag{9}$$

It is now possible to relate the random noise power to the total received power, P_0:

$$P_0 = \frac{\alpha^2}{2} + \sigma_F^2 = \sigma_F^2 \left[\frac{\gamma^2}{2} + 1\right] \tag{10}$$

or

$$\sigma_F^2 = \frac{P_0}{\frac{\gamma^2}{2} + 1} \tag{11}$$

The carrier-to-noise input ratio is then,

$$\left(\frac{C}{N}\right)_{IF} = \frac{\gamma^2/2}{1 + \frac{2N_0 W_{IF}}{P_0/(\frac{\gamma^2}{2}+1)}} \tag{12}$$

considering the random component as noise.

It is convenient to express the direct and random component with in-phase and quadrature components.

$$S_D(t) = \alpha \left\{ I_{CXD}(t) \cos\left[(\omega_0 + \Delta\omega)t + \theta_1\right] - I_{SXD}(t) \sin\left[(\omega_0 + \Delta\omega)t + \theta_1\right] \right\} \tag{13}$$

where

$$\theta_1 = \omega_0 b + \theta \tag{14}$$

and

$$S_R(t) = R(t)\left\{I_{CXR}(t)\cos[\omega_0 t + S(t)] - I_{SXR}(t)\sin[\omega_0 t + S(t)]\right\} \tag{15}$$

The functions I_{CXD} and I_{SXD} are given by:

$$\begin{aligned} I_{CXD}(t) = &\left\{J_0(m_1) + 2\sum_{n_1=1}^{\infty} J_{2n_1}(m_1)\cos 2n_1\left[\omega_1(at+b)+\theta_{1D}\right]\right\}\cdot \\ &\cdot\left\{J_0(m_2) + 2\sum_{n_2=1}^{\infty} J_{2n_2}(m_2)\cos 2n_2\left[\omega_2(at+b)+\theta_{2D}\right]\right\} \\ &-\left\{2\sum_{n_1=0}^{\infty} J_{2n_1+1}(m_1)\sin(2n_1+1)\left[\omega_1(at+b)+\theta_{1D}\right]\right\}\cdot \\ &\cdot\left\{2\sum_{n_2=0}^{\infty} J_{2n_2+1}(m_2)\sin(2n_2+1)\left[\omega_2(at+b)+\theta_{2D}\right]\right\} \end{aligned} \tag{16}$$

$$\begin{aligned} I_{SXD}(t) = &\left\{2\sum_{n_1=0}^{\infty} J_{2n_1+1}(m_1)\sin(2n_1+1)\left[\omega_1(at+b)+\theta_{1D}\right]\right\}\cdot \\ &\cdot\left\{J_0(m_2) + 2\sum_{n_2=1}^{\infty} J_{2n_2}(m_2)\cos 2n_2\left[\omega_2(at+b)+\theta_{2D}\right]\right\} \\ &+\left\{J_0(m_1) + 2\sum_{n_1=1}^{\infty} J_{2n_1}(m_1)\cos 2n_1\left[\omega_1(at+b)+\theta_{1D}\right]\right\}\cdot \\ &\cdot\left\{2\sum_{n_2=0}^{\infty} J_{2n_2}(m_2)\sin(2n_2+1)\left[\omega_2(at+b)+\theta_{2D}\right]\right\} \end{aligned} \tag{17}$$

where $J_S(x)$ are Bessel functions of order S in the variable X. The functions I_{CXR} and I_{SXR} are identical to the ones described in (16) and (17) except for the arguments for the sines and cosines which are now $\omega_j t + \theta_{jR}$.

We now have to consider the random component. Defining

$$\begin{cases} I_{CF}(t) = R(t) \cos S(t) \\ I_{SF}(t) = R(t) \sin S(t) \end{cases} \tag{18}$$

the power spectrum of I_{CF} is called the fading spectrum. Its bandwidth B_F is a measure of the fading rate. We distinguish three possibilities.

(A) Slow fading, $B_F = 0$

(B) Fast fading, $B_F > W$ where W is the bandwidth of the band pass filter,

and (C) Intermediate fading, $0 < B_F < W$

The IF output $X(t)$ is first passed through a narrow band carrier extraction filter. Hence the BPF (band-pass filter) input is given by:

$$d(t) = \alpha \cos\left[(\omega_0 + \Delta\omega)t + \theta_1\right] + R(t)\cos\left[\omega_0 t + S(t)\right] + n_0(t) \tag{19}$$

where $n_0(t)$ is derived from the IF additive noise.

For slow and intermediate fading the STN ratio at the end of the BPF is given by:

$$\rho = \frac{\alpha^2/2}{\frac{\langle R^2(t)\rangle}{2} + 2N_0 B_L} = \frac{\gamma^2}{\langle R^2(t)\rangle + \frac{4N_0 B_L}{\sigma_F}} \tag{20}$$

where we normalized R to $\tilde{R}$

$$\tilde{R} = \frac{R}{\sigma_F} \tag{21}$$

which has the probability distribution:

$$P(R) = R\, e^{-\frac{R^2}{2}} \tag{22}$$

Hence

$$\rho = \frac{\gamma^2}{2 + \frac{4 N_0 B_L}{P_r \left(\frac{\chi^2}{2}+1\right)}} \tag{23}$$

For fast fading the random component is reduced in power by the multiplicative factor W/B_F in the BPF.

The BPF output signal-to-noise ratio is

$$\rho = \frac{\gamma^2}{\frac{2W}{B_F} + \frac{4 N_0 B_L}{\frac{W}{B_0}\frac{B_0}{\left(\frac{\chi^2}{2}+1\right)}}} \tag{24}$$

Since for both slow and intermediate fading, the random signal is passed unchanged in the BPF, we will combine the analyses for these two situations.

6G.1 SLOW AND INTERMEDIATE FADING

The signal entering the BPF is given in (19):

$$d(t) = \alpha \cos\left[(\omega_0+\Delta\omega)t+\theta_1\right] + R(t)\cos\left[\omega_0 t + \zeta(t)\right] + n_0(t) \tag{25}$$

For slow fading ΔW must of necessity be negligible, however for intermediate fading we have to keep this term.

The bandpass filter output is:

$$r(t) = \alpha \sin\left[(\omega_0+\Delta\omega)t+\theta_1\right] + \varepsilon(t) \tag{26}$$

where we treat the random component as noise, thus:

$$\begin{aligned}
\varepsilon(t) &= n_F(t) + n_B(t) \\
n_F(t) &= R(t)\sin\left[\omega_0 t + \zeta(t)\right] \\
n_B(t) &= I_{cB}\sin(\omega_0+\Delta\omega)t - I_{sB}\cos(\omega_0+\Delta\omega)t
\end{aligned} \tag{27}$$

When $r(t)$ and $\chi(t)$ are processed in a product detector and the low frequency portion extracted, the resulting signal plus noise is given by:

$$\begin{aligned}
z(t) &= LF\left[\chi(t)\, r(t)\right] \\
&= -\frac{\alpha^2}{2} I_{sx0}(t) + \varepsilon_{sxn}(t) + \varepsilon_{nxs}(t) + \varepsilon_{nxn}(t)
\end{aligned} \tag{28}$$

The last three terms describe noise.

The function $z(t)$ is passed through the tone filters F_j which are centered at $\mp f_j$, $j=1,2$, double sided power spectra and have a width W_{0j}. These filters are assumed to be unity gain filters. If the tone filter outputs are denoted by $Y_j(t)$:

$$Y_j(t) = -\alpha^2 J_0(m_k) J_1(m_j) \sin\left[\omega_j t + \eta_{j1}\right] + n_{SXn,j}(t) + \eta_{nxS_{jj}}(t) + \eta_{nxn_{jj}}(t) \quad (29)$$

$$j \neq k = 1,2$$

where we approximated

$$\omega_j a = \omega_j \left[1 + \frac{\Delta\omega}{\omega_0}\right] \approx \omega_j \quad (30)$$

and defined

$$\eta_{j1} = \omega_j b + \theta_{jD} \quad (31)$$

and we will also define

$$\eta_{j2} = \theta_j R$$

$$\theta_{10} = \theta_1 - \left[\theta(t) - \Delta\omega t\right] = \theta_1 - \theta_2 \quad (32)$$

If the filters are sufficiently narrow, all harmonics and intermediate frequencies of the tone frequencies are rejected.

The first noise term is due to $\varepsilon_{SXn}(t)$

$$\varepsilon_{SXn}(t) = LF\left\{S_0(t)\left[n_F(t) + n_B(t)\right]\right\}$$

$$= \frac{\alpha R}{2}\left\{I_{cxD}(t)\sin(-\theta_{10}) - I_{SXD}(t)\cos\theta_{10}\right\}$$

$$+ \frac{\alpha}{2}\left\{I_{cxd}(t)\left[-I_{cB}\sin\theta_1 - I_{SD}\cos\theta_1\right] - I_{SXD}(t)\left[I_{cB}\cos\theta_1 - I_{SD}\sin\theta_1\right]\right\} \quad (33)$$

which results in a tone filter output

$$n_{SXnjz}(t) = -\alpha J_0(m_k) J_1(m_j) R\cos\theta_{10}\sin(\omega_j t + \eta_{j1})$$

$$-\alpha J_0(m_k) J_1(m_j)\left[I_{cB}\cos\theta_1 - I_{SD}\sin\theta_1\right]\sin(\omega_j t + \eta_{j1}) \quad j \neq k = 1,2 \quad (34)$$

The noise power associated with this term is:

$$N_{6G-6SXn_{1j}} = \alpha^2\left[J_0(m_k) J_1(m_j)\right]^2 \frac{1}{2}\left\{\frac{\langle R^2\rangle}{2} + \langle I_{cB}^2(t)\rangle\right\} \quad (35)$$

under the assumption that θ_{1o} is uniformly distributed over $[0, 2\pi]$ for small $\Delta\omega$, and since I_{CB} and I_{SB} are zero mean Gaussian distributions.

In passing we note that the power spectrum of the stationary IF noise is independent of the frequency about which it is expanded. For a double sided unity gain filter

$$\langle I^2_{CB}(t)\rangle = 2N_0 \cdot \begin{cases} \omega\,; & \omega_{oj} > \omega \\ \omega_0\,; & \omega_{oj} < \omega \end{cases} \tag{36}$$

while the mean value of R^2 is:

$$\langle R^2(t)\rangle = \int_0^\infty R^2 \frac{R}{\sigma^2} e^{-\frac{R^2}{2\sigma^2}} dR$$

$$= 2\sigma^2_F \tag{37}$$

Hence:

$$N_{SXn_jj} = \frac{\sigma_F^4 \gamma^2 [J_0(m_k) J_1(m_j)]^2}{2}\left[1 + \frac{2N_0}{\sigma^2_F} \cdot \begin{cases} \omega\,; & \omega_{oj} > \omega \\ \omega_{oj}\,; & \omega_{oj} < \omega \end{cases}\right] \tag{38}$$

The second tone filter noise function is derived from $\varepsilon_{nxs}(t)$. Since

$$\varepsilon_{nxs}(t) = LF\{[S_R(t) + n(t)]\, r(t, \text{signal term})\}$$

$$= \frac{\alpha R}{2}\left[I_{CXR}(t)\sin\theta_{10} - I_{SXR}(t)\cos\theta_{10}\right]$$

$$+ \frac{\alpha}{2}\left[I_C \sin\theta_1 - I_S\cos\theta_1\right] \tag{39}$$

the resulting tone filter output noise is:

$$n_{SXn_jj}(t) = -\alpha R J_0(m_k) J_1(m_j) \sin[\omega_j t + \theta_{j2}]$$

$$+ \frac{\alpha}{2}[I_c \sin\theta_1 - I_S\cos\theta_1] \tag{40}$$

of bandwidth W_{oj}, with noise power:

$$N_{SXn_jj} = \frac{\sigma_F^4 \gamma^2}{2}[J_0(m_k) J_1(m_j)]^2 + \sigma^2_F[\gamma^2 N_0 \omega_{oj}] \tag{41}$$

where

$$\langle I_o^2(t)\rangle \longrightarrow 4N_0\omega_{oj} \tag{42}$$

for a double sided power spectrum filtered through 2 filters of width W_{oj} provided the tones f_j are well within the IF bandwidth. The last noise term is $n_{nxn}(t)$.

$$\varepsilon_{nxn}(t) = LF\{[S_R(t)+n(t)][n_I(t)+n_B(t)]\}$$

$$= -\frac{k^2}{2} I_{SXR}(t) + \frac{R}{2}[I_c(t)\sin\theta_2 - I_s(t)\cos\theta_2]$$

$$+ \frac{R}{2}\{I_{cxR}(t)[I_{cB}\sin(-\theta_2) - I_{SB}\cos\theta_2]$$

$$- I_{SxR}(t)[I_{cB}\cos\theta_2 - I_{SB}\sin\theta_2]\}$$

$$+ LF[n(t)n_B(t)] \qquad (43)$$

The last term $LF[n(t)n_B(t)]$ is analyzed in C_{12}.

It has noise power $N_0^2 \omega \omega_{oj}$. The tone filter output of $\varepsilon_{nxn}(t)$ is:

$$n_{nxn_j}(t) = -R^2 J_0(m_k) J_1(m_j)\sin[\omega_j t + \eta_{j2}] + \frac{R}{2}[I_c\sin\theta_2 - I_s\cos\theta_2]$$

$$- R J_0(m_k) J_1(m_j)\sin(\omega_j t + \eta_{j2})[I_{cB}\cos\theta_2 - I_{SB}\sin\theta_2] + LF[n(t)n_B(t)] \qquad (44)$$

of bandwidth W_{oj} which has noise power:

$$N_{nxn_j}(t) = [J_0(m_k) J_1(m_j)]^2 \frac{\sigma_E^4}{8} + \frac{\sigma_E^2}{2}\cdot 4 N_0 W_{oj} + N_0^2 \omega \omega_{oj}$$

$$+ [J_0(m_k) J_1(m_j)]^2 \sigma_E^2 \cdot 2N_0 \begin{cases} \omega & ; \omega_{oj} > \omega \\ \omega_{oj} & ; \omega_{oj} < \omega \end{cases} \qquad (45)$$

The signal power is

$$S_j = \alpha^4 [J_0(m_k) J_1(m_j)]^2 / 2 \qquad (46)$$

Hence the tone filter output (S/N) ratio is:

$$\left(\frac{S}{N}\right)_{oj} = \begin{cases} \dfrac{\frac{\gamma^2}{2}}{1 + \frac{1}{8\gamma^2} + \frac{N_0\omega}{\sigma^2}\left[1+\frac{2}{\gamma^2}\right] + \frac{N_0\omega_{oj}}{\sigma^2[J_0(m_k)J_1(m_j)]^2}\left(1+\frac{2}{\gamma^2}+\frac{N_0\omega}{\sigma^2}\right)} & ; \omega_{oj} > \omega \\ \dfrac{\frac{\gamma^2}{2}}{1 + \frac{1}{8\gamma^2} + \frac{N_0\omega_{oj}}{\sigma^2}\left[1+\frac{2}{\gamma^2}+\frac{\sigma_E^2 + N_0\omega}{\gamma^2\sigma^2[J_0(m_k)J_1(m_j)]^2}\right.} & ; \omega_{oj} < \omega \end{cases} \qquad (47)$$

The tone filter output $y_j(t)$ is

$$y_j(t) = -\alpha^2 J_0(m_k) J_1(m_j) \left\{ \left[1 + \frac{R(t)}{\alpha} \cos\theta_{10} + \frac{I_{CR}\cos\theta_1 - I_{SR}\sin\theta_1}{\alpha} \right] \sin(\omega_j t + \eta_{j1}) \right.$$

$$\left. + \left[\frac{R}{\alpha}\cos\theta_{10} + \left(\frac{R}{\alpha}\right)^2 + \frac{R}{\alpha} \frac{I_{CR}\cos\theta_2 - I_{SR}\sin\theta_2}{\alpha} \right] \sin(\omega_j t + \eta_{j2}) \right\}$$

$$+ \frac{\alpha}{2}\left[I_C \sin\theta_1 - I_S \cos\theta_1 \right] + \frac{R}{2}\left[I_C \sin\theta_2 - I_S \sin\theta_2 \right] + LF\left[n(t) n_0(t) \right]$$

$j \neq k = 1, 2$ (48)

If we write $y_j(t)$ with in-phase and quadrature components, about the tone frequency $\omega_j t + \eta_{j1}$, we have:

$$y_j(t) = I_{cj} \cos(\omega_j t + \eta_{j1}) + I_{sj} \sin(\omega_j t + \eta_{j1}) \quad (49)$$

where

$$I_{sj}(t) = -\alpha^2 J_0(m_k) J_1(m_j) \left\{ 1 + \frac{R}{\gamma}\cos\theta_{10} + \left[\frac{R}{\gamma}\cos\theta_{10} + \left(\frac{R}{\gamma}\right)^2 \cos(\eta_{j2} - \eta_{j1}) \right. \right.$$

$$\left. \left. + \left[\frac{1 + \frac{R}{\gamma}}{\sqrt{2}\rho_{DL}} + \sqrt{\rho_2} \right] I_{sT}(t) \right\}$$

$$I_{cj}(t) = -\alpha^2 J_0(m_k) J_1(m_j) \left\{ \left[\frac{R}{\gamma}\cos\theta_{10} + \left(\frac{R}{\gamma}\right)^2 \right] \sin(\eta_2 - \eta_1) \right.$$

$$\left. - \left[\frac{1 + \left(\frac{R}{\gamma}\right)}{\sqrt{2}\rho_{DL}} + \sqrt{\rho_2} \right] I_{cT}(t) \right\} \quad (50)$$

where R is a Rayleigh distributed random variable, ρ_{DL} is the direct signal power to random noise power at the bandpass filter output

$$\rho_{DL} = \frac{\alpha^2}{4 N_0 W} \quad (51)$$

The random variables I_{CT} and I_{ST} are normally distributed with zero mean and variance unity. They are due to the last three terms and the stationary portion of the bandpass filter noise.

If we define

$$\rho_T = \frac{\alpha^2 \left[J_0(m_k) J_1(m_j) \right]^2}{2 N_0 \omega_{0j}} \quad (52)$$

ρ_2 is given by

$$\rho_2 = \frac{N}{S} = \frac{1}{2}\left[\frac{1}{\gamma_{nL}} + \frac{1+\left(\frac{R}{\gamma}\right)^2}{\gamma}\right] \tag{53}$$

The phase error δ due to multipath and additive noise is thus given by:

$$\delta = \text{Arctan}\left\{\frac{1+\frac{R}{\gamma}\cos\theta_{10}\left[\frac{R}{\gamma}\cos\theta_{10}+\left(\frac{R}{\gamma}\right)^2\cos(\eta_{j2}-\eta_{j1})+\left[\frac{1+\frac{R}{\gamma}}{\sqrt{2}\,\delta_{n}}+\sqrt{\rho_2}\right]I_{ST}(t)\right]}{\left[\frac{R}{\gamma}\cos\theta_{10}+\left(\frac{R}{\gamma}\right)^2\sin(\eta_{j2}-\eta_{j1})-\left[\frac{1+\frac{R}{\gamma}}{\sqrt{2}\,\delta_{n}}+\sqrt{\rho_2}\right]I_{CT}(t)\right]}\right\} - \frac{\pi}{2} \tag{54}$$

Since we wish δ to have zero mean in the absence of multipath and additive noise and since we wish to write $\eta_j(t)$ of (49) with a sine rather than a cosine we subtracted a $\frac{\pi}{2}$ from δ in eq. (54) and add $\frac{\pi}{2}$ in (49).
Note that ρ_2 is noise-to-signal ratio.

FAST FADING

The random component is said to be fast fading whenever its bandwidth exceeds the bandwidth of the bandpass filter W. The input to the BPF is given in (19).

$$d(t) = \alpha\cos\left[(\omega_0+\Delta\omega)t+\theta_1\right]+R(t)\cos\left[\omega_0 t+\Sigma(t)\right]+n_0(t) \tag{55}$$

We write the output as

$$r(t) = \alpha\sin\left[(\omega_0+\Delta\omega)t+\theta_1\right]+\varepsilon(t) \tag{56}$$

where $\varepsilon(t)$ is noise which includes the random component.

$$\varepsilon(t) = n_F(t)+n_0(t)$$
$$n_0(t) = R_0(t)\sin\left[\omega_0 t+\Sigma(t)\right]$$
$$n_F(t) = I_{CB}\sin(\omega_0+\Delta\omega)t - I_{SB}\cos(\omega_0+\Delta\omega)t \tag{57}$$

where R_0 is still Raleigh distributed but $n_F(t)$ has bandwidth W, and variance

$$\sigma_{nF}^2 = \frac{W}{B_F}\sigma_0^2 \tag{58}$$

i.e., it is reduced by the "relative fading rate" $\frac{W}{B_F}$. The product of the extracted reference $X(t)$ and the IF output are processed together in a low pass filter, yielding as before

$$z(t) = -\frac{\alpha^2}{2} I_{SXD}(t) + \varepsilon_{SXn}(t) + \varepsilon_{nXS}(t) + \varepsilon_{nXn}(t) \tag{59}$$

which is then passed through unity gain tone filters of bandwidths W_{oj} and centered at the tones $\pm f_j$ for double sided spectra. These filters are assumed to be so narrow that only the tone frequencies are passed, while all harmonics and intermodulation frequencies are rejected. Proceeding as in the first part of this matrix element the tone filter output is found to be:

$$\eta_j(t) = -\alpha^2 J_0(m_k) J_1(m_j) \left\{ \left[1 + \frac{R_0}{\alpha} \cos\theta_{10} + \frac{I_{cn}\cos\theta_1 - I_{SD}\sin\theta_1}{\alpha} \right] \sin(\omega_j t + \eta_{j1}) \right.$$
$$\left. + \left[\frac{R_1}{\alpha} \cos\theta_{10} + \frac{R_1 R_0}{\alpha^2} + \frac{R_2}{\alpha} \frac{I_{cn}\cos\theta_2 - I_{SD}\sin\theta_2}{\alpha} \right] \sin(\omega_j t + \eta_{j2}) \right\}$$
$$+ \frac{\alpha}{2} \left[I_c \sin\theta_1 - I_S \cos\theta_1 \right] + \frac{R_0}{2} \left[I_c \sin\theta_2 - I_S \cos\theta_2 \right] + LF\left[n(t)\, n_0(t) \right] \tag{60}$$

If we now write $\eta_j(t)$ with in-phase and quadrature components about $\omega_j t + \eta_{j1}$

$$\eta_j(t) = I_{cj} \cos(\omega_j t + \eta_{j1}) + I_{Sj} \sin(\omega_j t + \eta_{j1})$$
$$= E_j \cos(\omega_j t + \eta_{j1} - \delta) \tag{61}$$

where δ is the instantaneous phase angle error due to multipath and additive noise.

The desired output would be a sine, rather than a cosine. We also want δ to have zero mean in the absence of multipath and additive noise.

If therefore we write

$$\eta_j(t) = E_j \sin(\omega_j t + \eta_{j1} - \delta) \tag{62}$$

we have to write δ as $\delta = A\tan\frac{I_{sj}}{I_{cj}} - \frac{\Pi}{2}$

$$= \tan^{-1}\left\{\frac{1+\frac{\beta R_1\cos\theta_{12}}{\gamma}+\left[\frac{R\cos\theta_{12}}{\gamma}+\frac{R_0\beta}{\gamma_1}\right]\cos(\eta_{j2}-\eta_{j1})+\left[\frac{1+\beta R_0}{\sqrt{2}\rho_B}+\sqrt{\rho_2}\right]I_{sT}}{\frac{R\cos\theta_{12}}{\gamma}+\frac{\beta R R_0}{\gamma^2}\sin(\eta_{j2}-\eta_{j1})-\left[\frac{1+\frac{\beta R_0}{\gamma}}{\sqrt{2}\rho_B}+\sqrt{\rho_2}\right]I_{cT}}\right\}$$

(63)

where

R is Raleigh distributed: $p(R) = R\,e^{-\frac{R^2}{2}}$

R_o is Raleigh distributed: $p(R_0) = R_0 e^{-\frac{R_0^2}{2}}$

$$\beta = \sqrt{\frac{\alpha}{B_T}}$$

$$\rho_B = \frac{\alpha^2}{N_0\alpha}$$

(64)

Since R and R_o are similarly distributed over the width of the filter but not outside the filter bandwidth, they are correlated and we need to determine the joint probability distribution of R and R_o. After we obtain that, the only way to determine the mean and variance of δ is by analyzing it on the computer.

Here we are interested in determining the joint probability distribution of R and R_o. Their variances are respectively σ^2 and σ_0^2. Defining the following four variables:

$$X_1 = I_{c1}$$

$$X_2 = I_{s1}$$

$$X_3 = I_{c2}$$

$$X_4 = I_{s2}$$

(65)

where

$$R_1^2 = I_{c1}^2 + I_{s1}^2$$

$$R_2^2 = I_{c2}^2 + I_{s2}^2$$

(66)

The variables with the same leading subscripts (C or S) are coupled, while when the variables have different leading subscripts they are independent, we can write down the correlation matrix

$$\Sigma = \| \langle X_i X_j \rangle \|$$

$$= \begin{bmatrix} \sigma^2 & 0 & S_{12} & 0 \\ 0 & \sigma^2 & 0 & S_{12} \\ S_{12} & 0 & \sigma^2 & 0 \\ 0 & S_{12} & 0 & \sigma^2 \end{bmatrix} \qquad (67)$$

where

$$\langle X_1 X_3 \rangle = \langle X_3 X_4 \rangle = S_{12}$$

$$\langle X_2 X_4 \rangle = \langle X_4 X_1 \rangle = S_{12}$$

(68)

The joint probability distribution of the X_i is:

$$P(X_1, X_2, X_3, X_4) = K e^{-\frac{1}{2} X}$$

(69)

where

$$K = \frac{1}{(2\pi)^2 |\Sigma|}$$

and $|\Sigma|$ indicates the value of the determinant of Σ while

$$Q = \underline{X}^T \Sigma^{-1} \underline{X} \qquad (70)$$

where X^T means the transpose of the column vector

$$\underline{X} = \begin{pmatrix} X_1 \\ X_2 \\ X_3 \\ X_4 \end{pmatrix} \tag{71}$$

and Σ^{-1} is the inverse of the correlation matrix Σ, which is found to be

$$\Sigma^{-1} = \frac{1}{\sigma^2\sigma_0^2 - \delta_{12}^2} \begin{bmatrix} \sigma_0^2 & 0 & -\delta_{12} & 0 \\ 0 & \sigma_0^2 & 0 & -\delta_{12} \\ -\delta_{12} & 0 & \sigma^2 & 0 \\ 0 & -\delta_{12} & 0 & \sigma^2 \end{bmatrix} \tag{72}$$

It is straight forward to show that $\Sigma \cdot \Sigma^{-1}$ is the identity matrix, as a check.

If we now form Q, where Q is the product of three matrices of sizes (1,4), (4,4), and (4.1) Q is found to be:

$$Q = \left\{ \frac{X_1^2 + X_3^2}{\sigma^2} + \frac{X_2^2 + X_4^2}{\sigma_0^2} - \frac{2\delta_{12}}{\sigma^2\sigma_0^2}\left(X_1X_3 + X_2X_4\right) \right\} \Big/ \left(1 - \frac{\delta_{12}^2}{\sigma^2\sigma_0^2}\right) \tag{73}$$

We will define

$$\rho = \frac{\delta_{12}}{\sigma\sigma_0} \tag{74}$$

and write:

$$p(X_1, X_2, X_3, X_4) = \frac{1}{(2\pi)^2\left[1-\rho^2\right]^2(\sigma^2\sigma_0^2)^2} \exp -\left\{ \left[\frac{R^2}{\sigma_1^2} + \frac{R_0^2}{\sigma_0^2} - \frac{2\delta_{12}}{\sigma_1^2\sigma_0^2}\left(X_1X_3 + X_2X_4\right) \right] \Big/ 2\left(1-\rho^2\right) \right\} \tag{75}$$

We will now re-interpret the definitions of the X_i

$$\begin{cases} X_1 = I_{C1} = R\cos\theta_1 \\ X_2 = I_{S1} = R\sin\theta_1 \\ X_3 = I_{C2} = R_0\cos\theta_2 \\ X_4 = I_{S2} = R_0\sin\theta_2 \end{cases} \tag{76}$$

Hence

$$X_1 X_3 + X_2 X_4 = R R_0 \cos(\theta_1 - \theta_2)$$

we now wish to integrate out the undesirable θ_1 and θ_2.

Since

$$\prod_i X_i = R\,dR\;R_0\,dR_0\,d\theta_1\,d\theta_2$$

$$P(R, R_0)\,dR\,dR_0 = \int_{\theta_2}\int_{\theta_1} P(R, R_0, \theta_1, \theta_2)\,R R_0\,dR\,dR_0\,d\theta_1\,d\theta_2 \tag{77}$$

$$= \frac{\bar{R}\,\bar{R}_0}{1-\rho^2}\,d\bar{R}\,(\bar{R}_0\,\ldots)\,\exp-\left\{\frac{\bar{R}^2+\bar{R}_0^2}{2(1-\rho^2)}\right\} I_0\left[\frac{\rho\,\bar{R}\,\bar{R}_0}{1-\rho^2}\right] \tag{78}$$

where R and R_0 have been normalized to $\bar{R}$ and $\bar{R}_0$ respectively. Hence the joint probability distribution of R and R_0 is:

$$P(\bar{R}, \bar{R}_0) = \frac{\bar{R}\,\bar{R}_0}{1-\rho^2}\exp-\left\{\frac{\bar{R}^2+\bar{R}_0^2}{2(1-\rho^2)}\right\} I_0\left[\frac{\rho\,\bar{R}\,\bar{R}_0}{1-\rho^2}\right] \tag{79}$$

We now wish to inquire into ρ, and since

$$\rho = \frac{S_{12}}{\sigma\sigma_0} \tag{80}$$

we wish to find the value of S_{12}.

Recalling that

$$S_{12} = \langle X_1 X_3 \rangle \tag{81}$$

and if we write

$$n_1(t) = I_{c1}\cos\omega_0 t - I_{s1}\sin\omega_0 t$$

$$n_2(t) = I_{c2}\cos\omega_0 t - I_{s2}\sin\omega_0 t \tag{82}$$

we find that

$$\langle n_1 n_2 \rangle = \langle I_{c1} I_{c2} \rangle \cos^2\omega_0 t + \langle I_{s1} I_{s2} \rangle \sin^2\omega_0 t$$

$$= \langle I_{c1} I_{c2} \rangle \tag{83}$$

Since c and s subscripted variables are mutually uncorrelated. Now $n_1(t)$ is the filter response to $n_1(t)$. If $h(\tau)$ is the fourier transform of the filter response function $H(f)$

$$h(\tau) = \int_{-\infty}^{\infty} H(f)\, e^{j2\pi f\tau}\, df \tag{84}$$

and

$$= \int_{-\infty}^{\infty} h(\tau)\, n_1(t-\tau)\, d\tau \tag{85}$$

so that

$$\begin{aligned} \langle n_1(t)\, n_2(t)\rangle &= \int_{-\infty}^{\infty}\left[\int_{-\infty}^{\infty} H(f)\, e^{j2\pi f\tau}\, df\right]\langle n_1(t)\, n_1(t-\tau)\rangle\, d\tau \\ &= \int_{-\infty}^{\infty} H(f)\, df \int_{-\infty}^{\infty} R_{n_1}(\tau)\, e^{j2\pi f\tau}\, d\tau \\ &= \int_{-\infty}^{\infty} H(f)\, P_1(f)\, df \\ &= \sigma_0^2 \end{aligned} \tag{86}$$

where $R_{n_1}(\tau)$ is the autocorrelation function of $n_1(t)$ and $P_1(f)$ is its power spectrum. The result is independent of the response function of the filter.

Hence

$$\begin{aligned} S_{12} &= \langle X_1 X_2 \rangle \\ &= \sigma_0^2 \quad ; \quad B_F > \omega \end{aligned} \tag{87}$$

Therefore

$$\begin{aligned} \rho &= \frac{\sigma_0^2}{\sigma\sigma_0} \\ &= \frac{\sigma_0}{\sigma} \end{aligned} \tag{88}$$

and since σ^2 and σ_o^2 measure the power of the random component

$$\sigma^2 = 2N_o B_F$$
$$\sigma_o^2 = 2N_o W \tag{89}$$

where B_F is the bandwidth of the random component and W the bandwidth of the filter, we find that

$$\rho = 1 \quad \text{Slow and intermediate fading}$$
$$= \sqrt{\frac{W}{B}} \quad \text{Fast fading} \tag{90}$$

Hence the equations of interest are:

Tone filter output:

$$y_j = \sin(\omega_j t + n_{j1} - \delta) \tag{91}$$

where we wish to estimate the phase angle n_{j1} which results in a phase error due to multipath and additive noise given by:

$$\delta = \text{Arctan} \left\{ \frac{1 + \frac{\sqrt{\frac{W}{B_F}} R_o \cos\theta_{10}}{\gamma} + \left[\frac{R\cos\theta_{10}}{\gamma} + \frac{\sqrt{\frac{W}{B}} R R_o}{\gamma}\right]\cos(n_{2j} - n_{1j}) + \left[1 \sqrt{\frac{W}{B_F}} \frac{R_o}{\gamma} + \sqrt{\rho_2}\right] I_{ST}}{\left[\frac{R\cos\theta_{10}}{\gamma} + \frac{\sqrt{\frac{W}{B_F}} R R_o}{\gamma^2}\right]\sin(n_{2j} - n_{1j}) - \left[\frac{1 + \sqrt{\frac{W}{B_F}} \frac{R_o}{\gamma}}{\sqrt{2\rho_B}} + \sqrt{\rho_2}\right] I_{CT}} \right\} \tag{92}$$

The joint probability function of R and R_o is given by

$$p(R, R_o) = \frac{R R_o}{1-\rho^2} \exp - \left\{\frac{R^2 + R_o^2}{2(1-\rho^2)}\right\} I_o\left(\frac{\rho R R_o}{1-\rho^2}\right) \tag{93}$$

R and R_o are normalized Raleight distribtdions

where the normalized covariance is given by

$$\gamma = 1; \quad \text{Slow and intermediate fading}$$

$$= \sqrt{W/B_F}; \quad \text{Fast fading} \tag{94}$$

We see that upon comparing δ of (92) with δ of (54) we can obtain the slow fading case from the fast fading by identifying R and R_o as R, which is consistent.

Figures 6G-1 and 6G-2 show the dependence of the mean and standard deviation of the phase error in equation (92) on the fading ratio.

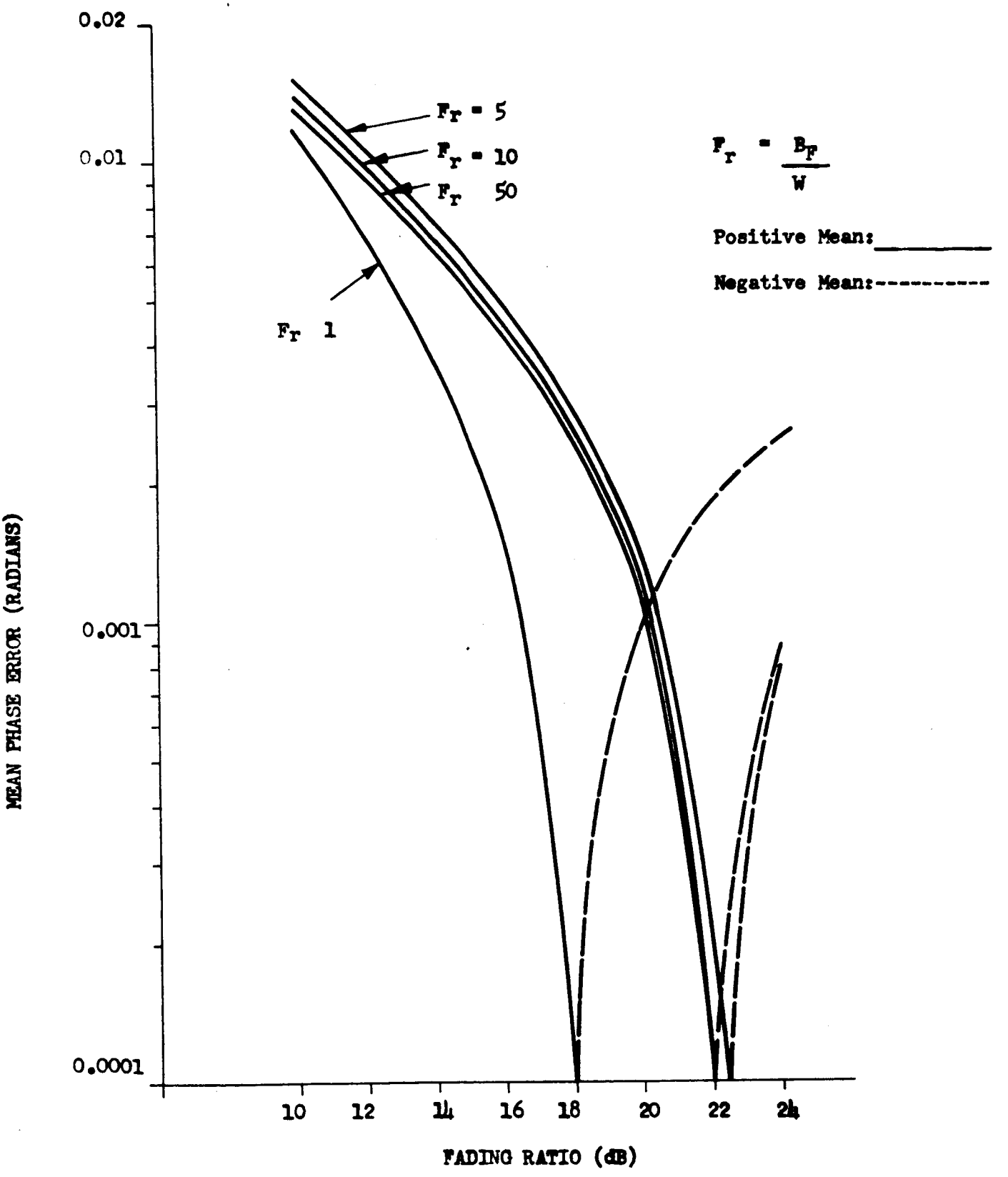

Figure 60-1 MEAN PHASE ERROR VS. FADING RATIO

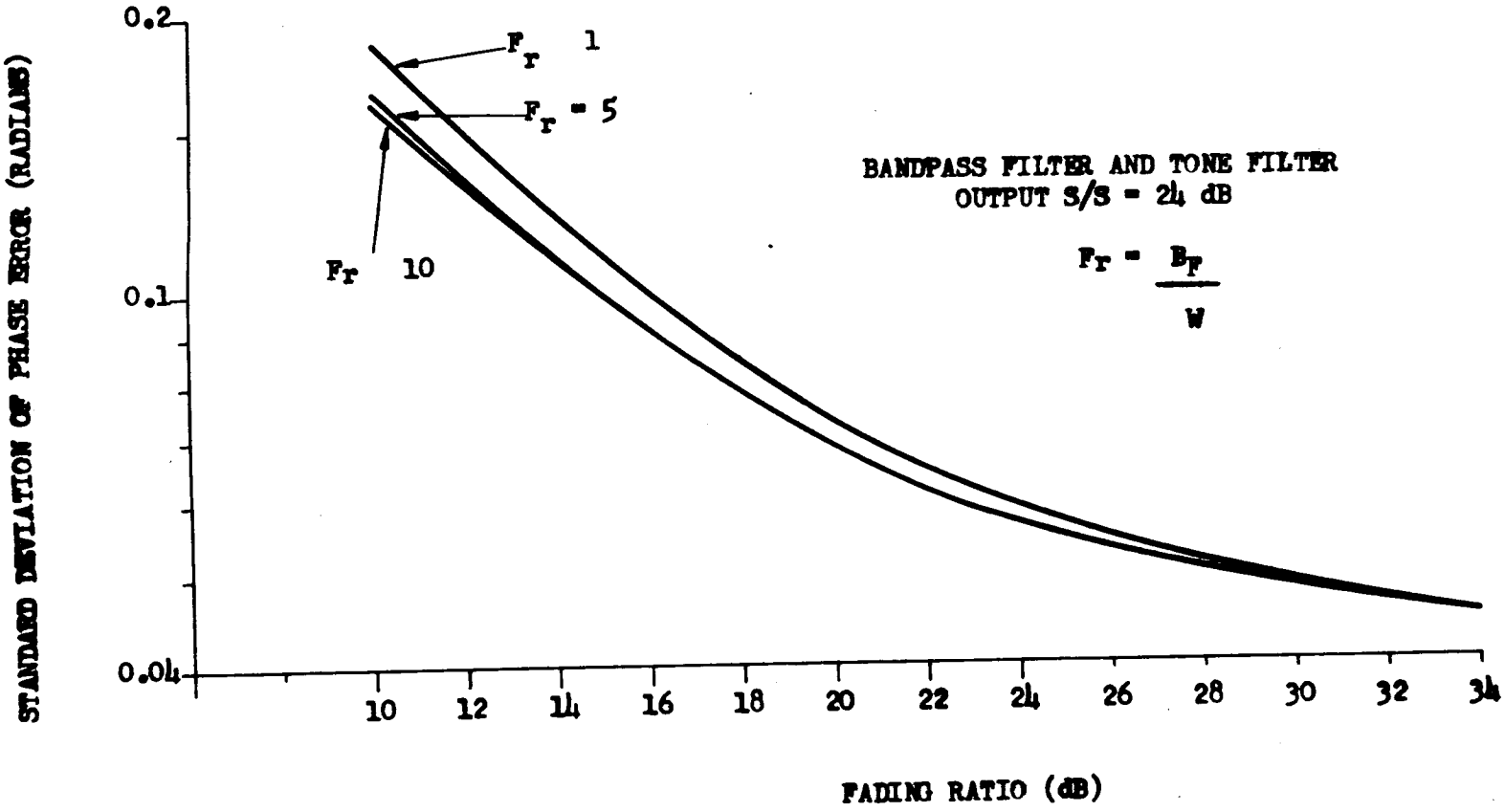

Figure 60-2 STANDARD DEVIATION OF PHASE ERROR VS. FADING RATIO

Appendix 6H

COMPARISON OF FOUR PHASE DETECTORS IN THE PRESENCE OF WHITE NOISE

6H.1 OPTIMUM PHASE ESTIMATION IN THE PRESENCE OF WHITE NOISE

Let the received signal be of the form:

$$x(t) = A \cos(\omega_o t + \theta) + n(t) \quad ; -\frac{T}{2} \leq t \leq \frac{T}{2} \tag{1}$$

$$s(t) = A \cos(\omega_o t + \theta) \tag{2}$$

By means of the Karhunen-Loéve (K-L) Orthonormal expansion,[1] we can write:

$$\begin{aligned} x(t) &= \sum_i x_i \phi_i(t) \\ s(t) &= \sum_i s_i \phi_i(t) \\ \frac{\partial s(t)}{\partial \theta} &= \sum_i \frac{\partial s_i}{\partial \theta} \phi_i(t) \end{aligned} \tag{3}$$

Approximating in terms of N expansion coefficients,

$$x_i = s_i + n_i \quad ; i = 1, 2, 3, \text{-----}, N \tag{4}$$

The likelihood function corresponding to the data vector

$$\underline{X} = (x_1, x_2, x_3, - - , x_N) \tag{5}$$

is

$$L(\underline{X}) = \prod_{i=1}^{N} \frac{1}{\sigma\sqrt{2\pi}} \exp\left\{ - \frac{(x_i - s_i)^2}{2\sigma^2} \right\} \tag{6}$$

since the noise has zero mean, and is normally distributed. In the white noise case, the variance σ^2 is the only eigenvalue of the K-L integral equation.[1] It may be interpreted physically as the spectral density of a one-sided power spectrum. For our analysis, where spectra are double sided and the total noise power is $2 N_o W$

$$\sigma^2 = 2 N_o \tag{7}$$

The Cramer-Rao inequality states that the minimum variance of an estimate $\hat{\theta}$ is:

$$\sigma^2_{min}(\hat{\theta}) = \left[\frac{\partial E(\hat{\theta})}{\partial \theta}\right]^2 \Big/ E\left[\left(\frac{\partial \log L}{\partial \theta}\right)^2\right] \tag{8}$$

The method of maximum likelihood will yield the minimum expected variance if it exists. Therefore, the efficiency of any parameter estimator can be measured by comparing its variance with this minimum variance.

From Equation (6):

$$\log L = \sum_i^N \frac{1}{\sigma\sqrt{2\pi}} - \sum_{i=1}^N \frac{(x_i - s_i)^2}{2\sigma^2} \tag{9}$$

$$\frac{\partial \log L}{\partial \theta} = -\frac{1}{\sigma^2} \sum_{i=1}^N m_i \frac{\partial s_i}{\partial \theta} \tag{10}$$

and

$$E\left[\left(\frac{\partial \log L}{\partial \theta}\right)^2\right] = \frac{1}{\sigma^2} \sum_{i=1}^N \left(\frac{\partial s_i}{\partial \theta}\right)^2 \tag{11}$$

since the noise has zero mean.

We now make use of the following fundamental relationship. If:

$$z(t) = \sum_{m=1}^{\infty} z_m \phi_m(t) \quad ; \quad z_m = \int_a^b z(t)\, \phi_m^*(t)\, dt$$

and

$$\int_a^b \phi_m(t) \phi_m^*(t)\, dt = \delta_{mm} \tag{12}$$

---

* indicates complex conjugate

$$E\left(\frac{\partial \log L}{\partial \theta}\right)^2 = \frac{1}{\sigma^2} \sum_{i=1}^{N} \int_{-T/2}^{T/2} \left(\frac{\partial s}{\partial \theta}\right)^2 \phi_i \phi_i^* \, dt$$

$$= \frac{1}{\sigma^2} \int_{-T/2}^{T/2} \left(\frac{\partial s}{\partial \theta}\right)^2 dt$$

$$= \frac{A^2}{\sigma^2} \int_{-\frac{T}{2}}^{T/2} \left[1 - \cos 2(\omega_0 t + \theta)\right] d\theta$$

$$\approx \frac{A^2 T}{2\sigma^2} \qquad (13)$$

if $N_0 T$ is large.

Hence

$$\sigma^2_{min}(\hat{\theta}) = \left[\frac{\partial E(\hat{\theta})}{\partial \theta}\right]^2 \Big/ \frac{A^2 T}{2\sigma^2}$$

$$= \left[\frac{\partial E(\hat{\theta})}{\partial \theta}\right]^2 \Big/ \left[\frac{A^2}{4 N_0 W_i} \cdot WT\right]$$

$$= \left[\frac{\partial E(\hat{\theta})}{\partial \theta}\right]^2 \Big/ 2\left(\frac{E}{N_0}\right) \qquad (14)$$

where E/N_0 is the ratio of signal energy to noise spectral density.

6H.2 ANALYSIS OF THE USE OF INDEPENDENT SAMPLES FOR SIGNAL PARAMETER ESTIMATION

As before, the received signal is of the form:

$$x(t) = A \cos(\omega_0 t + \theta) + n(t); \; -T/2 \leq t \leq T/2$$

$$S(t; \theta) = A \cos(\omega_0 t + \theta) \qquad (1)$$

Suppose $x(t)$ is sampled at times $t_1, t_2, ----, t_N$ assuming values $x_1, x_2, ---, x_N$ such that the noise values are uncorrelated.

For the same likelihood function as before:

$$L(x_1, x_2, \cdots, x_m; \theta) = (\sqrt{2\pi}\sigma)^{-N} \exp\left\{-\frac{1}{2\sigma^2}\sum_i [x_i - S(t_i;\theta)]^2\right\} \quad (2)$$

The minimum variance of an estimate is:

$$\sigma^2_{min}(\hat{\theta}) = \left[\frac{\partial E(\hat{\theta})}{\partial \theta}\right]^2 \Big/ E\left[\left(\frac{\partial \log L}{\partial \theta}\right)^2\right]$$

$$= \sigma^2 \left[\frac{\partial E(\hat{\theta})}{\partial \theta}\right]^2 \Big/ \sum_{i=1}^{N}\left(\frac{\partial S(t_i;\theta)}{\partial \theta}\right)^2 \quad (3)$$

For band-limited white noise with bandwidth W, the samples are independent if taken 1/2W apart. Hence we have N = 2WT observations.

Taking σ^2 to be equal $N_o W$, and applying (3),

$$\sigma^2_{min}(\hat{\theta}) = \frac{\left[\frac{\partial E(\hat{\theta})}{\partial \theta}\right]^2 \sigma^2}{N\left\{\frac{A^2}{2N}\sum_{i=1}^{N}[1 - \cos 2(\omega_o t + \theta)]\right\}}$$

$$\approx \left[\frac{\partial E(\hat{\theta})}{\partial \theta}\right]^2 \Big/ \left\{2WT \cdot \frac{A^2}{2\sigma^2}\right\} = \left[\frac{\partial E(\hat{\theta})}{\partial \theta}\right]^2 \Big/ \frac{2E}{N_o} \quad (4)$$

But this is the same as Equation (14) on page 6H-3.

6H.3 ANALYSIS OF ZERO-CROSSING PHASE DETECTION

The zero-crossing measurement consists of calculating the time at which the waveform crosses the zero axis. The measured times, t_{oi} of $H_i(t)$, are not equal to the true signal zero-crossing times, $t_o^{(i)}$, due to the noise.

Let H(t) represent $H_1(t)$ or $H_2(t)$.

In a neighborhood of the measured zero-crossing time t_o, approximate H(t) by a straight line (see Figure 6H-1).

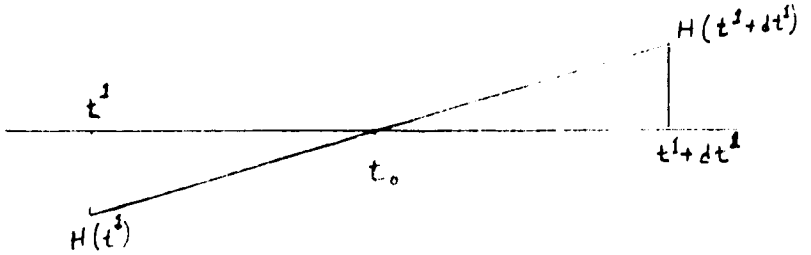

Figure 6H-1. Straight line approximation to H(t) about a zero crossing.

The straight line approximation is:

$$H(t) = H(t^1) + H^1(t^1)\ (t-t^1) \tag{1}$$

for any t in the interval $(t^1,\ t^1 + dt^1)$

If we let $t = t_o$ and solve (1) for t_o we have:

$$0 = H(t^1) + H^1(t^1)\ (t_o-t^1) \tag{2}$$

$$t_o = t^1 - H(t^1)/H^1(t^1) \tag{3}$$

If $t_o^{(i)}$ represents the true positive-slope zero-crossing time of the signal component of $H_i(t)$, it follows that:

$$\begin{aligned} t_{oi} &= t_o^{(i)} - H_i(t_o^{(i)}) / H_i^1(t_o^{(i)}) \\ &= t_o^{(i)} - \varepsilon_i \end{aligned} \tag{4}$$

and

$$\begin{aligned} \varepsilon_i &= H_i(t_o^{(i)}) / H_i^1(t_o^{(i)}) \\ &= \frac{n_i(t_o^{(i)})}{-A_i w_o + n_i^1(t_o^{(i)})} \\ &= -\frac{n_i(t_o^{(i)})}{A_i w_o} \end{aligned} \tag{5}$$

for high signal to noise ratios.

The estimate of phase difference, $\hat{\varphi}$, is based upon the zero-crossing times which are contaminated by noise.

$$\hat{\varphi} = [\omega_0 (t_{o1} - t_{o2})]_{mod \pm 2\pi} \tag{6}$$

i.e., if the quantity in brackets is positive we take it mod + 2π and mod - 2π otherwise. This ordering, and the definition of (6) is one of consistency (see (10)).

From Equation (4)

$$\omega_0(t_{o1} - t_{o2}) = \omega_0(t_o^{(1)} - t_o^{(2)}) + \omega_0(-\varepsilon_1 + \varepsilon_2) \tag{7}$$

Letting

$$\delta = \omega_0(-\varepsilon_1 + \varepsilon_2)$$

$$\approx \frac{n_1(t_o^{(1)})}{A_1} - \frac{n_2(t_o^{(2)})}{A_2} \tag{8}$$

From (1) the conditions for positive slope signal crossings are:

$$\begin{cases} \omega_0 t_o^{(1)} + \theta = 2n_1\pi - \pi/2 \; ; \; n_1 = 0, \pm 1, \pm 2, \ldots \\ \omega_0 t_o^{(2)} + \theta + \varphi = 2n_2\pi - \pi/2 \; ; \; n_2 = 0, \pm 1, \pm 2, \ldots \end{cases} \tag{9}$$

Therefore:

$$\omega_0(t_o^{(1)} - t_o^{(2)}) = 2(n_1 - n_2)\pi - \theta + \theta + \varphi \tag{10}$$

It follows then from (6) and (10) that in the absence of noise

$$\begin{aligned} \hat{\varphi} &= [2(n_1 - n_2)\pi + \varphi]_{mod \pm 2\pi} \\ &= \varphi_{mod \pm 2\pi} \\ &= \varphi_0 \end{aligned} \tag{11}$$

In the presence of noise

$$\hat{\varphi} = [\varphi + \delta]_{\text{mod} \pm 2\pi} \tag{12}$$

Since the noise functions are zero mean, Gaussian and independent

$$\sigma^2(\delta) = E\left\{ \frac{n_1(t_0^{(1)})}{A_1} - \frac{n_2(t_0^{(2)})}{A_1} \right\} = \frac{N_1}{A_1^2} + \frac{N_2}{A_2^2} \tag{13}$$

The mean value of the phase estimate $\hat{\varphi}$ is:

$$E(\hat{\varphi}) = \int_{-\infty}^{\infty} \frac{1}{\sigma\sqrt{2\pi}} e^{-\delta^2/2\sigma^2} [\varphi + \delta]_{\text{mod} \pm 2\pi} \, d\delta \tag{14}$$

It is easily shown that if we write

$$\varphi = \varphi_{\text{mod} \pm 2\pi} + 2l\pi$$

$$= \varphi_0 + 2l\pi \tag{15}$$

$$(\varphi + \delta)_{\text{mod} \pm 2\pi} = (\varphi_0 + \delta)_{\text{mod} \pm 2\pi} \tag{16}$$

If we let

$$y = \delta + \varphi_0 \tag{17}$$

we can evaluate the integral of (14).

$$E(\hat{\varphi}) = \varphi_0 + b(\varphi_0, \sigma) \tag{18}$$

where $b(\varphi_0, \sigma)$ represents a bias,

$$b(\varphi_0,\sigma) = 2\pi \sum_{n=1}^{u} n\left[\Phi\left(\frac{2(n+1)\pi + \phi_0}{\sigma}\right) - \Phi\left(\frac{2n\pi + \phi_0}{\sigma}\right) - \Phi\left(\frac{\phi_0 - 2n\pi}{\sigma}\right) + \Phi\left(\frac{\phi_0 - 2(n-1)\pi}{\sigma}\right)\right] \tag{19}$$

u is the largest integer less than or equal to $\left|\frac{3\sigma - \phi_0}{2\pi}\right|$

$$\Phi(x) = \int_{-\infty}^{x} \frac{1}{\sqrt{2\pi}} e^{-t^2/2}\, dt \tag{20}$$

The bias error is small when

$$|\varphi_0| < 2\pi - 3\sigma \tag{21}$$

We therefore have the following conclusions:

$$\begin{cases} E(\hat{\varphi}) = \varphi_{\text{mod}\pm 2\pi} \\ \sigma^2(\hat{\varphi}) = \sigma^2(\delta) \\ \qquad\qquad \approx \frac{1}{2}\left[\frac{1}{\left(\frac{S}{N}\right)_1} + \frac{1}{\left(\frac{S}{N}\right)_2}\right] \end{cases} \tag{22}$$

whenever

$$\left|\varphi_{\text{mod}\pm 2\pi}\right| < 2\pi - \frac{3\sqrt{2}}{2}\sqrt{\frac{1}{\left(\frac{S}{N}\right)_1} + \frac{1}{\left(\frac{S}{N}\right)_2}} \tag{23}$$

6H.4 LIMITER-MULTIPLIER PHASE DETECTION

The noise can be written as:

$$n_i(t) = I_{ci}(t)\cos\omega_o t - I_{si}(t)\sin\omega_o t \quad ; i = 1, 2 \tag{1}$$

The inputs to the phase detector (see Figure 6H-2) can thus also be written as:

$$\left.\begin{aligned} H_1(t) &= [A_1\cos\theta + I_{c1}(t)]\cos\omega_o t - [A_1\sin\theta + I_{s1}(t)]\sin\omega_o t \\ H_2(t) &= [A_1\cos(\theta+\varphi) + I_{c2}(t)]\cos\omega_o t - [A_1\sin(\theta+\varphi) + I_{s2}(t)]\sin\omega_o t \end{aligned}\right\} \tag{2}$$

Observe that if a signal a(t) cos ($\omega_o t + \alpha$) is passed through a bandpass limiter, the output is cos ($\omega_o t + \alpha$)

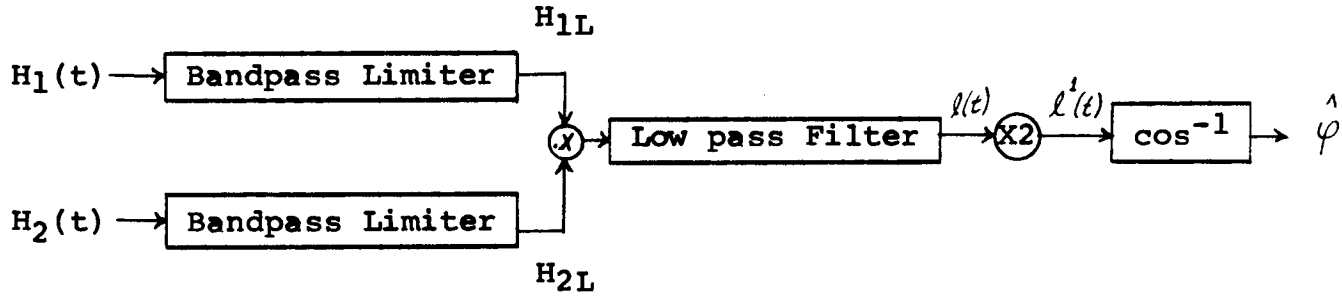

Figure 6H-2. Block Diagram of the Limiter-Multiplier Phase Detector

So passing $H_i(t)$ through such a bandpass limiter we obtain outputs

$$H_{iL}(t) = \cos[\omega_o t + \alpha_i(t)] \tag{3}$$

Now $\ell(t)$ is the low frequency position of the product detector output:

$$\ell(t) = LF\left[H_{1L}(t)\, H_{2L}(t)\right] = \frac{1}{2}\cos\left[\alpha_1(t) - \alpha_2(t)\right] \tag{4}$$

and passing $\ell(t)$ through a voltage multiplier we obtain $\ell'(t)$

$$\ell'(t) = \cos\left[\alpha_1(t) - \alpha_2(t)\right] \tag{5}$$

From Equation (2), we find that:

$$\begin{cases} \cos\alpha_1 = \dfrac{A_1\cos\theta + I_{c1}}{\left[A_1^2 + R_1^2 + 2A_1 I_{c1}\right]^{1/2}} \\ \sin\alpha_1 = \dfrac{A_1\sin\theta + I_{s1}}{\left[A_1^2 + R_1^2 + 2A_1 I_{c1}\right]^{1/2}} \\ \cos\alpha_2 = \dfrac{A_1\cos(\theta+\varphi) + I_{c2}}{\left[A_2^2 + R_2^2 + 2A_2 I_{c2}\right]^{1/2}} \\ \sin\alpha_2 = \dfrac{A_1\sin(\theta+\varphi) + I_{s2}}{\left[A_2^2 + R_2^2 + 2A_2 I_{c2}\right]^{1/2}} \end{cases} \tag{6}$$

where

$$\begin{cases} R_i = \sqrt{I_{ci}^2 + I_{si}^2} \quad ; i = 1, 2 \\ R_i\cos\varphi_i = I_{ci} \\ R_i\sin\varphi_i = I_{si} \end{cases} \tag{7}$$

We will now normalize in the following way:

Equations (6) are divided through by A_1 or A_2; I_{ci} and I_{si} are replaced by $\sqrt{N}\,I_{ci}$ and $\sqrt{N}\,I_{si}$ respectively, while R_i^2 is replaced by NR_i^2. Letting $\rho_i = A_i^2/2N_i$ we can write:

$$\cos\alpha_1 = \frac{\cos\theta + I_{c1}/\sqrt{2\rho_1}}{\sqrt{1 + \frac{R_1^2}{2\rho_1} + \frac{2\,I_{c1}}{\sqrt{2\rho_1}}}}$$

$$\approx \left[\cos\theta + I_{c1}/\sqrt{2\rho_1}\right]\left[1 - \frac{R_1^2}{4\rho_1} - \frac{I_{c1}}{\sqrt{2\rho_1}}\right] \qquad (8)$$

etc.

If we now form $\cos(\alpha_1 - \alpha_2)$ and separate out $\cos\varphi$ we have:

$$\varphi'(t) = \cos\varphi + \varepsilon(t) \qquad (9)$$

where $\varepsilon(t)$ is the error in measurement.

$$\varepsilon(t) = \cos\varphi\left[-\frac{R_1^2}{4\rho_1} - \frac{R_2^2}{4\rho_2} - \frac{I_{c1}}{\sqrt{2\rho_1}} \cdot \frac{I_{c2}}{\sqrt{2\rho_2}} - \frac{I_{c1}\,I_{c2}}{\sqrt{\rho_1\rho_2}}\right] +$$

$$\left[\frac{I_{c1}}{\sqrt{2\rho_1}} + \frac{I_{c2}}{\sqrt{2\rho_2}} - \frac{R_1R_2\cos(\varphi_1+\varphi_2)}{2\sqrt{\rho_1\rho_2}} - \frac{I_{c1}^2}{2\rho_1} - \frac{I_{c2}^2}{2\rho_2}\right] \qquad (10)$$

accurate to $1/\rho$.

If we now pass $\ell'(t)$ through an arc-cosine device we have

$$\hat{\varphi} = \cos^{-1}\left[\cos\varphi + \varepsilon(t)\right] \qquad (11)$$

If the measurement could be made without error, i.e., in the absence of noise

$$\hat{\varphi} = \varphi_{\text{mod} \pm 2\pi} \tag{12}$$

but in the presence of noise we have to work from (11).

Consider this equation. It is immediate that $\varphi = n\pi$, $n = 0, \pm 1, \pm 2, \ldots$ are possible singular points.

This same difficulty is also expressed in the first order Taylor's series approximation:

$$\hat{\varphi} = \varphi_{\text{mod} \pm 2\pi} - \varepsilon(t) \Big/ \sqrt{1 - \cos^2\varphi} \tag{13}$$

The mean of the estimate $\hat{\varphi}$ is

$$\langle \hat{\varphi} \rangle = \varphi_{\text{mod} \pm 2\pi} - \langle \varepsilon \rangle \Big/ \sqrt{1 - \cos^2\varphi} \quad ; \quad \langle \varepsilon \rangle = \left[-\frac{1}{2\rho_1} - \frac{1}{2\rho_2} \right] [\cos\varphi + 1]$$

$$\langle \hat{\varphi} \rangle = \varphi_{\text{mod} \pm 2\pi} + \left[\frac{1}{2\rho_1} + \frac{1}{2\rho_2} \right] \sqrt{\frac{\cos\varphi + 1}{\cos\varphi - 1}} \tag{14}$$

Equation (14) is derived from Equation (5-17.6) of Reference 2.

Also the variance of $\hat{\varphi}$

$$\sigma^2(\hat{\varphi}) \simeq \left[\frac{\partial \hat{\varphi}}{\partial \cos\varphi} \right]^2 \sigma^2(\cos\varphi) + \left[\frac{\partial \hat{\varphi}}{\partial \varepsilon} \right]^2 \sigma^2(\varepsilon)$$

$$\simeq \frac{1}{1 - [\cos\varphi + \langle \varepsilon \rangle]^2} \left[(\cos\varphi - 1)^2 \left(\frac{1}{2\rho_1} + \frac{1}{2\rho_2} \right) \right]$$

$$= \frac{[\cos\varphi - 1]^2 \left[\frac{1}{2\rho_1} + \frac{1}{2\rho_2} \right]}{\sin^2\varphi - 2\cos\varphi [\cos\varphi + 1] \left[\frac{1}{2\rho_1} + \frac{1}{2\rho_2} \right]} \tag{15}$$

6H.5 QUADRATURE PHASE DETECTOR

As in Equation 2 on page 6H-5.

$$\begin{cases} H_1(t) = [A_1\cos\theta + I_{c1}]\cos\omega_0 t - [A_1\sin\theta + I_{s1}]\sin\omega_0 t \\ \quad = R_1(t)\cos[\omega_0 t + \alpha_1] \\ H_2(t) = [A_2\cos(\theta+\varphi) + I_{c2}]\cos\omega_0 t - [A_2\sin(\theta+\varphi) + I_{s2}]\sin\omega_0 t \\ \quad = R_2(t)\cos[\omega_0 t + \alpha_2] \end{cases} \tag{1}$$

The low frequency portion of the first product detector output (see Figure 6H-3) is

$$L_1(t) = LF[H_1(t)H_2(t)] = \frac{R_1R_2}{2}\cos[\alpha_1 - \alpha_2] \tag{2}$$

while the low frequency portion of the second product detector output, where one of the signals underwent a 90° shift, is:

$$L_2(t) = -\frac{R_1R_2}{2}\sin(\theta_1 - \theta_2) \tag{3}$$

If now $L_1(t)$ and $L_2(t)$ are put through the divider we have

$$\frac{\sin(\theta_1-\theta_2)}{\cos(\theta_1-\theta_2)} = \frac{\frac{1}{2}R_1R_2\sin(\theta_1-\theta_2)}{\frac{1}{2}R_1R_2\cos(\theta_1-\theta_2)} \tag{4}$$

The estimate $\hat{\varphi}$ of phase difference is $\hat{\varphi} = \theta_2 - \theta_1$

$$\hat{\varphi} = -\tan^{-1}\frac{R_1R_2\sin(\theta_1-\theta_2)}{R_1R_2\cos(\theta_1-\theta_2)}$$

$$= \tan^{-1}\frac{R_1R_2\sin(\theta_2-\theta_1)}{R_1R_2\cos(\theta_2-\theta_1)}$$

$$= \tan^{-1}\left[\frac{\sin\varphi - \frac{I_{s1}}{\sqrt{2\rho_1}} + \frac{I_{s2}}{\sqrt{2\rho_2}} + \frac{I_{c1}I_{s2} - I_{s1}I_{c2}}{2\sqrt{\rho_1\rho_2}}}{\cos\varphi + \frac{I_{c1}}{\sqrt{2\rho_1}} + \frac{I_{c2}}{\sqrt{2\rho_2}} + \frac{I_{c1}I_{c2} + I_{s1}I_{s2}}{2\sqrt{\rho_1\rho_2}}}\right] \tag{5}$$

From Equation 5-17.6 of Reference 2,

if $\hat{\varphi} = f(I_{c1}, I_{s1}, I_{c2}, I_{s2})$ is approximately linear over the range of significant variation of ($I_{c1}, I_{s1}, I_{c2}, I_{s2}$), it can be approximated by a Taylor's series,

$$\langle \hat{\varphi} \rangle \cong f\left[\langle I_{c1} \rangle, \langle I_{s1} \rangle, \langle I_{c2} \rangle, \langle I_{s2} \rangle \right]$$

$$= \varphi_{mod \pm 2\pi} \qquad (6)$$

and

$$\sigma^2(\hat{\varphi}) \cong \left[\left(\frac{\partial f}{\partial I_{c1}}\right)^2 \sigma^2(I_{c1}) + \cdots + \left(\frac{\partial f}{\partial I_{s2}}\right)^2 \sigma^2(I_{s2}) \right] \qquad (7)$$

All covariance terms are zero because the in phase and quadrature components are uncorrelated as well as $n_1(t)$, $n_2(t)$.

By definition,

$$\sigma^2(I_{ci}) = \sigma^2(I_{si}) = 1 \quad , \quad i = 1, 2 \qquad (8)$$

Since

$$\frac{\partial}{\partial \cdot} \tan^{-1}\left(\frac{p}{q}\right) = \frac{q\frac{\partial p}{\partial \cdot} - p\frac{\partial q}{\partial \cdot}}{p^2 + q^2} \quad , \qquad (9)$$

for large signal-to-noise ratios, Equation (7) becomes:

$$\sigma^2(\hat{\varphi}) = \frac{\frac{1}{2\rho_1} + \frac{1}{2\rho_2} + \frac{1}{4\rho_1\rho_2}\left[R_1^2 + R_2^2\right] + \frac{1}{\sqrt{2}\rho_1\rho_2}\left[\frac{I_{c1}}{\sqrt{2}\rho_1} + \frac{I_{c2}}{\sqrt{2}\rho_2}\right]}{\left[\sin\varphi - \frac{I_{s1}}{\sqrt{2}\rho_1} + \frac{I_{s2}}{\sqrt{2}\rho_2} + \frac{I_{c1}I_{s2} - I_{s1}I_{c2}}{2\sqrt{\rho_1\rho_2}}\right]^2 + \left[\cos\varphi + \frac{I_{c1}}{\sqrt{2}\rho_1} + \frac{I_{c2}}{\sqrt{2}\rho_2} + \frac{I_{c1}I_{c2} + I_{s1}I_{s2}}{2\sqrt{\rho_1\rho_2}}\right]^2}$$

$$\approx \frac{1}{2}\left(\frac{1}{\rho_1} + \frac{1}{\rho_2}\right) \qquad (10)$$

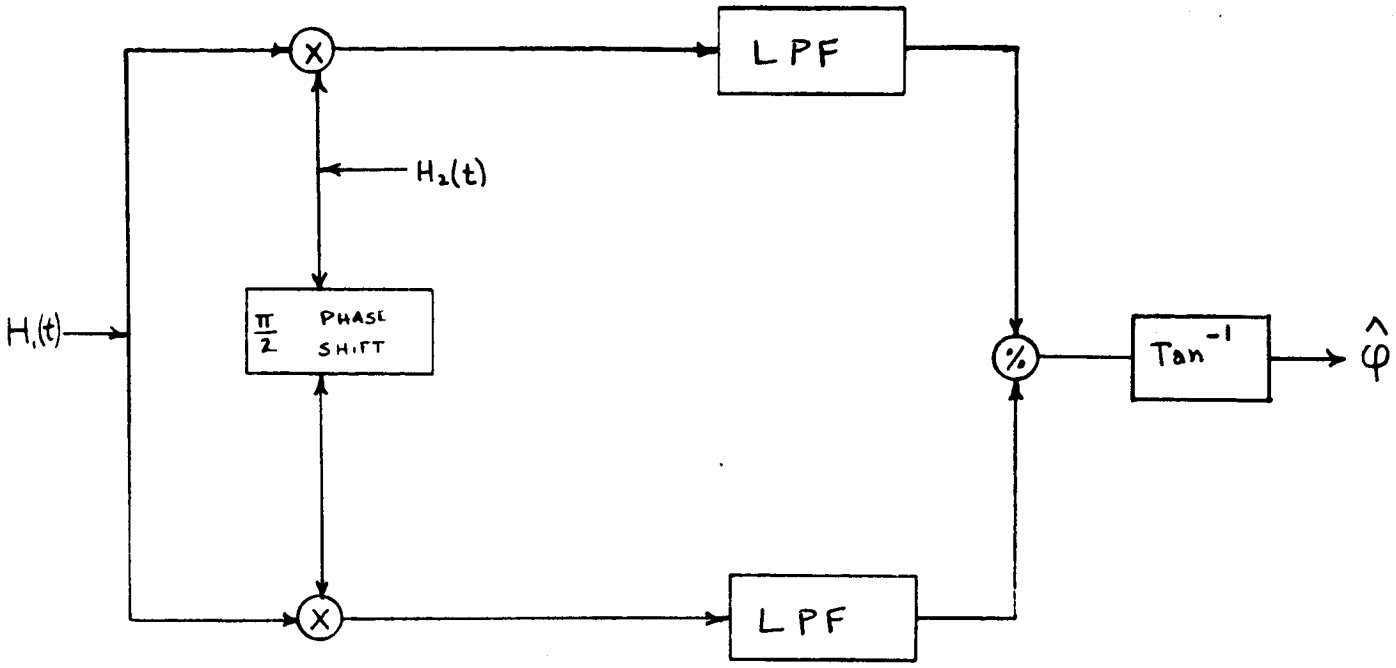

Figure 6H-3. Block Diagram of a Quadrature Phase Detector

6H.6 PRODUCT-DEMODULATOR-ENVELOPE-DIVISION PHASE DETECTOR

We write $H_1(t)$ and $H_2(t)$ as

$$\left.\begin{aligned} H_1(t) &= A_1 \cos[\omega_0 t + \theta] + n_1(t) \\ &= a_1 \cos[\omega_0 t + \alpha_1] \\ H_2(t) &= A_2 \cos[\omega_0 t + \theta + \varphi] + n_2(t) \\ &= a_2 \cos[\omega_0 t + \alpha_2] \end{aligned}\right\} \quad (1)$$

The output of the low pass filter (see Figure 6H-4) is $\ell(t)$:

$$\ell(t) = \tfrac{1}{2} a_1 a_2 \cos(\alpha_1 - \alpha_2) \quad (2)$$

and then pass $\ell(t)$ through a multiplier and phase shifter

$$\ell'(t) = a_1 a_2 \sin(\alpha_1 - \alpha_2) \quad (3)$$

The output of the envelope detector of the product $H_1(t)$ $H_2(t)$ is a_1 a_2.

The output of the divider is v(t):

$$V(t) = \sin(\alpha_1 - \alpha_2) \tag{4}$$

The estimate of phase difference is defined by

$$\hat{\varphi} = \alpha_2 - \alpha_1 \tag{5}$$

Thence

$$\begin{aligned}\hat{\varphi} &= -\sin^{-1}\left[\sin(\alpha_1 - \alpha_2)\right] \\ &= \sin^{-1}\left[\sin(\alpha_2 - \alpha_1)\right]\end{aligned} \tag{6}$$

and

$$\sin(\alpha_2 - \alpha_1) = \sin\alpha_2\cos\alpha_1 - \cos\alpha_2\sin\alpha_1$$

$$= \left[1 + \frac{R_1^2}{2\rho_1} + \frac{2I_{c1}}{\sqrt{2\rho_1}}\right]^{-1}\left[1 + \frac{R_2^2}{2\rho_2} + \frac{2I_{c2}}{\sqrt{2\rho_2}}\right]^{-1} \cdot$$

$$\cdot\left\{\left[\sin(\theta+\varphi) + \frac{I_{s2}}{\sqrt{2\rho_2}}\right]\left[\cos\theta + \frac{I_{c1}}{\sqrt{2\rho_1}}\right] - \left[\cos(\theta+\varphi) + \frac{I_{c2}}{\sqrt{2\rho_2}}\right]\left[\sin\theta + \frac{I_{s1}}{\sqrt{2\rho_1}}\right]\right\}$$

$$= \sin\varphi + \varepsilon(t) \tag{7}$$

where

$$\varepsilon(t) = -\sin\varphi\left[\frac{R_1^2}{4\rho_1} + \frac{R_2^2}{4\rho_2} + \frac{I_{c1}}{\sqrt{2\rho_1}} + \frac{I_{c2}}{\sqrt{2\rho_2}} + \frac{I_{c1}I_{c2}}{\sqrt{\rho_1\rho_2}}\right]$$

$$+\left[\frac{I_{s2}}{\sqrt{2\rho_2}} - \frac{I_{s1}}{\sqrt{2\rho_1}} + \frac{I_{c1}I_{s1}}{2\rho_1} - \frac{I_{c2}I_{s2}}{2\rho_2}\right] \tag{8}$$

In the absence of noise

$$\begin{aligned}\hat{\varphi} &= \sin^{-1}\left[\sin\varphi\right] \\ &\simeq \varphi_{\text{mod}\,\pm 2\pi}\end{aligned} \tag{9}$$

As before, we use Hald's work and obtain in the presence of noise:

$$\langle \hat{\varphi} \rangle = \sin^{-1}\left[\langle \sin\varphi \rangle + \langle \varepsilon(t) \rangle \right]$$

$$\cong \varphi_{mod \pm 2\pi} + \frac{\langle \varepsilon(t) \rangle}{\sqrt{1 - \sin^2\varphi}} \qquad (10)$$

The mean of $\varepsilon(t)$ is found to be:

$$\langle \varepsilon \rangle = -\sin\varphi \left[\frac{1}{2\rho_1} + \frac{1}{2\rho_2} \right] \qquad (11)$$

so that

$$\langle \hat{\varphi} \rangle \cong \varphi_{mod \pm 2\pi} \pm \tan\varphi \left[\frac{1}{2\rho_1} + \frac{1}{2\rho_2} \right] \qquad (12)$$

The variance of $\hat{\varphi}$ can be estimated for large S/N by

$$\sigma^2(\hat{\varphi}) \approx \left[\frac{\partial \hat{\varphi}}{\partial \varepsilon}\Big|_{\langle\rangle} \right]^2 \sigma^2(\varepsilon)$$

$$= \frac{\sin^2\varphi \left[\frac{1}{2\rho_1} + \frac{1}{2\rho_2} \right]}{\cos^2\varphi + 2\sin^2\varphi \left[\frac{1}{2\rho_1} + \frac{1}{2\rho_2} \right]} \qquad (13)$$

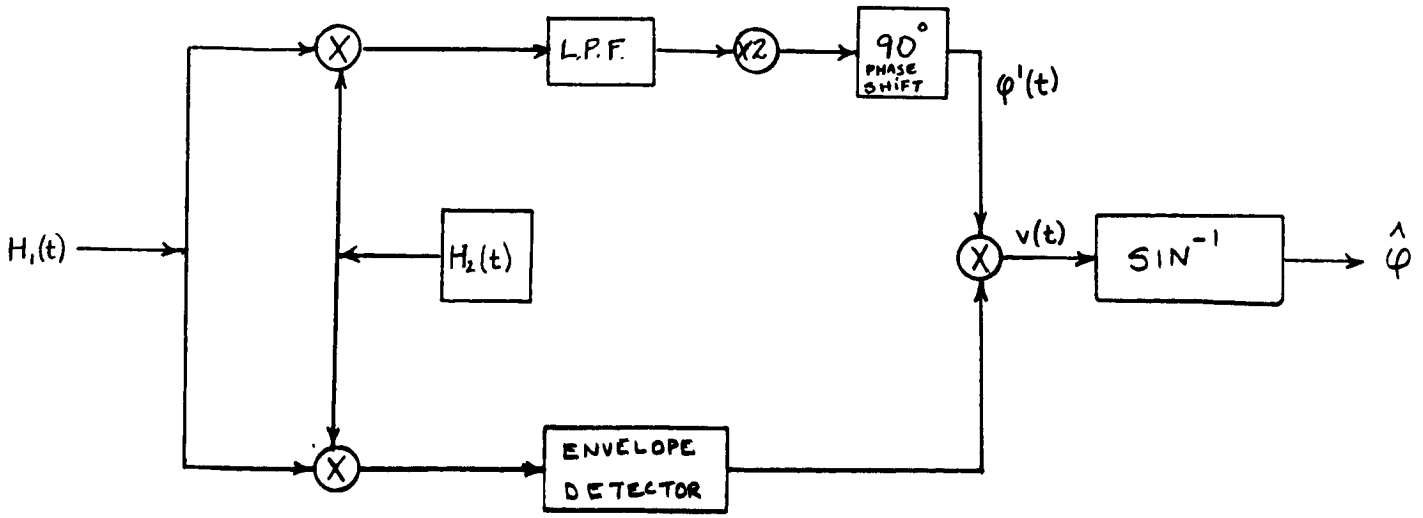

Figure 6H-4. Block Diagram of the Product-Demodulator-Envelope-Division Phase Detector

6H.7 REFERENCES

1. K. Karhunen, "Uber Lineare Methoden in der Wahrscheinlichkeitsrechnung," Ann. Acad. Sci. Flnn. 37 (1947); M. Loéve, "Fonctions Aleatoires de Second Ordre," Appendix to "Processus Stochastiques", by P. Levy, Gauthier - Villars 1948; M. Loéve, Probability Theory, D. Van Nostrand, 2nd Edition 1960 (there is a more recent edition); U. Grenander, "Stochastic Processes and Statistical Inference," Arkiv for Matematik, Stockholm 1950; W.B. Davenport and W.L. Root, Random Signals and Noise, McGraw-Hill 1958; and D. Slepian, "Estimation of Signal Parameters," IRE Transactions of the Professional Group on Information Theory, March 1954.

2. A. Hald - Statistical Theory with Engineering Applications, Wiley 1952.